STRENGTH OF SLENDER REINFORCED CONCRETE WALLS

BY

ISRAEL BESSER AVILA

A thesis presented in fulfilment of the requirements
of the Degree of Doctor of Philosophy

at

The University of Leeds

April, 1983

ACKNOWLEDGEMENTS

The writer would like to express his sincere thanks to Professor A.R. Cusens, Head of Civil Engineering at the University of Leeds, for making his stay in Leeds possible and for his ready assistance and helpful supervision throughout the course of this work.

The author wishes to express his gratitude to the University for his employment as Research Assistant, which largely enabled him to carry out this research.

He also extends his thanks to the following: the technical staff of the Department for their assistance in the manufacture, preparation and test of specimens, his friends and colleagues, Messrs. Choon Jin Tay and Monir Kamal for their help with the tests, Miss Wendy Bates and Mr. Roy Duxbury for their diligent contribution with matters related to photography, and especially Miss Wendy Beadle for her help with text proofing. The author is greatly indebted to Mrs. Janis Hickey and Mrs. Aileen Warren for their help and "rescue" in typing this work.

Finally, he would like to thank his parents for their encouragement.

ABSTRACT

This study is concerned with the behaviour of single span slender reinforced concrete members with depth/span ratios equal to and larger than 1. A series of deep panels with depth/span ratios between 1 and 4 was studied experimentally. These elements were tested under third point loads at the top level. Aspects such as stress development, in-plane and out-of-plane deformations, cracks and modes of failures were thoroughly investigated. Experimental stresses are compared with solutions given by the Finite Element technique. It is shown that the shear strength of deep panels increases for depth/span ratios beyond unity, in disagreement with present design recommendations.

A second group of walls was tested under five different combinations of uniformly distributed top and bottom vertical in-plane loads. A range of percentages of vertical web reinforcement was used. The quantity of reinforcement showed no effect in retarding the formation of horizontal cracks but their widths were progressively reduced.

The effect of soffit load on crack formation and failure of these walls is analysed. Test results are compared with current design recommendations. Soffit load causes tensile cracking of the concrete to occur earlier than under top loads only. It also reduces the bearing strength of the specimens.

Crushing of the bearing zone was the commonest mode of failure. This problem is studied and a general introduction to its understanding is presented.

Reinforced concrete deep members, when cast in their vertical position, present problems of segregation, which cause a variable quality of concrete within the depth. A large difference in the strength of concrete (up to 40 per cent) was observed between the upper and lower levels in specimens 1 m deep. Some attention is given to this problem, in order to analyse more accurately the experimental results.

TABLE OF CONTENTS

PRINCIPAL NOTATION

A	Area of individual bar
A_{hs}	Area of steel carrying hanging load
A_{sl}	Area of main reinforcement in tension
A_{sw}	Steel area of web reinforcement
A_v	Area of shear reinforcement perpendicular to flexural tension reinforcement
A_{vh}	Area of shear reinforcement parallel to flexural reinforcement
b	Thickness of beam
B	H/L ratio
d	Effective depth of beam
D	Flexural rigidity of a plate
d'	Diameter of concrete cores
E	Modulus of elasticity
E_c	Static modulus of elasticity of concrete
E_{ct}	Modulus of elasticity of concrete in tension
E_s	Modulus of elasticity of steel
E'	w/L ratio
F	An Airy stress function
f_b	Estimated bearing strength
f_{bu}	Tested ultimate bearing strength
f_c	Stress in concrete
f_{cu}	Cube compressive strength of concrete
f_{cb}	Prism strength of concrete
f'_c	Cylinder compressive strength of concrete
f_{ct}	Cylinder splitting strength of concrete

f_s	Stress in steel
f_y	Steel yield strength
f_{yw}	Stirrup yield stress
H	Height of beam or wall
h_a	Effective height of deep beam
h'	Height of concrete core
I	Second moment of area
K_1	$P_t/(P_t + P_b)$ ratio
L	Span of beam
l_o	Clear span of beam
M	Moment at a section
m	Experimental-to-estimated values of bearing strength
M_s	Negative (hogging) moment
M_t	Positive (sagging moment)
M_u	Ultimate bending moment
M_x, M_y	Bending moments per unit length perpendicular to the x and y axes respectively
M_{xy}	Twisting moment per unit length, perpendicular to the x axis
n	Bearing strength-to-compressive strength ratio
n_c	Bearing stress-to-compressive strength ratio at cracking
p	Ratio of reinforcement to concrete area
P_b	Load applied on the bottom
P_c	Ultimate load causing shear failure of a beam
P_{cr}	Cracking load
P_t	Load applied on the top level
q	Uniformly distributed load per unit length
R	Ratio of block area to contact area

s	Distance of the bearing plate from the edge of the specimen
s_1	Spacing of vertical web reinforcement
s_2	Spacing of horizontal web reinforcement
T	Resultant of all concrete tensile stresses
v	Nominal shear stress
v_c	Permissible shearing stress in concrete
V	Shear force
V_{ab}	Applied shear from bottom loads
V_{at}	Applied shear from top loads
V_c	Nominal shear strength provided by concrete
V_{cb}	Shear capacity assuming bottom loads
V_{cr}	Cracking strength of section
V_{ct}	Shear capacity assuming top loads only
V_n	Nominal shear strength of section
V_s	Nominal shear strength provided by shear reinforcement
w	Length of support
W	Total load
W_{cr}	Total uniformly distributed cracking load
x_e	Clear shear span
x_s	Shear span
x, y, z	Rectangular coordinates
Y	Depth of bar from top of beam
z	Lever arm
α	Angle of inclination of reinforcement to the axis of the beam
α_e	Modular ratio = E_s/E_{ct}
γ_{xy}	Shear strain component in rectangular coordinates

ε_c	Concrete strain
ε_s	Steel strain
ε_x, ε_y	Strains in x and y directions respectively
λ	Length/diameter ratio of core
λ_1, λ_2	Constants
ν	Poisson's ratio
σ_x, σ_y	Normal components of stress parallel to x and y axes
τ_{xy}	Shearing stress component in rectangular coordinates
ϕ_{cr}	Ratio of the stress in the reinforcement to the yielding stress (f_s/f_y) at the cracking load

CHAPTER 1

INTRODUCTION

1.1 GENERAL

In order to cater for large spans in buildings, new structural systems consisting of frames and deep beams have evolved leading to the development of wall-beams. The term wall-beam implies that the element functions as a wall and has load carrying capacity between discrete support points.

Certain characteristics, which are not present in slender beams, are exhibited by these members, owing to their depth. For instance, in deep beams, the non-linear stress distribution in vertical sections means that the normal theory of flexure based on Navier-Bernoully principles is not applicable. This property has been used by some authors to classify deep and slender beams. For example, Cheng and Pei (1954) stated that a "deep beam may be defined as a beam whose bending stresses deviate appreciably from the straight line distribution assumed in the elementary beam theory". Another quality of deep beams is their greatly enhanced shear capacity arising from the direct transfer of compressive stresses between loaded points and supports.

A 3-dimensional interpretation of the stress distribution in a deep flexural member loaded and supported as shown in Fig. 1.1(a) is illustrated in the following figures: Fig. 1.1(b), horizontal stresses, x direction; Fig. 1.1(c), vertical stresses, y direction and Fig. 1.1(d), shear stresses. These values were calculated using the Finite Element method of elastic analysis.

It can be observed that the flexural tensile stresses (Fig. 1.1(b) are concentrated at the very bottom of the wall and that

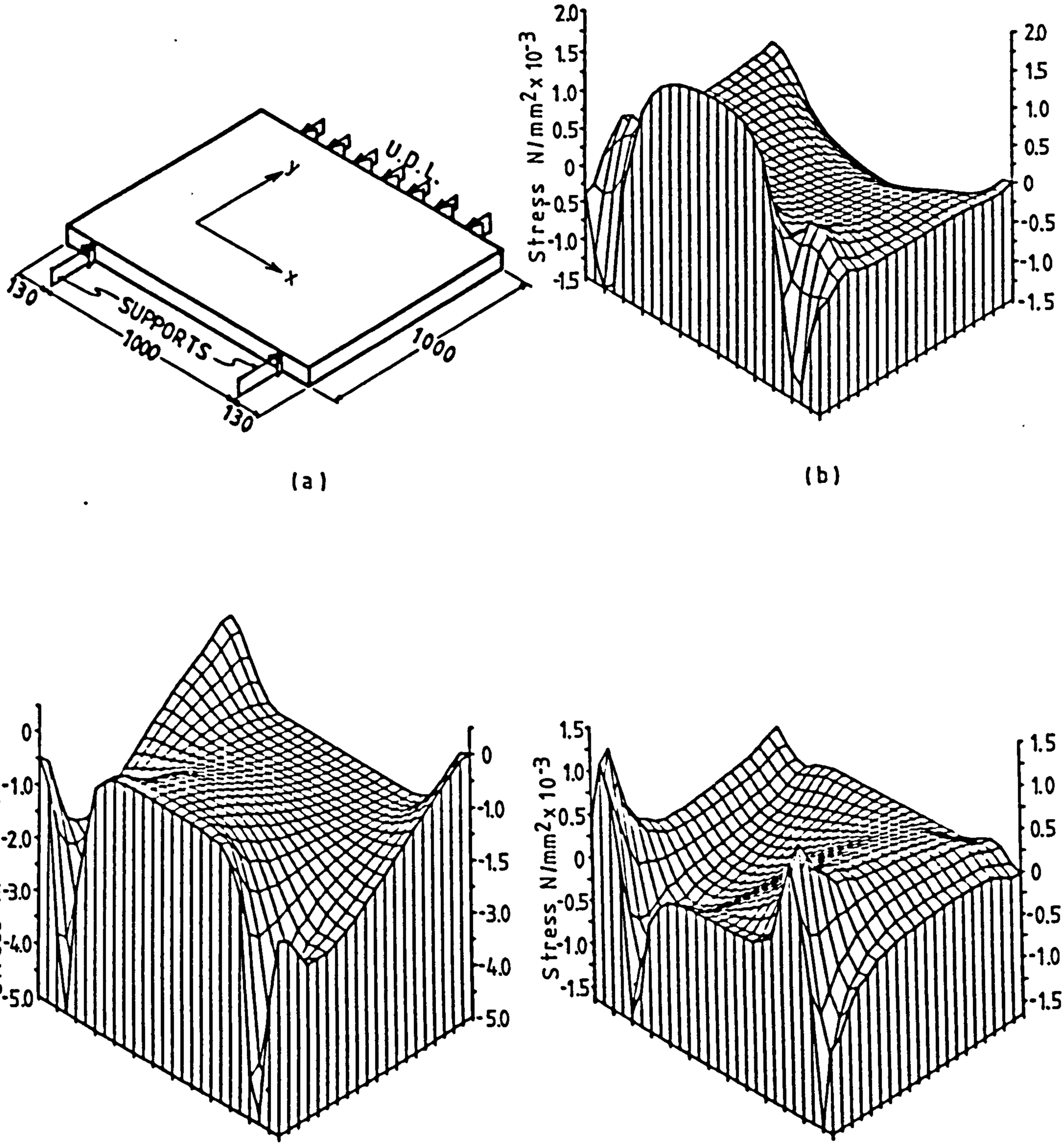

Fig. 1.1 Three-dimensional representation of stresses calculated by finite element analysis.
a) Isometric view of specimen, load, support and orthogonal co-ordinates system.
b) Stresses in x-direction.
c) Stresses in y-direction.
d) Shear stresses.

this tends to have a relatively uniform value along a large section of the span. The non-linear distribution of stresses in vertical sections is clearly demonstrated. Figure 1.1(c) shows the transfer of forces between the supports and the upper section of the wall giving rise to the arch action widely associated with deep beams. In Fig. 1.1(d), large shear stresses are illustrated in the area adjacent to the supports and at the bottom of the wall.

Deep beams are known to be sensitive to the position of loads in relation to their depth and the type of supports; these can be direct or indirect. Figure 1.2 provides an example of a combination of deep beams where direct and indirect supports together with direct and indirect loads are illustrated.

Although a clear division between slender and conventional deep beam behaviour does not exist, most documents dealing with this subject recognize deep beam action at span/depth ratios less than 2.5 for

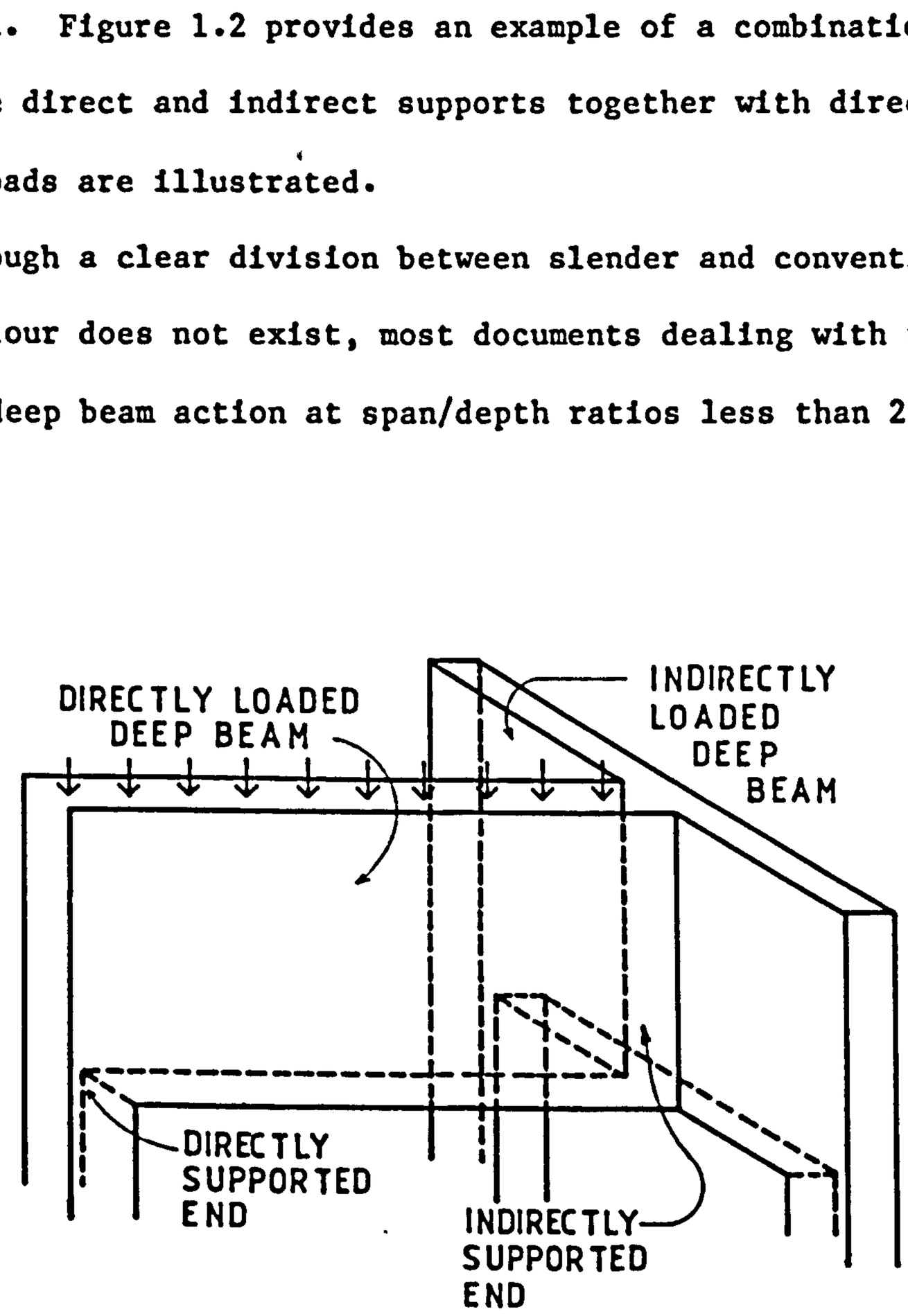

Fig. 1.2 Direct and indirect supports and loads

simply supported members. Features of deep beam behaviour have been found in column brackets, pile caps and in the end bearing blocks of prestressed concrete I beams. Geer (1960) considered that these end blocks were analogous to a deep beam turned on its side.

1.2 OBJECTIVES

In this investigation, an attempt has been made to study experimentally the influence of depth on the behaviour of deep beams with depth/span ratios beyond unity. Members subjected to combined top and bottom loads have also been considered. Particular attention was devoted to the following:

1) Surface crack formation and development of crack width.
2) Stress development.
3) In-plane deformation and out-of-plane horizontal deformation.
4) Vertical reinforcement influence on deep beam behaviour under top and bottom loads.
5) Bearing strength.

This experimental work aims to contribute towards the understanding of deep flexural members, to clarify certain aspects of earlier research and to provide information on previously unconsidered features.

1.3 THESIS OUTLINE

For a better understanding of deep flexural members behaviour and to be able to interpret test results, a survey of knowledge in this field to date was necessary. Therefore, a review of literature related to the subject was carried out and is presented in Chapter 2.

Chapter 3 is concerned with the manufacture and testing of the specimens. Material characteristics, particulars of test equipment and

test procedure are all incorporated.

Results obtained from the wall specimens are detailed in Chapter 4. Included are: crack patterns, crack widths, deformations and stress measurements taken on both large surfaces of the members.

Deep panel test results comprising in-plane displacements, crack patterns, out-of-plane displacements and strain measurement are contained in Chapter 5.

The problem of concrete quality variation within the wall specimens' depth due to segregation of the fresh concrete during casting is dealt with in Chapter 6.

Chapter 7 refers to the behaviour of deep flexural members under combined top and bottom loads. Additional analyses of results from Chapter 4 are also incorporated.

A study of the bearing capacity of deep flexural elements is covered in Chapter 8. Special attention is directed towards the bearing strength of these members under combined top and bottom loads.

A synopsis of the main observations and conclusions obtained from this experimental work is presented in Chapter 9, together with a number of suggestions for further research.

CHAPTER 2

REVIEW OF PREVIOUS WORK AND RESEARCH ON DEEP FLEXURAL ELEMENTS

2.1 GENERAL

In this chapter, an overall review of the research in the field of deep flexural members is presented. It has been subdivided, with the purpose of guiding the reader through the widely varied subjects in this field.

2.2 NUMERICAL SOLUTIONS

The stress distribution in deep members of homogeneous materials has been studied and well established by many authors, using analytical models. These models are based on the classical theory of elasticity, details of which can be obtained from Timoshenko and Goodier (1970). A common method for solving two-dimensional problems involves the determination of the Airy stress function, F, to satisfy the boundary conditions and comply with the biharmonic equation:

$$\partial^4 F/\partial x^4 + 2\partial^4 F/\partial x^2 \partial y^2 + \partial^4 F/\partial y^4 = 0 \qquad 2.1$$

Once the Airy stress function has been found, the stresses arise from the subsequent derivatives of the function as follows:

$$\sigma_x = \partial^2 F/\partial y^2,\ \sigma_y = \partial^2 F/\partial x^2 \text{ and } \tau_{xy} = -\partial^2 F/\partial x\ \partial y \qquad 2.2$$

Dischinger (1932) used hyperbolic Airy stress functions to analyse the stress distribution in continuous deep beams. Loads were represented by Fourier series. Tabulated results were given by Dischinger for different load cases and various ratios of height/span. These mathematical results were later used by the Portland Cement Association (1946) for the development of rules for concrete deep beam design. Dischinger's data was also used by Uhlman (1952) to complement

his own results for simply supported girder-walls, obtained by the finite difference method. Uhlman also provided data and some recommendations for the design of reinforced concrete deep beams.

Cheng and Pei (1954) used a similar method to that applied by Dischinger for the solution of planar-stress problems. They considered fixed supports, whereas Dischinger's solutions were based on supports with free in-plane rotations. The distribution of stresses at different sections at mid-span and above the supports was illustrated by graphs. Another similar numerical model was put forward by Thon (1958), which was also only applicable to continuous deep girders.

The numerical methods mentioned above were valid for multi-span deep beams only, due to the inability of the stress functions used to satisfy all the boundary conditions. Top and bottom edge boundary conditions were satisfied but not those at the vertical edges of the beam, eliminating the possibility of analysing single span deep members or end spans.

Problems related to the vertical boundaries of deep members have been overcome in different ways. Numerical solutions of single span deep beams with depth/span ratios of 0.5, 0.75, 1.0 and 1.5 were presented by Guzman and Luisoni (1948), based on two combined Airy stress functions. The first polynominal function satisfied all the boundary conditions but not necessarily the biharmonic equation; this was achieved by the contribution of the second stress function.

Conway et al (1951) used the superimposition of two stress functions to analyse the stress distribution in deep beams. The first stress function was a trigonometric series which did not satisfy one of the boundary conditions. This was satisfied by the second stress function, obtained by applying the principle of least work. Results from this method were compared to finite difference solutions and

reasonable agreement was reported. They showed that for depth/span ratios less than 0.5, the numerical methods provided results similar to those from simple-beam theory.

A stress function expressed as two parts was also used by Archer and Kitchen (1960) for the solution of single-span deep beams. One part was chosen so as to provide stress in accordance with the elementary beam theory and the other for stress components which accommodated the solution for the stress distribution of deep beams, considering the effect of vertical forces. Tabulated stresses for eight top loading conditions using span/depth ratios of 1, 1.5 and 2.0 were published. The analytical solution for one load case was compared to actual stresses measured on steel plates and was found to compare very well.

Coull (1966) presented a numerical method for the analysis of plane stresses, applicable to deep beams or any structure in which the stress system can be considered planar. In this method the stresses are given by a Fourier series as a function of one direction; the coefficients of the series depend upon the other co-ordinate. By utilising the principle of least work the coefficients are determined. This procedure differs from the methods using Airy stress functions in that the stresses are obtained directly from the solution of Fourier series, without the differentiation involved in the other methods. The series were chosen to satisfy the boundary conditions in every direction and loads were considered as superpositions of symmetric and anti-symmetric cases. A close agreement was found when solutions of an isotropic cantilever beam with a depth-to-span ratio equal to 1 were compared to results obtained from photoelastic tests performed by Kazimi and Coull (1964).

The finite difference method, a simplified procedure for the

numerical solution of the biharmonic equation, has also been employed for the analysis of deep flexural members. Conway et al (1951) verified its effectiveness and compared its results to values predicted by traditional strain energy methods. It was found that finite difference results were acceptable but not as accurate in the case of shear stresses.

Chow et al (1952) used the finite difference method to analyze the stress distribution in single-span deep beams under the five loading conditions shown in Fig. 2.1. Three height/span ratios were studied, i.e. 0.5, 1.0 and 2.0. It was observed that for all the types of loading, the stress curve agrees reasonably well with the linear distribution of the simple flexure theory when the depth/span ratio was 0.5. As this ratio increased, the difference between the linear distribution and the finite difference stresses became more significant. Three points of zero bending stress were noticed for depth/span ratios equal to 2. Results from the mathematical analysis

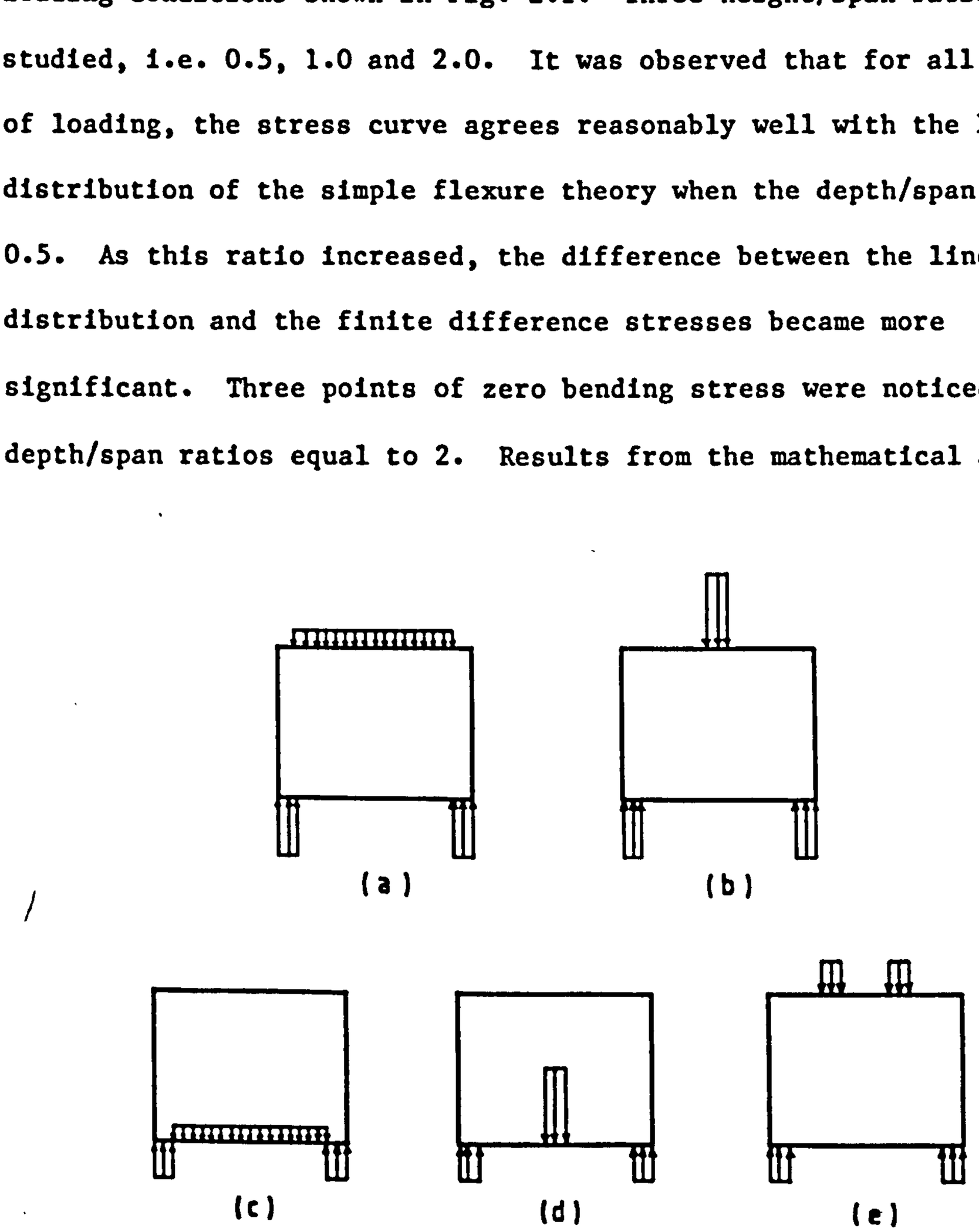

Fig. 2.1 Types of loading analysed by Chow (1952)

under each loading case were provided in graphical form and it was pointed out that the stresses for any combination of loading could be computed by means of the principle of superposition. It was further suggested that these results could be used for the design of tensile and shear reinforcement of concrete deep beams and procedures for determining the amount of reinforcement required were given.

Reinforced concrete is certainly not a homogeneous material, hence one of the principal assumptions of the linear elastic analysis is not satisfied. The cracking of the tension zone is another characteristic of concrete structures, which modifies the distribution of stresses as obtained from the classical theory of elasticity. Cracking of concrete at design loads causes stress redistribution, producing uncertainties about the validity of reinforcement design from elastic stresses. This is a challenge for more sophisticated methods of analysis to be developed which should aim to solve the problem of the inelastic behaviour of reinforced concrete.

With the aim of providing a mathematical model capable of dealing with the nonhomogenity of reinforced concrete, Cervenka and Gerstle (1971) presented a Finite Element analysis which considered the cracked state of this material. Their study was concerned with the inelastic analysis of reinforced concrete planar elements which were subjected to in-plane forces. Basically, the method is a Finite Element analysis which treats the uncracked concrete as an isotropic homogeneous material. The cracked concrete is considered anisotropic and capable of resisting only normal stresses parallel to the crack direction, which is taken to be perpendicular to the principal tension in the concrete, just prior to crack formation. The uniaxial stress-strain relationship for concrete is assumed to be elastic-perfectly plastic in compression and elastic and brittle in tension. For the

reinforcement, the stress-strain relationship is assumed to be elastic-perfectly plastic. By superposition of the stress-strain relationships of the individual material components, i.e. concrete and reinforcement, the stress-strain relationships of an infinitesimal element can be obtained.

In a second paper, Cervenka and Gerstle (1972) compared the analytical results from their method with experimental results of their own. They used deep beams as specimens and the aspects investigated were mainly: load-displacement, crack patterns and crack propagation and failure mechanisms. Specimens were tested under static and cyclic loading and in both cases crack patterns and forces compared well with the mathematical and experimental analyses.

The procedure presented by Cervenka and Gerstle is a definite step forward in the analysis of concrete structures in that a closer idealization of the actual behaviour of the material is observed. By taking different material stiffnesses into account, i.e. concrete and reinforcement and superimposing them, a more realistic overall stiffness of the member can be deduced at different load stages. Nevertheless, the problem of analysing reinforced concrete does not only involve the stiffness of the constitutive materials but other actions such as bond between reinforcement and concrete and friction between aggregates at cracked sections. Ideally, all these factors should be modelled by an efficient numerical analysis in order to provide an improved picture of the structure's actual behaviour. This is not an easy task and the only precise method of analysis is the actual test of concrete elements.

2.3 EXPERIMENTAL ANALYSES

Solutions based on the theory of elasticity do not always yield good results, because of problems linked with the idealization of the boundary conditions and in other cases details of the actual structure cannot be included in the analysis, reducing the degree of accuracy of the prediction. Therefore, model tests have an important role as a technique to study structural behaviour and also to verify those numerical methods aiming to predict the stress field of structures. This section presents a general review of experimental research carried out on deep flexural models.

2.3.1 Experimental analyses of homogeneous materials

A brief summary of experimental analyses performed on deep flexural members made from homogeneous materials follows.

Sciammarella and Palacio (1949) reported the photo-elastic test of a perspex deep beam with height/span ratio equal to 1. Later, the same authors (1951) published an additional test on a deep panel with a height/span ratio of 1.5. Both specimens were tested under uniformly distributed load on the top edge. In both tests, the largest tensile stress occurred on the internal edge of the supports and not at mid-span.

Saad and Hendry (1961) produced results from a series of photoelastic tests on simply supported deep beams made of Catalin with depth/span ratios of 0.67, 1.0 and 1.59. A point load at mid-span was applied on the top edge of each beam. They found that the simple-beam theory was adequate for beams in which the span exceeds 1.5 times the depth. The photo-elastic results compared well with those from the Finite Difference method. In another publication, Saad and Hendry (1961b) applied gravitational stresses to deep beams by means of a

centrifuge and measured stresses using the frozen stress method of photo-elasticity. Details of this method are given by Dally and Riley (1978). For this experimental work, the centrifuge produced an acceleration field equivalent to 100 times that of gravity. Beams having depth/span ratios of 0.54, 1.12, 1.49 and 2.23 were tested. The results confirmed that the Finite Difference method provides an accurate analysis of the gravitational stresses in a deep beam. It was found that a beam with depth larger than its span acts as a beam of depth equal to the span with the top part resting on it. The upper section hardly contributes to the resistance of the moment caused by the dead weight. Saad and Hendry stressed the importance of horizontal restraints at the supports of deep panels; they claimed that the arch action arose from the nature of the support conditions. This is not necessarily valid in reinforced concrete deep beams, since the main reinforcement forms a horizontal tie between supports and the arch action is effective under any support conditions.

Kaar (1957) tested a series of aluminium beams with height/span ratios ranging from 1 to 3 and a series of steel beams with height/span ratios from 0.5 to 2.0. The specimens were loaded at mid-span and electrical gauges were used to measure strains. Nonlinearity of stresses in deep beams was illustrated in these tests. It was pointed out for height/span ratios larger than 0.67, the stresses calculated by the ordinary Euler-Bernoully theory were in serious error. The lattice analogy, developed by McHenry (1943) was applied as a check on experimental results.

Archer and Kitchen (1960) reported the test of three steel single-span deep beams, with dimensions 305 x 305 mm, 305 x 203 mm and 305 x 152 mm, corresponding to span/depth ratios of 1.0, 1.5 and 2.0. All the plates were 13 mm thick and were tested under a point load at

mid-span on the top edge. Strains were mesured on the lower edge by means of electrical resistance strain gauges. Stresses were calculated from these strain measurements and compared successfully with mathematical predictions based on elastic theory. As the depth/span ratio increased, the experimental values were found to be markedly different from those given by simple flexure theory.

These tests on simply supported deep beams of homogeneous materials have contributed towards a better understanding of their behaviour. They have been used in the verification of numerical methods based on the theory of elasticity; reasonable agreement has been observed. This is to be expected, since these elements consist of isotropic materials, which obey Hooke's law. The effect of normal forces on the stress distribution has been shown, with larger depth/span ratios being more significantly affected when these forces are applied to the compression face of the beam. In general, the opinion presented in past documents is that the traditional flexure theory is valid for depth/span ratios less than 0.5. Beyond this limit, the stress distribution in vertical sections becomes increasingly non-linear.

2.3.2 Experimental analyses of reinforced concrete deep flexural elements

Although experimental analyses of elastic models provide excellent information on the behaviour of structures made out of isotropic homogeneous materials, for reinforced concrete, the information is limited to the early stages of loading, when the concrete behaves in an elastic manner. Under tensile stresses concrete becomes brittle, developing cracks in the tension zones, altering the stiffness of the member and redistributing stresses. Due to these

characteristics of reinforced concrete, "realistic models", as defined by Rowe and Base (1966), have often been used for the analysis of deep flexural members; some of these tests are summarized forthwith.

Graf et al (1943) tested a deep panel with dimensions and reinforcement details as shown in Fig. 2.2. It had a height/span ratio

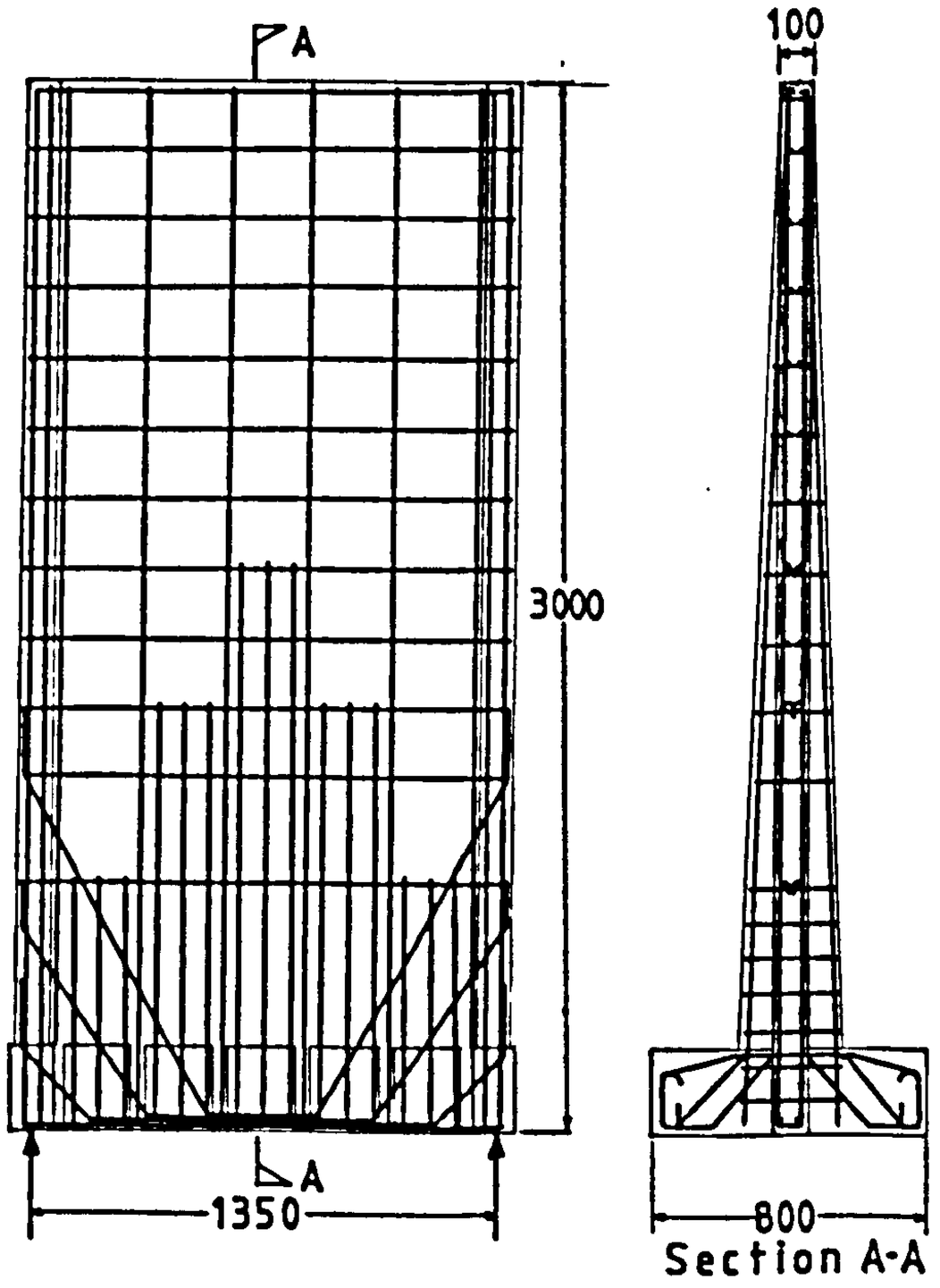

Fig. 2.2 Geometrical and reinforcement details of specimen tested by Graf et al (1943)

of 2.2 and the load was applied through built-in brackets at the bottom of the specimen. Cracks observed first were horizontal ones above the / brackets. Under larger loads, additional cracks appeared at increased distances from the bottom, sloping towards the side strips. Failure occurred due to yielding of the main reinforcement and the deterioration of the section between the wall and the support strip. Cracks in the wall remained very fine even under the maximum load applied.

The side strips were employed in order to avoid an early bearing failure and were successful. Their presence modified the classical arch action developed when direct supports are used, resulting in a hybrid combination of direct and indirect support. Large cracks and deterioration exhibited in the vicinity of the side strips indicates the shear type support provided in this case. Bending of some main bars was not a positive measure, since the tensile force tends to be uniform along the span. Also, the lower section of the wall had no horizontal reinforcement other than the main reinforcement, leaving no provision for the tensile forces between the wall and the side strips. This experiment was the first recorded document dealing with this type

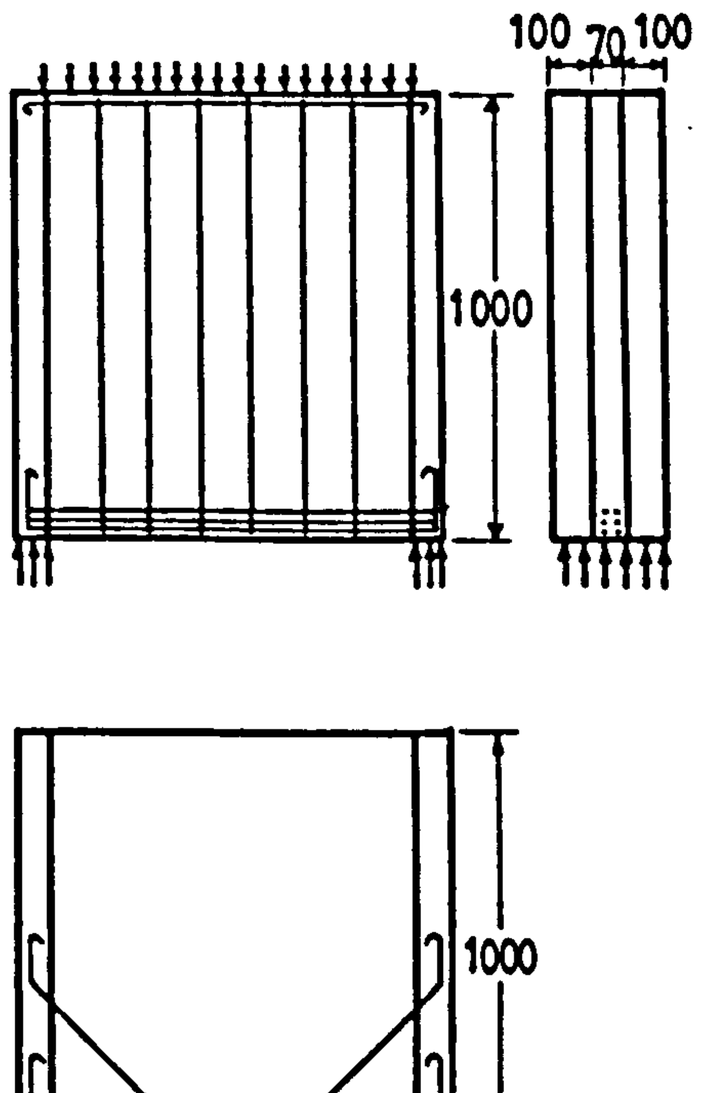

Fig. 2.3 Details of specimens used by Schütt (1956)

of loading in reinforced concrete.

Schütt (1956) tested a series of reinforced concrete walls under uniformly distributed load on the top and bottom edges. Dimensions and reinforcement details of those walls tested under load on the top are shown in Fig. 2.3; those under load on the lower edge were similar to those tested by Graf et al (1943). Side strips were also used by Schütt for both types of loading. The thicknesses of the walls used were 60 and 70 mm. Reinforcement was the main variable examined. Load was applied at the bottom of the specimen by means of brackets fixed to it. Based on these results and other analytical studies, Schütt proposed some design rules which are presented in Section 2.4.3. In these rules the combined action of top and bottom loads is considered. It should be noted that Schütt's results are obtained from walls supported by a combined direct and indirect action. The type of failure for those specimens loaded on top demonstrated the inefficiency of the reinforcement adopted. Some members had vertical stirrups as web reinforcement and others did not have any web reinforcement apart from bent up main bars. This left the section between the side strips and the wall vulnerable to the shear forces generated here.

De Paiva and Siess (1965) described an experimental investigation on the shear strength and behaviour of some moderately deep reinforced concrete beams. The main variables involved in the study were the amount of tension reinforcement, the concrete strength, the amount of web reinforcement and the span/depth ratios. The beams were loaded at third points. Panel thicknesses were 50, 76 and 102 mm and the span/depth ratios were 3.4, 2.7 and 1.8. They concluded that for moderately deep reinforced concrete beams without web reinforcement there was a high load capacity beyond diagonal cracking. Also shown was the fact that the addition of vertical and inclined stirrups had

no effect on the formation of inclined cracks and had little effect on the ultimate strength of beams failing in either flexure or shear. Web reinforcement tended to reduce the deflection at ultimate load. Concrete quality had no effect on the ultimate strength of beams failing in flexure but increased the strength of those specimens failing in shear.

With respect to the inability of vertical reinforcement to improve the strength of deep beams, Leonhardt (1966b) commented that this should be expected since the direction of principal tensile stresses in top loaded deep beams is almost horizontal.

Leonhardt and Walther (1966) reported the tests of simply supported, continuous and indirectly supported walls. The simply supported specimens had a height/span ratio of 1, both dimensions being 1600 mm; the thickness was 100 mm and the bearing length was 160 mm, leaving a span of 1440 mm. A group of 5 specimens were tested under uniformly distributed top loads; dimensions and reinforcement details are shown in Fig. 2.4. In one of these walls (WT4), the bearing area was increased by a transverse strip extending up to a height of 600 mm from the bottom. Dimensions and reinforcement details for those walls loaded at the bottom edge are given in Fig. 2.5. These walls had 18 vertical stirrups each, placed 69 mm apart and diameters as shown in Fig. 2.5. Walls WT5 and WT6 had 0.134 percent of main bending reinforcement, while specimen WT7 had 0.268 percent. These tests disclosed that the best way of providing main reinforcement is by means of well anchored bars from support to support and that horizontal hooks are suitable for anchorage. It was found that the cracking load was increased considerably by using this reinforcement procedure. Also proposed was the distribution of main reinforcement over a height of H/5. The bending up of main reinforcement was discouraged for both top

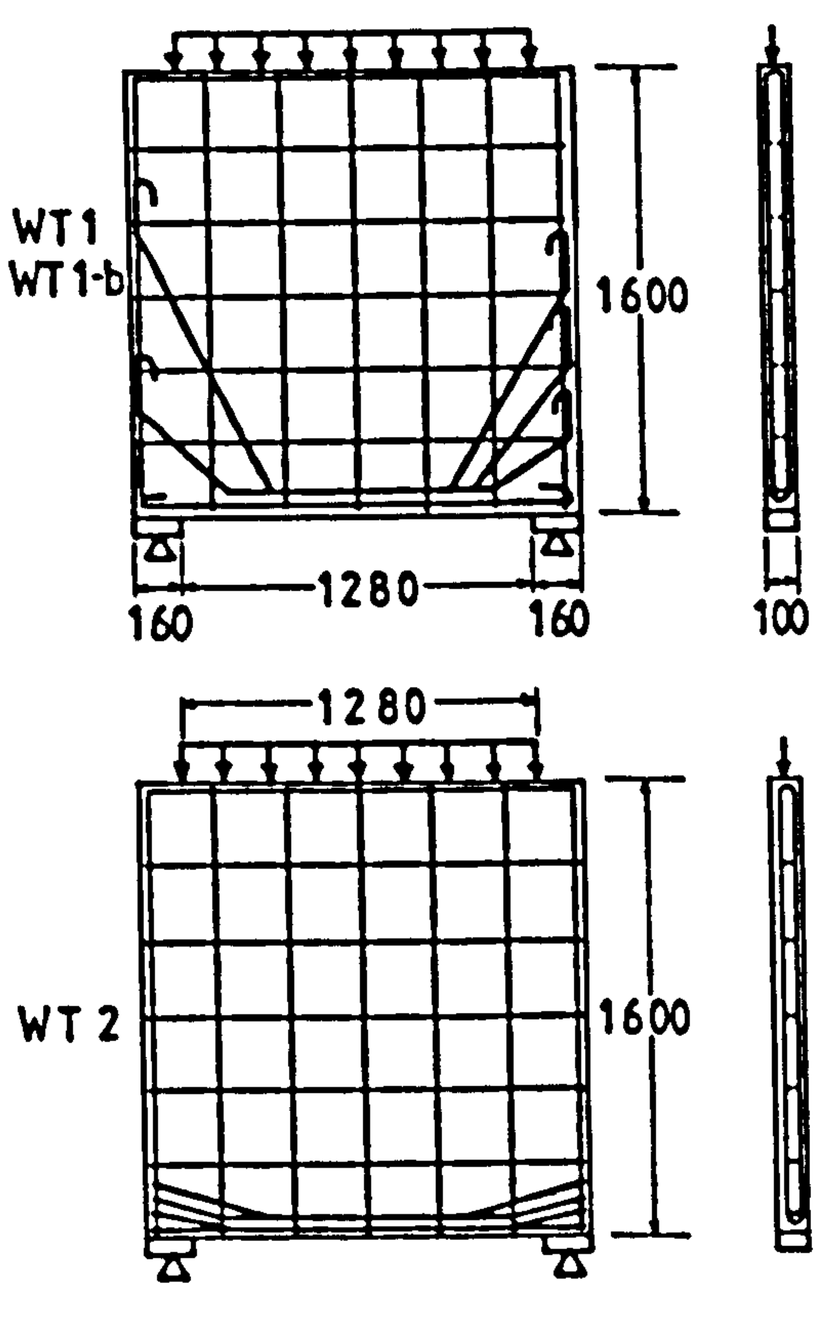

Fig. 2.4 Dimensions and reinforcement details in deep beams with load on top. From Leonhardt and Walther (1966)

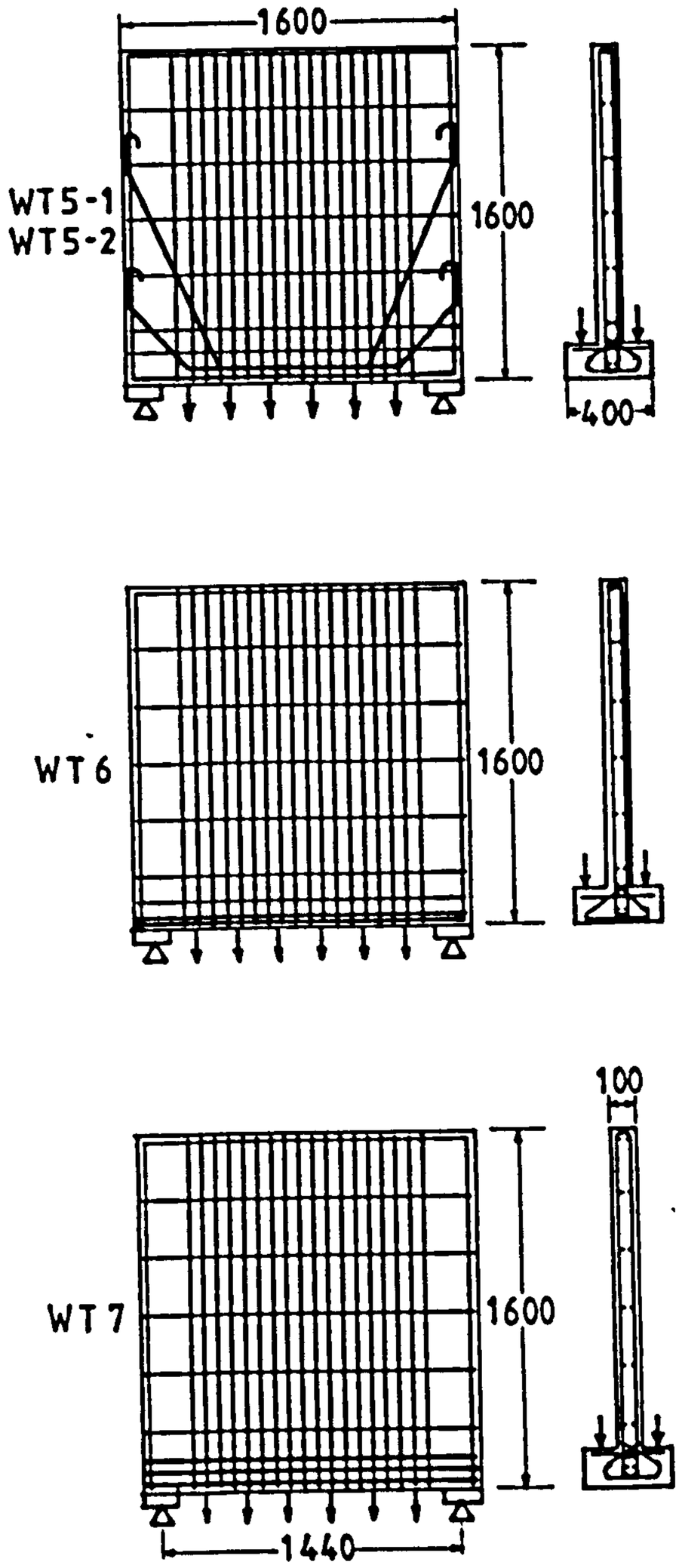

Fig. 2.5 Dimensions and reinforcement details of deep beams with suspended load. From Leonhardt and Walther (1966)

and bottom loads. With suspended loads, cracks occurred up to a height of 0.9L. Therefore, it was suggested that the vertical stirrups should extend to a height equal to the span and that hooks should be provided at the ends as anchorage. Close reinforcement was recommended

in order to reduce the width of cracks with the distance between stirrups limited to 100 mm. It was also observed that the tensile stress in the steel should not be too high, keeping it to a maximum of 200 N/mm^2 and that the vertical stirrups in the zones close to the supports could be taken to a height of 0.8 H but in the central zone of the span, within 0.7L, they should be carried throughout the height of the beam.

Leonhardt and Walther also reported the test of two single span beams which were indirectly supported over transverse panels and indirectly loaded by a transversal panel at the centre. The two beams had the same dimensions which are shown in Fig. 2.6 and consisted of a main deep beam with a span of 2400 mm. All the panels were 100 mm thick and 1600 mm in height. The specimens differed only in the arrangement of the reinforcement. Specimen IWT-1 had 50 percent of the main reinforcement bent up at an angle of 60°. Additional bent bars were positioned on top for the indirect introduction of the load. Specimen IWT-2 had the main steel straight from support to support distributed over a height of H/5 and vertical stirrups were provided

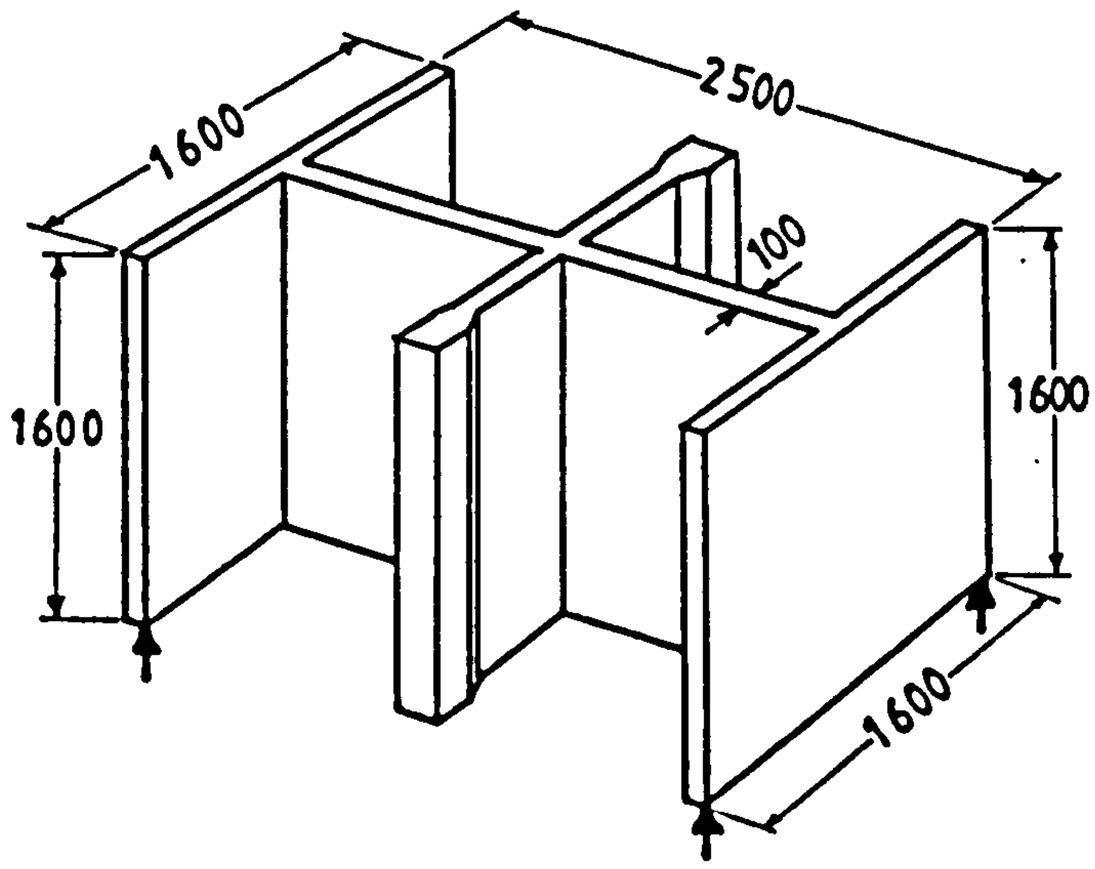

Fig. 2.6 External details of the indirectly loaded and indirectly supported specimens. Leonhardt and Walther (1966)

for the indirect introduction of the load. End walls were reinforced in a similar way to the main panels. Each specimen was supported at four points at the extremes of the end-walls and loaded at two points at the ends of the central, transverse wall. The arrangement of the panels and the way in which the load was applied allowed the analysis of both the behaviour of walls under indirect loading and indirect supports. Failure of both beams when tested occurred due to excessive compressive stresses in the inclined compressive struts. The deflection, it was reported, was hardly influenced by the arrangement of the reinforcement. Crack widths were considerably narrower in specimen IWT-1 than in specimen IWT-2 for the main panel and the bearing panels, but the opposite was observed in the loading transverse beam. Forces in the main bending reinforcement are reported to have higher values than in beams loaded on top. It was suggested that the main reinforcement should be continuous over the supports and distributed over a height of 0.1 to 0.15 H. Although the specimen IWT-1 with inclined reinforcement performed slightly better than the orthogonal reinforcement with regard to crack control, both specimens showed approximately the same safety factor. Leonhardt and Walther concluded that the simpler orthogonal reinforcement of IWT-2 was cheaper, due to the saving in labour by avoiding the complicated inclined reinforcement of IWT-1.

Kong et al (1970) presented on experimental study on the effectiveness of different web reinforcement in 35 normal weight concrete deep beams. The types of web reinforcement tested are shown in Fig. 2.7. Each of the specimens were rectangular deep elements, 915 mm overall length, 762 mm span, 76 mm width and with span/depth ratios ranging from 1 to 3. The beams were tested under two-point loading. It was found that the effectiveness of the various types of

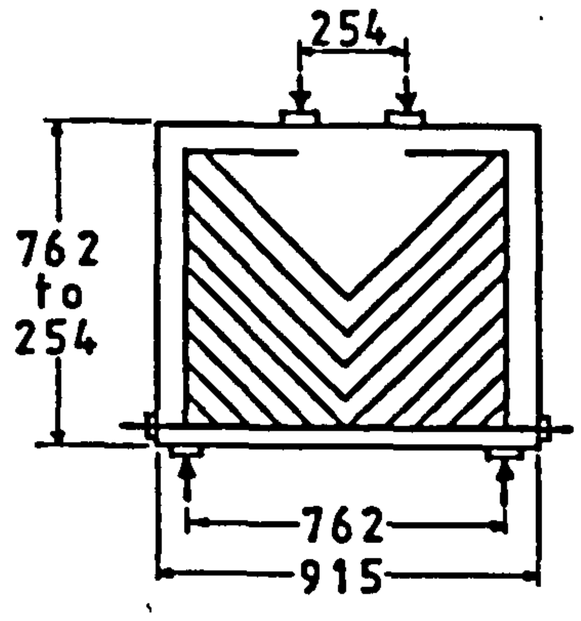

Fig. 2.8 Details of web reinforcement of specimens tested by Kong et al (1972)

strength, control of deflection and control of cracking, this was an effective type of web reinforcement. These results agree with those from Leonhardt and Walther (1966) in that inclined bars give the best control of cracks and deflections but they pointed out the economical impracticality of using this type of web reinforcement.

Kong and Robins (1971) carried out tests on simply supported lightweight concrete deep beams with dimensions and web reinforcement similar to those explained in the two previous reports and in the same manner. Deformed bars were used for the reinforcement. Inclined bars were found to be the most effective for controlling cracks and deflections and also provided greater strength. It was also observed that the strength formulas for normal weight concrete deep beams were not necessarily suitable for lightweight concrete beams.

Further experimental work on lightweight concrete deep beams was reported by Kong and Singh (1972). Here the results from 45 specimens using sintered fly ash lightweight aggregate are published. Different types and amounts of web reinforcement were used. Experimental cracking and ultimate loads were compared to those calculated from various formulas. De Paiva and Siess's formula (Eq. 2.23) was found to

be adequate for estimating ultimate shear loads, although not as accurate for calculating ultimate shear of normal weight beams. Tests showed that the ratio x_e/H had a greater effect on cracking and ultimate loads than L/H. For all the x_e/H ratios studied (0.23 to 0.70), inclined web reinforcement was the most effective.

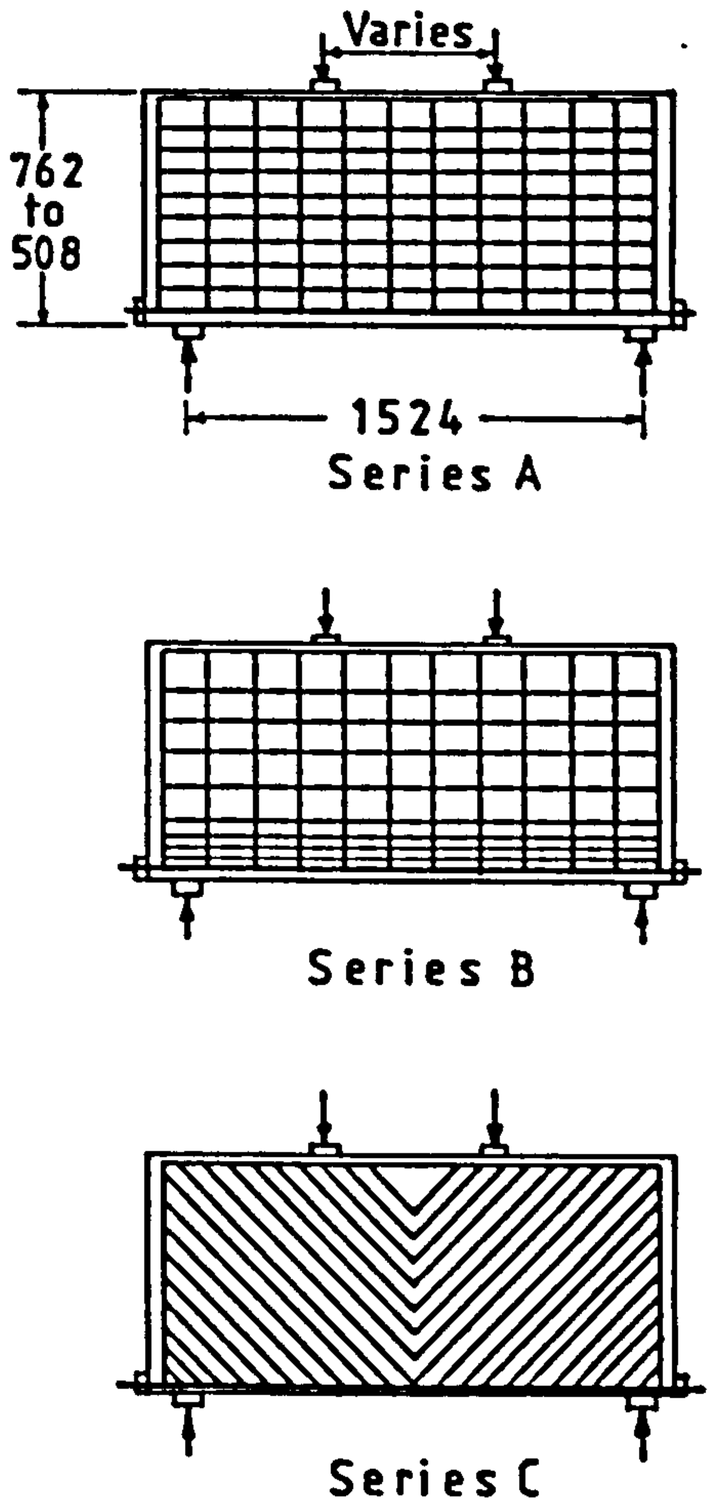

Fig. 2.9 General arrangement and details of web reinforcement (Kong and Singh, 1974)

Kong and Singh (1974) tested the effectiveness of the three web reinforcements shown in Fig. 2.9, under repeated loads. The specimens were cast with lightweight concrete, using sintered-fly-ash aggregate. Inclined web reinforcement was found to be the superior type and that Eq 2.23, for static shear by de Paiva and Siess, produced the most accurate prediction for those deep beams with a repeated-load history.

Smith and Vantsiotis (1982) reported results from tests on 52 deep reinforced concrete beams under two symmetrical point loads. The specimens were rectangular beams with 356 mm depth, 102 mm thickness and varying lengths from 1420 to 2080 mm. The span varied from 813 to 1470 mm. Ratios of shear span to effective depth (x_s/d) of 0.77, 1.01, 1.34 and 2.01 were used. Five beams did not have web reinforcement and the remaining specimens had variable vertical and horizontal web reinforcement. Vertical reinforcement varied from 0.23 percent to 0.91 percent, while horizontal web reinforcement varied from 0.18 percent to 1.25 percent. All 52 beams tested failed in shear. A definite decrease in inclined cracking and ultimate loads with increasing x_s/d ratio was reported. The increase in ultimate shear strength and in diagonal cracking load was attributed to the arch action for specimens with a shear span/depth ratio less than 2.5. It was found that vertical stirrups became more effective with greater shear span/depth ratios. Horizontal web reinforcement was more efficient in beams with shear span/depth ratio less than 1.0. Concrete quality exerted a greater influence on beams with low shear span/depth ratios. Web reinforcement was unsuccessful at controlling the diagonal cracking load and the cracking patterns were the same for beams with or without it; however, when present less damage was observed at failure.

From the research on deep beams summarised above, the following main points have been extracted:

a) These beams show high load capacity beyond diagonal cracking.

b) Vertical reinforcement has no effect on the formation of inclined cracks nor on the ultimate strength.

c) Concrete quality had no effect on the ultimate strength of beams failing in flexure but increased the strength of those specimens failing in shear.

d) Inclined cracking and ultimate loads increase as the shear span/depth ratio (x_s/H) decreases below 2.5.

e) The shear span/depth ratio (x_s/H) had a greater effect on cracking and ultimate load than span/depth ratio (L/H).

f) The effectiveness of the various types of web reinforcement depends on the shear span/depth ratio. For low x_s/H ratios, horizontal reinforcement is appropriate and for large x_s/H, vertical reinforcement is advantageous.

g) For strength, control of deflection and control of cracking, inclined bars were the most effective web reinforcement but they are economically impractical, leading to the recommendation of an orthogonal bar arrangement for web reinforcement.

2.3.3 Experimental analyses of reinforced concrete deep beams with openings

In modern construction, large openings in structural elements are often required in order to allow the installation of ducts and services. In other cases, openings are needed to serve as doors and windows. Some research has been performed, covering slender beams, of which the analysis of Nasser et al (1967) is an example. Fintel et al (1968) presented an extensive study on "staggered wall beams", as a structural system for multistorey buildings; here the problem of large openings for doors had to be considered. To prove the recommendations given by Fintel et al, Carpenter and Hanson (1969) tested two concrete beams with openings in their webs. It must be noted that, although these walls have large, vertical dimensions, they do not necessarily fall into the category of deep beams.

In order to answer questions arising from the need to have openings in deep flexural members, Kong and Sharp (1973) tested 24

simply supported lightweight deep beams with dimensions as shown in Fig. 2.10. Two clear shear spans were used, giving x_e/H ratios of 0.4 and 0.25. The span/depth ratio was kept constant at a value of 2.0. The test beams were divided into two groups: one had no web reinforcement and the second had a rectangular mesh. Rectangular web

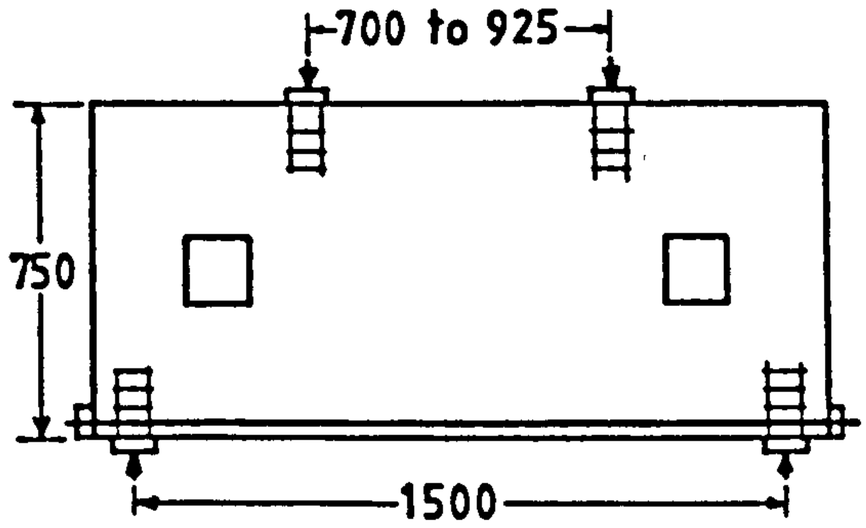

Fig. 2.10 Dimensions of specimens tested by Kong and Sharp (1973)

openings were placed at different positions within the beam. The effect of the openings on the ultimate shear strength depended on their position and was largely detrimental to the beam strength when coinciding with the line joining the support with the loading point. Web reinforcement did not have any significant effect on the crack pattern and mode of failure.

Additional experimental work on lightweight deep beams with web openings was reported by Kong and Sharp (1977). Specimens had L/H ratios of 1.5 and 1 and x_e/H ratios of 0.3 and 0.2. A group of beams had no web reinforcement and the rest were reinforced in seven different forms, as shown in Fig. 2.11. Inclined web reinforcement (W6 in Fig. 2.11) was found to be the most efficient. Some design recommendations were propounded, based on the experimental results of this work.

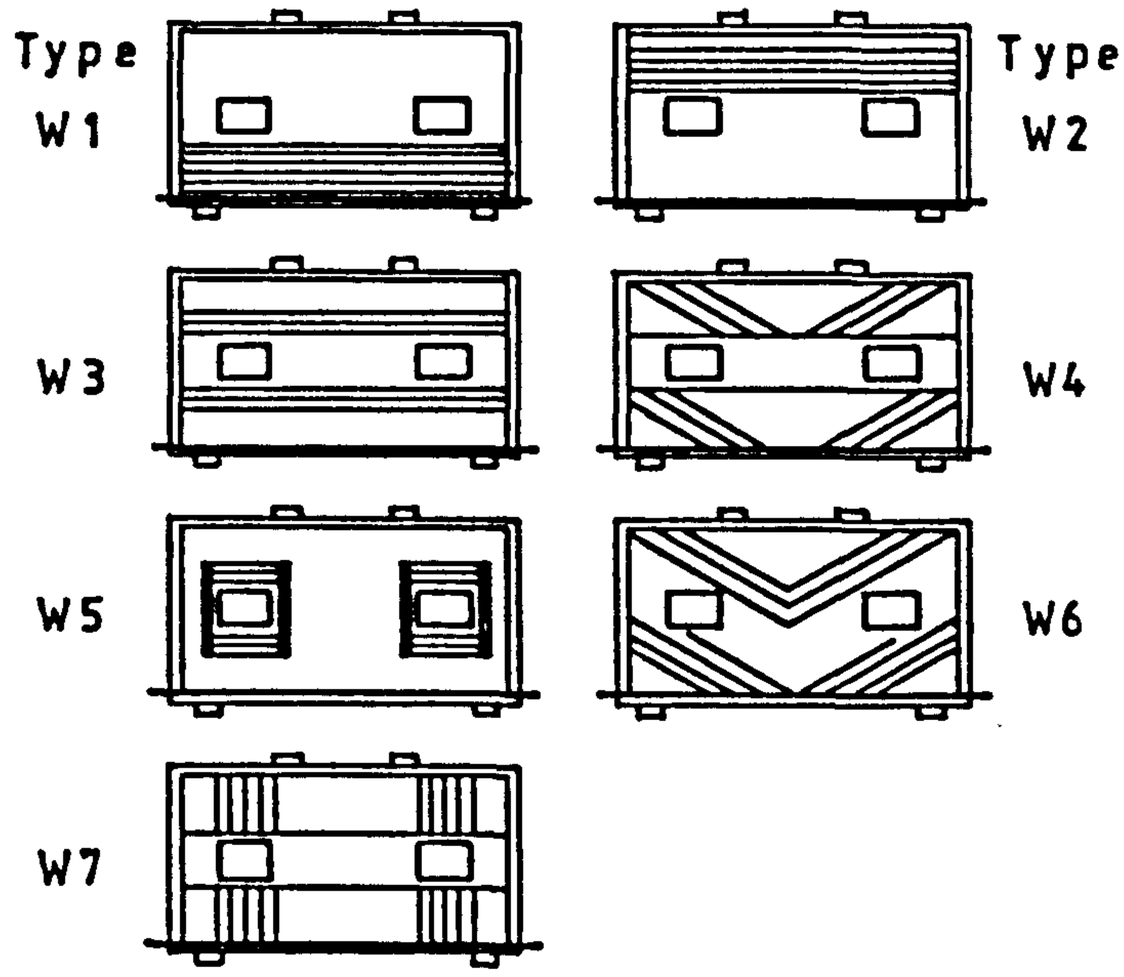

Fig. 2.11 Web reinforcement details. Kong and Sharp (1977)

The same experimental analysis was repeated on normal weight concrete beams and reported by Kong et al (1978). Here, 16 beams of sizes comparable to those discussed above and one large beam were tested. The full size beam had a span of 3500 mm, depth of 1800 mm and thickness of 250 mm with web reinforcement consisting of vertical and horizontal stirrups. The findings of this experimental work were consistent with those previously discussed.

The above documents imply that openings affect the ultimate shear strength and that where coincident with the line joining support and loading point are especially harmful to beam strength. Inclined web reinforcement above and below the openings was the most successful; members made with normal and lightweight aggregate demonstrated the same results.

2.4 RECOMMENDATIONS FOR DESIGNING REINFORCED CONCRETE DEEP FLEXURAL MEMBERS

A brief summary of the outstanding documents providing guidance for the design of reinforced concrete deep flexural members follows.

2.4.1 Portland Cement Association (1946)

This report proposed a design procedure applicable to reinforced concrete beams with height-to-span ratios (H/L) larger than 2/5 or 4/5 for continuous and single-span girders respectively.

Two ratios are essential for the use of this procedure: the height-to-span ratio, H/L, denoted as B and the support-to-span ratio, w/L, denoted as E'. These two ratios are ued as parameters in all calculations and charts which are based on Dischinger's (1932) tabulated values. Stresses are presented in figues for sections at mid-span and for sections at intermediate supports. The analysis was carried out for values of height-to-span ratios equal to 1/2, 2/3 and 1. The support-to-span ratio, w/L, investigated had the following values: 1/20, 1/10, 1/5 and 1/2.

Those loading cases considered were:

1) continuous beam with a) uniform load at bottom, b) concentrated load at bottom and at centre of all spans, and c) concentrated load at top and at centre of spans.

2) single-span beam with a) uniform load at bottom and b) concentrated load at centre of span.

The design method is as follows: since the characteristic ratios B and E'are known, the stress coefficients can be selected from figures given and then the stresses calculated. From another figure, a coefficient is obtained to calculate the resultant of all concrete tensile stresses, T. After this, the area of reinforcement (A_{sl}) can

be deduced from the expression:

$$A_{sl} = T/f_s \qquad 2.3$$

where f_s is the working stress of the steel. It was advised that the main tensile reinforcement should be placed as close as possible to the lower edge of the beam.

Suggestions were given for verification of shear strength. Due to the limited data available, it was tentatively recommended that the unit shear, v, be computed as

$$v = 8V/7bd \qquad 2.4$$

Also, it was suggested that the permissible shearing stress of the concrete could be considered as v_c (1 + 5 H/L)/3 where v_c is the permissible shearing stress for shallow beams.

Chow et al (1953) considered that the area of tensile steel as calculated by Eq. 2.3 should be increased and proposed the following alteration:

$$A_{sl} = 1.5T/f_s \qquad 2.5$$

They also advised that the area of steel should be distributed within the whole of the tension zone, by spreading half of the area of steel ($A_{sl}/2$) uniformly throughout the tension zone and the other half should have a progressively linear distribution with increasing distance from the neutral axis.

The method proposed by the Portland Cement Association for shear design of deep beams was considered sensible by Chow et al. In it, the additional shear strength of deep beams above slender ones was widely acknowledged.

2.4.2 Uhlman (1952)

Based on data obtained from Dishinger's elastic analysis and his own application of Finite Difference method, Uhlman provided some

recommendations for the design of reinforcement in deep beams. This method establishes the minimum thickness of an element simply supported and loaded in its own plane as

$$b = 0.06\ L/\sqrt{K} \qquad 2.6$$

where L = span of panel

K = a function of H/L given in tabular form in Uhlman's report

H = height of panel

The area of the main reinforcement is calculated from

$$A_{s1} = M/f_s z \qquad 2.7$$

where M = bending moment at mid-span

f_s = permissible steel stress

z = lever arm

The lever arm value varies for different loading conditions and could be obtained from graphs as a function of the overall length and the height.

In the case of deep beams with loading along the lower edge, the required area of hanging steel is provided by

$$A_{hs} = W/f_s \qquad 2.8$$

where W = applied load between the supports.

For uniformly distributed loading, it recommends that the bars should be vertical and uniformly spaced. For concentrated loads, the vertical steel should be concentrated in the region of the applied load. Additional inclined reinforcement is also provided for both distributed and concentrated loads on the lower edge. This is given as a percentage of the hanging steel area and is calculated as a function of H/L from a graph.

In the case of a combination of loading, superposition of the reinforcement calculated for each case is advised.

Design recommendations were also produced for continuous deep

beams and special provisions were given for the differential settlement of supports. It was stated that for the case of deep beams loaded on the top, no web reinforcement was necessary. Although Uhlman's recommendations were based mainly on evidence from elastic analysis, they demonstrated overall very sound engineering concepts.

2.4.3 Schütt (1956)

In this report, the following procedure was recommended for the safe design of deep flexural elements under top and lower edges loading. The calculation of the area of bending reinforcement was based on the equation

$$A_s = M/f_s z = qL^2/8f_s z \qquad 2.9$$

where f_s = working stress of steel, kg/cm^2

z = internal lever arm, cm

L = effective span (centre to centre of supports), cm

q = load per unit length, kg/cm

For deep beams with height/span ratios less than 1, the lever arm value used is calculated as for normal slender beams. In the case of walls with height/span ratios between 1 and 2 the following lever arm value was proposed

$$z = 0.9L\sqrt{H/L} \qquad 2.10$$

where H = total height of wall, cm

giving an area of main reinforcement required equal to

$$A_{sl} = 0.14\ qL/f_s\sqrt{H/L} \qquad 2.11$$

and in walls with height/span ratios larger than 2, the main reinforcement area is obtained from

$$A_{sl} = 0.1\ qL/f_s \qquad 2.12$$

For equations 2.10, 2.11 and 2.12 it was assumed that the main reinforcement was distributed over a height equal to 0.1 L.

Considering that 1/2 to 2/3 of the main flexural reinforcement is bent (as shown in Fig.2.3), the ultimate shear capacity of the section can be predicted from

$$V_u = 0.54\ f_{cb}\ b^2\sqrt{H/b} \qquad 2.13$$

where f_{cb} = strength of concrete (prism strength), kg/cm^2

b = width of wall, cm.

A safe limit for the shear capacity of the wall was considered as 1/3 of the figure predicted by Eq. 2.13, given by

$$V_{gr} = 0.18\ f_{cb}\ b^2\sqrt{H/b} \qquad 2.14$$

This allowed a maximum safe load on the top edge as predicted by the following expression

$$w^o_{gr} = (0.36\ f_{cb}\ b^2/L)\sqrt{H/b} \qquad 2.15$$

A limit to the load hanging capacity is provided by

$$w^u_{gr} = (0.30\ f_{cb}\ b^2/L)\sqrt{L/b} \qquad 2.16$$

Note that the load capacity is given as a function of the span, the thickness of the wall and the strength of the concrete.

Where a wall is loaded simultaneously from the top and bottom, the total load accepted is given by

$$w_{gr} = w^o_{gr}\ w^o/(w^o+w^u) + w^u_{gr}\ w^u/(w^o+w^u) \qquad 2.17$$

where w^o = load per unit length applied on top

w^u = load per unit length applied on the soffit.

Selfweight was considered as part of the load applied on the top. It should be noted that the procedure required vertical reinforcement for both top and bottom loads. This reinforcement was controlled by the depth/span (H/L) ratio in the following form: for H/L ratios less than 1.0, the amount of vertical reinforcement was provided by

$$A_{sv} = V/f_s\ \sqrt{2} \qquad 2.18$$

For H/L ratios larger than 1.0 the area of this reinforcement is given by

$$A_{sv} = V/f_s\sqrt{2H/L} \qquad 2.19$$

and when H/L is larger than 2.0, the vertical reinforcement becomes

$$A_{sv} = V/2f_s \qquad 2.20$$

In the case of specimens under bottom load, the vertical reinforcement could be increased by the factor $\sqrt{w^u \times w^u_{gr}}$.

Equations 2.18 to 2.20 show the author's faint recognition of the reduction in efficiency of vertical bars as the depth/span ratio increases. At the time when these proposals were published, information related to the contribution of vertical reinforcement to the strength of deep beams was scarce, hence the overestimation of their importance.

2.4.4 De Paiva and Siess (1965)

Results from experimental work on deep beams were reported by de Paiva and Siess (1965). They described three modes of failure, called "flexure", "flexure-shear" and "shear-proper". Previously, Laupa et al (1955) used the term "shear-proper" to describe the failure of slender beams loaded close to the support, and developed an expression for their strength, which is as follows:

$$v = V/bH = 200 + 0.188\ f'_c + 21300\ p_t \qquad 2.21$$

where V = shear force

f'_c = cylinder compressive strength of concrete, psi

v = nominal shear stress

H = depth of beam

b = width of beam

and $p_t = A_{sl}(1 + \sin\alpha)/bH$

in which A_{sl} = area of steel crossing a vertical section between the load point and support.

α = angle of inclination of reinforcement to the axis of the beam.

In those beams tested by de Paiva and Siess, the nominal shearing stress was expressed in terms of a load P'_s as

$$P'_s = 2\ vbH \qquad 2.22$$

in which P'_s = load at failure in shear proper, lb.

By comparing data calculated from Eq 2.22 with experimental results, the next expression was obtained for the computed shear strength P''_s

$$P''_s = 0.80\ (1 - 0.6\ x_e/H)\ P'_s \qquad 2.23$$

where x_e/H = clear shear span/depth ratio.

This expression represents a lower bound to the test values and is valid for values of x_e/H between 0 and 1.

De Paiva and Siess concluded that the presence of vertical or inclined reinforcement did not affect the load at which diagonal cracks appear and had hardly any influence on the ultimate strength. For beams with or without web reinforcement there was a high load capacity beyond the cracking load.

2.4.5 Ramakrishnan and Ananthanarayana

Based on experimental results, Ramakrishnan and Ananthanarayana (1968) came to the conclusion that shear failure in a deep beam is essentially a diagonal tension failure and that the ultimate shear strength of the beam could be taken as the load producing a diagonal tension failure. Therefore, they developed equations to predict the ultimate shear strength of reinforced concrete deep beams on the basis of the splitting strength of concrete.

It has been established that in an indirect tension test the splitting strength of the concrete f_t can be expressed as:

f_t = Maximum splitting force/K(area resisting the splitting force) 2.24

where K is a coefficient equal to 1.57 for a cylinder.

For a deep beam under two-point load on the top (Fig. 2.12(a)), the splitting component of the load P is

$$P = W \text{ cosec } \theta \qquad 2.25$$

This expression in equation 2.24 gives

$$W = Kf_t bH \qquad 2.26$$

and the ultimate load P_c on the beam becomes

$$P_c = 2W = 2Kf_t bH \qquad 2.27$$

The failure plane is fixed by $\tan \theta = H/x_s$.

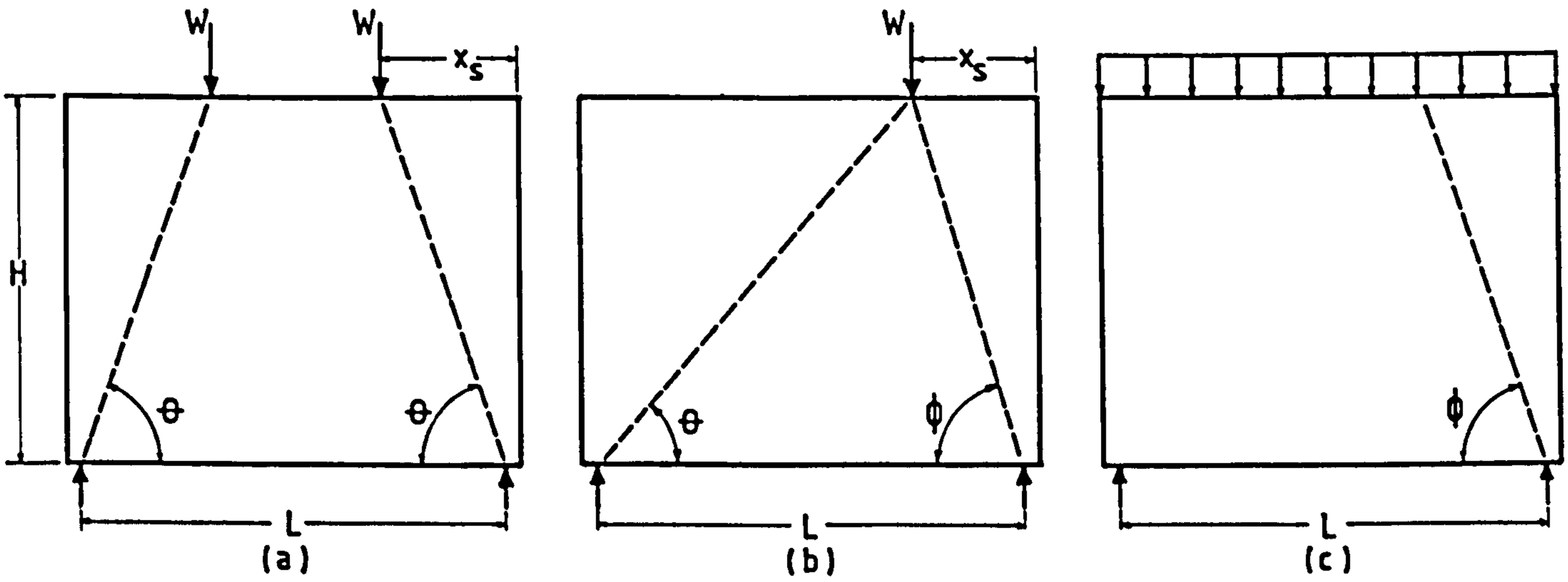

Fig. 2.12 Effect of load on deep beams; a) two-point load, b) eccentric load, c) uniformly distributed load

The same procedure was used to find the ultimate load for a concentrated force (Fig. 2.12(b)). The ultimate load of the beam is given by

$$P_c = K\,(1 + \tan \theta \cot \phi')\, f_t bH \qquad 2.28$$

where $\phi \geq \theta$. The failure plane for this case is determined by:

$$\tan \phi = H/x_s \qquad 2.29$$

For a central concentrated load $\theta = \phi$ and $x_s = L/2$ producing the following expression for the ultimate load:

$$P_c = 2K f_t bH \qquad 2.30$$

and the failure plane is

$$\tan \phi = 2H/L \qquad 2.31$$

In the uniformly distributed load case (Fig. 2.12(c)) it was found that the splitting force P reached a maximum when the diagonal crack plane was fixed by

$$\tan \phi = 3H/L \qquad 2.32$$

The ultimate load P_c on the beam is given by

$$P_c = qL = 2K f_t bH \qquad 2.33$$

In the derivation of the above expressions, the effect of the web reinforcement has been neglected. It was shown that the value of K generally lies between 1.0 and 1.75 and that a value of 1.12 is a reasonable lower bound for beams that fail exclusively in diagonal tension.

The specimens tested by these authors were reinforced longitudinally and had little or no web reinforcement; thus these equations may prove to be an acceptable tool to estimate cracking load but its prediction of ultimate strength might be questionable for members reinforced with the normally accepted orthogonal arrangement of bars. Varghese and Krishnamoorthy (1966) reported "shear or sliding cracks" in reinforced concrete panels tested under three different top loads. This conflicts with the diagonal tension failure discussed above.

2.4.6 Comité Européen du Béton - FIP

The Comité Européen du Béton (1970) have defined a deep beam as a

straight beam, generally of constant cross-section with a span-to-depth ratio (L/H) less than 2 for simple beams and 2.5 for continuous beams.

For the purpose of their design, the bending moments due to permanent loads and imposed loads are calculated as for normal slender beams. The same applies for shear forces.

a) Design for flexure

To counteract the ultimate bending moment M_u, the area of principle reinforcement in tension is calculated as the reinforcement required for a normal beam in which the lever arm z is taken as

$$z = 0.2\ (L + 2H) \quad \text{for } 1 \leq L/H < 2 \qquad \text{(a)}$$

or $$z = 0.6\ L \quad \text{for } L/H < 1 \qquad \text{(b)} \qquad 2.34$$

where H = total depth of deep beam

L = span of beam

When L/H exceeds 2, the relationship gives the same lever arm as for normal beams. In these expressions the maximum value of H is limited to L.

The principal tensile reinforcement must be extended throughout the span and uniformly distributed over a depth equal to (0.25H - 0.05L), measured from the soffit of the beam.

In the instance of continuous beams with M_t and M_s being the extreme positive and negative moments, the area of principal reinforcement is calculated as explained earlier but the lever arm z must be deduced from

$$z = 0.2\ (L + 1.5\ H) \quad \text{for } 1 \leq L/H < 2.5 \qquad \text{(a)}$$

or $$z = 0.5\ L \quad \text{for } L/H < 1 \qquad \text{(b)} \qquad 2.35$$

The importance of supplying small diameter bars is stressed, in order to limit the width and development of cracks. Provision of adequate anchorages to the main reinforcement at the supports is also crucial. Anchorage achieved by vertical hooks must be avoided because

of its tendency to promote cracking in the anchorage zone.

This document reports that in deep beams the compressive stresses due to bending are rarely critical and it is usually unnecessary to verify the compression zone. Further to this, it recommends that the lateral buckling in this zone should be examined; however, a method is not offered.

b) Shear design recommendations

The procedure for calculating the shear force in a deep beam follows the same recommendations given for a normal beam and the maximum shear force imposed on the section is given by

$$V_{max} = 0.1bH\ f_c \qquad 2.36$$

where f_c = design strength of concrete, N/cm^2

In this expression, the maximum value for H corresponds to the length of the span, L.

c) Web reinforcement

For beams with load applied on the upper portion, the document proposes the use of orthogonal reinforcement in the web, consisting of vertical stirrups and horizontal bars on both faces of the element.

The area of reinforcement should be not less than $0.0025\ bs_1$ for a smooth round bar or $0.002\ bs_1$ for a high-bond bar, where b is the thickness of the beam and s_1 the distance between bars.

When the load is applied to the lower portion of the beam, the vertical stirrups should be designed to transmit the total load to the upper portion of the beam. The maximum spacing of bars allowed is 150 mm.

In addition to these provisions, recommendations are given for reinforcing deep beams with indirect supports and indirect loading. Dimensioning of support zones is also considered. Most of the C.E.B. recommendations appear to be based on the findings and conclusions from

Leonhardt and Walther (1966).

2.4.7 Kong

Kong and Robins (1972) propounded an experimental formula for calculating the ultimate shear strength of deep beams for both normal weight and lightweight concrete. This formula allows for the effect of web reinforcement and stands as follows:

$$V_u = C_1 f_c bH + C_2 \sum^{n} A\,(Y/H)\,\sin^2\alpha \qquad 2.37$$

where V_u = ultimate shear strength of the beam

C_1 = coefficient equal to 0.14 for normal weight concrete and 0.096 for lightweight concrete

C_2 = coefficient equal to 83 N/mm^2 for normal weight concrete and 247 N/mm^2 for lightweight concrete

f_c = cube strength or 10 times the cylinder splitting, whichever is less, N/mm^2

b = thickness of beam, mm

H = overall depth of beam, mm

A = area of an individual web bar, mm^2

Y = depth of bar, measured from top of beam to the point where it intersects the line joining the adjacent sides of the load bearing block and the support block.

α = angle between bar and the line described above

n = number of web bars, including the main reinforcement that crosses the line between support and loading block.

The authors reported that the computed ultimate loads predicted by Eq. 2.37 compared fairly well with experimental results.

Later, Kong et al (1972) presented a modified version of Eq. 2.37 in which the x_e/H ratio was explicitly included and the cylinder splitting strength of concrete is used instead of the cube strength.

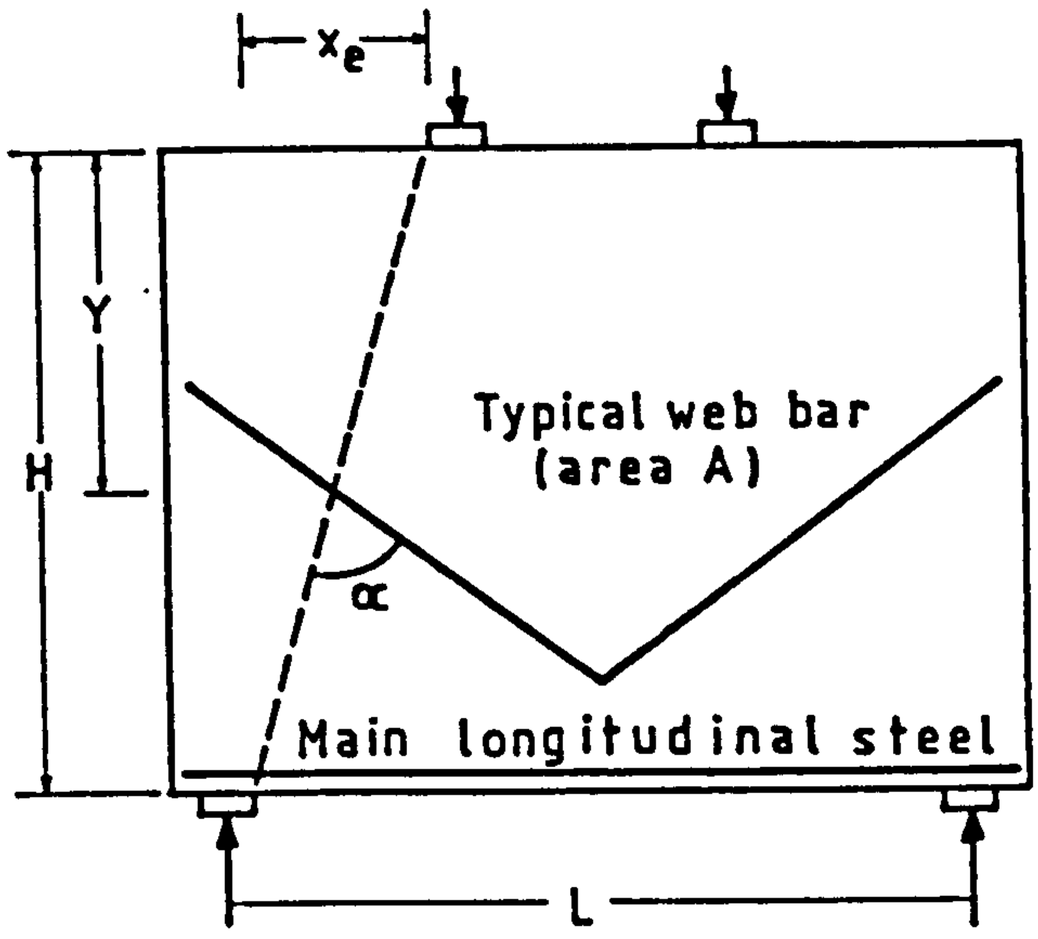

Fig. 2.13 Meaning of symbols for Eq. 2.38 (Kong et al, 1972)

The revised formula became

$$V_u = C_1 \, [1-0.35 \, x_e/H] \, f_t b H + C_2 \Sigma \, A \, Y/H \, \sin^2\alpha \qquad 2.38$$

where C_1 = coefficient equal to 1.4 for normal weight and 1.0 for lightweight concrete.

C_2 = coefficient equal to 130 N/mm^2 for plain round bars and 300 N/mm^2 for deformed bars

f_t = cylinder splitting strength, N/mm^2

The significance of the other factors remains as explained previously.

2.4.8 A.C.I. Standard 318-77

This document specifies that flexural members with overall depth to clear span ratios greater than 2/5 and 4/5 for continuous and simple spans respectively, shall be designed as deep flexural members. It does not contain a detailed procedure for designing deep members for flexure, but expresses that nonlinearity of strain distribution and lateral buckling must be considered.

a) Flexural reinforcement

The recommendations of the Code for flexural tension reinforcement are limited to the rules given for general flexural members. It is stated that where positive reinforcement is required, the ratio p of reinforcement provided shall not be less than

$$p = 200/f_y \qquad 2.39$$

where $p = A_{s1}/bd$

b) Shear design recommendations

The Code presents a series of rules applicable to members with clear span to effective depth ratio (l_o/d) less than 5 and loaded at the top or compression face when designed for shear. For members subjected to shear and flexure only, the nominal shear strength, V_n, is computed from the nominal shear strength provided by concrete, V_c, and the nominal shear strength provided by shear reinforcement, V_s, so that

$$V_n = V_c + V_s \qquad 2.40$$

In general, the horizontal reinforcement shall not be less than 0.0025 times the gross area of web. The area of vertical shear reinforcement, A_{sv}, shall not be less than $0.0015\ bs_1$, and s_1, the spacing of bars, shall not exceed d/5, nor 450 mm.

The last proposals are intended for members loaded at the top. If the loads are applied through the bottom of a member, design for shear should be the same as for ordinary members.

Full details of the recommendations for design for shear are given in Section 7.3.1 where special attention is paid to this aspect.

2.4.9 CIRIA Guide 2 (1977)

This extensive study presents the most comprehensive set of rules and recommendations available until now for designing deep flexural

concrete members. These recommendations are directed at beams with span/depth ratios less than 2 for single span or less than 2.5 for multi-span members. A short summary of these propositions follows:

a) Design for flexure

The area of reinforcement needed to resist positive or negative moments due to ultimate load is calculated from

$$A_s > M_u/0.87\ f_y\ z \qquad 2.41$$

where f_y = characteristic strength of reinforcement,

M_u = design moment at ultimate limit state,

and z = lever arm at which the reinforcement acts, given by the following equations:

$$z = 0.2\ L + 0.4\ h_a \qquad 2.42$$

for single span beams and

$$z = 0.2\ L + 0.3\ h_a \qquad 2.43$$

for multi-span beams at mid-span and support sections,

where L = effective span

and h_a = effective height.

Curtailment of the positive reinforcement within the span is not advised but the distribution of it over a depth of $0.2h_a$ is.

b) Shear design recommendations

Design for shear is controlled by the web reinforcement requirements, considering the position of forces either at the top or bottom of the beam. A full analysis of the method is presented in Section 7.3.2 where this aspect is examined in detail.

c) Web reinforcement

This guide advocates that the web reinforcement should consist of vertical and horizontal bars, placed at each face of the beam. This reinforcement should satisfy the recommendations of CP110 (1972) for minimum reinforcement in walls (Clause 3.11) and for temperature and

shrinkage effects (Clause 5.5.9.2). In a wall, when the vertical reinforcement is used to resist compression, the horizontal reinforcement should be at least 0.25 percent or 0.30 percent if high yield or mild steel is used respectively. For shrinkage and temperature effects, the same amount of steel is advised. Clause 3.11.4.1 says that unless 0.4 percent of vertical reinforcement is provided, a wall cannot be considered as a reinforced concrete wall. On the other hand, for fire resistance purposes, a reinforced concrete wall should not contain less than 1.0 percent of vertical reinforcement.

An additional proposition is given in this guide for the web reinforcement. It is stated that in areas of a deep beam stressed in tension, the proportion of the steel area, related to the local area of concrete shall comply with the following condition:

$$A_{sw} > 0.52\sqrt{f_{cu}}/0.87f_y \qquad 2.44$$

From above, it seems that fire resistance and Eq. 2.44 control the minimum requirements for web reinforcement of deep beams.

2.4.10 General remarks

In the above sections, the development of recommendations for design of deep beams has been followed; from the early rules provided by the Portland Cement Association (1946), based mainly on results from numerical models using elastic theory, to the more comprehensive regulations of the CIRIA Guide 2 (1977), which compiles the knowledge of the 30 succeeding years.

Recommendations have been mainly dedicated to design for flexure and shear strength. In the field of design for flexure, the same principles have been maintained but changes have occurred in the estimation of the lever arm z and the distribution of the main

reinforcement.

Most developments have taken place with respect to shear design. A better understanding of the effect of web reinforcement contribution to the shear capacity of deep beams has allowed the latter document to present sound proposals in this field. However, should the designer ignore the strength of the upper section of a wall above a height equal to the span? This is an aspect which has not been fully investigated and perhaps this is the reason why the most recent documents have adopted this limit as a safe measure.

The documents studied are rich in rules for beam design under top load but they tend to be vague when dealing with suspended loads or combinations of top and bottom loads. This is another field in which very little research has been carried out.

The bearing capacity of deep beams has hardly been analysed except by a few authors and then only in an indirect way when the specimens suffered an early or unexpected bearing failure. Bearing strength of these deep members is controlled by allowing a maximum contact stress, depending on the support position, i.e., either external or internal.

2.5 CONCLUSIONS

a) Numerical methods based on the theory of elasticity can predict the stress field in flexural planar elements made of homogeneous materials and subjected to in-plane forces. These procedures can be used for the analysis of reinforced concrete with limited accuracy. More sophisticated methods, such as Finite Element, have been implemented to consider the stiffnesses of the constitutive materials, improving the predictions of the stress distribution for reinforced concrete. Since this is a complex material, the only precise method of analysis

is the actual test of structural members.

b) Tests carried out on deep beams made of homogeneous materials, which obey Hooke's law, have contributed towards a better understanding of their behaviour. The general opinion extracted from research in this field is that the traditional flexure theory is valid for span/depth ratios larger than 2.0. Beyond this limit, the stress distribution in vertical sections becomes increasingly non-linear. These tests have also been used in the verification of numerical methods of analysis, based on elastic theory, aiming to predict stresses in deep flexural members.

c) In top loaded deep beams, the vertical reinforcement does not contribute greatly to the shear strength and can hardly be efficient, because the direction of the principal tensile stresses is almost horizontal.

d) With suspended loads, vertical stirrups should be employed to take this load and should reach to a height equal to the span.

e) Inclined web reinforcement for deep beams loaded on top was found to be effective for strength and control of deflection and cracking. However, this type of reinforcement is uneconomical due to the difficulties of placing it.

f) It has been considered that the main reinforcement should be distributed over a height about 0.2 times the overall depth of the deep beam and this should be extended along the whole span, without being bent. The anchorage over supports should be provided by horizontal hooks.

g) Openings affect the shear strength of deep beams, depending upon their position. The most detrimental effect to the beam strength occurs where they are coincident with the line joining support and loading point. Inclined web reinforcement above and below the opening

is the most efficient for beams with either lightweight or normal aggregate.

h) Those aspects which still need to be examined further are the following: contribution to the shear strength by the upper section of walls with height/span ratios larger than 1, behaviour of these structures under combinations of top and bottom loads and their bearing strength under different types of loading and ways of improving it.

CHAPTER 3

EXPERIMENTAL WORK

3.1 DESCRIPTION OF TEST SPECIMENS

Two types of specimen were used in this experimental investigation. Both were basically thin rectangular elements made out of reinforced concrete. One had constant dimensions and its particular geomentrical feature was the presence of a nib on the lower edge. This type of specimen will be referred to as WALLS in the text. The second type of specimen had a variable dimension (height) which made it deep in relation to the span. These rectangular, flat elements will be referred to as DEEP PANELS.

3.1.1 Description of Walls

The test specimens consisted of 17 walls of 72 mm thickness, 1000 mm depth, 1260 mm overall length, and 1000 mm simple span. In the lower section of the wall a nib was formed on both sides, measuring 90 and 72 mm in the horizontal and vertical directions respectively. Six vertical holes 25 mm in diameter were formed on each side of the nib. On top of the wall, at both ends, a step 5 mm deep and 130 mm long was formed leaving a central section of 1000 mm over which the uniformly distributed load was to be applied. Details of the specimens are provided in Fig. 3.1.

The main longitudinal reinforcement consisted of 10 plain bars of 10 mm nominal diameter with 332 N/mm^2 average yield stress. This reinforcement was placed in five layers, consisting of five closed stirrups. The web reinforcement was provided by an orthogonal arrangement of bars on both faces of the wall. This reinforcement was 6 mm diameter plain bars with 367 N/mm^2 average yield stress. The nib was reinforced with closed stirrups made out of 10 mm diameter plain

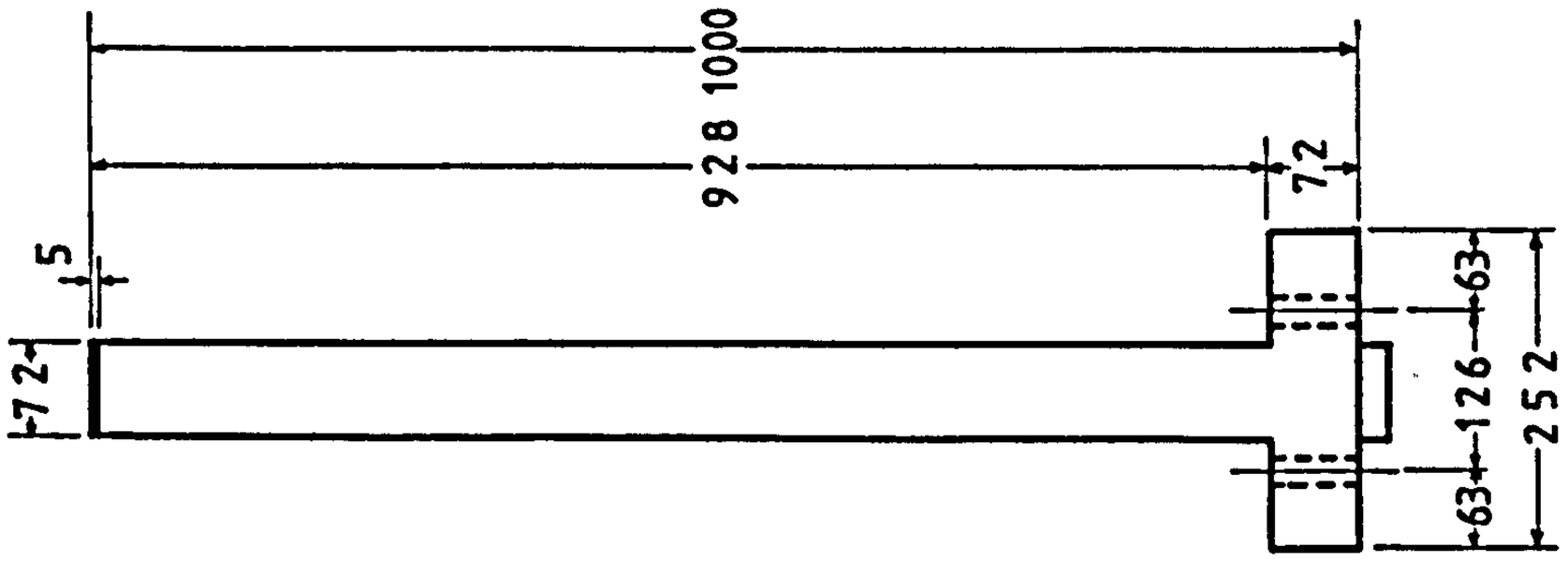

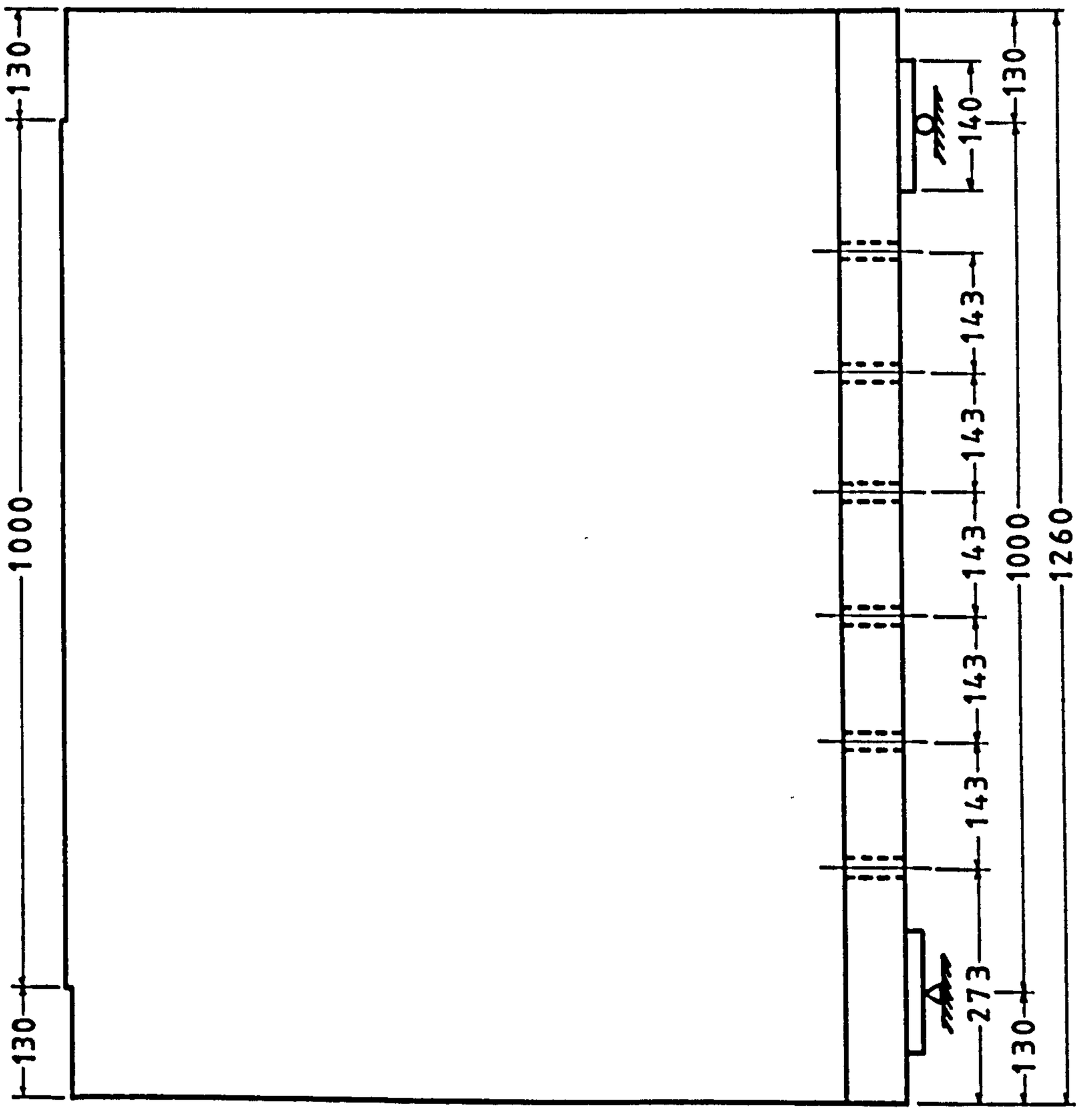

Fig. 3.1 Dimensions and details of walls specimens

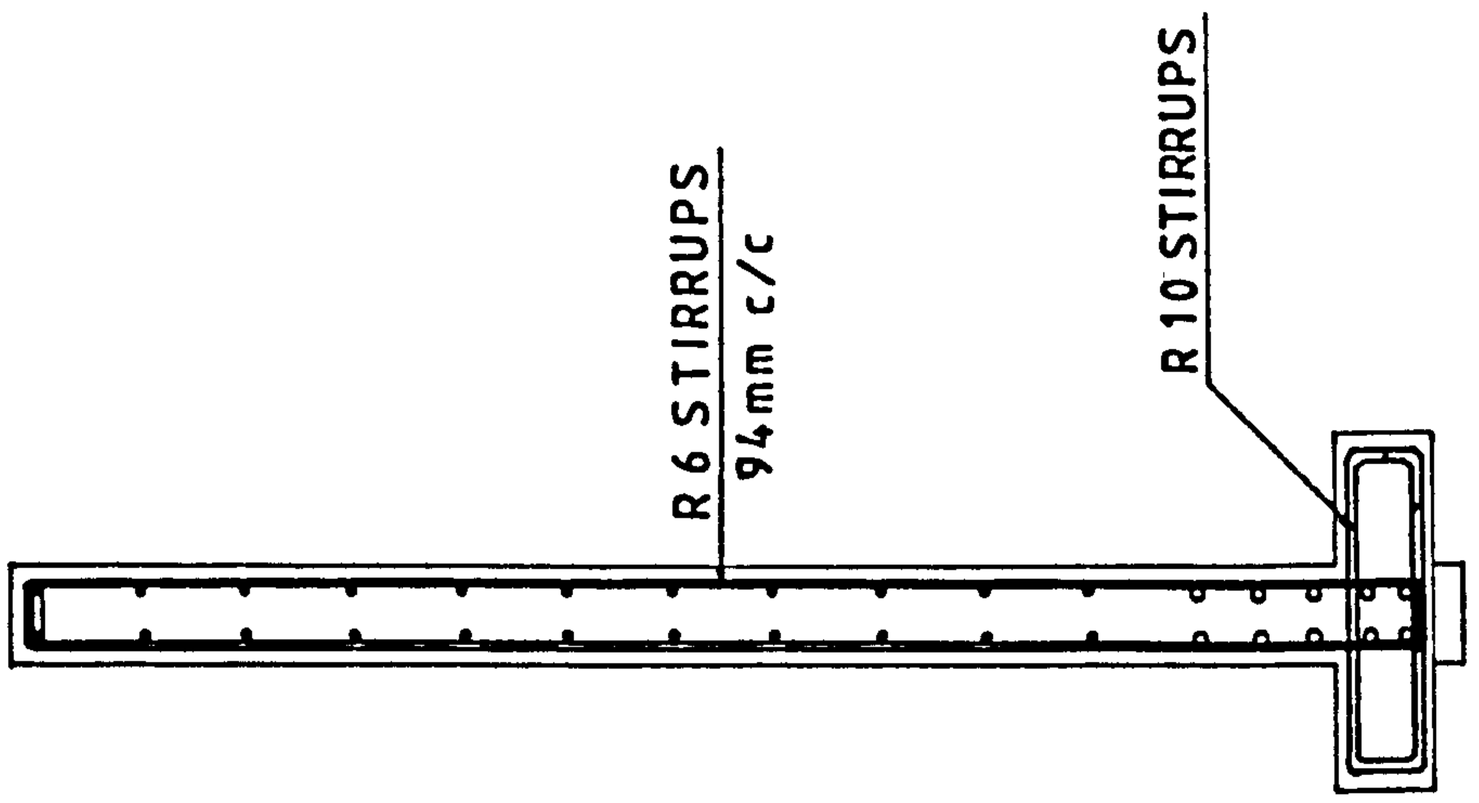

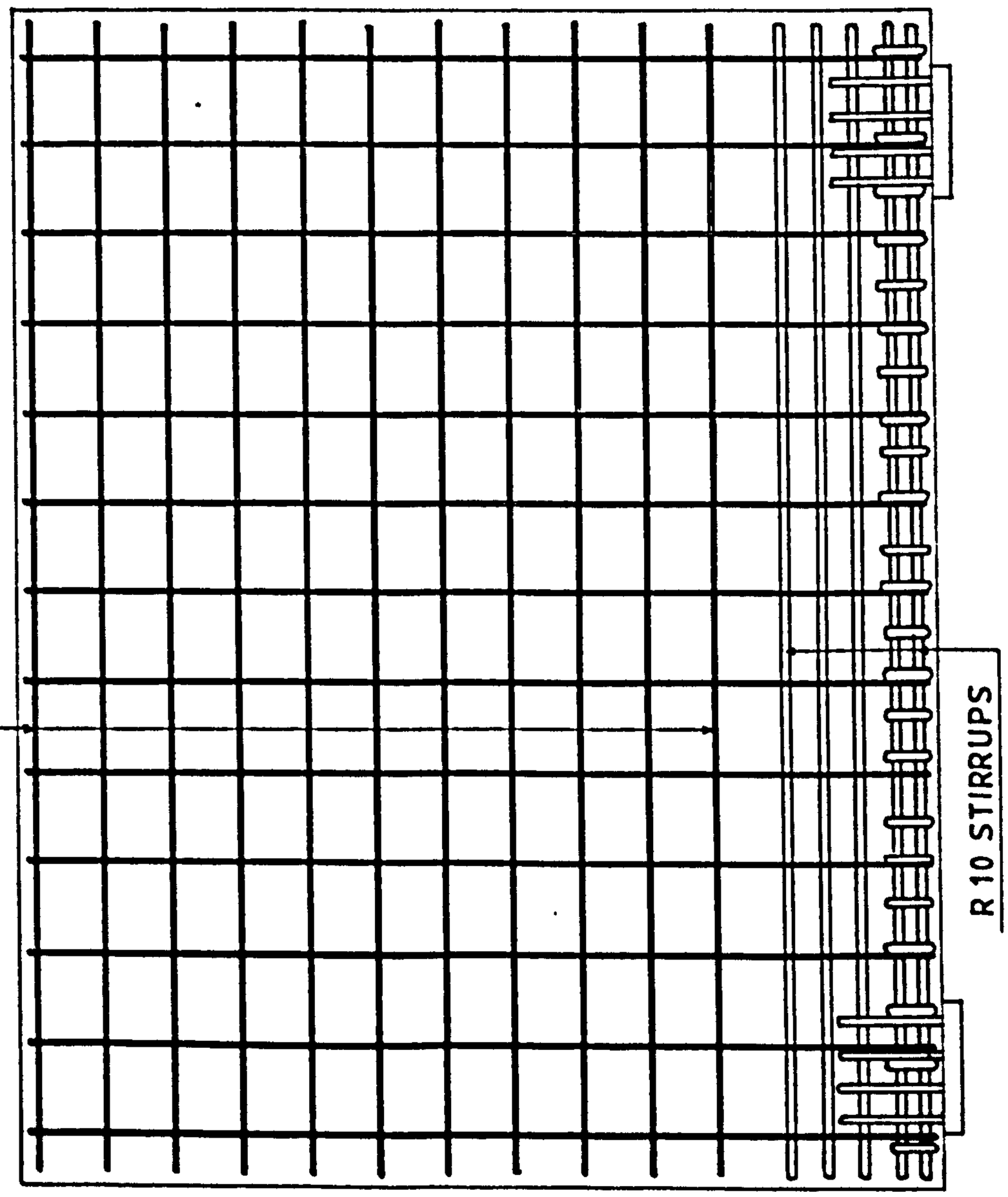

Fig. 3.2 Details of typical reinforcement used in walls W2

bars with 332 N/mm^2 average yield stress. Additional diagonal bars were used in the nibs. These consisted of 6 mm diameter deformed bars with 560 N/mm^2 yield stress. Details of the reinforcement are given in Fig. 3.2.

The anchorage to the main steel and the web reinforcement was provided by the hooks at the end of the stirrups.

3.1.2 Description of Deep Panels

The test specimens consisted of 7 panels of 72 mm thickness, 720 mm simple span, 872 mm overall length, and depth/thickness ratio

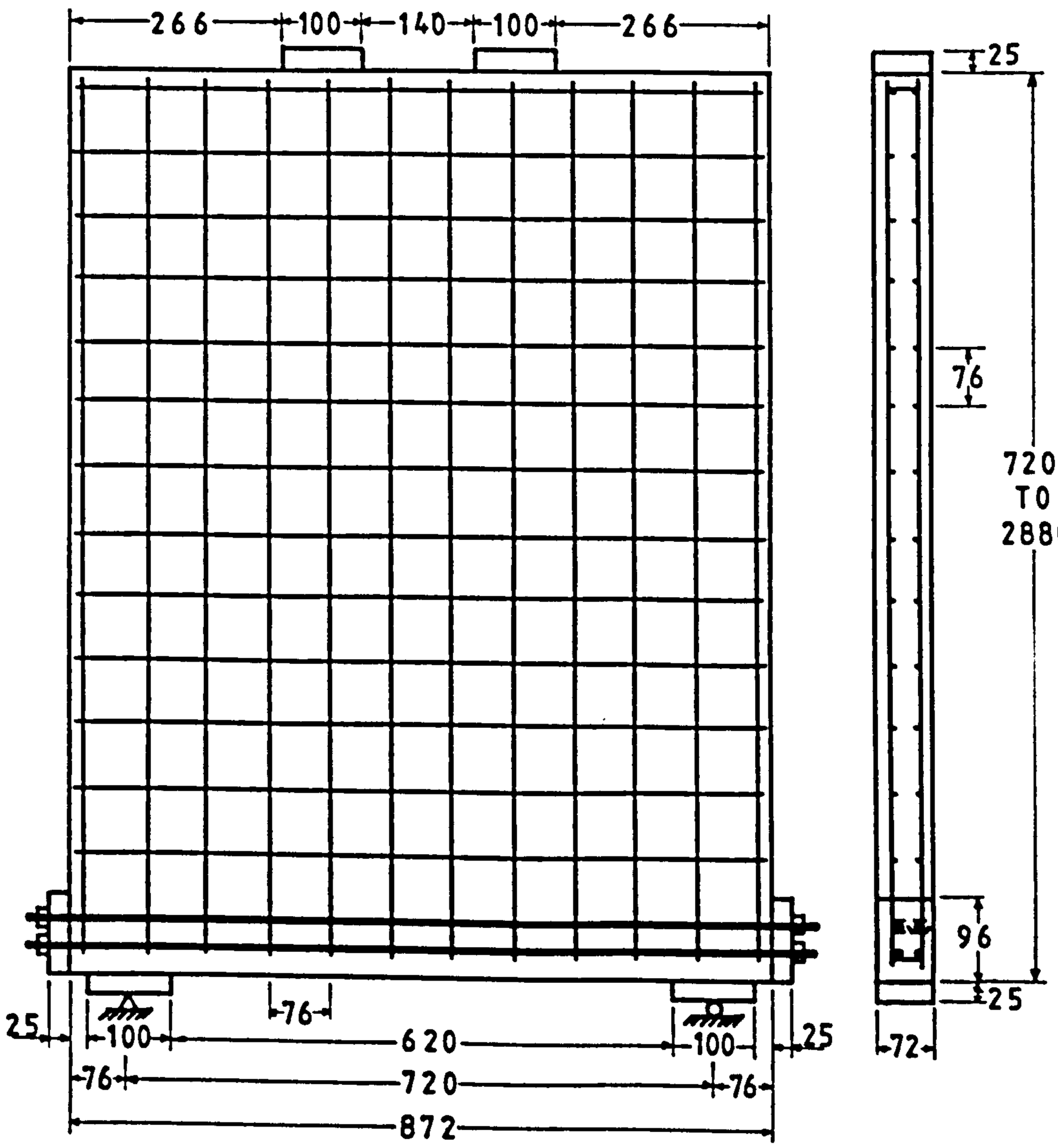

Fig. 3.3 Typical reinforcement detail of Deep Panels

ranging from 10 to 40, corresponding to depths of 720 to 2880 mm. The specimens were all cast in normal weight concrete.

The main longitudinal reinforcement consisted of 4 bars of 10 mm nominal diameter with 420 N/mm^2 average yield stress. This reinforcement was placed in two layers (Fig. 3.3). The web reinforcement was provided by using BRC Weldmesh, which consists of plain bars 5.3 mm diameter in both directions at 76.2 mm centres. The yield stress of this steel was found to be 425 N/mm^2. One layer of mesh was placed at each face of the specimen. The main bars were anchored to steel blocks at their ends to prevent bond failure. To achieve this, the reinforcing bars were left protruding from the beam and the ends threaded. A 96 x 72 x 25 mm steel block with holes for passing the main bars through was bedded to each end of the panel with cement paste. Nuts were threaded on to the bars at both ends and tightened. Details of the end-blocks are shown in Fig. 3.4.

3.2 MATERIALS

3.2.1 Cement

The cement used for all the specimens was ordinary Portland Cement, supplied by the Blue Circle Group.

3.2.2 Aggregate

The coarse aggregate used was North Notts quartzite gravel with a maximum size of 10 mm, "irregular" shape and "smooth" surface texture as classified by BS 812: Part 1:1975. The sand used as fine aggregate was obtained from the same quarry. The grading curves for the fine and coarse aggregates are shown in Fig. 3.5.

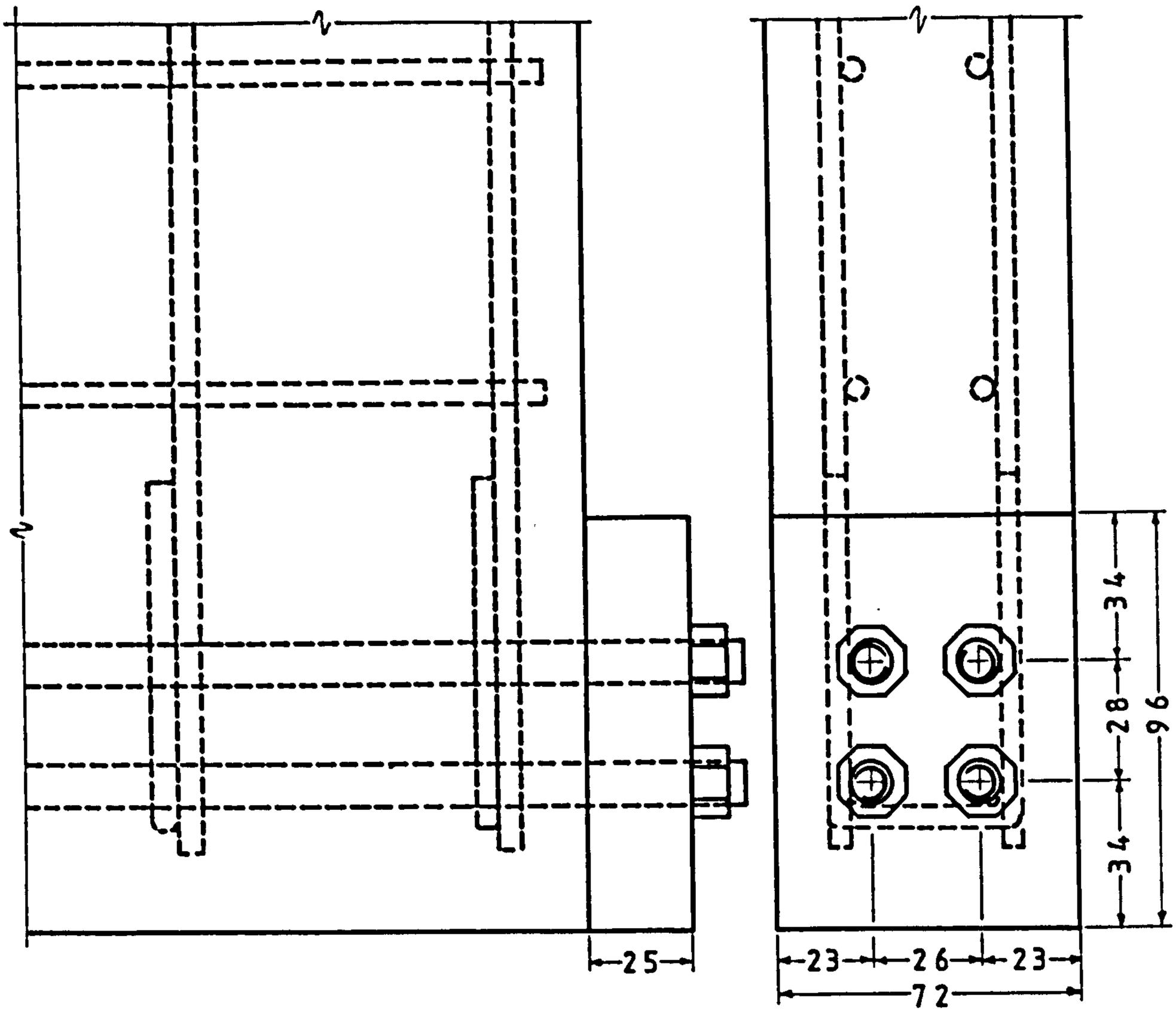

Fig. 3.4 End block and steel reinforcement detail

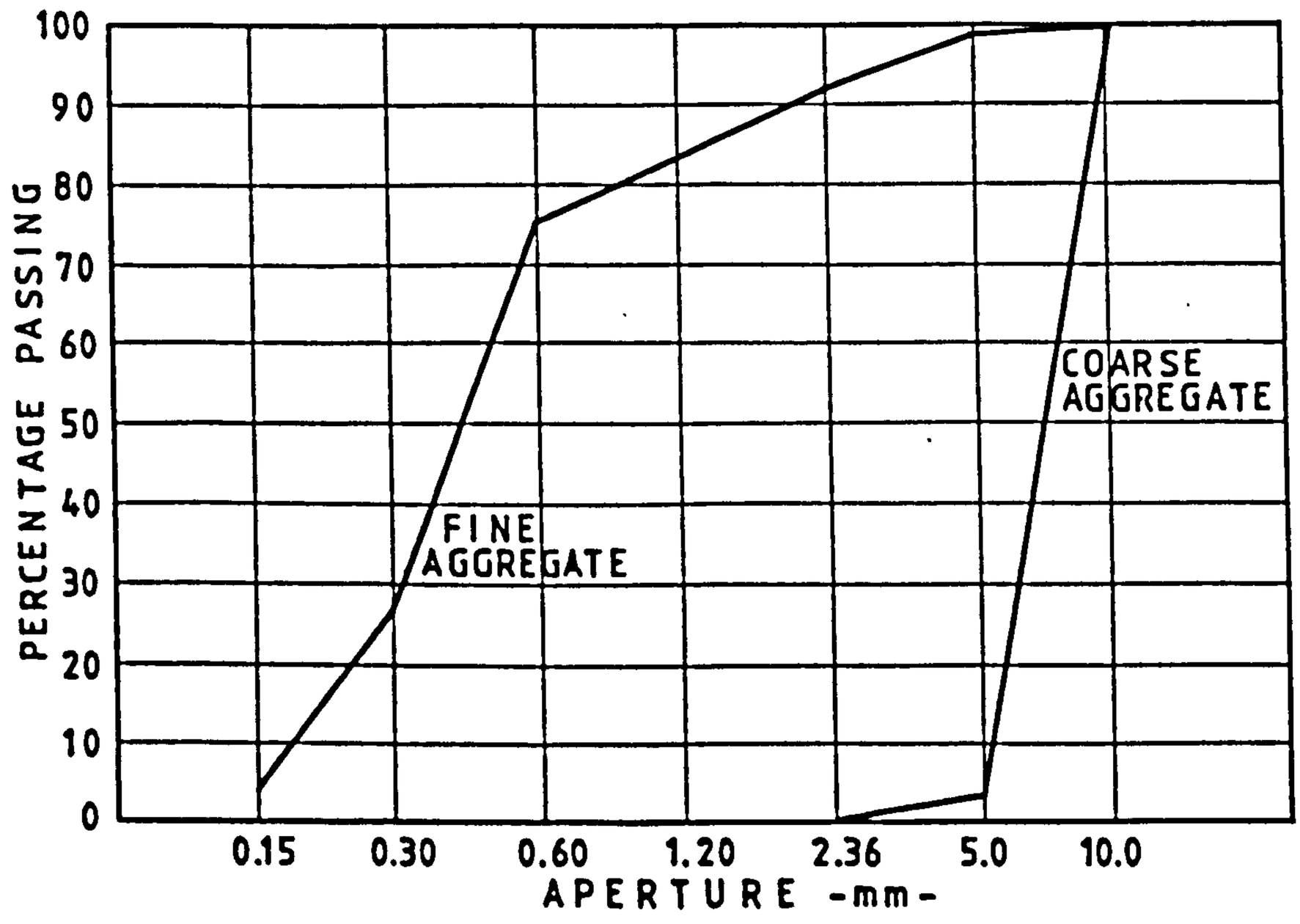

Fig. 3.5 Grading curves for fine and coarse aggregates

3.3 MIX DETAILS

3.3.1 Mix Details of Walls

Two mixes were used for the casting of these specimens. The first five specimens were cast using mix A; the mix proportion by weight was 1 : 2.5 : 4.4 with water/cement ratio of 0.62. The rest of the specimens were cast using mix B, with mix proportions by weight of 1 : 1.99 : 3.59 and with a water/cement ratio of 0.53. Both mixes were improved by using additives. 200 cubic centimetres of Sikament Superplasticiser and 20 cubic centimetres of Sikament Air Entraining Agent were used in every mix, with the purpose of increasing the cohesion of the mix while casting and to improve the workability of the material (Neville, 1981). A flowing concrete was needed in order to pass through the heavily reinforced section. Workability tests carried out gave average values of 150 mm slump, V-B time less than 1 second and compacting factor equal to 0.96 for mix A. Mix B gave average values of 130 mm slump, V-B time less than 1 second and compacting factor of 0.94.

Details of the concrete strength for each specimen are given in Table 3.1.

3.3.2 Mix Details of Deep Panels

The mix used was identical for all the specimens in order to obtain similar strengths of concrete. The mix proportion by weight was 1 : 2.5 : 4 with water/cement ratio of 0.65.

Workability tests gave average values of 75 mm slump, V-B time of about 2 seconds and compacting factor of 0.94.

The concrete properties of each specimen are provided in Table 3.2.

Table 3.1 Concrete Properties of Walls

Specimen	f_{cu} N/mm^2	f_{ct} N/mm^2	ν	E_c kN/mm^2	Density kg/m^3
W1-L1	41.7	2.47	0.148	32.054	2271.0
W1-L2	38.9	2.47	0.132	29.571	2301.0
W1-L3	34.2	2.22	0.185	32.660	2328.0
W1-L4	38.3	2.52	0.176	27.738	2315.0
W1-L5	41.0	2.69	0.164	33.551	2308.0
W2-L1	45.3	2.49	0.156	32.114	2285.0
W2-L2	42.2	2.55	0.141	31.793	2316.0
W2-L3	36.0	2.45	0.184	29.123	2270.0
W2-L4	34.8	2.34	0.180	27.577	2277.0
W2-L5	43.4	2.68	0.140	34.749	2327.0
W3-L1	50.3	2.76	0.146	34.267	2310.0
W3-L2	44.9	2.74	0.152	33.391	2328.0
W3-L3	43.6	2.40	0.145	31.668	2318.0
W3-L4	48.6	2.83	0.146	31.896	2346.0
W3-L5	48.9	2.88	0.142	33.594	2327.0
W4-L2	41.7	2.58	0.140	32.527	2325.0
W5-L2	47.3	2.87	0.147	33.400	2336.0

Table 3.2 Concrete Properties of Deep Panels

Panel	f_{cu} 7 days N/mm^2	f_{cu} 28 days N/mm^2	f_{cu} day of test N/mm^2	f_{ct} day of test N/mm^2	E_c day of test kN/mm^2
DB1	29.0	41.0	49.6	3.36	34.7
DB2	32.7	45.6	53.0	3.30	33.2
DB3	28.7	40.5	49.3	3.13	31.1
DB4	31.9	45.0	48.0	2.50	31.7
DB5	28.5	39.6	49.4	3.86	35.1
DB6	33.0	46.7	51.6	3.46	34.8
DB7	29.0	40.5	46.9	3.47	36.6

3.4 FABRICATION AND CURING

3.4.1 Fabrication and Curing of Walls

All specimens were cast in a vertical position, using oiled moulds made from plastic-coated Wisaboard. The mould was made in such a way that it was easily assembled for casting and it came apart in five sections to take the specimen out. Due to the awkward shape of the nib, the specimens were cast vertically but up-side-down as shown in Fig. 3.6. All the reinforcement was prepared and the cage put together out of the mould (Fig. 3.7). Once the cage was ready it was put into the mould and held in place by spacers. Due to this procedure of casting it was necessary to provide a mix with special characteristics to avoid excessive segregation and ensure proper compaction of the concrete. The ingredients of the mix were weighed and placed into a 0.2 cubic metre Cumflow horizontal drum mixer, except the water, which was mixed with

the air entraining agent and added to the other dry ingredients after 30 seconds or more of mixing. After 2 minutes the superplasticiser was added and all the ingredients mixed for a further minute. Only one specimen was cast at a time. Slump and compacting factor tests were carried out for each mix. The concrete was poured into the mould which rested on a vibrating table for compaction. The process of filling the mould took about five minutes. Immediately after casting, the specimen was removed from the vibrating table. The exposed face of the concrete was made good and then covered with wet sacks and polythene sheets.

Control specimens were cast with each mix and also compacted on the vibrating table. At 24 hours after casting, the wall and the control specimens were stripped from the moulds and placed in the curing room until they were needed for testing. The curing room was kept at a temperature of 20°C and a relative humidity of 95-100 percent.

3.4.2 Fabrication and Curing of Deep Panels

All specimens were cast in a horizontal position, using oiled moulds made from plastic-coated Wisaboard. One side of the mould was adjustable and its position easily altered to allow varying panel depths. The web reinforcement was held in place by spacers and by the main reinforcement which passed through the sides of the formwork.

The concrete was mixed in a 0.2 cubic meter capacity Cumflow horizontal drum mixer. Slump and compacting factor tests were carried out for each mix. The concrete was placed in the mould and the specimen was compacted using an external vibrator.

Control specimens were cast with each mix and compacted on a vibrating table. 24 hours after casting, the control specimens were stripped from the moulds and placed in the curing room. The panel was kept covered with damp hessian for at least 3 days, watered constantly

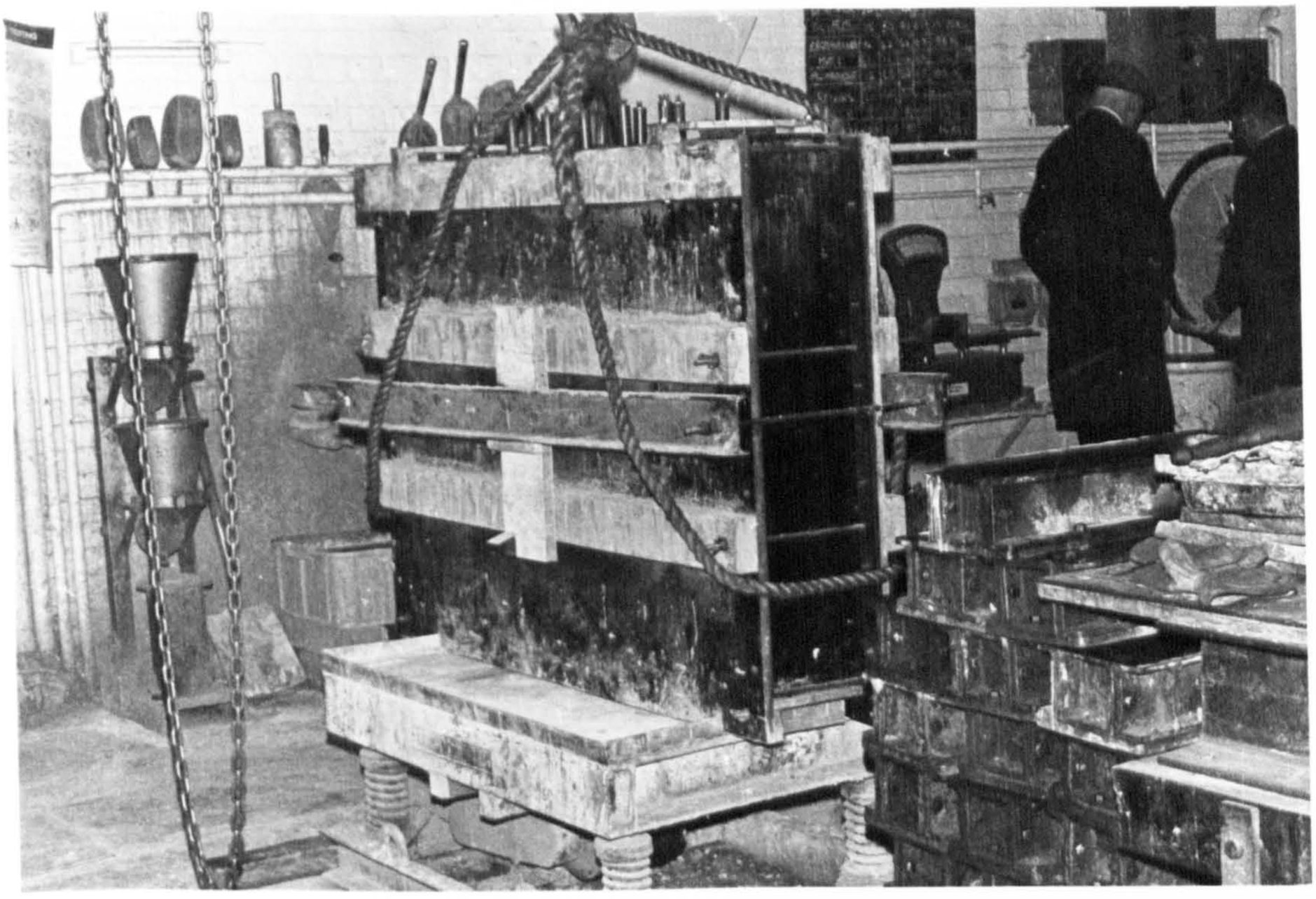

Fig. 3.6 Mould on vibrating table

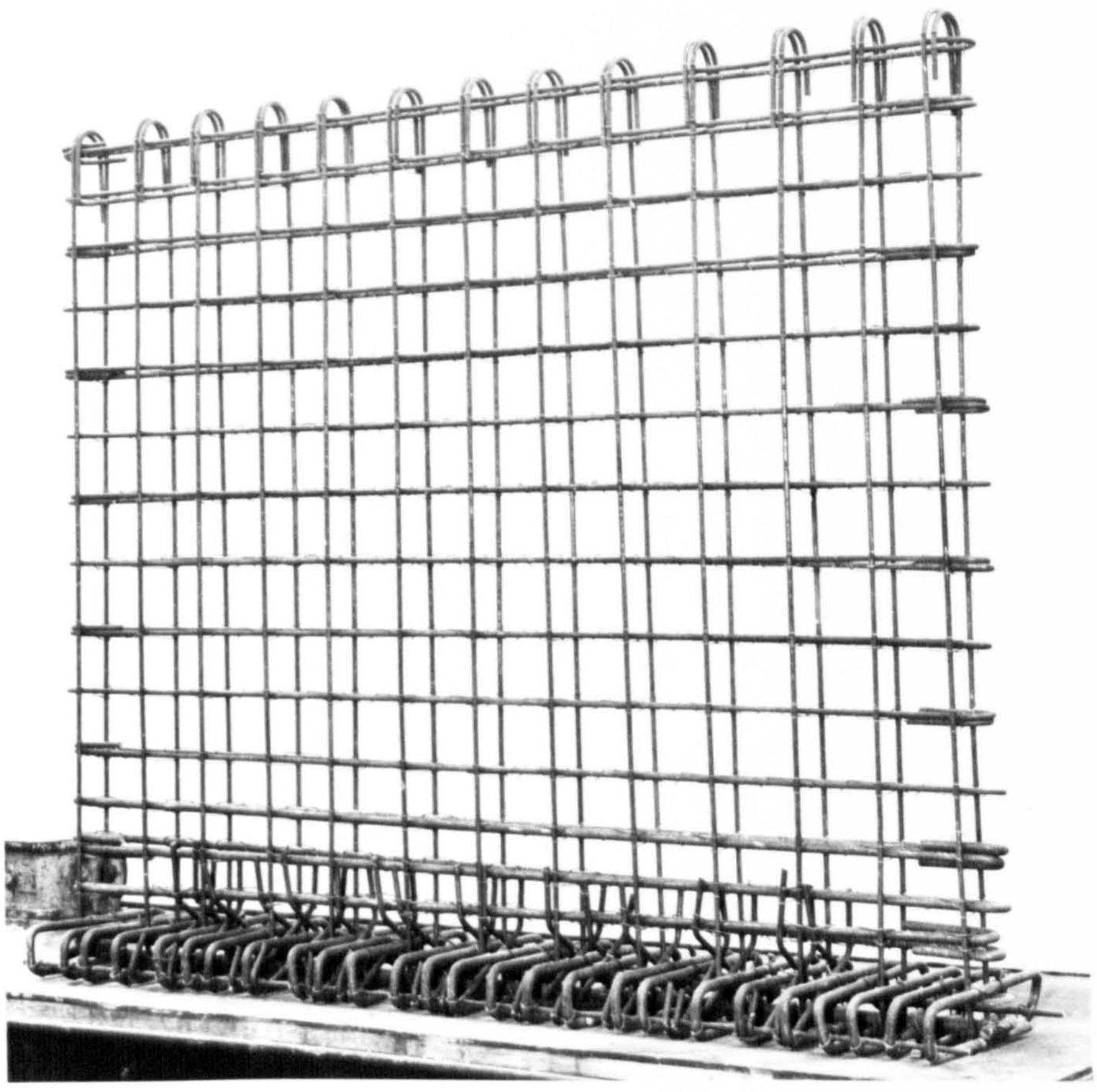

Fig. 3.7 Typical cage reinforcement for walls

and then transferred to the curing room until the day of the test.

3.5 CONTROL SPECIMENS

The control specimens for each mix consisted of 9 standard 100 x 100 x 100 mm cubes, four 300 x 150 mm diameter cylinders and three 100 x 100 x 500 prisms. Cubes were used to determine the crushing strength of the concrete at 7 days, 28 days and the day of the main test. The cylinders were used to determine the splitting strength on the day of the main test. The prisms provided the data for the stress-strain relationship of the concrete on the day of the main test.

In order to minimize differences in the strength of concrete between the test specimen and the control specimens, the same procedure was applied for casting and curing both. There are several factors which can contribute to different strengths of the concrete in the actual specimen and the control specimens. Among these factors, casting and storage conditions are the most important. The ambient conditions during casting, the compaction in moulds, curing during the first 24 hours and during the subsequent period are decisive with regard to the strength of the concrete as reported by Bhargava (1969). All these conditions were kept constant as far as it was possible during casting and curing.

The control specimens were tested in accordance with BS 1881 : 1970.

3.6 INSTRUMENTS

Instruments were provided to measure vertical and horizontal displacements and strains. Loading of the specimen was applied by means of hydraulic testing machines and frames. The systems for loading the deep panels and the walls are described in the following sections.

3.6.1 Loading System for Walls

The loading apparatus for testing the walls (Fig. 3.9) consisted essentially of a high rig which had two cross-heads and two independent hydraulic and mechanical systems to apply the loads.

The upper cross-head held the hydraulic jack and equipment used to apply the uniformly distributed load on top of the wall. The load from the jack was carried by a steel beam which transmitted that load equally onto two other smaller beams. In this way, the load applied by the hydraulic jack was carried by four rollers onto four steel blocks welded to a stiffened channel which provided the uniformly distributed load onto the upper section of the specimen through a rubber pad 25 mm thick. Details of this part of the equipment are given in Fig. 3.8.

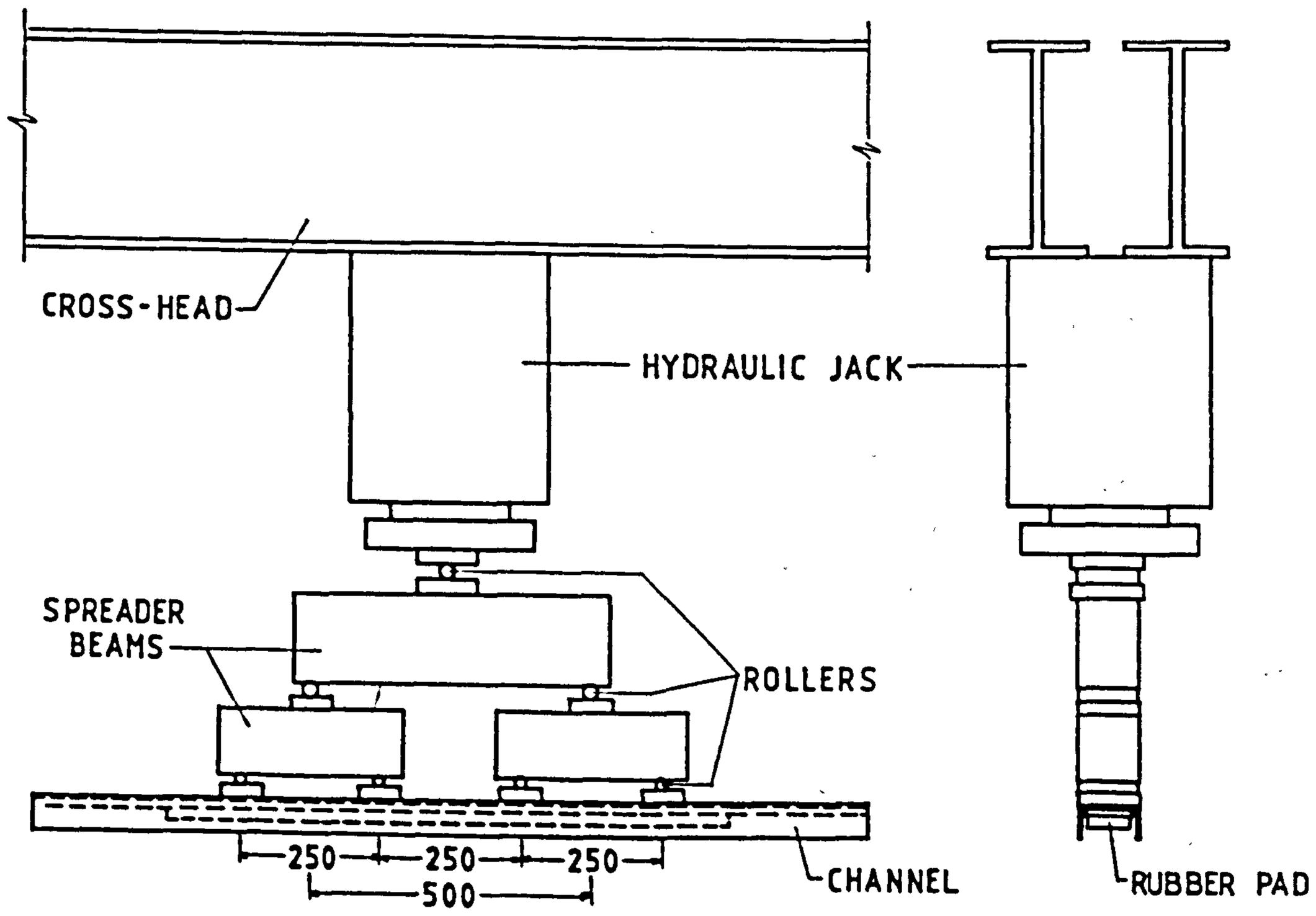

Fig 3.8 Top loading system

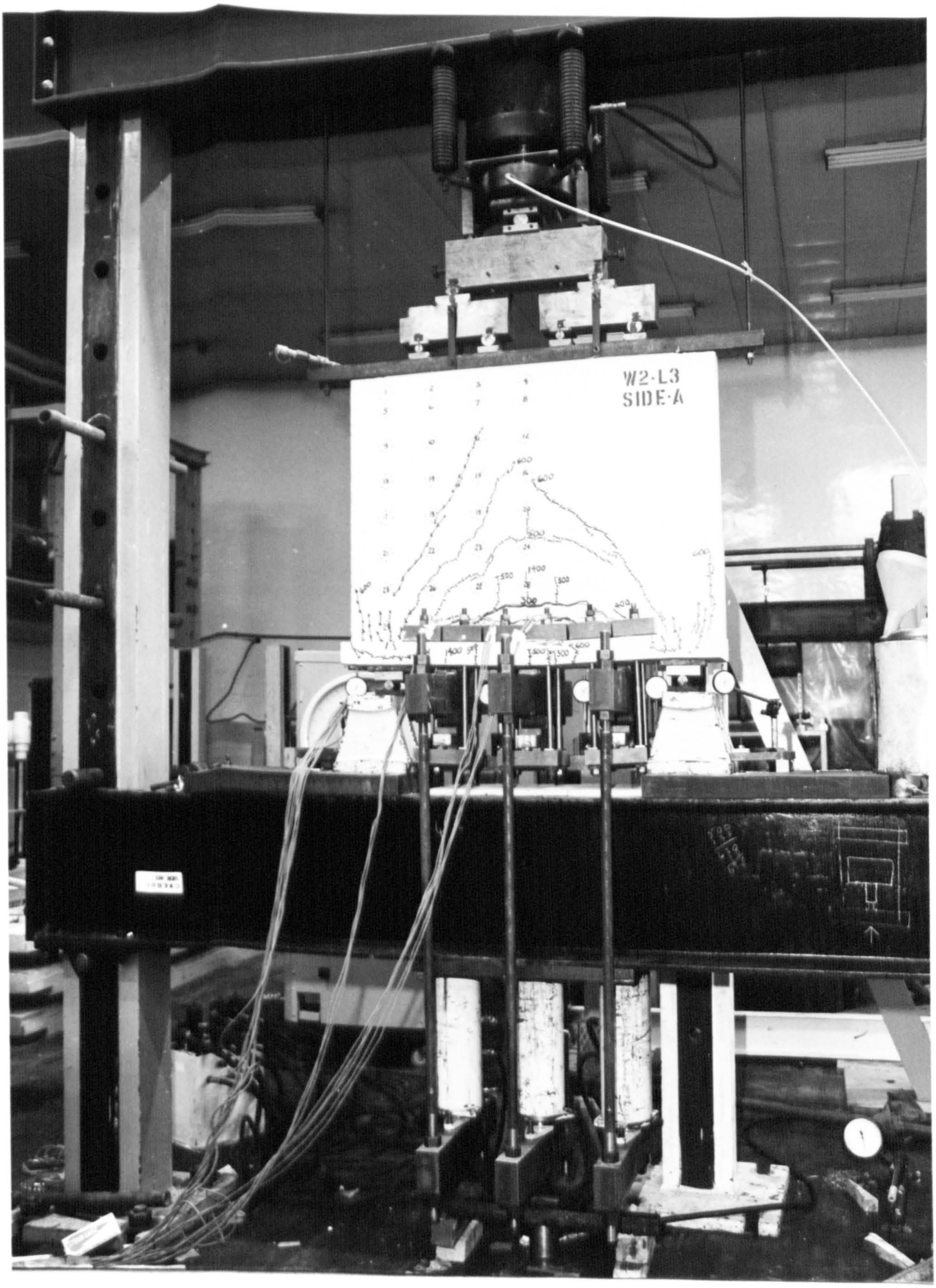

Fig. 3.9 Loading system for testing walls

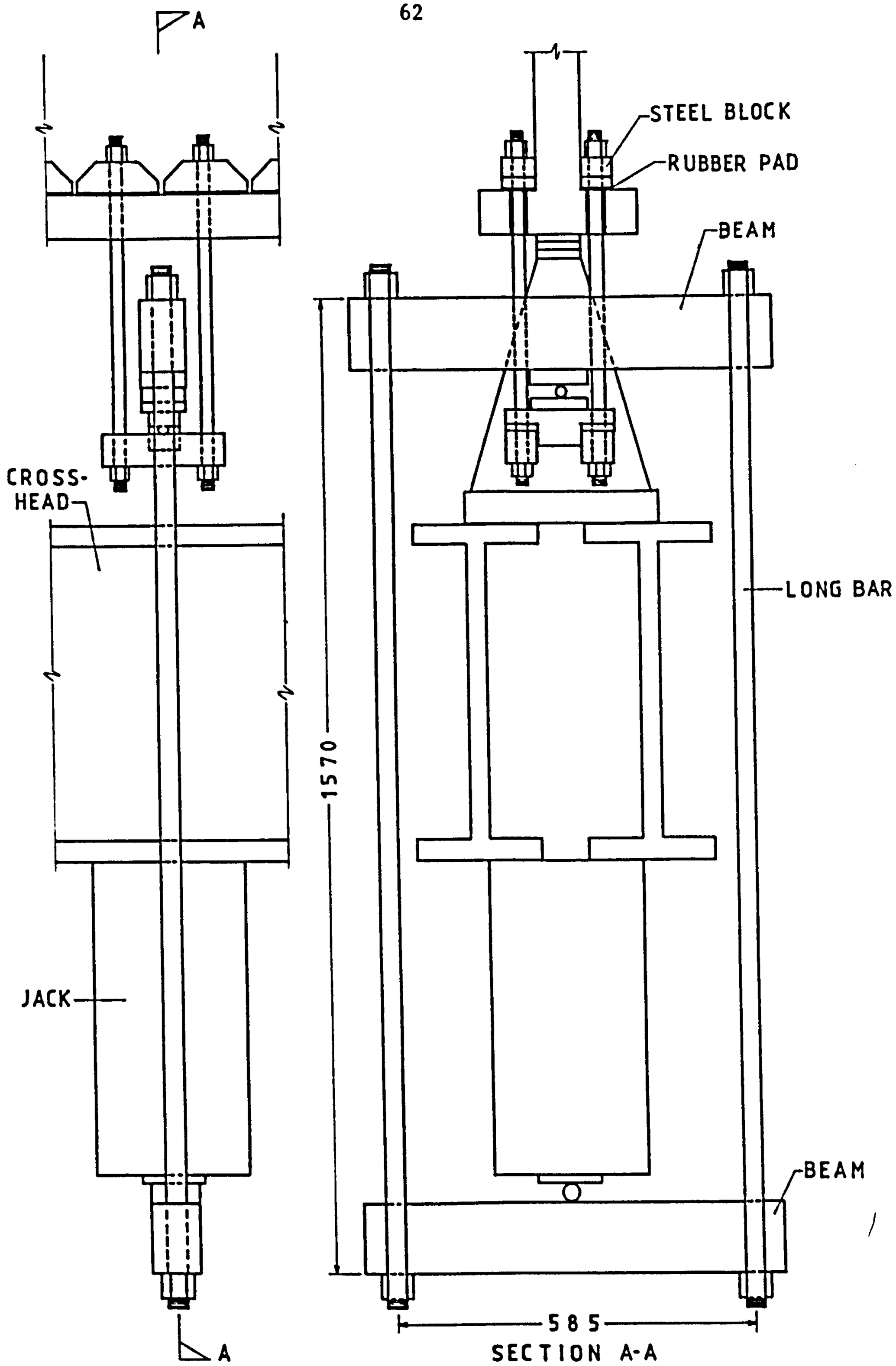

Fig. 310 Loading system for lower section of walls

The lower cross-head of the rig provided support to the specimen. It also held the jacks used for the application of suspended load on the walls.

The load on the lower section of the wall was provided by three systems working in line, each of them having one or two hydraulic jacks and tie-rods to transmit the load to the nib (Fig. 3.10). The jacks were attached under the cross-head and pushed against it on to a steel frame. The frame consisted of two parallel beams and two tie-rods. One of the beams was attached to the hydraulic jack and the other passed under the specimen. Here a mechanism of rollers and steel sections transferred the load onto the nib at four points through steel blocks mounted on rubber pads 6 mm thick (Fig. 3.10).

3.6.2 Loading System for Deep Panels

The specimens were tested under two-point top-loading at third-span points. The load was applied hydraulically by means of a Scriven testing machine and frame. The panels were simply supported over a single span (Fig. 3.11).

3.6.3 Dial Gauges

Dial gauges (Mercer, 1 division = 0.001 in) were used to measure vertical (in-plane) and horizontal (out-of-plane) displacements of the specimens.

3.6.4 Demec Gauge

The strain measurements on the concrete were taken by means of a mechanical strain gauge, known as a Demec Gauge, developed by the Cement and Concrete Association and described by Morice (1953). This

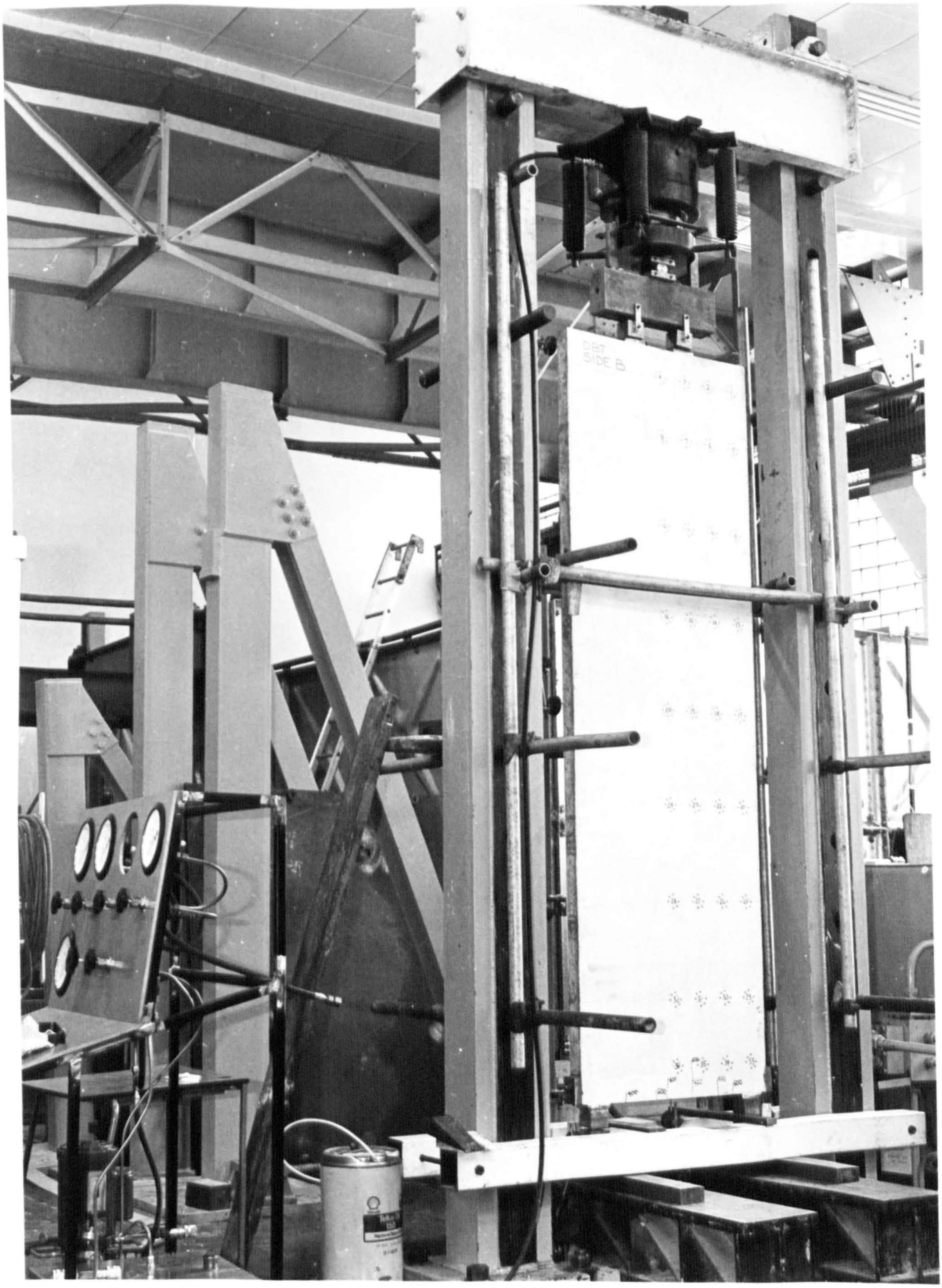

Fig. 3.11 Arrangement of machine and frame used for testing deep panels

instrument had a 50 mm gauge length in which the least measurable strain was 1.99×10^{-5} mm/mm. The measurements were taken on stainless steel discs cemented on to the concrete surface using Amco F88 dental cement and solvent.

3.7 TESTING PROCEDURE

3.7.1 Testing Procedures of Walls

At least two days before testing, the wall with all the control specimens were removed from the curing room into the laboratory. The specimen was mounted on to the rig and made safe. The faces of the

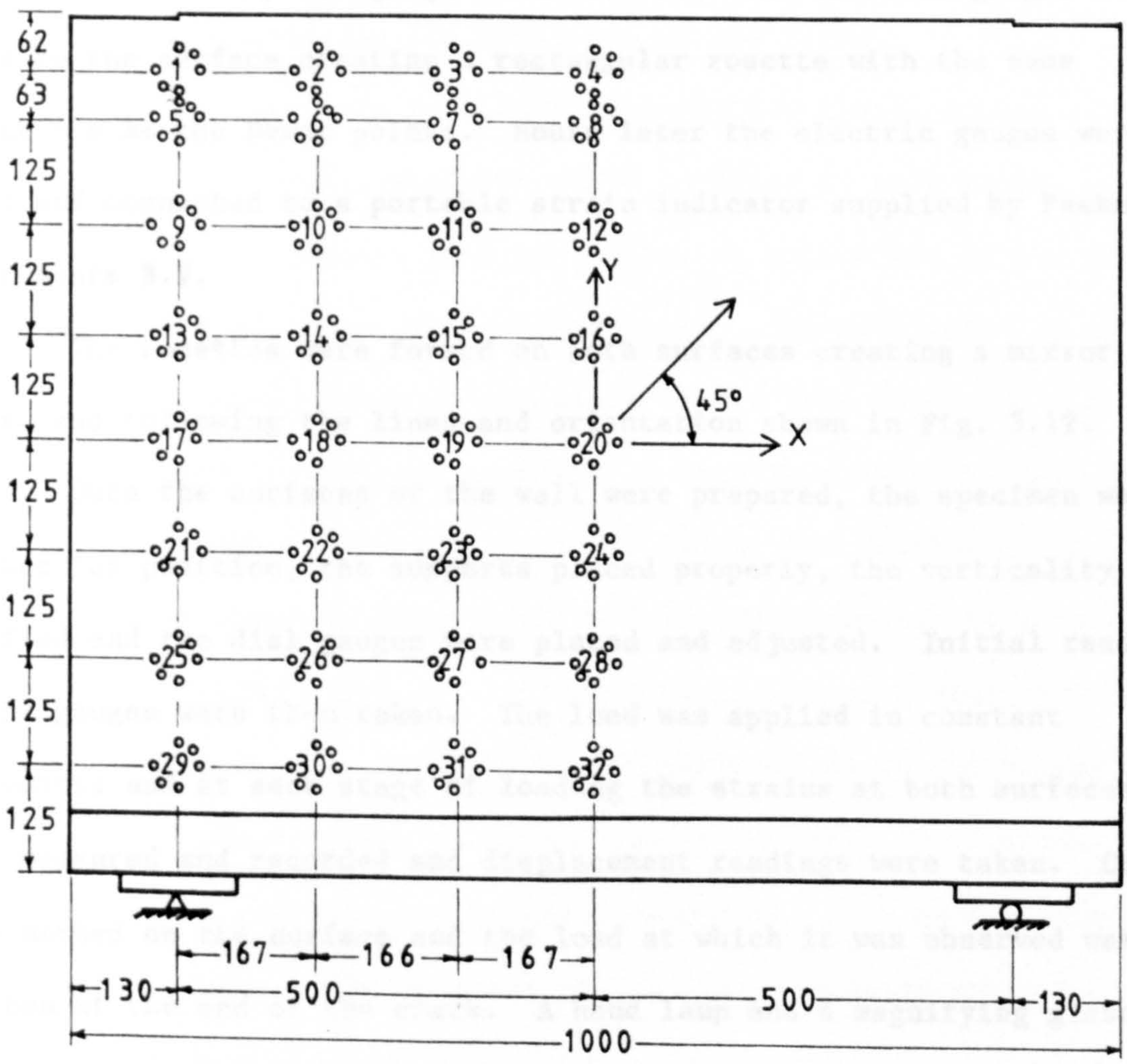

Fig. 3.12 Distribution and position of strain rosettes on wall specimens

specimen were painted with a coat of non-drip white emulsion to facilitate the detection of cracks. A grid was marked on both faces of the specimen, establishing the position and direction of the strain gauges and Demec points. At each position on the surface of the panel, where strain measurements were required, 6 Demec points were fixed to create a rectangular rosette. At those places where the measurement of strains by means of the Demec gauge was not possible, electrical-resistance strain gauges were used. This required the preparation of the concrete surface with Araldite. When the Araldite dried the surface was polished with sand paper and the remaining dust and dirt was removed with acetone. The gauges were then fixed to the model using P-2 adhesive provided by the gauge manufacturer. The electric gauges were fixed to the surface creating a rectangular rosette with the same directions as the Demec points. Hours later the electric gauges were wired and connected to a portable strain indicator supplied by Peekel Instruments B.V.

The rosettes were formed on both surfaces creating a mirror image, and following the lines and orientation shown in Fig. 3.12.

Once the surfaces of the wall were prepared, the specimen was checked for position, the supports placed properly, the verticality verified and the dial gauges were placed and adjusted. Initial readings of the gauges were then taken. The load was applied in constant increments and at each stage of loading the strains at both surfaces were measured and recorded and displacement readings were taken. Cracks were marked on the surface and the load at which it was observed was written at the end of the crack. A hand lamp and a magnifying glass were used to aid crack detection. The width of the cracks was measured and a record of the crack-width was taken. A hand microscope with a magnification of 40 was used. The graduation in the eyepiece scale of

the microscope corresponded to a crack width of 0.02 mm. This procedure was repeated up to the failure load or until it was obvious that the specimen was close to failure due to yielding of the reinforcement.

When the test was over, the specimen was removed and photographed to record the final crack pattern. The control specimens were tested the same day in which the main test took place. Each test took about eight hours.

3.7.2 Testing Procedure of Deep Panels

After 28 days or more under curing conditions, the specimen to be tested was mounted on the supports under the frame of the testing machine. The height of the hydraulic jack was adjusted to the size of the specimen by moving the top crossbeam of the frame.

When the panel was secured to the testing frame, it was painted with a thin coat of white emulsion paint in order to make crack detection easier. A square grid was marked on both sides of the panel to establish the position of the Demec Points. At each point on the surface of the panel, where strain measurements were required, 6 Demec points were fixed to create a rectangular rosette. These rosettes were fixed on both surfaces creating a mirror image, and following the lines and orientation shown in Figs. 3.13 to 3.19 corresponding to panels DB1 to DB7 respectively. Line A coincides with the support line, line C coincides with a loaded point and line D corresponds to the centre line of the panel. The distance between lines is 120 mm. The specimen was then checked for position and verticality and the dial gauges were placed and adjusted. The position of the dial gauges is shown in Figs. 3.13 to 3.19 and are identified as D1, D2, etc.

Loads were usually applied in steps of 100 kN and strains at both surfaces were measured and recorded and displacement readings were

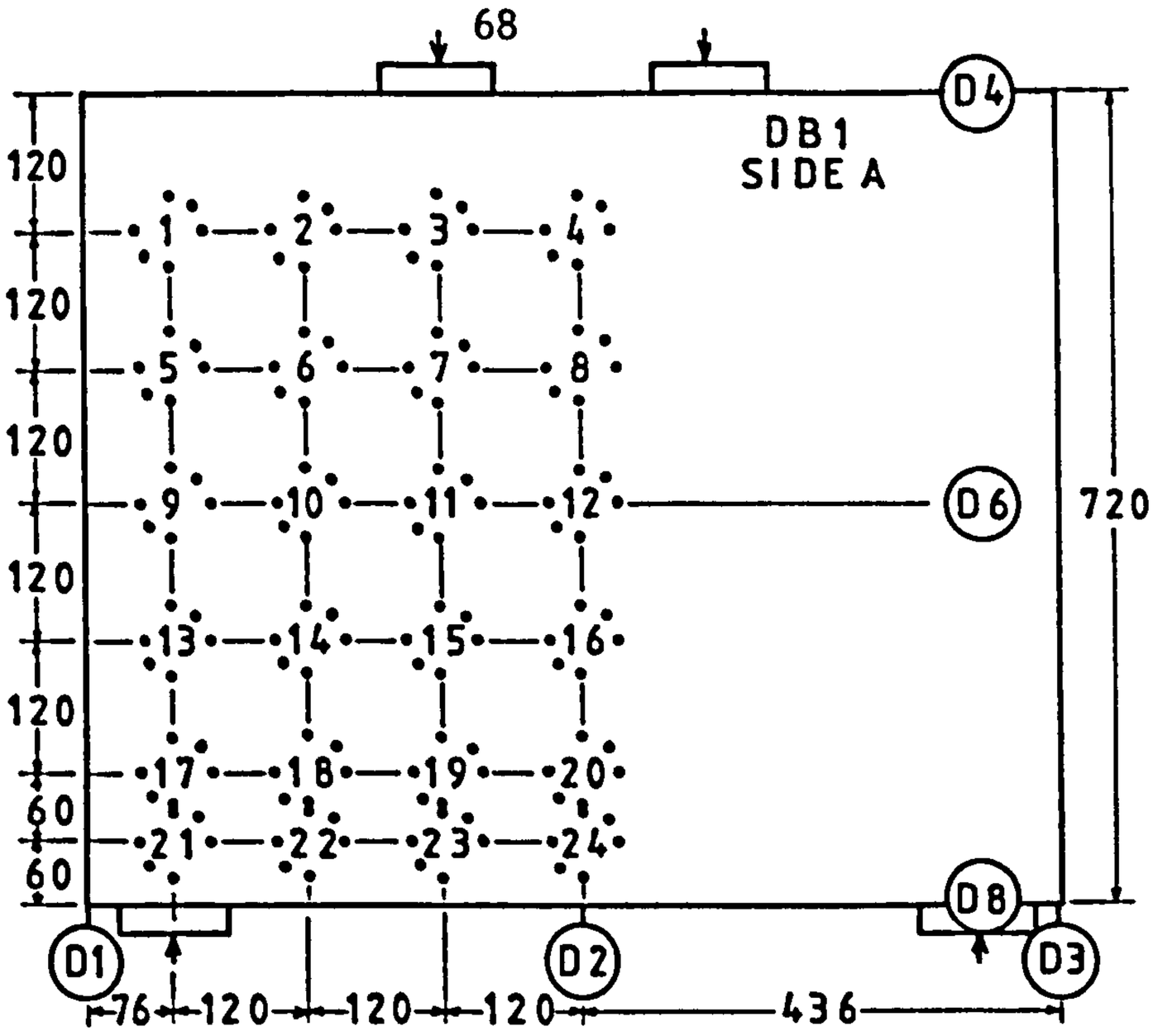

Fig. 3.13 Distribution and position of rosettes and dial gauges on specimen DB1

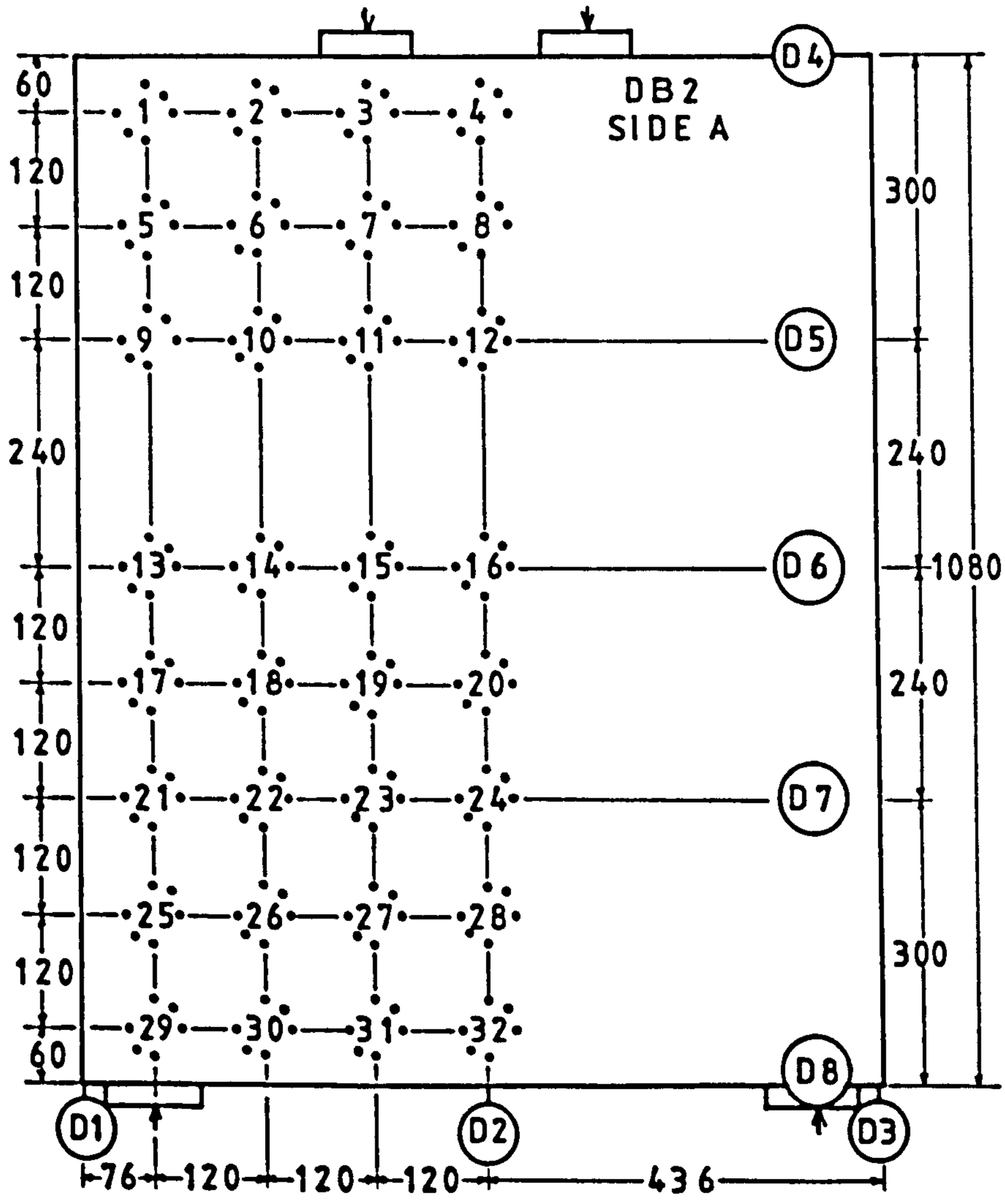

Fig. 3.14 Distribution and position of strain rosettes and dial gauges on specimen DB2

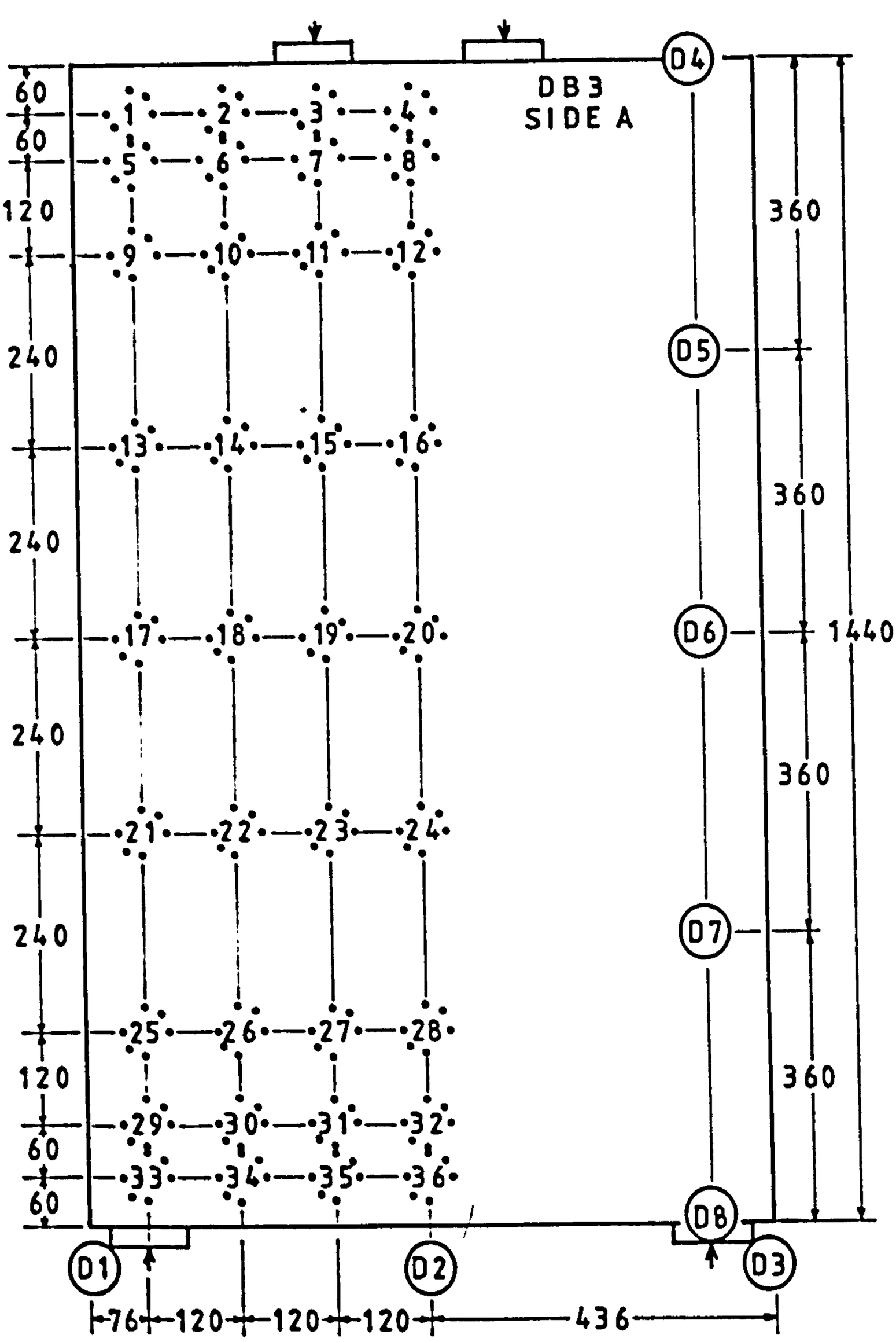

Fig. 3.15 Distribution and position of strain rosettes and dial gauges on specimen DB3

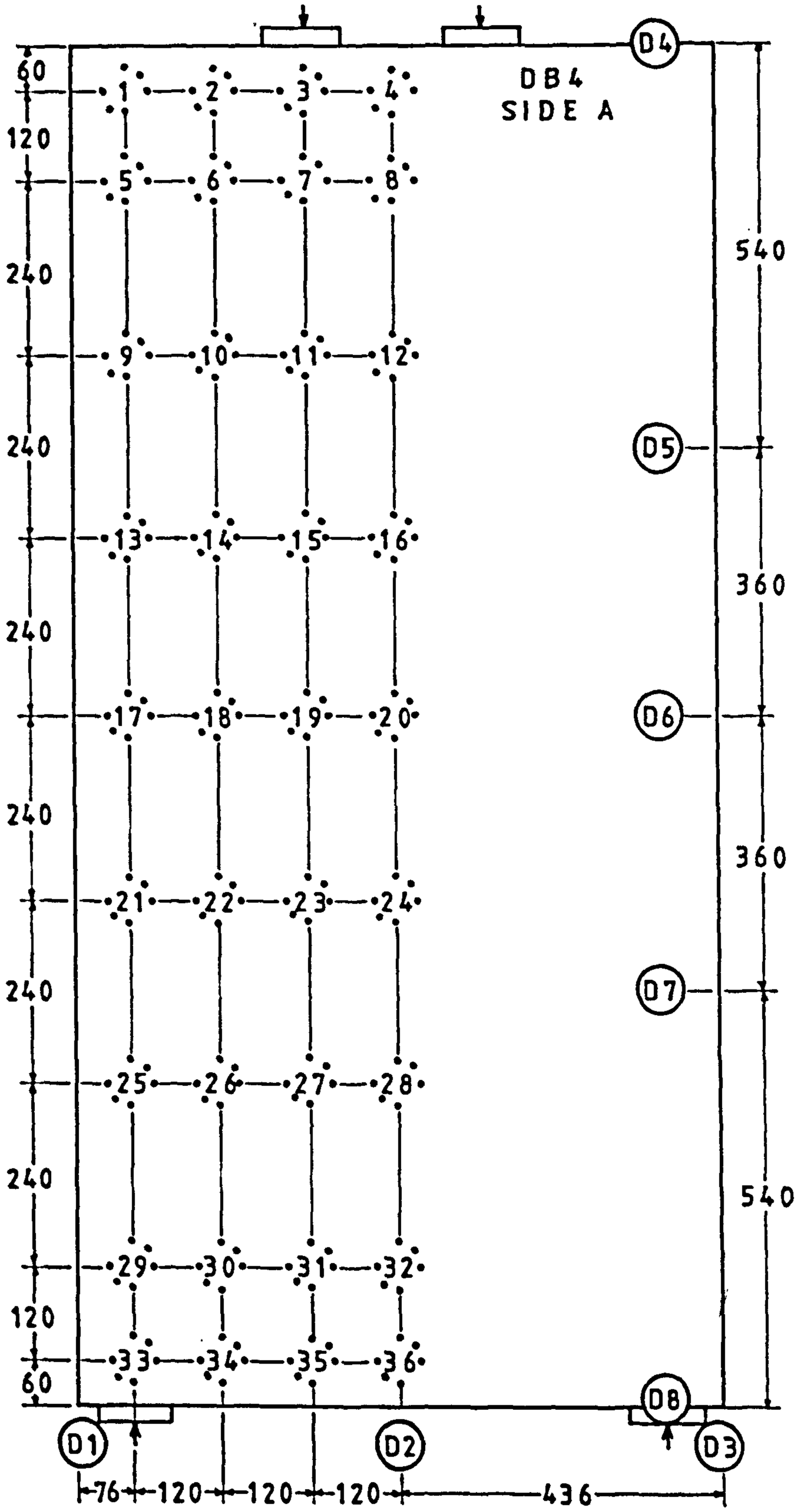

Fig. 3.16 Distribution and position of strain rosettes and dial gauges on specimen DB4

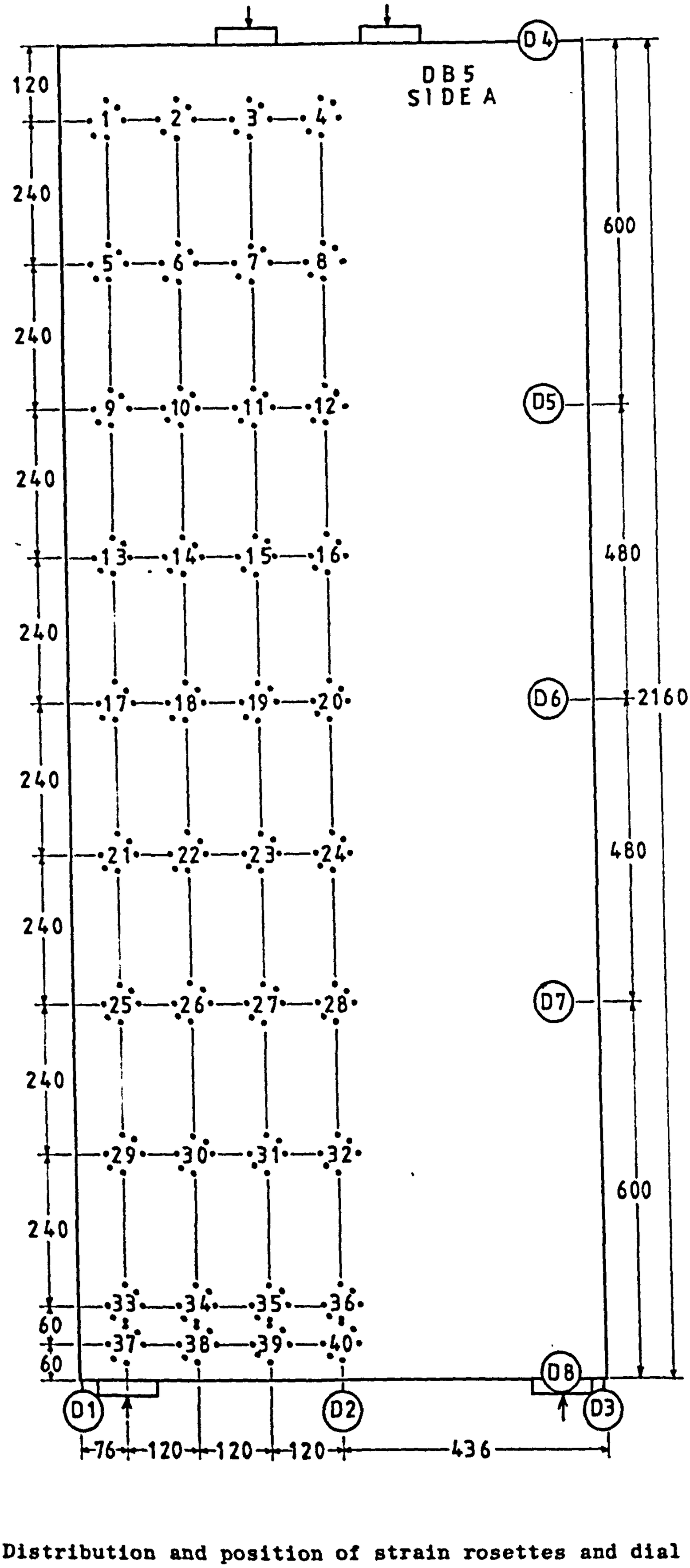

Fig. 3.17 Distribution and position of strain rosettes and dial gauges on specimen DB5

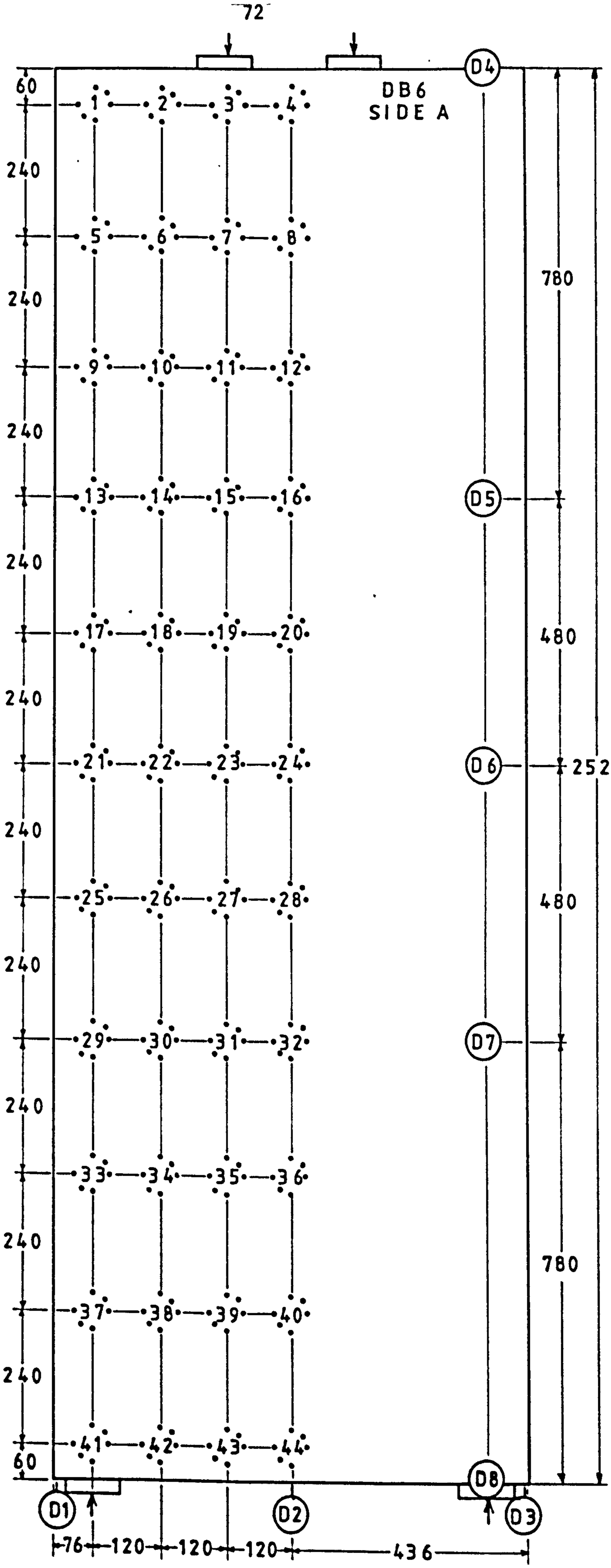

Fig. 3.18 Distribution and position of strain rosettes and dial gauges on specimen DB6

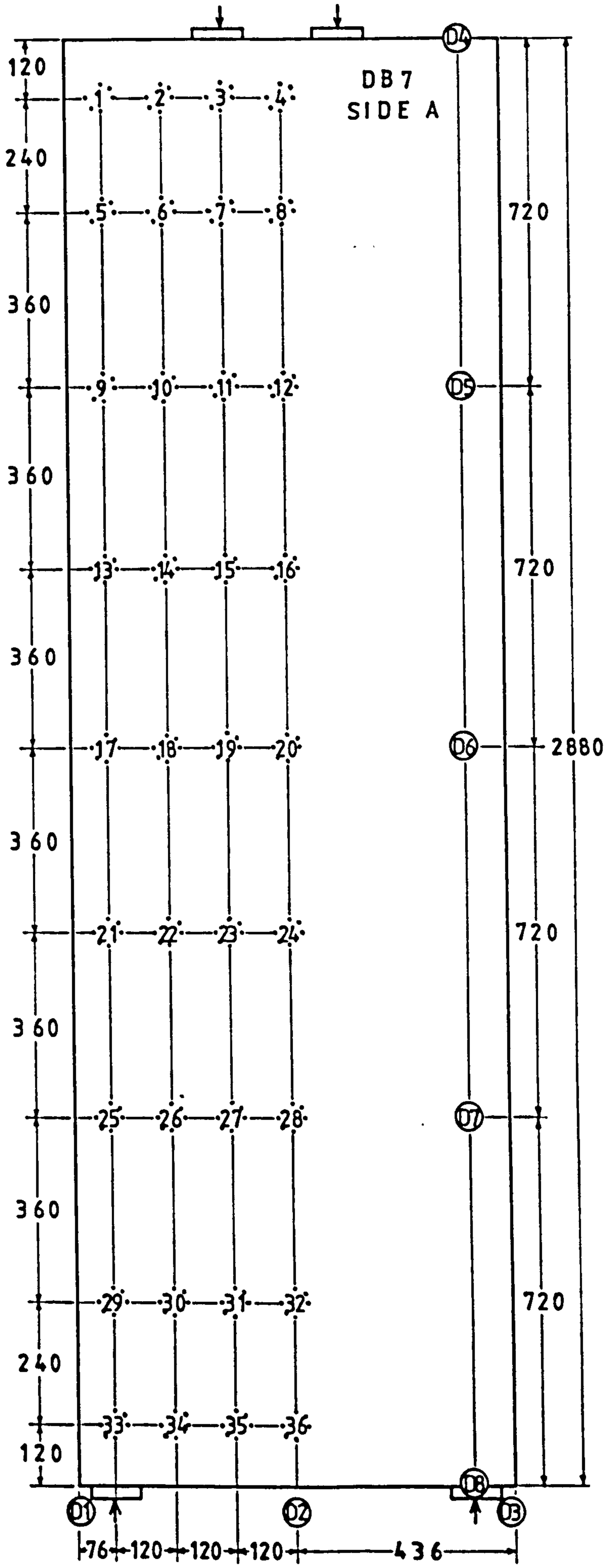

Fig. 3.19 Distribution and position of strain rosettes and dial gauges on specimen DB7

taken. At each load stage the appearance of cracks was monitored. A hand lamp and a magnifying glass were used to aid crack detection. The position and extent of each crack was marked on the surface and the load at which it occurred was written at the extremity of the crack. This procedure was repeated up to the failure load.

When failure occurred, the panel was removed and photographed to record the final crack pattern.

The control specimens were tested on the same day in which the main test took place. Each test took about eight hours.

3.8 SPECIMEN NOTATION

3.8.1 Notation of Walls

The 17 specimens tested in this series had equal geometry and main reinforcement but different vertical reinforcement. A simple code is used to identify each specimen. The first letter, W, is common to all the specimens referred to as "walls". The number which follows, 1 to 5, identifies the percentage of vertical reinforcement in the wall, corresponding to the values given in Table 3.3.

The next two characters (L1, L2, L3, L4 or L5) correspond to the loading to which the specimen was subjected.

Five different combinations of top and bottom loads were used in this experimental phase. The first load type, identified as L1, corresponds to a uniformly distributed load on top of the specimen. Load type L2 identifies the case of uniformly distributed load applied at the bottom of the specimen. Load type L3 corresponds to a combination of top and bottom-load in a ratio 1 to 1. Load type L4 represents the combination of top and bottom-loads in a ratio 2 to 1 and load type L5 identifies the combination of top and bottom loads in a

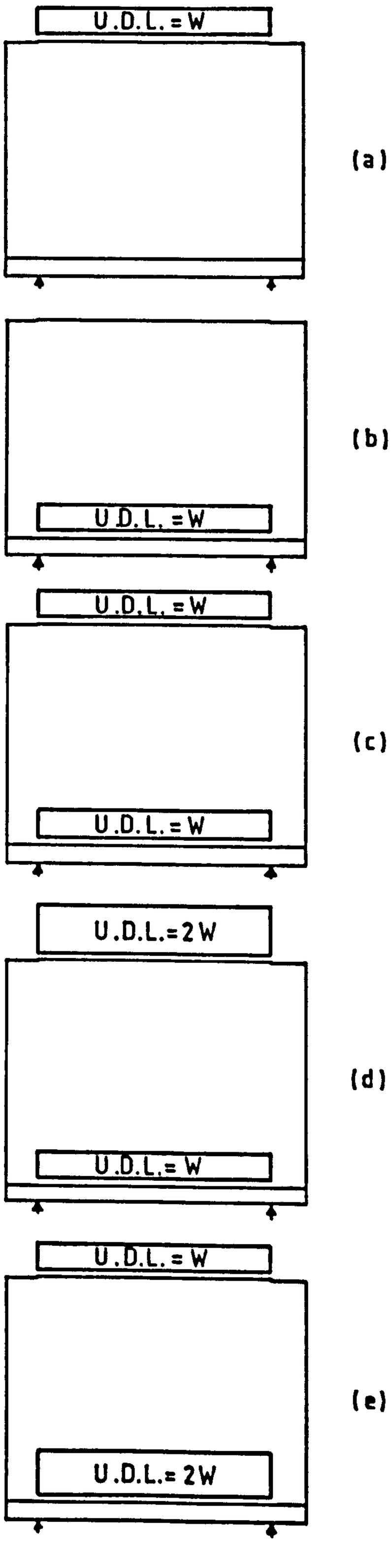

(a)

(b)

(c)

(d)

(e)

Fig. 3.20 Load types
(a) L1, (b) L2, (c) L3,
(d) L4, (e) L5.

ratio 1 to 2. Figure 3.20 shows diagramatically the load types explained above.

As an example, W1-L4 refers to a specimen with 1.06 percent of vertical reinforcement and loaded under uniformly distributed load on top and bottom in a ratio 2 to 1.

Table 3.3 Percentage of vertical reinforcement in the walls

Notation	Vertical Reinforcement Percentage
W1	1.06
W2	0.8
W3	1.4
W4	0
W5	2.0

3.8.2 Notation of Deep Panels

The 7 specimens tested had different depths. The other dimensions and characteristics were similar and the load was applied in the same manner for each one. The notation used consists of 3 characters, the last being numerical and varying from 1 to 7. Table 3.4 shows the identification for each deep panel and the corresponding depth.

As an example, DB5 identifies the deep panel which had a depth of 2160 mm.

Table 3.4 Vertical Dimensions of Deep Panels

Specimen	DB1	DB2	DB3	DB4	DB5	DB6	DB7
Depth (mm)	720	1080	1440	1800	2160	2520	2880

3.9 PROCESSING OF EXPERIMENTAL RESULTS

The experimental figures obtained from the Demec gauge readings were stored on the magnetic tape of the computer and then processed by a programme written in Fortran 10 for that purpose. This programme calculates the strain, stresses, curvatures, bending and twisting moments, and principal moments. The computer graphic facilities were used for most of the analysis and comparison of results.

3.10 EXPERIMENTAL METHOD

In order to define completely the stress field at discrete points on both faces of the concrete panel, rectangular rosettes were formed with Demec points as shown in Fig. 3.21. Each rosette consisted of 6 Demec points placed in pairs at the 0^{o}, 45^{o} and 90^{o} positions, 50 mm apart.

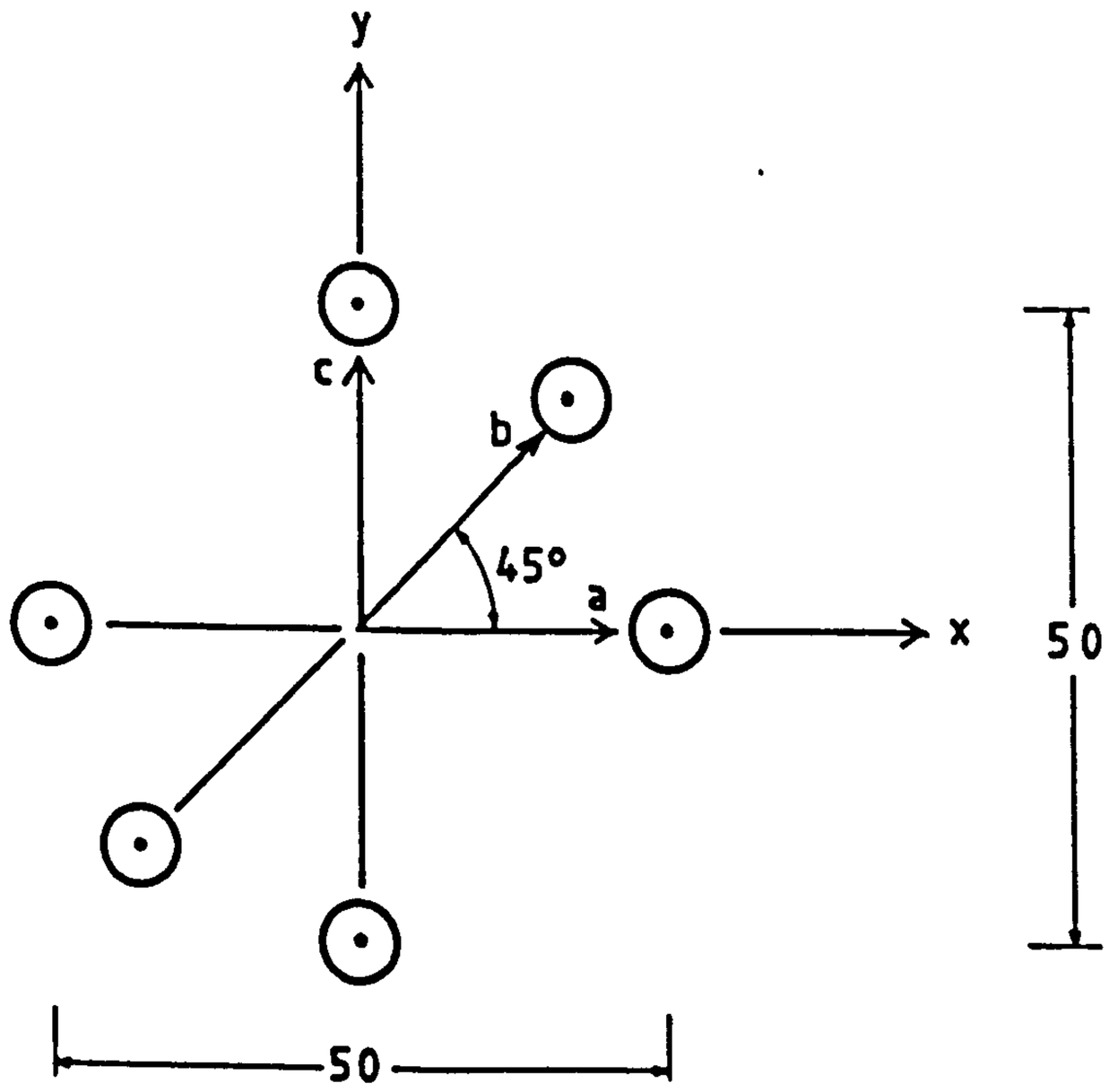

Fig. 3.21 Position of Demec-points of Rectangular rosettes

For this particular rosette, the cartesian components of strain are:

$$\varepsilon_x = \varepsilon_a \qquad \text{(a)}$$

$$\varepsilon_y = \varepsilon_c \qquad \text{(b)} \qquad 3.1$$

$$\gamma_{xy} = 2\varepsilon_b - \varepsilon_a - \varepsilon_c \qquad \text{(c)}$$

as given by Dally and Riley (1965). The corresponding linear elastic stresses on the plane of strain measurement are:

$$\sigma_x = \frac{E}{1-\nu^2}(\varepsilon_x + \nu\varepsilon_y) \qquad \text{(a)}$$

$$\sigma_y = \frac{E}{1-\nu^2}(\varepsilon_y + \nu\varepsilon_x) \qquad \text{(b)} \qquad 3.2$$

$$\tau_{xy} = \frac{E}{2(1+\nu)}\gamma_{xy} \qquad \text{(c)}$$

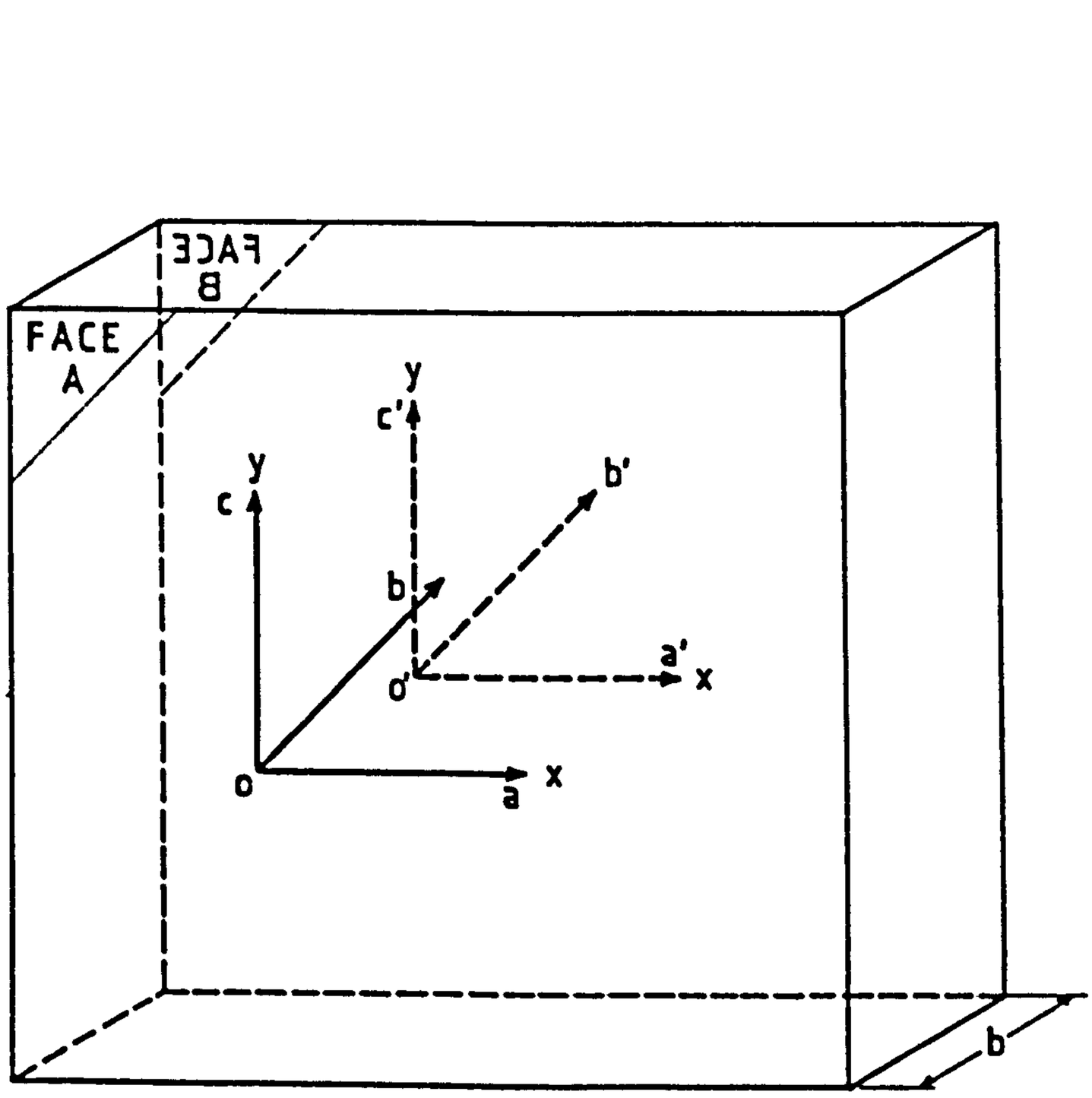

Fig. 3.22 Direction of strains measured at both faces of panel

3.10.1 Derivation of Curvatures

Assuming that the distribution of strains across any section of a thin panel is linear, the curvature at that section and at any direction is given by:

$$\frac{1}{R} = \frac{\varepsilon_B - \varepsilon_A}{b} \qquad 3.3$$

where ε_A = strain measured on side A,

ε_B = strain measured on side B

and b = thickness of the panel as shown in Fig. 3.22.

Applying equation 3.3, the curvatures in the three directions shown are:

$$\frac{1}{R_a} = \frac{1}{R_{oa}} = \frac{\varepsilon_{oa'} - \varepsilon_{oa}}{t} \qquad \text{(a)}$$

$$\frac{1}{R_b} = \frac{1}{R_{ob}} = \frac{\varepsilon_{ob'} - \varepsilon_{ob}}{t} \qquad \text{(b)} \qquad 3.4$$

$$\frac{1}{R_c} = \frac{1}{R_{oc}} = \frac{\varepsilon_{oc'} - \varepsilon_{oc}}{t} \qquad \text{(c)}$$

Knowing the curvatures in three directions, the curvature parallel to the planes O_x and O_y and the twist with respect to the x and y axes are given by:

$$\frac{1}{R_x} = \frac{1}{R_a} \qquad \text{(a)}$$

$$\frac{1}{R_y} = \frac{1}{R_c} \qquad \text{(b)} \qquad 3.5$$

$$\frac{1}{R_{xy}} = \left(2\,\frac{1}{R_b} - \frac{1}{R_a} - \frac{1}{R_c}\right)\left(\frac{1}{2}\right) \qquad \text{(c)}$$

3.10.2 Derivation of Bending Moments

Using the curvature at any point of a prismatic member, the bending moment at that section is given by:

$$M = \frac{1}{R} EI \qquad (a)$$

or

$$M = \frac{\varepsilon_B - \varepsilon_A}{t} EI \qquad (b) \qquad 3.6$$

where EI is the flexural rigidity.

Equations 3.6 are valid for the case of a prismatic member, in which the effects of transverse moments are neglected or do not exist.

Considering the effect of Poisson's ratio, the bending and twisting moments in a non-prismatic member are expressed by Timoshenko and Woinowsky-Krieger (1959) as follows:

$$M_x = D \left(\frac{1}{R_x} + \nu \frac{1}{R_y}\right) \qquad (a)$$

$$M_y = D \left(\frac{1}{R_y} + \nu \frac{1}{R_x}\right) \qquad (b) \qquad 3.7$$

$$M_{xy} = D (1 - \nu) \frac{1}{R_{xy}} \qquad (c)$$

where $D = \dfrac{Et^3}{12(1-\nu^2)}$

CHAPTER 4

EXPERIMENTAL RESULTS FOR WALLS

4.1 GENERAL

In this chapter, results concerned with crack patterns, crack widths and in-plane displacements of the wall specimens will be presented and discussed. These results will be presented in groups, based on the five types of loading as described in section 3.8.2.

4.2 CRACK PATTERNS

4.2.1. Crack Patterns of Walls Loaded on Top (L1)

Despite differences in the vertical web reinforcement, the crack patterns were similar for walls W1, W2, and W3 when loaded on top. In general, the first cracks to appear were small flexural cracks within the depth of the nib. These did not propagate to a large extent with increased load. The next cracks to form were diagonal cracks, initiating near the supports and above the nib, spreading rapidly upwards and towards the middle of the wall. At higher loads, these cracks lengthened and new cracks were formed near the supports, propagating parallel or at wider angle than the previous cracks. Finally, the failure of the specimens was brought about by crushing of the concrete at the support points.

The development of cracks in wall W1-L1 can be followed in Figure 4.1. Up to a load of 500 kN (Fig. 4.1(a)) the few cracks detected were flexural cracks within the depth of the nib. The largest cracks were those above the support lines, created by the negative moment in this area. They began on the top of the nib and then extended downwards. The first diagonal cracks were detected under a load of 600 kN (Fig. 4.1(b)) forming an angle of about 67^{o} with the horizontal and extending to a

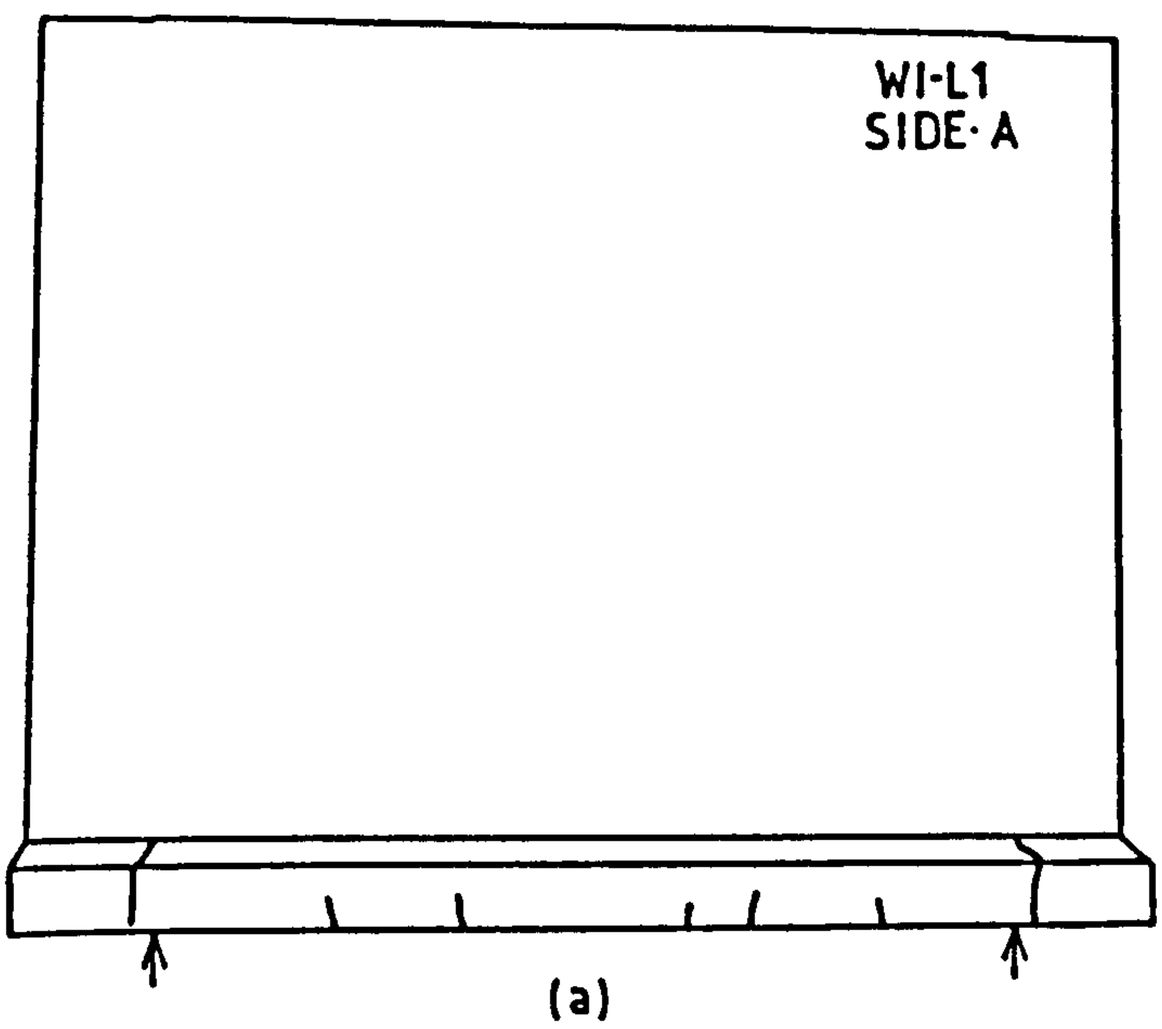

(a)

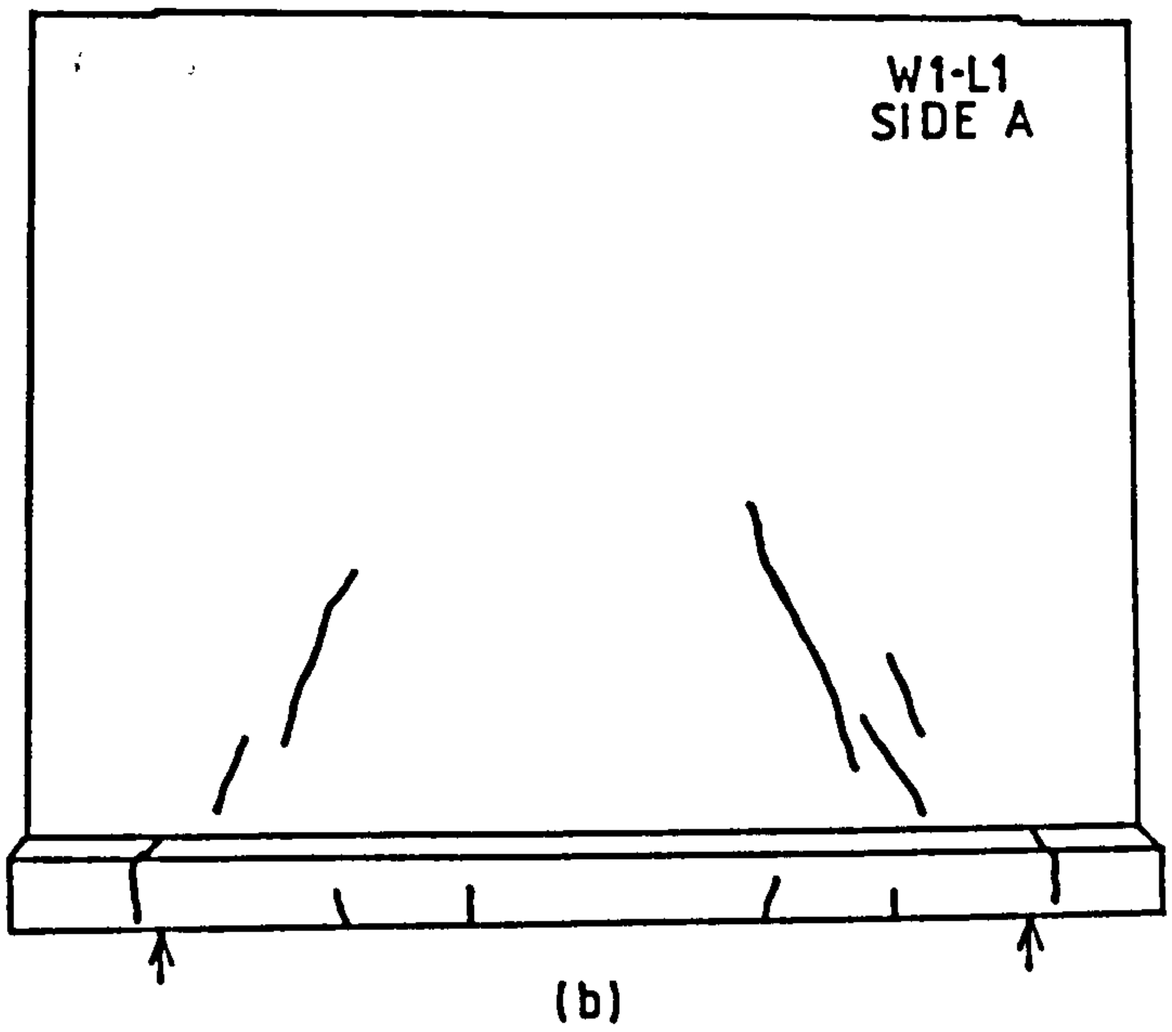

(b)

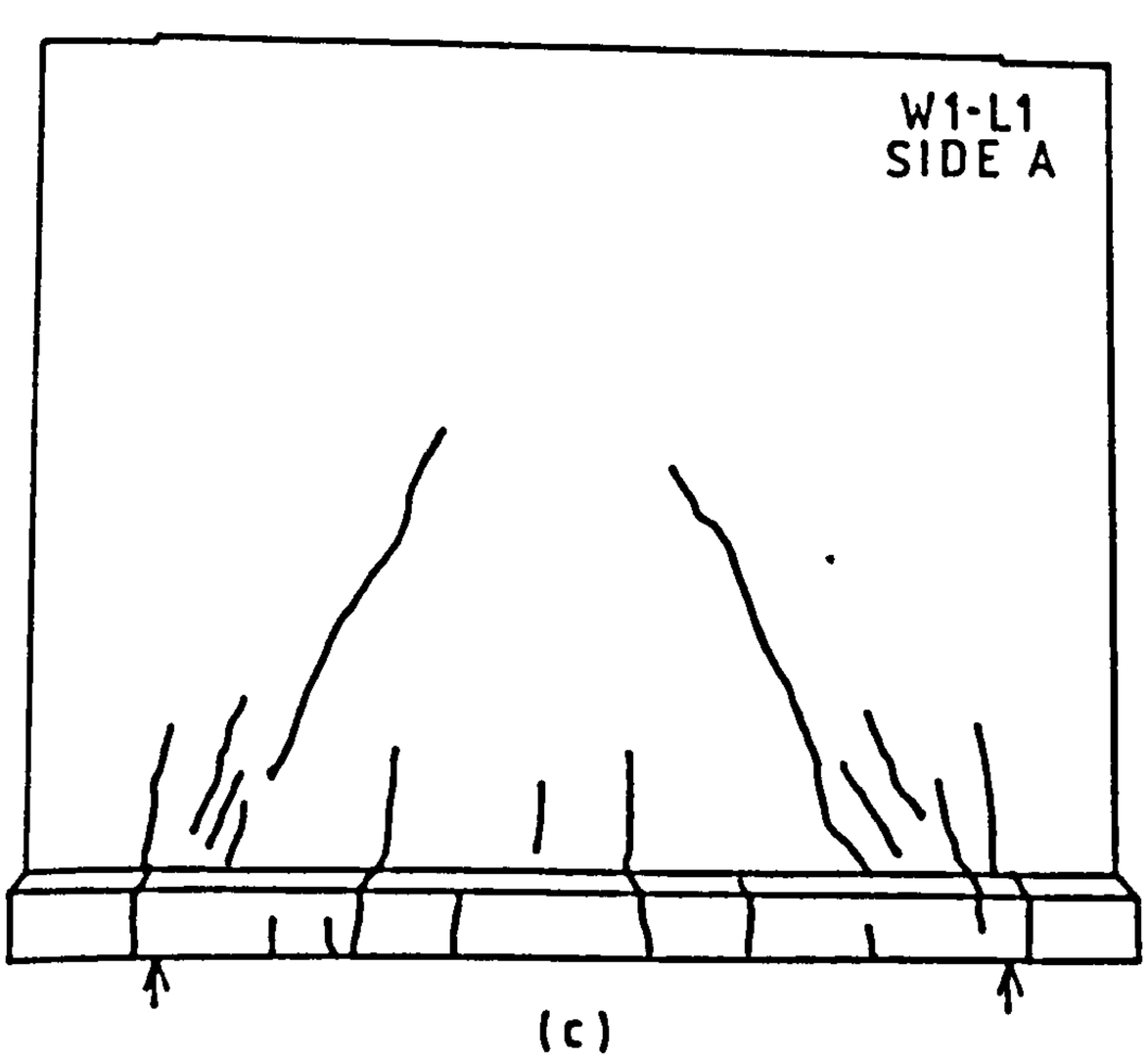

(c)

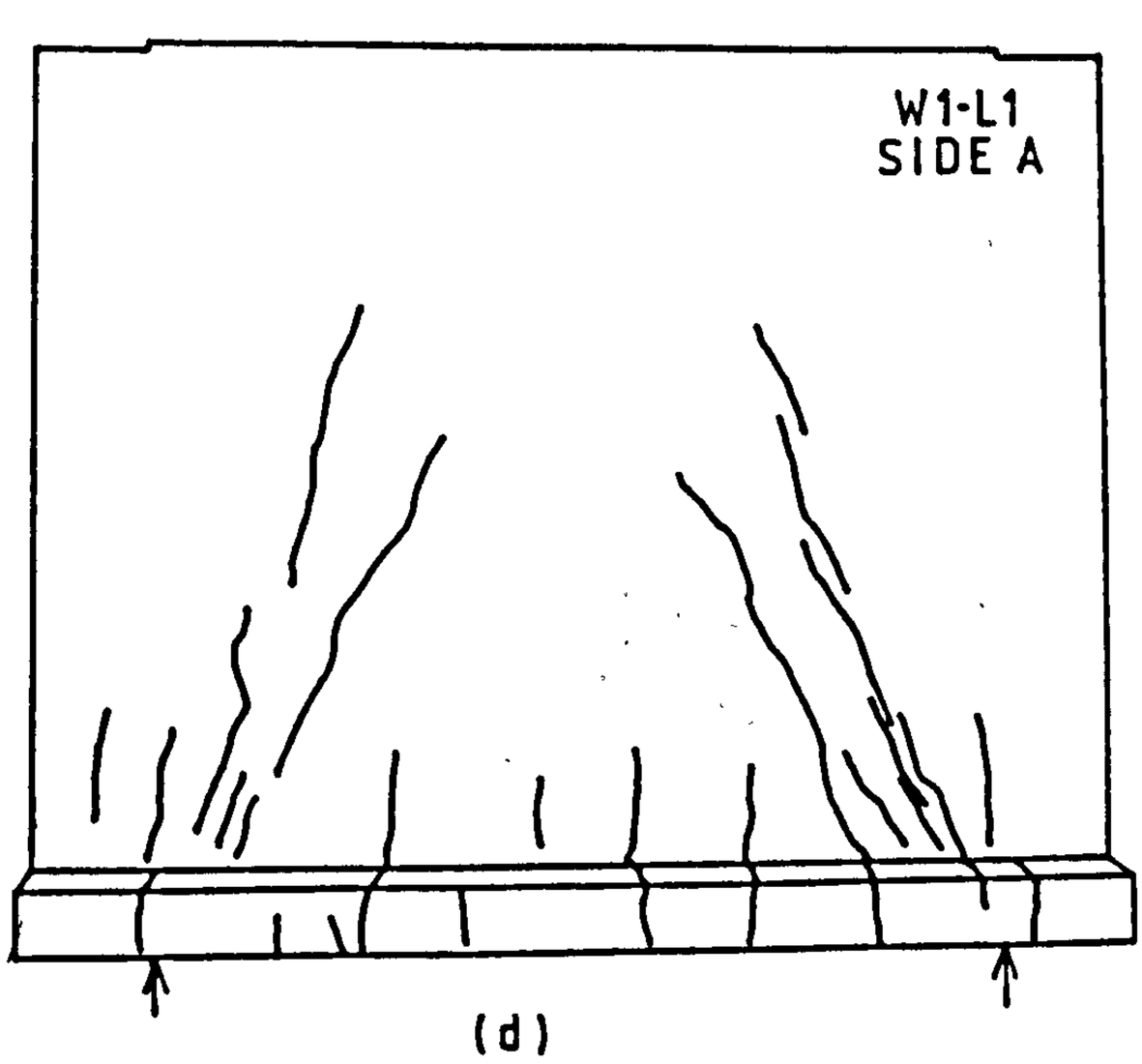

(d)

Fig. 4.1 Development of cracks in wall W1-L1

(a) Crack pattern at a load of 500 kN
(b) Crack pattern at a load of 600 kN
(c) Crack pattern at a load of 750 kN
(d) Crack pattern at a load of 950 kN

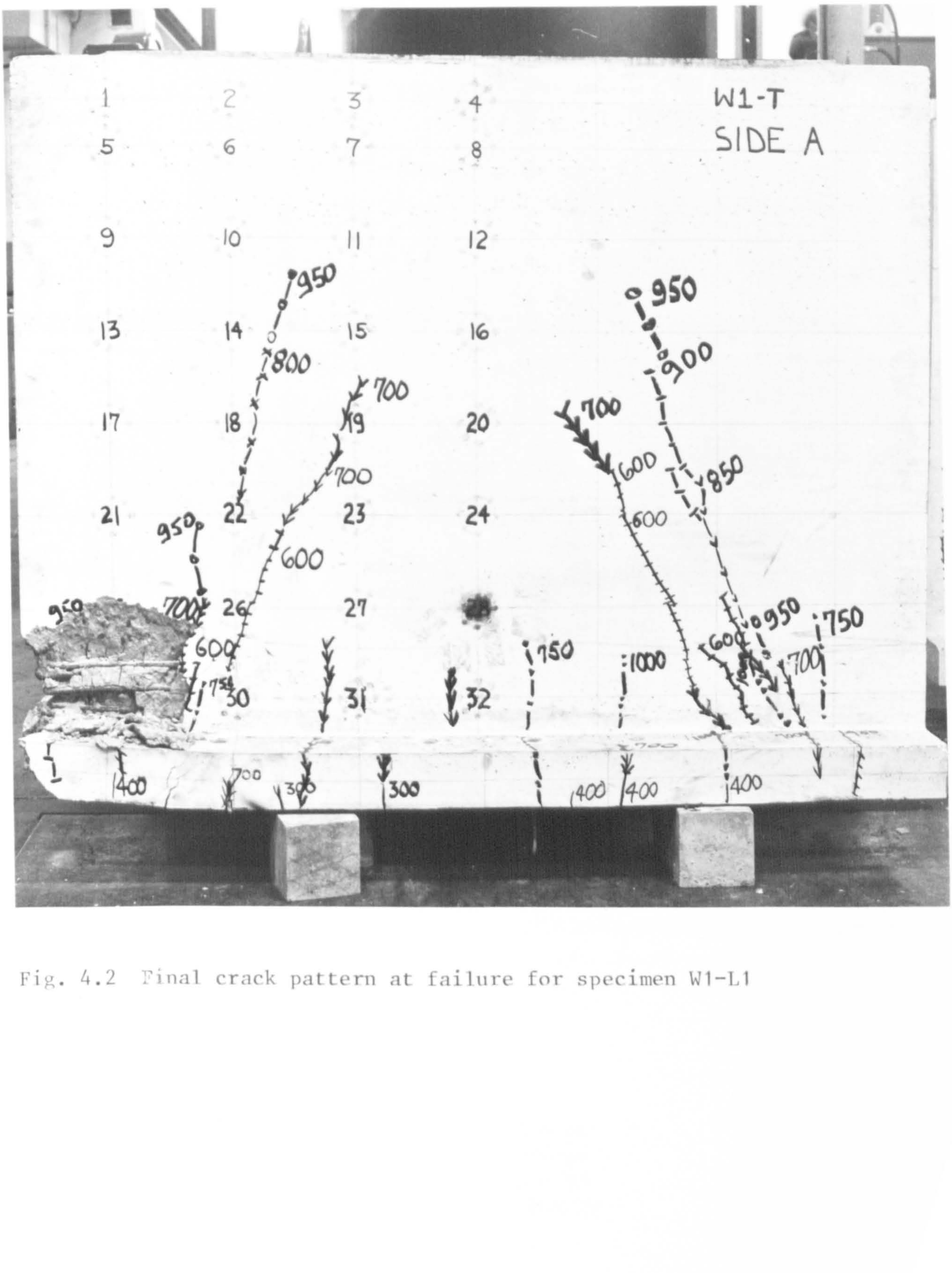

Fig. 4.2 Final crack pattern at failure for specimen W1-L1

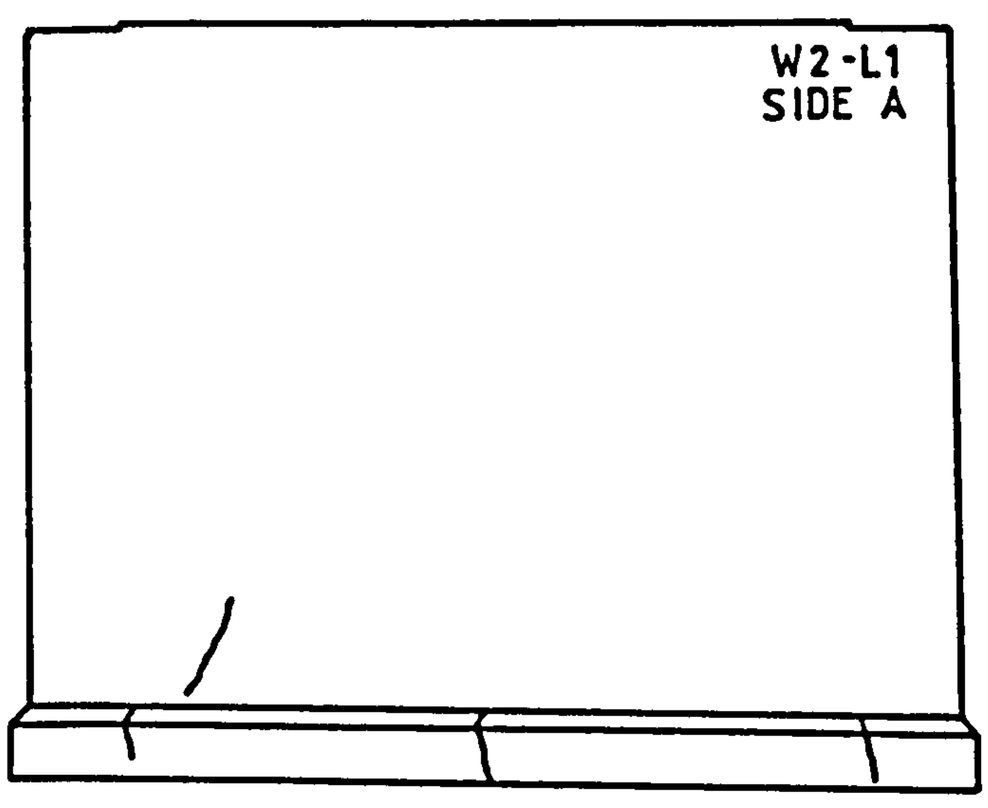

(a)

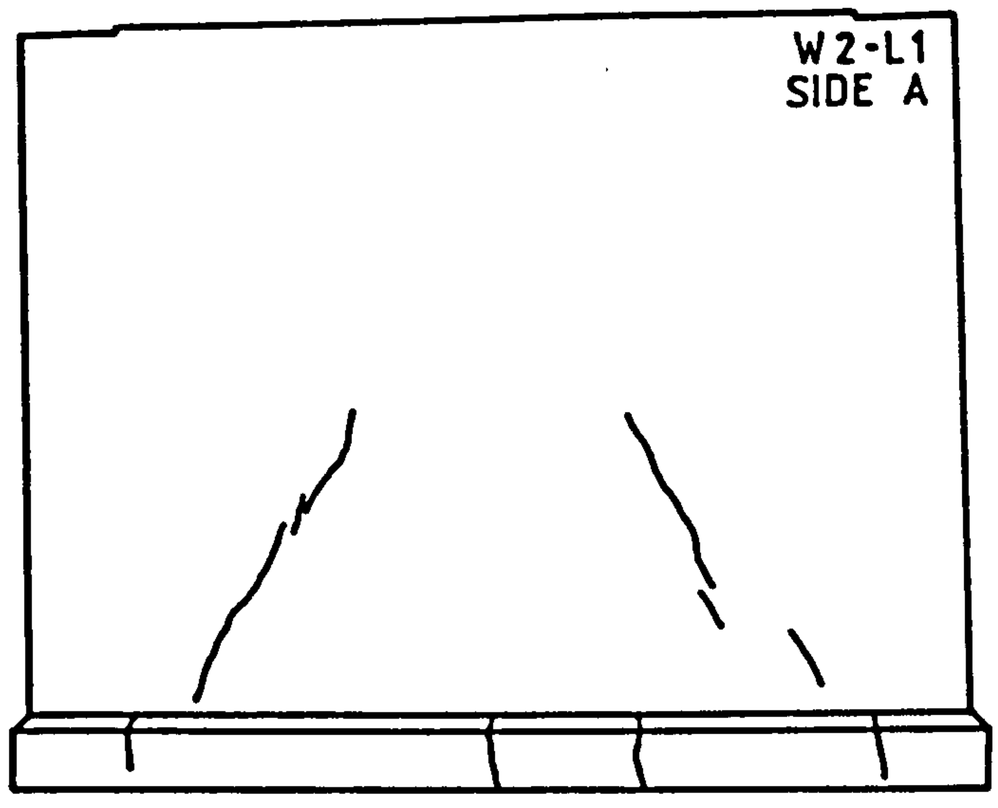

(b)

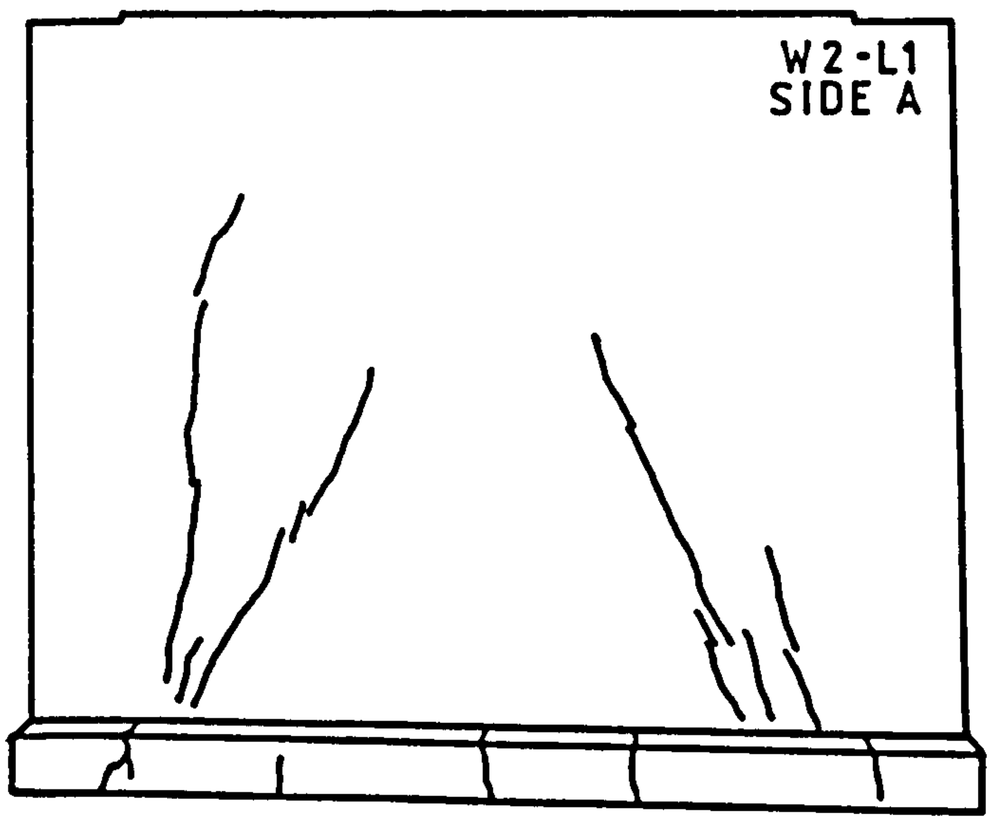

(c)

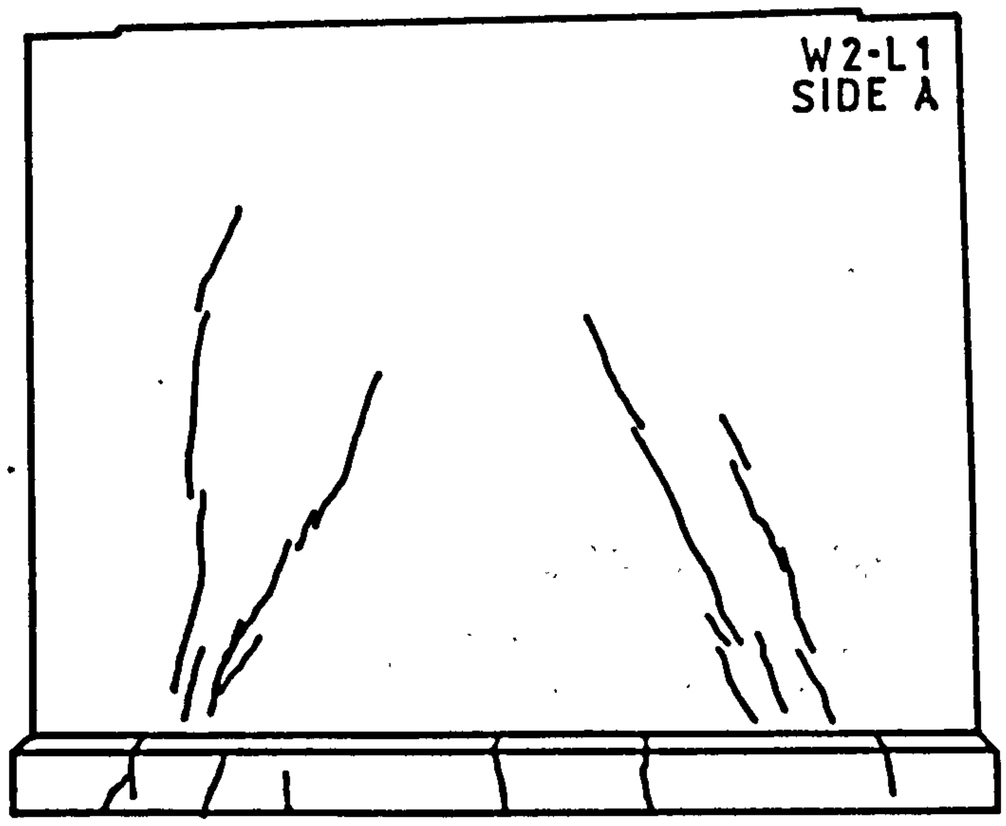

(d)

Fig. 4.3 Development of cracks in Wall W2-L1

(a) Crack pattern at a load of 500 kN
(b) Crack pattern at a load of 700 kN
(c) Crack pattern at a load of 900 kN
(d) Crack pattern at a load of 1000 kN

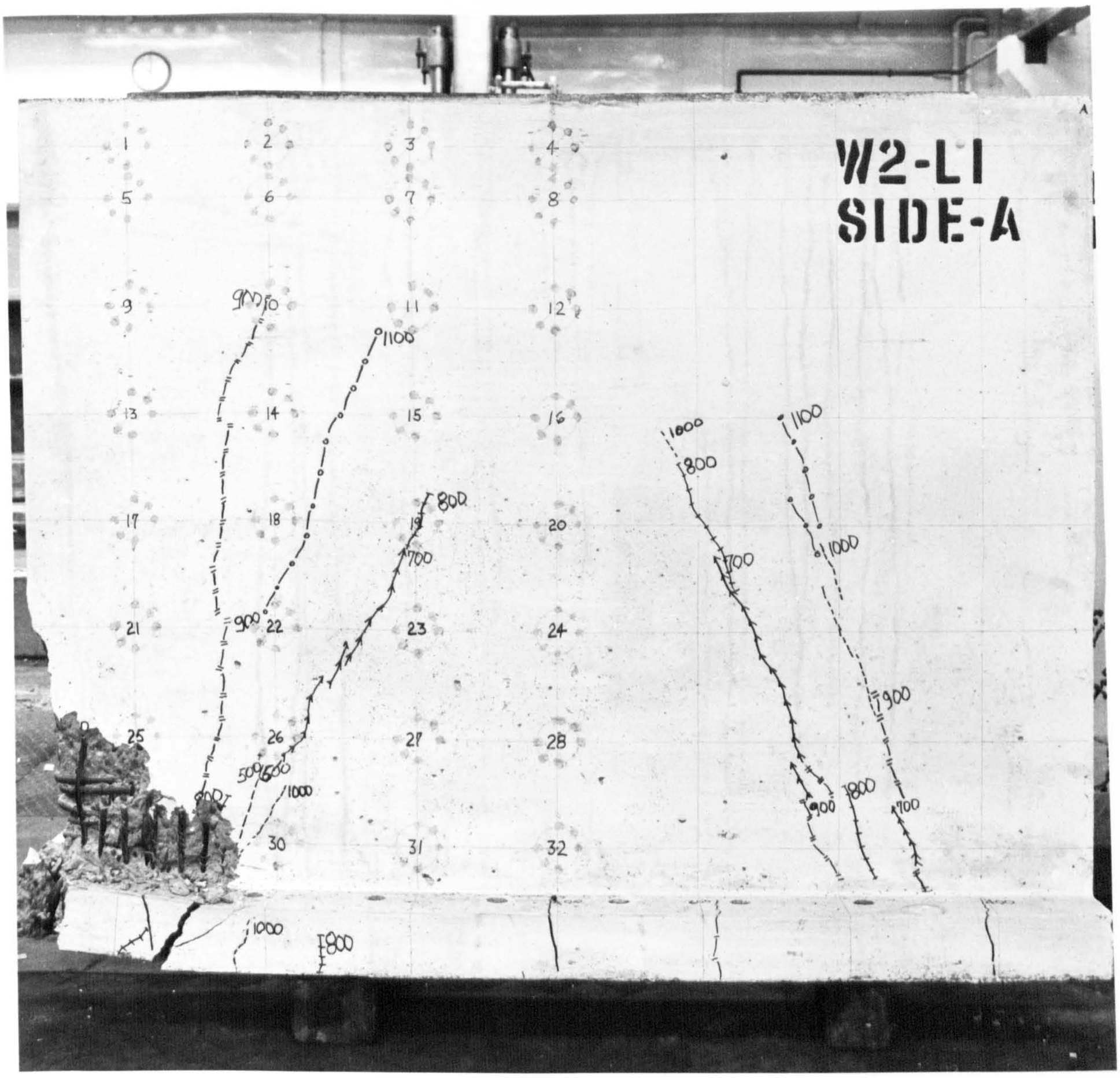

Fig. 4.4 Final crack pattern at failure for specimen W2-L1

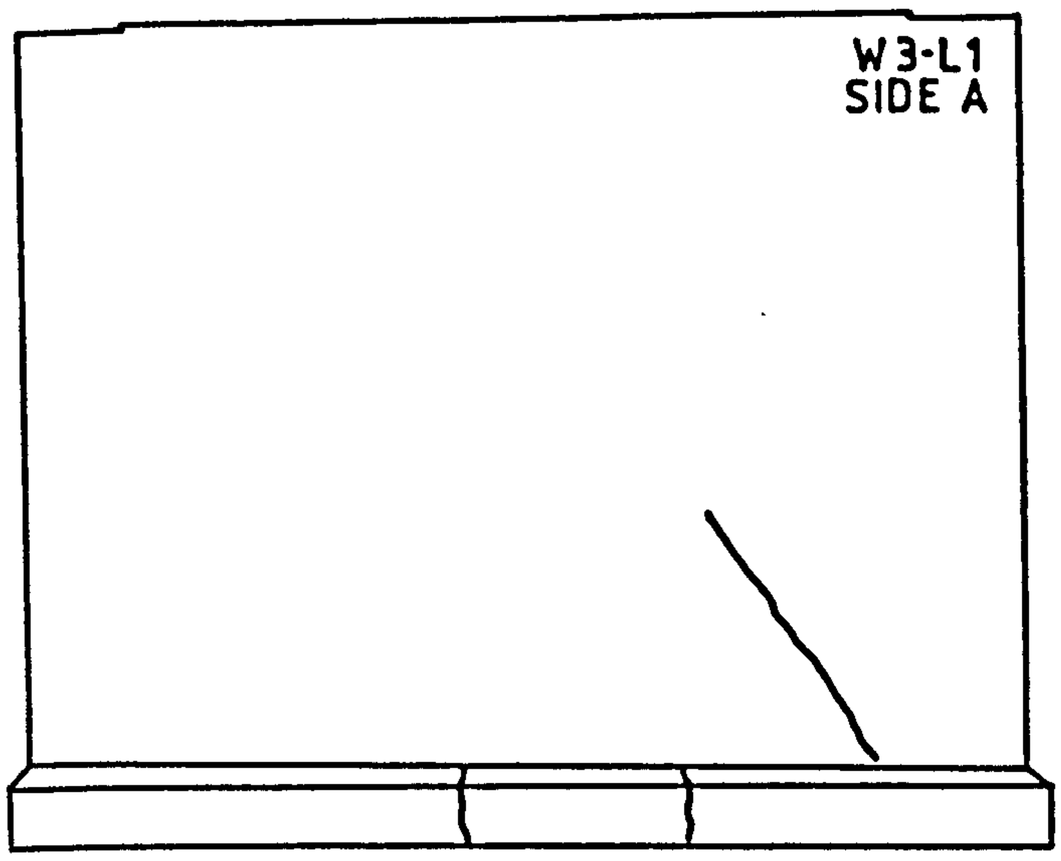

(a)

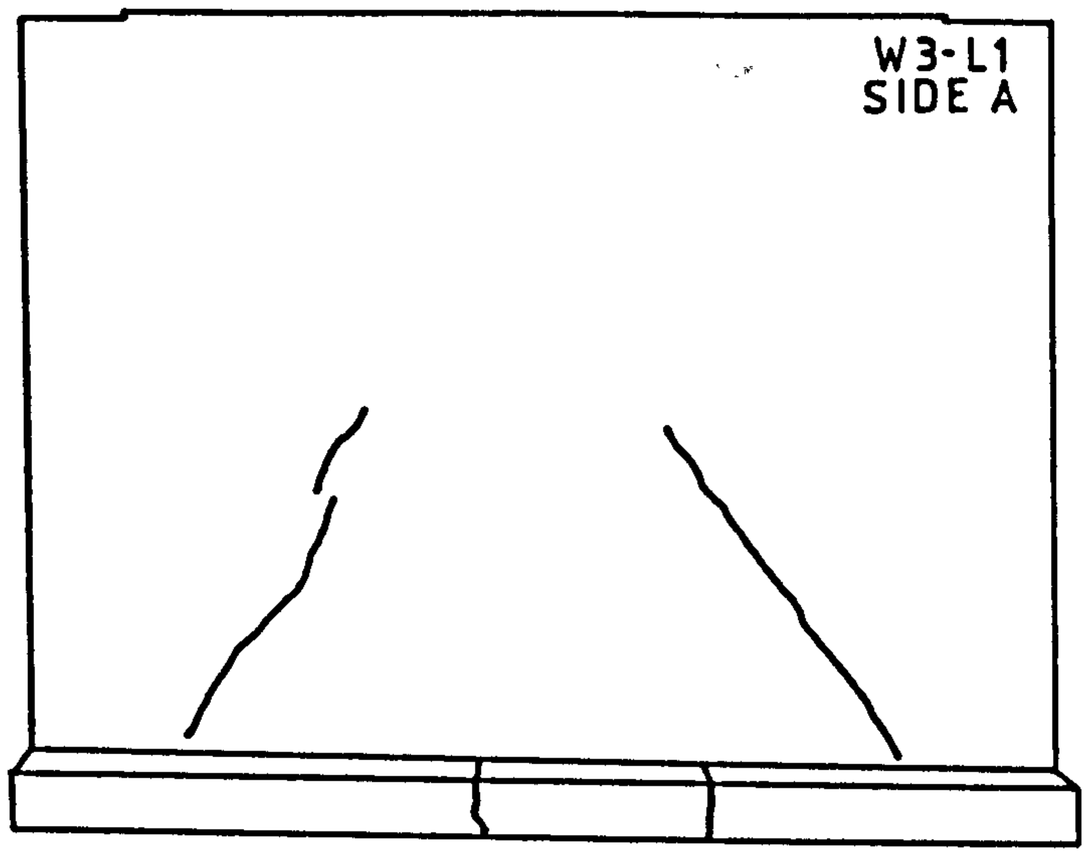

(b)

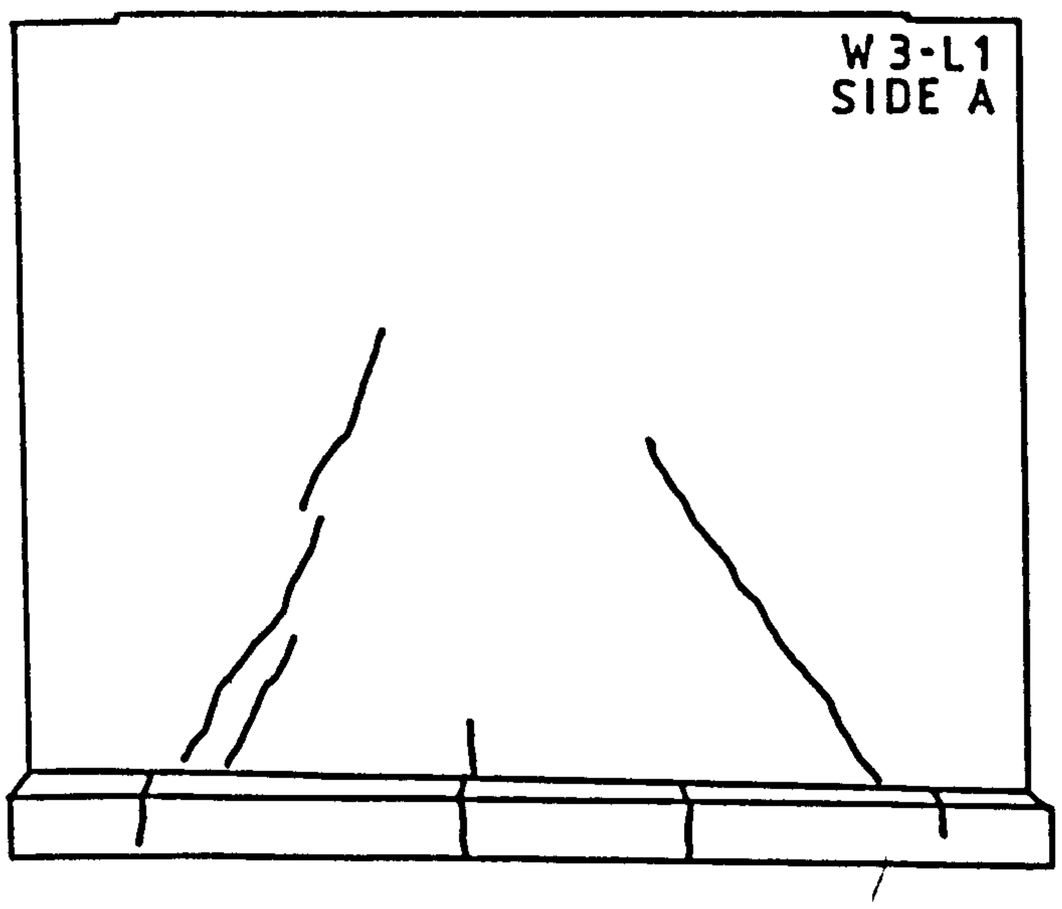

(c)

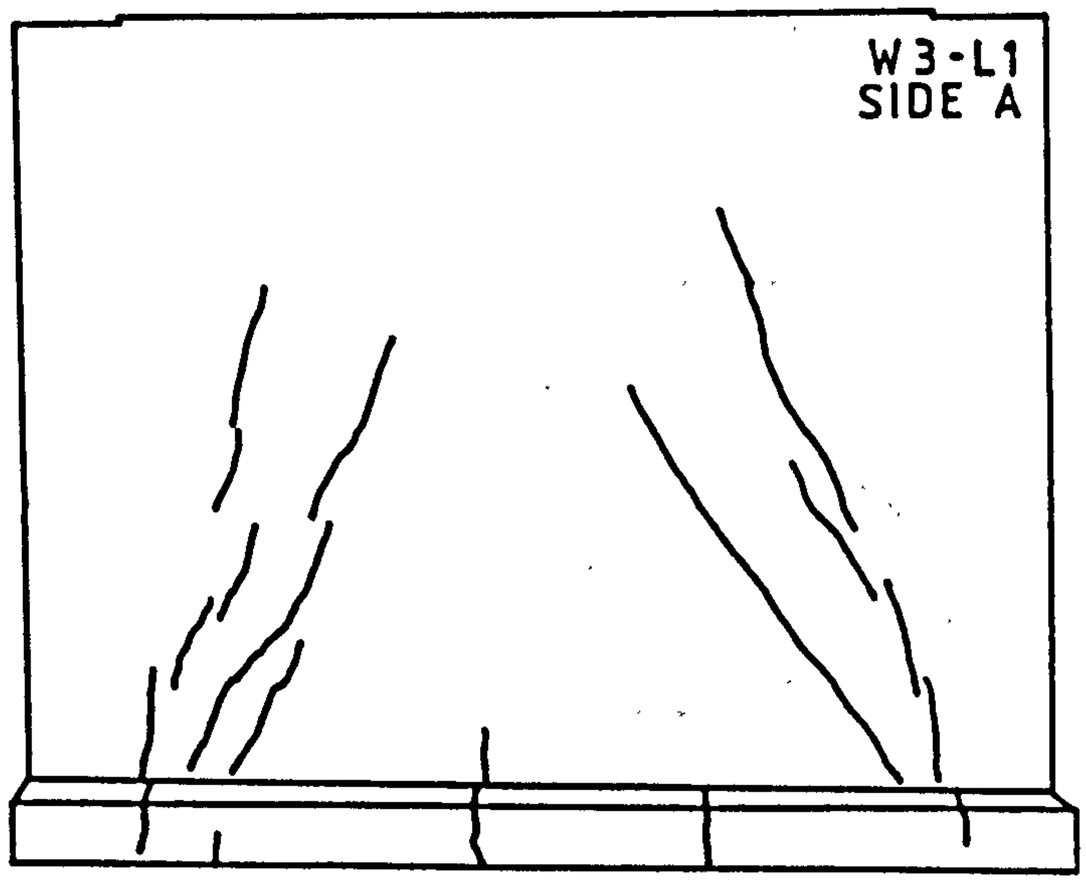

(d)

Fig. 4.5 Development of cracks in wall W3-L1

(a) Crack pattern at a load of 600 kN
(b) Crack pattern at a load of 700 kN
(c) Crack pattern at a load of 800 kN
(d) Crack pattern at a load of 1000 kN

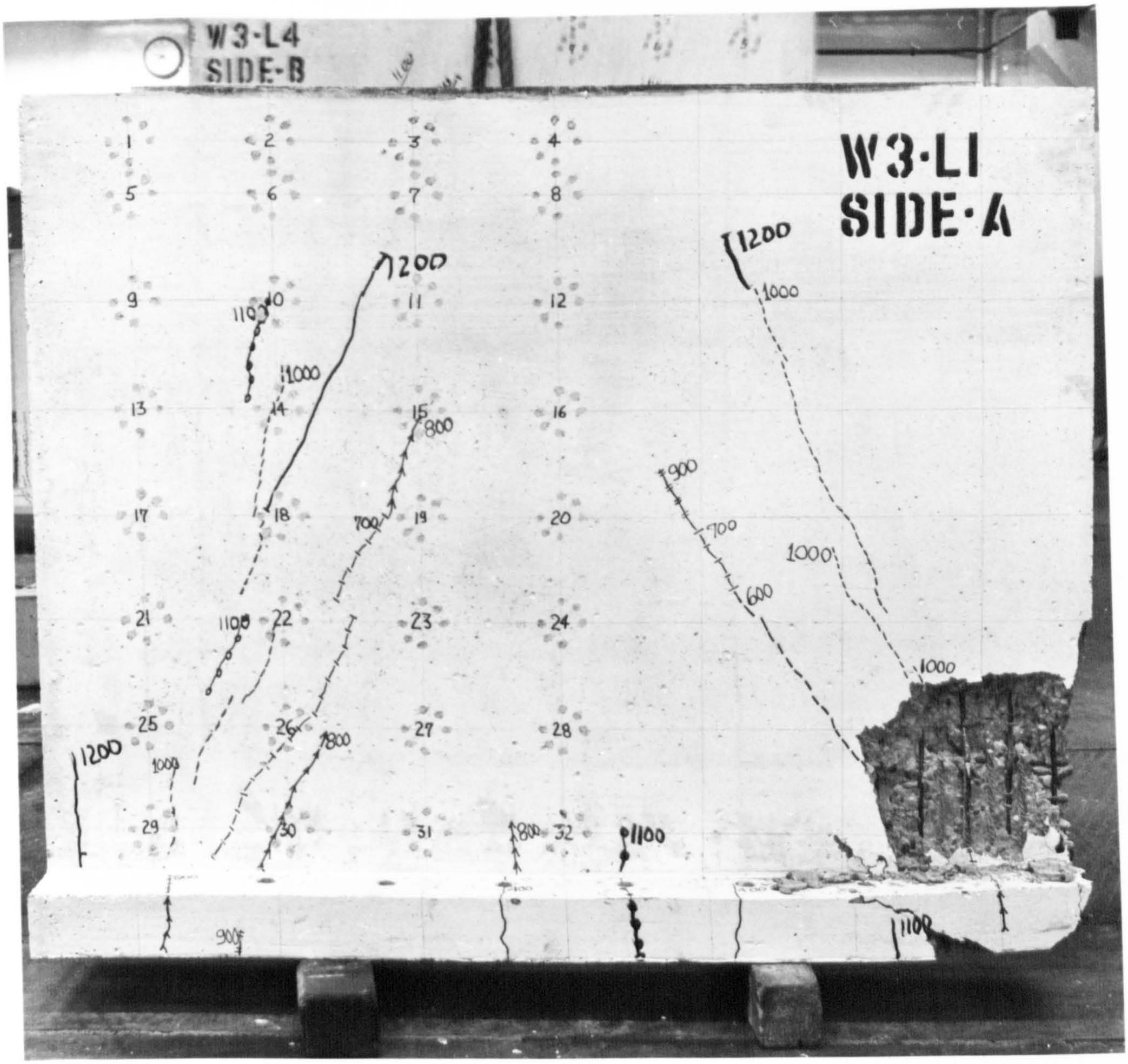

Fig. 4.6 Final crack pattern at failure for specimen W3-L1

height of 450 mm. At 750 kN (Fig. 4.1(c)) the diagonal cracks spread to a height of about 550 mm and new small cracks were detected in the region above the supports. At 950 kN (Fig. 4.1(d)) extensive new diagonal cracks had spread at an angle of about 72° with the horizontal and outside the first diagonal cracks, reaching a height of 700 mm. Finally, Fig. 4.2 shows the pattern of cracking of wall W1-L1 after failure at a load of 1100 kN.

The development of cracks in walls W2-L1 and W3-L1 was similar to that described for specimen W1-L1. Figures 4.3 and 4.4 illustrate the history of cracking for specimen W2-L1 in the same way as Figs. 4.5 and 4.6 describe that for wall W3-L1.

4.2.2 Crack Patterns of Walls Loaded on the Soffit (L2)

Crack development for walls W1, W2, W3, W4 and W5, when loaded on the soffit, was influenced largely by the percentage of vertical reinforcement present. In general, the first crack was observed at a depth of 200 mm and extended horizontally along at least the middle third of the span. With increased load, new cracks were formed above the first one, creating a series of arch-shaped cracks. The following discussion of crack development under this type of loading begins with those specimens having little or no vertical reinforcement and continues with those having a significant amount.

Wall W4-L2 was not reinforced apart from the main bending reinforcement, this being the same as the other specimens. At a load of 130 kN, the first crack was formed, accompanied by a loud noise. This horizontal crack (Fig. 4.7) found at a depth of about 200 mm propagated along the whole span. Flexural cracks were observed on the nib together with vertical cracks outside both supports. A quasi-vertical crack appeared above and outside both supports at a load of 140 kN, and diagonal

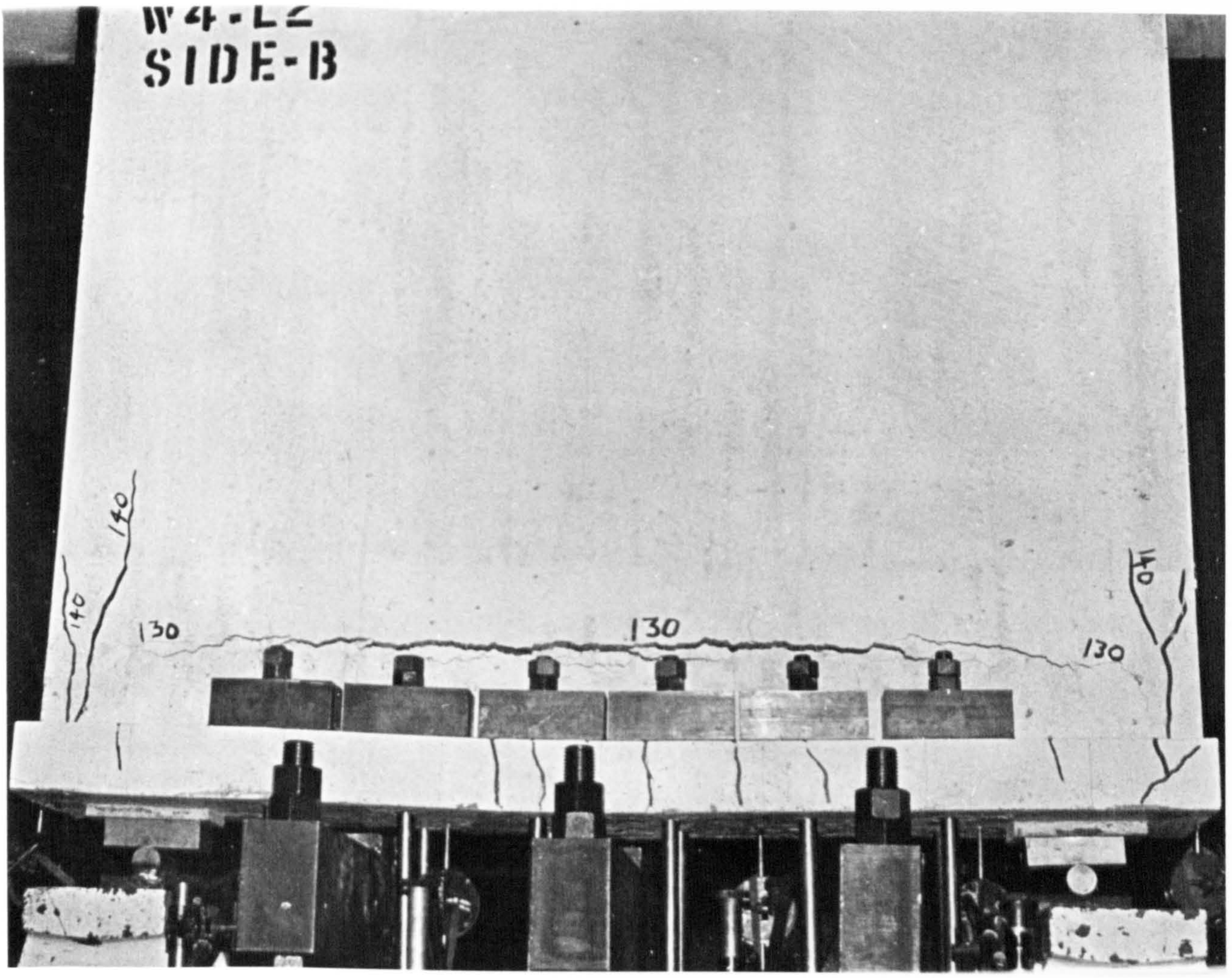

Fig. 4.7 Crack pattern at a load of 140 kN for specimen W4-L2

cracks were seen on the nib. The load was increased up to 150 kN, but no new cracks were observed. At this stage, the section under the large horizontal crack was behaving as a normal slender beam.

The first crack in specimen W2-L2 (Fig. 4.8) became visible at a load of 167 kN, was horizontal, at a height of about 200 mm, and extended over nearly the whole span. At 200 kN, only a minor flexural crack appeared on the nib. A crack creating almost a complete arch was seen at a load of 233 kN. This crack was horizontal in the middle third of the span and was formed at a height of 375 mm, 175 mm above the first crack. Additional flexural cracks were formed within the depth of the nib. Diagonal cracks were also seen on the nib, at both sides, above the support lines. When the load was increased up to 267 kN, another crack appeared at about 520 mm. At this stage of loading, extensive deflection of the bottom of the wall was taking place. No new cracks or extension of cracks were observed on the upper section of the wall at 300 kN load, except those vertical cracks on the external sides of both supports. Many new cracks appeared between the nib and the first horizontal crack formed at 167 kN, and after sustaining the load of 300 kN for a short period, large deterioration of this section was seen. Fig. 4.8 illustrates the final condition of this specimen after testing. Average spacing between cracks along the central vertical line in the wall was 174 mm.

Crack development in specimen W1-L2 is presented in Figures 4.9 and 4.10. The first horizontal and flexural cracks were noticed at a load of 167 kN (Fig. 4.9(a)); the horizontal appeared at a height of about 200 mm from the soffit and covered the whole span. At a load of 200 kN (Fig. 4.9(b)), diagonal cracks appeared between the horizontal crack formed previously and the nib. When the load was increased to 233 kN, a crack forming a complete arch was observed (Fig. 4.9(c)) having its central flat section at a height of about 310 mm from the soffit. At 267 kN load

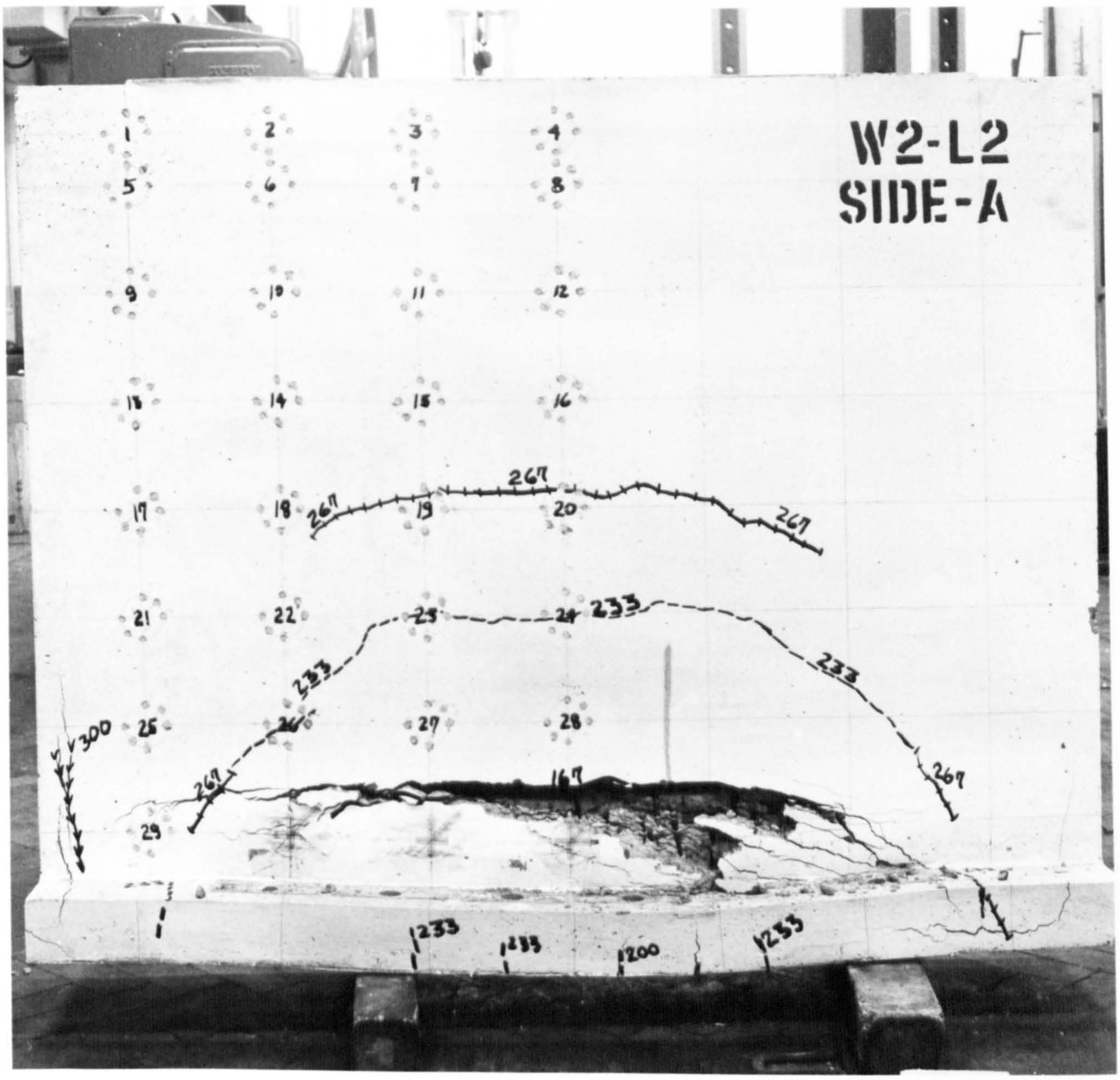

Fig. 4.8 Final crack pattern for specimen W2-L2

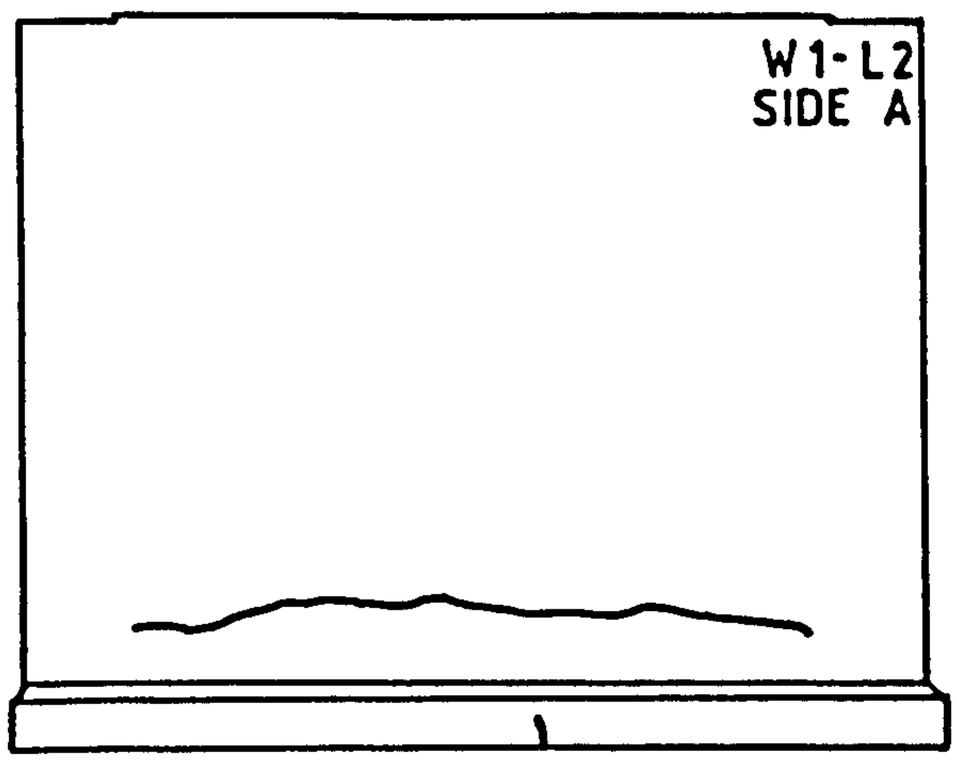

(a)

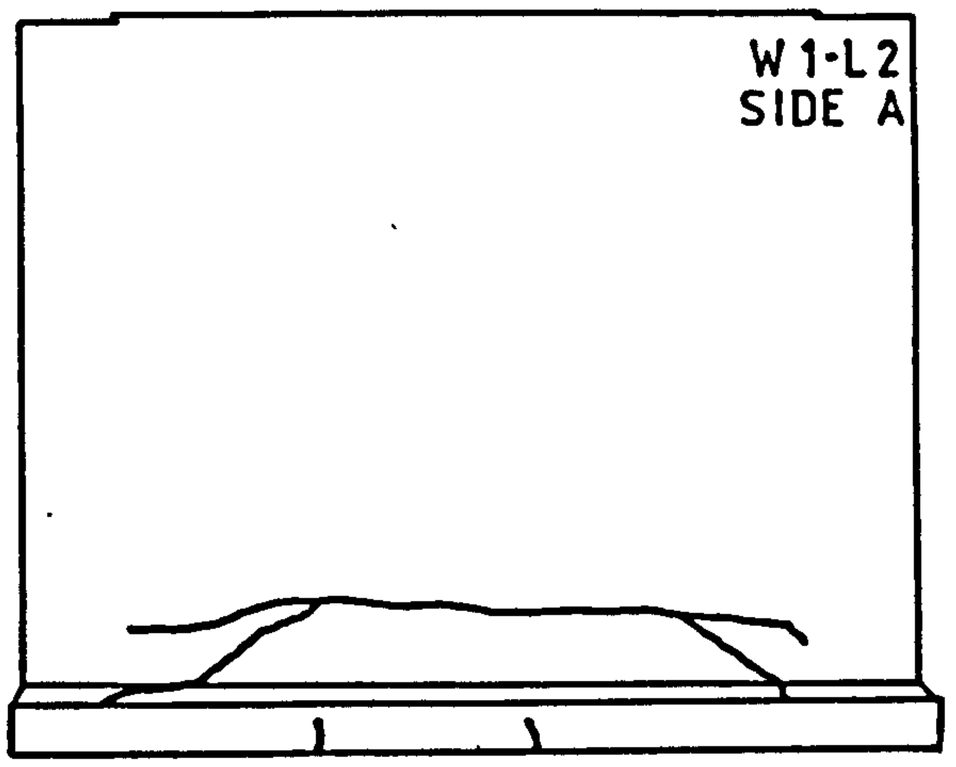

(b)

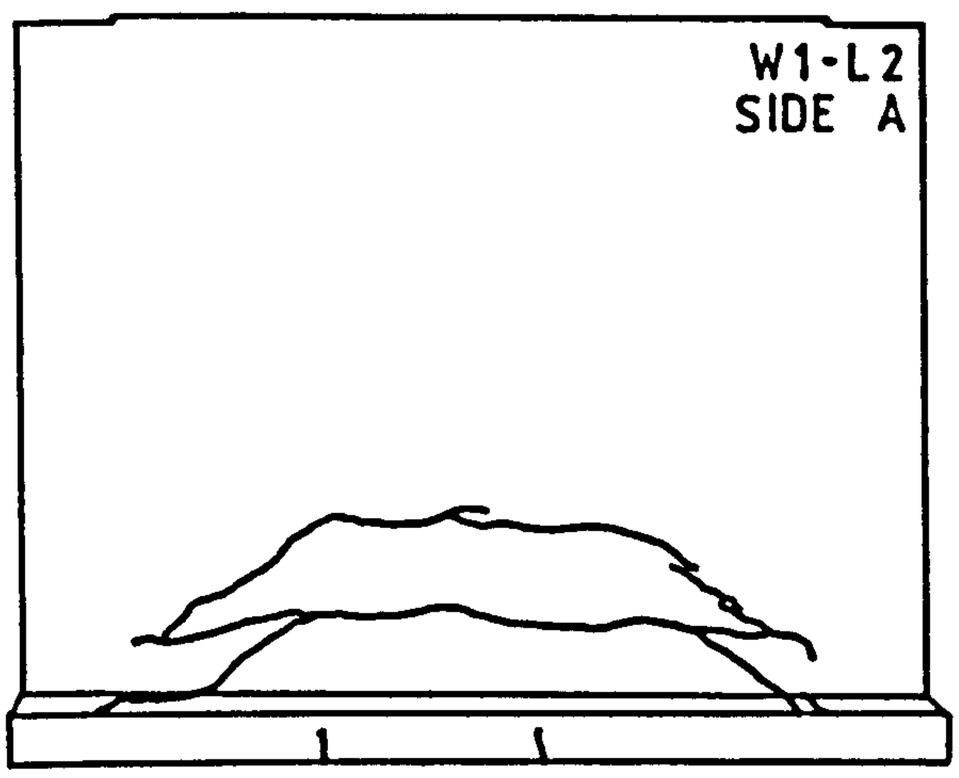

(c)

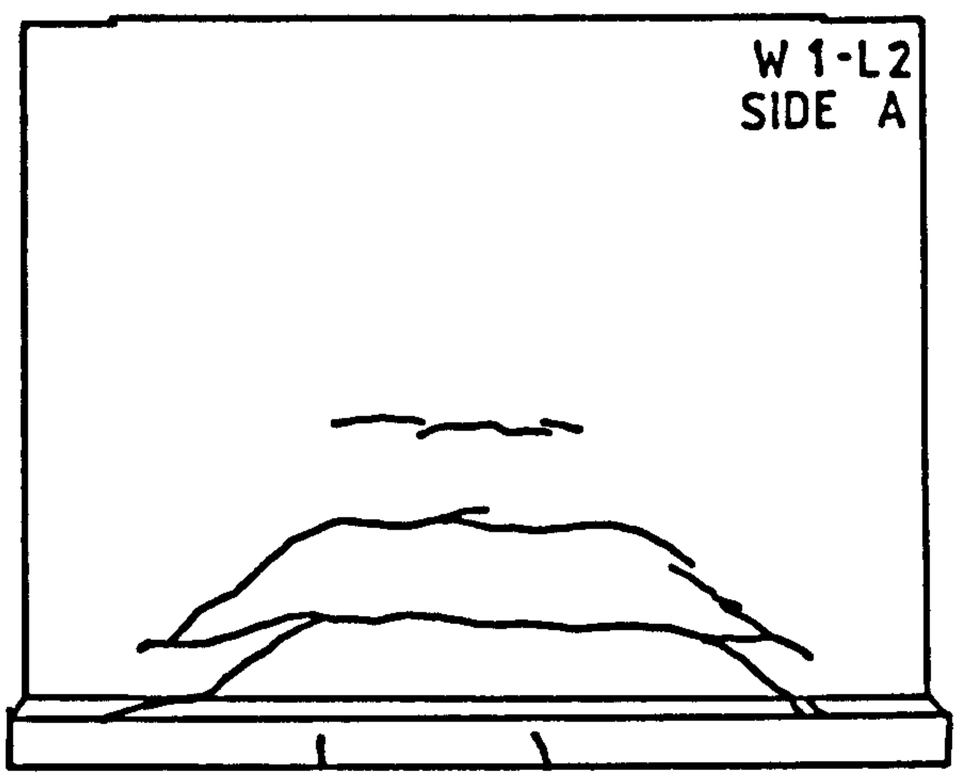

(d)

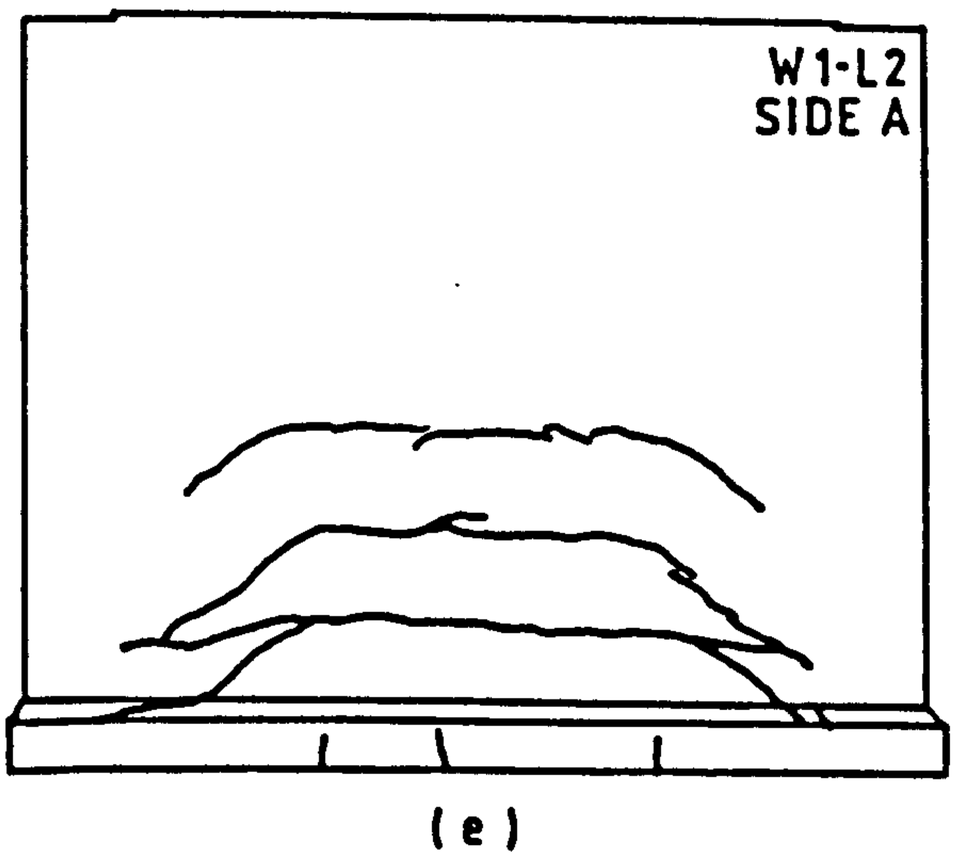

(e)

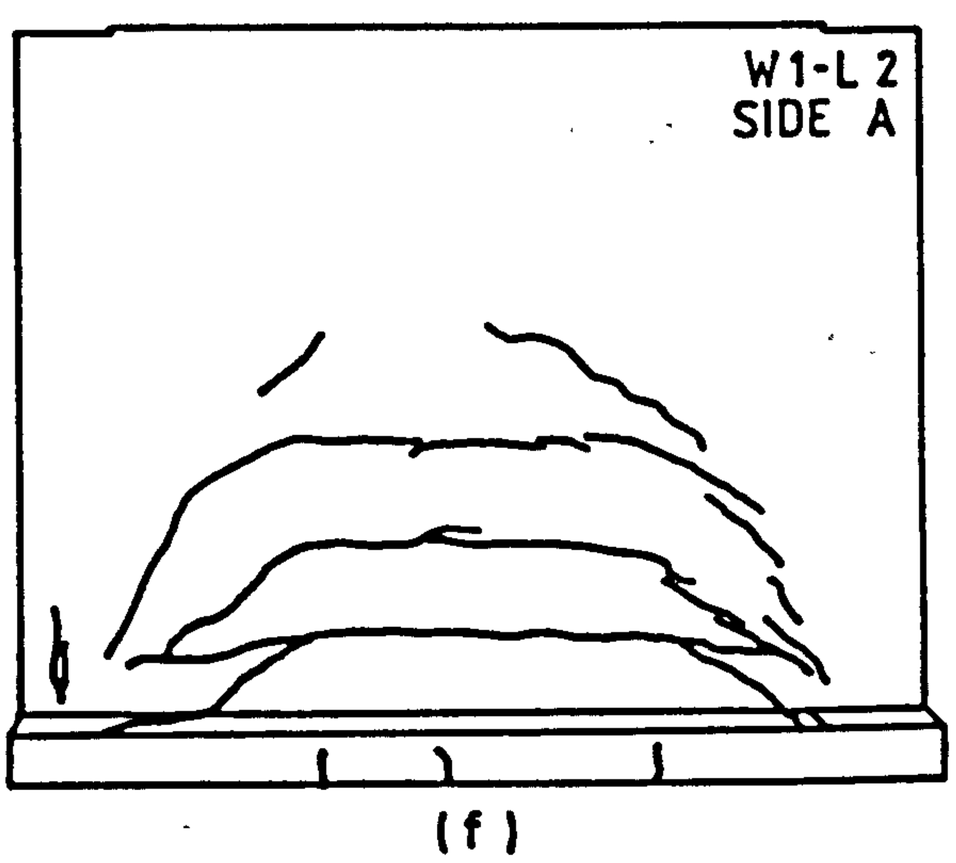

(f)

Fig. 4.9 Development of cracks in wall W1-L2

(a) Crack pattern at a load of 167 kN
(b) Crack pattern at a load of 200 kN
(c) Crack pattern at a load of 233 kN
(d) Crack pattern at a load of 267 kN
(e) Crack pattern at a load of 300 kN
(f) Crack pattern at a load of 333 kN

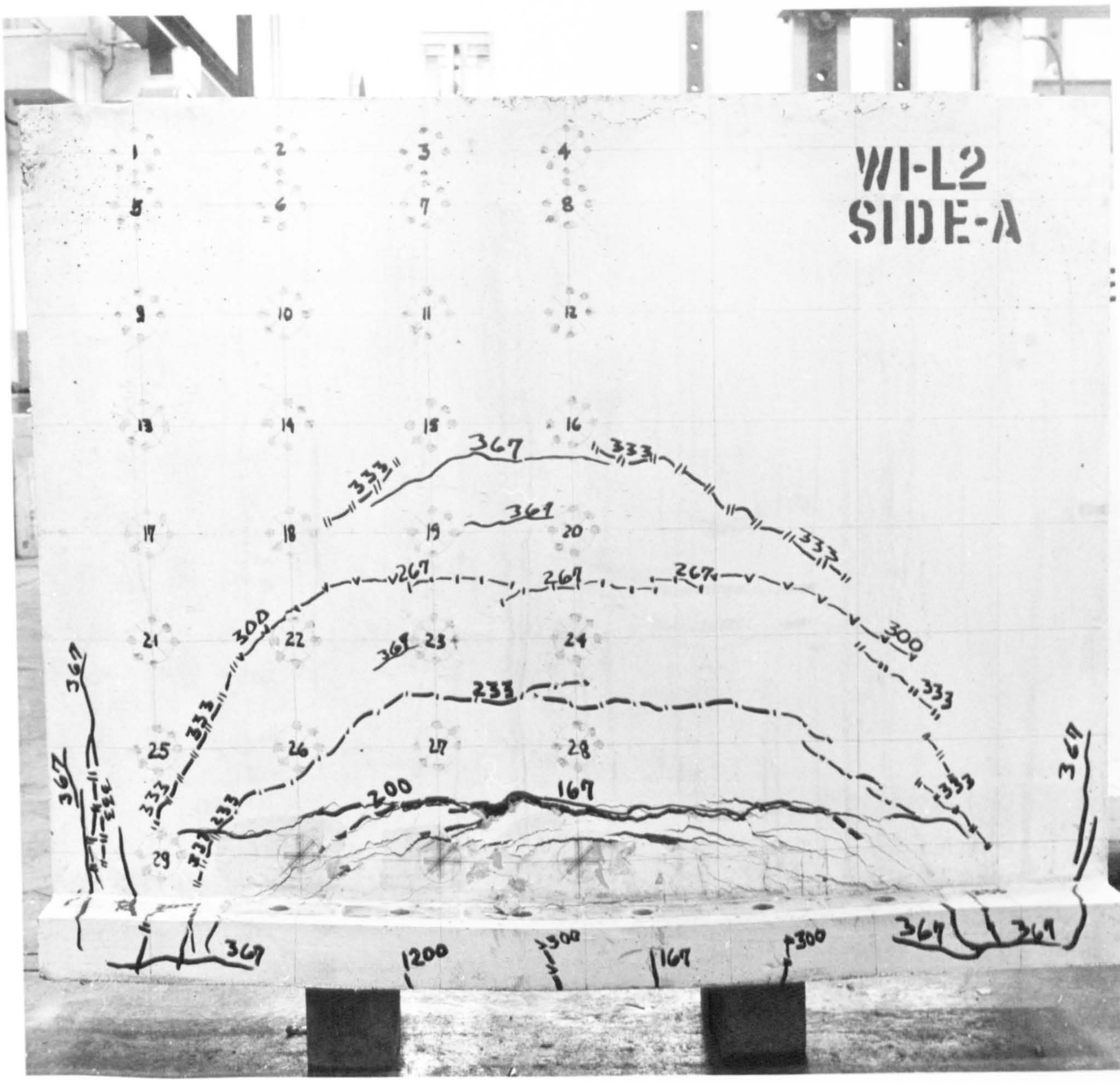

Fig. 4.10 Final crack pattern for specimen W1-L2

(Fig. 4.9(d)) the flat section of a third arch-like crack was observed at a height of 435 mm from the soffit; lengthening of this crack was observed at 300 kN load (Fig. 4.9(e)), creating a complete arch. Under 333 kN (Fig. 4.9(f)) the first vertical crack on the outside of the supports was detected and the inclined part of an additional arch-shaped crack appeared. At this load a large number of cracks started to appear between the first horizontal crack and the nib. The maximum load applied on this specimen was 375 kN and Fig. 4.10 illustates the final crack pattern. Average spacing between cracks was 138 mm, measured along the vertical central line on the wall.

Figure 4.11 shows the development of cracks with increasing load in specimen W3-L2. The first cracks were observed at a load of 200 kN (Fig. 4.11(a)). Two large horizontal cracks appeared, one at a depth of about 200 mm and a second at a depth of about 260 mm. Vertical cracks were observed on both sides of the wall outside the supports, at 467 kN (Fig. 4.11(f)). Figure 4.12 shows the final crack pattern and the condition of the specimen after sustaining a load of 500 kN. Extensive damage occurred in the lower section, caused by excessive deflection. Cracks appeared on the wall up to a depth of 875 mm from the soffit. The average spacing between cracks on the central vertical section of the wall was 82 mm.

In the case of specimen W5-L2, the first crack appeared at a load of 160 kN; subsequent crack development (Fig 4.13) had a pattern similar to the previous specimens. The maximum load applied was 375 kN, when the test had to be halted due to technical problems when the cracks reached a height of 680 mm. Average crack spacing was 64 mm, as measured along the vertical centre line.

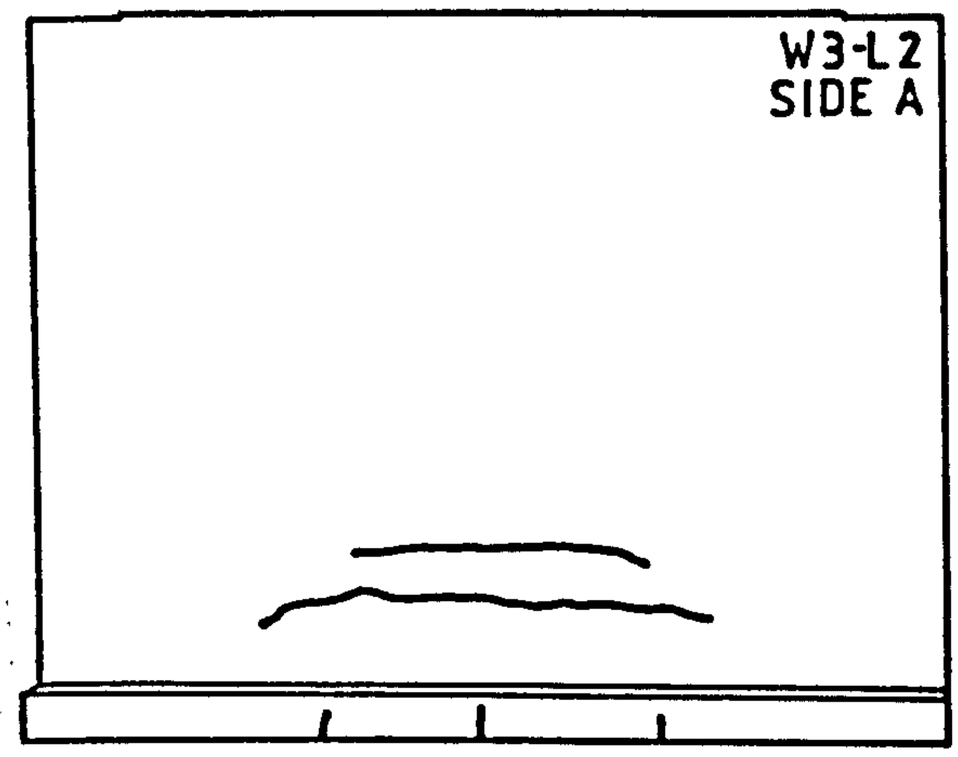

(a)

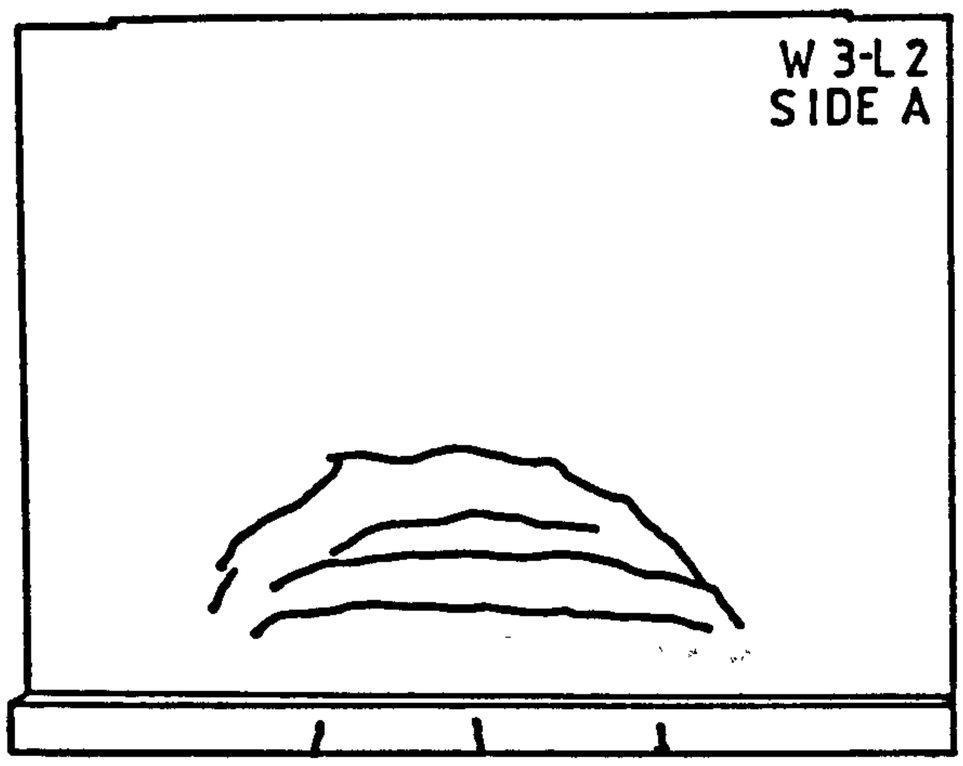

(b)

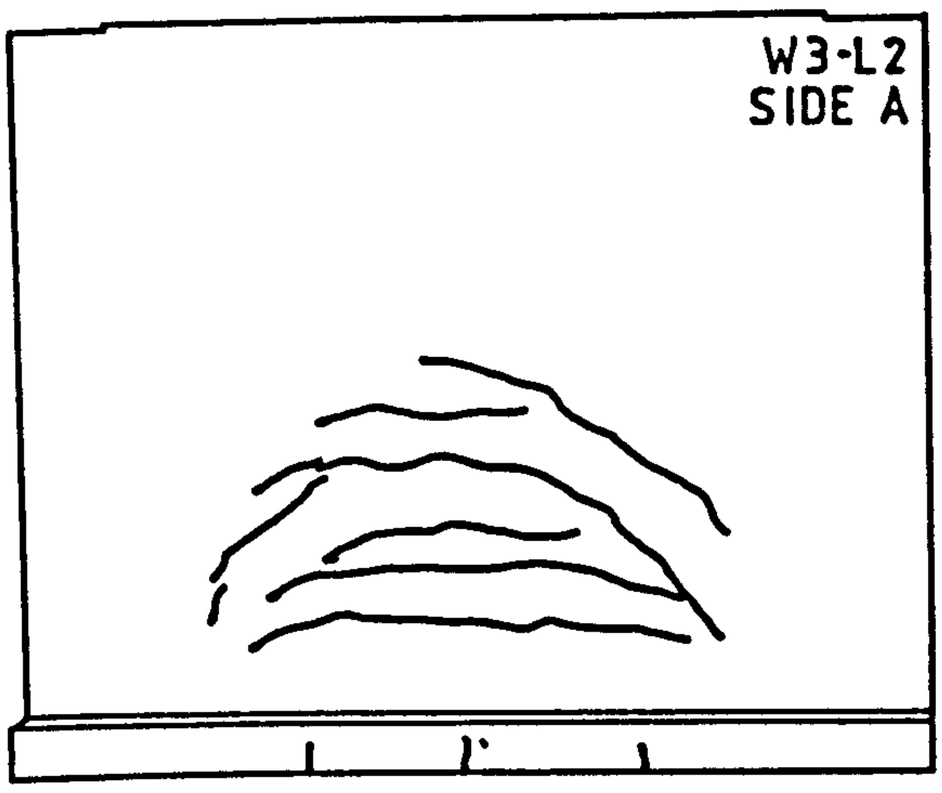

(c)

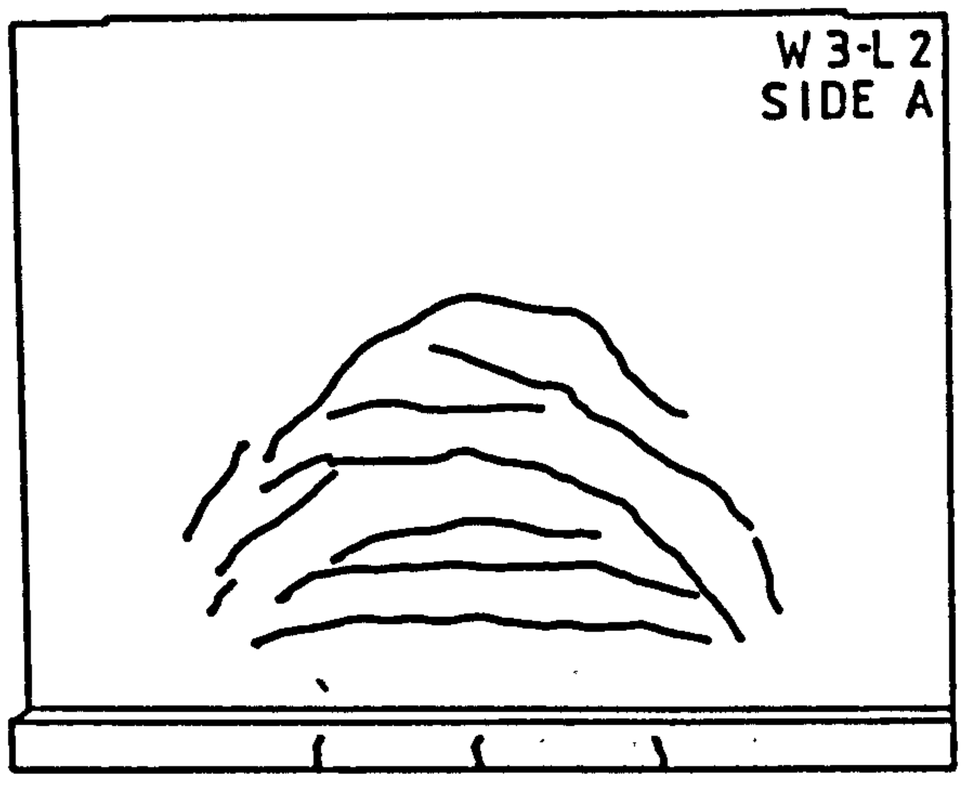

(d)

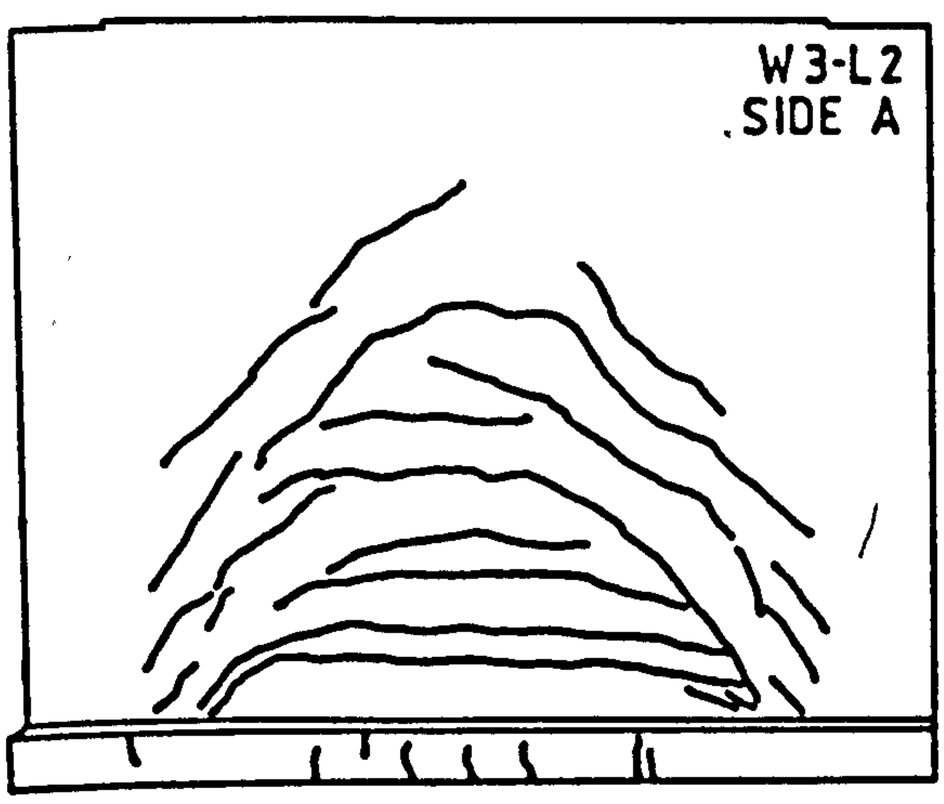

(e)

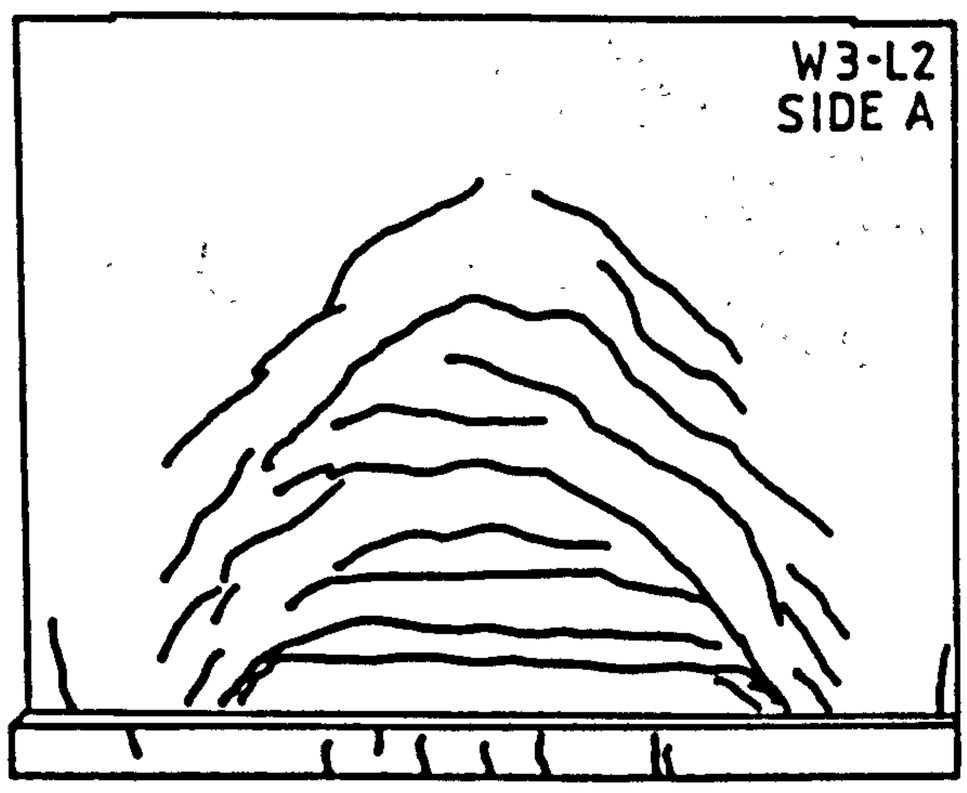

(f)

Fig. 4.11 Development of cracks in wall W3-L2

(a) Crack pattern at a load of 200 kN
(b) Crack pattern at a load of 267 kN
(c) Crack pattern at a load of 300 kN
(d) Crack pattern at a load of 367 kN
(e) Crack pattern at a load of 433 kN
(f) Crack pattern at a load of 467 kN

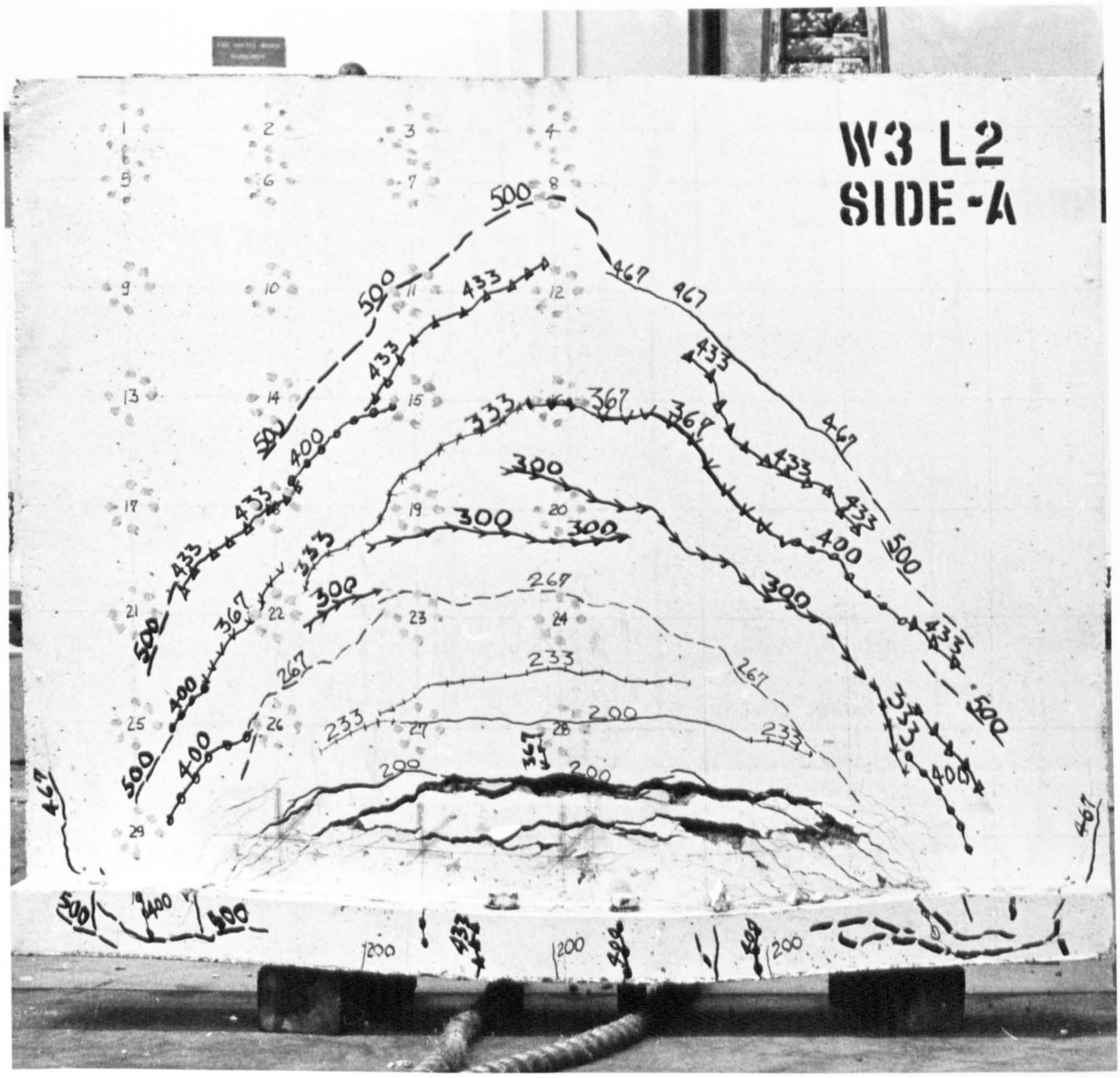

Fig. 4.12 Final crack pattern for specimen W3-L2

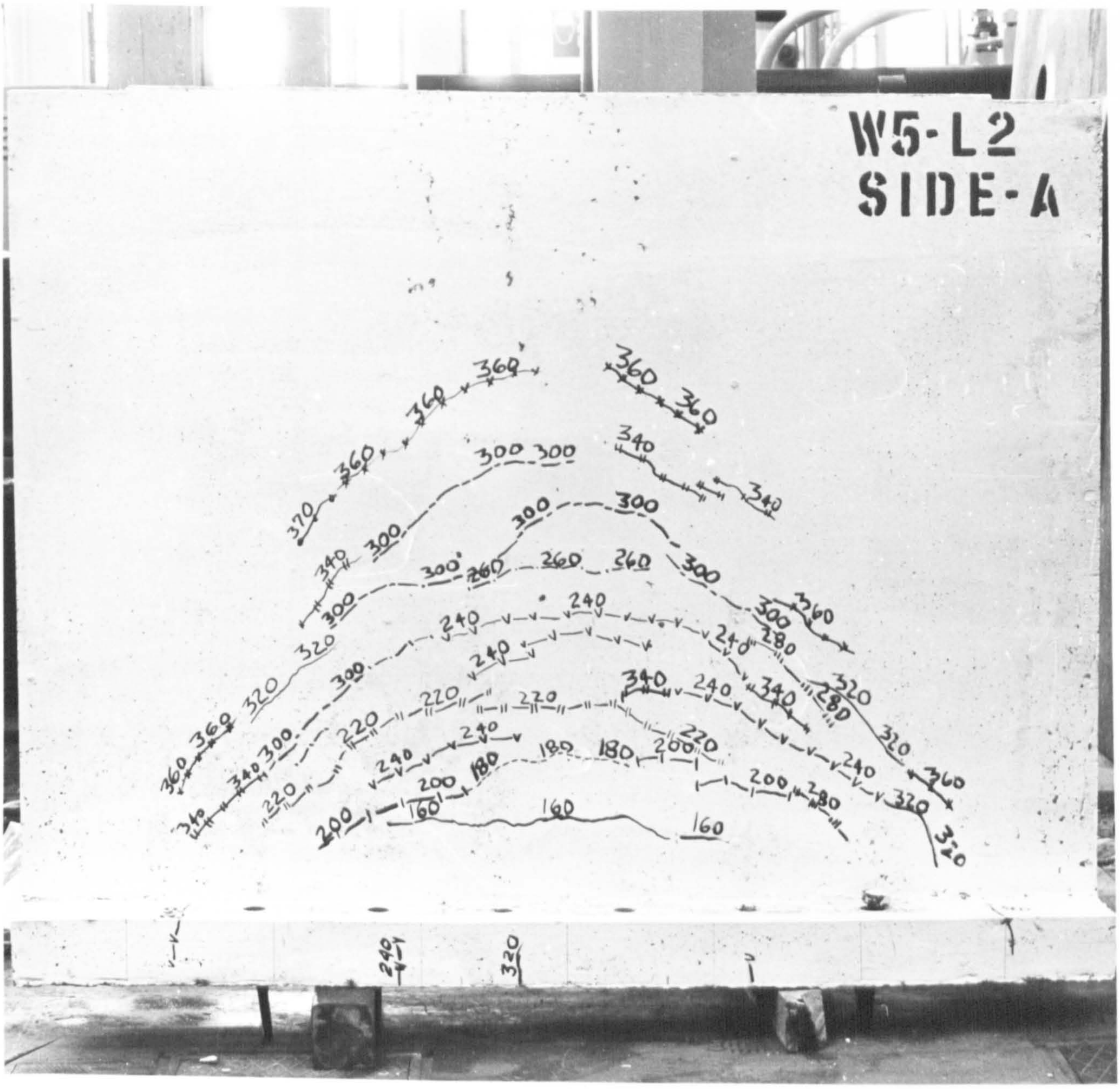

Fig. 4.13 Final crack pattern for specimen W5-L2

4.2.3 Crack Patterns of Walls Loaded Under Load Type 3 (L3)

Fig. 4.14 illustrates the final crack pattern observed in specimen W2-L3. The first crack appeared at a total load of 300 kN; it was horizontal and at a height of 190 mm from the soffit. Above the horizontal crack, an arch-like crack formed at 500 kN load, leaving a large uncracked gap between them, apart from three vertical cracks. The spacing and position of these three cracks corresponds to the spacing and position of the vertical bars. Extensive damage to the lower section of the wall started to take place at the maximum load applied of 600 kN. The highest crack reached 750 mm from the soffit with average crack spacing measured as 210 mm on the central vertical section. The last diagonal cracks formed were inclined at 62^{o} to the horizontal.

In specimen W1-L3, the first crack appeared at a combined load of 300 kN (Fig. 4.15(a)). This was a horizontal crack at a height of 180 mm from the soffit. At a load of 400 kN, the first arch-like crack was seen (Fig. 4.15(b)), leaving a central gap of 190 mm between both cracks. New arch-like cracks appeared at loads of 500 kN (Fig. 4.15(c)) and 600 kN (Fig. 4.15(d)). Under 700 kN load, extensive cracks appeared between the first crack and the nib (Fig. 4.16) as well as diagonal cracks inclined at 50-56 degrees with the horizontal. Average spacing between cracks along the vertical central line was 117 mm and the maximum load applied on this specimen was 750 kN.

Crack development in specimen W3-L3 is demonstrated by Figs. 4.17 and 4.18. The first cracks were detected at a load of 400 kN; they were a horizontal and a diagonal crack as shown in Fig. 4.17(a)). The horizontal crack was formed at 180 mm from the soffit. Some small flexural cracks were observed on the nib. Under a load of 500 kN, two major cracks were present, forming a quasi-arch which was incomplete in the central section. A large uncracked section was left between these new

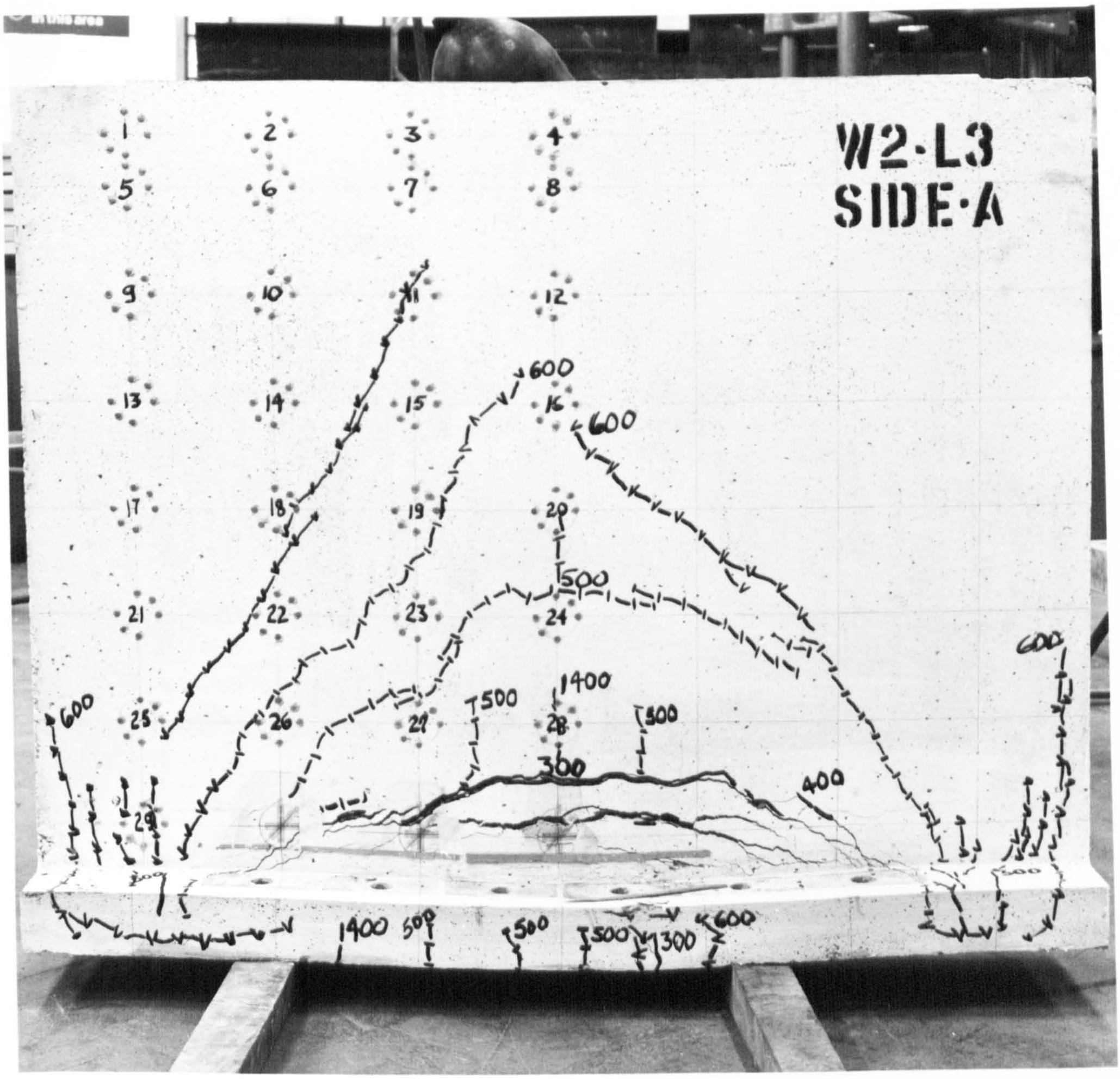

Fig. 4.14 Final crack pattern for specimen W2-L3

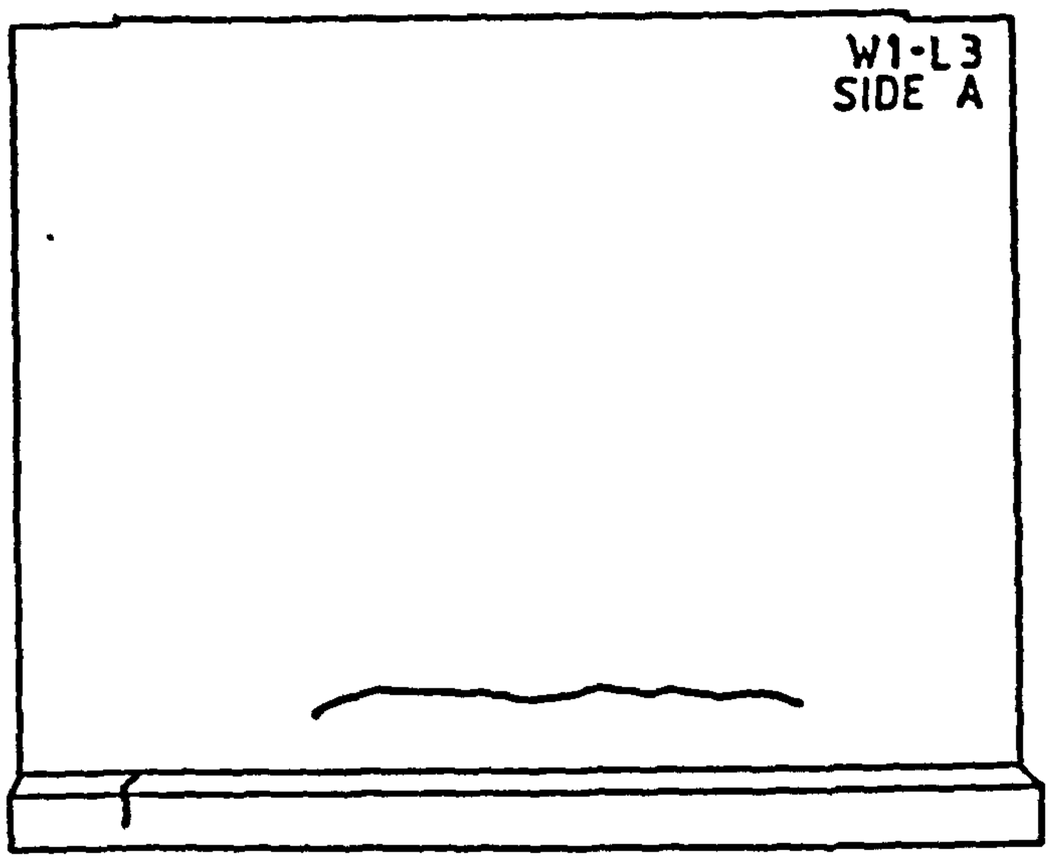

(a)

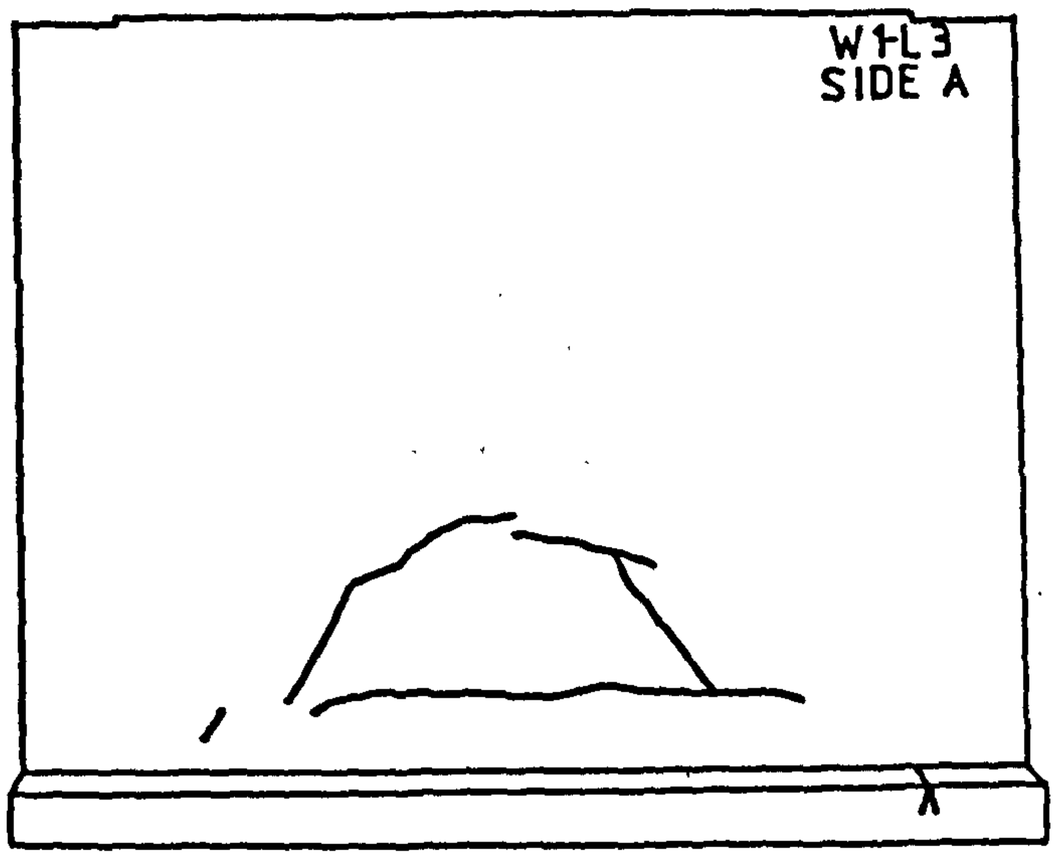

(b)

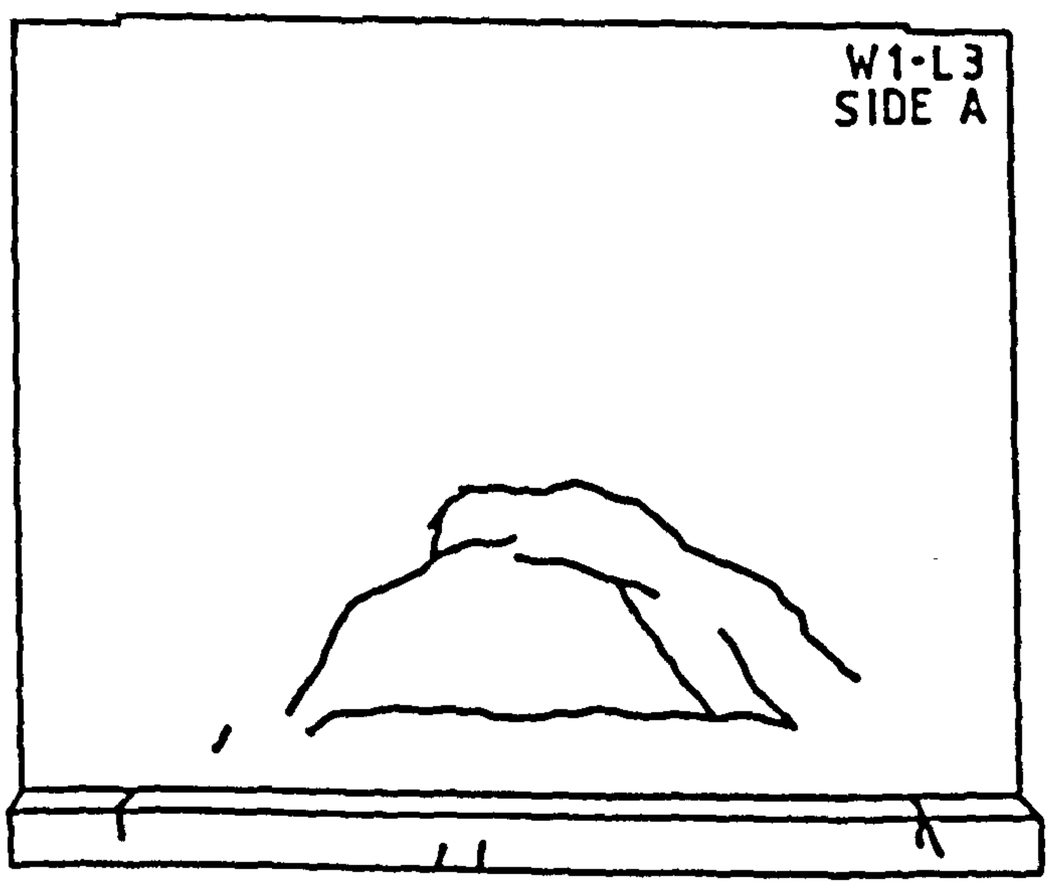

(c)

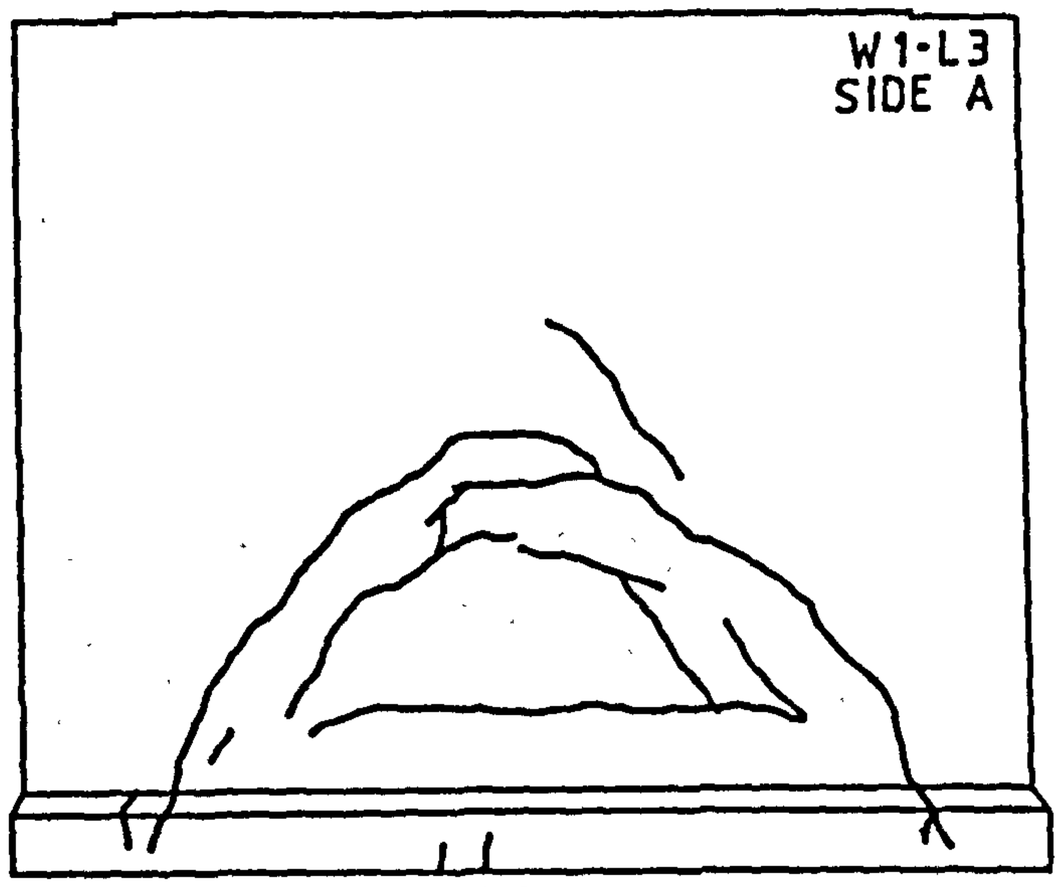

(d)

Fig. 4.15 Development of cracks in wall W1-L3

(a) Crack pattern at a load of 300 kN
(b) Crack pattern at a load of 400 kN
(c) Crack pattern at a load of 500 kN
(d) Crack pattern at a load of 600 kN

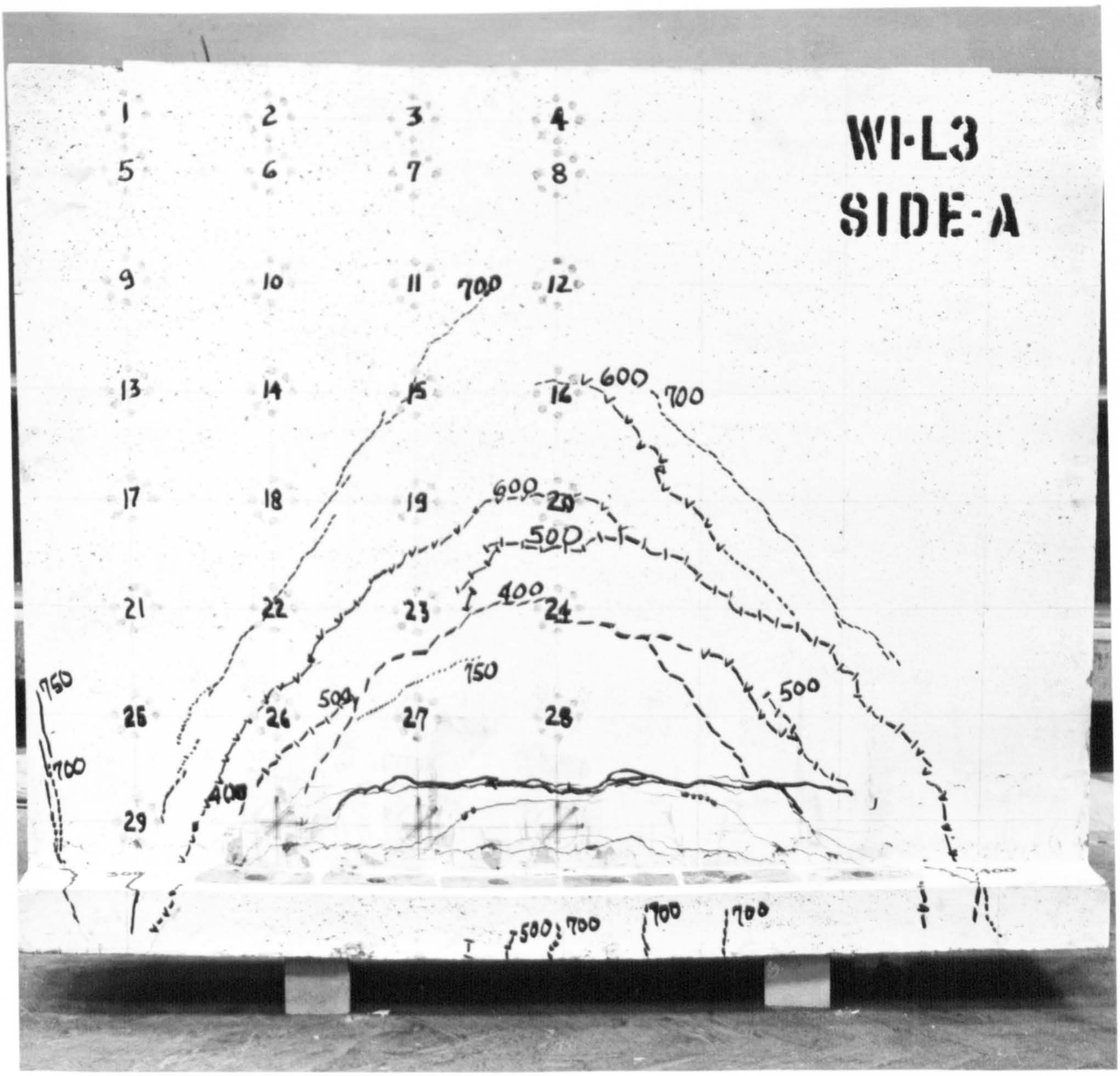

Fig. 4.16 Final crack pattern for specimen W1-L3

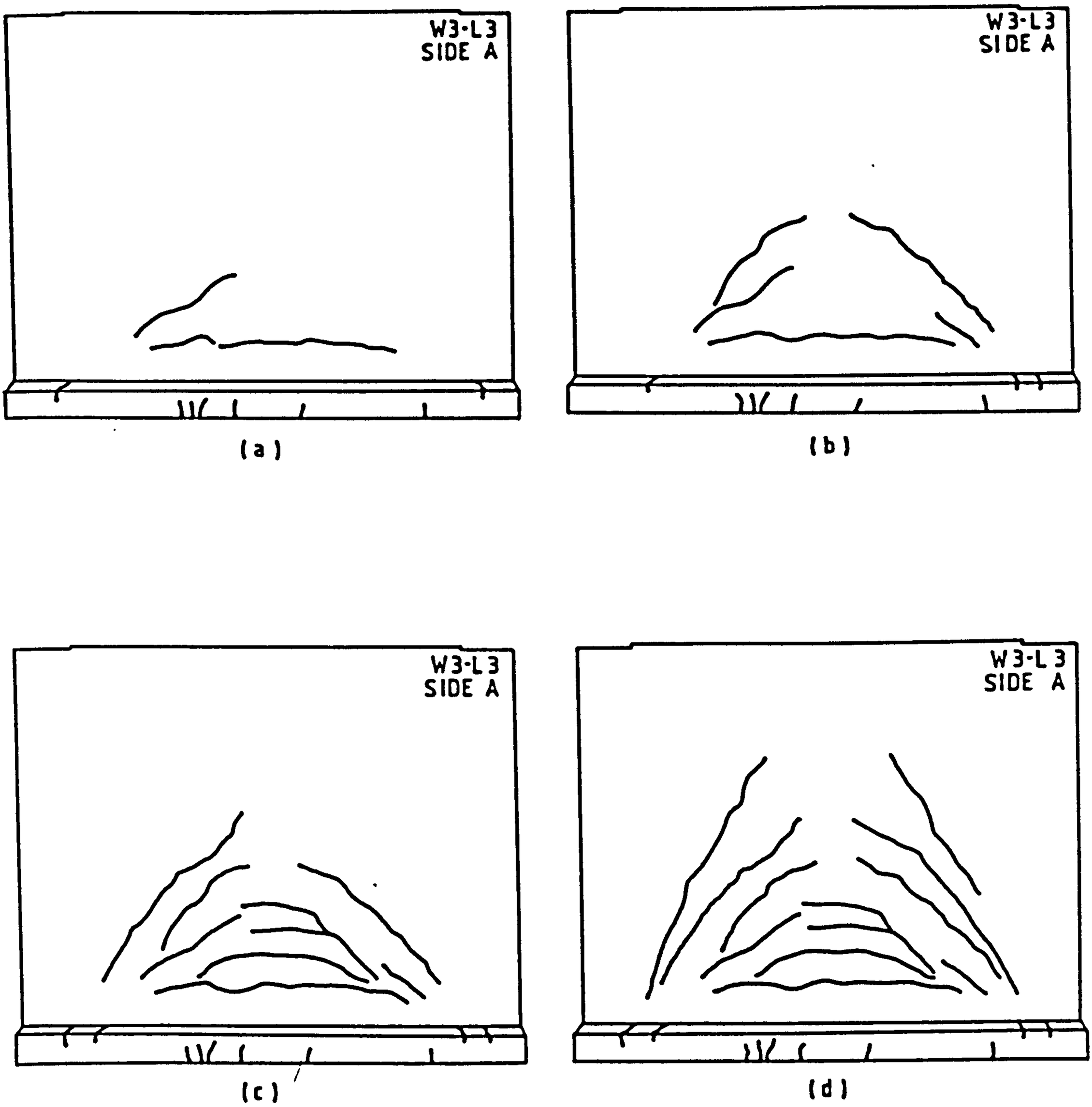

Fig. 4.17 Development of cracks in wall W3-L3

(a) Crack pattern at a load of 400 kN
(b) Crack pattern at a load of 500 kN
(c) Crack pattern at a load of 600 kN
(d) Crack pattern at a load of 700 kN

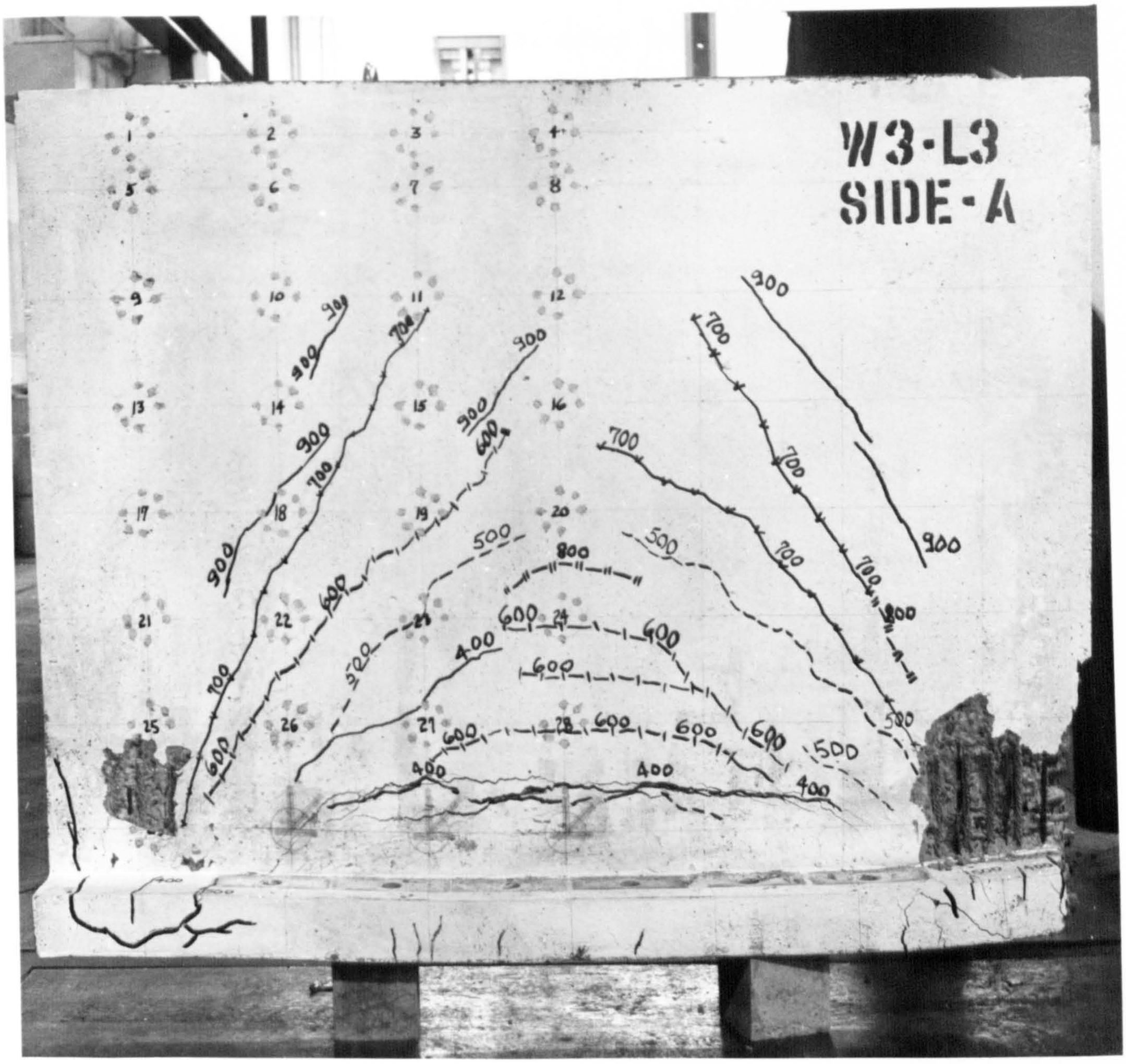

Fig. 4.18 Final crack pattern for specimen W3-L3

cracks and the primary crack. At a load of 600 kN, several cracks appeared in the space mentioned earlier. Large diagonal cracks were visible at 700 kN load, at an angle of 58-60 degrees with the horizontal. The average crack spacing in the central section was 64 mm. Fig. 4.18 shows the final pattern of cracks after failure at a load of 940 kN.

4.2.4 Crack Patterns of Walls Loaded Under Load Type 4 (L4)

In specimen W2-L4, the first crack observed was vertical, at mid-span and extended along the depth of the nib under a load of 200 kN. At 300 kN load (Fig. 4.19(a)) a diagonal crack appeared at an angle of 56 degrees with the horizontal, reaching a height of 340 mm from the soffit. A slightly arched crack (Fig. 4.19(b)) became visible at 400 kN load, positioned 190 mm from the soffit, measured at mid-span. Under 500 kN load few vertical cracks were observed within the nib. At mid-span and above the first horizontal crack, a vertical crack was observed coinciding with a vertical reinforcing bar. Several diagonal and arched cracks appeared at 600 kN load, as shown in Fig. 4.19(c), reaching a height of about 500 mm. At a load of 700 kN (Fig. 4.19(d)), a long diagonal crack appeared on the right-hand side of the specimen, extending to a height of 625 mm and at an angle of 56 degrees. A new horizontal crack appeared above the nib, at a level of about 130 mm from the soffit. Two additional vertical cracks were visible within the middle third of the span and between two horizontal cracks, coinciding with reinforcing bars. Some of the diagonal cracks lengthened at 800 kN load (Fig. 4.20) and a large crack appeared on the left hand side of the wall at an angle of 56 degrees. Other cracks appeared on the outside of the supports. The load was increased up to 900 kN; here the width of the horizontal crack last formed increased rapidly while the first horizontal crack (seen at a load of 400 kN) decreased in width considerably. Vertical crack

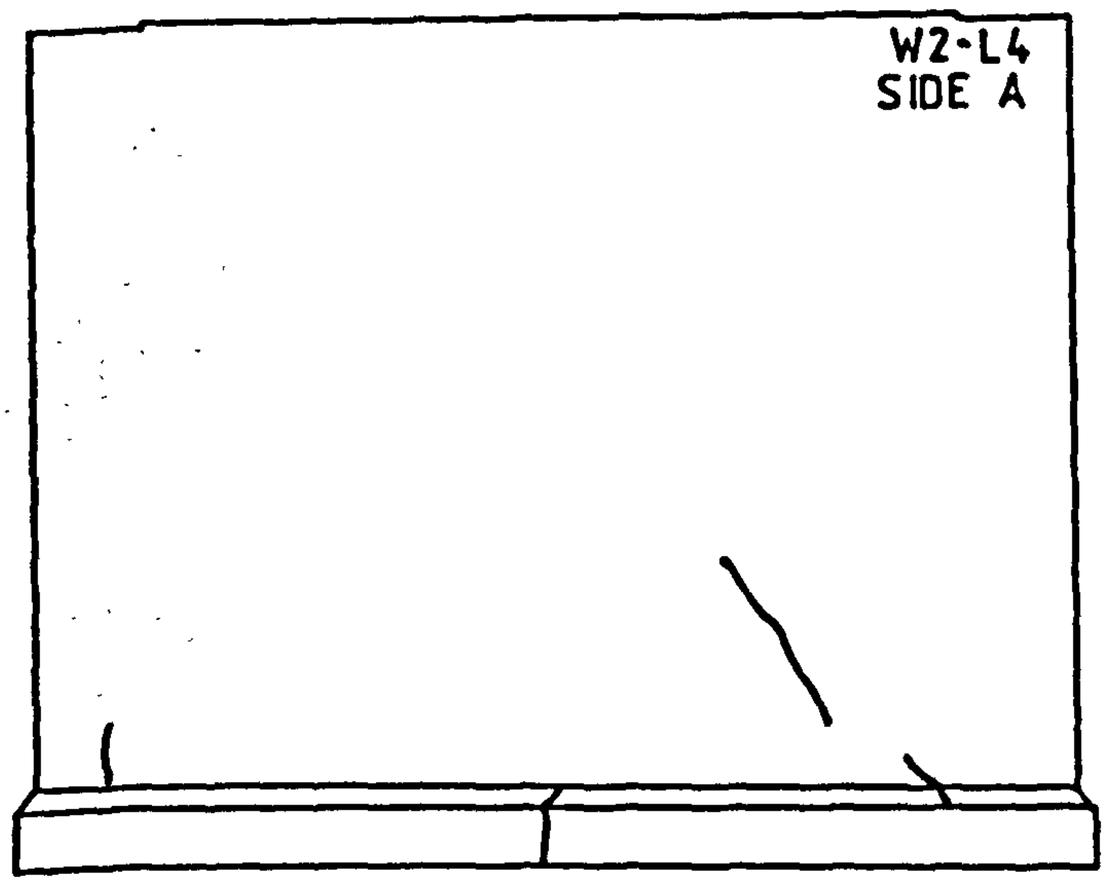

(a)

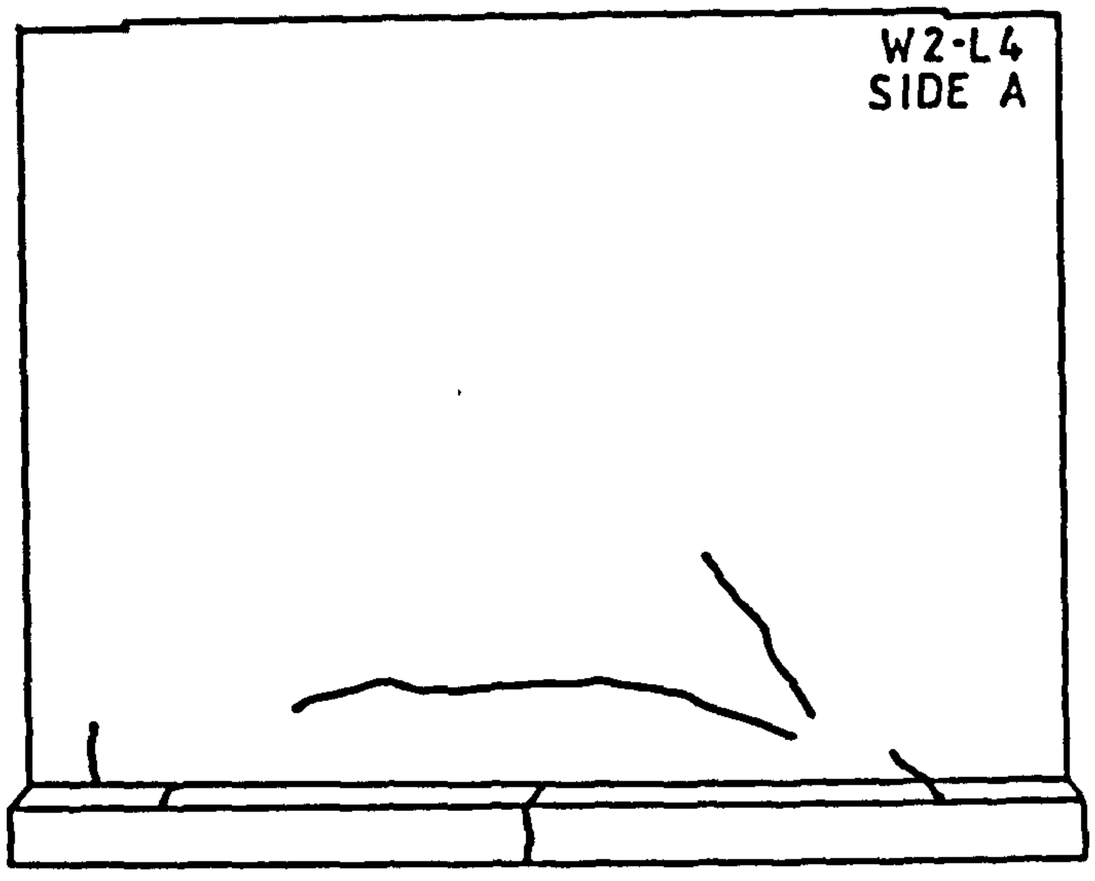

(b)

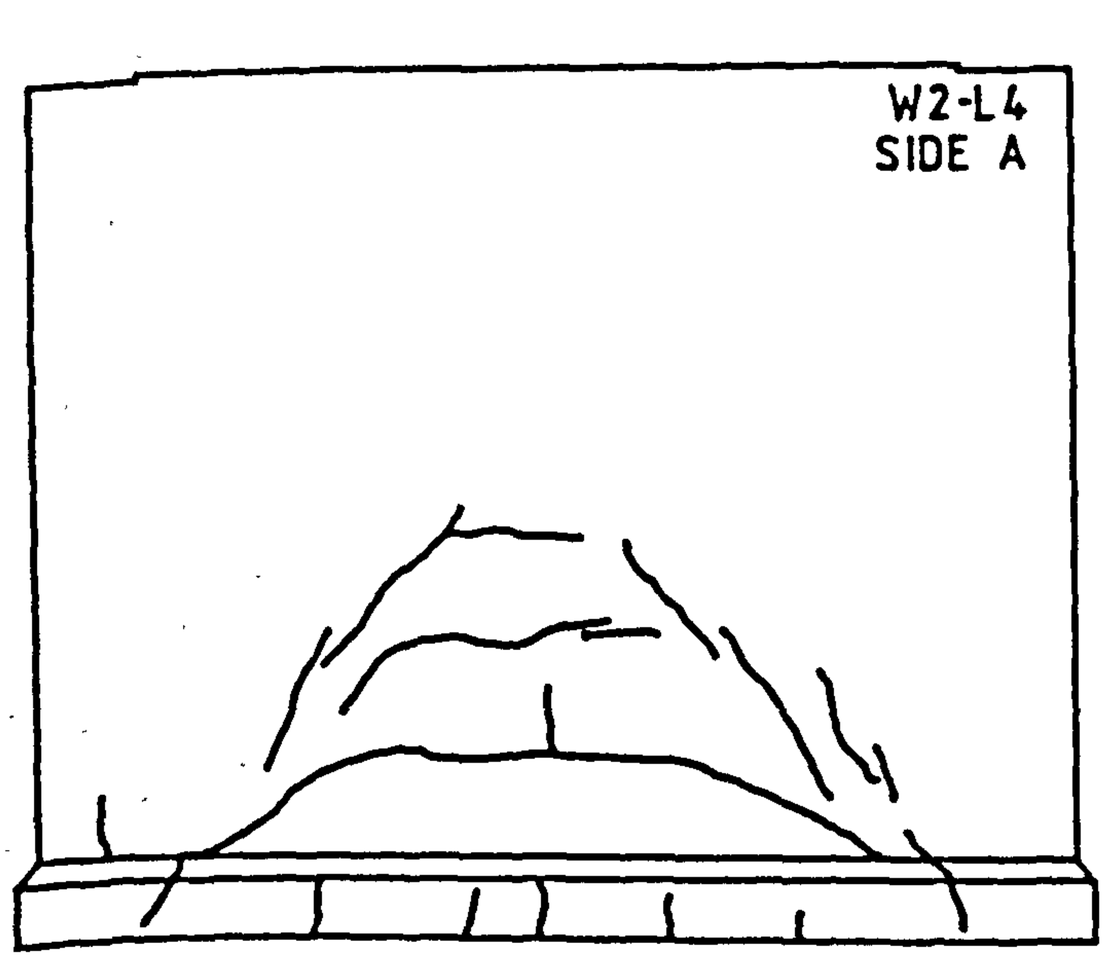

(c)

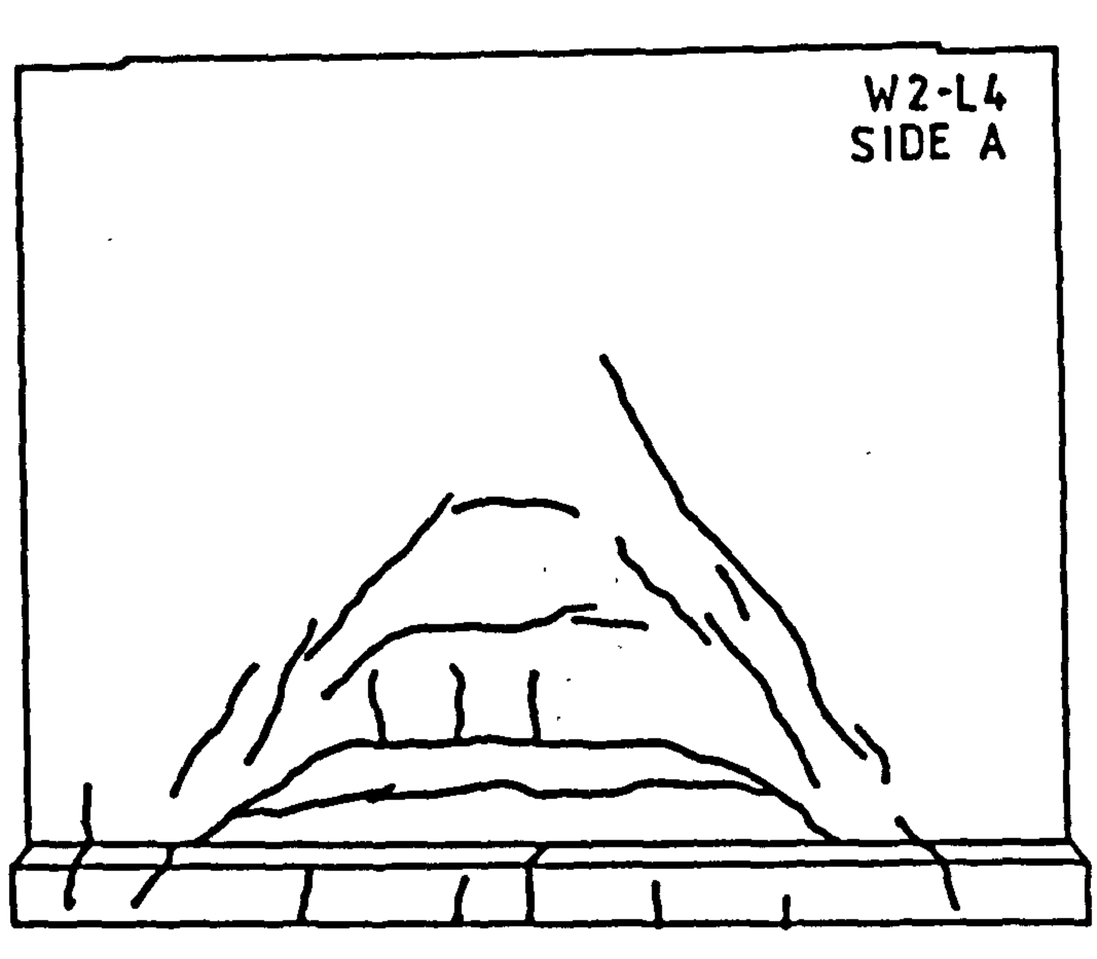

(d)

Fig. 4.19 Development of cracks in wall W2-L4

(a) Crack pattern at a load of 300 kN
(b) Crack pattern at a load of 400 kN
(c) Crack pattern at a load of 600 kN
(d) Crack pattern at a load of 700 kN

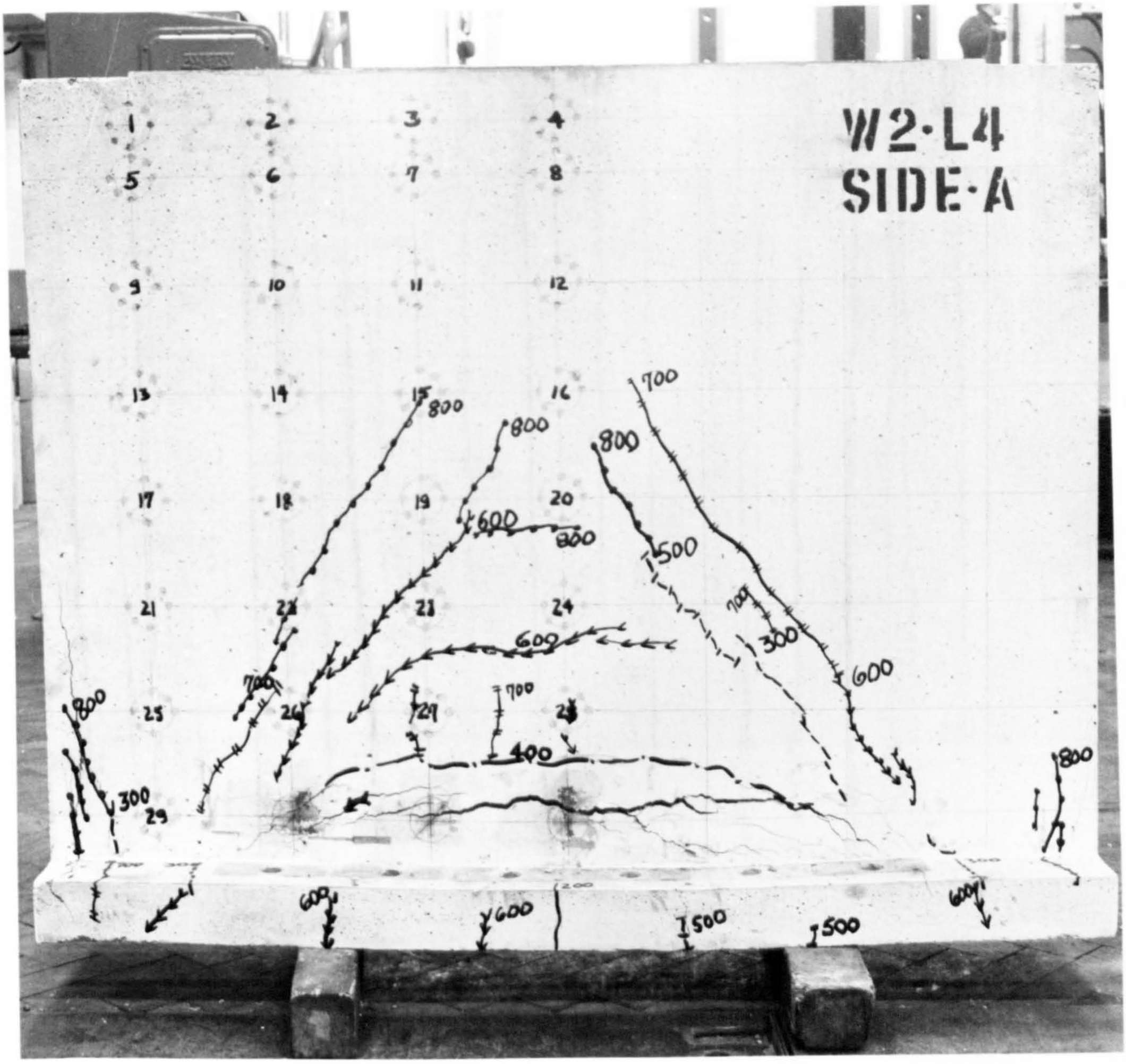

Fig. 4.20 Final crack pattern for specimen W2-L4

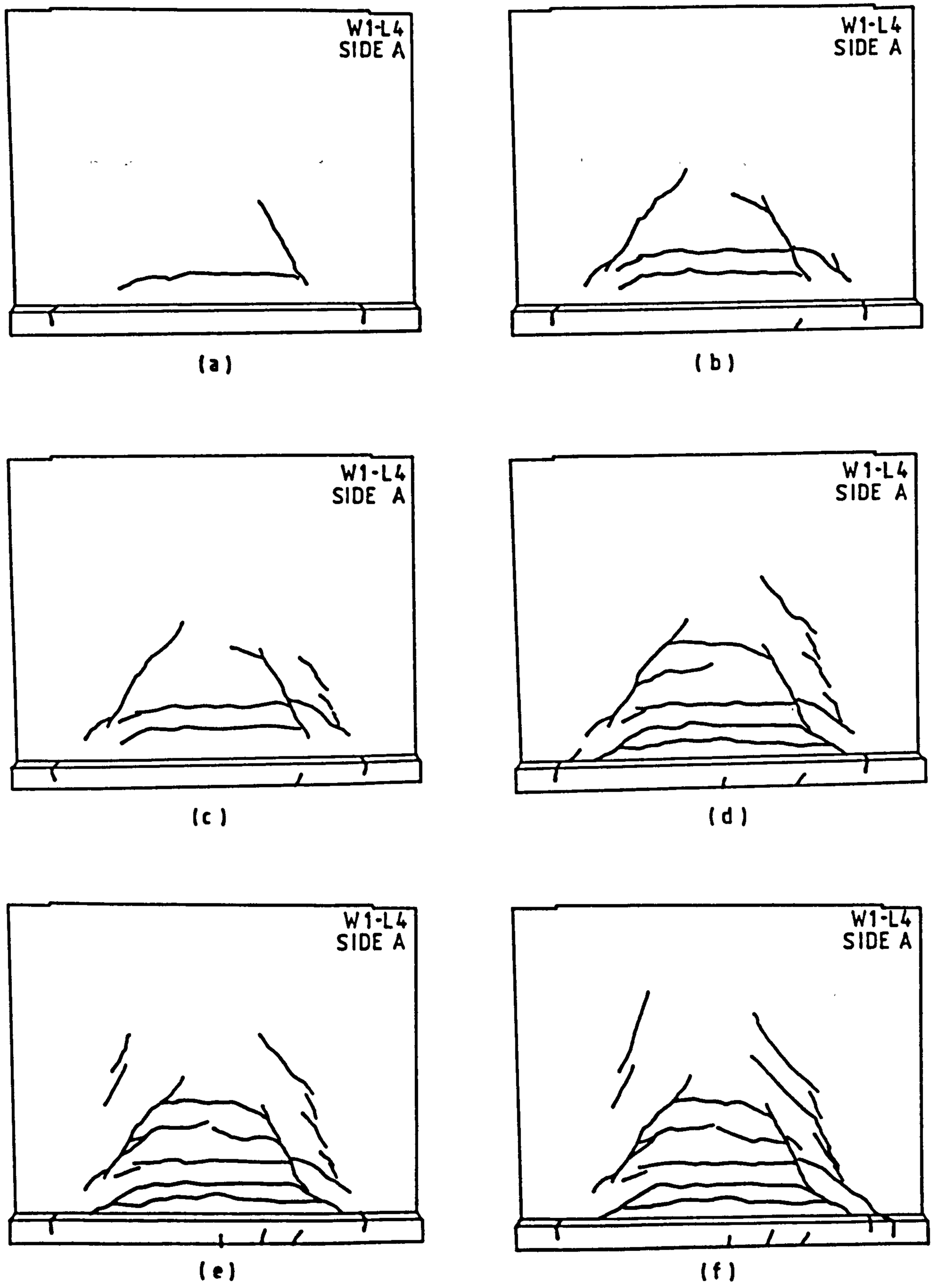

Fig. 4.21 Development of cracks in wall W1-L4

(a) Crack pattern at a load of 400 kN
(b) Crack pattern at a load of 500 kN
(c) Crack pattern at a load of 600 kN
(d) Crack pattern at a load of 700 kN
(e) Crack pattern at a load of 800 kN
(f) Crack pattern at a load of 900 kN

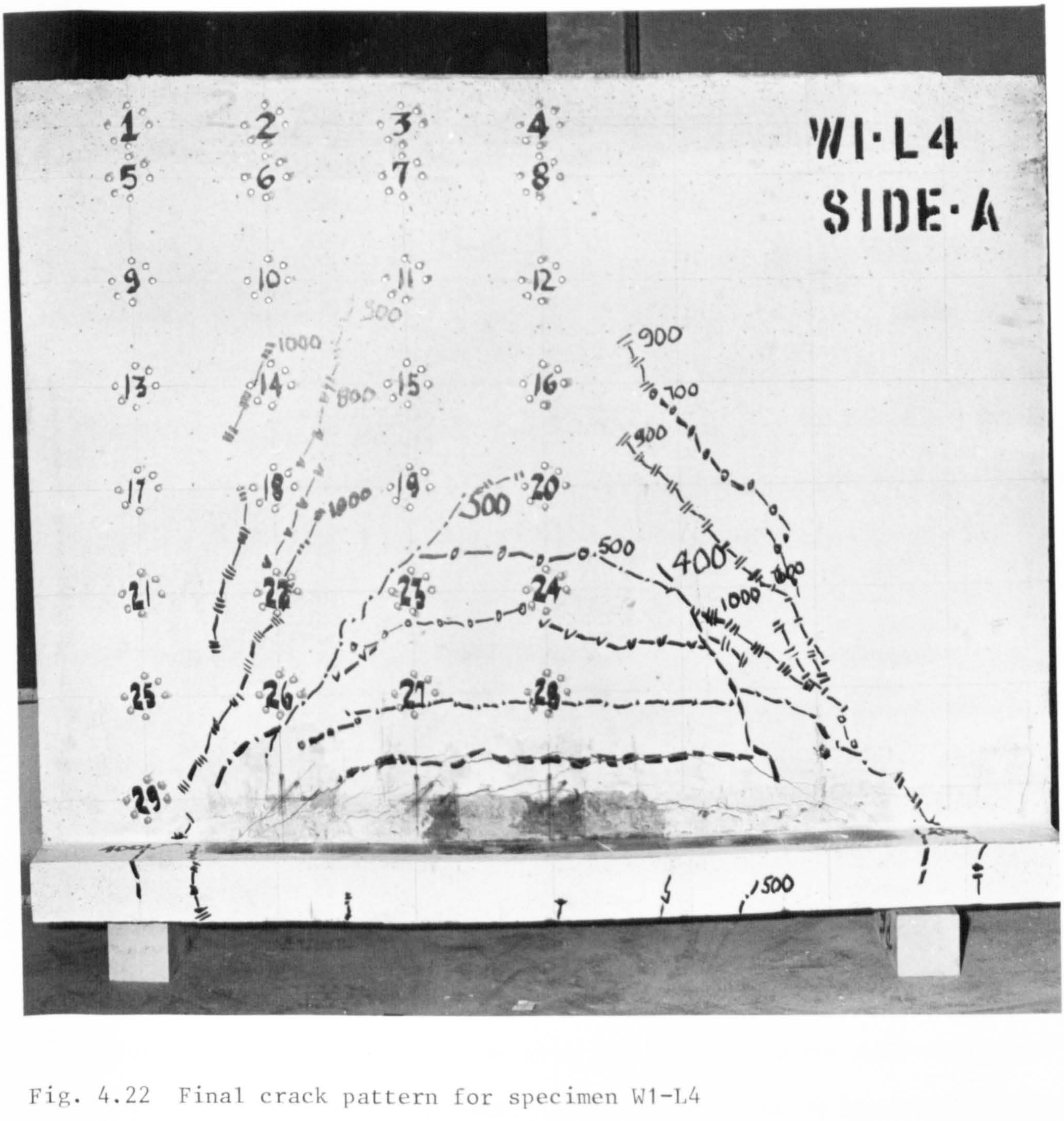

Fig. 4.22 Final crack pattern for specimen W1-L4

development above the supports indicated that the specimen was close to failure due to crushing of the concrete at the supports and no additional load was applied. The mean crack spacing measured on the central vertical section was 139 mm; in calculating this, the last horizontal crack formed above the nib was ignored.

Crack development in specimen W1-L4 can be followed in Figs. 4.21 and 4.22. Initial cracks observed were the horizontal and diagonal cracks shown in Fig. 4.21(a) at a load of 400 kN. The diagonal crack was inclined at 62 degrees and extended to a height of 400 mm; the horizontal crack was 175 mm from the soffit. Crack patterns at higher loads, i.e. 500, 600 and 700 kN, can be observed in Figs. 4.21(b), 4.21(c) and 4.21(d) respectively. At 700 kN, a new horizontal crack was formed above the nib, at about 125 mm from the soffit. The pattern of cracks at 800 and 900 kN are shown in Figs 4.21(e) and 4.21(f) respectively. Figure 4.22 illustrates the final pattern of cracks. The maximum load applied to this specimen was 1100 kN; here vertical cracks started to appear above the supports and damage to the region above the nib was also observed. Mean crack spacing in the central vertical section was 83 mm. The highest cracks on the wall were diagonal cracks reaching a height of about 750 mm from the soffit.

In specimen W3-L4, at a load of 400 kN (Fig. 4.23(a)), a horizontal and a diagonal crackwere seen. The horizontal crack was positioned at a height of 160 mm from the soffit and the diagonal crack had an inclination of 55 degrees. Figure 4.23(b) shows the development of additonal diagonal cracks and the extension of the previous one to a height of about 600 mm from the soffit under a load of 500 kN. These diagonal cracks on the left hand side of the wall were inclined at about 50 degrees. Figs. 4.23(c), 4.23(d), 4.23(e) and 4.23(f) show the development of arch-like and diagonal cracks at different loading stages. An interesting feature is the formation of a large number of nearly

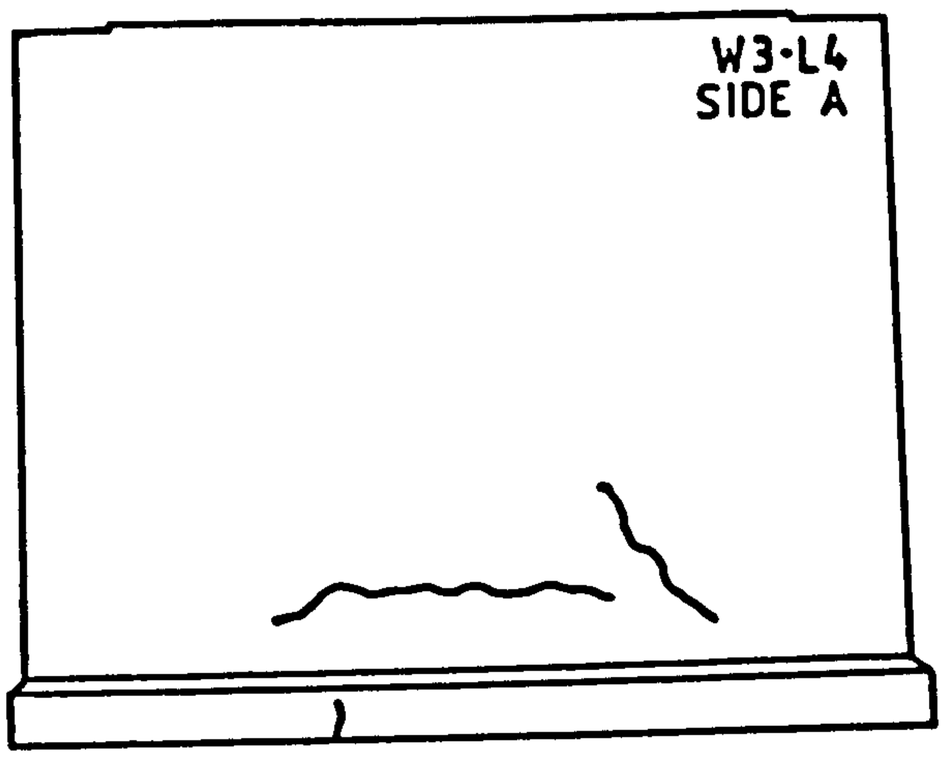

(a)

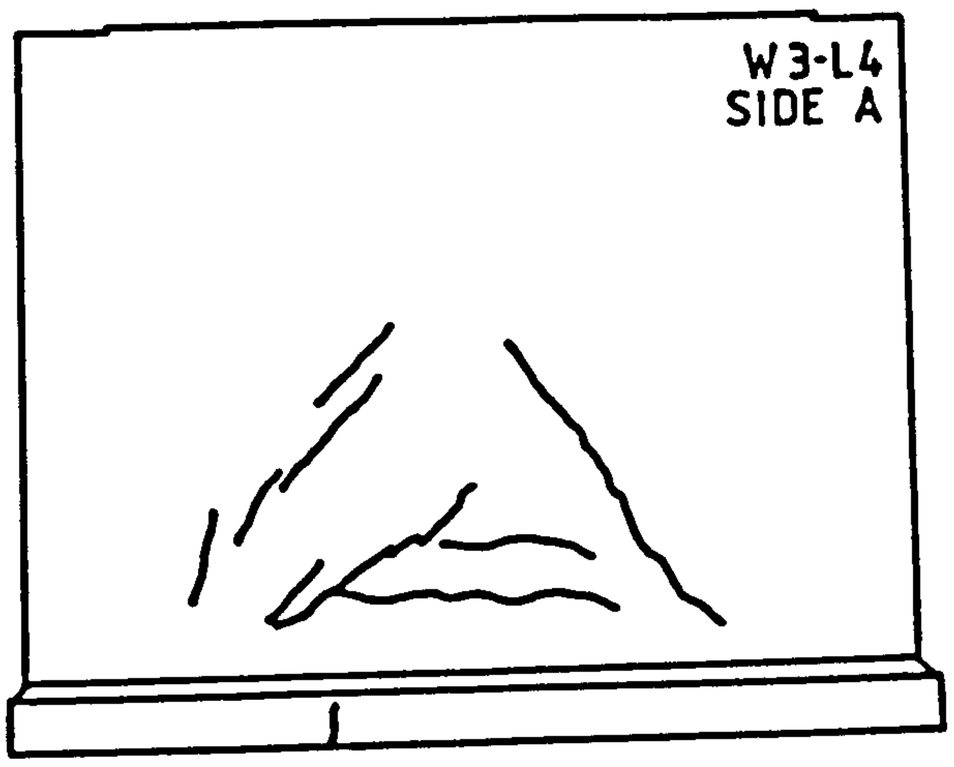

(b)

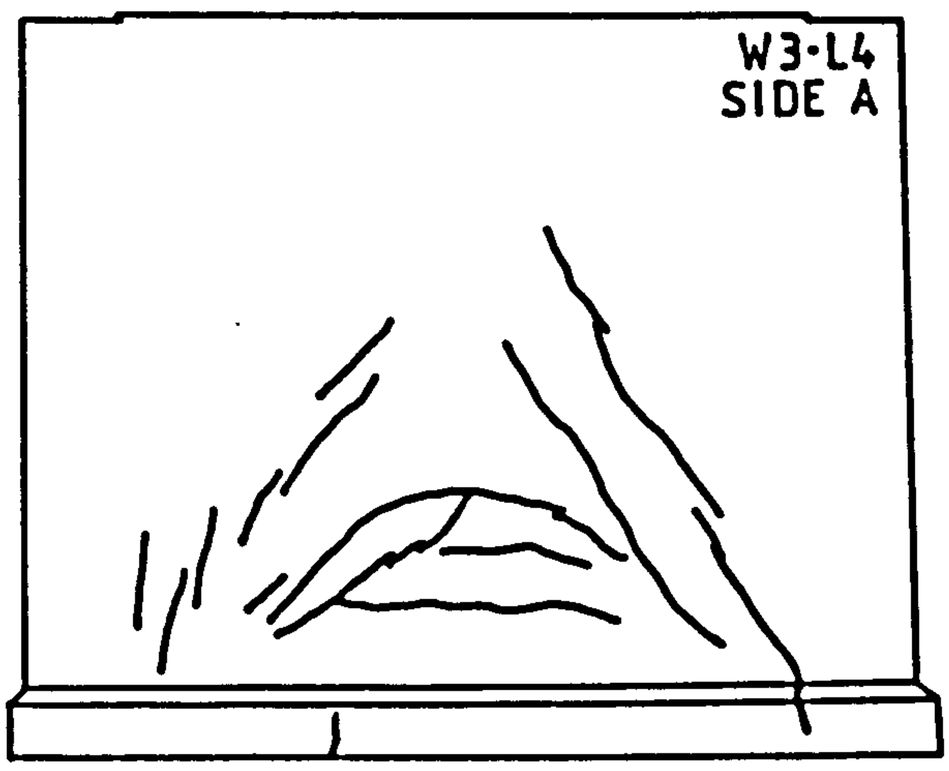

(c)

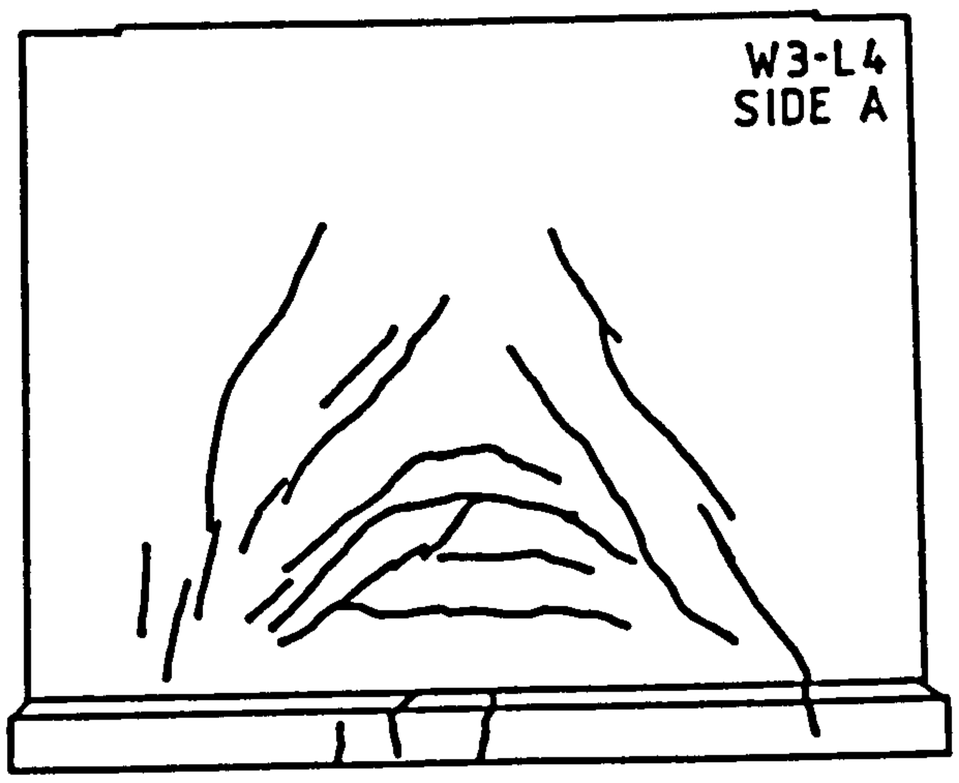

(d)

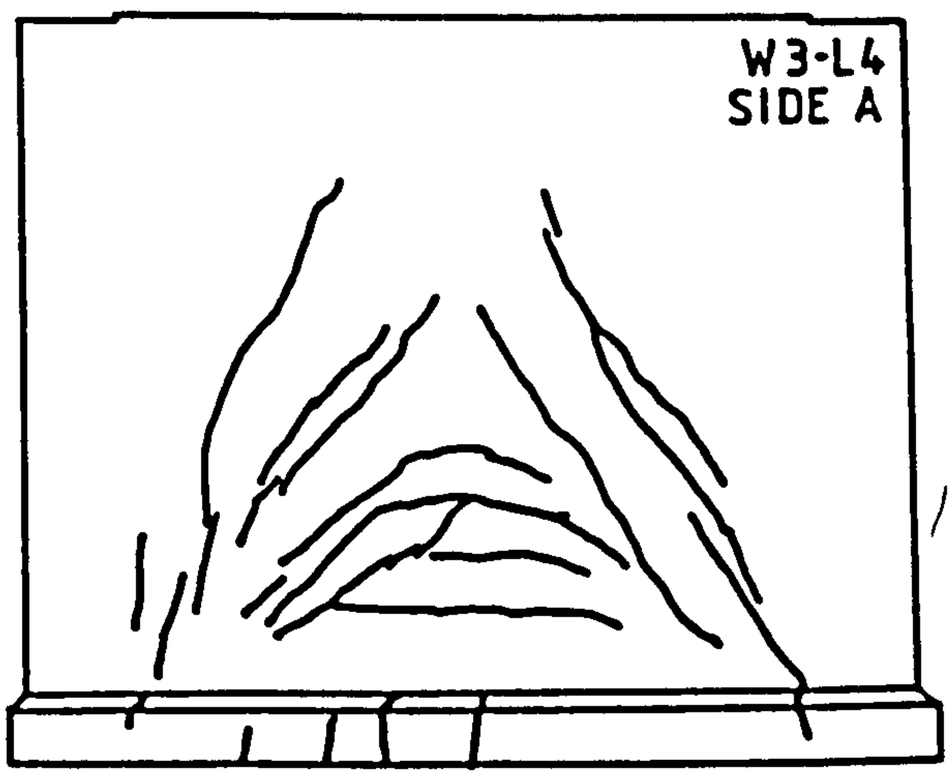

(e)

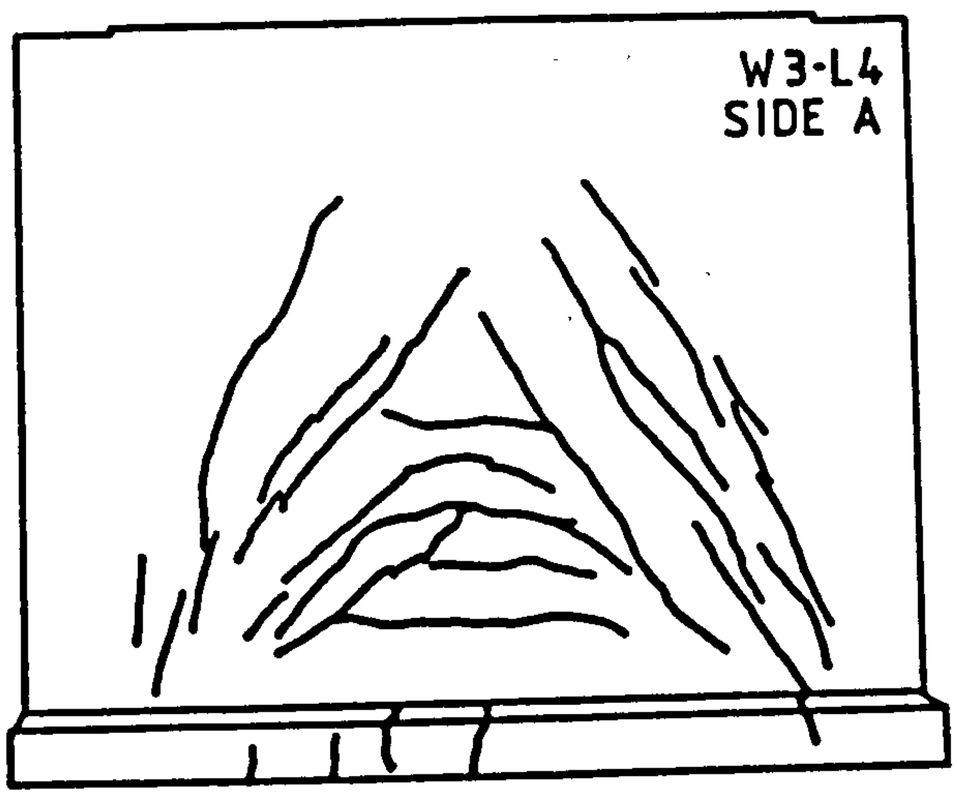

(f)

Fig. 4.23 Development of cracks in wall W3-L4

(a) Crack pattern at a load of 400 kN
(b) Crack pattern at a load of 500 kN
(c) Crack pattern at a load of 600 kN
(d) Crack pattern at a load of 700 kN
(e) Crack pattern at a load of 800 kN
(f) Crack pattern at a load of 900 kN

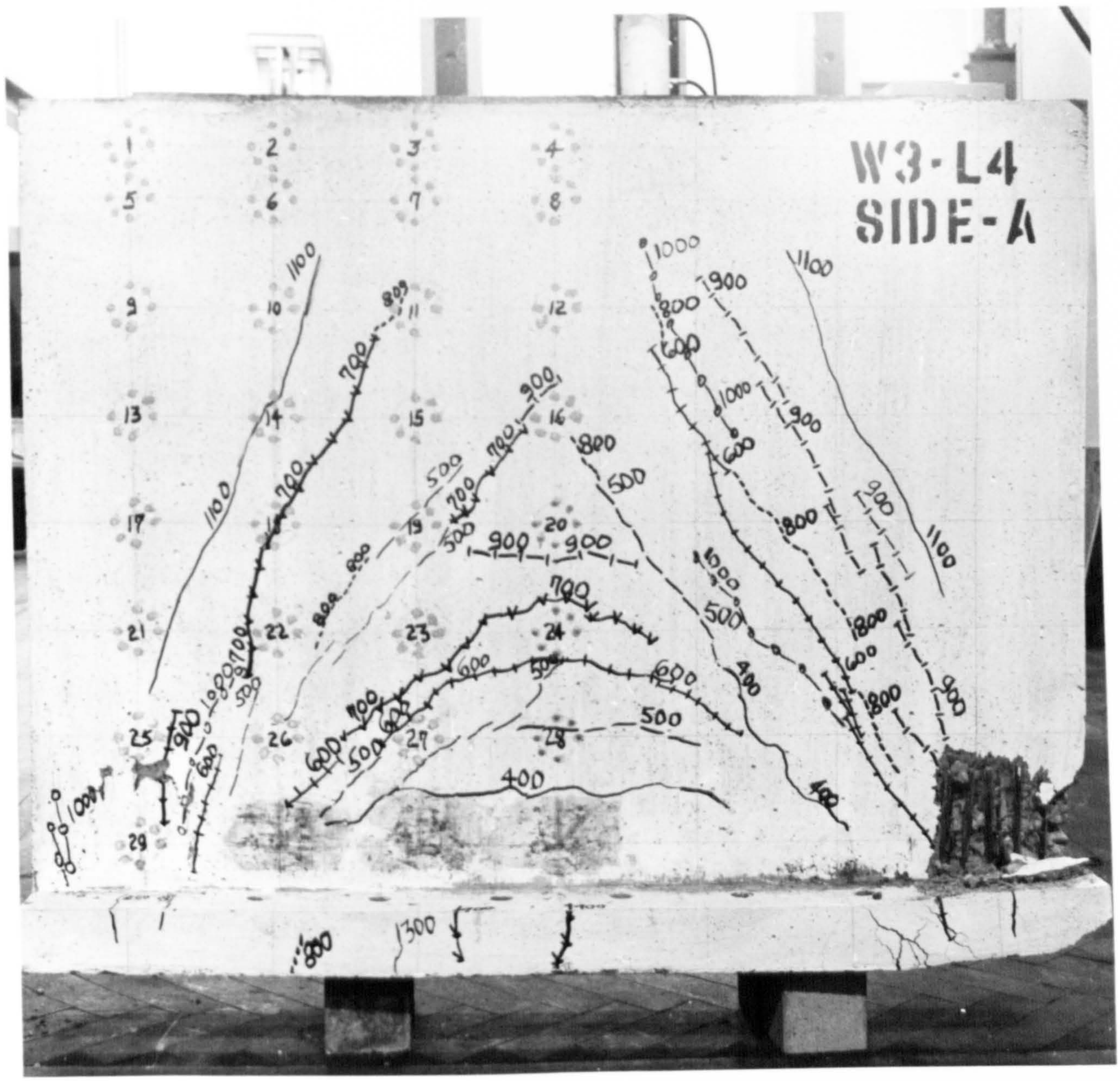

Fig. 4.24 Final crack pattern for specimen W3-L4

parallel diagonal cracks. The final pattern of cracks after failure is shown in Fig. 4.24. Average crack spacing along the vertical central section of the wall was 66 mm with the largest cracks reaching 820 mm from the soffit.

4.2.5 Crack Patterns of Walls Loaded Under Load Type 5 (L5)

Crack evolution in wall W2-L5 can be easily followed in Fig. 4.25. At 200 kN load a long horizontal crack was formed at a height of 190 mm from the soffit. Subsequently, with each increase in load, new horizontal cracks and arch-like cracks were formed. Extensive damage was inflicted on the lower section of the wall when the maximum load of 450 kN was applied. The highest crack extended about 600 mm from the soffit and the average crack spacing along the vertical central section of the wall was 134 mm.

Crack propagation in specimen W1-L5 is summarized graphically in Figs. 4.26 and 4.27. At a load of 200 kN, the first horizontal crack (Fig. 4.26(a)) was formed 163 mm from the soffit. Figure 4.26(b) shows the composition of cracks at a load of 400 kN and Fig. 4.26(c) at 500 kN. Complete arch-like cracks were formed up to the load of 500 kN. Under 570 kN load (Fig. 4.26(d)) diagonal cracks evolved at an angle of 67-72 degrees on the right hand side and 60-80 degrees on the left hand side of the specimen. The uppermost crack reached 750 mm from the soffit and average crack spacing along the vertical central section was 140 mm. Failure occurred at a load of 570 kN and the ultimate crack pattern is depicted in Fig. 4.27.

Initial crack formation was recorded at a load of 300 kN for specimen W3-L5, when the cracks shown in Fig. 4.28(a) were observed. The lower horizontal crack was produced 195 mm from the soffit. At 400 kN load the crack pattern was as shown in Fig. 4.28(b). Here the appearance of a horizontal crack above the nib, 150 mm from the soffit provided an

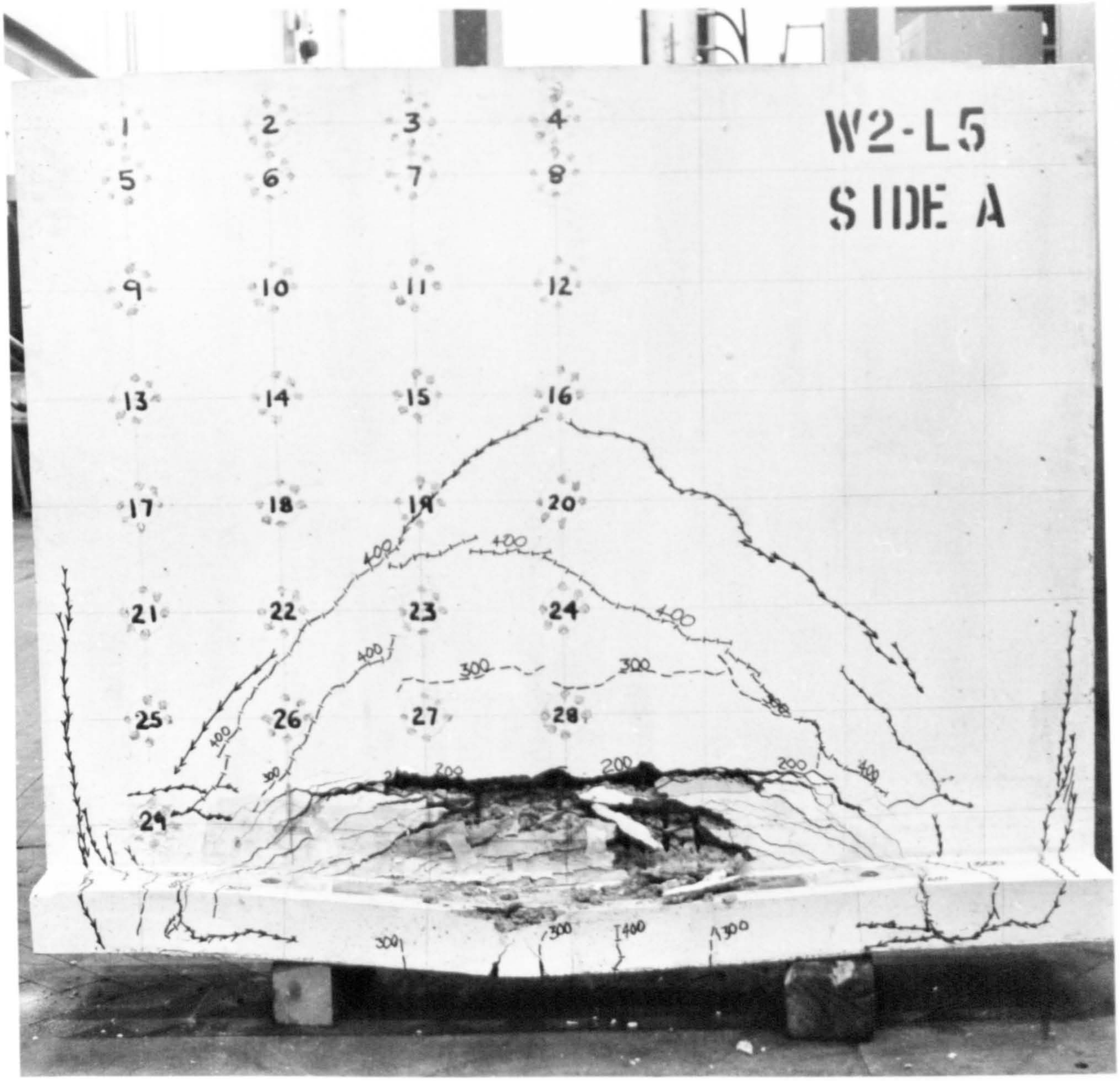

Fig. 4.25 Final crack pattern for specimen W2-L5

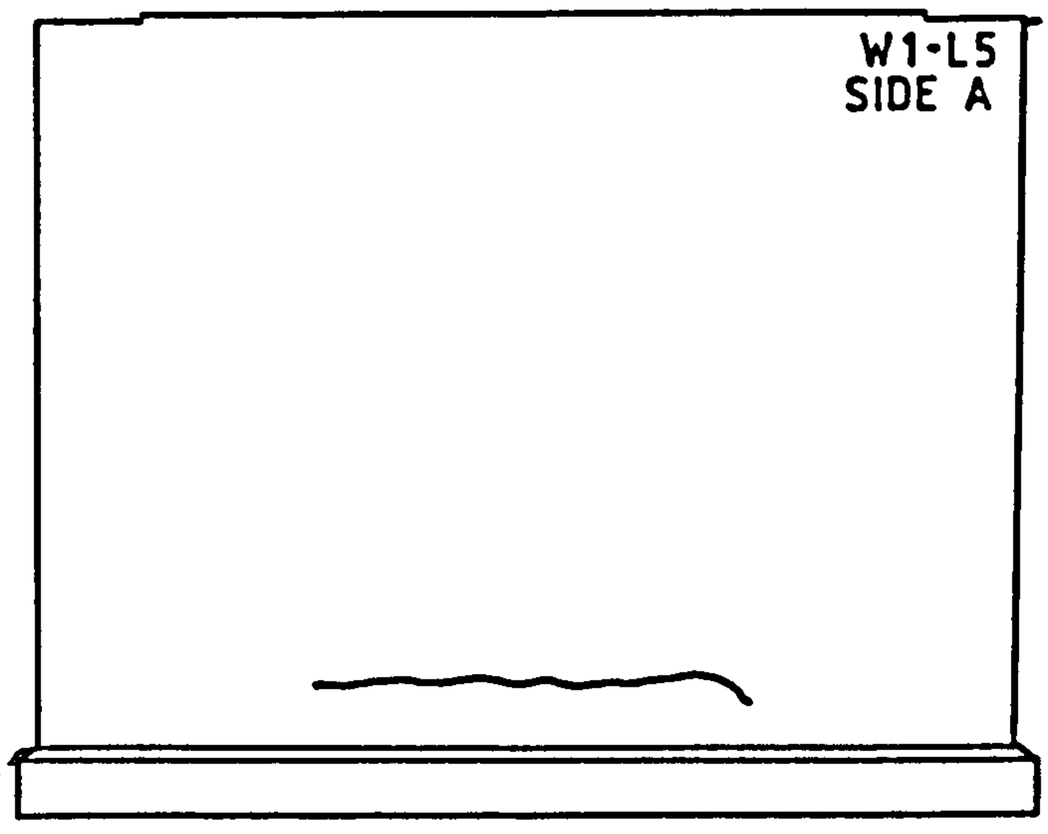

(a)

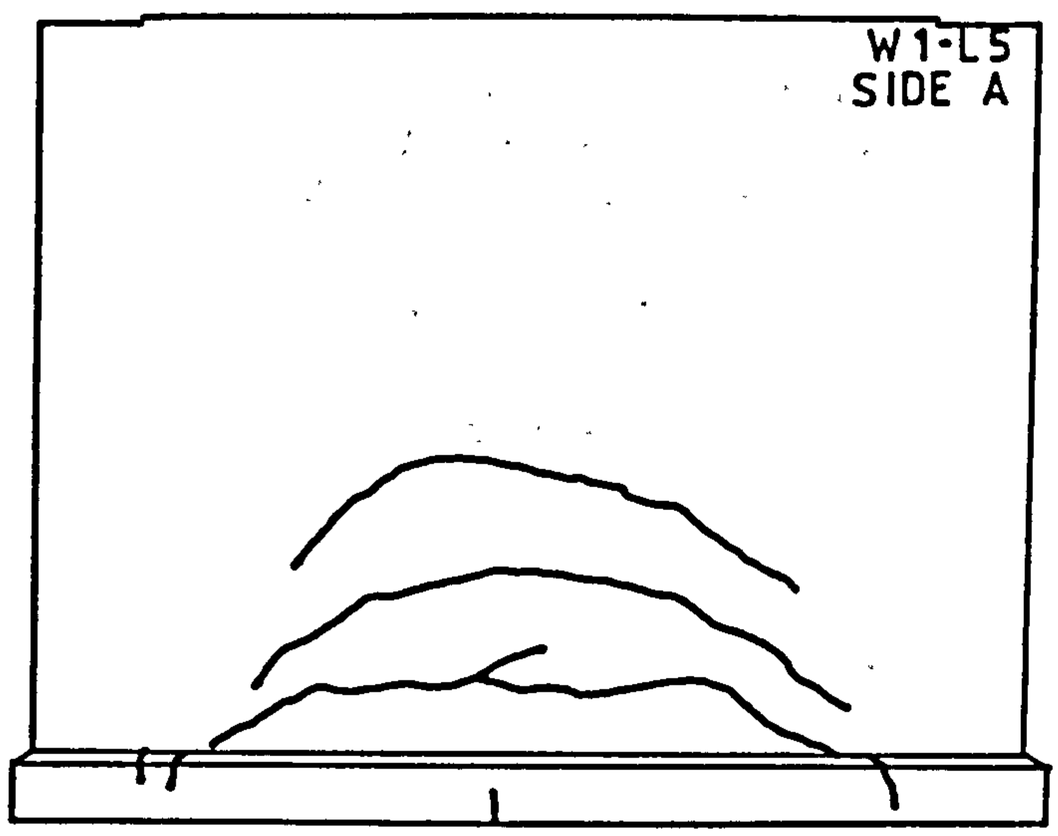

(b)

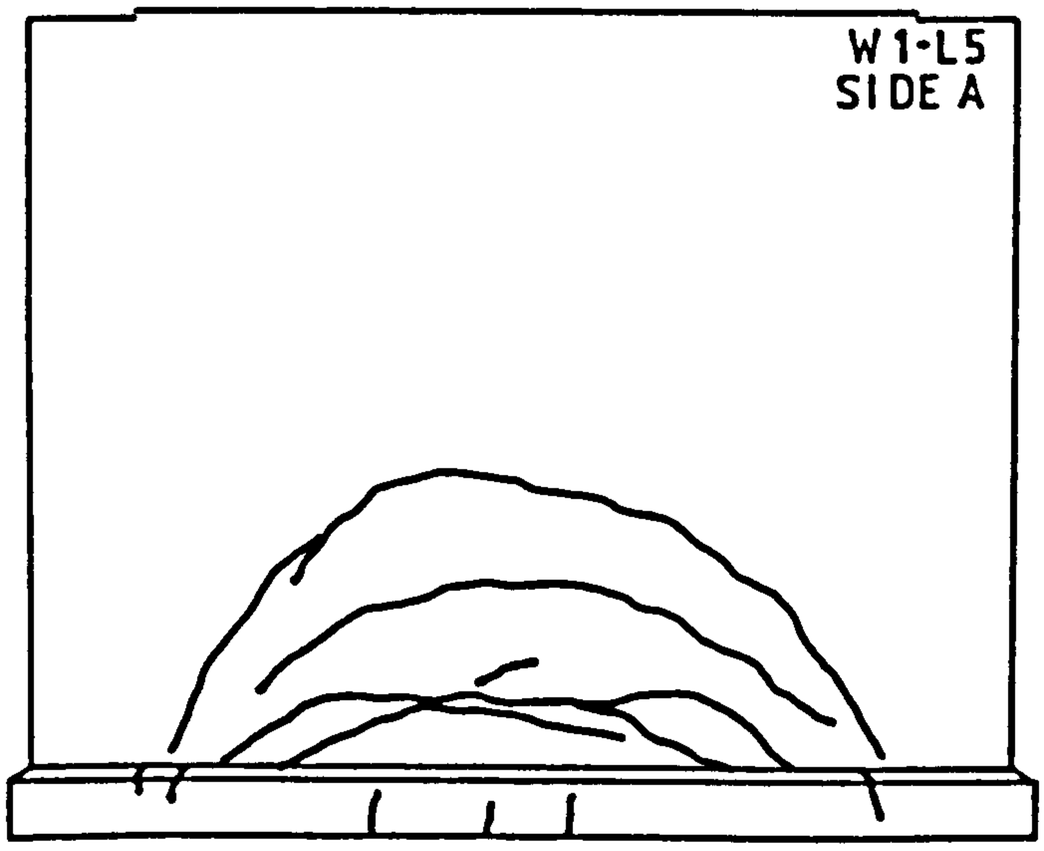

(c)

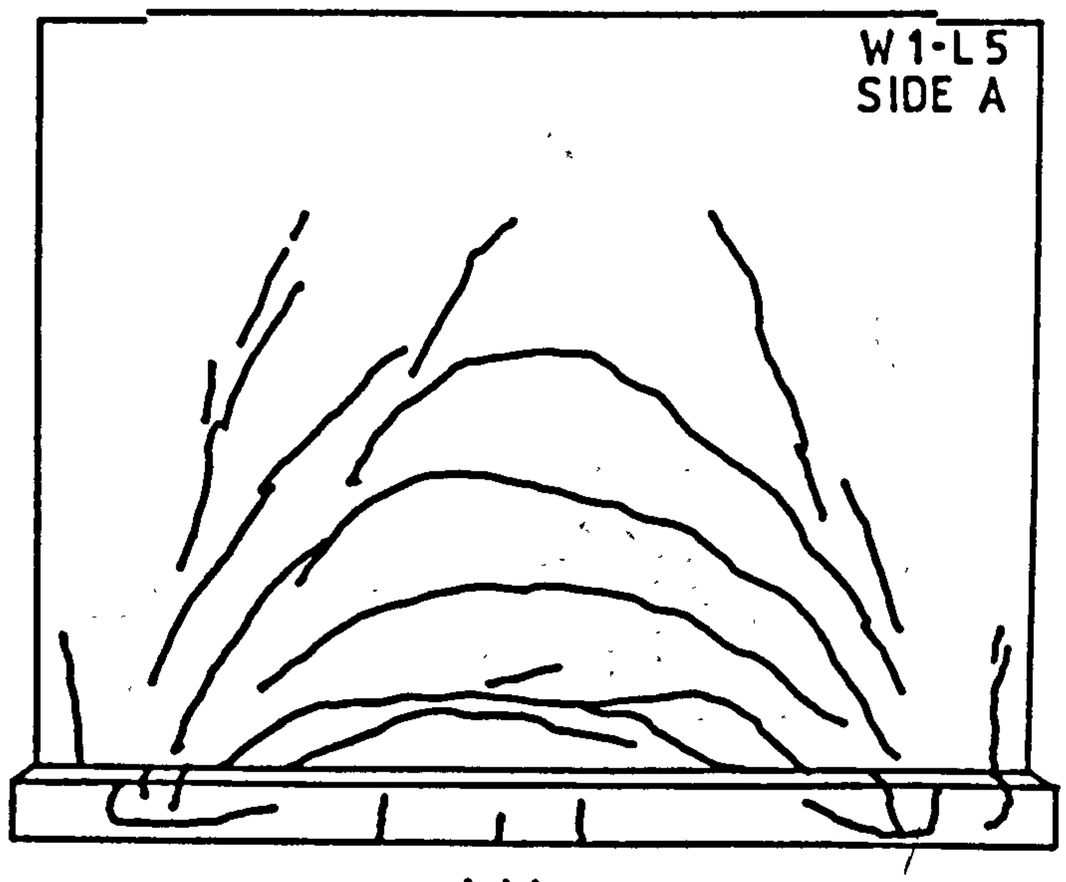

(d)

Fig. 4.26 Development of cracks in wall W1-L5

(a) Crack pattern at a load of 200 kN
(b) Crack pattern at a load of 400 kN
(c) Crack pattern at a load of 500 kN
(d) Crack pattern at a load of 570 kN

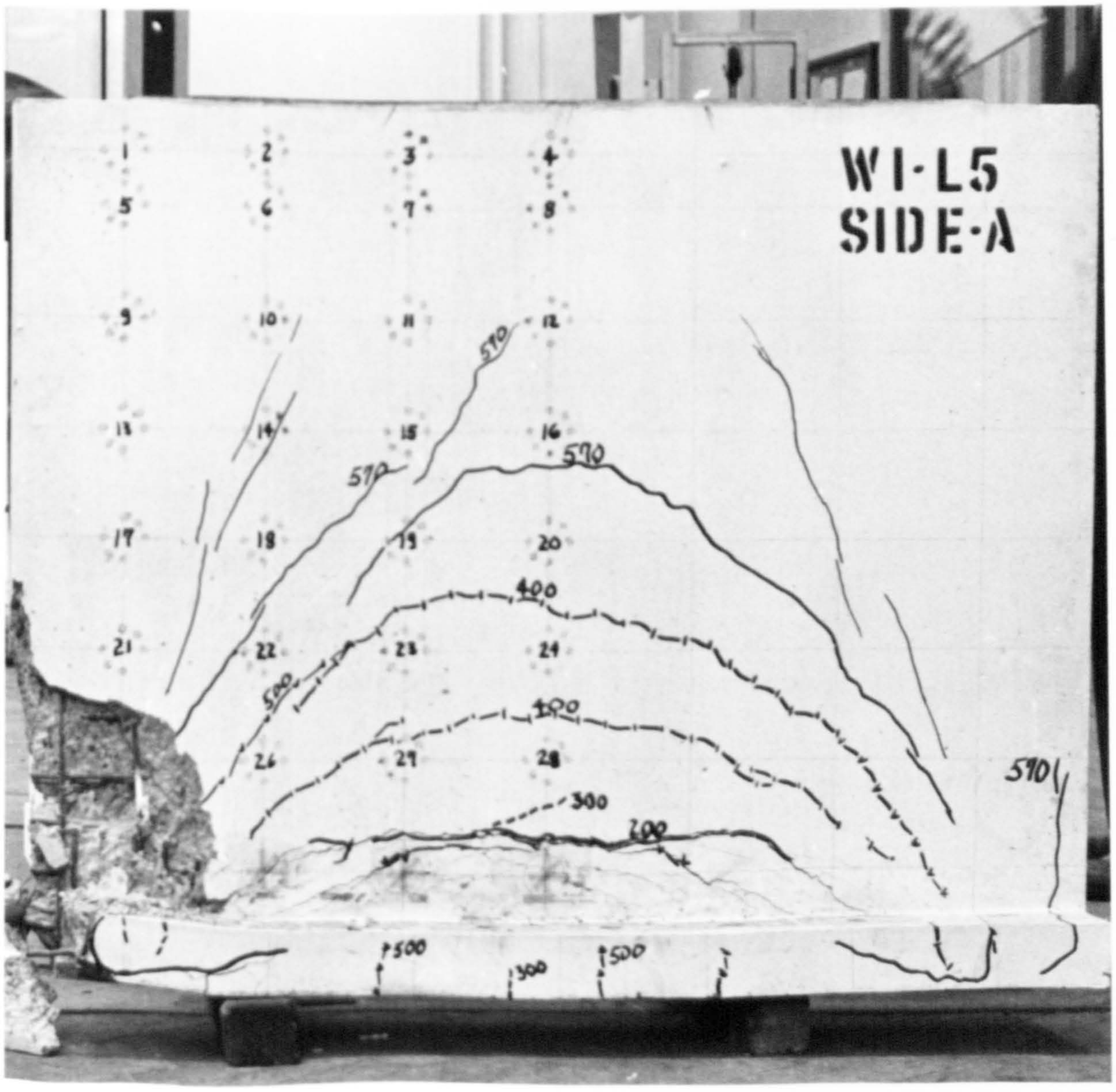

Fig. 4.27 Final crack pattern for specimen W1-L5

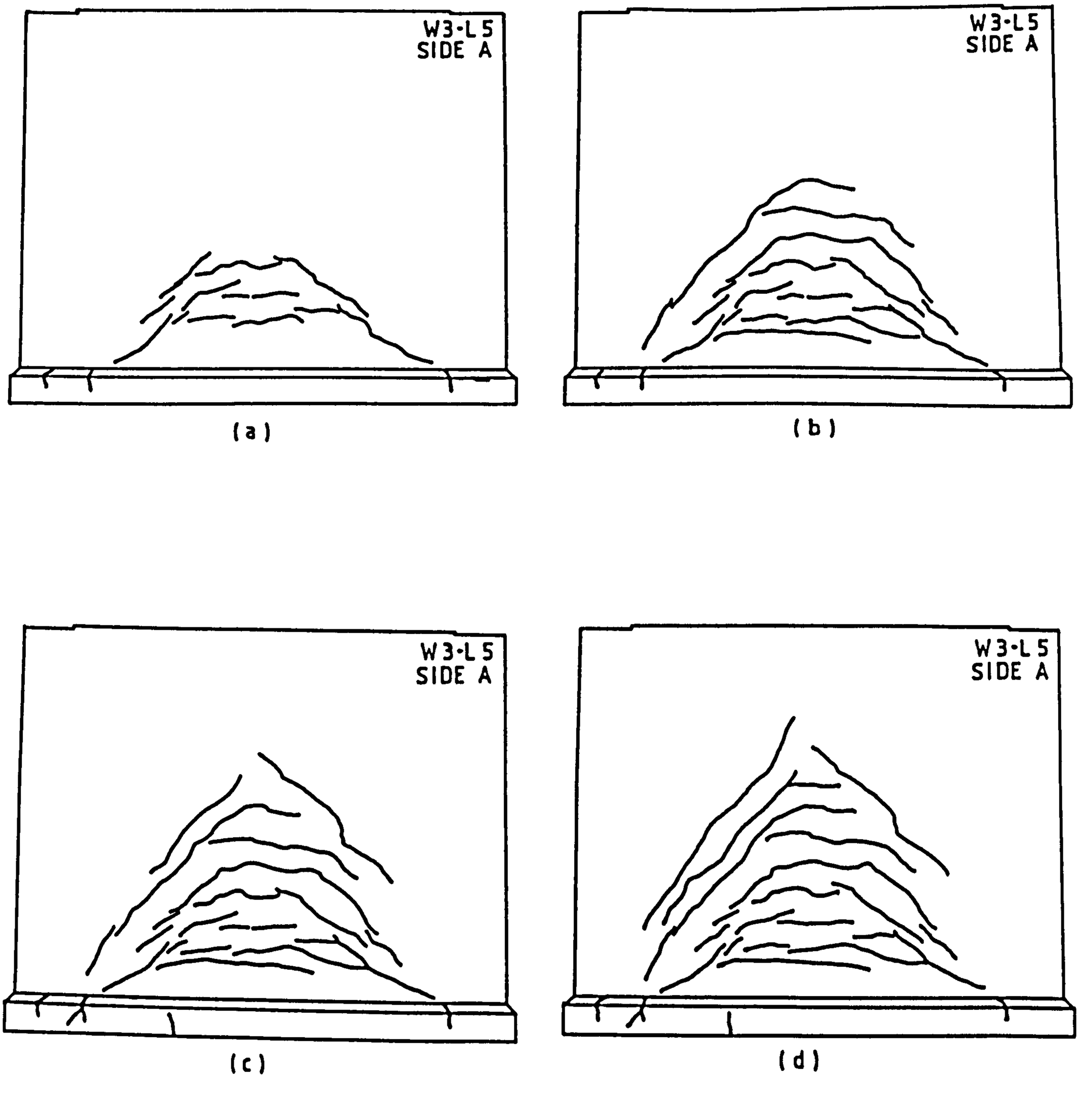

Fig. 4.28 Development of cracks in wall W3-L5

(a) Crack pattern at a load of 300 kN
(b) Crack pattern at a load of 400 kN
(c) Crack pattern at a load of 500 kN
(d) Crack pattern at a load of 600 kN

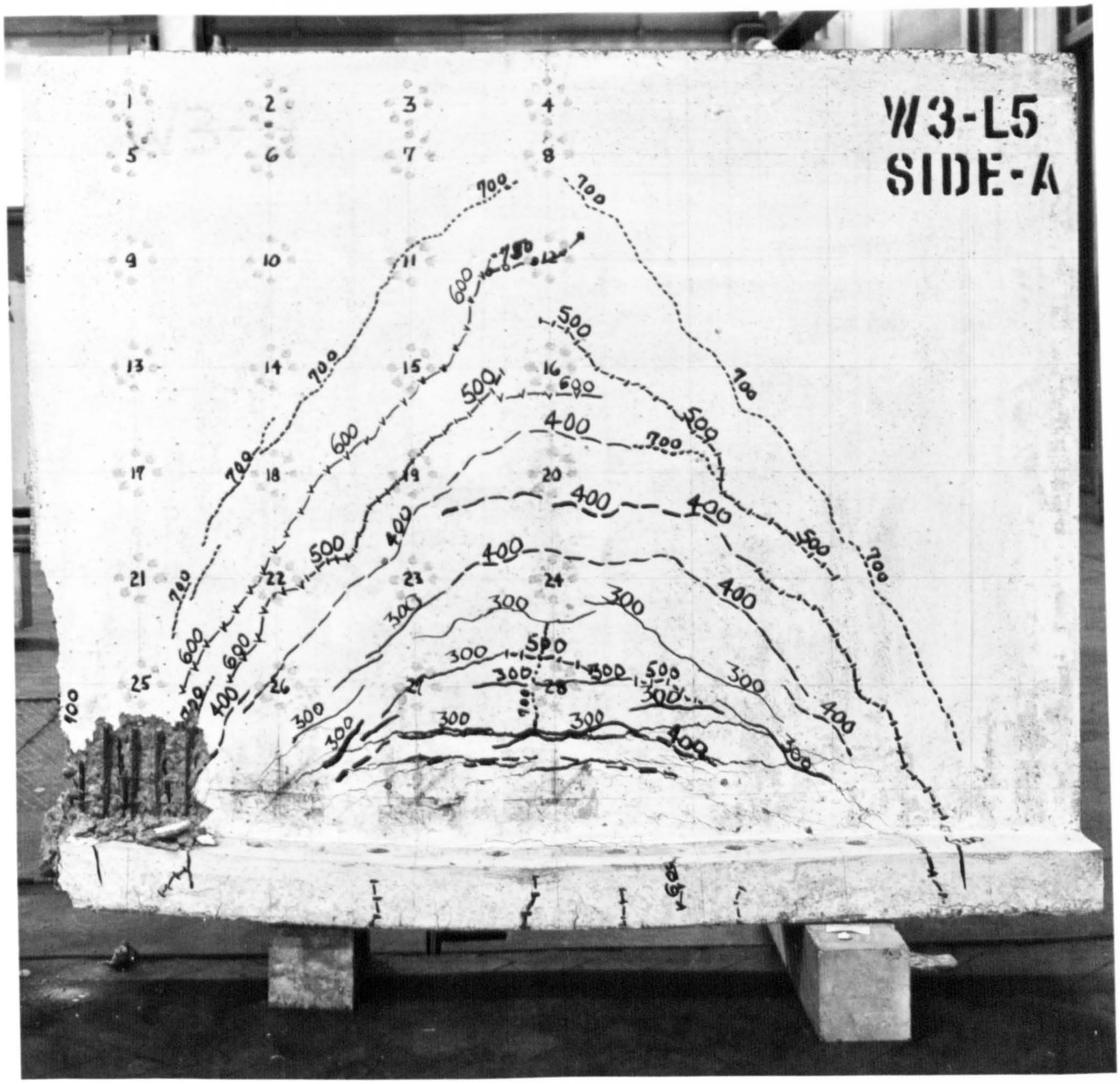

Fig. 4.29 Final crack pattern for specimen W3-L5

interesting feature. Under loads of 500 and 600 kN, the arrangement of cracks appeared as shown in Figs. 4.28(c) and 4.28(d). Figure 4.29 presents the final crack pattern. Note that at a load of 700 kN, large cracks were observed, enveloping those cracks formed earlier. The angle of inclination of these cracks altered as they propagated higher in the wall. In the lower third, the cracks were inclined at 65-70 degrees; in the middle third the angle was about 52 degrees and at the higher section, the slant of the crack was 30-40 degrees. Maximum load applied to this wall was 800 kN, when it failed due to crushing of the support zone as seen in Fig. 4.29. The average crack spacing along the vertical central section was 67 mm.

4.3 CRACK WIDTHS

In general, cracks were detected when their widths were between 0.02 and 0.06 mm. With each load increment the cracks were measured in order to discover the greatest crack width. In most cases, the first crack possessed the largest width throughout the test. With some specimens a diagonal crack provided the greatest crack width, especially those loaded on the top. For those members loaded at the bottom or under combinations of top and bottom loads, a horizontal crack invariably gave the largest crack width. Flexural cracks were insignificant in these specimens. They rarely propagated beyond the depth of the nib and their width was less than 0.1 mm. Cracks observed within the nib were not considered in the analysis of crack widths, since the evolution of cracks in this area is influenced by the local reinforcing details and the geometry. One example of this is the vertical crack formed in the nib, directly above the supports, in all the specimens with load on the top. These particular cracks can be seen in Figs. 4.1(a) and 4.3(a) and are created by the negative moment in this region. The nib was not designed

for bending moment, either positive or negative. Its purpose was to transfer the load on to the wall efficiently, without contributing to a large extent to the in-plane stiffness of the lower section of the wall. The behaviour of the nib is beyond the scope of this analysis.

4.3.1 Crack Width of Walls Loaded on Top (L1)

Figure 4.30 presents the maximum crack widths for the specimens loaded on the top. Specimens W1-L1 and W3-L1 had diagonal cracks first observed at a load of 600 kN. Maximum initial crack width in specimen W1-L1 was 0.06 mm and in specimen W3-L1, 0.04 mm. In wall W2-L1 the first diagonal crack was detected at an earlier load of 500 kN, measuring 0.02 mm. For the three specimens, this measurement took place at a height of about 250 mm from the soffit. The difference in the load at which the first crack was detected and the various crack widths of the first crack can be attributed to two factors; firstly, that specimen W2-L1 was reinforced less than the other two and was therefore more susceptible to cracking at earlier loads, and secondly, to human error in failing to detect the cracks on specimen W1-L1 and W3-L1 earlier. If we extrapolate in Fig. 4.30 the values for loads of 600 and 700 kN for speciemns W1-L1 and W3-L1, they would coincide at the same point as wall W2-L1 at a load of 500 kN.

On examining Fig 4.30, the maximum crack width seems to have developed similarly in specimens W1-L1 and W2-L1 except at the load stages of 800 and 850 kN. Crack widths in specimen W3-L1 were slightly narrower than those in the other two walls for every given load. This could be due to the larger percentage of vertical reinforcement in specimen W3-L1.

The maximum crack width measured was 0.20 mm at a load of 1000 kN on wall W2-L1. At the same load the crack width on specimen W3-L1 was 0.16 mm. In general, the results indicate that up to the 1000 kN load the

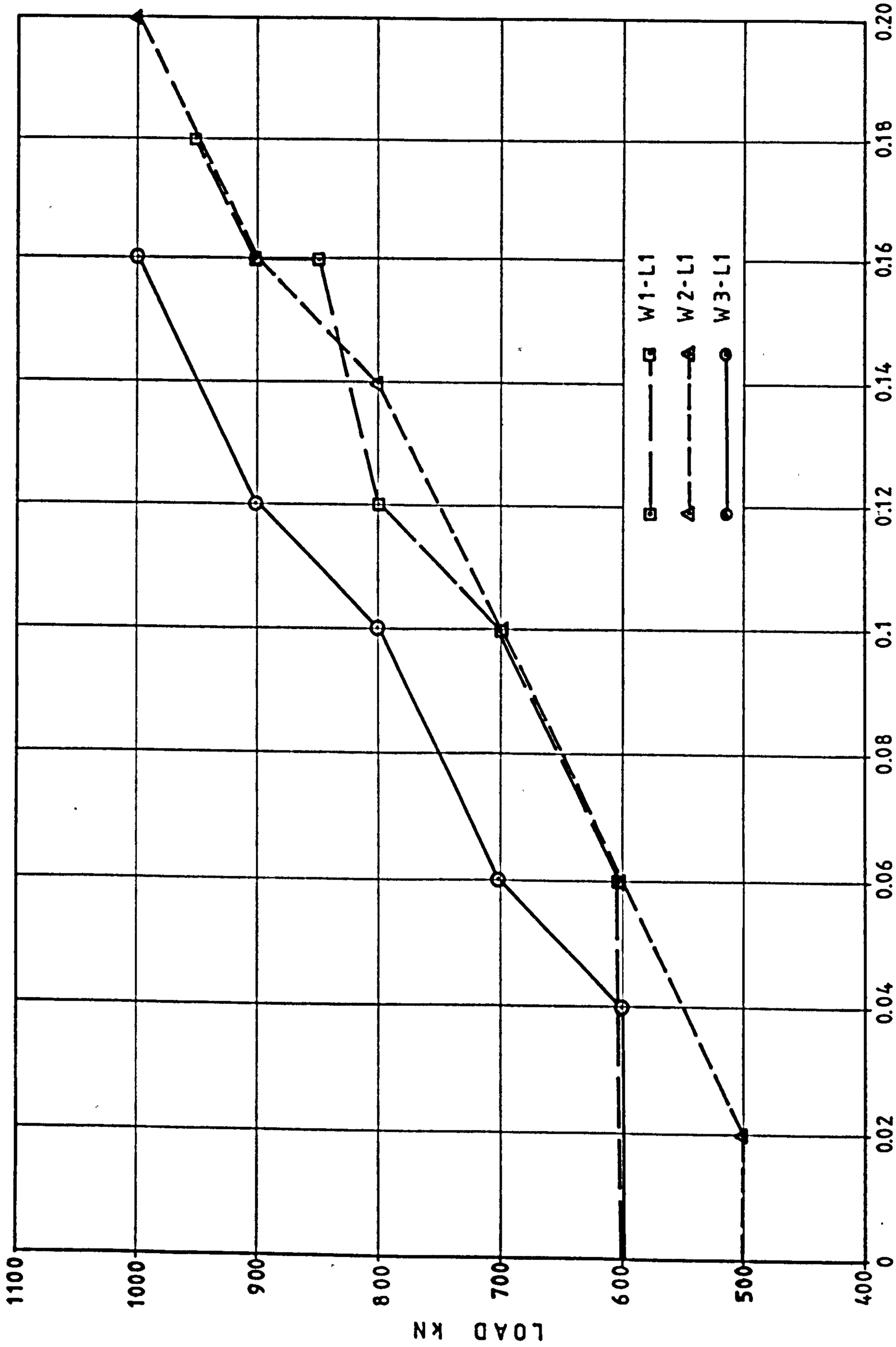

Fig. 4.30 Crack width development for walls loaded on the top - L1

crack width in the three specimens exhibited relatively linear behaviour.

4.3.2 Crack Width of Walls Loaded at the Bottom (L2)

The values of maximum crack widths for those walls loaded at the bottom is summarized in Fig. 4.31. This figure presents the crack width measurements up to 1.2 mm; a complete set of data is given in Tables 4.1 and 4.2. Invariably, the measurements of crack widths in these specimens were taken at the centre of the span. In specimen W4-L2, the first crack appeared at a load of 130 kN and measured 3.5 mm. This large crack width was expected because of the omission of vertical reinforcement. Under a load of 150 kN, the crack width increased to about 8.5 mm.

The initial horizontal crack width in specimen W2-L2 measured 0.06 mm at a load of 167 kN. It increased under subsequent loads as shown in Fig. 4.31 and its last measurement read 4.0 mm at a load of 300 kN.

Wall W1-L2 had its first horizontal crack at a load of 167 kN which measured 0.04 mm. The same crack opened to a width of about 6.0 mm at a load of 367 kN.

In specimen W3-L2 the first horizontal crack was detected at a load of 200 kN and had a width of 0.02 mm. Up to 267 kN load the crack width increased linearly. At a load of 433 kN the crack width became 2.50 mm.

For wall W5-L2, the first crack was observed at a load of 160 kN and its maximum width measured 0.02 mm. Maximum load applied to this specimen was 370 kN and up to this load, the crack width-to-load ratio was almost linear as shown in Fig. 4.31. The detection of the first horizontal crack in wall W5-L2 at an earlier load than specimen W1-L5, W2-L5 and W3-L5 was surprising, since it possessed the heaviest reinforcement.

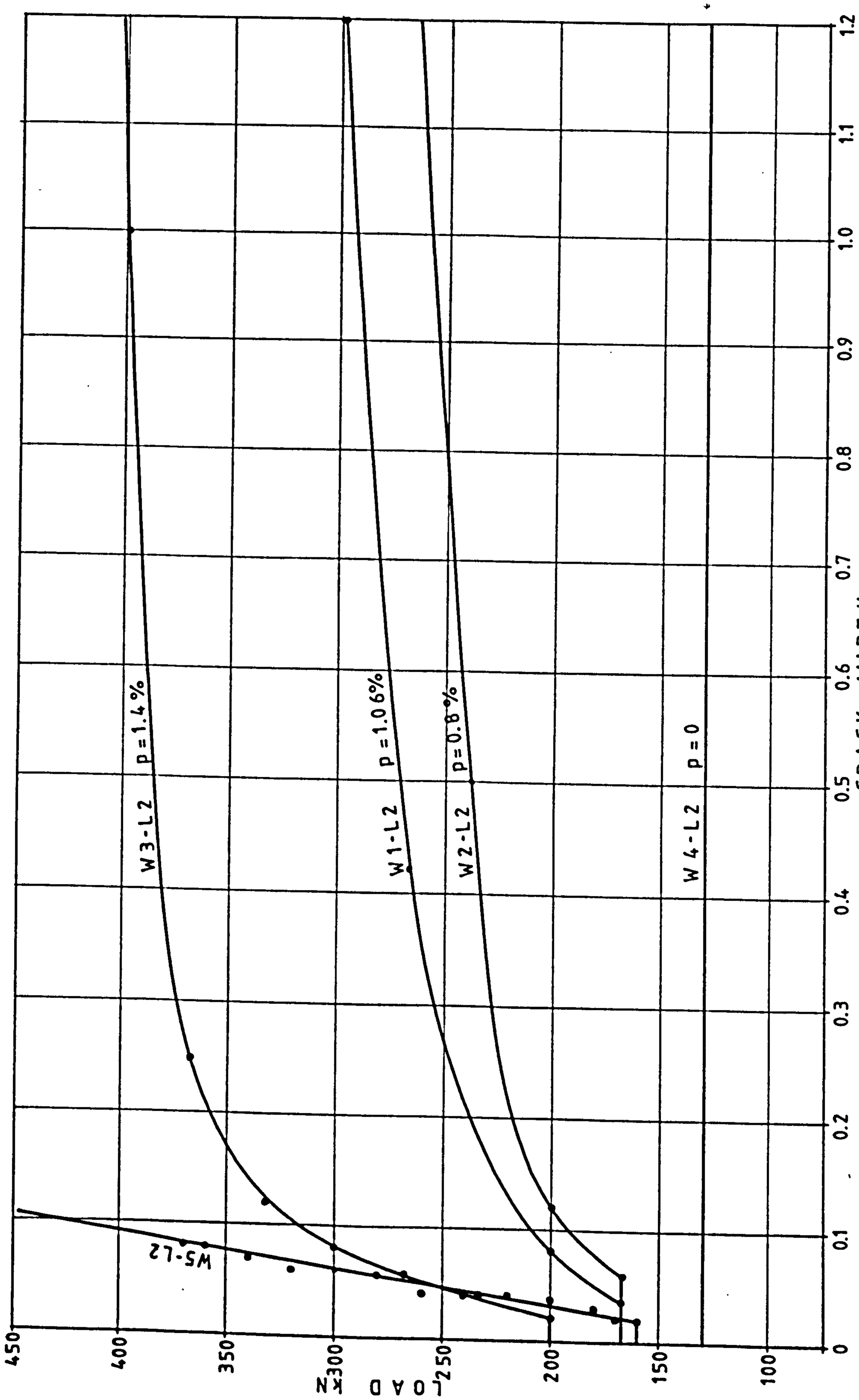

Fig. 4.31 Crack width development for walls loaded on the bottom only - L2

Table 4.1 Maximum crack widths (mm) measured in walls W1, W2 and W3 loaded on the soffit (L2)

LOAD kN	SPECIMEN W1-L2	W2-L2	W3-L2
167	0.04	0.06	-
200	0.08	0.12	0.02
233	0.20	0.50	0.04
267	0.42	1.40	0.06
300	1.20	4.00	0.08
333	2.50	-	0.12
367	6.00	-	0.25
400	-	-	1.00
433	-	-	2.50

Table 4.2 Maximum crack widths (mm) measured in walls W4 and W5 loaded on the soffit (L2)

LOAD kN	SPECIMEN W4-L2	W5-L2
130	3.5	-
140	4.0	-
150	8.5	-
160	-	0.02
180	-	0.03
200	-	0.04
260	-	0.04
280	-	0.06
320	-	0.06
340	-	0.07
360	-	0.08
370	-	0.08

4.3.3 Crack Width of Walls Loaded Under Load Type 3 (L3)

Maximum values for crack widths measured in specimens W1-L3, W2-L3 and W3-L3 are summarized in Table 4.3. Figure 4.32 shows these values for crack widths up to 1.2 mm. Initial horizontal cracks in specimens W1-L3 and W2-L3 were observed at a load of 300 kN and these measured 0.02 and 0.04 mm respectively. In specimen W3-L3 the first horizontal crack was detected at 400 kN and measured 0.02 mm.

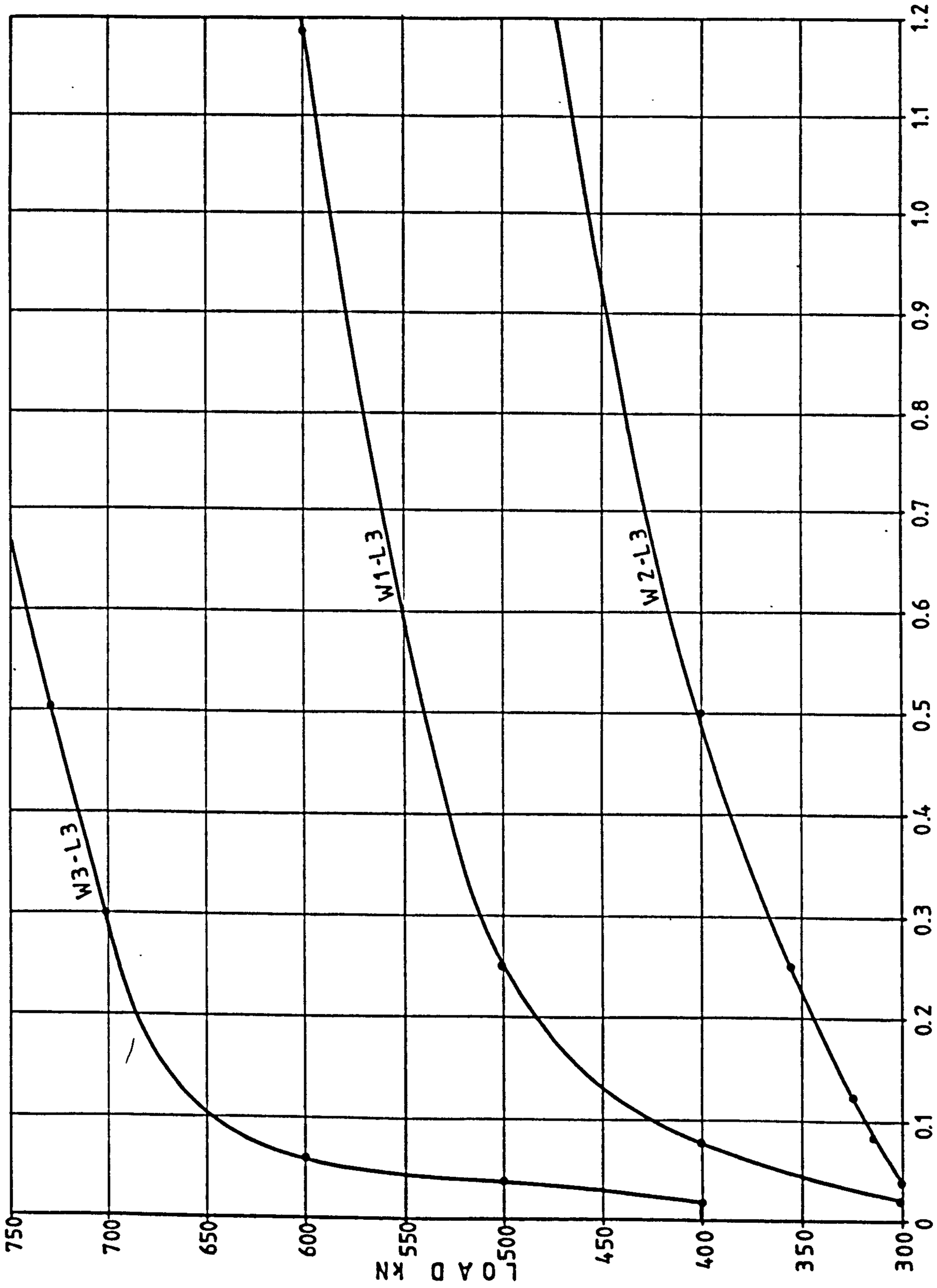

Fig. 4.32 Crack width development for walls loaded under load type 3 - L3

Table 4.3 Maximum crack widths (mm) measured in walls loaded under load type 3 (L3)

LOAD kN	SPECIMENS W1-L3	W2-L3	W3-L3
300	0.02	0.04	-
400	0.08	0.50	0.02
500	0.25	1.75	0.04
600	1.20	7.00	0.06
700	3.25	-	0.30
750	5.50	-	-
800	-	-	2.00

4.3.4 Crack Width of Walls Under Load Type 4 (L4)

The varying values for maximum crack width in specimens W1-L4, W2-L4 and W3-L4 up to a crack width of 0.7 mm shown in Fig 4.33. Table 4.4 presents the data concerned with the maximum crack width measured in these specimens under load type 4. It can be observed that in the three specimens, the first crack was detected at the same load (400 kN) and the crack width was 0.02 mm for speciemns W1-L4 and W3-L4, and in specimen W2-L4 measured 0.04 mm.

Table 4.4 Maximum crack widths (mm) measured in walls loaded under load type 4 (L4).

LOAD kN	SPECIMENS W1-L3	W2-L3	W3-L3
400	0.02	0.04	0.02
500	0.04	0.06	0.02
600	0.08	0.14	0.02
700	0.18	0.70	0.04
800	0.40	2.00	0.04
900	1.15	6.00	0.06
1000	2.00	8.00	0.10

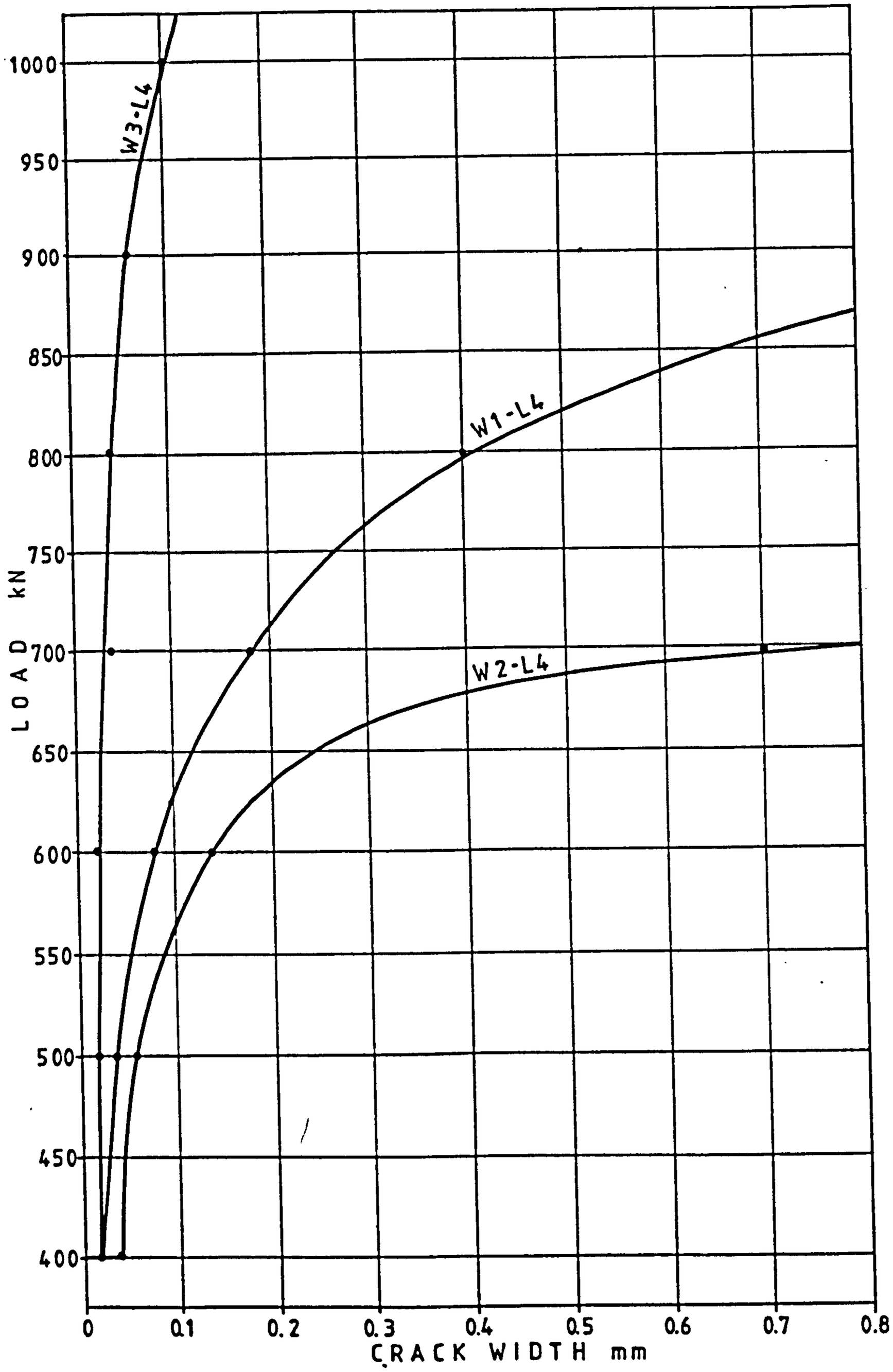

Fig. 4.33 Crack width development for walls loaded under load type 4 - L4

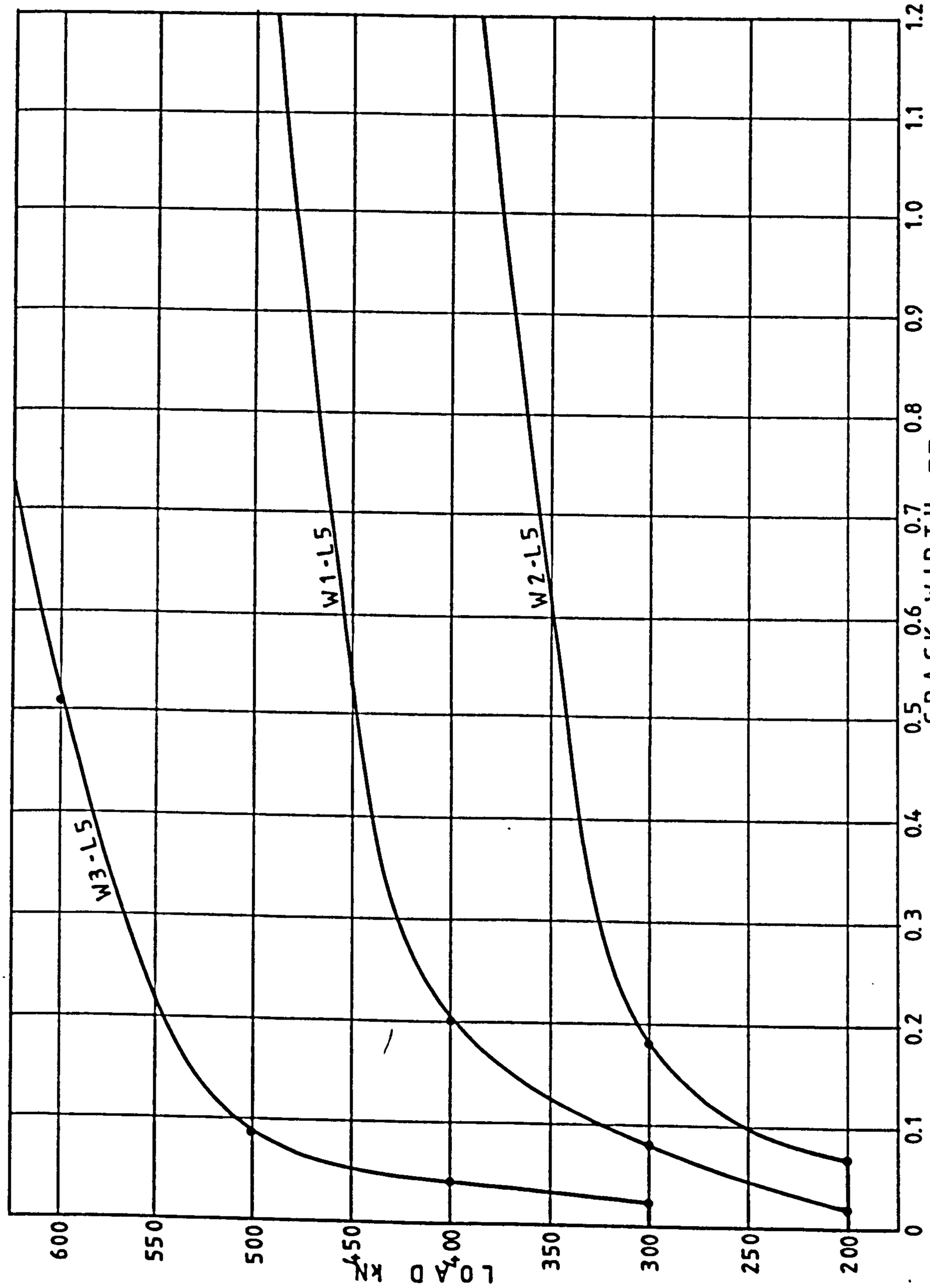

Fig. 4.34 Crack width development for walls loaded under load type 5 – L5

4.3.5 Crack Widths of Walls Under Load Type 5 (L5)

Changes in maximum crack width for specimens W1, W2 and W3 are shown graphically in Fig. 4.34 up to a crack width of 1.2 mm. Data for the three specimens loaded under load type 5 (L5) is provided in Table 4.5. The first horizontal cracks in specimens W1 and W2 were detected at 200 kN load and measured 0.02 and 0.07 mm respectively. In specimen W3 the first crack was observed at 300 kN load and measured 0.02 mm.

Table 4.5 Maximum crack widths (mm) measured in walls loaded under load type 5 (L5).

LOAD kN	SPECIMENS W1-L5	W2-L5	W3-L5
200	0.02	0.07	-
300	0.08	0.18	0.02
400	0.20	1.60	0.04
500	1.50	-	0.08
570	6.50	-	-
600	-	-	0.50
700	-	-	1.60
750	-	-	3.00
800	-	-	6.00

4.4 DISPLACEMENTS

The in-plane displacement was measured at 5 or 6 points along the soffit of each specimen. Presentation of this topic will be mainly based on the measurements recorded by the dial gauge at the centre of the span or the gauges most immediate to mid-span. In some cases, whenever it is convenient, the displacement measured by all the gauges will be shown graphically. The following discussion of results will be subdivided into five groups, based on the type of load.

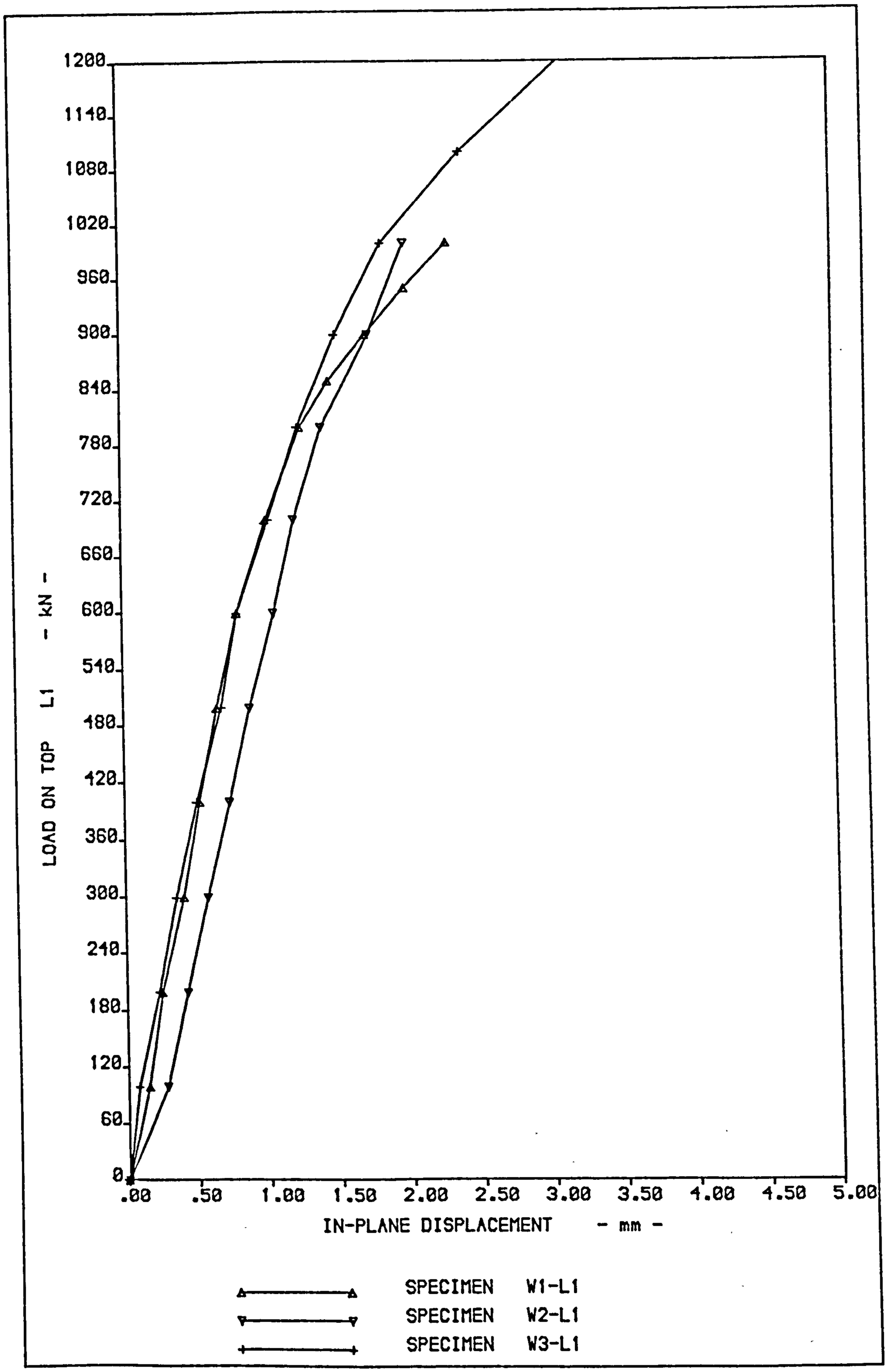

Fig 4.35 Comparison of displacement at mid-span for walls loaded on top (L1)

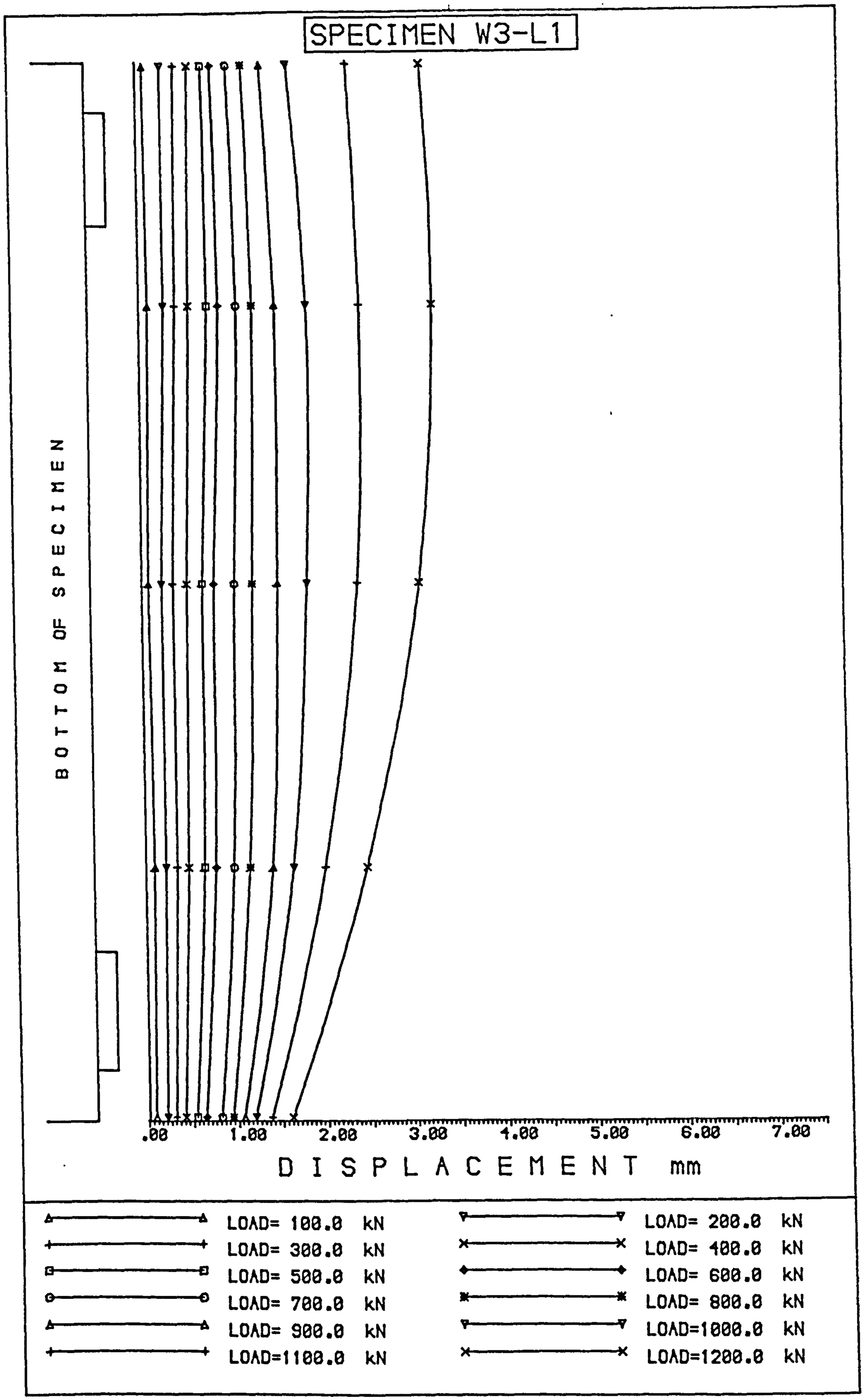

Fig. 4.36 Displacement measured at the soffit on specimen W3-L1 under different loads

4.4.1 Displacement of Walls Loaded on Top (L1)

Load-displacement curves for specimens W1-L1, W2-L1 and W3-L1 are exhibited in Fig. 4.35. These displacements were measured at mid-span. Wall W2-L2 gave the largest initial displacement and the difference between this and the values for the two other specimens remained almost constant up to a load of 800 kN. A linear relationship exists at the early stages of load and becomes non-linear after a load of 600 kN for specimens W1-L1 and W3-L1 and after 700 kN for specimen W2-L1.

Fig. 4.36 shows the displacements measured at 5 points on the soffit of wall W3-L1. These points are joined by curved lines, making the distinction of values for each load case easier. On examining this figure it appears that deflection of early loads is minimal and that the wall experiences a nearly uniform in-plane displacement. At higher loads some deflection was observed, which is shown graphically in the curve corresponding to the displacement at a load of 1200 kN (Fig. 4.36). In this case, the deflection calculated was about 16 percent of the total displacement of mid-span.

4.4.2 Displacement of Walls Loaded Under Load Type 2 (L2)

A total of five walls were treated under load at the bottom. Each of these specimens had different percentages of vertical reinforcement as explained in Section 3.1.1.

Fig 4.37 shows the in-plane displacement at the soffit of specimen W4-L2, which had no vertical reinforcement. It can be observed that up to a load of 120 kN the deformation was almost uniform along the soffit. At this stage of loading the stiffness of the wall was largely dependent on the capacity of the concrete to resist direct tension. Cracking of the wall took place at 130 kN load, producing a large deformation as

illustrated in Fig. 4.37. The section of the wall between the soffit and the horizontal crack was transformed into a slender beam with its capacity for carrying load depending on its bending rigidity only.

Fig. 4.38 demonstrates the effect of vertical reinforcement on the in-plane deformation once the concrete section cracks, together with the displacement exhibited by specimen W2-L2 having 0.8 percent reinforcement in the vertical direction. Up to 133 kN load, this wall deformed almost uniformly with hardly any perceptible deflection in the middle third of the wall. At a load of 167 kN (the load at which the first horizontal crack was detected), a substantial deformation was shown by dial gauges 3 and 4. Nevertheless, this deformation was relatively modest when compared with the deformation experienced by specimen W4-L2 (Fig. 4.37) at the cracking load. Evidently, in-plane deformation of the soffit of walls loaded under hanging loads is controlled mainly by the amount of vertical reinforcement, once the concrete cracks. Displacements measured by dial gauge 3 are shown for the five walls tested under this loading condition in Fig. 4.39. The load-displacement relation was almost linear for all the specimens, before the formation of horizontal cracks and it seems that the stiffness of all the walls was similar. Specimen W5-L2 was the exception, showing larger stiffness even before cracking of the concrete occurred due to the increased percentage of reinforcement. After cracking, the load-displacement relation was directly dependent on the percentage of reinforcement, i.e. the stiffness of each wall was proportional to the amount of reinforcement. This second region in the load-displacement curve was again linear but showed a smaller stiffness compared to that of the uncracked region. A third stage on the load-deformation curve is the non-linear part up to failure due to yielding and fracture of the vertical reinforcement.

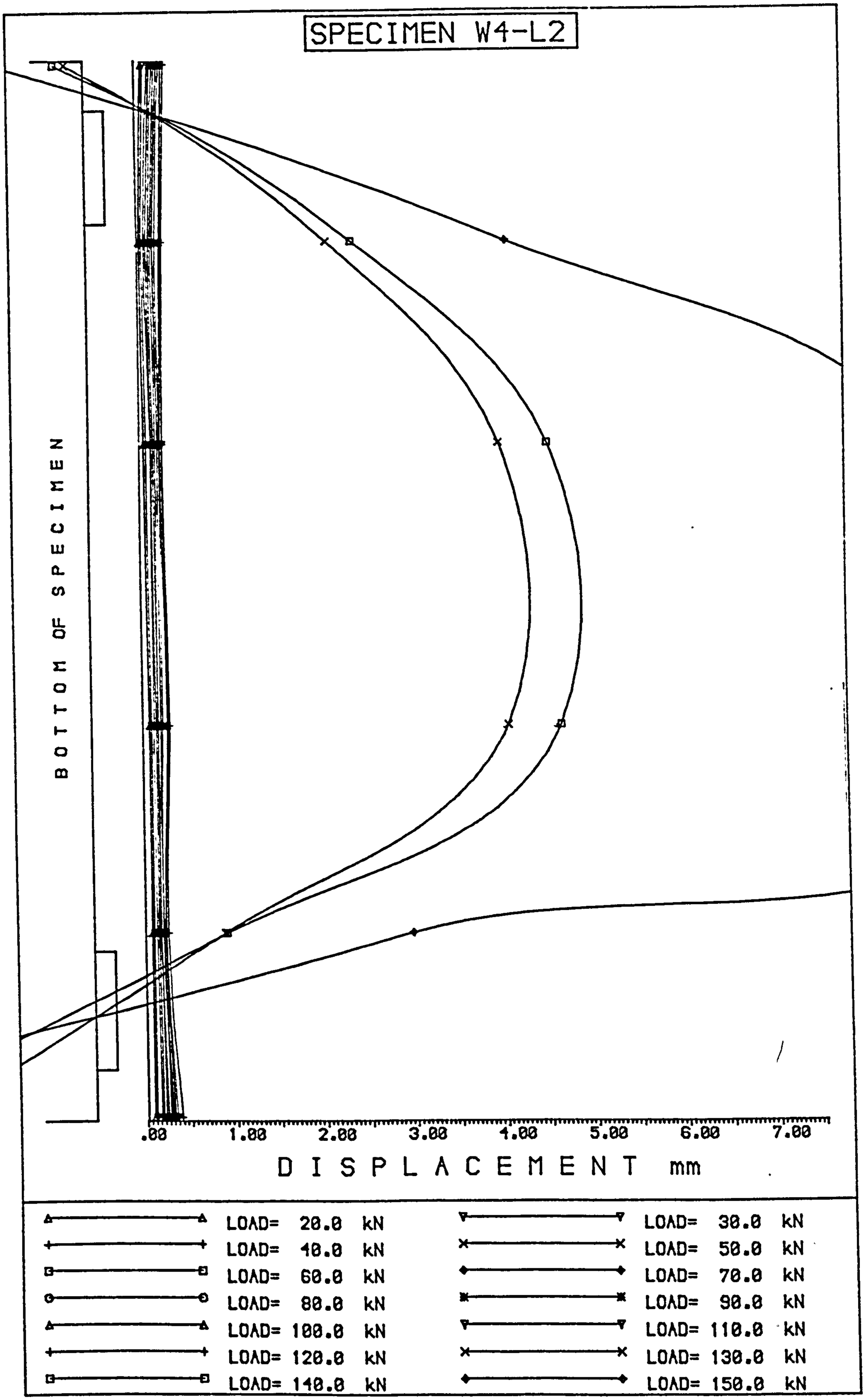

Fig. 4.37 Displacement measured at the soffit on specimen W4-L2 under different loads

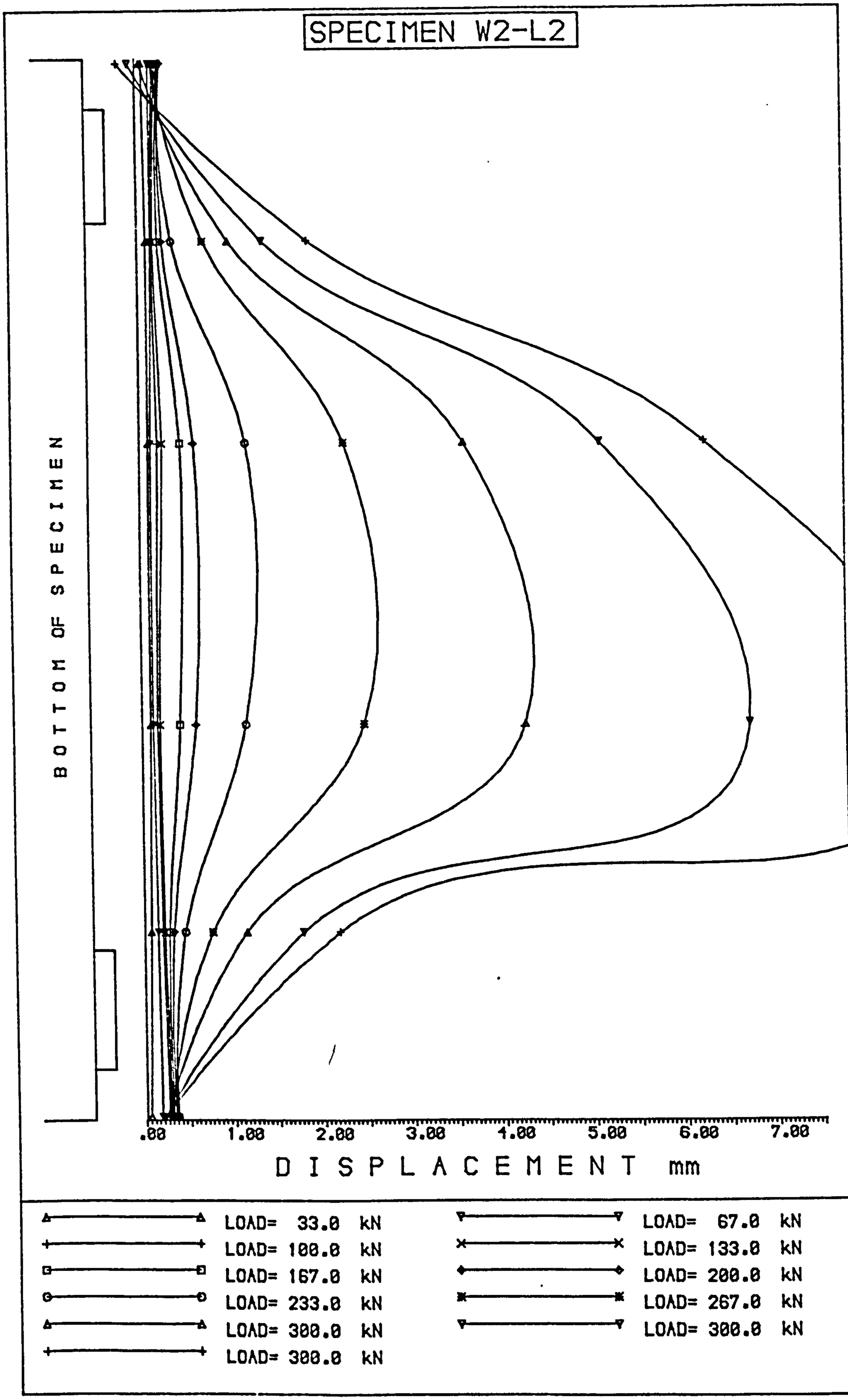

Fig. 4.38 Displacement measured at the soffit on specimen W4-L2 under different loads

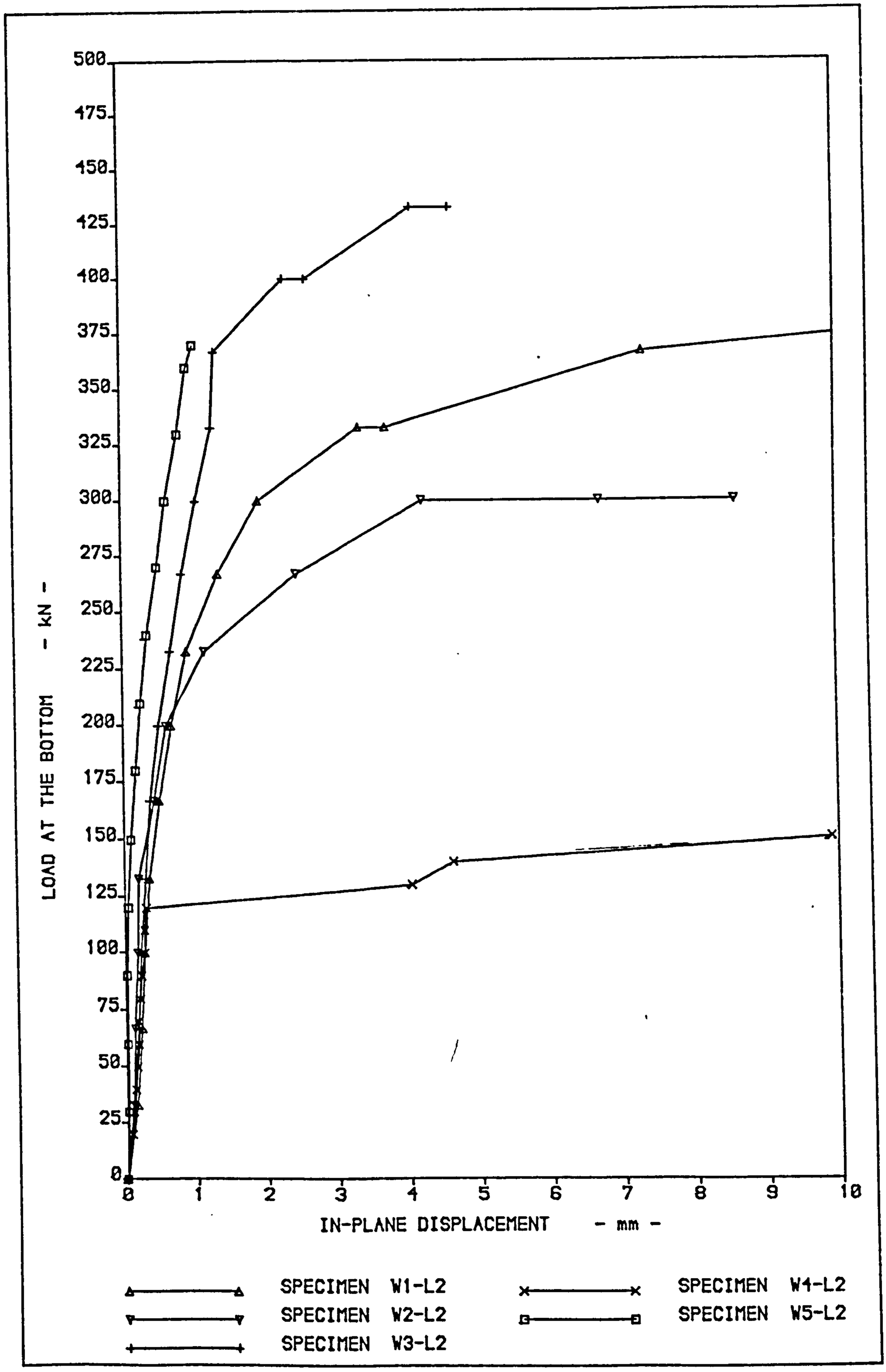

Fig. 4.39 Comparison of displacement at mid-span for walls loaded at the bottom (L2)

4.4.3 Displacement of Walls Under Combined Top and Bottom Loads (L3, L4 and L5)

In-plane displacements measured by dial gauge 3 on the soffit of the three walls tested under load type 3 are presented in Fig. 4.40. Stiffness was proportional to the percentage of vertical reinforcement in these walls, although at early stages of load the difference in the stiffness was not prominent. The same behaviour can be observed in Fig. 4.41 for load type 4 and in Fig. 4.42 for load type 5. For all these cases, the stiffness is not consistently proportional to the percentage of reinforcement at early stages of loading and before cracking takes place. Instead, it depends on the concrete section and the concrete properties.

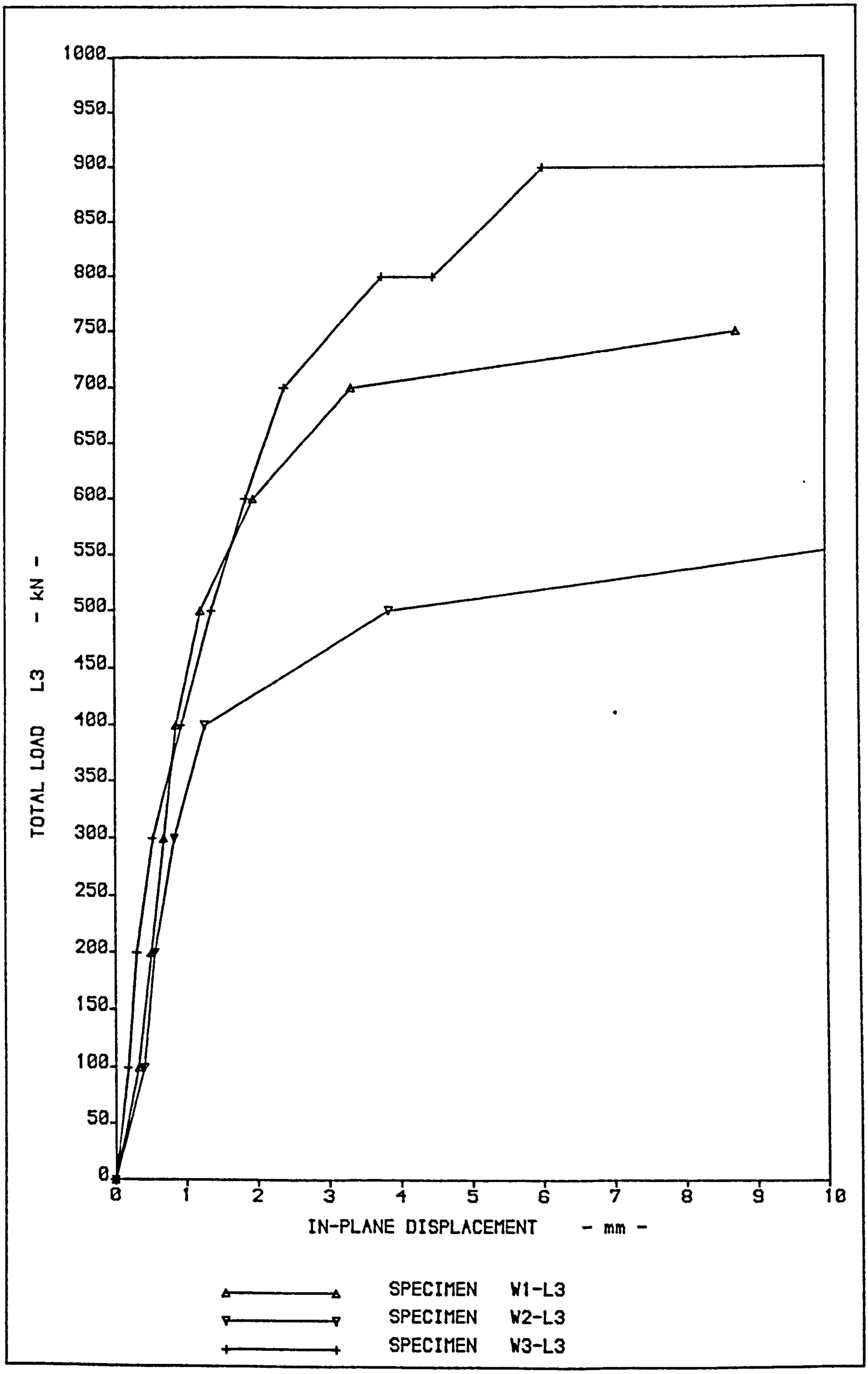

Fig. 4.40 Comparison of displacements at mid-span for walls loaded under load type 3 (L3)

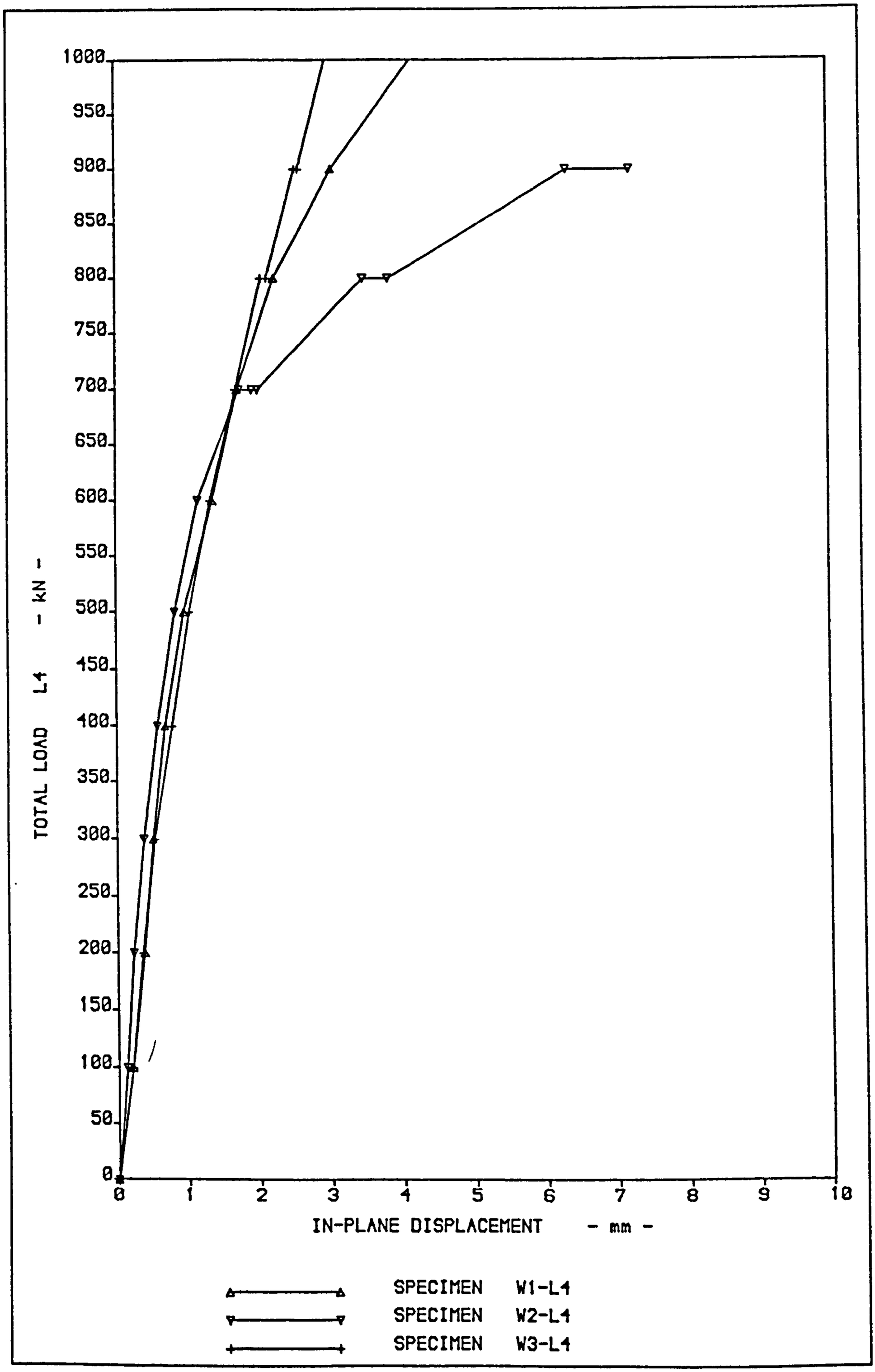

Fig. 4.41 Comparison of displacement for walls loaded under load type 4 (L4

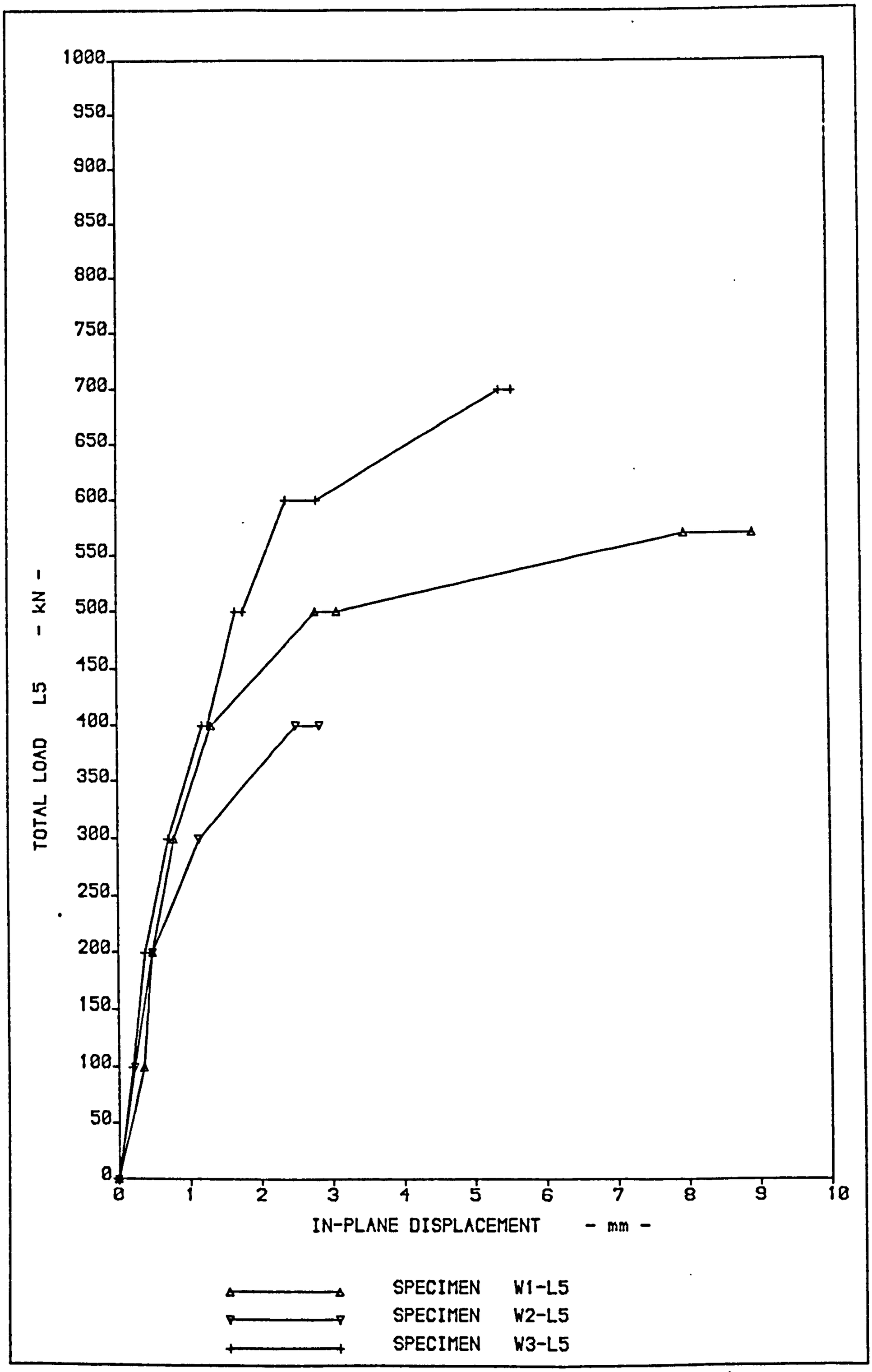

Fig. 4.42 Comparison of displacement for walls loaded under load type 5 (L5)

CHAPTER 5

EXPERIMENTAL RESULTS OF DEEP PANELS

5.1. INTRODUCTION

In this chapter, the experimental results obtained from the deep panels are presented and analysed. Data from tests are given in tabular form. For the purpose of analysis and comparison, graphs have been employed in most cases.

5.2 CRACK PATTERNS AND MODES OF FAILURE

Crack patterns at failure of specimens DB1 to DB7 are shown in Figs.5.1 to 5.7 respectively, illustrating the extent of the cracks and the load at which first observed. The numbers shown at the end of the cracks must be multiplied by 10 in order to obtain the load in kN, except in Figs.5.6 and 5.7 where they already represent kN.

Specimen DB1 (Fig. 5.1) first showed cracks at an early load of 150 kN within the central third of the span, these being flexural cracks.

These vertical cracks propagated quickly as the load increased, penetrating to approximately 2/3 of the depth of the panel. Next to appear at 400 kN load were inclined cracks within the shear span and at the soffit of the specimen, extending inwards and towards the top third of the beam. Further inclined cracks initiated close to the supports with increased load, and spread towards the loading points. When the inclined cracks appeared, the vertical cracks ceased to spread and those new cracks formed were the shear cracks between supports and loading points. At a load of 700 kN, the entire section joining the supports and the loaded points was cracked and, after sustaining 800 kN load for a short period of time, total failure occurred. Failure of specimen DB1 was a typical diagonal cracking failure with final

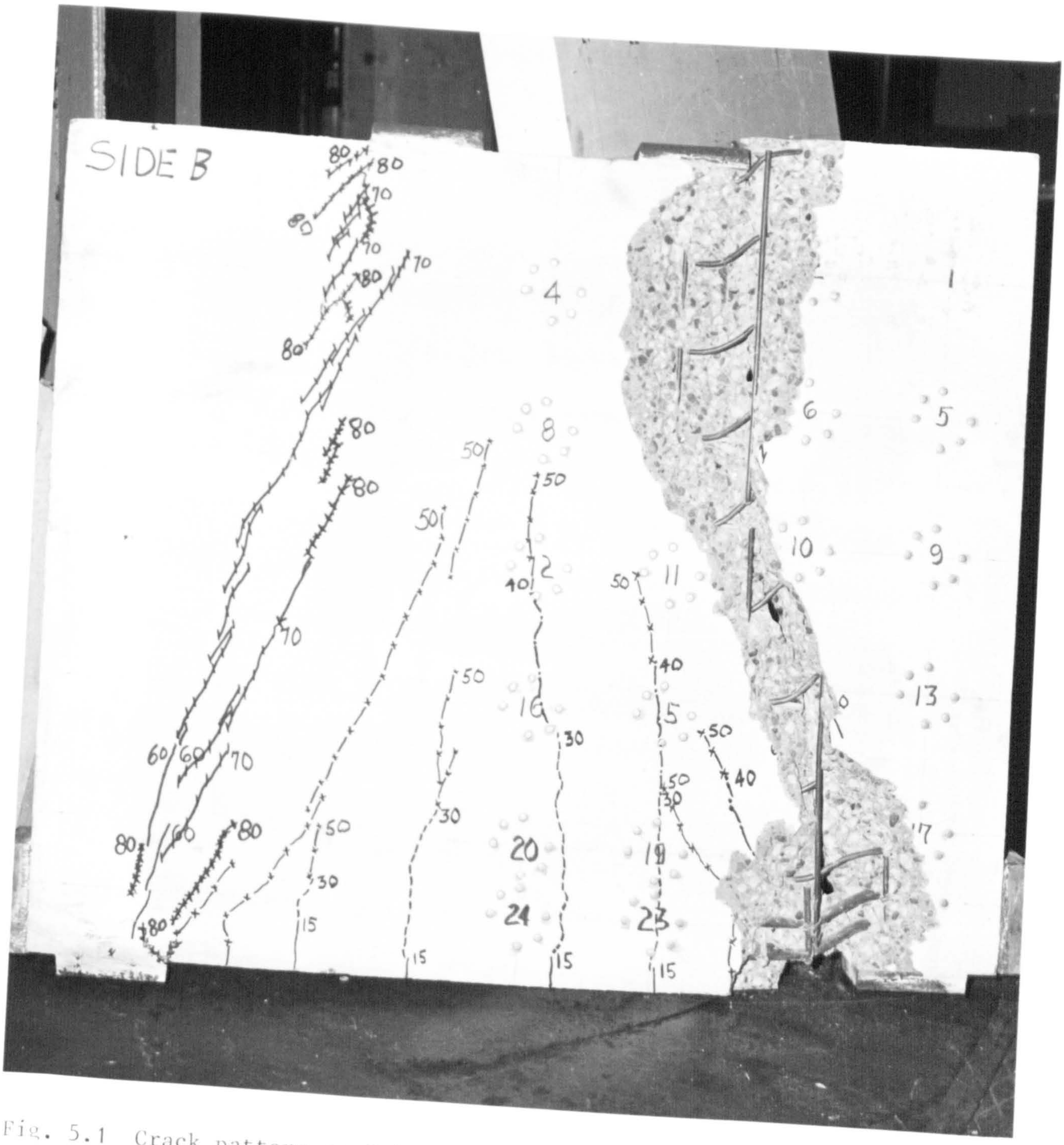

Fig. 5.1 Crack pattern at failure for specimen DB1

extensive crushing of the concrete between support and loading point.

Three of the methods described in Section 2.4 were used to calculate the shear capacity of the panel DB1. The results are as follows: Ramakrishnan and Ananthanarayana's method predicted a total force of 390 kN by using Eq. 2.27 and the recommended lower bound value of K = 1.12; the CIRIA method predicted a top load shear capacity of 384 kN (Eq. 7.14); ACI-77 (Eq. 7.8) gives an ultimate shear capacity of 397 kN. It is interesting to note that of these three procedures, only the ACI-77 method considers the presence of vertical and horizontal web reinforcement, but its prediction does not differ much from that of the other two methods in the case of the specimen analysed. Another interesting point is that in the shear calculations for specimen DB1 using the ACI-77 recommendations, the contribution of concrete is only 63 percent of the total shear capacity of the reinforced section. The three procedures employed agree in their predictions for ultimate load capacity of specimen DB1 and their predicted values corresponding to the load at which the first diagonal cracks appeared in the model tested.

Cracks in specimen DB2 (Fig. 5.2) started at 300 kN load in the central third of the span and at the soffit. Crack formation was similar to that of specimen DB1, but did not propagate at the same rate with increasing load. The first diagonal crack appeared at a load of 500 kN but its length was considerably less compared with the first diagonal crack that appeared in specimen DB1. Cracks near the supports were fewer and in general, the vertical and inclined cracks spread to a height approximately equal to 0.5 L. This specimen failed by crushing of the bearing block.

Vertical cracks first became visible in specimen DB3 (Fig. 5.3) at a load of 400 kN, and propagated slowly with increasing load.

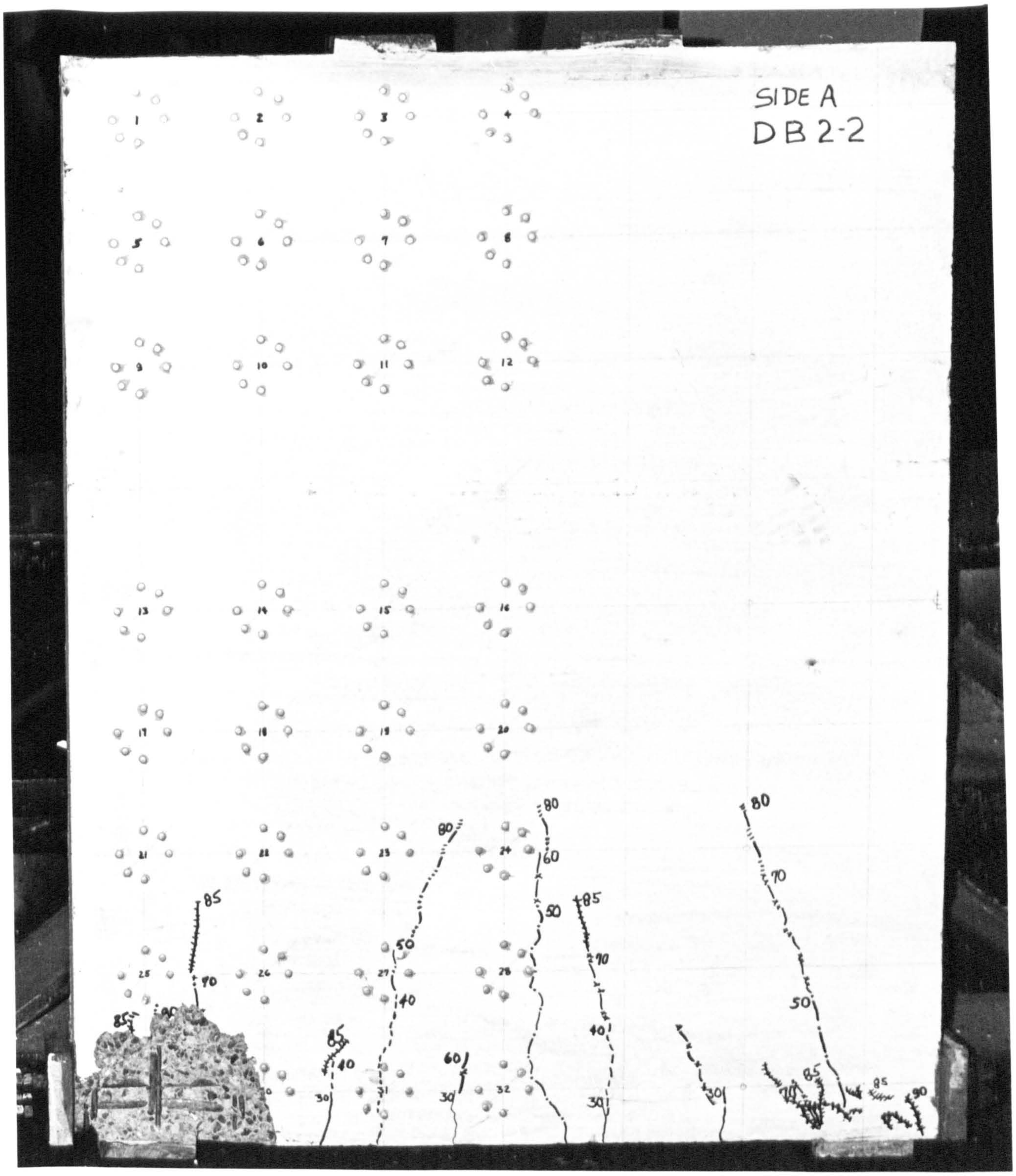

Fig. 5.2 Crack pattern at failure for specimen DB2

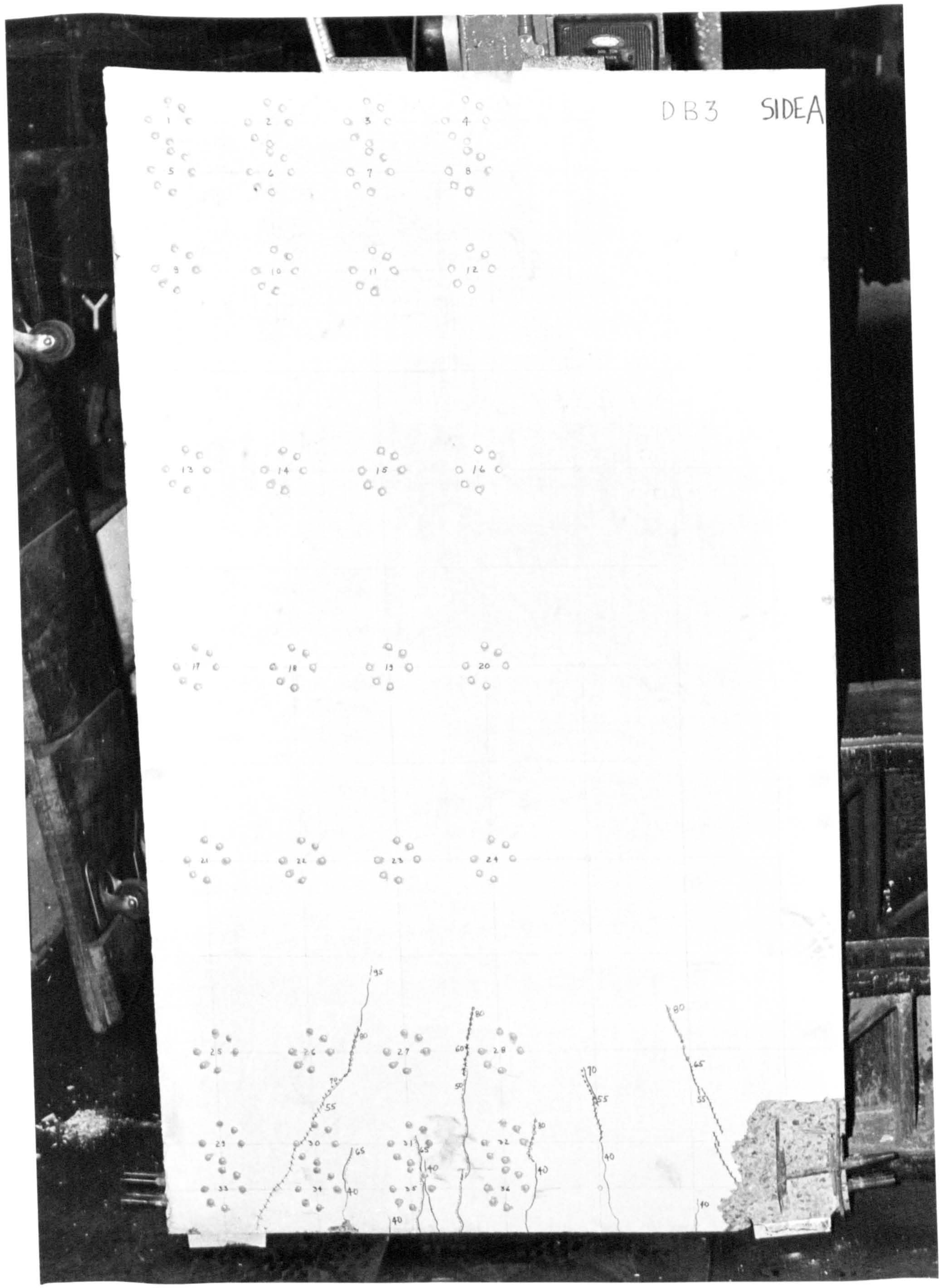

Fig. 5.3 Crack pattern at failure for specimen DB3

Diagonal cracks were first seen at a load of 550 kN, originating at the soffit of the specimen close to the load block. They extended very slowly with increasing load, reaching a maximum height of about 0.5 L. This element failed at a load of 950 kN by local crushing of the concrete at one of the supports.

In specimen DB4 (Fig. 5.4) the first cracks to form were flexural cracks within the central half of the span. These were observed at a load of 200 kN and extended from the soffit to the level of the main reinforcement. With increasing load these cracks propagated vertically, finally lengthening at a load of 650 kN. At 600 kN load, diagonal cracks appeared in the support region, just above the level of the uppermost main reinforcement bar. Failure of this panel occurred at a load of 800 kN by crushing of concrete on both supports simultaneously.

The crack pattern of specimen DB5 (Fig. 5.5) was similar to that of DB4. Flexural cracks were seen first at a load of 150 kN with diagonal cracks appearing at a load of 700 kN. The final mode of failure was also similar to DB4 and occurred at 940 kN load.

Panel DB6 showed fewer cracks than the previous specimens with its first diagonal crack visible at 700 kN load. Total failure happened under a load of 950 kN by crushing of the concrete in a bearing zone.

The modes of failure of specimens DB2 to DB6 were similar, in that,at the final stage of loading,the concrete of one or both load bearing zones failed in compression with outward buckling of the web reinforcement here,producing in some cases spalling of large sections of concrete cover.

Leonhardt and Walther (1966) reported tests on deep beams with depth/span ratio = 1 in which crushing of the bearing blocks was the

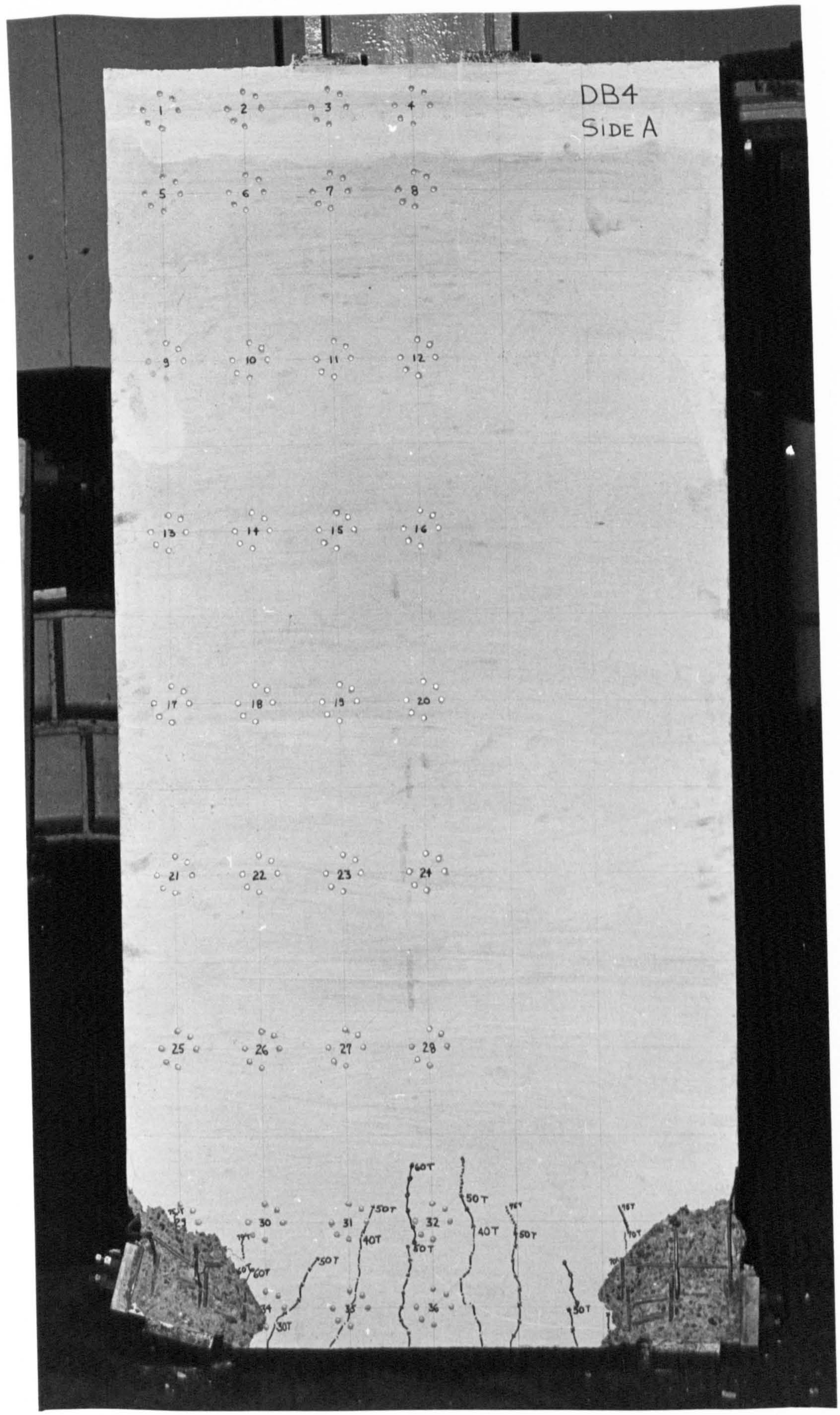

Fig. 5.4 Crack pattern at failure for specimen DB4

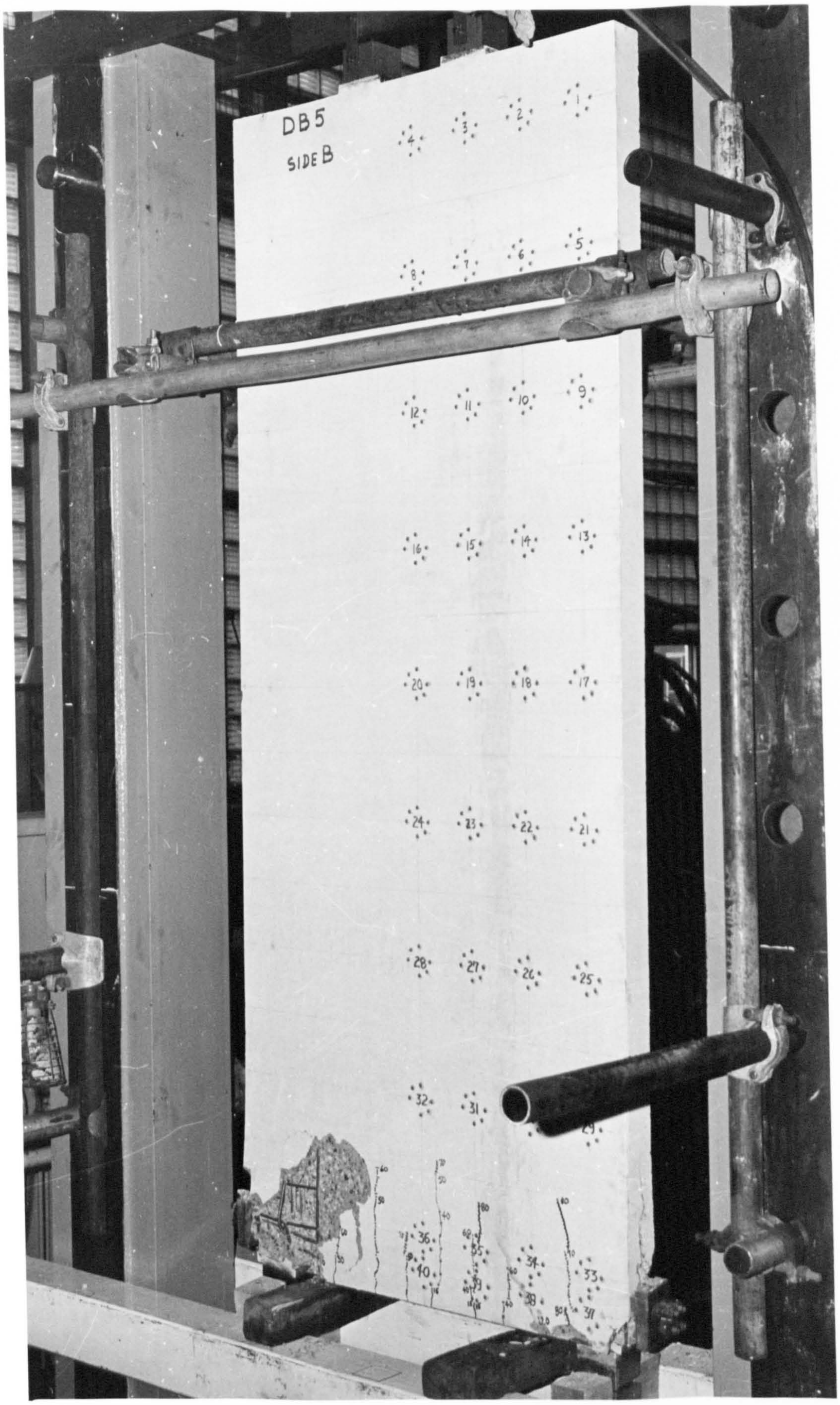

Fig. 5.5 Crack pattern at failure for specimen DB5

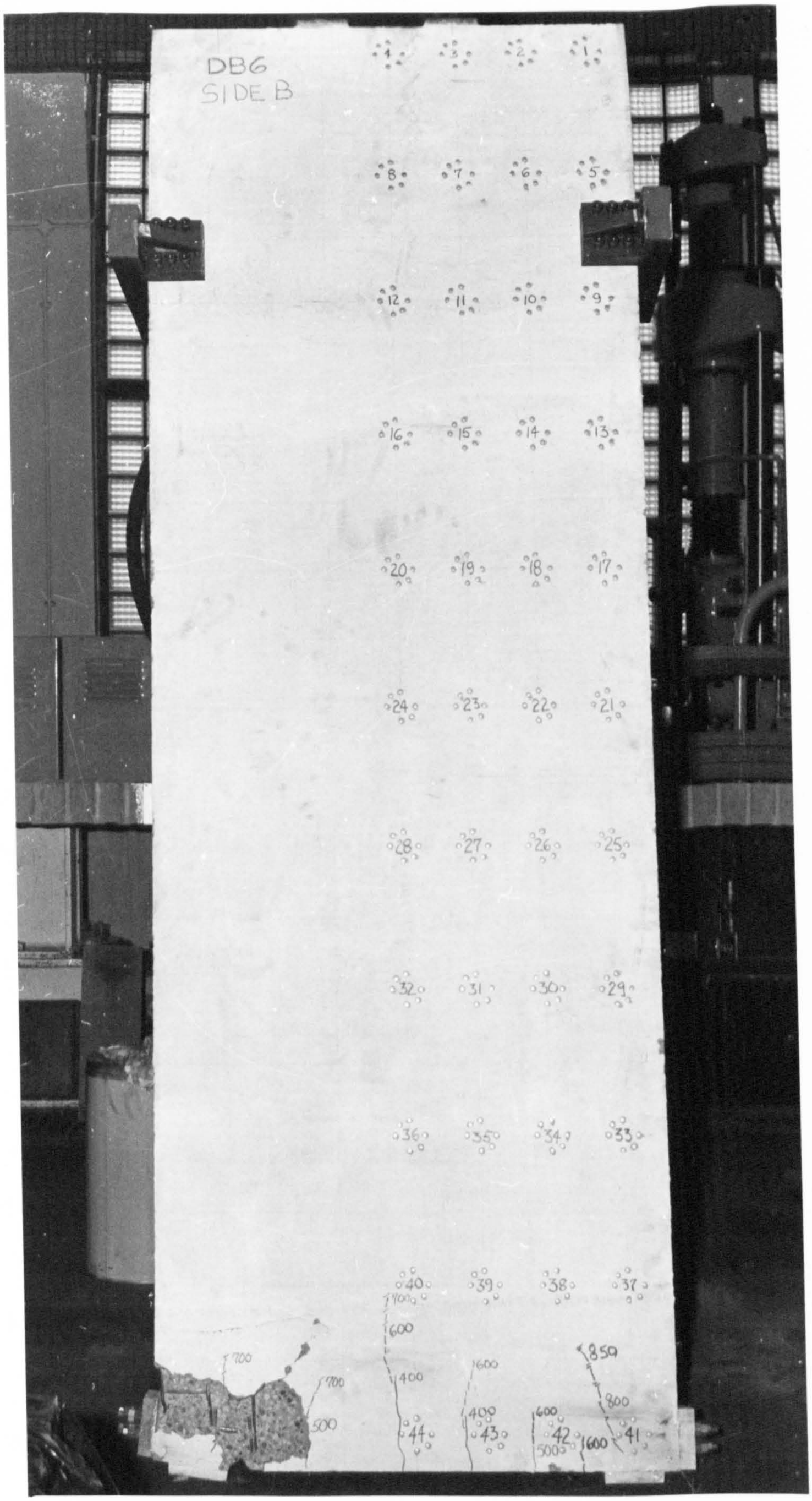

Fig. 5.6 Crack pattern at failure for specimen DB6

principal mode of failure. Leonhardt (1966) went further saying that for deep beams with span/depth ratio less than 2, one should not speak of shear and shear reinforcement, since such beams always fail because the concrete crushes near the bearing. Kong et al (1970) reported the test of deep beams with span/depth ratio of 1 to 3. Diagonal cracking was the primary cause of failure and crushing of concrete was only a secondary effect. For moderately deep flexural elements (span/depth ratio > 1), crushing of the bearing zone does not necessarily have to be the main failure mode. Strictly speaking, the failure mode for moderately deep flexural elements depends on such factors as web reinforcement and size of the bearing blocks. These structural elements when designed with adequate reinforcement to resist shear forces and bending moments are expected to fail at the supports due to the concentration of compressive stresses.

In cases where the span/depth ratio of flexural members is less than 1, the only mode of failure attained is crushing of the support blocks. This has been the failure mode of the five elements (DB2 to DB6) discussed in this chapter. Due to the importance shown by this failure mode, the matter is discussed further in Chapter 8.

Failure of specimen DB 7 (Fig. 5.7) was due to buckling. Up to failure load the cracks in the lower section of the panel were very few and short in length. The first flexural cracks were observed at a load of 400 kN and the only diagonal crack appeared at a load of 700 kN. Total failure took place at 900 kN load, demonstrating horizontal cracks at mid-height as shown in Fig. 5.7.

The loads and modes of failure of the deep panels tested are summarized in Table 5.1

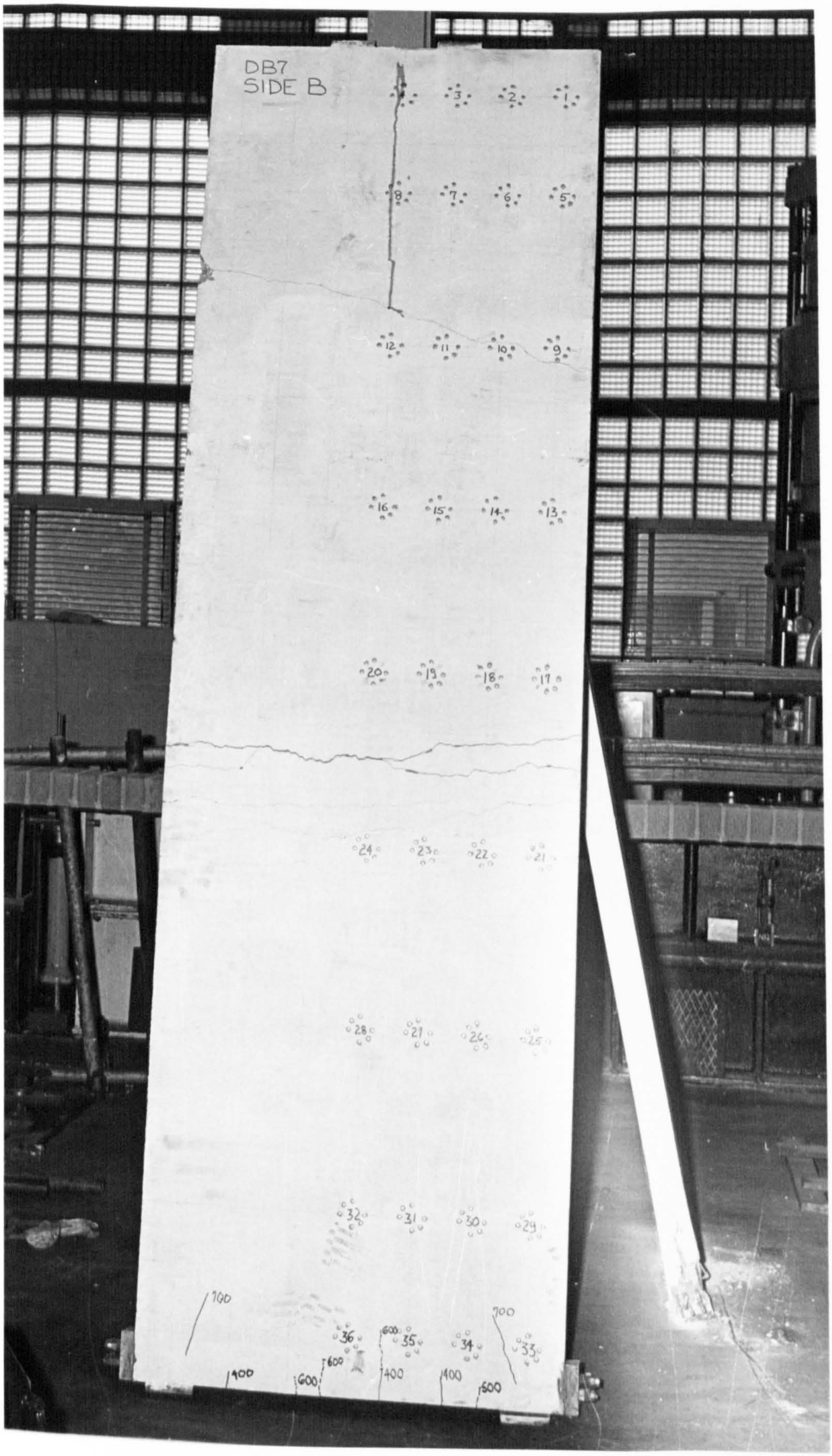

Fig. 5.7 Crack pattern at failure for specimen DB7

Table 5.1 Modes of failure and failure loads of the deep panels

SPECIMEN	FAILURE LOAD (kN)	MODE OF FAILURE
DB1	800	Shear - Diagonal cracking
DB2	900	Crushing of bearing block
DB3	950	-do-
DB4	800	-do-
DB5	940	-do-
DB6	950	-do-
DB7	900	Buckling

5.2.1 Discussion of Crack Patterns of Deep Panels

One of the aspects that this experimental analysis has followed is the load at which the first diagonal crack appeared in each specimen. Figure 5.8 presents a graphical summary of this observation, showing that the load at which diagonal cracks occurred became larger as the depth-to-span (H/L) ratio increased from 1 to 3. Thereafter, it appears that the diagonal cracking load was not affected by the depth-to-span (H/L) ratio. The relationship between the H/L ratio and the diagonal cracking load was almost linear for values of H/L from 1 to 3. This linear relationship is represented by the dashed line in Fig. 5.8, which corresponds to the following expression:

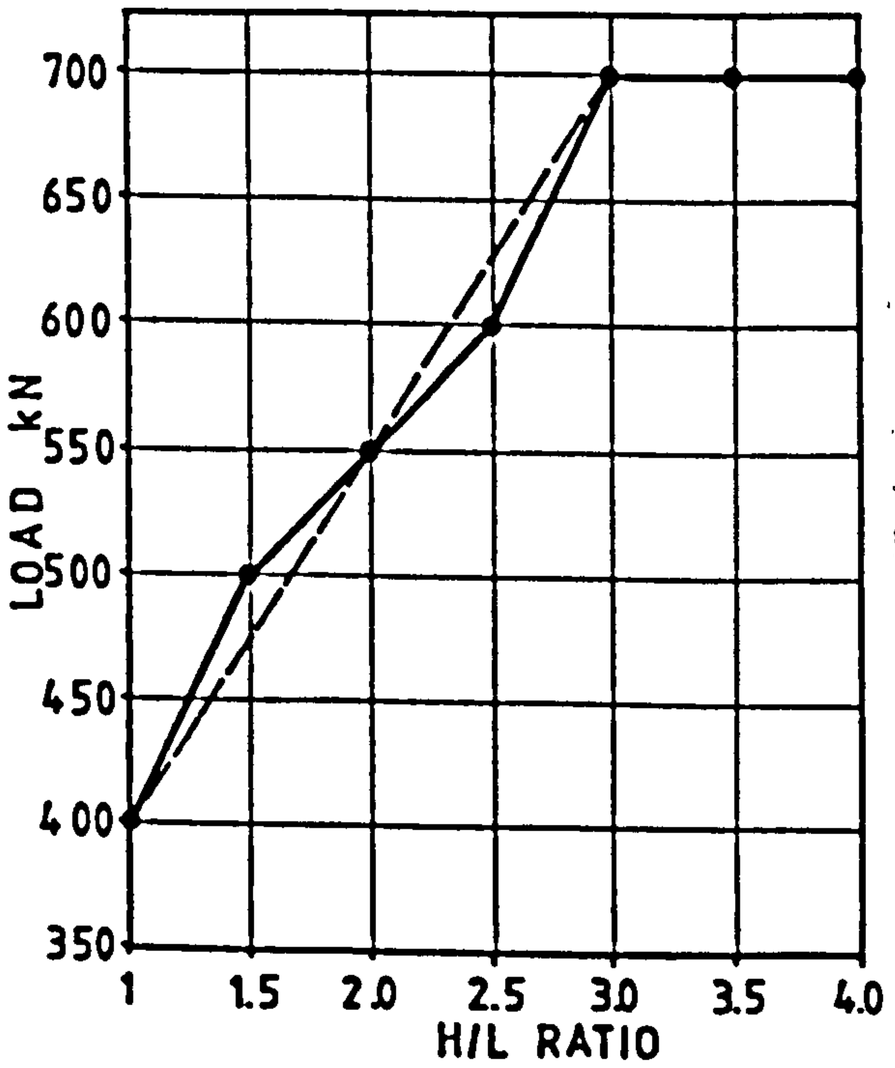

Fig. 5.8 Load at which first diagonal load was detected versus depth-to-span ratio

$$P_{cr} = 400 + (H/L - 1)150 \qquad 5.1$$

where (H/L - 1) should not exceed 2. Since these specimens were loaded at third points of the span, equation 5.1 can be expressed in terms of the shear strength of the section in the following form:

$$V_{cr} = V + (H/L - 1)75000 \qquad 5.2$$

where

V = cracking strength of the section for H/L = 1, N

V_{cr} = cracking strength of section for H/L > 1, N.

Comparing the height to which the cracks spread in each panel, it can be observed that the deeper the element, the lower the extension of the crack. This took place for both bending and diagonal cracks. Figure 5.9 compares the maximum height reached by the flexural cracks in each panel at a load of 800 kN, with the corresponding height-to-span ratio of each specimen. The tendency of the crack height to decrease with larger depth-to-span ratios is illustrated and the lessening of this decrease as this ratio increases. A certain amount of variation was

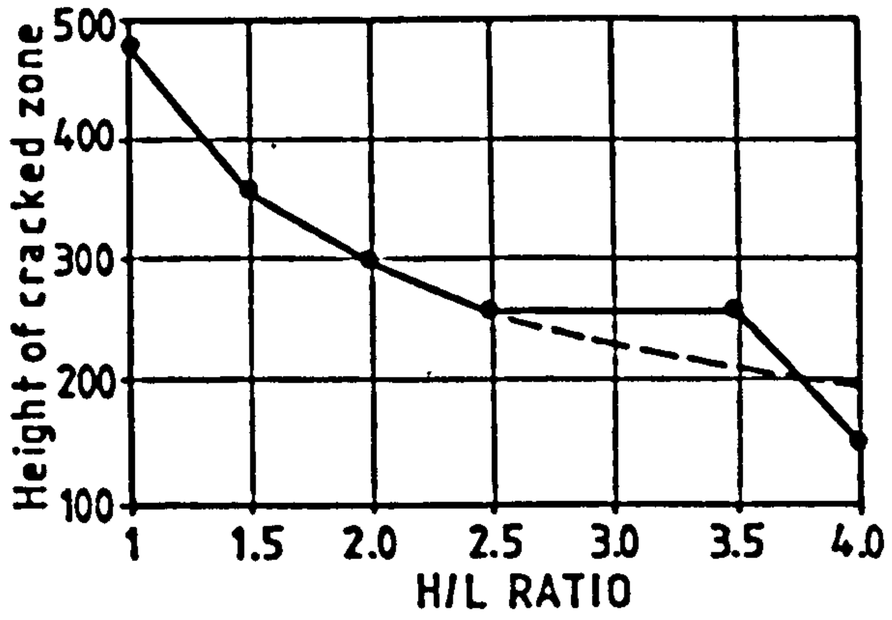

Fig. 5.9 Height of bending cracks on deep panels vs. depth-to-span ratio

shown by specimens DB6 and DB7 with H/L ratios of 3.5 and 4.0 respectively; this could be due to differences in the strength of concrete.

The relationship between the maximum height of the diagonal cracks to the depth-to-span (H/L) ratio of the panels tested is shown in Fig. 5.10. Generally the height of the diagonal cracks decreased as the H/L ratio augmented. The largest change was exhibited between the H/L ratios of 1 and 1.5. These results give clear evidence of the improvement of the bending and shear capacity of deep beams as their depth-to-span ratio extends beyond unity. This seems to contradict the practice of limiting the active height to a value equal to the effective span for elements with depth-to-span ratios larger than 1.

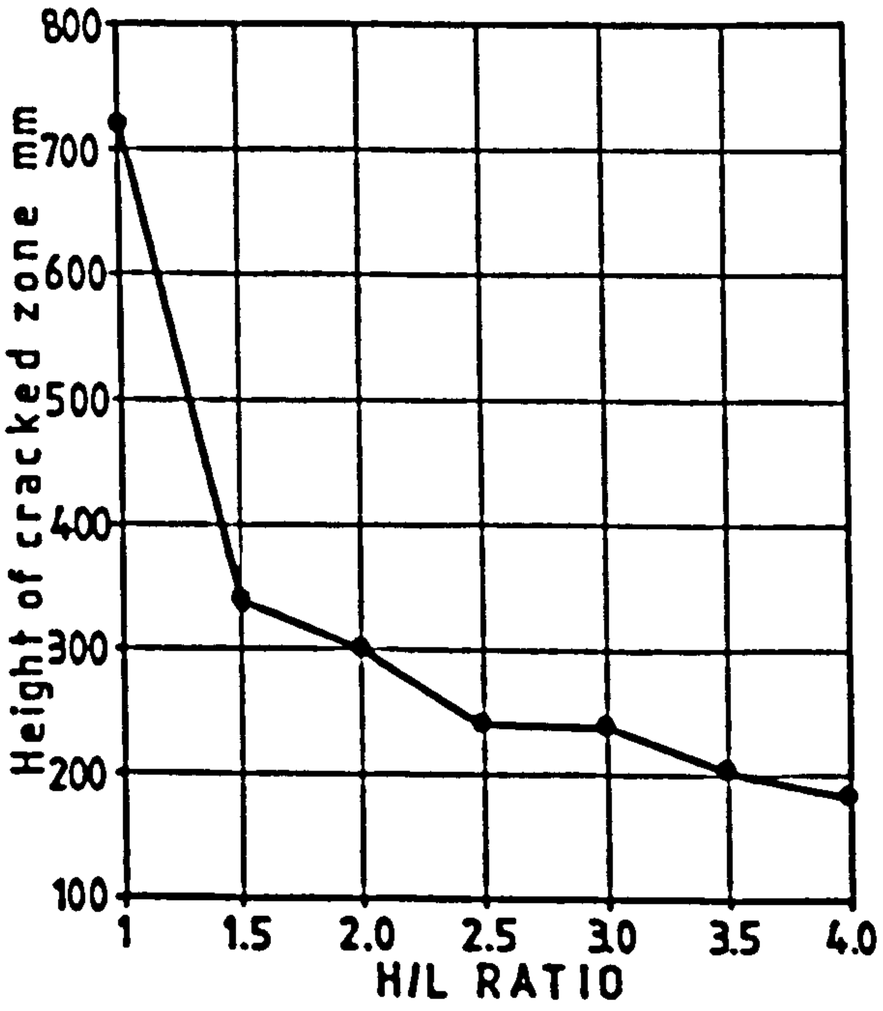

Fig. 5.10 Height of diagonal cracks on deep panels vs. depth-to-span ratio

5.3 DISPLACEMENTS

5.3.1 Vertical Displacements

The vertical (in-plane) displacement was measured at three points on the soffit of the specimens. These three points were at the centre of the panel (D2) and at the two edges (D1 and D3) outside the supports, as shown in Figs. 3.13 to 3.19. By measuring the vertical displacement the behaviour of the specimen could be observed, and the support mechanism, used to provide a simple support system, monitored.

Figure 5.11 shows the vertical displacement measured at mid-span for the panels tested. The maximum displacement measured was 2.57 mm in specimen DB1 at a load of 800 kN. No direct relationship can be deduced from Fig. 5.11 between the depth/span ratio and the displacement at mid-span. Figure 5.12 compares the load-deflection curves of the seven deep panels. Deflections were calculated by reducing the mean displacement of both supports from the displacement at mid-span. Although the largest deflection was experienced by specimen DB1, with the smallest depth/span ratio, no clear correlation can be deduced between the deflection and the depth of deep elements with depth/span ratios larger than unity.

The differential settlement of both supports is a matter of interest when testing this kind of element. This is an undesirable condition in the test, however, the maximum differential deformation measured was 0.88 mm in specimen DB7 under a load of 750 kN, hardly affecting the distribution of forces and stresses.

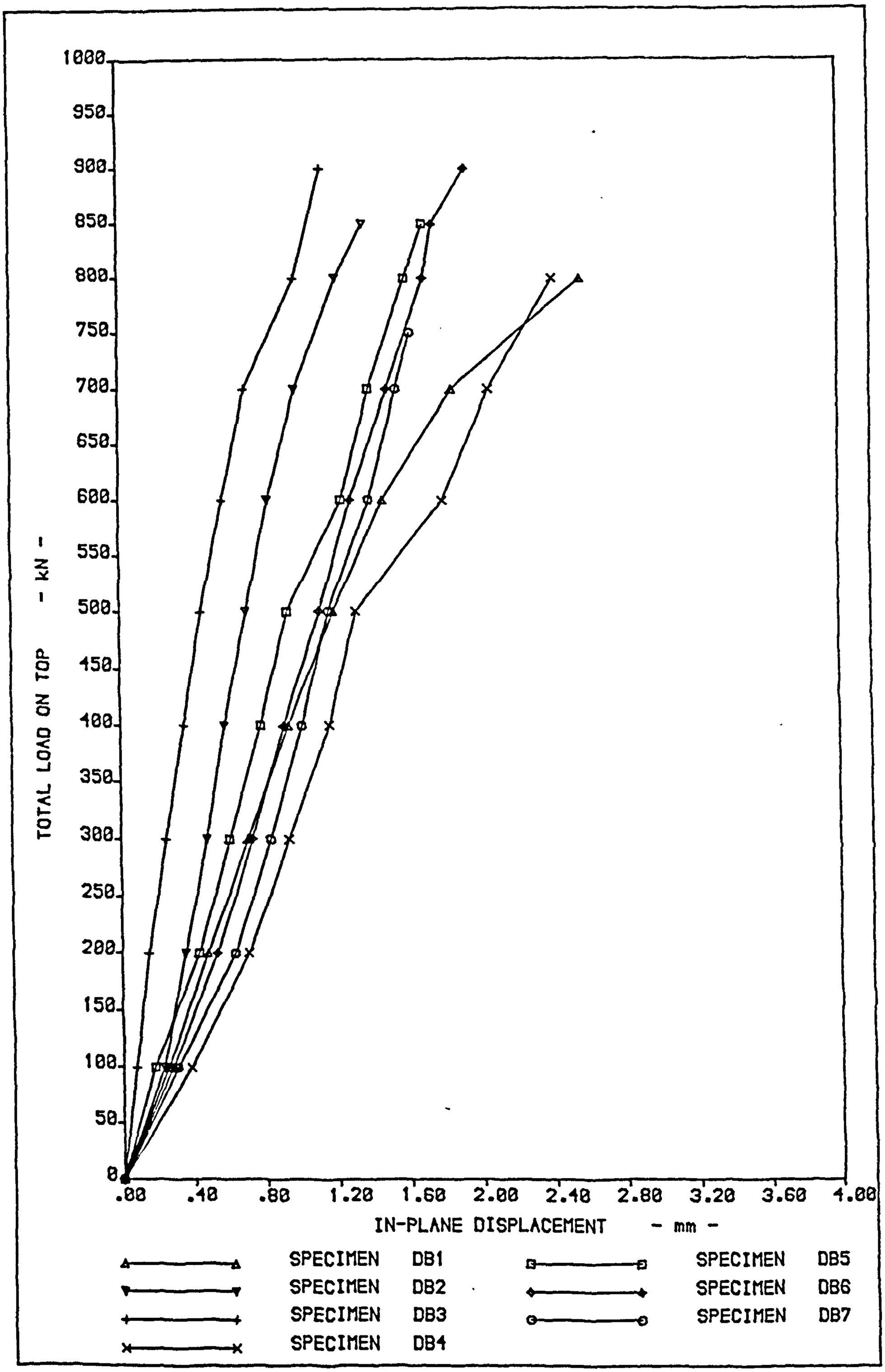

Fig. 5.11 Comparison of mid-span displacement of deep panels

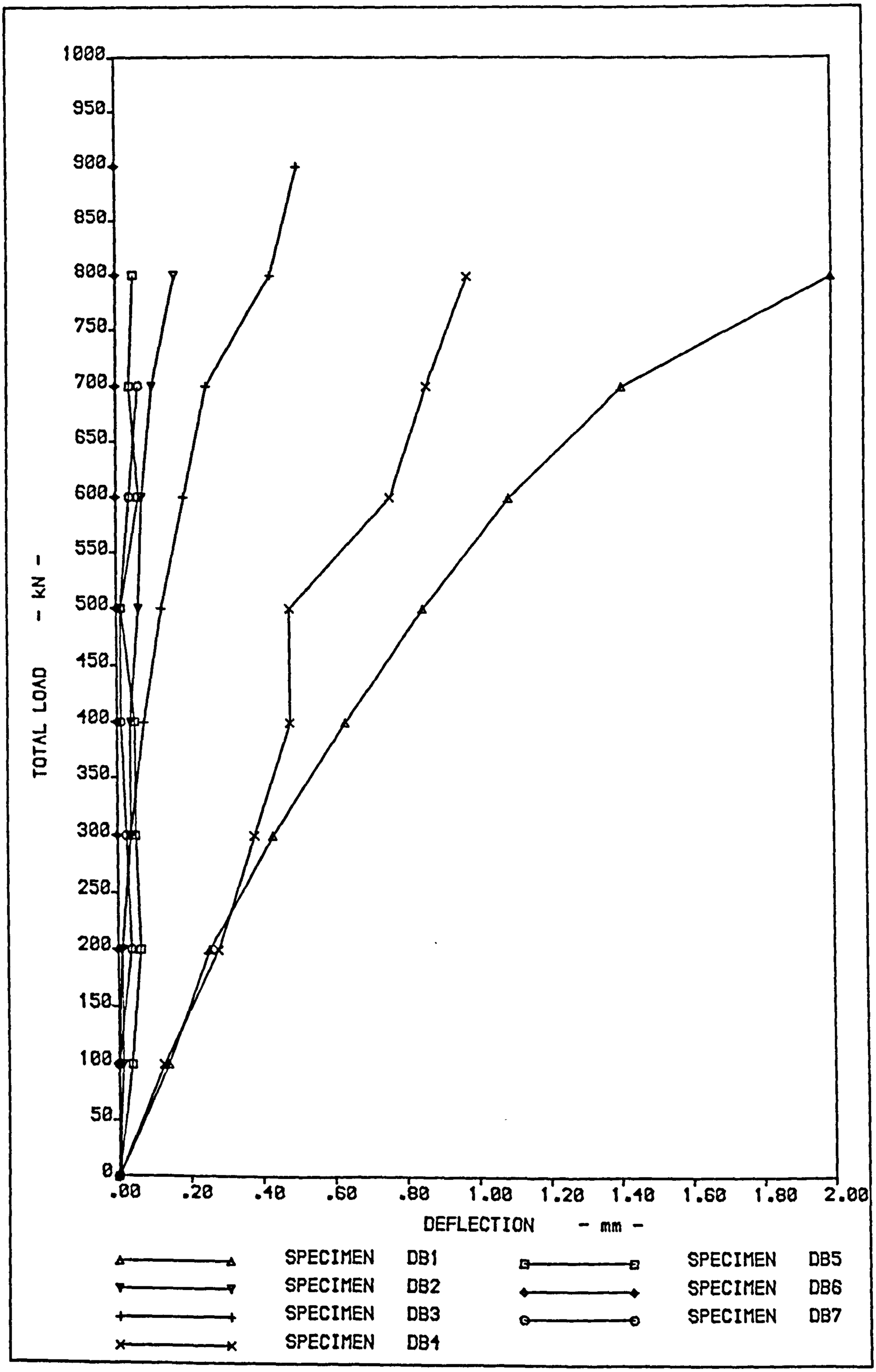

Fig. 5.12 Comparison of deflection of deep panels

Table 5.2 Deflection (mm) measured on Deep Panels

	LOAD (kN)								
	100	200	300	400	500	600	700	800	900
DB1	0.139	0.254	0.431	0.635	0.851	1.092	1.409	2.006	-
DB2	0.013	0.013	0.038	0.038	0.063	0.073	0.102	0.165	-
DB3	0	0.012	0.038	0.076	0.127	0.190	0.253	0.432	0.508
DB4	0.127	0.279	0.381	0.482	0.483	0.762	0.863	0.977	-
DB5	0.038	0.064	0.051	0.050	0.013	0.064	0.038	0.050	-
DB7	0	0.038	0.025	0.012	0.012	0.038	0.063	-	-

Differential settlement occurs mainly due to the different form of both supports in order to provide a simple supported mechanism for the specimens.

5.3.2 Horizontal Displacements

Horizontal displacements were measured at 5 points on the surface A of the specimens tested. These points were distributed along a line coinciding with the right hand support, as shown in Figs. 3.13 to 3.19. Specimen DB1 was the exception, having the horizontal displacement measured at 3 points only, i.e. D4, D6 and D8 (Fig 3.13).

The intention behind measuring the horizontal displacement was to detect bending or buckling of the panels in a vertical axis, and to make sure that the supports and loading mechanisms did not permit a substantial horizontal translation of the specimens under test. Figures 5.13 to 5.19 show the horizontal displacements measured experimentally on specimens DB1 to DB7 respectively.

By comparing Figs 5.13 to 5.19, it can be observed that no creditable bending occurs in specimens DB1 (Fig. 5.13) to DB4 (Fig 5.16), although some horizontal translation is shown. Figure 5.17 demonstrates that at a depth/thickness ratio of 30, the phenomenon of buckling is attainable and this had its maximum expression in Fig. 5.19, corresponding to specimen DB7.

Table 5.3 presents the relative horizontal displacement of the top of the specimens with respect to its bottom level. In general, this relative displacement was small, having the maximum value in specimen DB4 (Fig 5.16) equal to 4.826 mm at a load of 800 kN. The ratio of this maximum relative displacement to the depth of the specimen is 0.00268 mm/mm, which has been considered too small to cause any substantial effect on the behaviour of the specimens. Nevertheless, measures were adopted in order to restrict further the displacement at the top of the panels. Another hydraulic jack was used, which effectively reduced the horizontal displacement in the three tests carried out afterwards as can be seen in Figs. 5.17 to 5.19.

Table 5.3 Relative horizontal displacements (mm) of top with respect to bottom of specimens DB1 to DB7

SPECIMEN	LOAD kN								
	100	200	300	400	500	600	700	800	900
DB1	0.026	0.076	0.152	0.305	0.431	0.508	0.609	0.711	
DB2	0.533	0.914	1.092	1.193	1.321	1.499	1.677	2.032	
DB3	0.889	1.143	1.245	1.397	1.549	1.931	2.133	2.413	2.718
DB4	1.169	2.413	2.972	3.124	3.379	3.683	4.242	4.826	
DB5	0.025	0.254	0.508	0.768	1.016	1.194	1.371	1.498	
DB6	0.127	0.381	0.787	1.067	1.270	1.448	1.600	1.855	2.083
DB7	0.635	1.041	1.473	1.752	1.880	1.930	2.083		

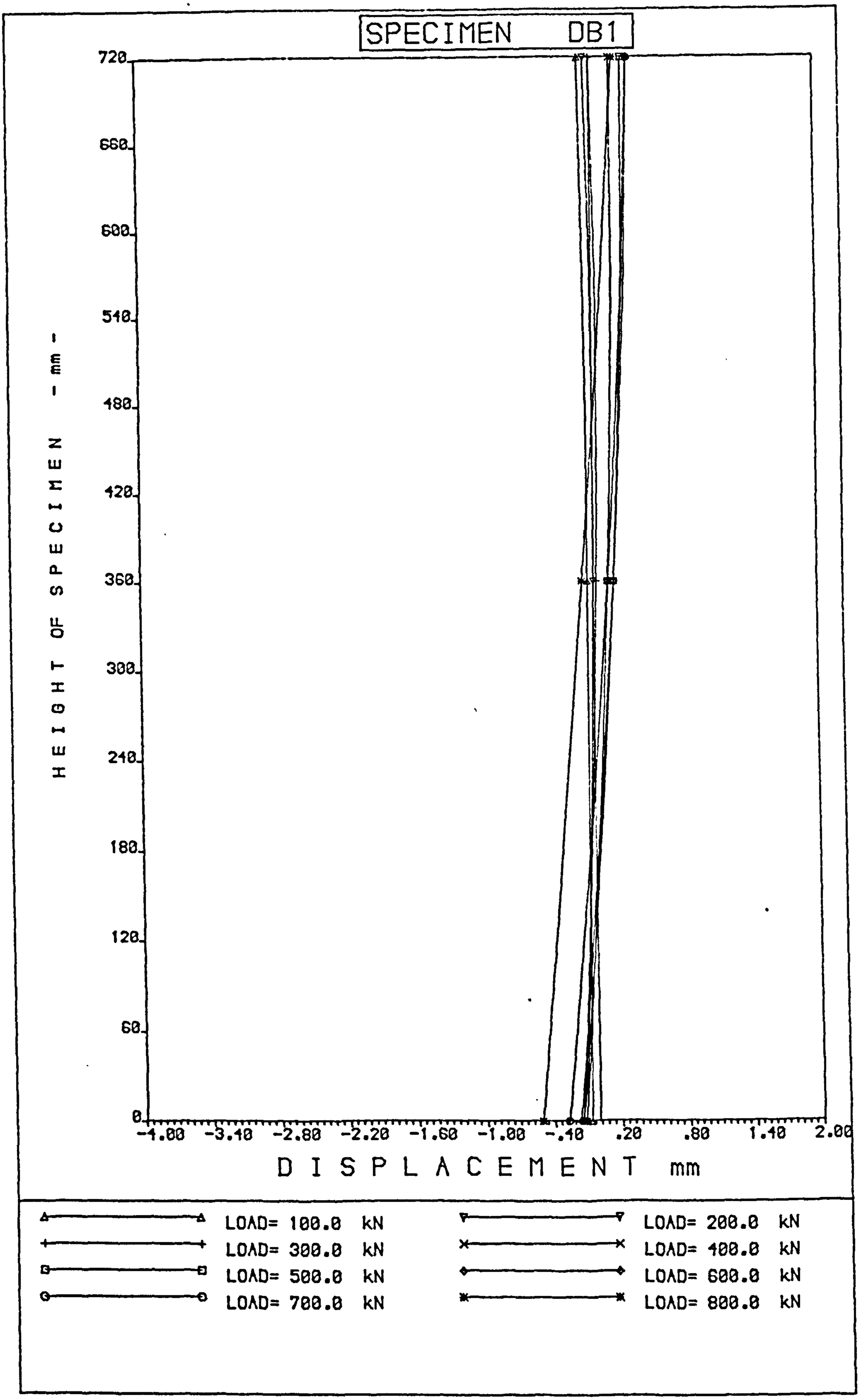

Fig. 5.13 Horizontal (out of plan) displacement for specimen DB1

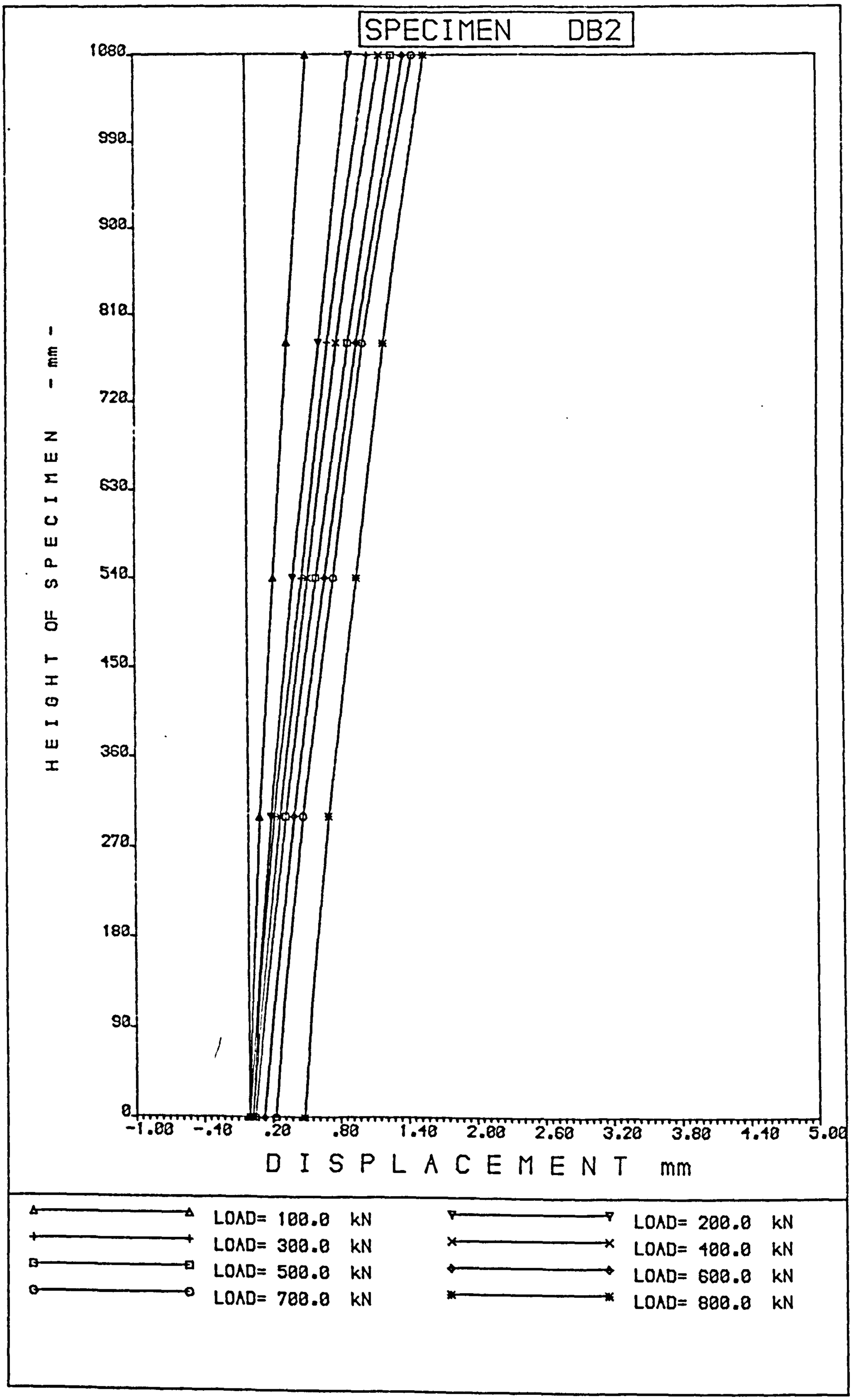

Fig. 5.14 Horizontal (out of plane) displacement for specimen DB2

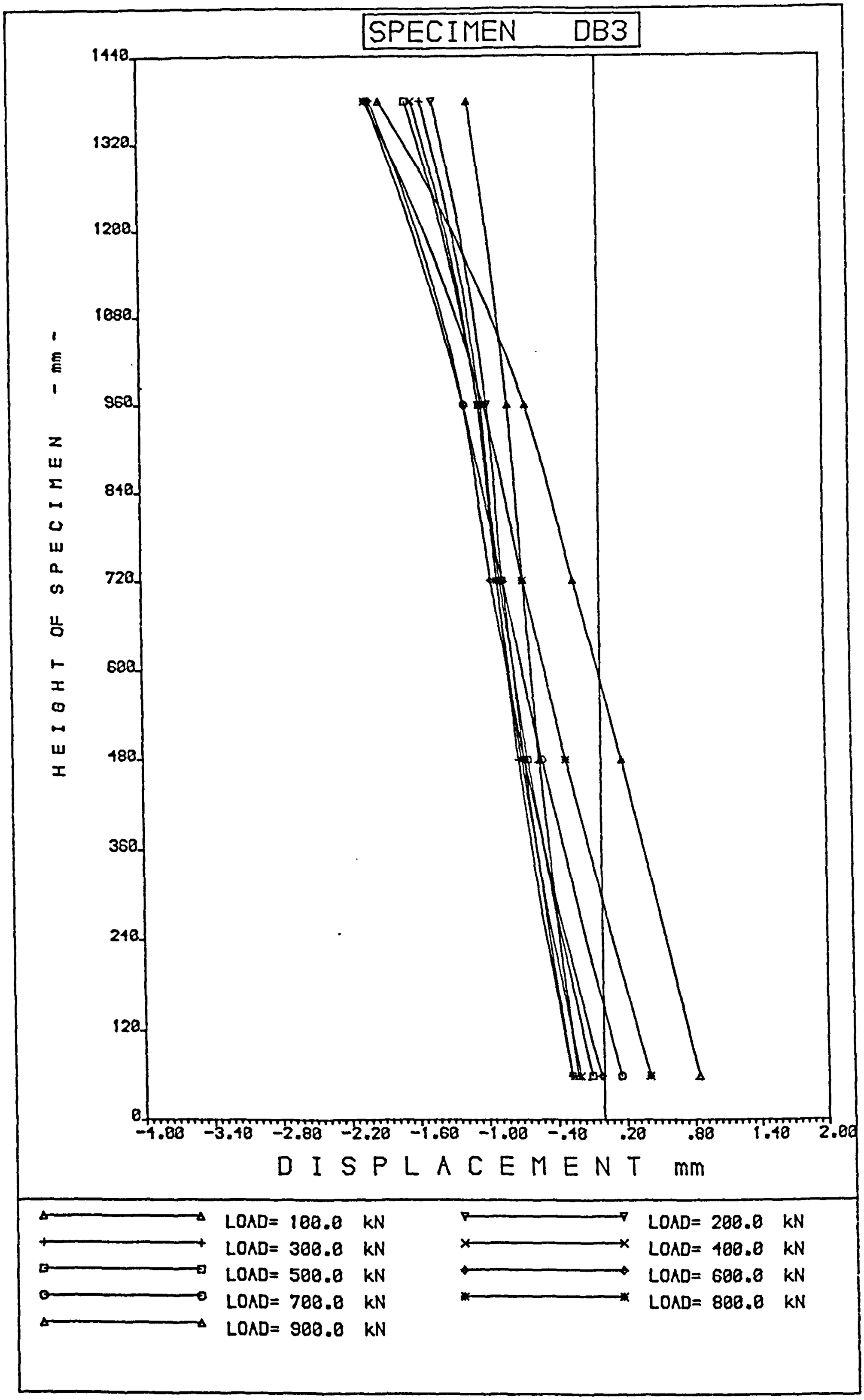

Fig. 5.15 Horizontal (out of plane) displacement for specimen DB3

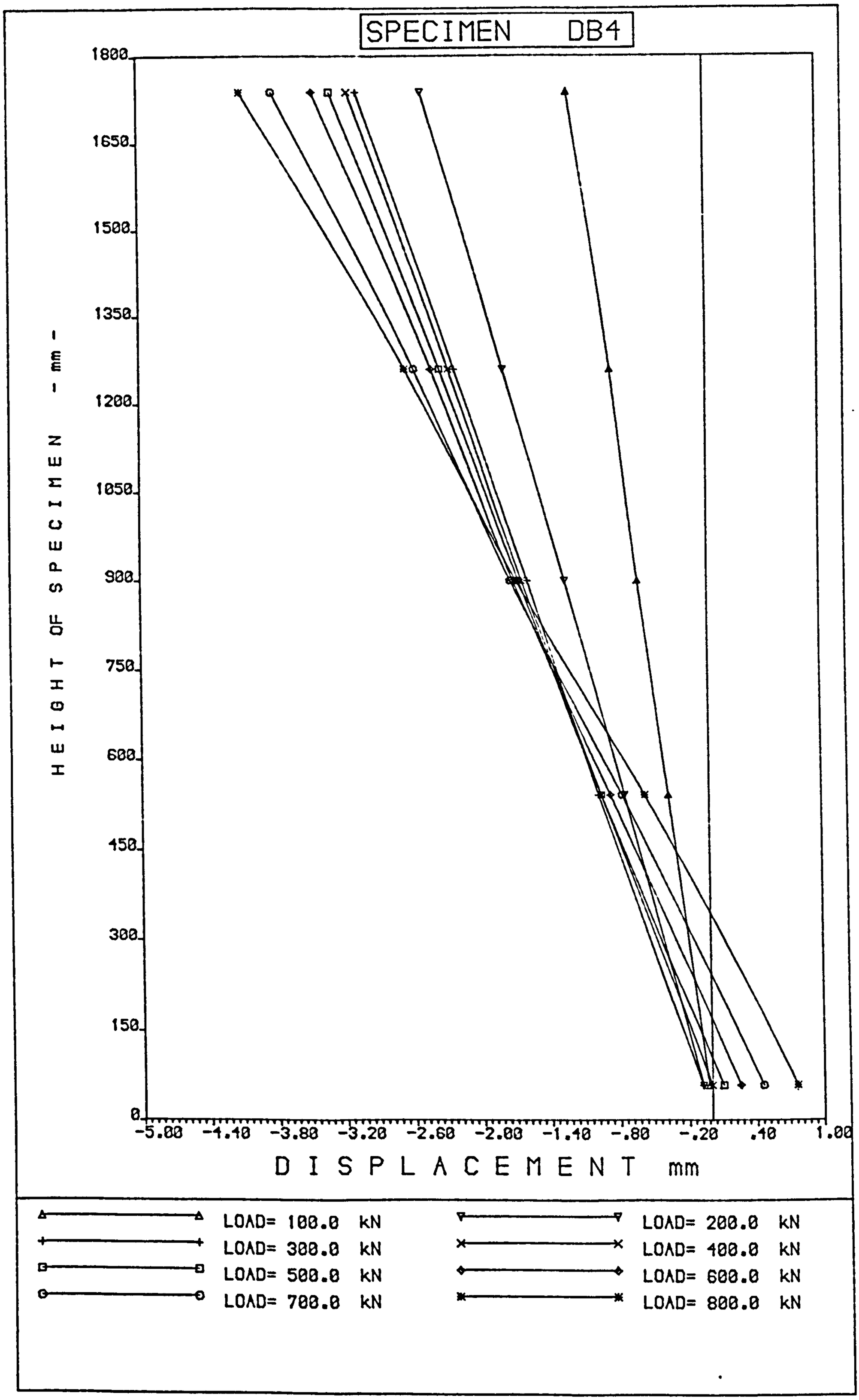

Fig. 5.16 Horizontal (out of plane) displacement for specimen DB4

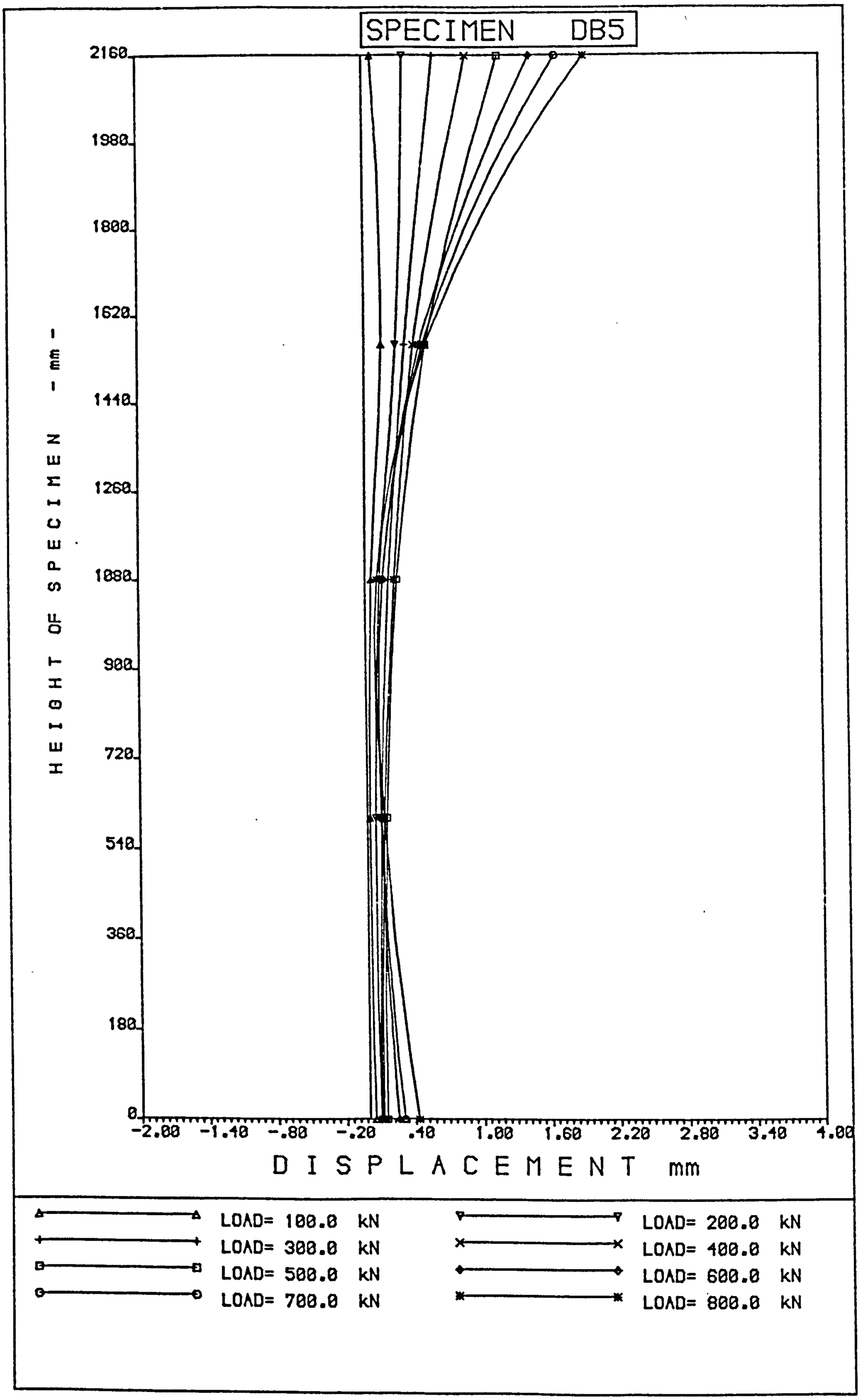

Fig. 5.17 Horizontal (out of plane) displacement for specimen DB5

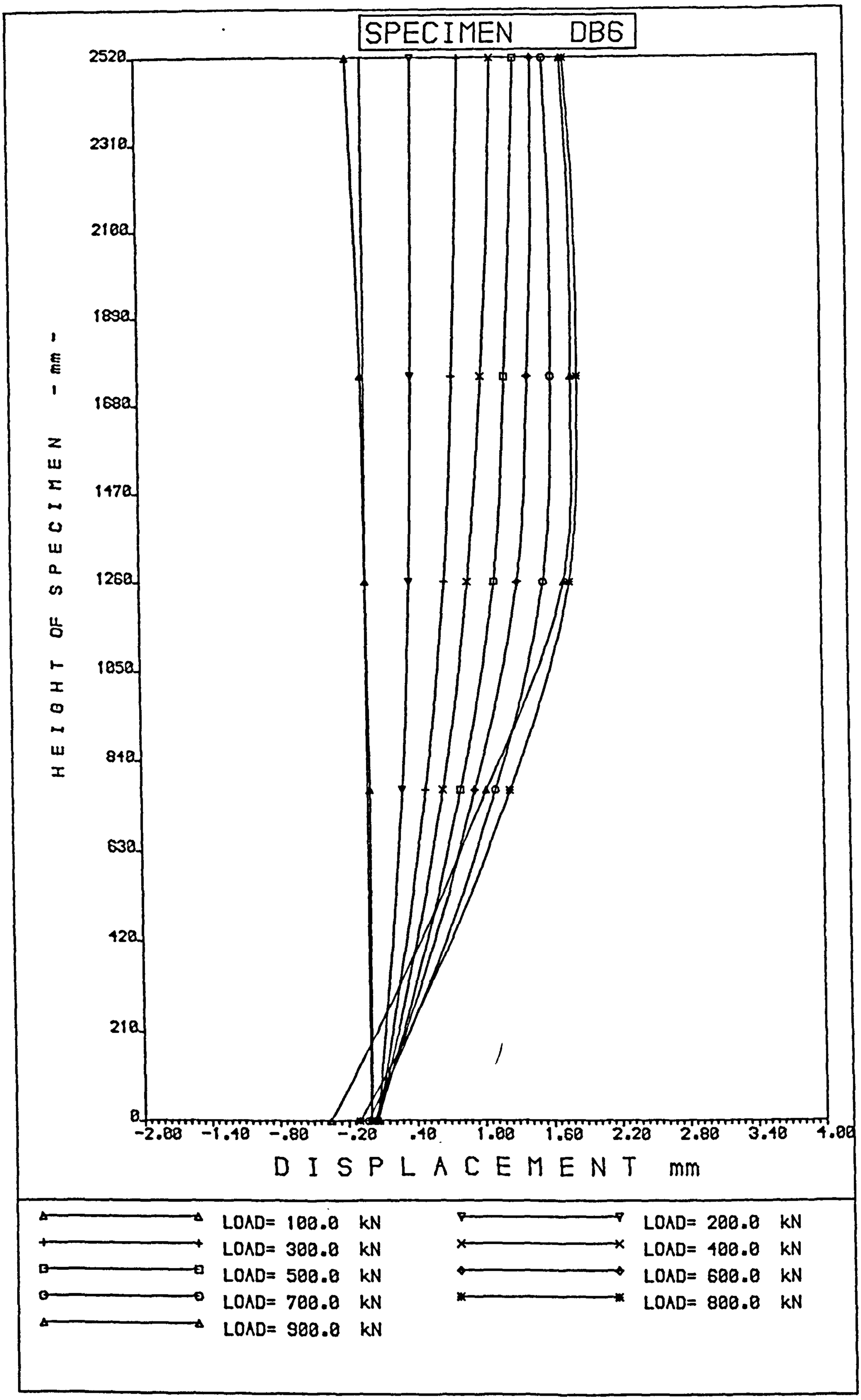

Fig. 5.18 Horizontal (out of plane) displacement for specimen DB6

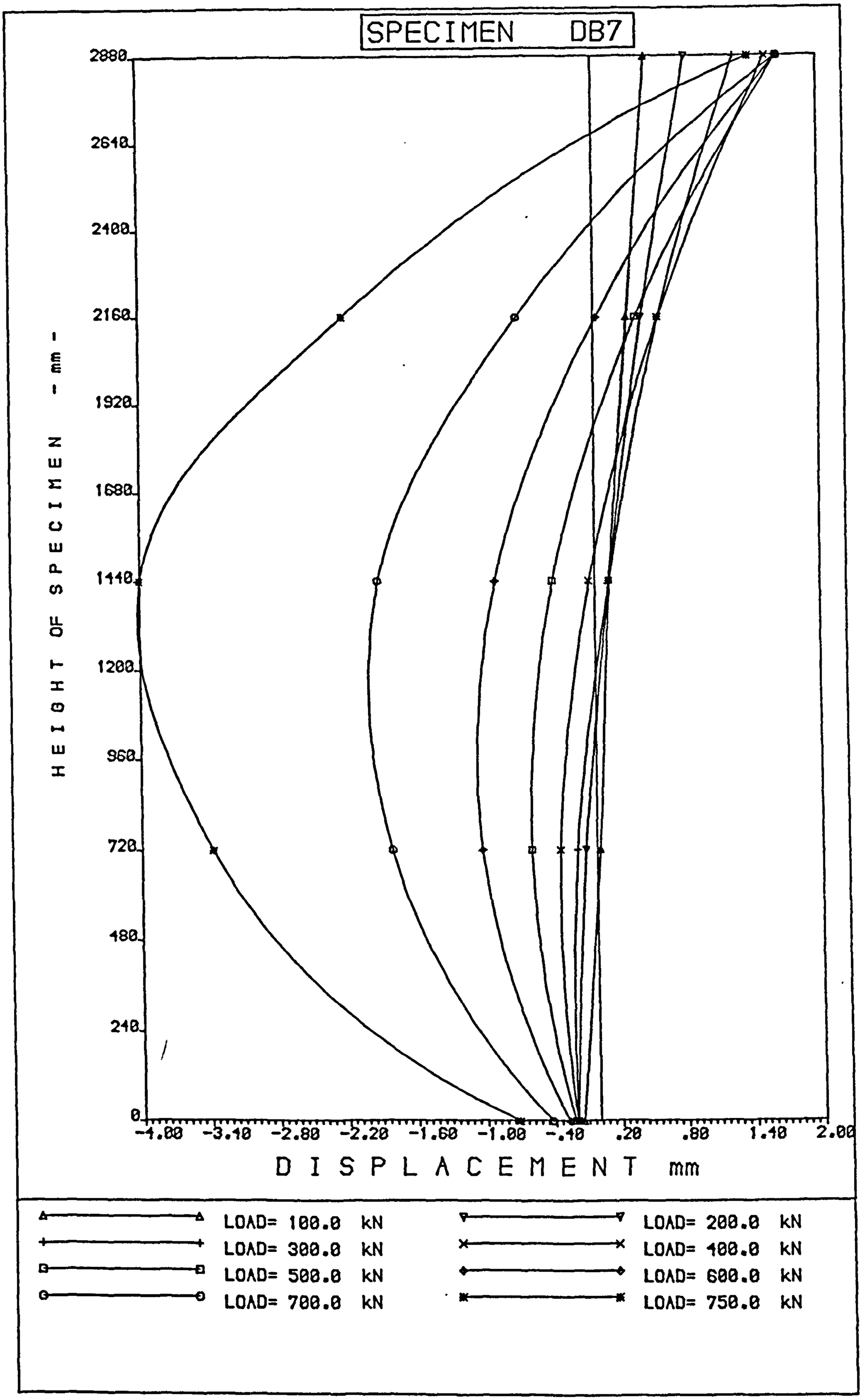

Fig. 5.19 Horizontal (out of plane) displacement for specimen DB7

5.4 STRESSES

The distribution of stresses in deep beams is affected by the normal pressures on the top and bottom edges due to loads and reactive forces, causing the distribution to be non-linear in vertical sections. Theoretical methods of analysis, based on simple linear theory of elasticity predict accurately the behaviour of deep beams made of isotropic and homogeneous materials. However, in the case of deep reinforced concrete beams, some doubts arise about the capability of these theoretical methods to predict the distribution of stresses, especially when cracks appear at relatively small tensile forces.

In order to establish an agreement between theoretical and experimental results, the longitudinal stresses (σ_x), vertical stresses (σ_y) and shear stresses (τ_{xy}) were compared as follows.

Experimental values for stresses were obtained from the strain measurements taken from the rectangular strain rosettes on each specimen. The stresses were calculated knowing the modulus of elasticity and Poisson's ratio for the concrete as explained in Section 3.10. Theoretical values were deduced using the program PSALM, discussed in the following section.

Included in the following figures are experimental results of the stresses obtained on both sides of the specimens and the mean value calculated from them at each point.

5.4.1 Program PSALM

Program PSALM was prepared by the Highway Engineering Computer Branch of the Department of the Environment (1976). PSALM is part of the package of programs called Strand-Version 2. The input for program PSALM, consisting of the finite element mesh and nodal coordinates, can be generated automatically by any of its data generation programs IPUT2, LOAD or PPUT. Program PSALM uses triangular and beam elements for the plane stress and the plate bending analysis. The program may be used

for the linear elastic analysis of slab decks of arbitrary plan with isotropic or orthotropic material and it may be used for either plate bending or plane stress analysis. The number of degrees of freedom per node is three, i.e., the displacement w, and the two rotations about the x and y axes. A linear variation of bending and twisting moments is obtained across each element independently, and from this variation of moments the shear forces are found. The support conditions are specified at each node and it includes rigid supports, elastic restraints, and/or specific displacements. The output includes centroidal and nodal values for each element. The nodal average moments are obtained by taking the mean of the values from the corners of the triangles meeting at the node, and the nodal average shear forces are obtained from the centroidal values of adjacent elements. The output from PSALM consists of printing of the input data, nodal displacements, reactions at both fixed and elastic supports, centroidal and nodal averaged moments, principal moments, centroidal and nodal shear forces. For plane stress it is the in-plane stress and principal stress which are printed out.

5.4.2 Longitudinal Stress

The presentation and comparison of the experimental and numerical longitudinal stresses is mainly based on the stresses along the mid-span section. When required, the stresses in any other vertical section are compared. Figure 5.20 shows the experimental and numerical values of longitudinal stresses for specimen DB1 at four different sections and under a load of 100 kN. The position of each section is shown within the figure. In general, the numerical prediction and the experimental measurements agree well. Some degree of variation is shown by the experimental values; this can be attributed to the fact that the device used for the measurement of strains was not sensitive enough.

The curvilinear distribution of stresses which is given in Fig. 5.20 is a feature widely recognised in deep flexural elements. In specimens with depth/span ratio larger than 1, the distribution of stresses is not only curvilinear, but also shows more than one neutral axis. This phenomenon can be observed in Figs. 5.21 to 5.26 where results for panels DB2 to DB7 are given at a load of 100 kN along the mid-span section. In all these cases the experimental values corroborate the analytical predictions, except for a few experimental measurements which deviated slightly mainly due to the inability of the gauge to read small strains accurately. Based on this successful comparison, it can be concluded that the prediction by the finite element method is accurate and reliable for the analysis of deep elements in their uncracked condition.

Finite element predictions have been used to observe the effect of the depth/span ratio on the position of the neutral axes in these deep panels. Table 5.4 compiles the position of the neutral axes observed in each element, as a function of the span and total depth of the panels; these values are given graphically in Fig. 5.27.

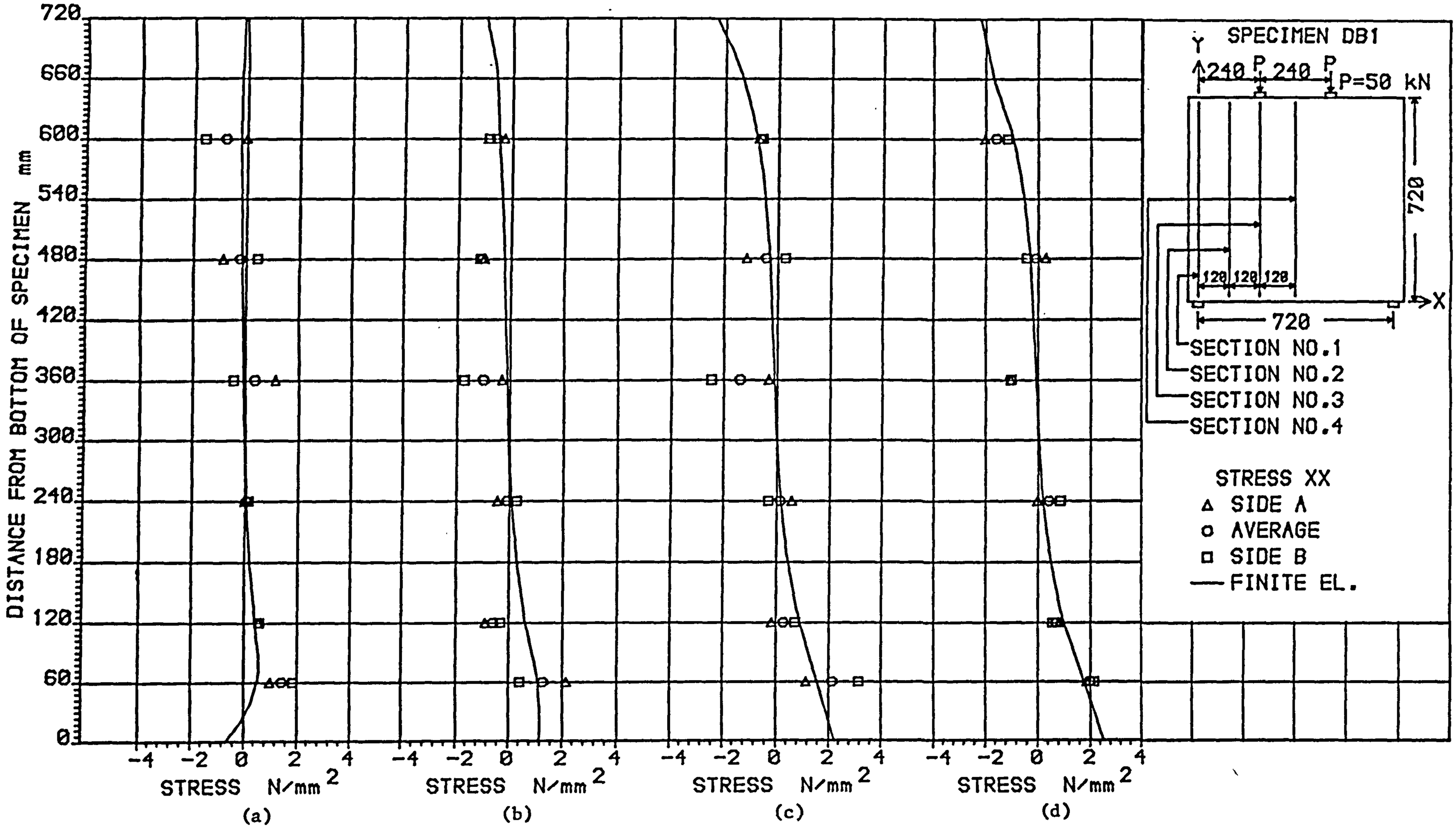

Fig. 5.20 Comparison of experimental and numerical longitudinal stresses at four sections on specimen DB1. Load = 100 kN. a) at section 1, b) at section 2, c) at section 3 and d) at section 4.

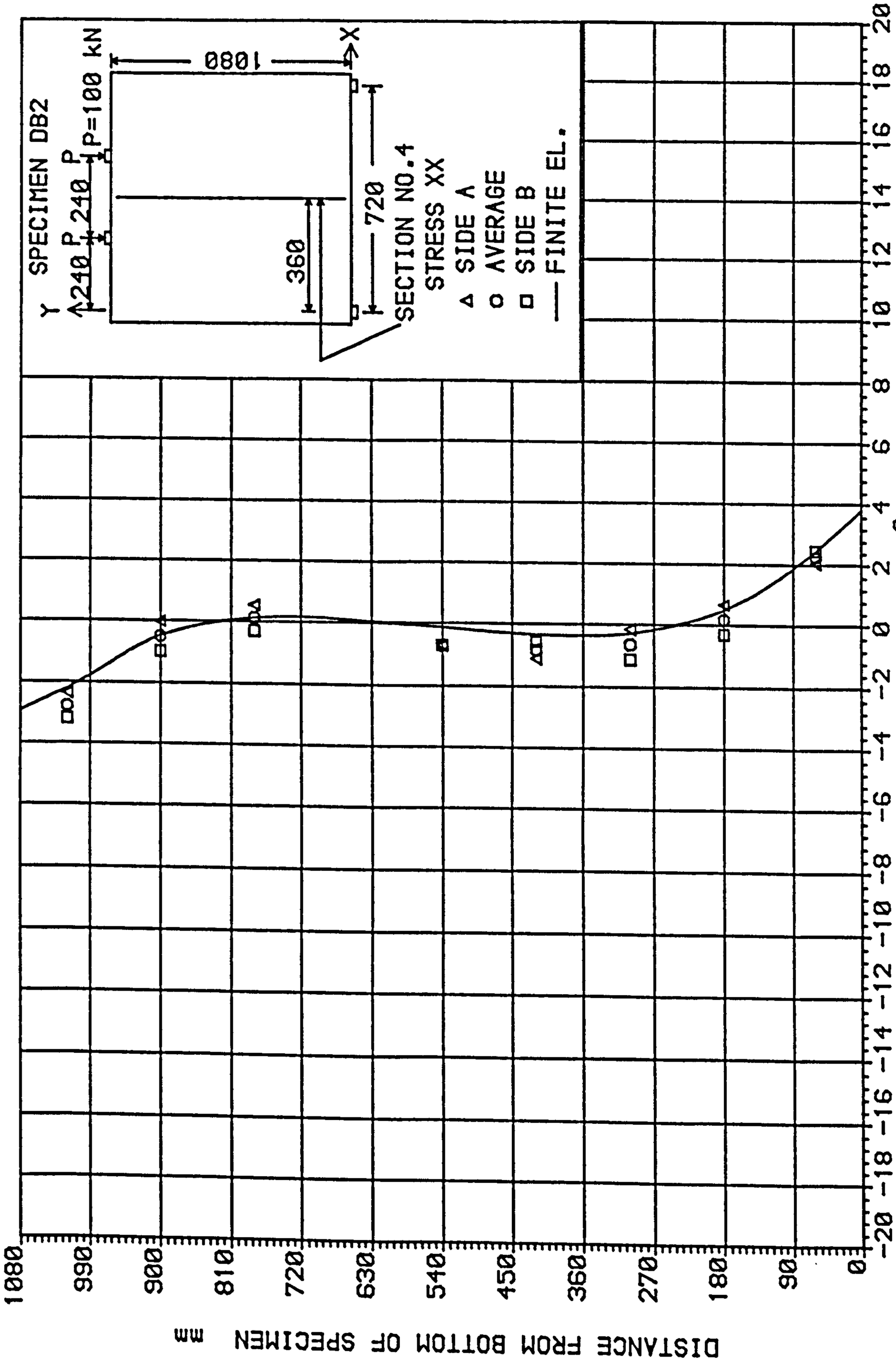

Fig. 5.21 Comparison of experimental and numerical longitudinal stresses at section 4 on specimen DB2 (load = 200 kN)

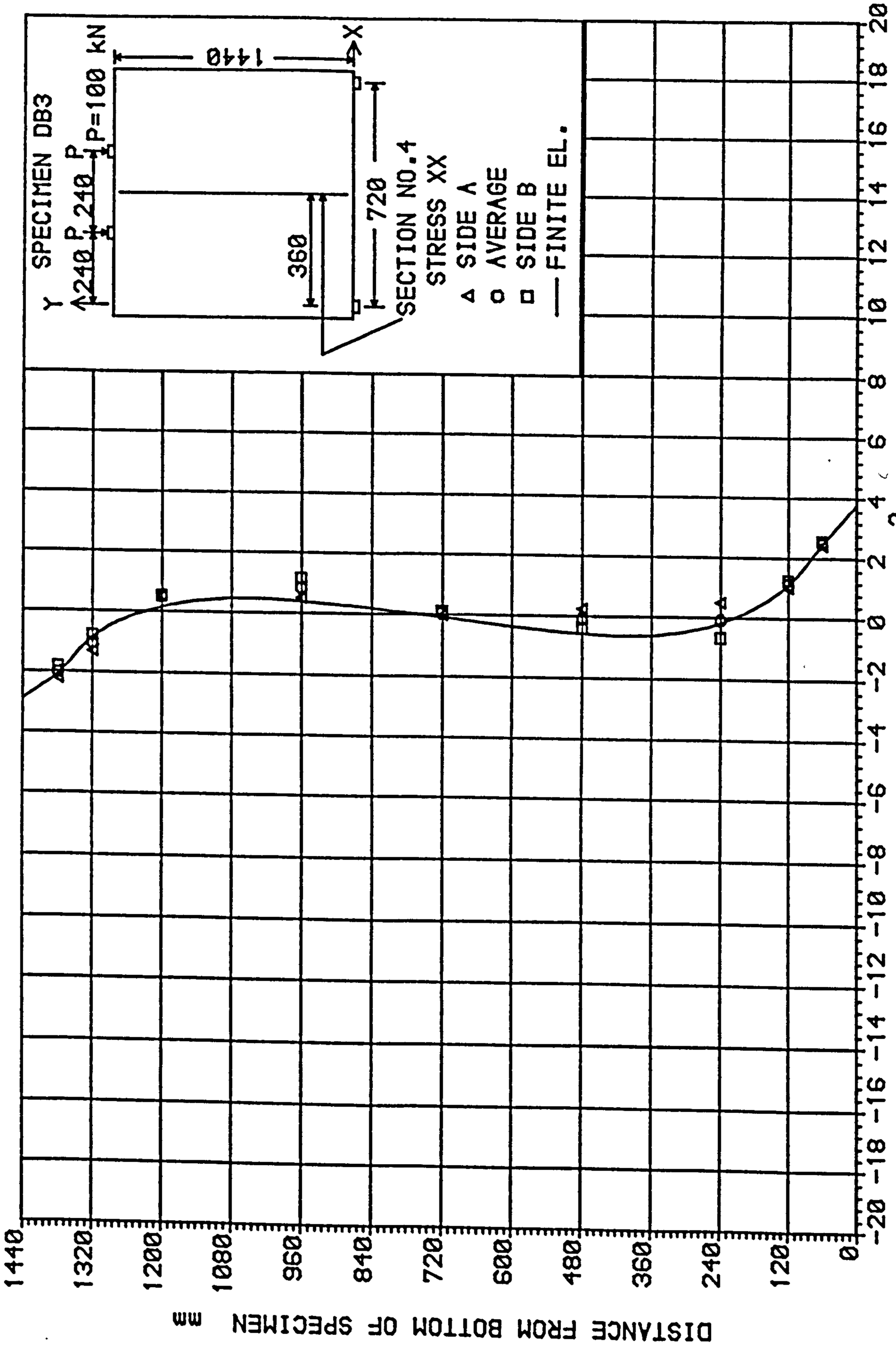

Fig. 5.22 Comparison of experimental and numerical longitudinal stresses at section 4 on specimen DB3 (load = 200 kN)

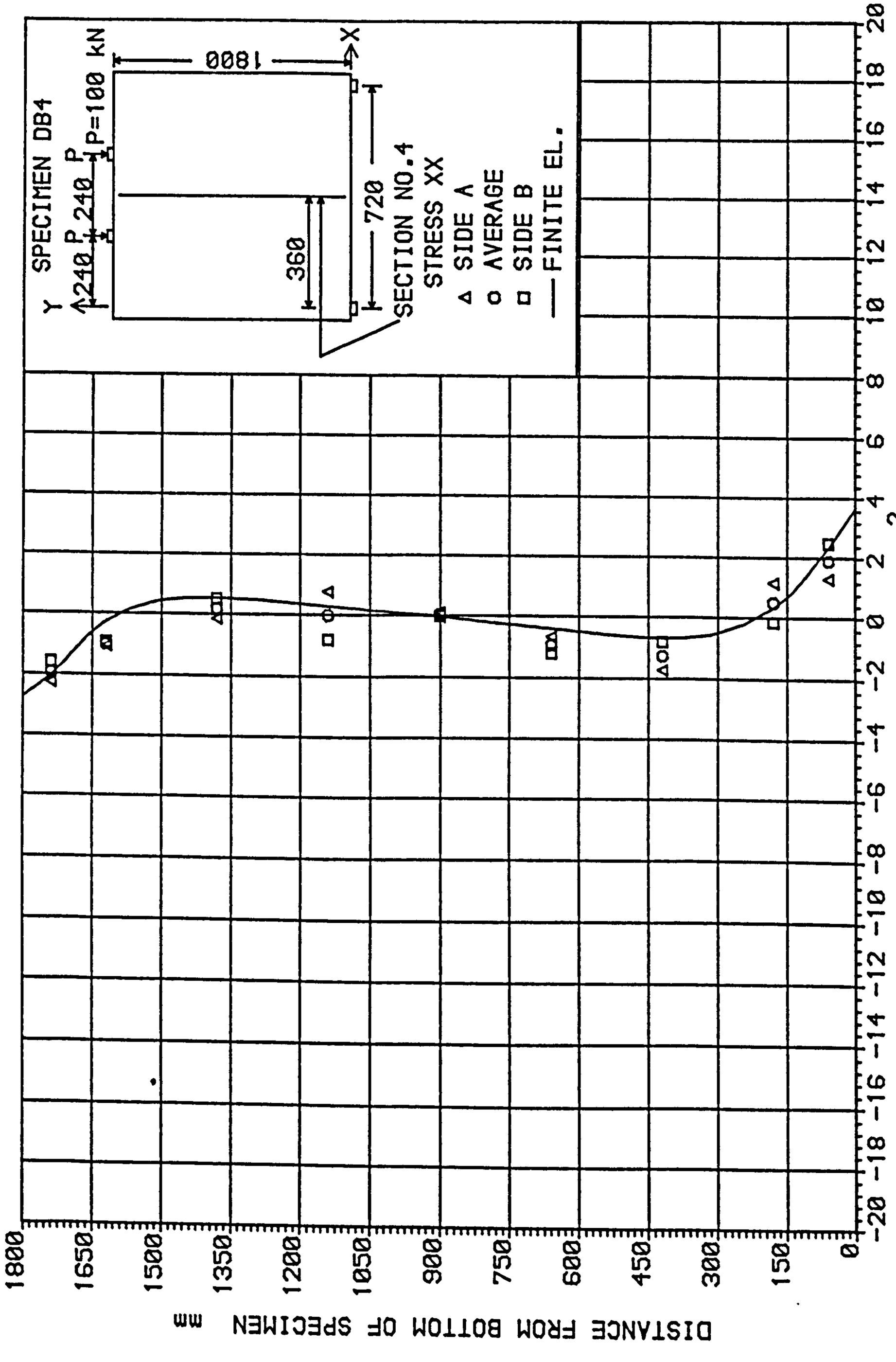

Fig. 5.23 Comparison of experimental and numerical longitudinal stresses at section 4 on specimen DB4 (load = 200 kN)

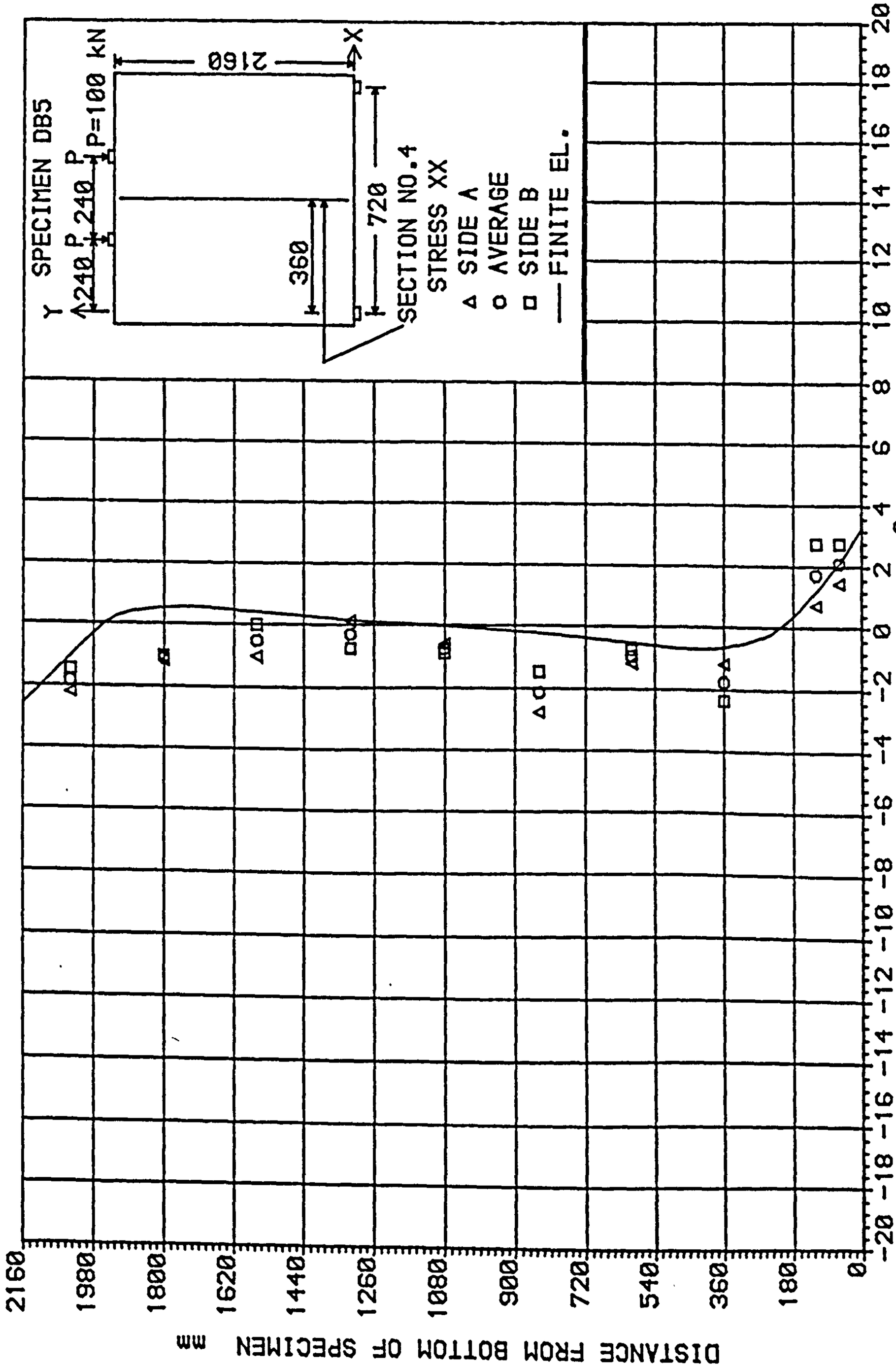

Fig. 5.24 Comparison of experimental and numerical longitudinal stresses at section 4 on specimen DB5 (load = 200 kN)

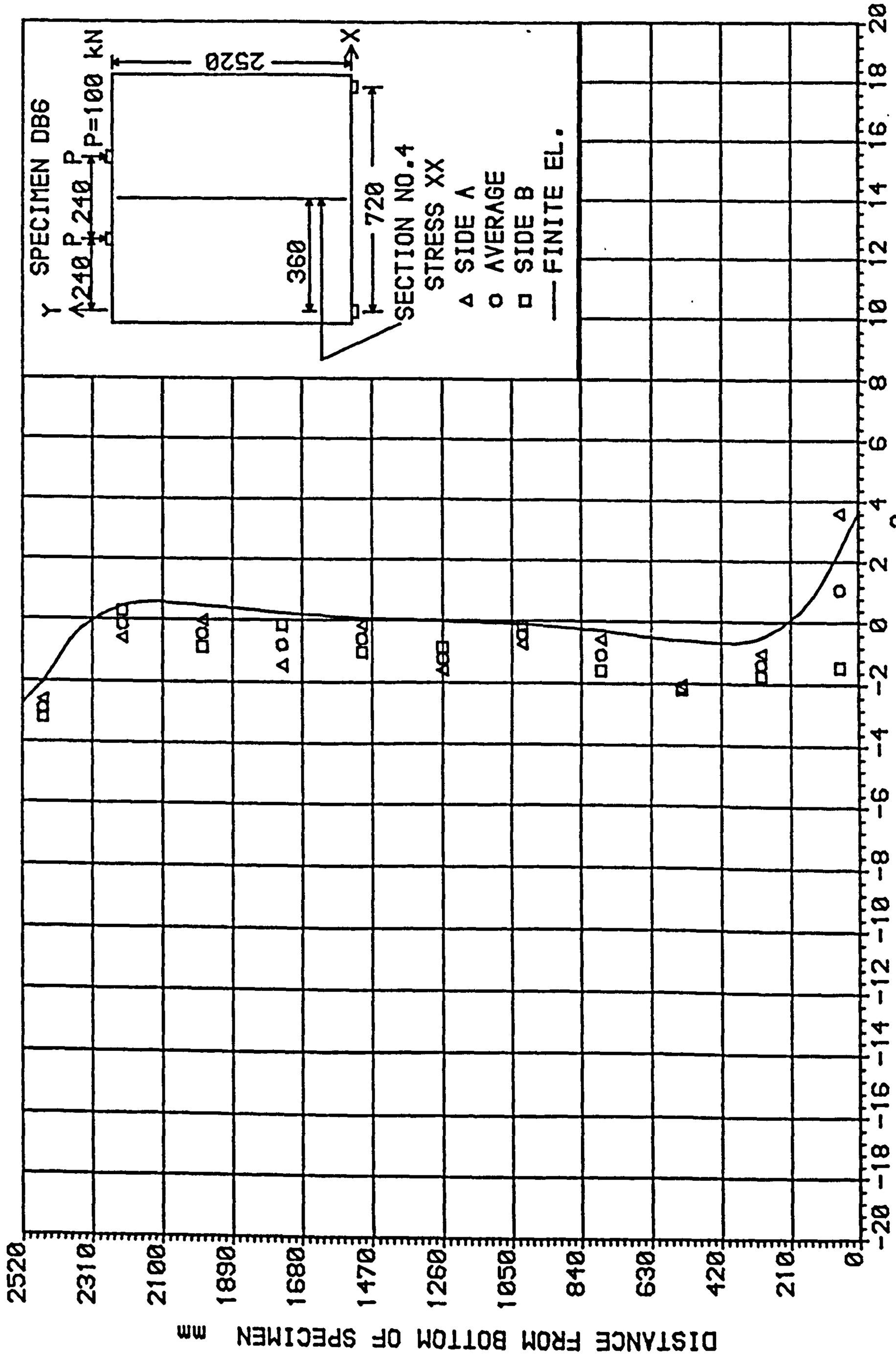

Fig. 5.25 Comparison of experimental and numerical longitudinal stresses at section 4 on specimen DB6 (load = 200 kN)

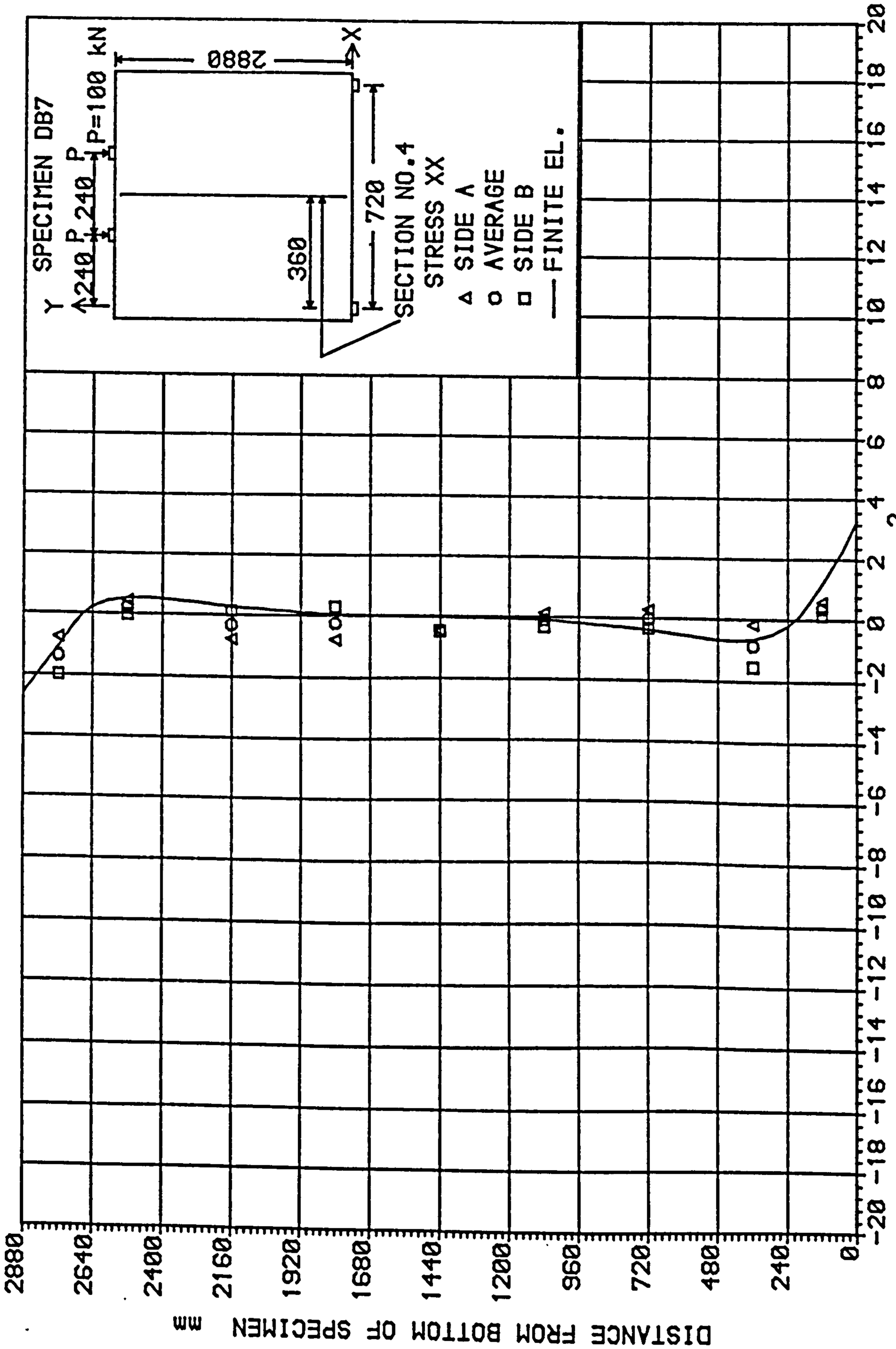

Fig. 5.26 Comparison of experimental and numerical longitudinal stresses at section 4 on specimen DB7 (load = 200 kN)

Table 5.4 Position of neutral axes for different depth/span ratios

SPECIMEN	H/L	LOWER N.A. measured from soffit mm		MIDDLE N.A. measured from soffit mm		UPPER N.A. measured from top mm	
DB1	1.0			325	0.45d		
DB2	1.5	240	0.33L	595	0.55d	255	0.35L
DB3	2.0	220	0.30L	755	0.53d	215	0.30L
DB4	2.5	220	0.30L	930	0.52d	215	0.30L
DB5	3.0	220	0.30L	1080	0.50d	210	0.29L
DB6	3.5	220	0.30L	1260	0.50d	210	0.29L
DB7	4.0	210	0.29L	1440	0.50d	210	0.29L

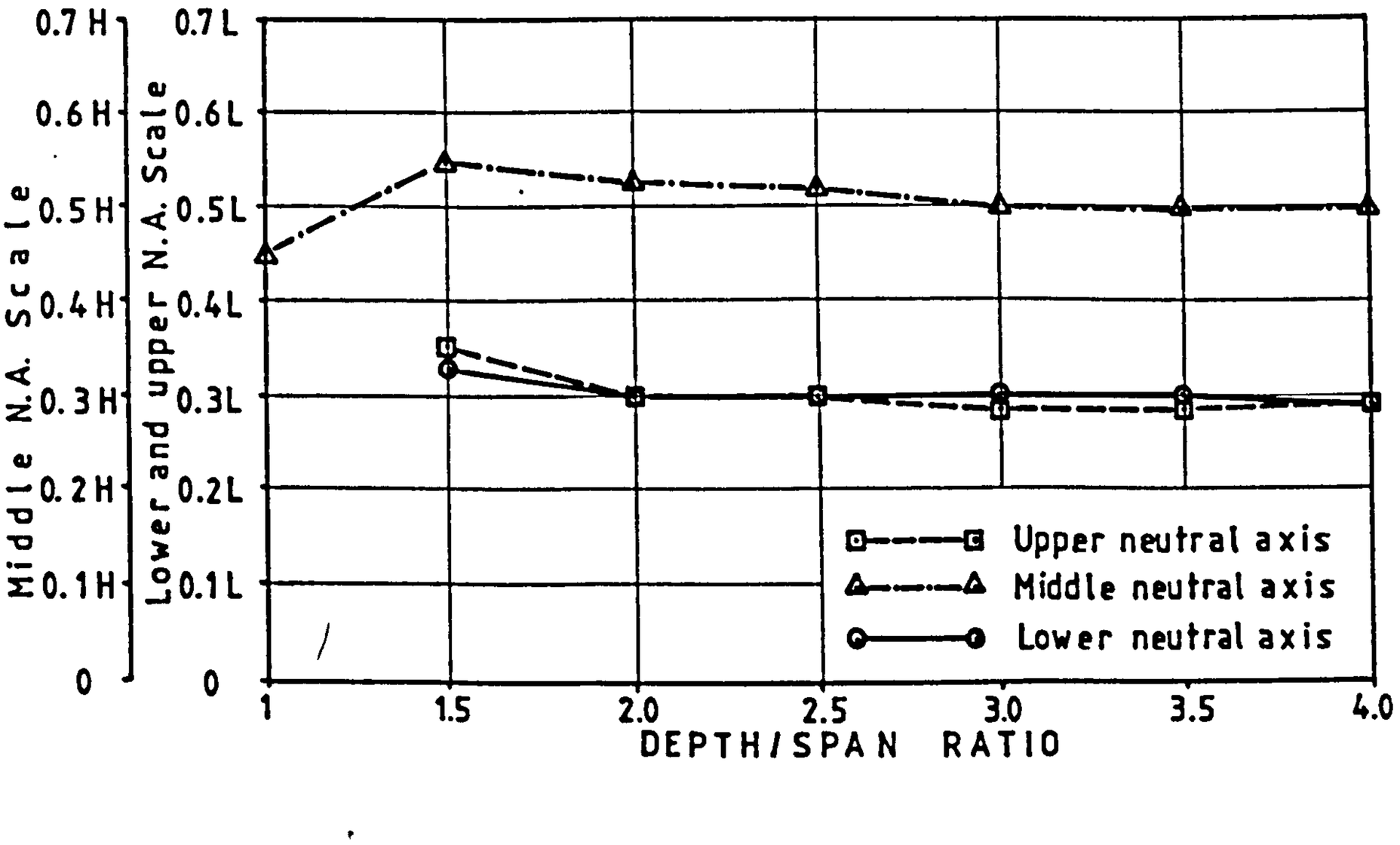

Fig. 5.27 Position of neutral axes for different depth/span ratios. Lower and middle N.A. measured from the soffit. Upper N.A. measured from top.

At depth/span ratios between 1 and 1.5 two additional neutral axes are formed and the middle neutral axis is displaced from 0.45d to 0.55d. The upper and lower neutral axes are formed at depths about 0.35L measured from the top and soffit respectively. As the depth/span ratio increases, the middle neutral axis tends to adopt a position equal to 0.5d and the other two neutral axes move towards a value close to 0.3L measured from the top and from the bottom of the deep element.

Until now the comparison of longitudinal experimental and theoretical stresses has been carried out for small loads, a condition in which reinforced concrete behaves almost elastically. Under larger loads, cracks might appear in those regions where tensile stresses develop. In fig. 5.28 the results for specimen DB1 are shown, under a load of 300 kN. The experimental values in the lower half of the wall present an erratic pattern; however, in the upper half the stresses measured seem reasonable , although they are about 60 percent larger than the theoretical ones. As the load increased to 600 kN (Fig. 5.29) the apparent deterioration of the experimental values was even greater. The neutral axis predicted by the theoretical method was displaced upwards, reducing the section under compression and causing the development of larger compressive stresses in the top section of the wall, in order to achieve equilibrium of forces.

Strains measured in regions affected by cracks were of no significance, since they often included the width of cracks. In other cases, the strains could be measured on a portion of concrete between two cracks. Often these measurements do not register any strain and in some cases, the strain recorded could be negative, i.e. compressive. This negative strain could be explained as the result of the relaxation of tensile forces on a limited mass of concrete due to total failure of

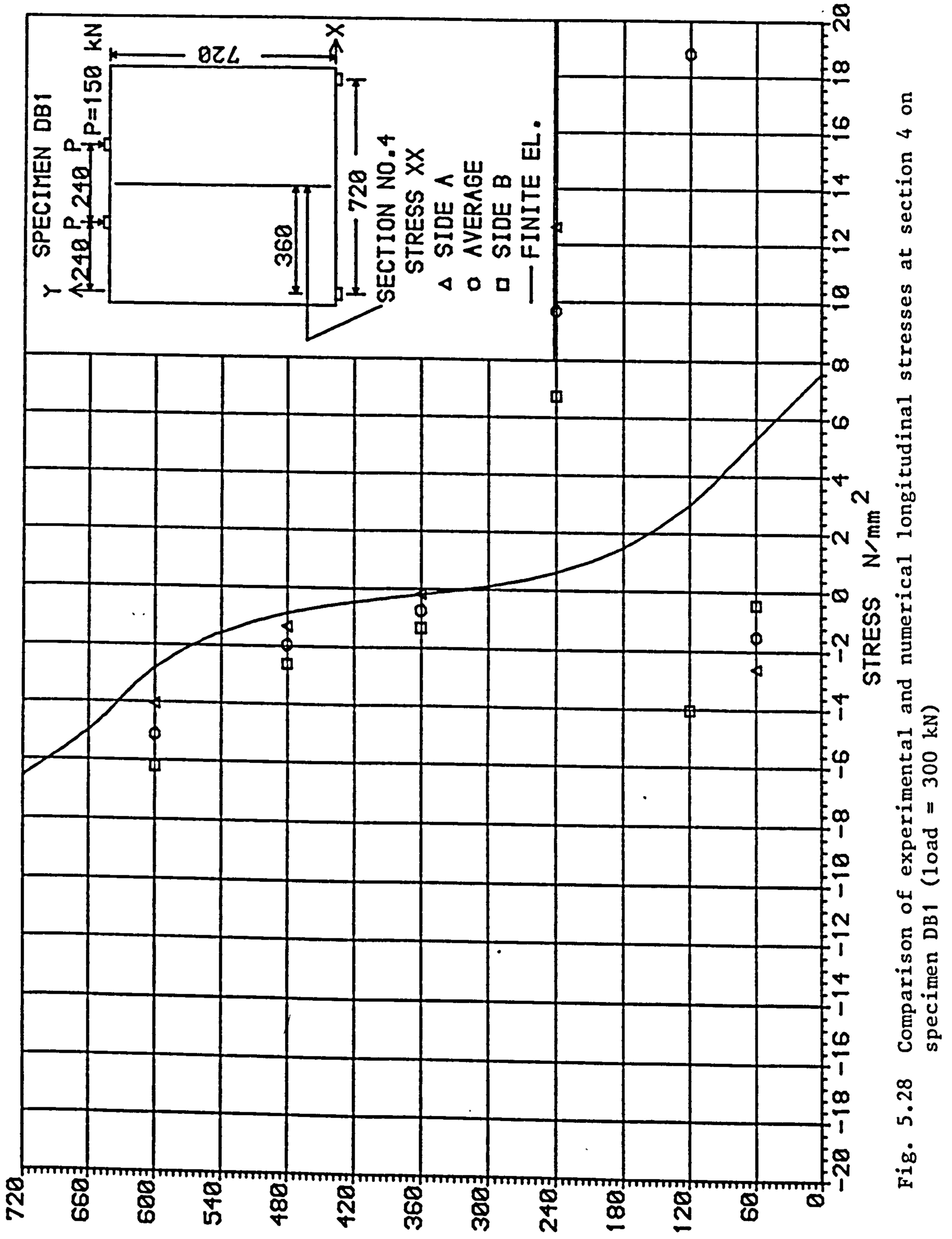

Fig. 5.28 Comparison of experimental and numerical longitudinal stresses at section 4 of specimen DB1 (load = 300 kN)

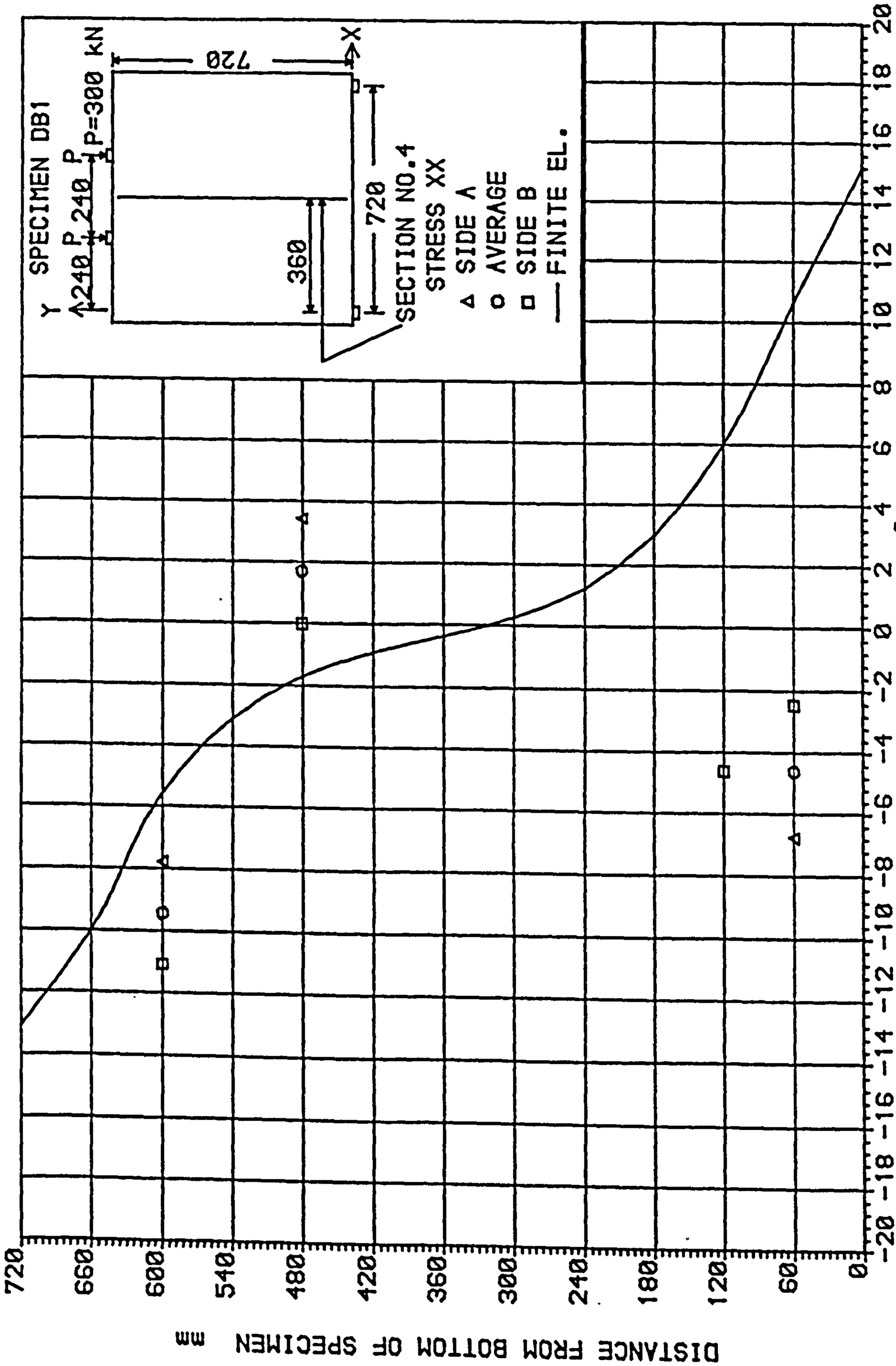

Fig. 5.29 Comparison of experimental and numerical longitudinal stresses at section 4 on specimen DB1 (load = 600 kN)

the bond between the bars and the concrete surrounding it. It is common practice to place the test specimen on the supports and then the readings corresponding to the unloaded condition taken, without any consideration of the strain already experienced by the material under its own weight and any other strains due to shrinkage. When local bond failure occurs all the strains are relieved in the concrete, including the initial strains not considered during the zero load reading, causing the origination of a fictitious negative strain. This could be the reason for the negative stresses measured experimentally at point 24 (the lowest in section 4) of specimen DB1 (Figs 5.28 and 5.29) in an area where tensile longitudinal stresses are obviously present.

Experimental and theoretical results for specimens DB2 to DB7 under loads of 600 kN or more are demonstrated in Figs. 5.30 to 5.35. It can be observed that the deeper the element, the less affected the experimental solution is by cracks. For all the specimens, the compressive stresses measured were larger than the theoretical values by about 30 to 60 percent. In specimen DB5 (Fig 5.33) this difference was about 100 percent, showing a large displacement of the measured values with respect to the analytical results along the whole depth of the panel. It is obvious that this difference was the result of an experimental error; although some attention has been given to this matter, there is no clear justification for these experimental results for panel DB5.

Generally the longitudinal stresses in the central section (within the height) of the deep panels have proved to be relatively small compared to the maximum tensile and compressive stresses at the bottom and top. It can be pointed out that the sections above the upper neutral axis and below the lower neutral axis are the critical sections with respect to longitudinal stresses. However more generally

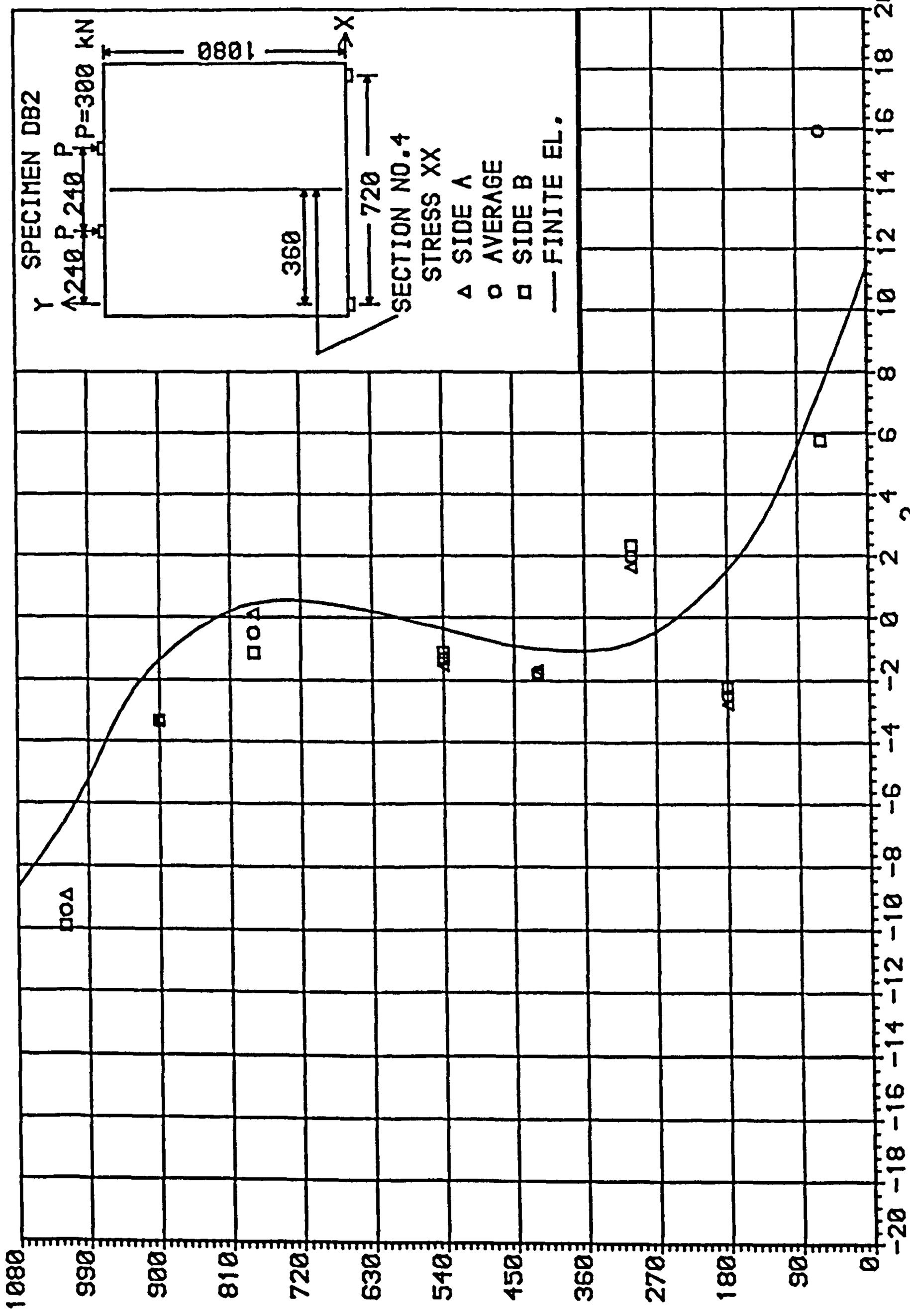

Fig. 5.30 Comparison of experimental and numerical longitudinal stresses at section 4 on specimen DB2 (load = 600 kN)

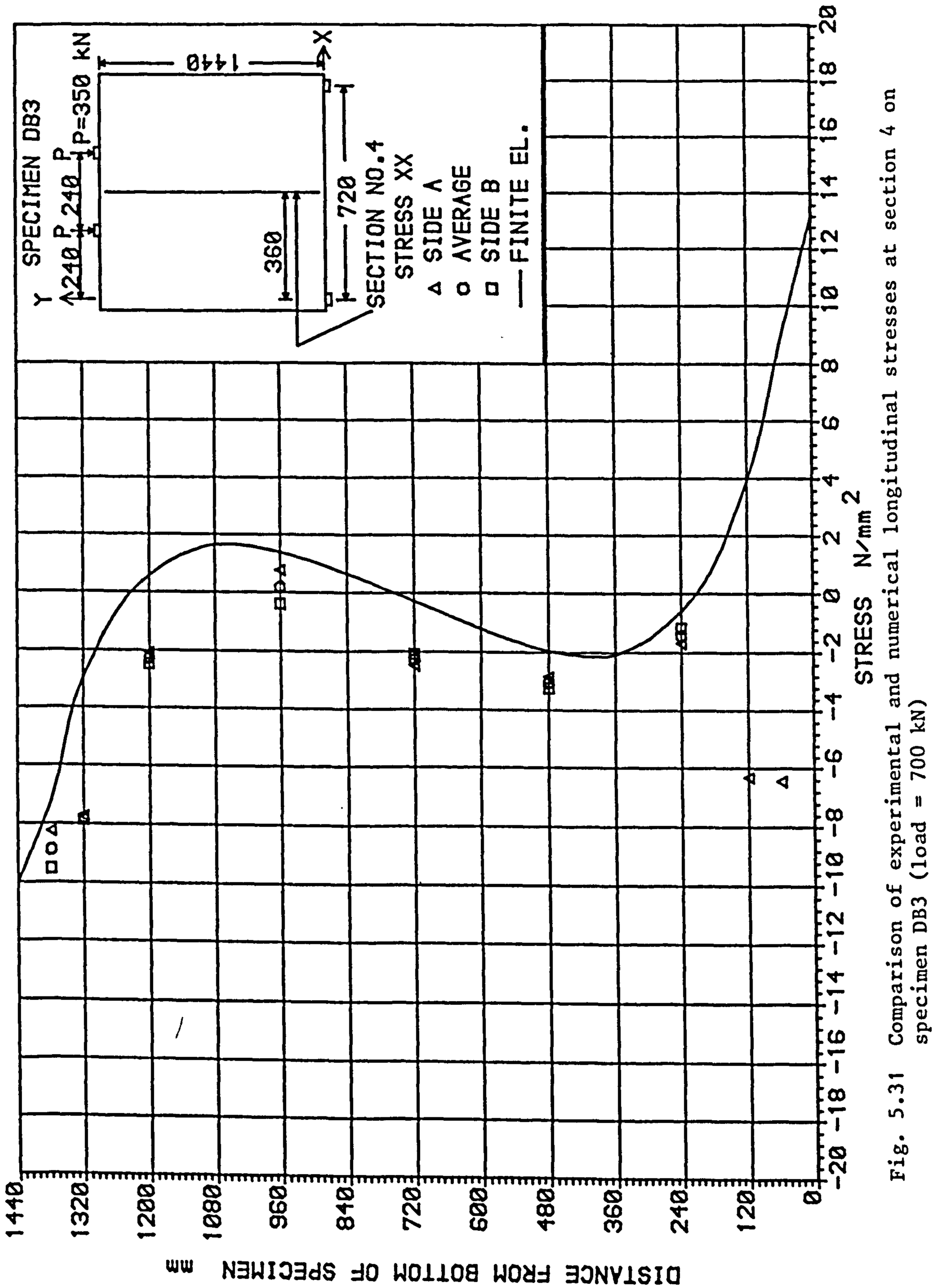

Fig. 5.31 Comparison of experimental and numerical longitudinal stresses at section 4 on specimen DB3 (load = 700 kN)

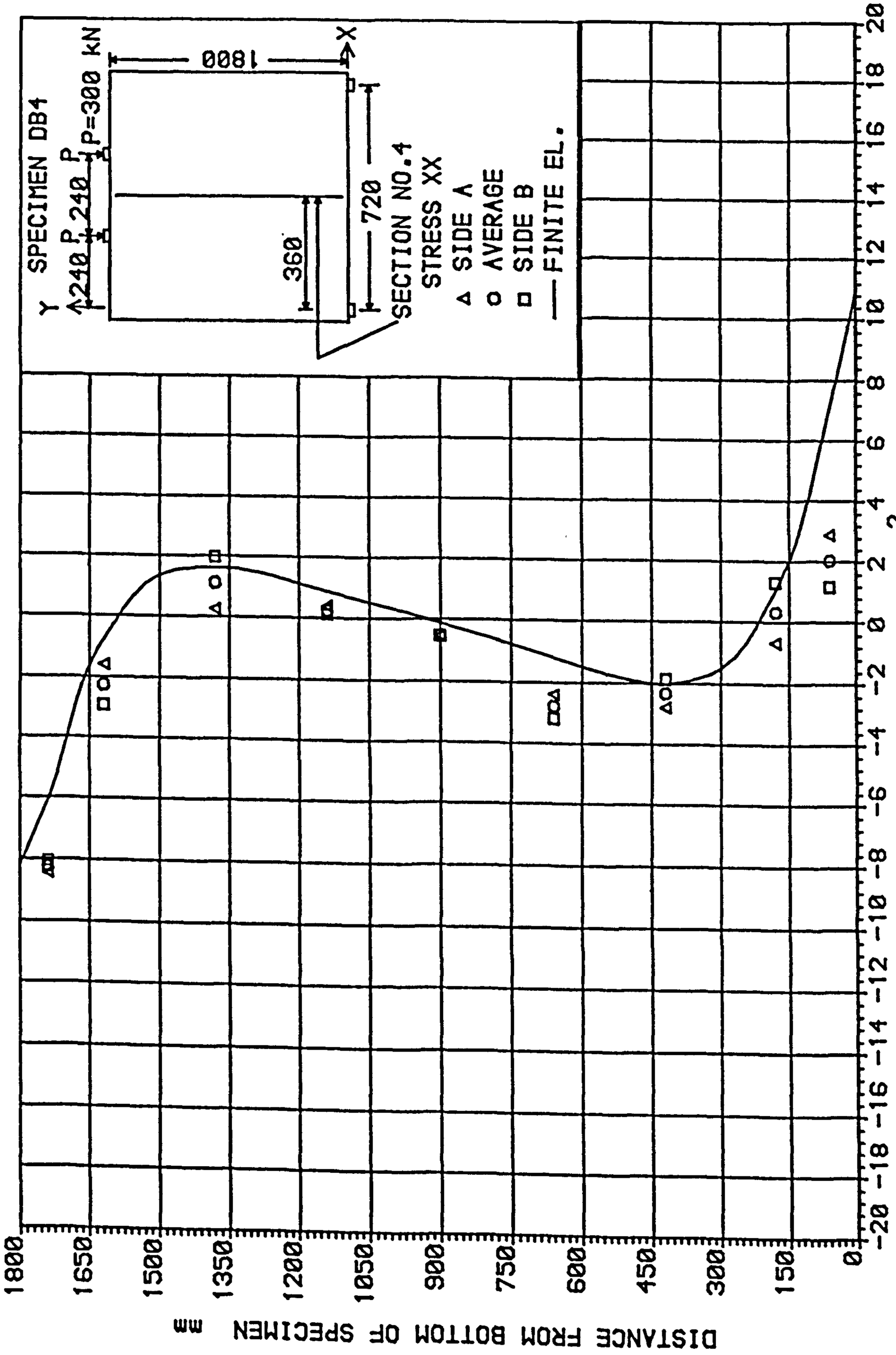

Fig. 5.32 Comparison of experimental and numerical longitudinal stresses at section 4 on specimen DB4 (load = 600 kN)

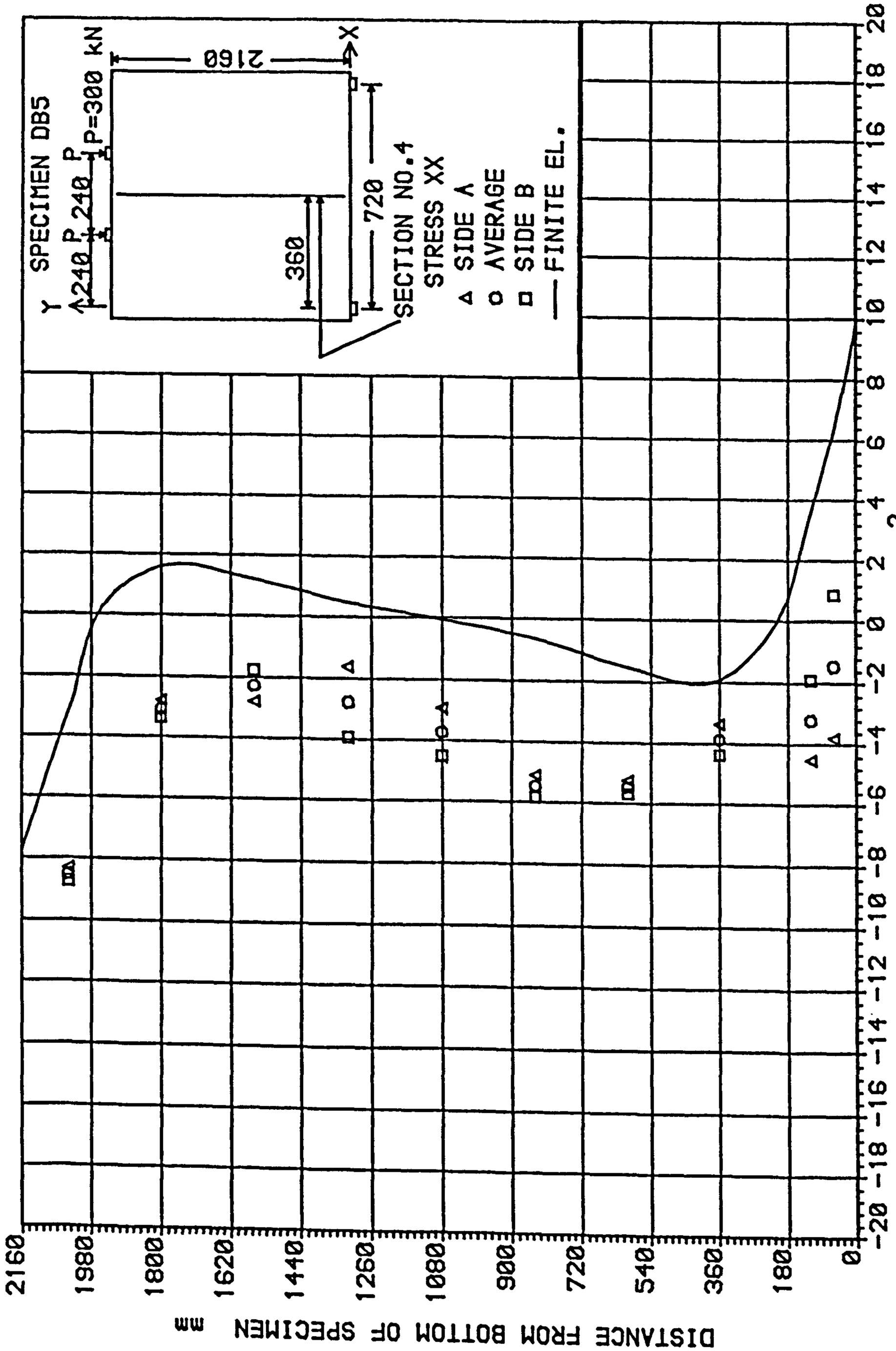

Fig. 5.33 Comparison of experimental and numerical longitudinal stresses at section 4 on specimen DB5 (load = 600 kN)

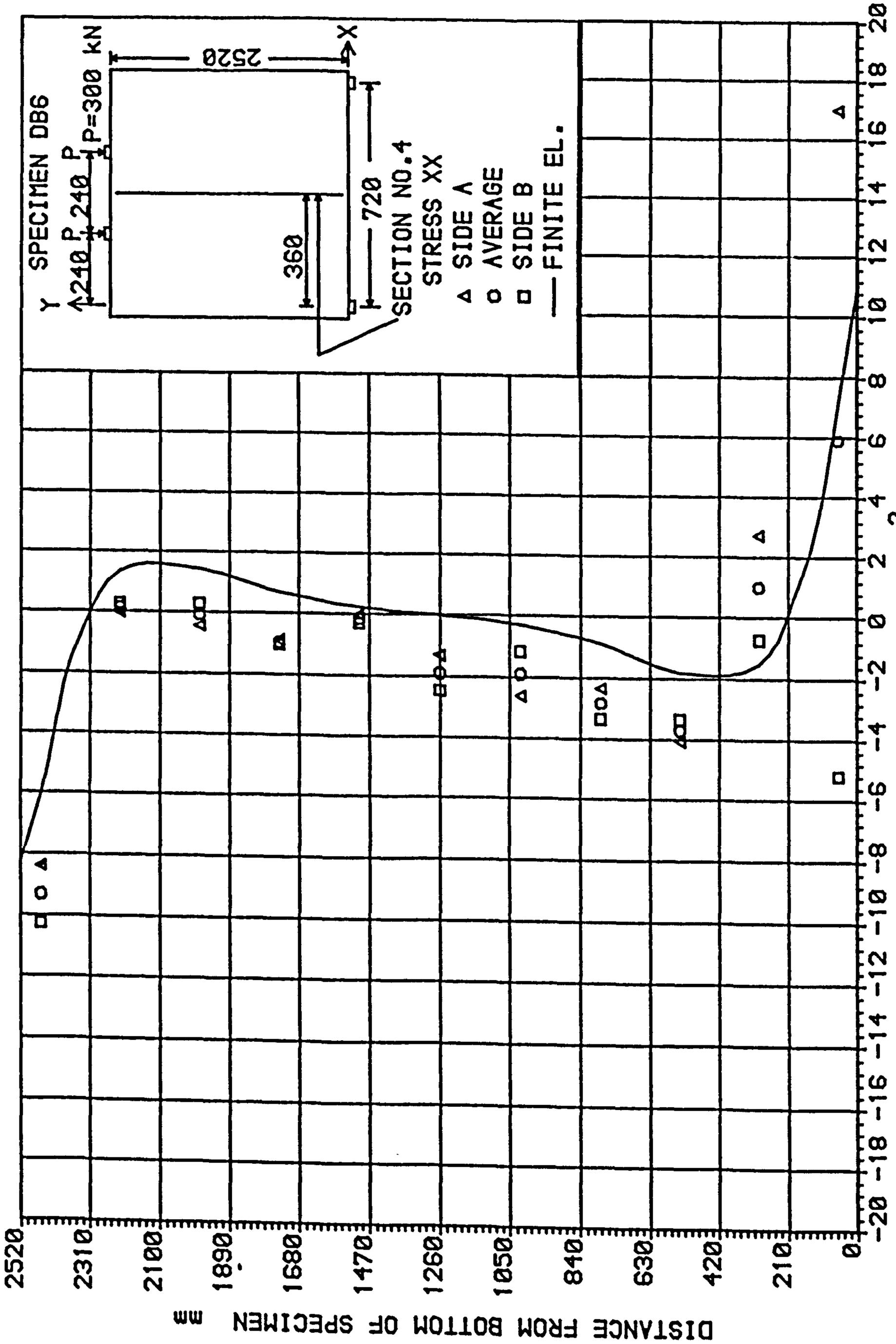

Fig. 5.34 Comparison of experimental and numerical longitudinal stresses at section 4 on specimen DB6 (load = 600 kN)

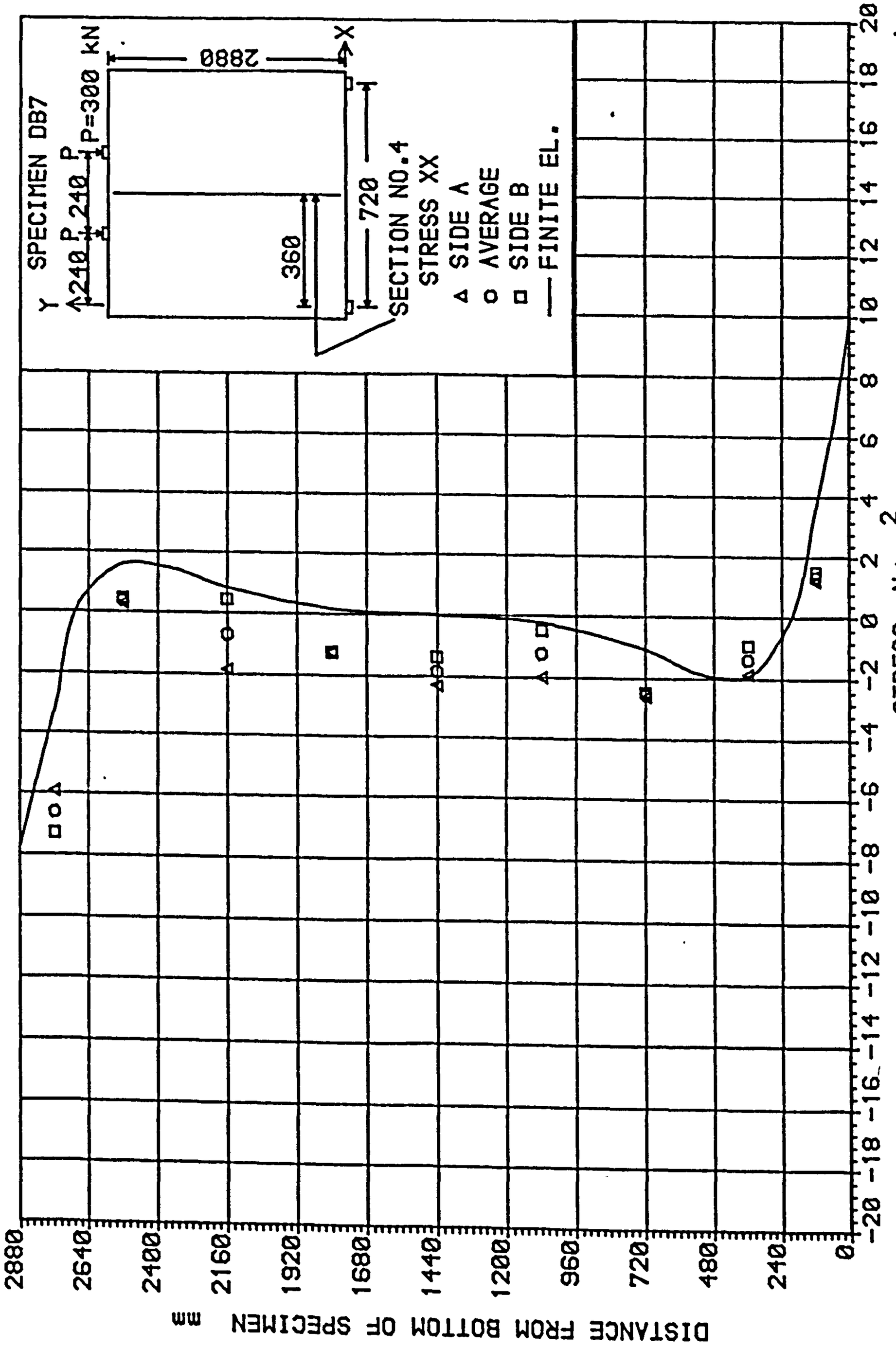

Fig. 5.35 Comparison of experimental and numerical longitudinal stresses at section 4 on specimen DB7 (load = 600 kN)

it can be said that the upper and lower sections extending to depths of span/3 from the top and bottom of the wall should be carefully considered for design purposes.

From Figs. 5.29 to 5.35 the observation can be made that the maximum compressive and tensile stresses vary considerably from specimen DB1 (Fig. 5.29) to DB2 (Fig. 5.30) and thereafter they appear altered little by changes in depth/span ratio. The effect of the depth on the maximum longitudinal stresses on deep flexural elements can be observed on Fig. 5.36; stresses shown correspond to those calculated by the finite element method and a constant total load of 100 kN. The elastic properties of the material used correspond to the average of those shown in Table 3.2. Figure 5.36 discloses a sharp reduction in stresses as the depth/span ratio increases up to a value of 1.5. On reaching a value of 2.0, the stresses reduce slightly and thereafter the effect of the depth is extremely small.

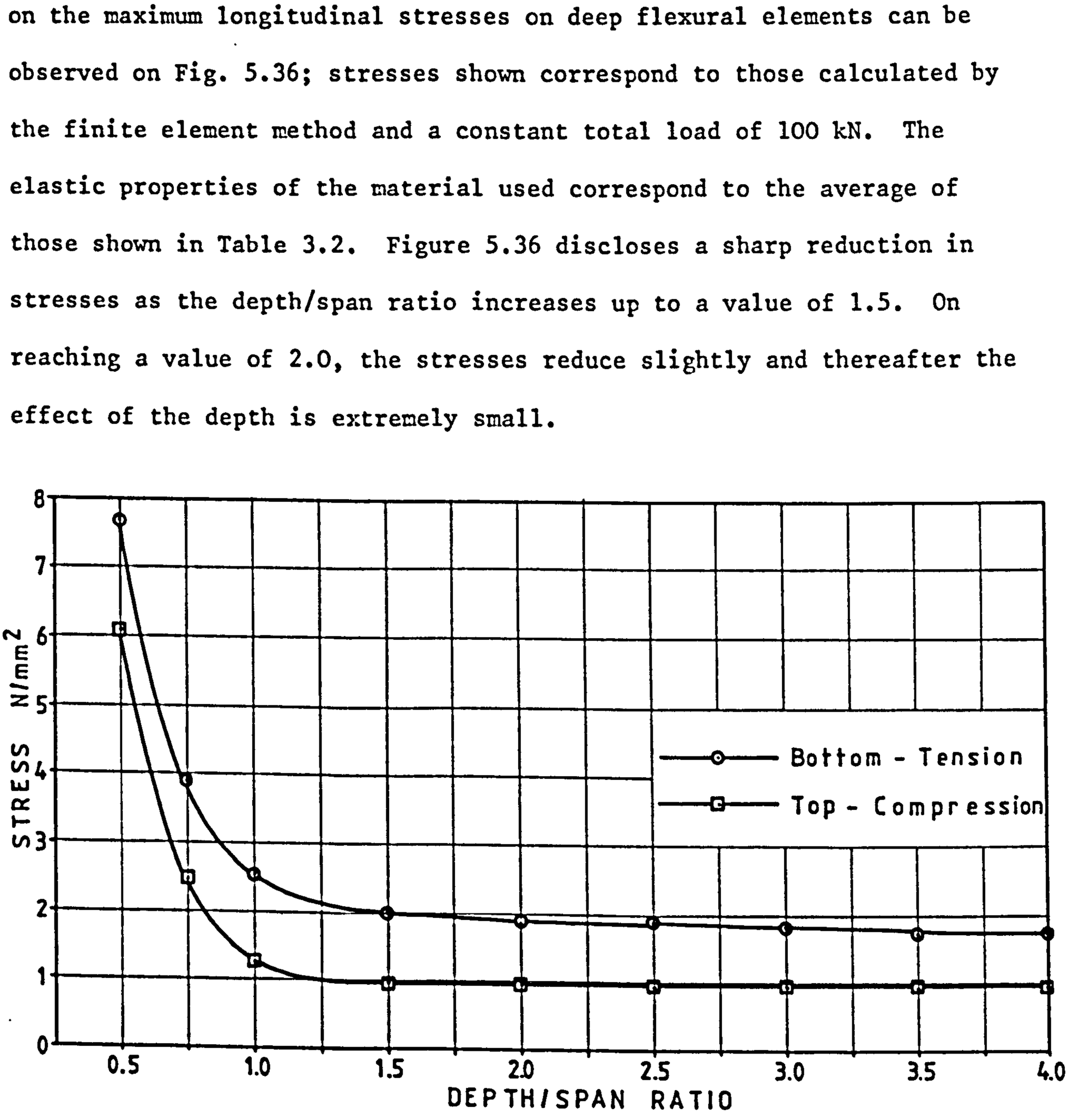

Fig. 5.36 Effect of depth/span ratio on maximum longitudinal stresses for deep panels under third points load

5.4.3 Vertical Stress

The presentation of theoretical and experimental vertical stresses is based mainly on those results from sections 1 and 4, which coincide with a support and mid-span respectively.

Figure 5.37 shows the values of vertical stresses at four sections in specimen DB1 under a total load of 100 kN. Generally, the experimental and the theoretical results agree well, except for a small number of points. In Fig. 5.37(b), the predicted vertical stress in the soffit has a relatively large value where zero stress was expected. A similar condition was observed in Fig. 5.37(d) at the uppermost level of the specimen where the vertical stress was also expected to have a value equal to zero. The theoretical results gave relatively large values at these points, but it is well known that this analytical method employed does not satisfy fully the boundary conditions, where this error occurs.

Figures 5.38 to 5.43 illustrate the excellent agreement between the experimental values and those predicted by finite element in Section 1 for specimens DB1 to DB7 under a total load of 200 kN.

Under larger loads, some differences between both methods are noticed. Figures 5.44 to 5.50 compare the experimental and analytical results for specimens DB1 to DB7 along Section 4 under a load of 600 kN or more. The experimental results shown for specimen DB1 (Fig. 5.44) are affected by cracks in the concrete. This effect was reduced in the other specimens with larger depths and the comparison of results was good. For specimens with larger depth/span ratios the experimental values were larger than the theoretical ones, although they follow the same general pattern. It is believed, that this difference, which in some cases is over 40 percent of the theoretical solution, results from inaccuracies introduced by assuming that the elastic properties of the test specimen correspond to those measured from cubes, cylinders and

prisms cast with the same concrete.

By comparing Figs. 5.44 to 5.50, it can be observed that a relatively large difference in vertical stresses between the sides of the specimen began to show in specimen DB5 (Fig. 5.48), with depth/thickness ratio equal to 30 and had its maximum effect in specimen DB7 as shown in Fig. 5.50. The differences in value between the vertical stresses measured on both sides of the panel are interesting because they reflect the discrepancy between the strains measured on both sides of the specimen and give the curvature in the vertical plane at any section as calculated by equation 3.4.

Figure 5.51 presents the erratic behaviour of the curvature in the vertical direction along the mid-span section in specimen DB4 for different loads. This behaviour was typical for the other specimens with depths smaller than DB4. In Fig. 5.52 the same values for specimen DB5 are given graphically. Here, a more definite pattern is observed, with the curvature increasing regularly with the load. The same observation can be made in Figs. 5.53 and 5.54 for panels DB6 and DB7 with the maximum value of curvature being provided by specimen DB7.

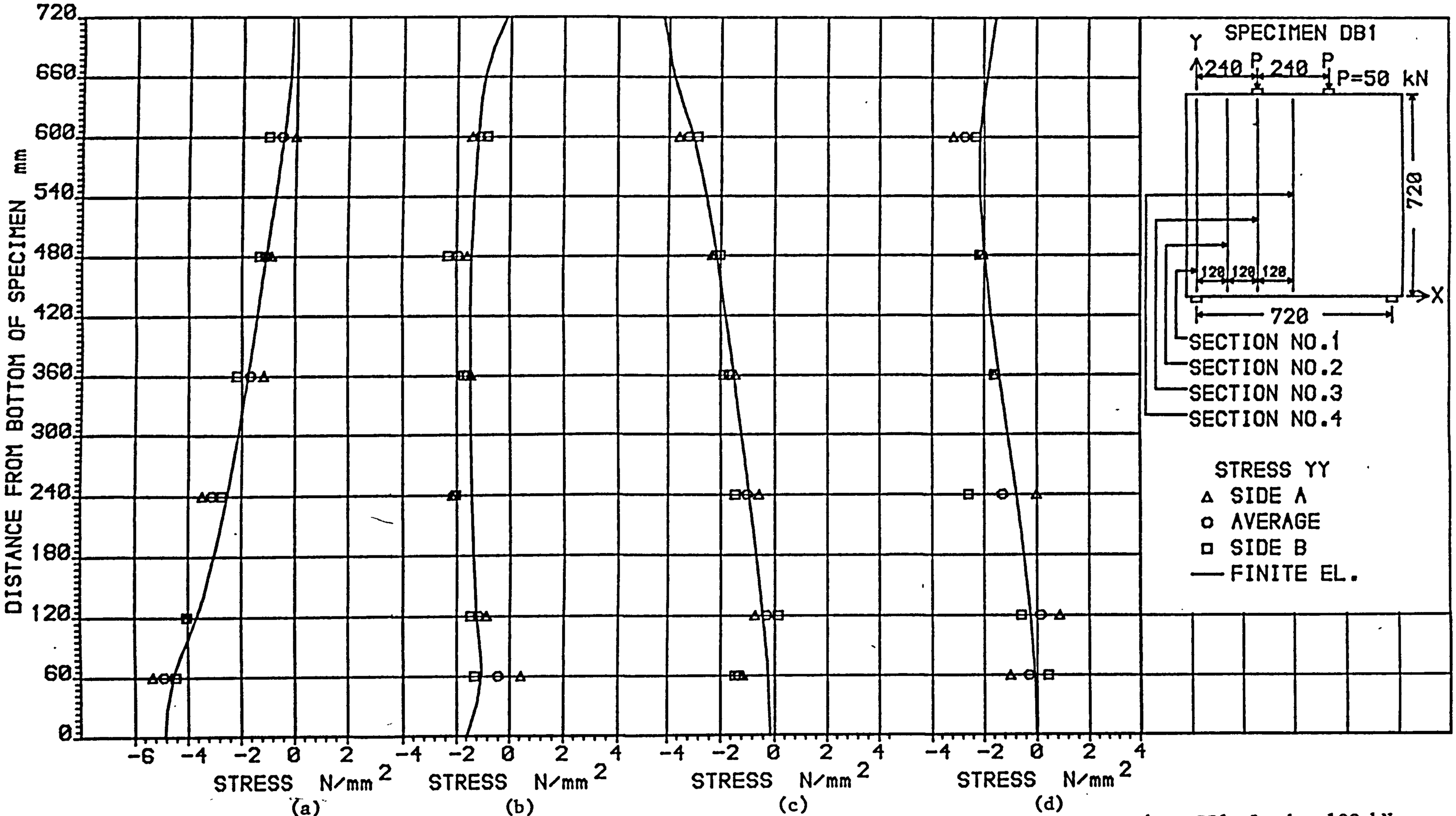

Fig. 5.37 Comparison of experimental and numerical vertical stresses at four sections on specimen DB1. Load = 100 kN. a) at section 1, b) at section 2, c) at section 3 and d) at section 4

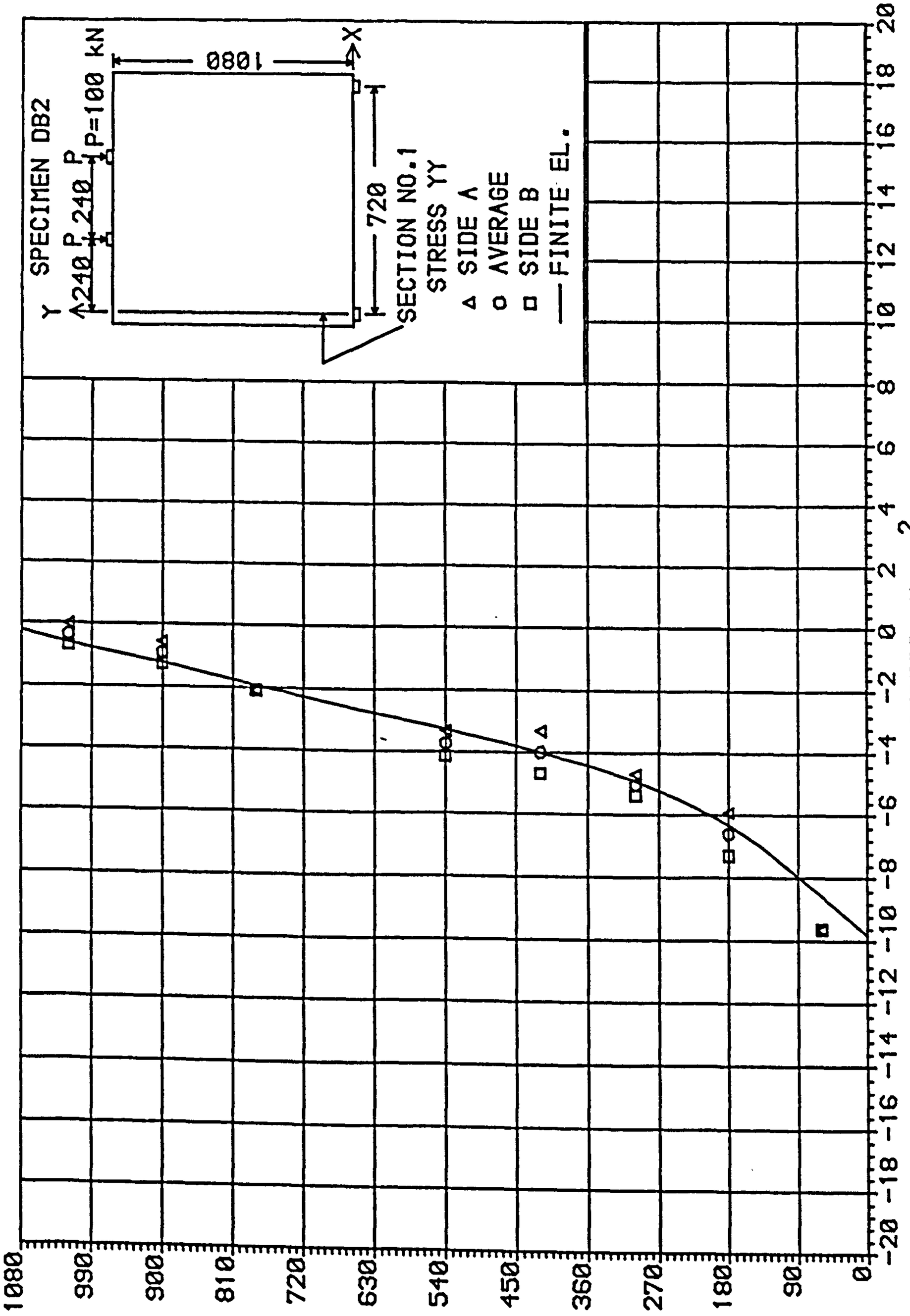

Fig. 5.38 Comparison of experimental and numerical vertical stresses at section 1 of specimen DB2 (load = 200 kN)

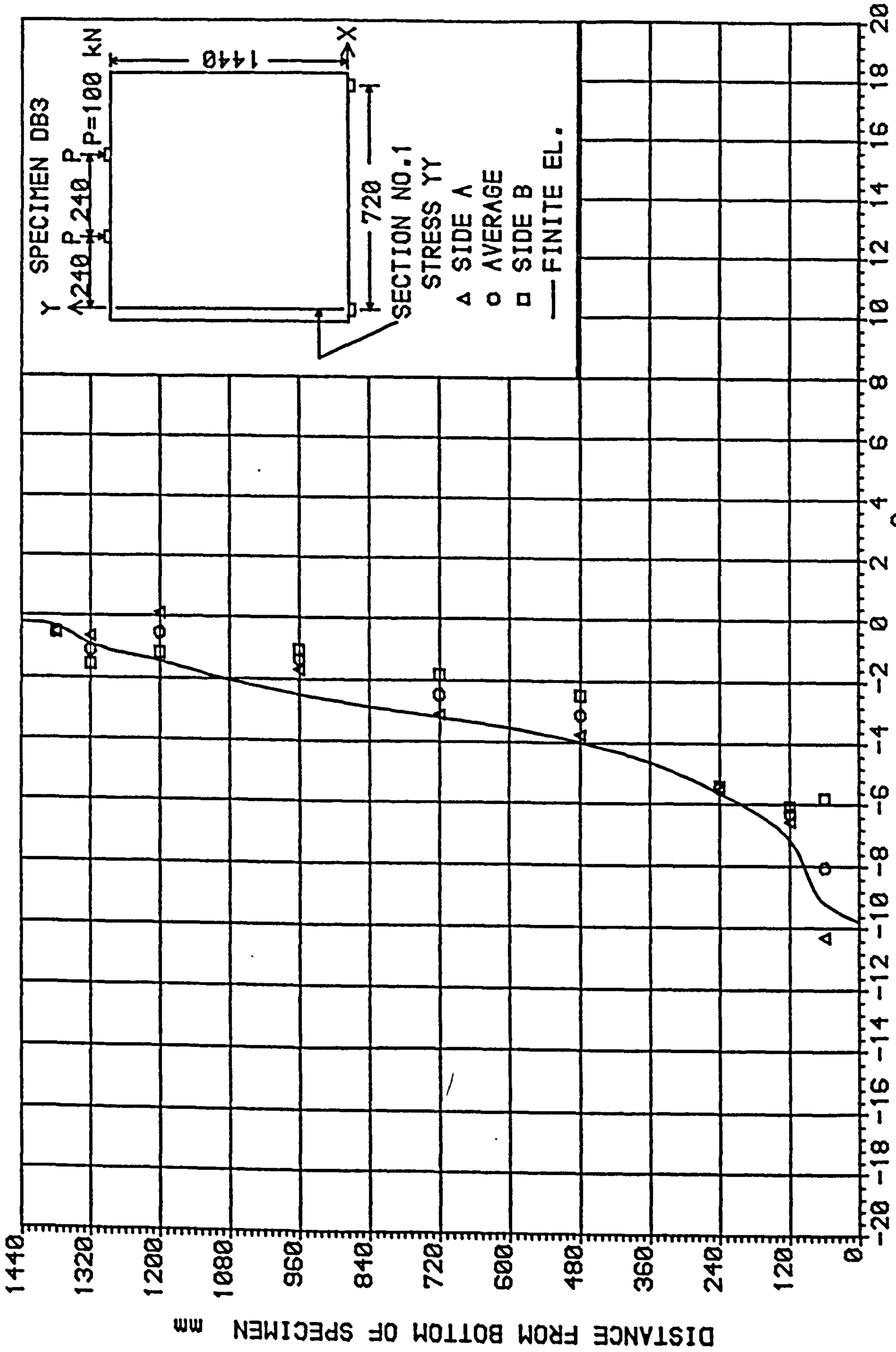

Fig. 5.39 Comparison of experimental and numerical vertical stresses at section 1 on specimen DB3 (load = 200 kN)

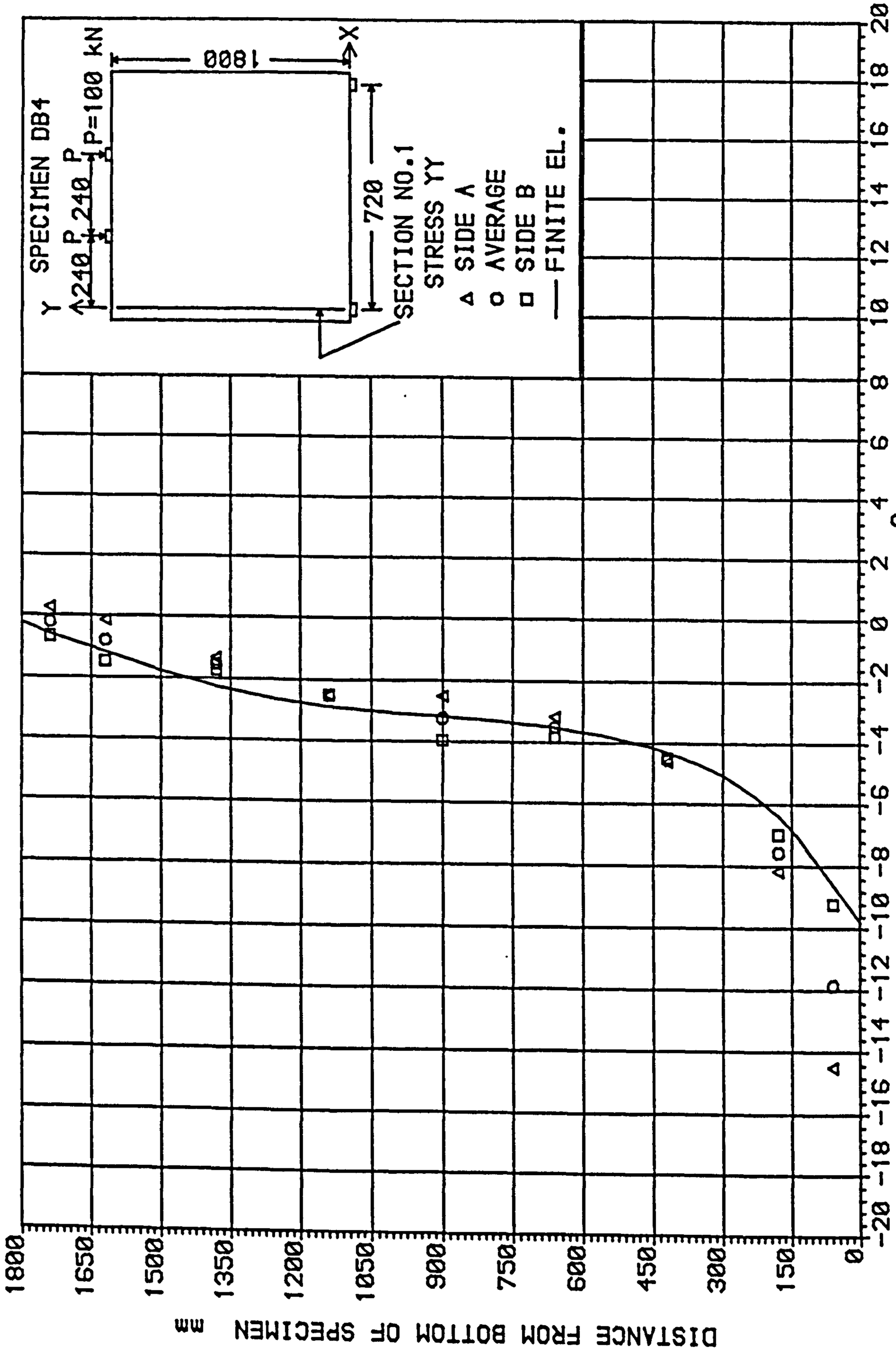

Fig. 5.40 Comparison of experimental and numerical vertical stresses at section 1 on specimen DB4 (load = 200 kN)

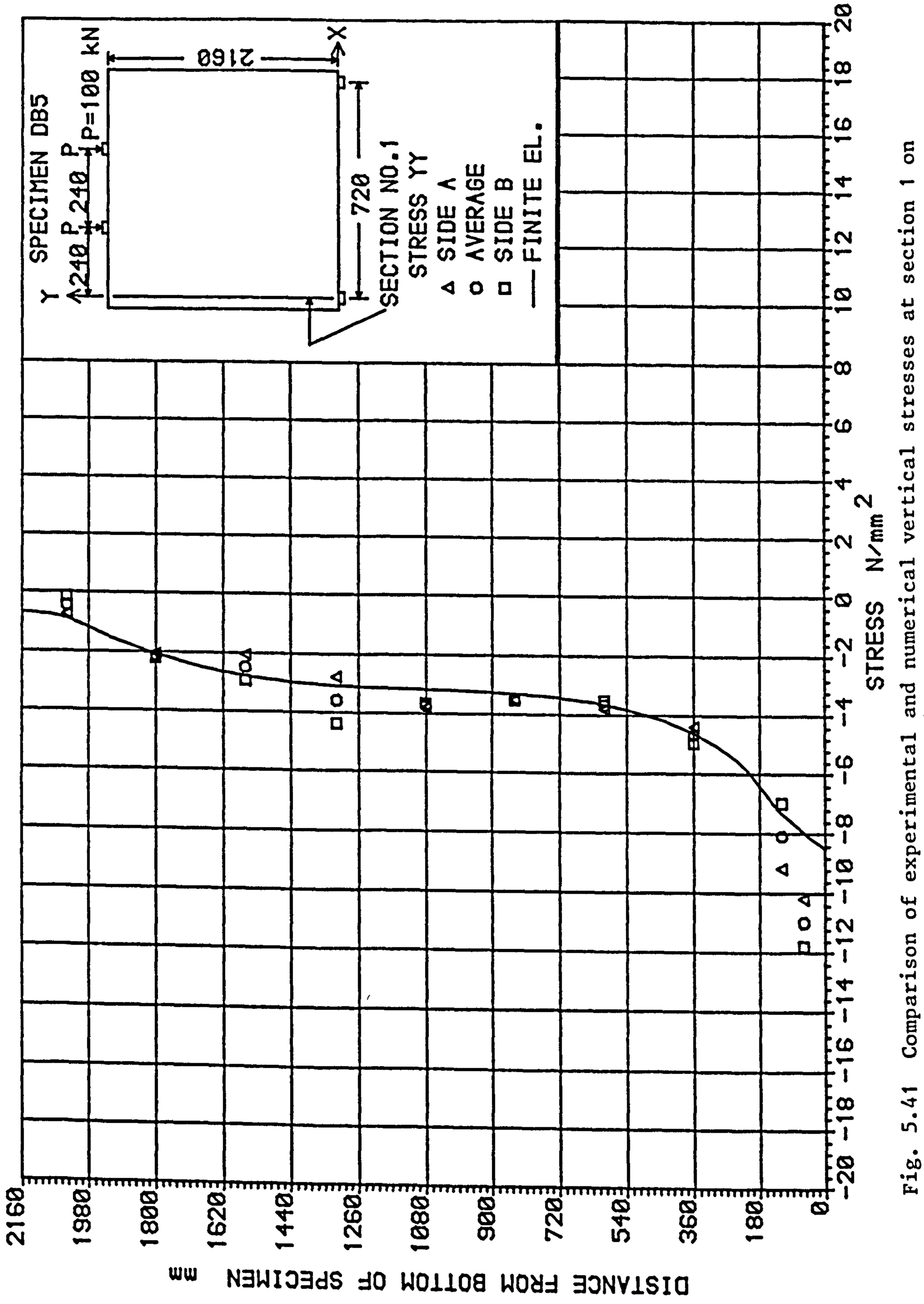

Fig. 5.41 Comparison of experimental and numerical vertical stresses at section 1 on specimen DB5 (load = 200 kN)

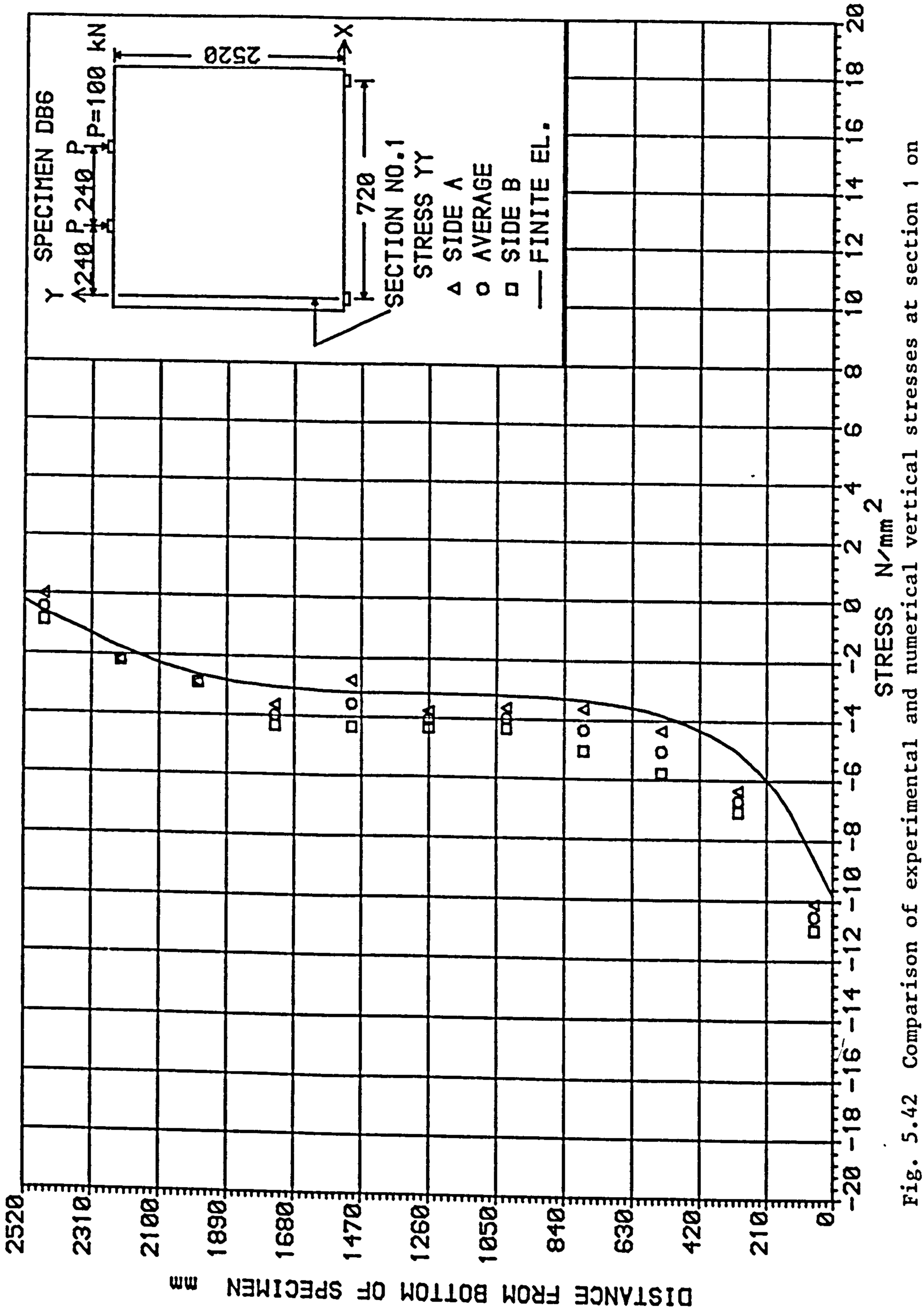

Fig. 5.42 Comparison of experimental and numerical vertical stresses at section 1 on specimen DB6 (load = 200 kN)

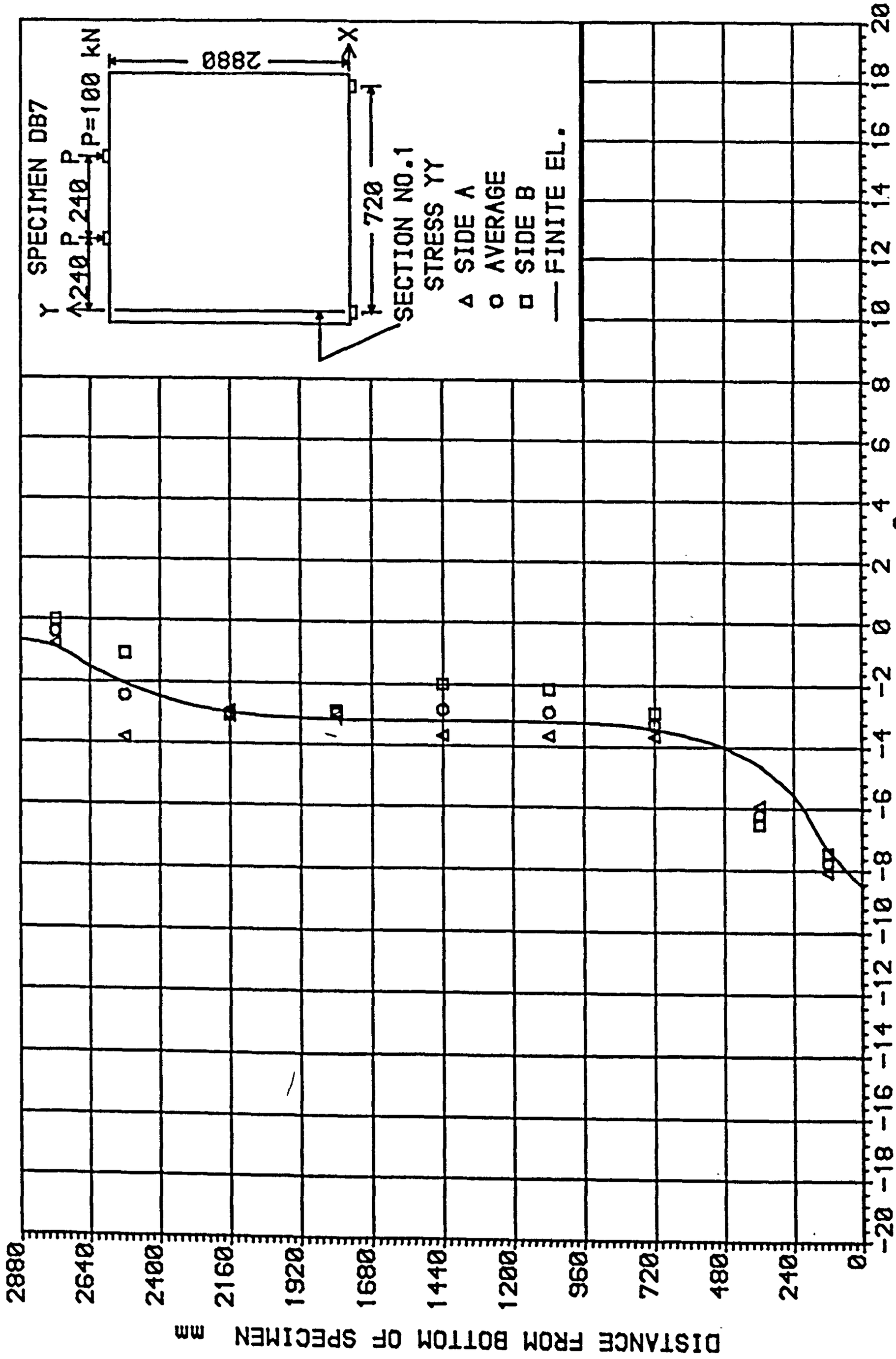

Fig. 5.43 Comparison of experimental and numerical vertical stresses at section 1 on specimen DB7 (load = 200 kN)

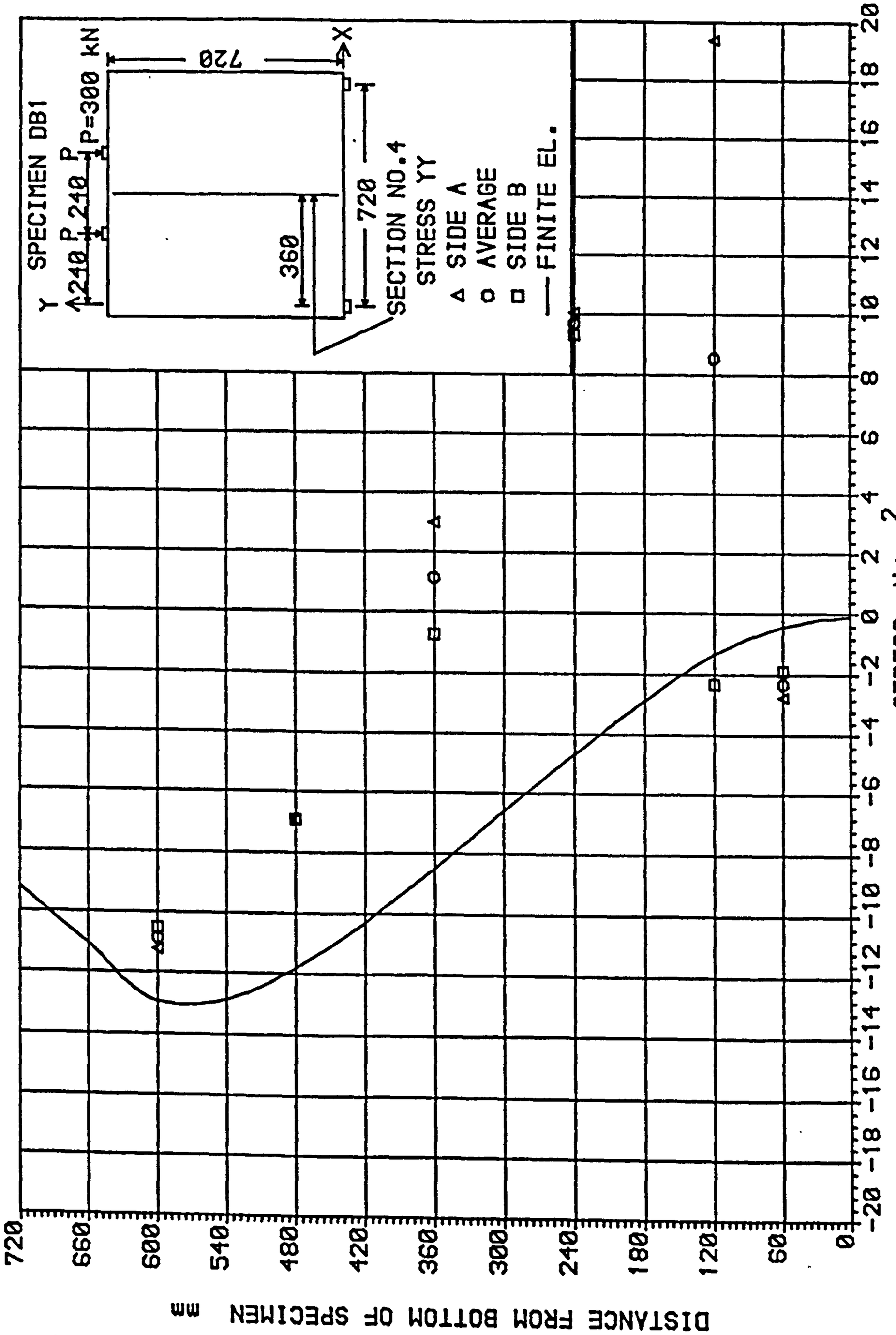

Fig. 5.44 Comparison of experimental and numerical vertical stresses at section 4 on specimen DB1 (load = 600 kN)

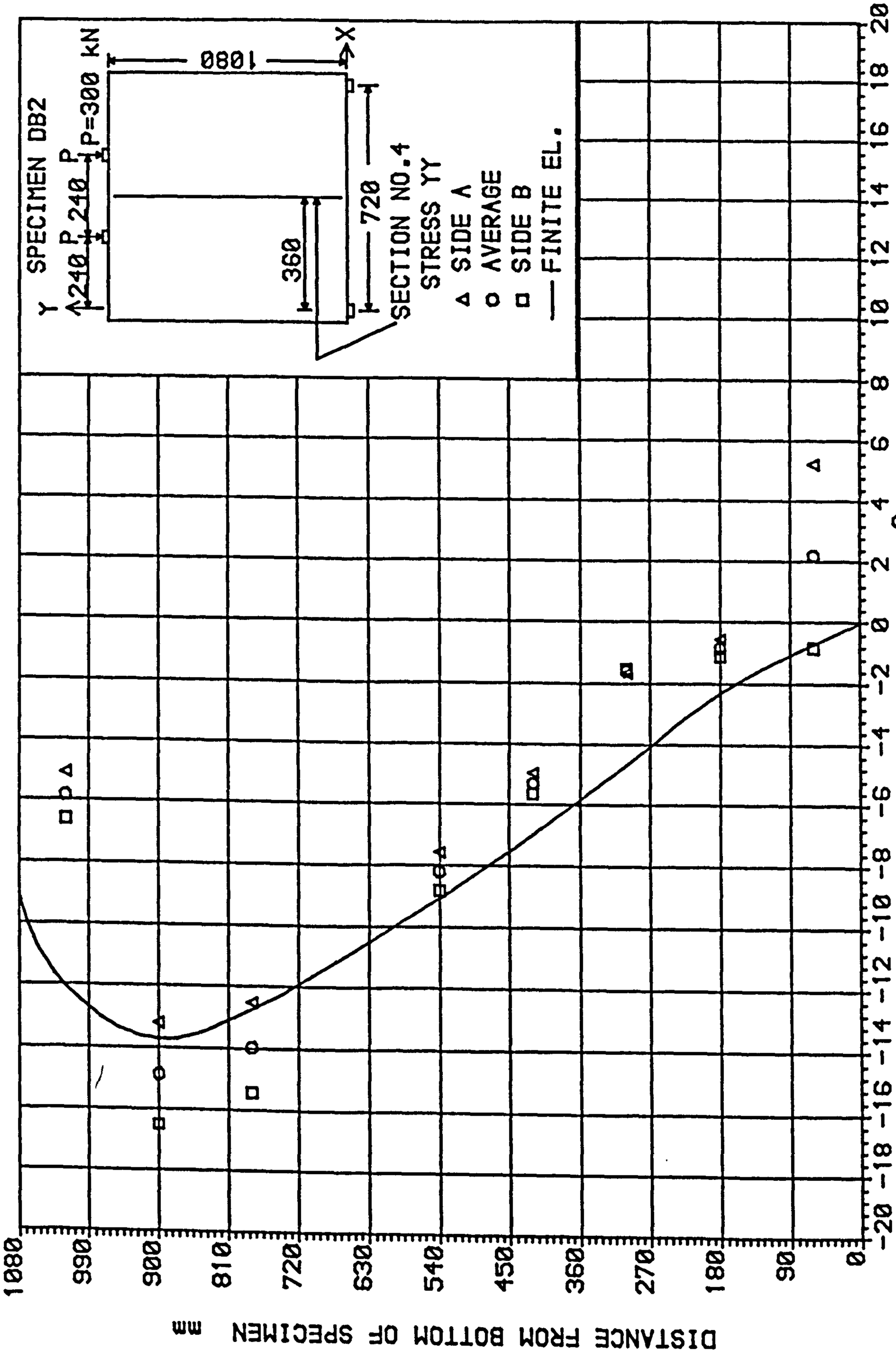

Fig. 5.45 Comparison of experimental and numerical vertical stresses at section 4 on specimen DB2 (load = 600 kN)

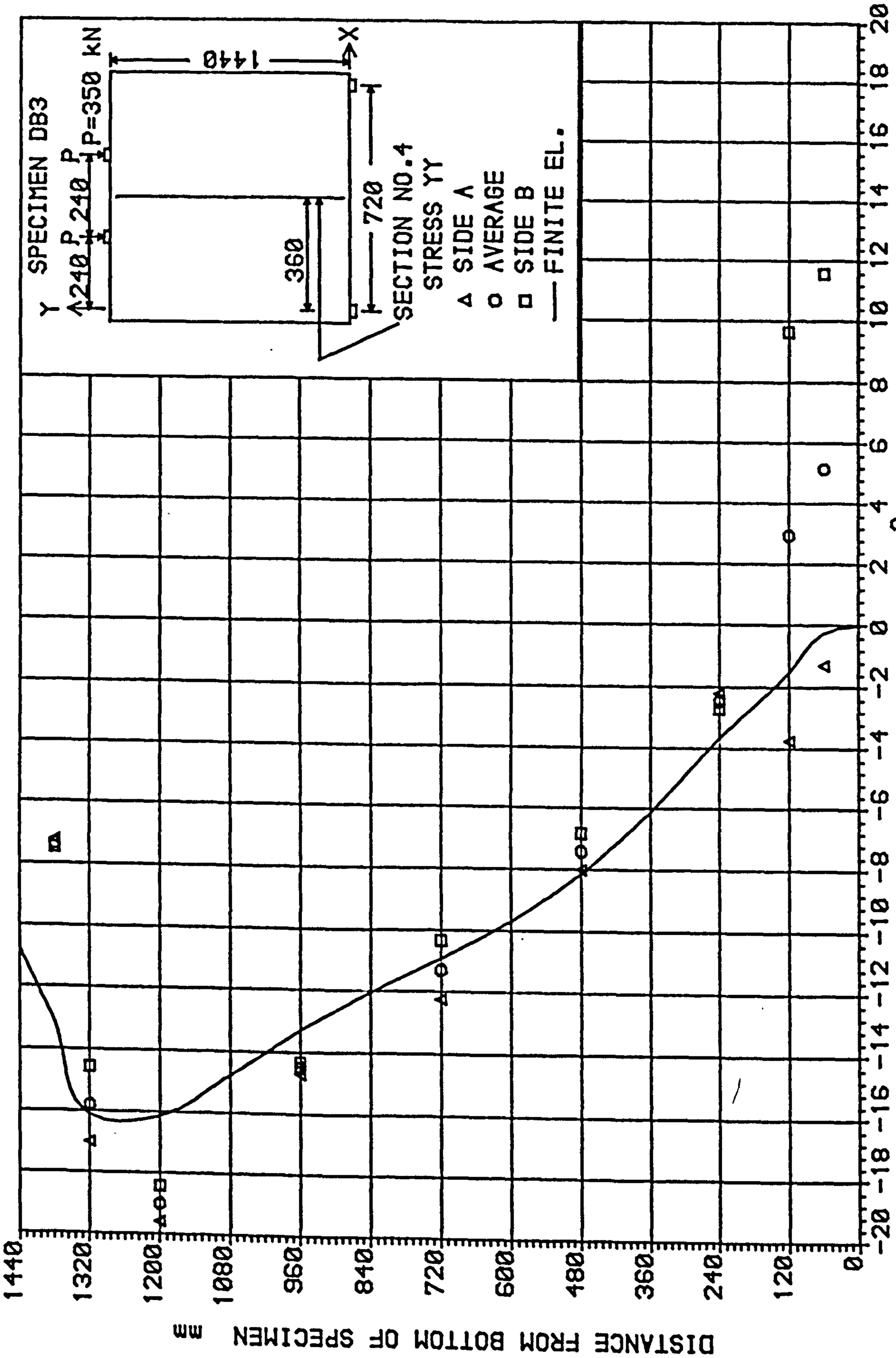

Fig. 5.46 Comparison of experimental and numerical vertical stresses at section 4 on specimen DB3 (load = 700 kN)

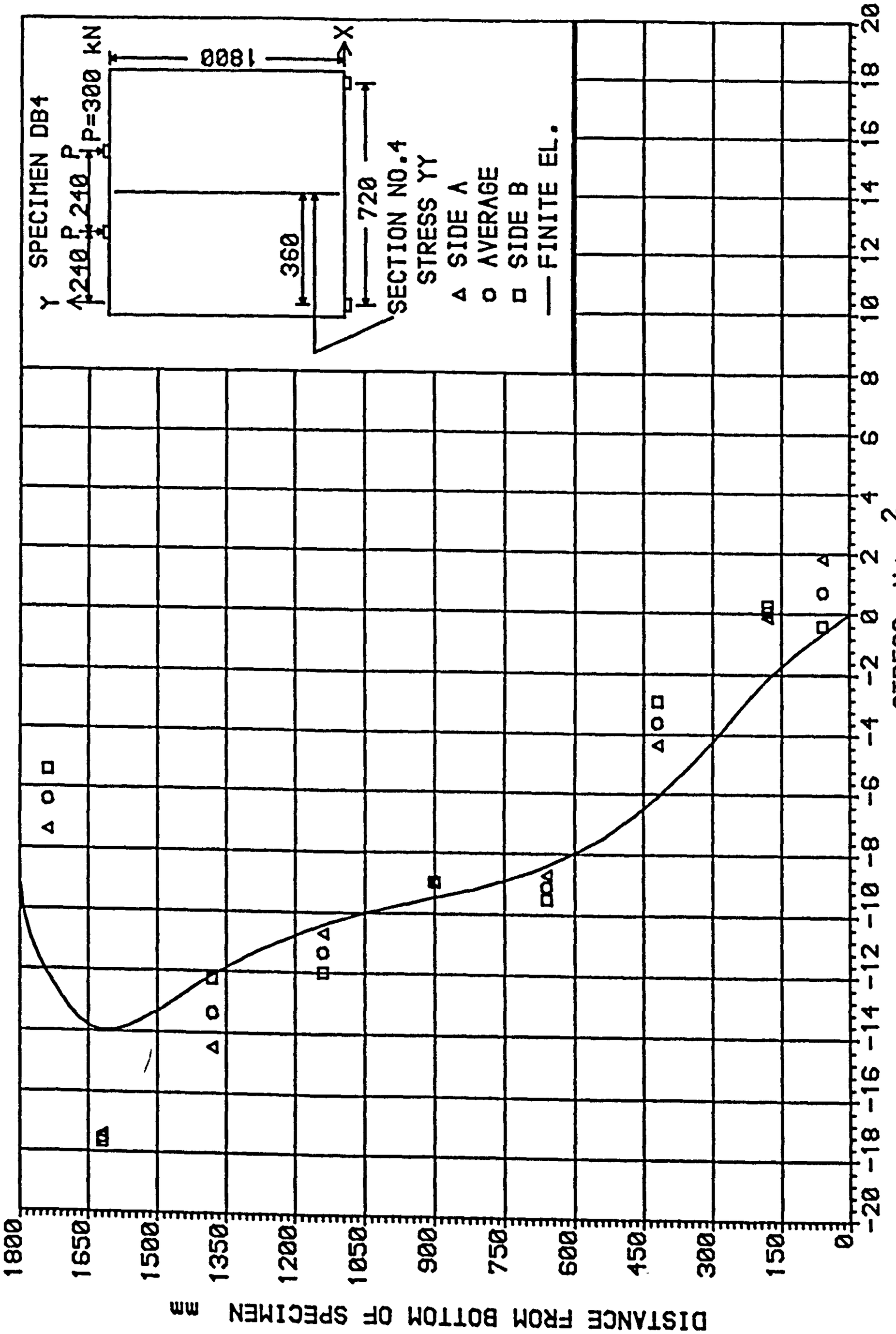

Fig. 5.47 Comparison of experimental and numerical vertical stresses at section 4 on specimen DB4 (load = 600 kN)

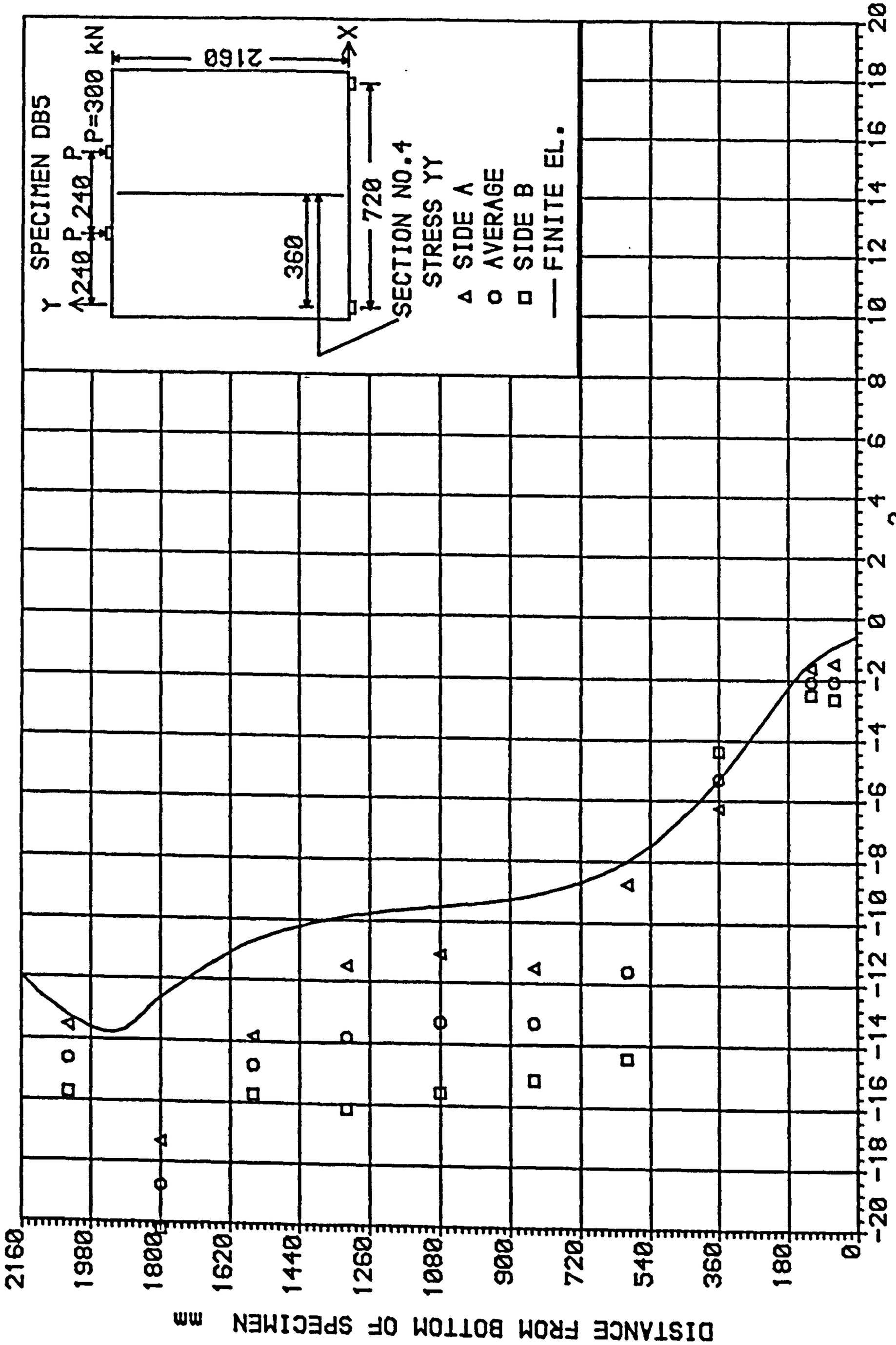

Fig. 5.48 Comparison of experimental and numerical vertical stresses at section 4 of specimen DB5 (load = 600 kN)

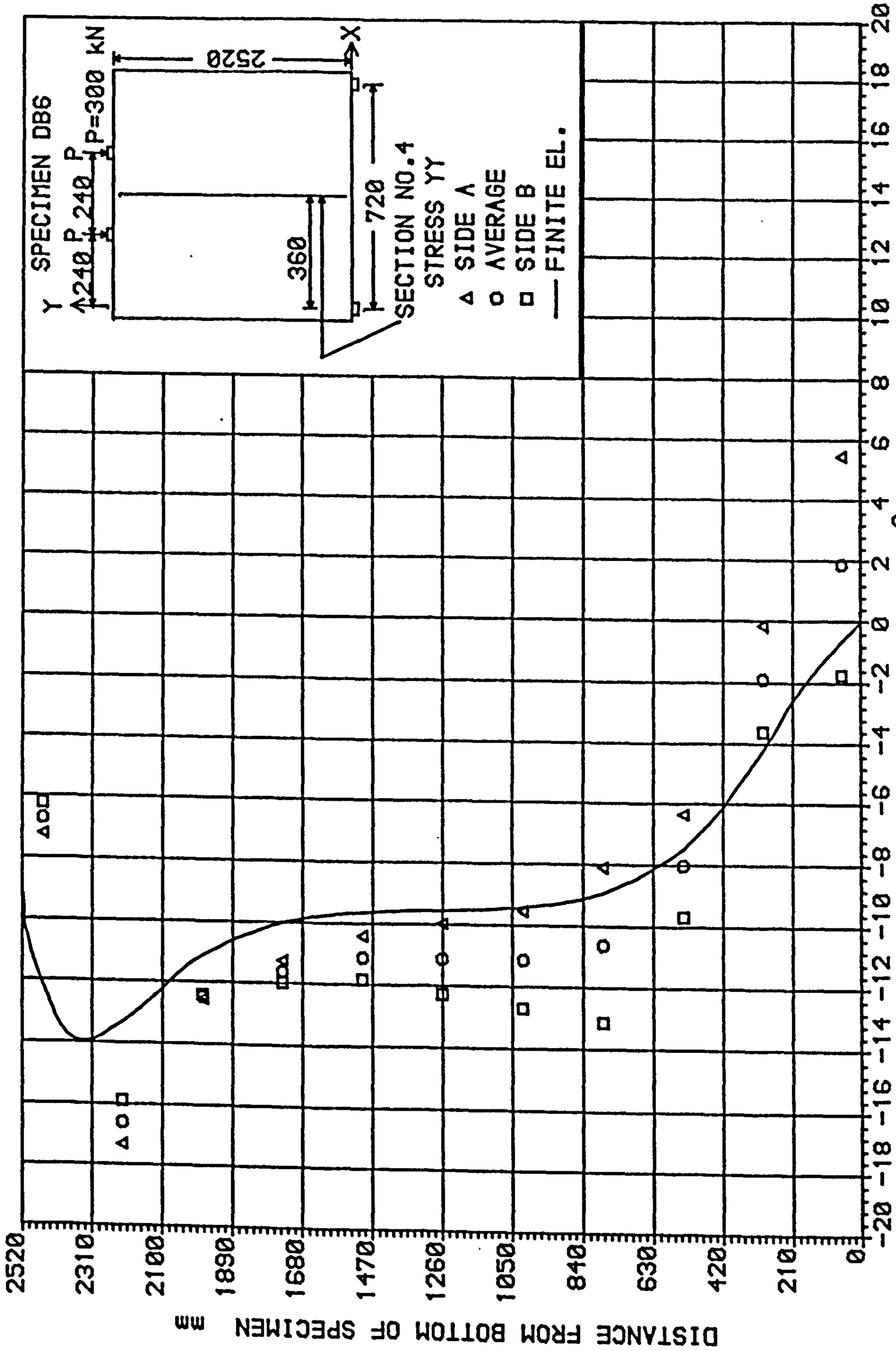

Fig. 5.49 Comparison of experimental and numerical vertical stresses at section 4 of specimen DB6 (load = 600 kN)

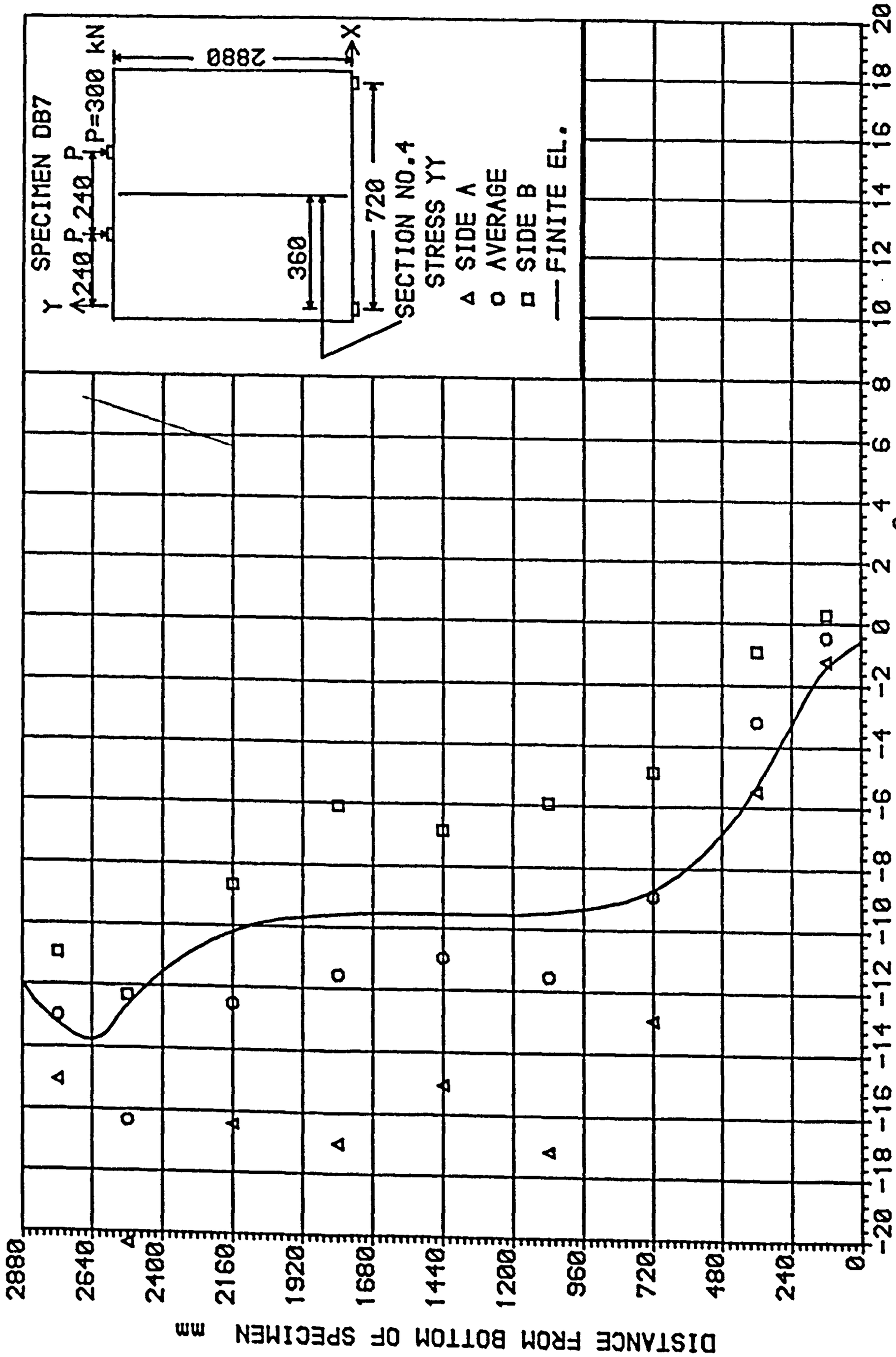

Fig. 5.50 Comparison of experimental and numerical vertical stresses at section 4 on specimen DB7 (load = 600 kN)

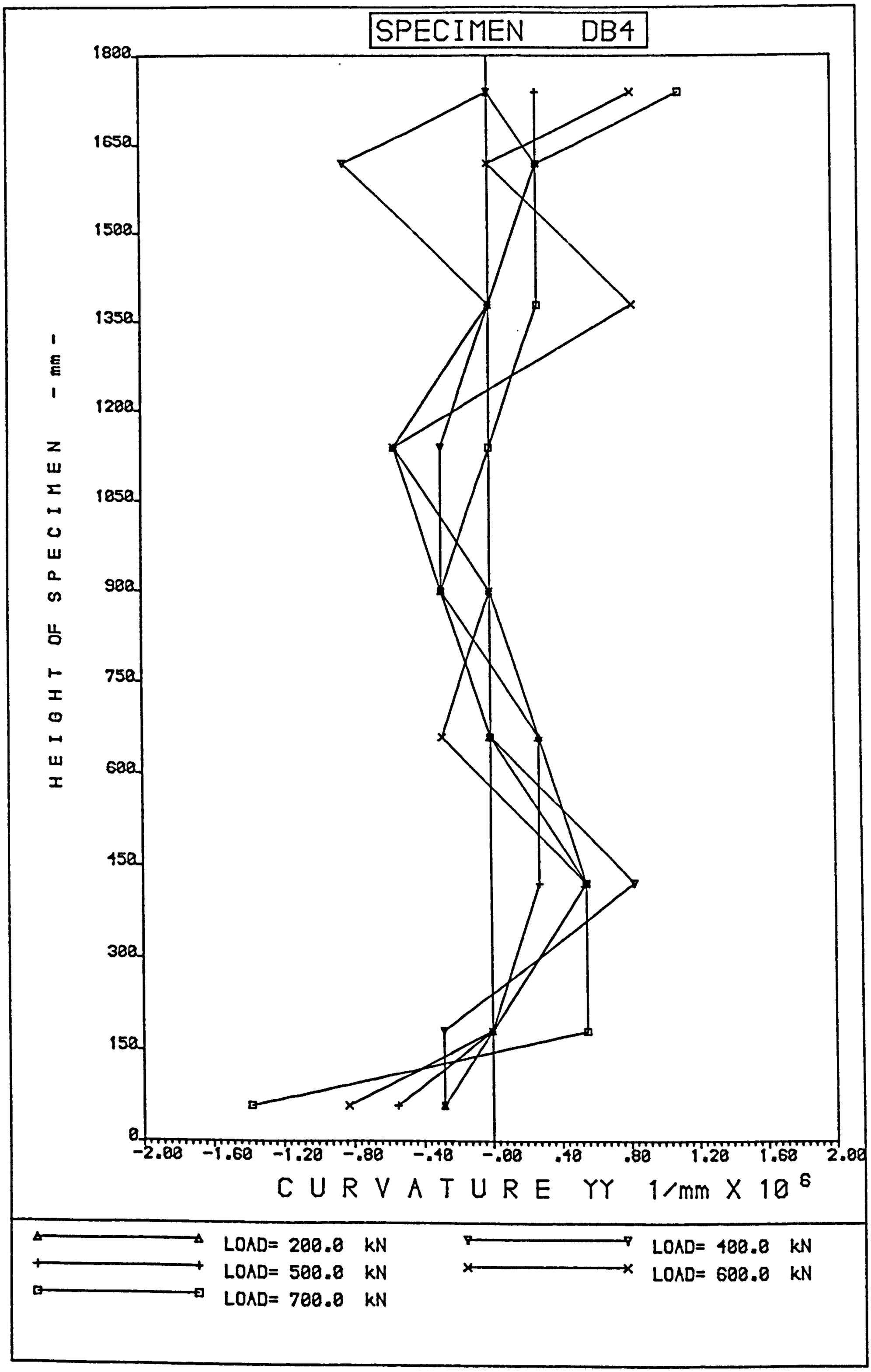

Fig. 5.51 Curvature measured experimentally at section 4 on specimen DB4

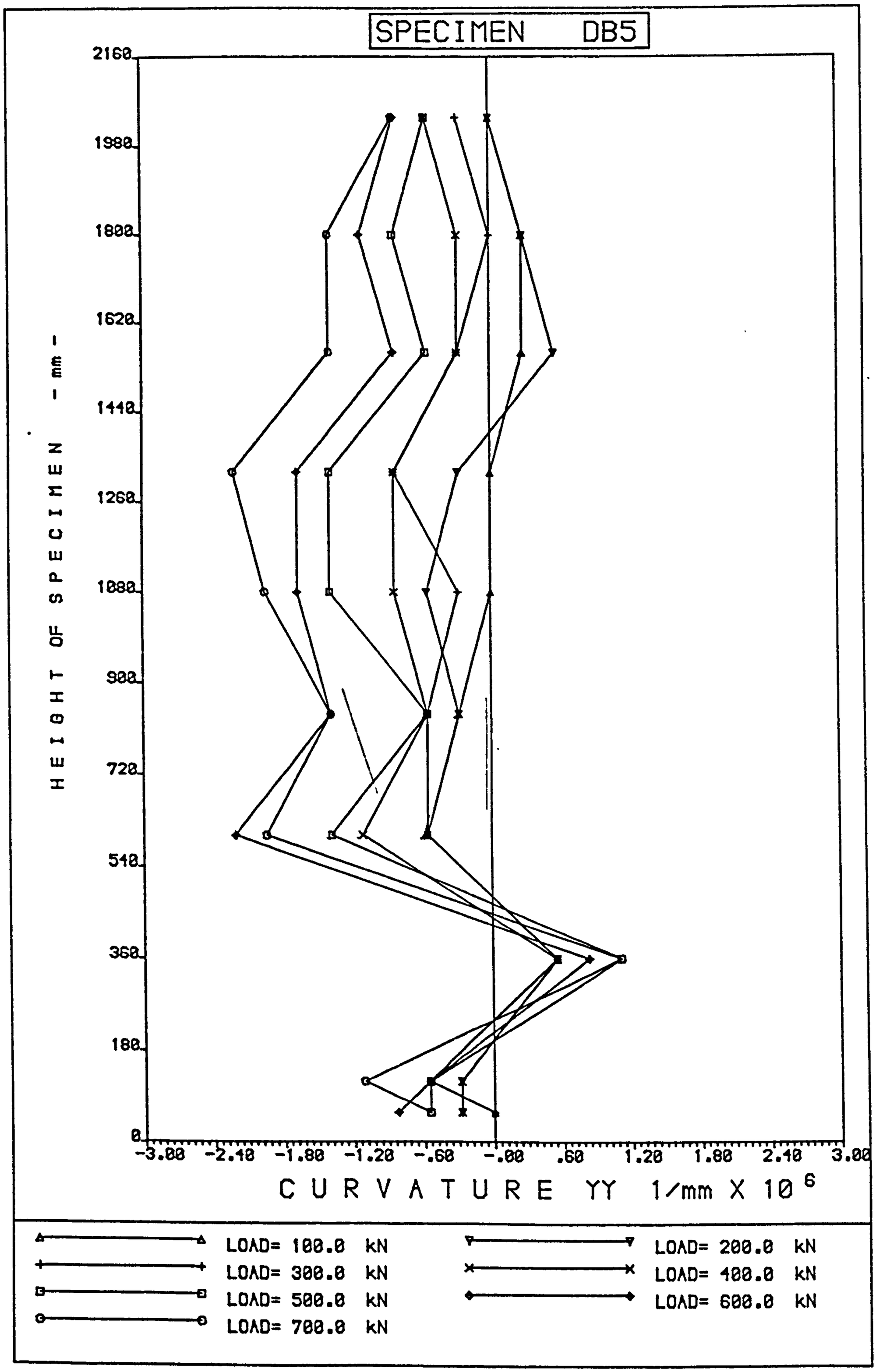

Fig. 5.52 Curvature measured experimentally at section 4 on specimen DB5

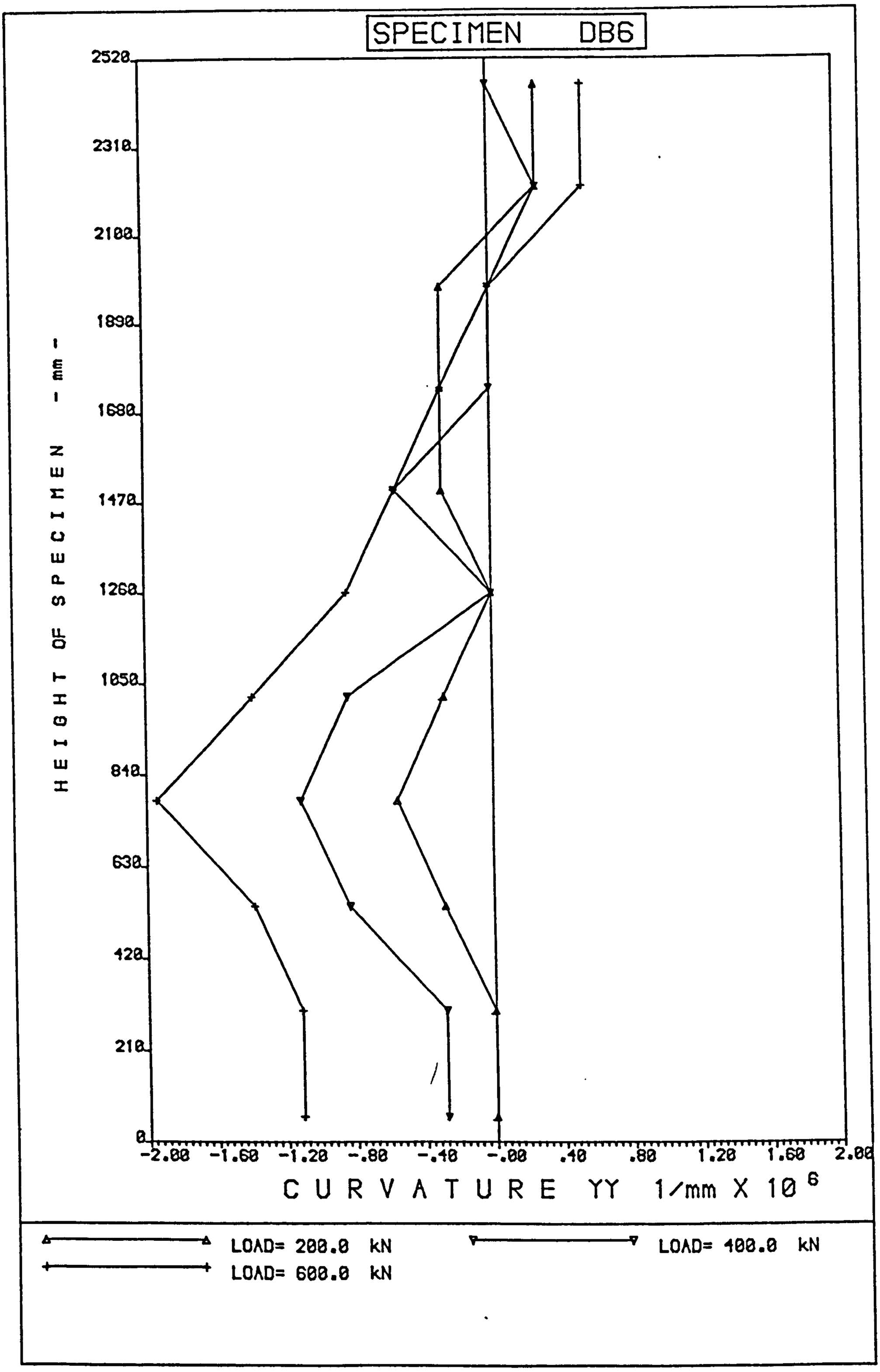

Fig. 5.53 Curvature measured experimentally at section 4 on specimen DB6

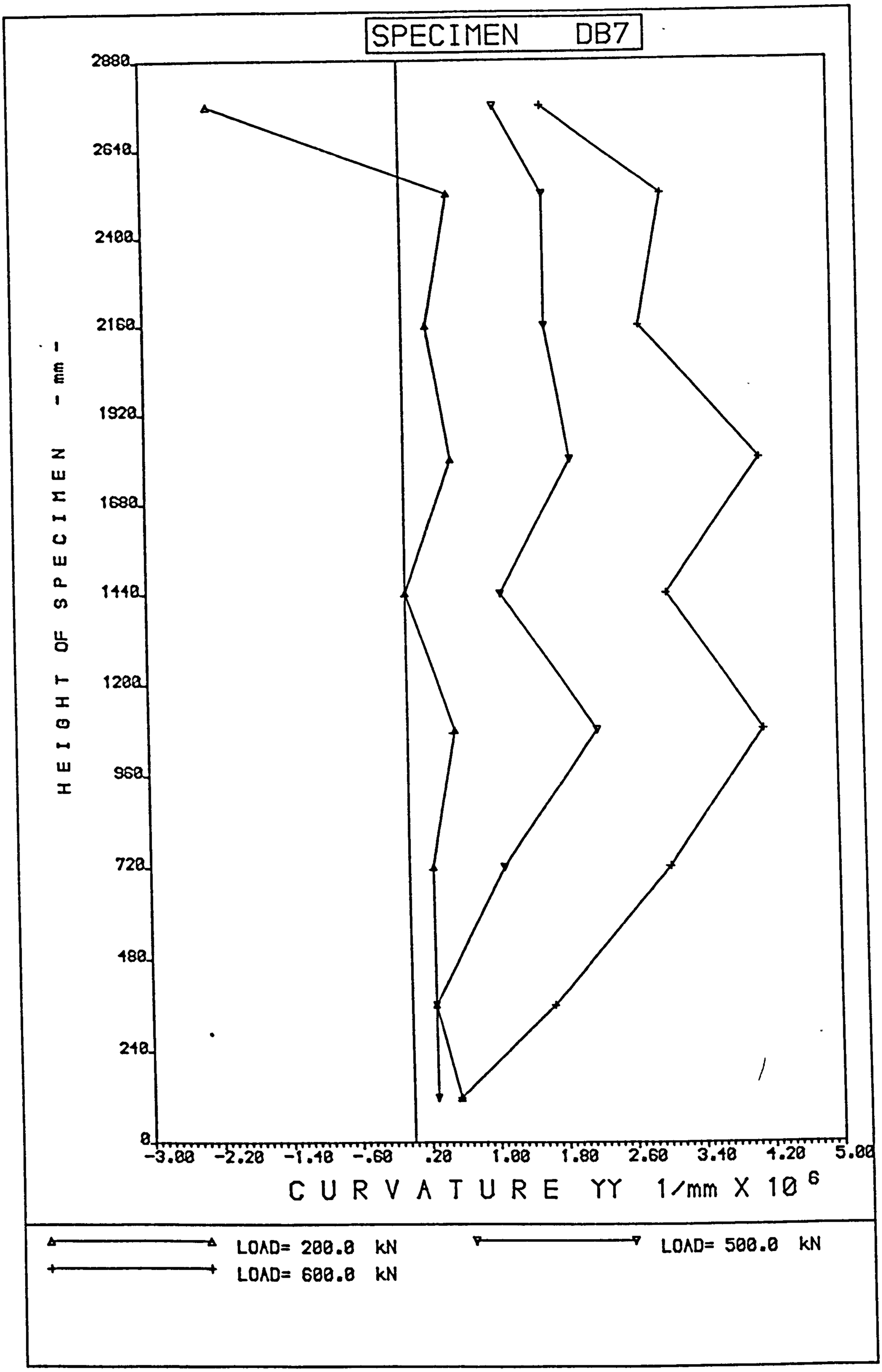

Fig. 5.54 Curvature measured experimentally at section 4 on specimen DB7

CHAPTER 6

STRENGTH OF CONCRETE IN VERTICAL STRUCTURES

6.1 INTRODUCTION

When the compressive strength of the concrete in a structure is mentioned, it normally refers to the compressive strength obtained from standard control specimens cast from the same concrete as the structure. The strength of the concrete is usually considered to be uniform throughout the member. Nevertheless, the strength of the concrete obtained from control specimens is only indicative of the quality of the material in the structure and it is well known that the compressive strength in the structure differs from that of the control specimens (Murphy, 1979). Furthermore, the quality of the concrete varies within the structural element and with the direction of loading (Neville, 1959). These differences occur due to factors such as curing conditions, variations in compaction and the type of structure, as explained by Bhargava (1969).

As it is necessary to know the actual strength of concrete in the structure, various procedures have been used for this purpose. In recent years, non-destructive test methods have been used, such as ultrasonic pulse velocity measurements (Kaplan, 1958) and rebound hammer method. Petersons (1964) presents a survey of procedures used to estimate the quality of concrete in finished structures. He points out that the most important method is drilling of core cylinders from finished structures and the testing of these cylinders. A detailed study and a comprehensive review of the current knowledge of core testing has been published by The Concrete Society (1976).

6.2 QUALITY OF CONCRETE IN VERTICAL STRUCTURES

The action of compacting the concrete in any structure causes migration of light components, such as air and water, towards the top, creating a weaker concrete on the upper levels. This phenomenon can be observed in slabs, as reported by Kemi and Hiraga (1979), but the difference in strength between the low and top levels of the member seems to be more drastic in structures with large vertical dimensions and cast in their vertical position, for example, walls and columns.

Mendoza and Casillas (1965) reported the test of 25 columns, 3.0 m high and diameters of 150 and 250 mm, cast vertically. Two concrete qualities were used, i.e. 14 and 35 N/mm^2 ultimate compressive strength. Each column was cut into 10 sections and tested for ultimate compressive strength and for tensile (splitting) strength. It was concluded that the difference in strength of the concrete within the height of the column was independent of the quality of the concrete. This conclusion might be questionable as we will see later on, when other authors findings will be noted. In those columns cast and compacted in sections of 500 mm, the ultimate compressive strength at the low level was 12 percent larger than the strength of the control specimen, and in the top it was 3 percent lower. The total difference of the compressive strength between the top and bottom levels was about 16 percent. In those columns cast and compacted in two sections only, the difference between the maximum and minimum strength rose to 21 percent. At the lower level, the concrete reached a strength 15 percent larger than the theoretical strength and in the top it was 6 percent lower. This demonstrates the effect of the casting and compacting procedures in the variation of the quality of the concrete within the depth of the structure. Unfortunately, the results from the tests related to the variation of the tensile strength of the concrete within

the depth of the column were irregular and will not be discussed.

Ramirez and Barcena (1979) extracted 100 mm cores from 250 x 250 x 2000 mm concrete columns in order to study the variation of the concrete strength within the height. The results showed an important difference in strength between the upper and lower part of the column. In columns with a theoretical concrete quality of 9 N/mm^2 the core strength at the upper level was less than 60 percent of the strength at the lower part, while in columns made out of a 13 N/mm^2 concrete quality, that ratio was less than 70 percent.

Bloem (1965) cast two columns 203 x 660 mm in cross section and 3 m high. Different curing conditions were given to each column. 43 cores, 100 mm in diameter were drilled from each column. It was found that the strength was reasonably uniform throughout the height, except the top 300 mm. The cores taken 100 mm from the top were 15 to 20 percent weaker than the rest. The strength of the cores extracted from the column cured in air was 3 to 4 percent lower than the cores drilled from the column cured under proper conditions.

Kemi and Hiraga (1979) reported an investigation of core strength of concrete walls. The investigation included light-weight concretes. It was found that for normal and light-weight concretes the difference in strength was increased in proportion to the rate of placing and slump. They explained that the strength of concrete increased proportionately to the depth of the wall as a result of segregation, sedimentation and consolidation. Light-weight concrete showed the same tendency to the strength as normal weight concrete. The strength of concrete was found to vary about 12 percent per meter depth. The standard specimen strength was found to be equal to the strength of concrete at a depth of about 400 mm from the top surface.

Bellander (1979) reports the test of 100 x 100 mm cores

extracted from 17 wall units (1.45 x 1.45 x 0.22 m) and 26 slabs (1.75 x 0.55 x 0.22 m), finding differences in strength between the top and lower sections in these units.

The strength in the top section was up to 20 percent lower than in the bottom part in the wall units and up to 17 percent in the slab units. It was also found that this difference increases with the strength level in the wall units but it was reduced for higher concrete qualities in slabs.

The splitting strength of the concrete was found to be affected in the same manner as the compressive strength and it was independent of the type and treatment of the structure. The larger compressive and splitting strength close to the bottom of the slab and wall units is explained as being caused by the relative increase in the aggregate content.

Bhargava (1969) tested cores extracted from walls 1.5 x 1.5 m in area and 120, 160 and 200 mm thick. Cores with 100 and 150 mm in diameter were used. It was found that the strength of concrete in the walls varied with height; it was lowest at the top and highest at the bottom. The strength of cores from the top was 77 percent of the strength of control specimens for concrete with a quality of 59 N/mm^2 and 96 percent for concrete with a quality of 25 N/mm^2. The strength of cores from the bottom was 102 percent of the strength of control specimens for concrete with a quality of 59 N/mm^2 and 99 percent for concrete with a quality of 25 N/mm^2. These results show that the dispersion in the strength of concrete in walls was significantly higher for concretes of higher quality.

6.3 EXPERIMENTAL ANALYSIS AND RESULTS

Although the experimental evidence on the strength of concrete in

vertical structures agrees with the fact that the concrete strength varies within the depth of the element, a definite conclusion in this aspect is not available yet. The uncertainty lies with the combination of various aspects which are reported as affecting the distribution of strength. In the experimental investigations briefly discussed above, several factors, e.g. the theoretical quality of concrete, curing conditions, workability, compaction, and rate of placing have been mentioned as being responsible, in one degree or another for the dispersion in the strength of the concrete.

Because of the special characteristics of the mixes used for casting the walls and due to the difficulties experienced during casting, it was felt that it was necessary to verify the actual strength of the concrete. Wall W4-L2 was selected for that purpose, since it did not have reinforcement in the upper section, giving the opportunity of extracting cores without the presence of steel bars.

The cores were drilled perpendicular to the plane of the wall, giving a maximum length equal to the thickness of the wall, i.e. 72 mm. The length dictated the size of the core, since BS 1881:Part 4:1970, Clause 3.1.1 demands that the length before capping shall be at least 95 percent of the diameter. This created difficulties, since British Standard 1881 states also that cores shall have a diameter of either 100 or 150 mm. The length, being limited to 72 mm, before capping, did not allow drilling cores of these recommended dimensions.

It was decided to extract cores 75 mm in diameter and another group of cores with a smaller cross section in order to help to assess the difference in strength due to the use of a smaller bit than that recommended by BS 1881.

Nine cores, 74 mm in diameter, were extracted from three different levels (1, 2 and 3) following three vertical bands (A, B and C) as shown

in Fig. 6.1. Nine additional cores (43 mm in diameter) were extracted from the same levels and within the same bands as shown in Fig. 6.1. The ratio of diameter to maximum aggregate size was 4.3 for these cores.

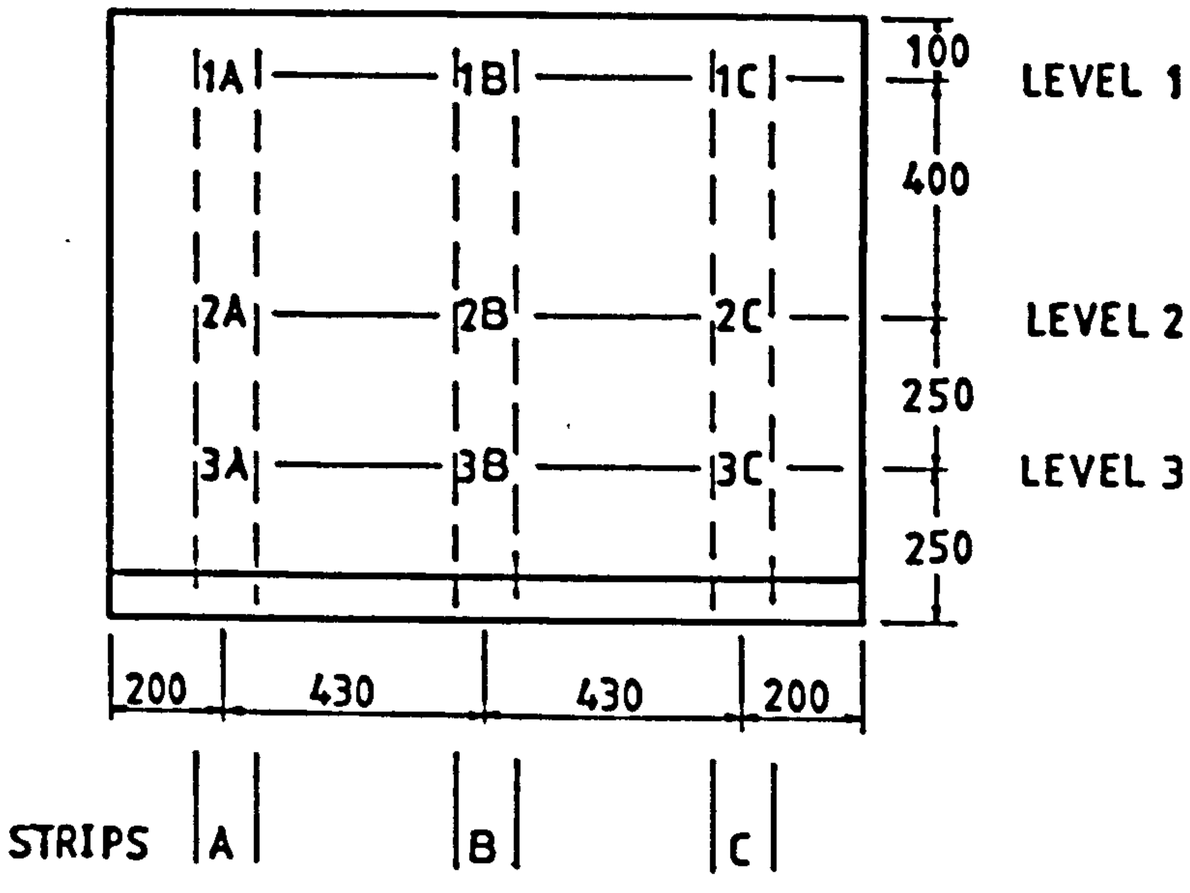

Fig. 6.1 Position of cores within specimen W4-L2

A Clipper machine, made by NORTON in Luxemburg was used for drilling the cores. It uses a Black and Decker drill, with a speed of 350 rpm. The bits used were diamond impregnated. Each core was identified by a simple code, using two characters. The first character refers to the level from which it was drilled (1, 2 or 3) and the second character identifies the vertical band (A, B or C).

The cores were capped with high-aluminia cement mortar in accordance with Clause 5.5.2 of BS 1881:Part 3 and kept under water for at least 48 hours before being measured and tested for ultimate compressive strength.

Tables 6.1 and 6.2 present the dimensions and details of results of the test for cores with 74 and 43 mm in diameter respectively.

Table 6.1 Dimensions and strength details of cores obtained from specimen W4-L2. Core diameter = 74 mm

	LEVEL 1			LEVEL 2			LEVEL 3		
Core	1A	1B	1C	2A	2B	2C	3A	3B	3C
Diameter	74	74	74	74	74	74	74	74	74
Length	81	81	81	81	81	81	81	83	81
λ = length/ diam.	1.09	1.09	1.09	1.09	1.09	1.09	1.09	1.12	1.09
Failure load (kN)	205	181	186	145	130	146	126	119	134
Core strength (N/mm^2)	47.7	42.1	43.2	33.7	30.2	33.9	29.3	27.7	31.2
Estimated actual strength N/mm^2	49.3	43.5	44.7	34.8	31.2	35.1	30.3	28.9	32.3
Average actual strength N/mm^2	45.8			33.7			30.5		

Table 6.2 Dimensions and strength details of cores obtained from specimen W4-L2. Core diameter = 43 mm

	LEVEL 1			LEVEL 2			LEVEL 3		
Core	1A	1B	1C	2A	2B	2C	3A	3B	3C
Diameter	43	43	43	43	43	43	43	43	43
Length	66	66	65	65	65	66	66	65	66
λ = length/ diam.	1.53	1.53	1.51	1.51	1.51	1.53	1.53	1.51	1.53
Failure load (kN)	38.3	33.2	37.0	32.2	31.4	36.2	29.0	26.4	32.2
Core strength (N/mm^2)	26.4	22.9	25.5	22.2	21.6	24.9	20.0	18.2	22.2
Estimated actual strength N/mm^2	30.6	26.6	29.6	25.8	25.1	28.9	23.2	21.1	25.8
Average actual strength N/mm^2	28.9			26.6			23.4		

The estimated actual strength of each core, corrected for the ratio λ (length/diameter) as recommended by The Concrete Society (1976), is given graphically in Figs. 6.2 and 6.3 for cores with 74 and 43 mm in diameters respectively. It is obvious that the strength of the concrete varied considerably with the depth of the wall, providing the lowest value at the bottom. The points at the three levels have been joined by straight lines, just to show the trend in variation. The average strength at each level is also provided.

Tables 6.3 and 6.4 give the estimated actual strength of the cores, 74 and 43 mm diameters respectively, expressed as a percentage of the strength of the cubes used as control specimens. The average of the percentage of the strength at each level is also given.

Table 6.3 Actual strength of concrete in wall W4-L2 expressed as a percentage of the cube strength obtained from control specimens. Core diameter = 74 mm

	Level 1			Level 2			Level 3		
Core	1A	1B	1C	2A	2B	2C	3A	3B	3C
Percentage	100	88	91	71	63	71	61	59	66
Average	93			68			62		

Table 6.4 Actual strength of concrete expressed as a percentage of the cube strength of control specimens. Core diameter = 43 mm

	Level 1			Level 2			Level 3		
Core	1A	1B	1C	2A	2B	2C	3A	3B	3C
Percentage	60	52	58	51	49	57	45	41	51
Average	57			52			46		

6.4 DISCUSSION OF RESULTS AND CONCLUSIONS

6.4.1. Strength of Concrete Within the Depth of the Wall

In general, the results of this test agree well with the findings of those investigations mentioned previously. Although these results show larger strength at the top of the specimen than at the bottom, while the literature surveyed shows the opposite, it does not imply any disagreement between both findings. It must be remembered that these walls were cast upside-down, as explained in Section 3.4.1.

It has been demonstrated in Figs. 6.2 and 6.3 that the maximum strength of concrete occurs at the top of the specimen. By extrapolating the values shown in Fig. 6.2, it can be predicted that at the top, the strength of the concrete would be equal to or perhaps larger than the characteristic strength obtained from the control specimens.

The average strength of concrete at the middle of the specimen was at least 68 percent of the characteristic value. At a depth of 750 mm the strength was at least 62 percent of the characteristic value and by extrapolation, it can be predicted to be less than 60 percent at the bottom.

The rate of change of strength of concrete with the depth was larger in the upper half of the specimen, while the lower half shows a tendency to a more moderate variation.

6.4.2 Effect of Core size in Measured Strength of Concrete

A large discrepancy exists between the strength shown in Fig. 6.2 and those of Fig. 6.3. The average strength of concrete obtained with cores 43 mm in diameter was 61 percent of the strength measured with 74 mm cores at level 1, 76 percent at level 2 and 74 percent at level 3. The largest disagreement between both results was observed at the upper

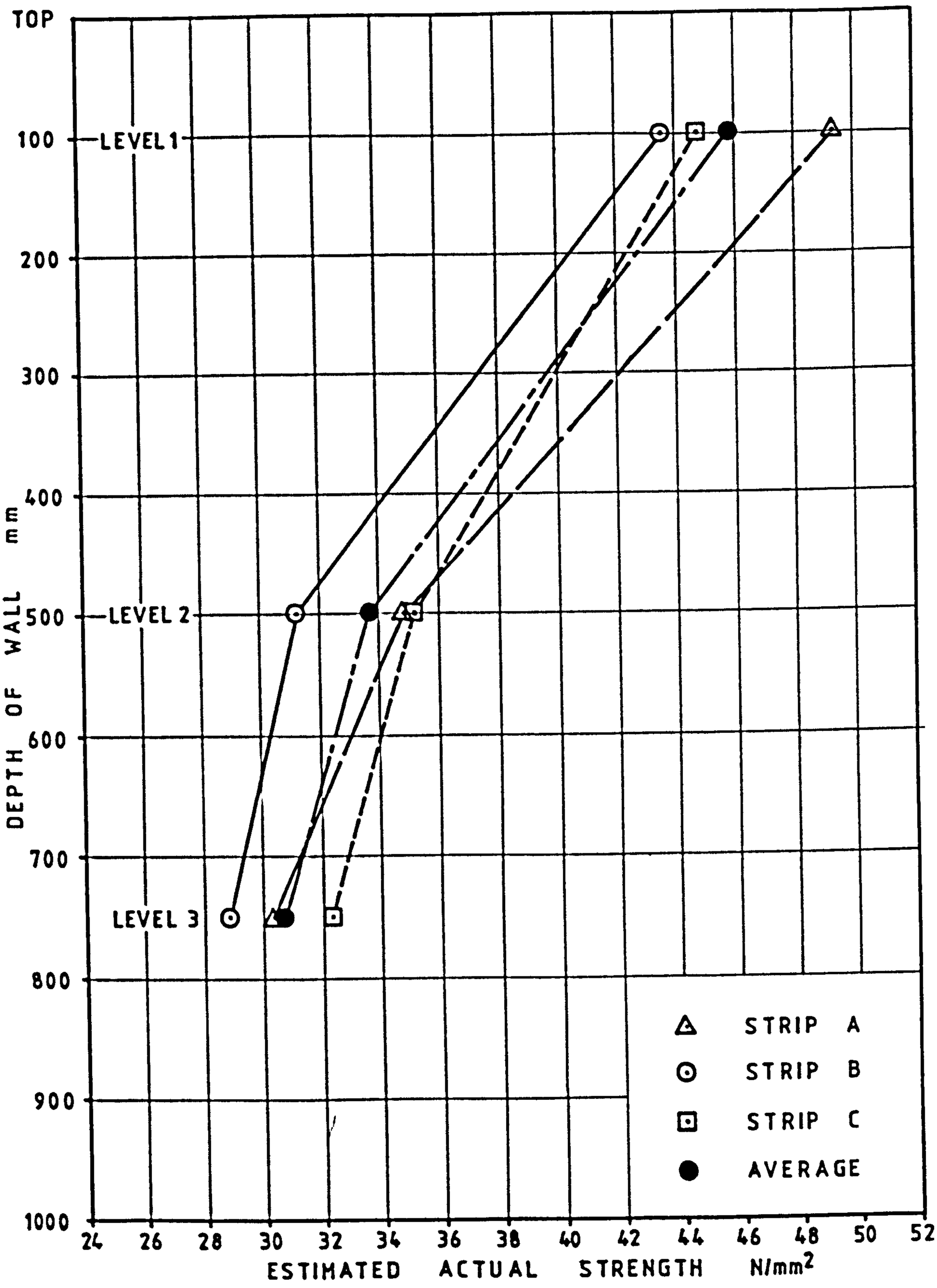

Fig. 6.2 Estimated actual strength of cores 74 mmØ and average value at three levels

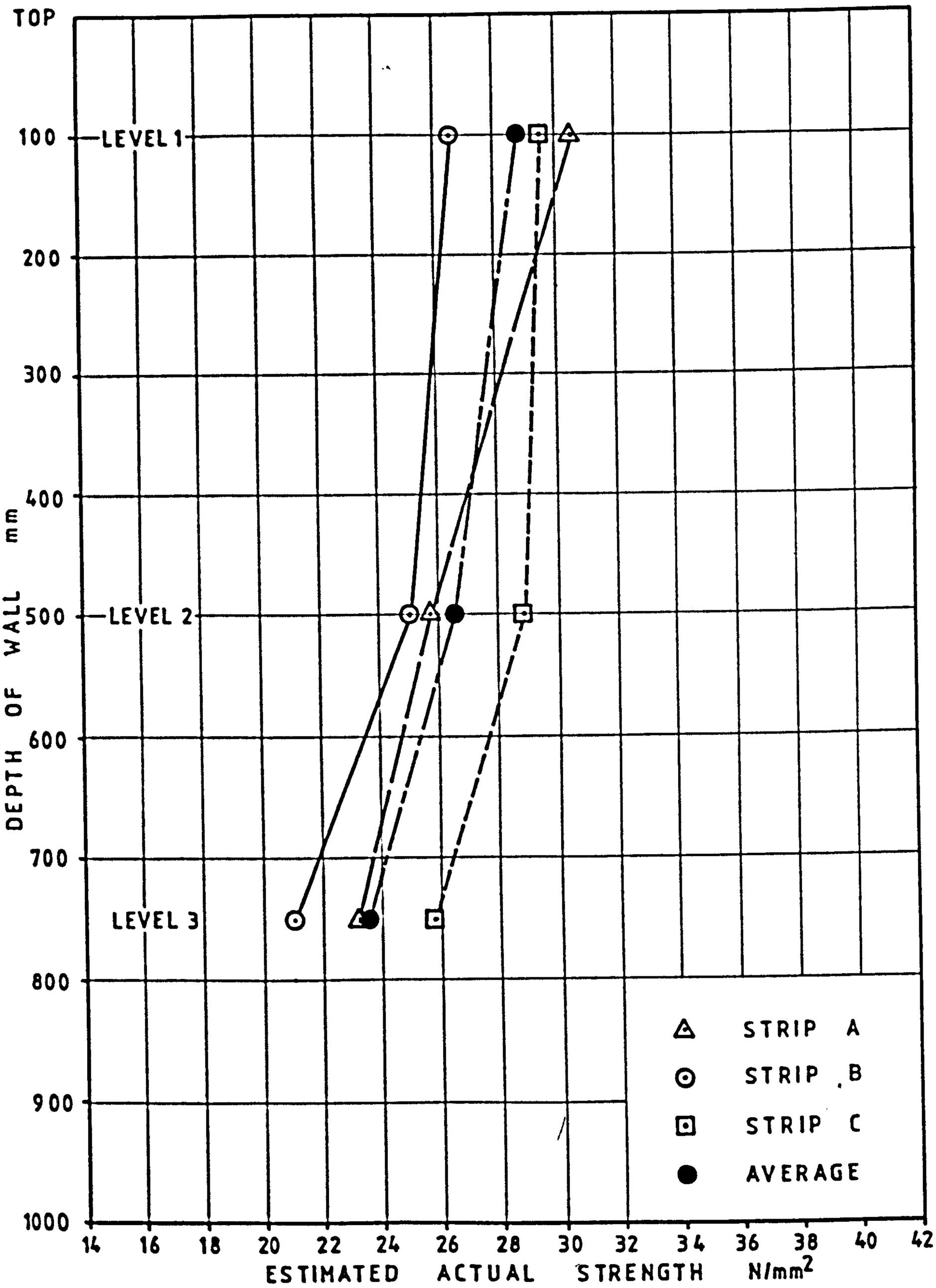

Fig. 6.3 Estimated actual strength of cores 43 mmØ and average value at three levels

level, where the concrete had the largest strength (Fig. 6.4).

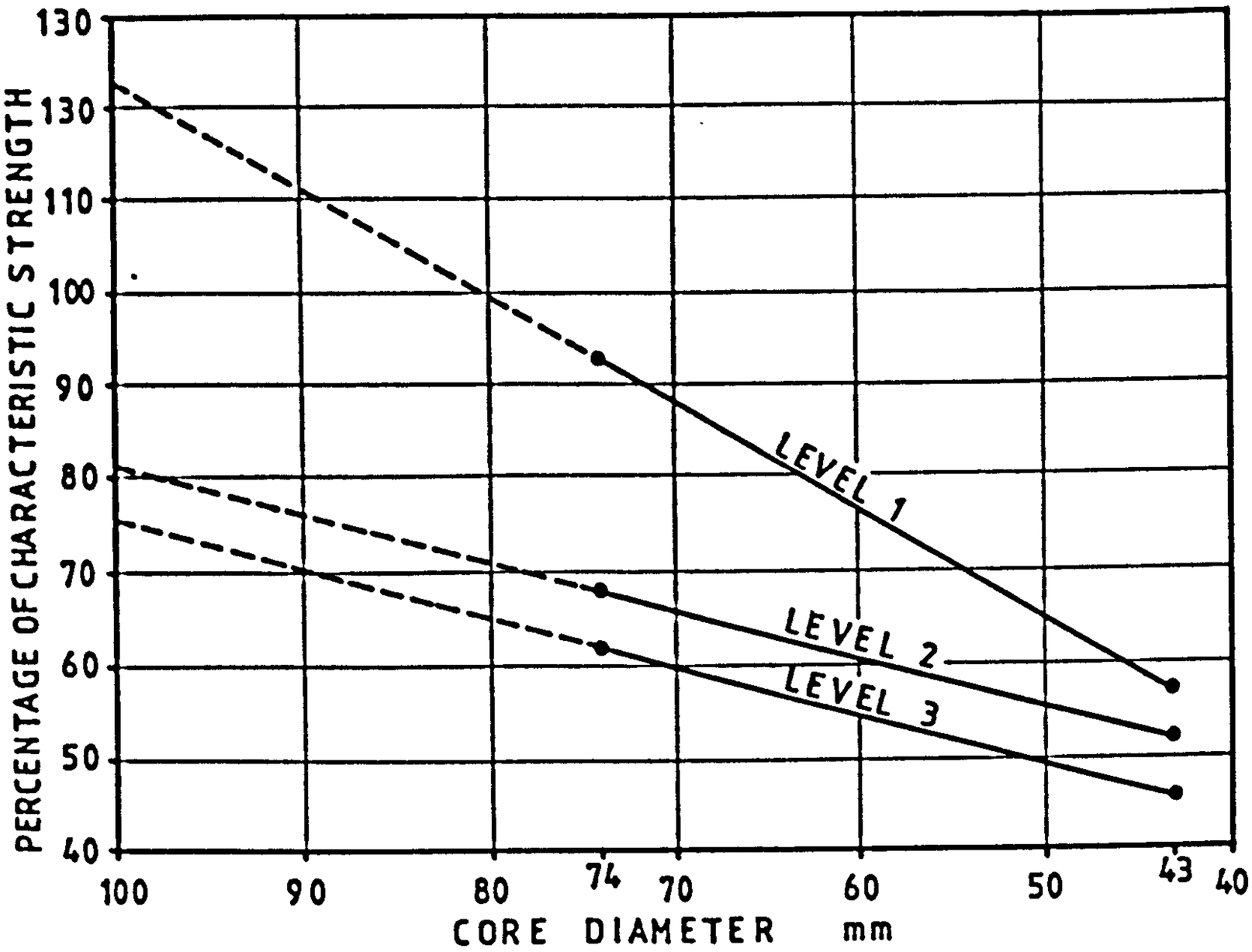

Fig. 6.4 Effect of core diameter on the strength of cores at three different levels on wall W4-L2

These results agree well with those given by Ramirez and Barcena (1979) who compared the strength of concrete from cores of three different diameters (50, 100 and 150 mm) to conclude that the smaller the core is, the less the expected strength due to damage of the concrete during drilling (Fig. 6.5). They considered that the actual strength of the concrete is given by cores with a diameter of 150 mm. It was found that the strength of cores with a diameter of 100 mm was up to 4.2 percent lower than the actual strength of the concrete. It varied depending on the concrete quality, from 0.5 percent for concrete of theoretical quality of 9 N/mm^2 to 4.2 percent for concrete of theoretical quality of 20 N/mm^2. The loss of strength was larger for cylinders of 50 mm. Their loss was 14.6 percent for concrete of theoretical quality of 9 N/mm^2 and 20.6 percent for concrete of 20 N/mm^2.

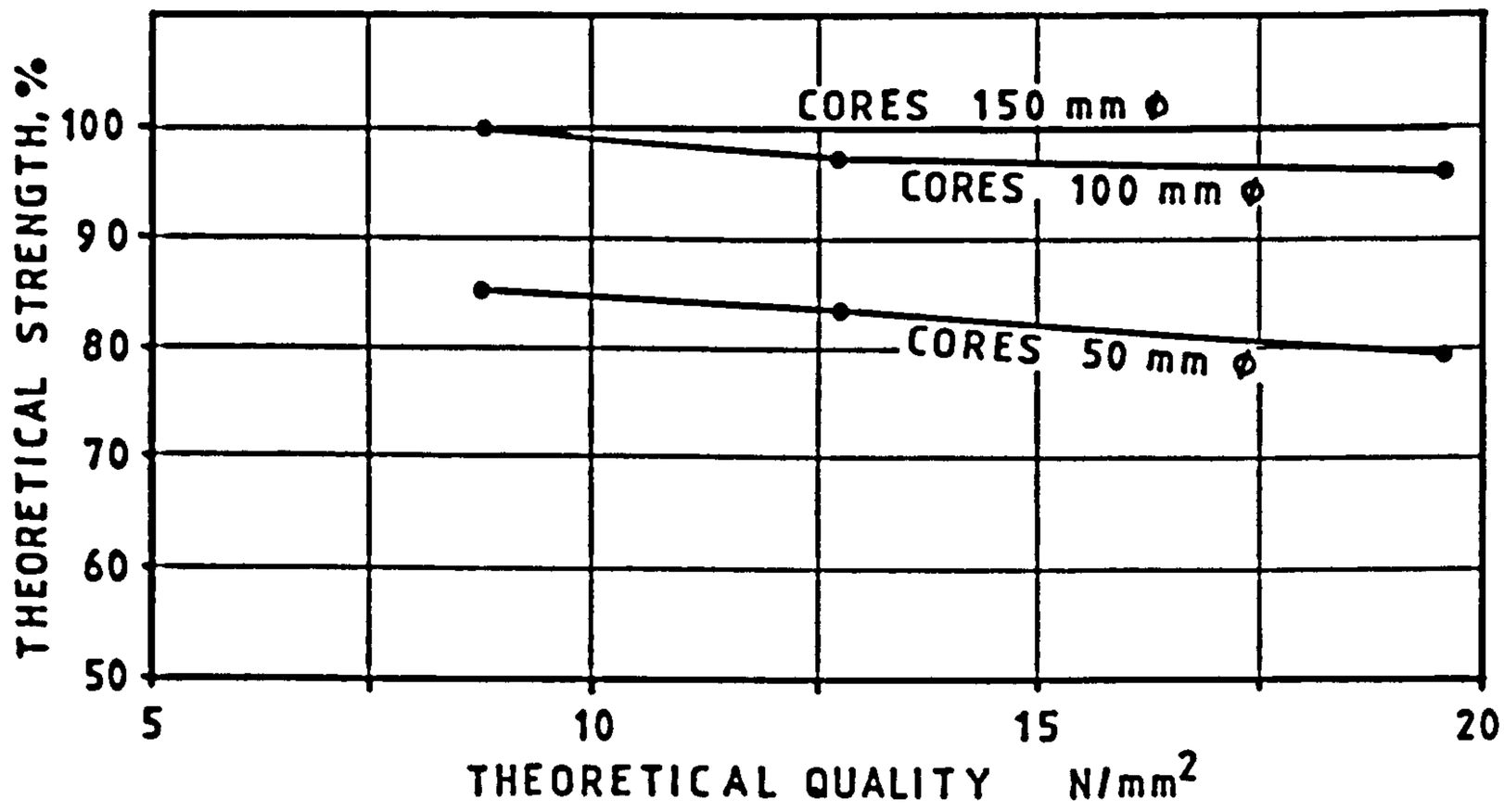

Fig. 6.5 Effect of the quality of concrete on the strength of cores. Ramirez and Barcena (1979)

Kemi and Hiraga (1979) found that in normal concrete, cores of 50 mm diameter gave approximately 90 percent of the strength given by cores 150 mm diameter. For light-weight concrete that ratio was 80 percent.

Campbell and Tobin (1967) carried out tests on nearly 500 cylinders and core samples of normal and light-weight concrete. Cores 100 and 150 mm diameter were tested after being cured under different conditions. The length-to-diameter ratio was kept constant ($h'/d' = 2.0$) in all the specimens. The maximum strength was provided by the control cylinders cured under the laboratory conditions. At 28 days, the 150 mm cores showed an average strength of 86.8 percent of the strength given by the control cylinders, while the 100 mm cores gave 65.4 percent, showing a tendency of the concrete strength to decrease as the core diameter becomes smaller. The average strength of the 100 mm cores was 75 percent of the average strength of the 150 mm cores.

Bungey (1979) examined the results of an investigation in which cores 44 mm in diameter were tested. Two aggregate sizes were investigated. For 10 mm gravel aggregate a factor of 1.14 was determined to convert the core strength (ratio h'/d' = 2.0) into cube strength (100 mm) for cores drilled horizontally. For 20 mm gravel aggregate that factor was found to be 1.22.

Although the results of the investigations mentioned above follow the trend of our findings, not all the literature available coincides in this matter. The following gives examples of this.

Lewis (1980) noted that the strength of cores was always less than the strength of standard cylinders and the smaller the core diameter, the lower the compressive strength. He used a factor of 1.07 and 1.11 to multiply the strength of cores 100 and 75 mm diameters, respectively, in order to estimate the strength of 150 mm dimeter cores. Lewis explains that the differences in strength from cores of various sizes were related to a strength gradient through the test slab and not due to the effect of the diameter. Where no gradient of strength existed, he observed that the strengths of the cores of different diameters did not vary significantly.

Meininger (1968) studied the aspect of core strength of cores having 50, 100 and 150 mm diameter. The cores were extracted from a wall and a slab 406 mm thick. All the cores had a length to diameter (h'/d') ratio of 2. The maximum aggregate size used was 19 mm. It was found that there is not a consistent relationship between the core size and the measured strength. For the slab, the three core sizes measured the same strength and for the wall the 50 mm cores averaged up to 8 percent higher strength than the 100 and 150 mm cores. Fig. 6.6 shows these results.

Bowman (1980) reports the test of 25 cores 50 mm diameter and 24 cores 150 mm diameter extracted from an actual structure, in order to

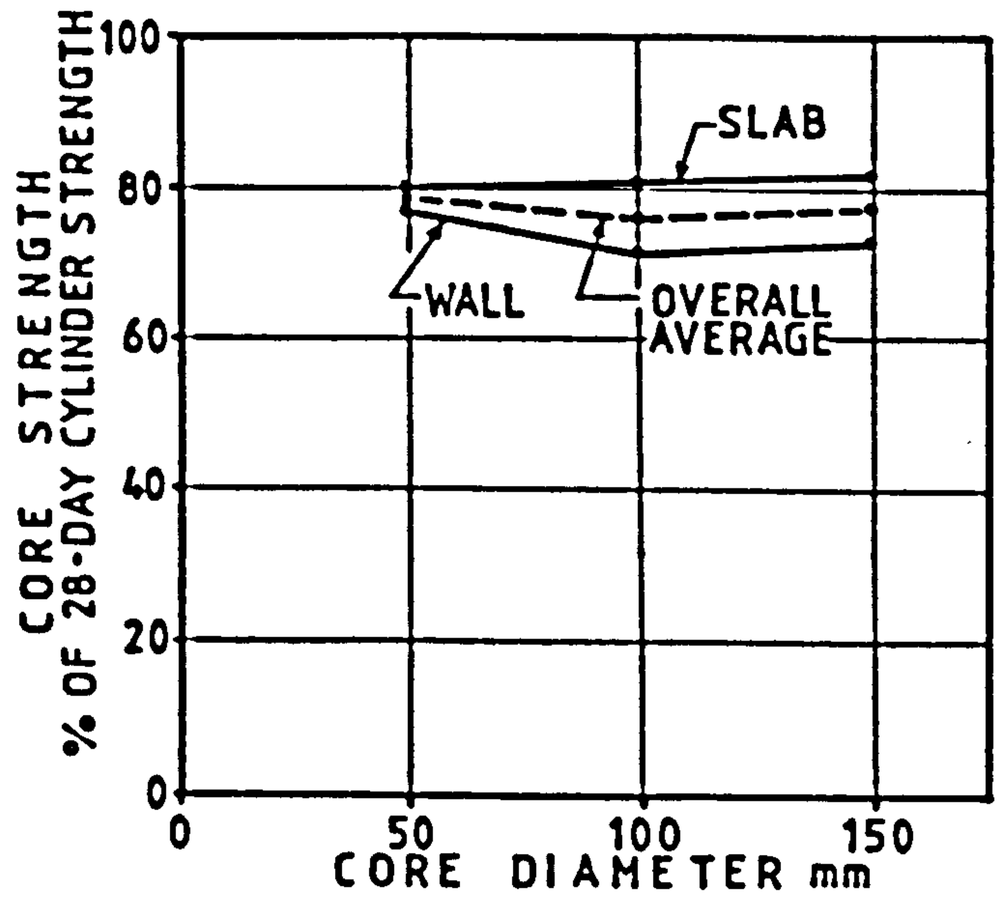

Fig. 6.6 Effect of core diameter on strength. From Meininger (1968)

compare the variability of results from small and large diameter cores. The 50 mm cores gave a mean strength of 44.7 N/mm^2 and a coefficient of variation of 28.9 percent. The 150 mm cores gave a mean strength of 41.4 N/mm^2 and a coeficient of variation equal to 19.5 percent. These findings show larger strength measured by the smaller cores and greater variability of results.

Mather and Tynes (1961) conducted an experiment to determine the relation between the 28-day compressive strength of 150 x 300 mm cylinders and that of 150, 200 and 250 mm diameter cores drilled from test structures. The results suggest that there is no significant difference between the strength of concrete of 150 x 300 mm moulded cylinders and of cores of the dimensions tested. But, for the smaller cores, a larger number of tests were required to obtain results of a given precision.

The above summarizes the results of some experiments which somehow disagree with our findings and of other authors previously mentioned. It was felt that some comments on these remarks were necessary and they follow.

Lewis's results do not contradict the trend of our experimental figures, although the explanation that he gives for the reduction of strength in smaller cores, does not have any positive ground in our

experiment. Our 43 mm cores were extracted by drilling the wall throughout its thickness (as for the 74 mm cores) and then the length of the cores was reduced by cutting about 5 mm off from both ends. there is no evidence to substantiate such a large gradient of strength across a wall 72 mm thick and cast vertically.

In the case of Meininger's results, the inconsistency reported between the measured strength and the core sizes is observed in the cores extracted from a wall. No effect on the core strength was revealed due to their vertical position in the wall, and perhaps, this factor has some connection with these results. Meininger's figures for the slab show a slight increase in strength for the larger cores, Fig. 6.6, which agrees well with the trend of our results.

The figures shown by Bowman are very interesting, but unfortunately no details about the structure, the concrete used, and the relative position of the cores within the structure were provided, leaving many questions unanswered.

The work of Mather and Tynes was conducted on large cores, in which the effect of damage during drilling could be insignificant, as their results have shown. It was not suggested that the same would apply for cores with diameters under 150 mm.

From the evidence obtained in the literature available and from our experimental results, it is concluded that the strength of cores is affected by their diameter. The measured strength is proportional to the core diameter. The effect of this on the strength is larger for smaller cores and this effect is increased for concretes of higher quality.

One of the aims of this analysis was to determine the actual strength of the concrete at different levels of the wall. It is with regret that we have to conclude that it was not achieved. The best

measurements obtained are the figures given by cores 74 mm in diameter. The actual strength would be larger (Fig. 6.4) and measured more accurately by 100 and 150 mm cores. These were not attainable and it is not possible to define the strength of 100 mm cores from smaller ones, since a statistical relationship for this purpose is not available yet. Therefore, the under-estimated figures provided by 74 mm cores will be used for assessing the compressive strength of concrete within the walls.

6.4.3 Strength of Concrete Within the Length of the Wall

The strengths of the cores extracted from the middle strip (B) of the wall were on average 91 percent of the strength of the cores extracted from the side strips (A and C) for 74 mm cores (Fig. 6.2). For cores 43 mm in diameter (Fig. 6.3) that ratio was 88 percent.

These results are similar to those obtained by Meininger (1968) who reported that cores extracted from the middle third of a wall were on average about 91 percent of cores extracted from the left and right thirds.

The same tendency in the strength of concrete within the length of the wall was observed by Bhargava (1979) although the ratio reported in that paper was about 70 percent.

6.5 CONCLUSIONS

For the wall tested, the following conclusions may be drawn.

a) The safe and under-estimated figures provided by 74 mm cores are adopted for assessing the compressive strength of concrete within the wall.

b) The maximum strength of concrete occurs at the top of the specimen, where the quality of concrete would be equal to that

obtained from the control specimens. At the bottom, the quality of concrete is less than 60 percent of the theoretical quality.

c) The rate of change of strength of concrete with the depth was larger in the upper half of the specimen, while the lower half shows a tendency to a more moderate variation.

d) The strength of cores is affected by their diameter. The effect of this on the strength is larger for smaller cores and this effect is increased for concretes of higher quality.

e) The strengths of the cores extracted from the middle vertical strip of the wall were on average 91 percent of the strength of the cores extracted from the side strips.

CHAPTER 7

STUDY OF THE BEHAVIOUR OF DEEP FLEXURAL ELEMENTS UNDER COMBINED TOP AND BOTTOM LOADS

7.1 INTRODUCTION

Substantial numerical and experimental analyses have been dedicated to reinforced concrete, from which extensive knowledge on the behaviour of structural members under static and dynamic loads has arisen. This knowledge mainly covers members under pure flexure, pure compression or under the combined action of flexure and axial compression. However, some members such as deep beams do not conform to the general flexure theory and they require special attention. The depth of these elements permits an additional action to take place, i.e., vertical direct tension from forces applied to the lower levels.

Information available on deep flexural members subjected to the combined action of flexure, shear and vertical direct tension is very limited. Previous research has mainly been directed towards the evaluation of shear strength and the contribution of web reinforcement to shear in specimens directly loaded on top and directly supported. However, no such informaton is obtainable with regard to the behaviour of these elements under other types of loads and supports. This point is stressed by the CIRIA Guide 2 (1977).

This chapter presents a brief summary of the understanding to date on the behaviour of deep flexural members under combinations of top and bottom loads. Experimental results concerning this aspect were presented in Chapter 4 and here are discussed and analysed further.

7.2 EFFECT OF SHORT SPANS ON SHEAR STRENGTH

The test programme performed by Kani (1966) using rectangular beams with two top point loads and directly supported at the bottom demonstrated a relatively drastic change in the ultimate shear stress when the shear span to depth ratio (x_s/d) fell below about 2.5. Similar findings were revealed in earlier work published by Leonhardt and Walther (1962) in which a series of rectangular beams with variable span and shear span were tested. This test included a set of beams loaded under two points and a uniformly distributed load. Based on the Stuttgart tests, Leonhardt (1965) shows that the shear strength of beams without shear reinforcement increases rapidly for concentrated loads when the shear span to depth ratio (x_s/d) falls below 3 and for distributed loads when the span to depth ratio falls below 12. He explains that this results from the arching action in the concrete.

A combination of dimensional and statistical regression analyses was used by Zsutty (1968) to provide a basis for the division of test beam behaviour into the arch action of deep beams and the usual beam action of slender beams. It was found from the analysis of all the data that the minimum coefficient of variation of error for the shear strength of simple rectangular beams was obtained when a separation value of 2.5 for the shear span to depth ratio was used. The beam action was attained for $x_s/d > 2.5$ and arch action for $x_s/d < 2.5$.

Effects of the x_s/d ratio on the shear capacity of reinforced concrete beams are well established. Ferguson (1956) suggested that the additional shear capacity provided by a small shear span was due to the compressive forces developed over the supports and under the load.

Whereas the shear strength of deep flexural members under direct top load has been extensively investigated, the behaviour of indirectly loaded or bottom loaded deep beams has not yet been clearly defined.

In order to inquire into the effect of indirect loading and indirect support on the shear capacity of reinforced concrete deep beams, Ferguson (1956) tested 6 beams (Fig. 7.1) without shear reinforcement and $x_s/d = 1.35$. One of the specimens, F4, was a normal rectangular beam, 100 mm wide, 250 mm deep and tested under symmetrical point loads over a simple span of 990 mm. Beams S1, S2, S3 and S4 had identical dimensions, but these were built with lateral cross members, for applying indirect loads and indirect reactions. Beam F6 was provided with lateral cross members which allowed the application of load within the lower half. Results from Ferguson's tests are shown in Fig. 7.1. The conclusion drawn from these tests was that when loads or reactions are introduced as shears, the extra strength associated with short shear spans is lost.

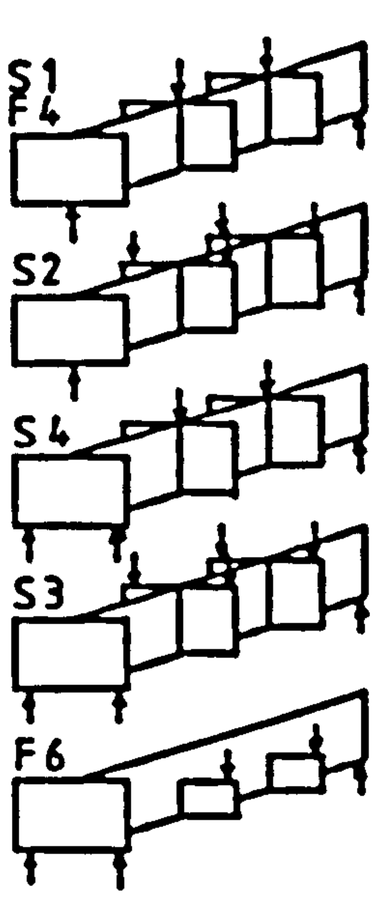

Fig. 7.1 Effect of loading conditions on shear capacity. $x_s/d = 1.35$ (Ferguson, 1956).

Taylor (1960) tested a series of rectangular reinforced concrete beams without shear reinforcement. One purpose of this test was to examine the effect of the support condition and load position on the beam's shear capacity. As with Ferguson's beams, Taylor's specimens were built with lateral cross members for indirect supports and

loading. The shear span varied from 457 to 1372 mm, corresponding to x_s/d ratios of 1.5 to 4.5. For each shear span, two beams were tested: one under direct loading and support and the second under indirect loading and support. Two beams from the series had short shear spans with x_s/d corresponding to 1.5 and 2.5. Results from these tests show that for all the x_s/d ratios tested, the manner of loading and supporting has very little effect on the load at which diagonal cracking occurs, but had an enormous effect on the beam's capacity to sustain load beyond the diagonal cracking load in beams with x_s/d below 2.5. Beams loaded and supported by means of the transverse members were capable of withstanding only the diagonal cracking load. Ferguson's and Taylor's results are concordant in that the large capacity of short shear spans to sustain load is reported to be due to the combination of top load and bottom pressure of support blocks.

Zsutty (1971) presented equations to predict the ultimate shear strength of rectangular beams with $x_s/d < 2.5$ under concentrated loads. In an earlier report, Zsutty (1968) gave the following empirical equation for predicting ultimate shear strength of slender beams, without shear reinforcement and under concentrated load:

$$v_{u1} = V_u/bd = 60\cdot(f'_c pd/x_s)^{1/3} \qquad 7.1$$

where f'_c = concrete cylinder strength, psi

p = steel ratio = As/bd

d = beam effective depth to steel, in

a = shear span, in

By multiplying Eq. 7.1 by the factor $2.5/(x_s/d)$, it becomes

$$v_{u2} = v_{u1}2.5/(x_s/d) \qquad 7.2$$

which includes the limit of the beam action from the arch mechanism and the shear span to depth ratio (x_s/d). Zsutty claims excellent

agreement between this last mathematical prediction (Eq. 7.2) and the empirical ultimate shear strength of rectangular beams without shear reinforcement and with $x_s/d < 2.5$.

For short beams ($x_s/d < 2.5$) without shear reinforcement, loaded and supported indirectly, Zsutty (1971) suggests that Eq. 7.1 predicts the ultimate shear strength. In other words, the shear strength of these beams was equal to the strength of the slender beams loaded and supported in the usual manner. Based on very limited experimental information, he recommends, for beams with $x_s/d < 2.5$, reinforced with vertical stirrups for shear and with indirect load and indirect supports, the following equation for ultimate shear strength:

$$v_u = v_{ul} + rf_{yw} \qquad 7.3$$

where v_{ul} = as Eq. 7.1

r = stirrup ratio = A_v/bs

s = stirrup spacing, in

b = beam width, in

f_{yw} = stirrup yield stress, psi.

When the specimens are under direct load and direct supports, Eq. 7.3 becomes:

$$v_u = v_{u2} + rf_{yw} \qquad 7.4$$

where v_{u2} = as Eq. 7.2.

An interesting point in Eq. 7.4 is the consideration of vertical reinforcement for shear in beams with $x_s/d < 2.5$ and directly loaded on top. The contribution of vertical shear reinforcement in these equations could create disagreement with the findings of other authors. It has been established that as the ratio x_s/d decreases, the vertical web reinforcement becomes less effective. The extent of the influence of this reinforcement in Eq. 7.4 is questionable in view of other authors' results.

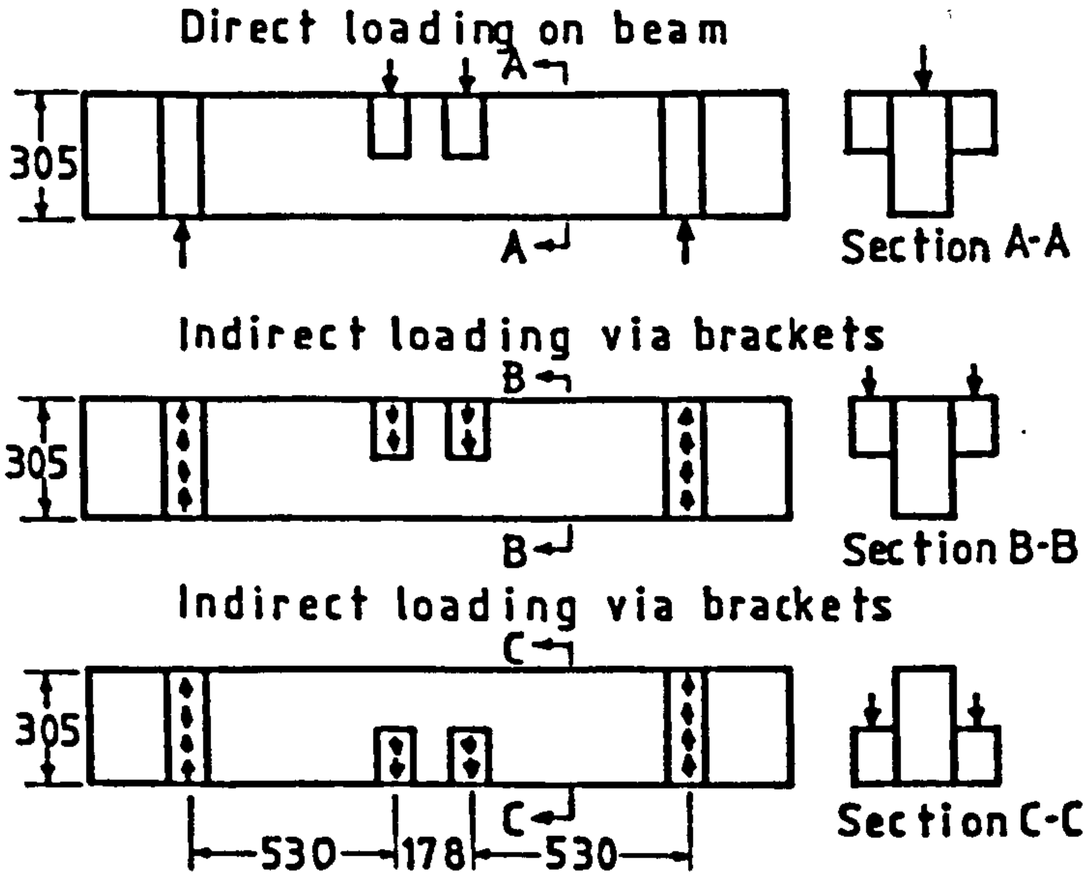

Fig. 7.2 Loading and specimen details (Fereig and Smith, 1977)

Fereig and Smith (1977) studied the effect of indirect loading and support conditions on the behaviour and ultimate shear strength of beams with short shear spans. Figure 7.2 shows the specimens and loading details used in these tests. It was claimed that the short span beams loaded indirectly did not show the same gain in strength as those directly loaded with x_s/d ratios less than 2.5. An increase in shear strength was observed at x_s/d ratios of about 1.5. The presence of vertical web reinforcement significantly improved the strength of those short span beams loaded indirectly but it did not affect the behaviour of those loaded directly on top. This contradicts the fundamentals upon which Eq. 7.4 is founded.

In addition to these experimental analyses which separate the beam action from the arch mechanism of short beams and from the effect of indirect loads, wall-beams have been tested under top and bottom loads. The work done by Graf et al (1943), Schütt (1956) and Leonhardt and Walther (1966) in this field has been presented and discussed in Section 2.3.2.

The main conclusions from the experimental reports analysed above are: 1) the shear strength of short span beams is larger than the

strength of slender beams, 2) this gain in shear strength is valid only for those specimens loaded directly on top and supported directly at the bottom, 3) the additional shear strength is created by the development of the so called "arch action", which generates compressive forces between the loaded points and the supports and 4) the arch action is observed in elements with shear span to depth ratios less than 2.5.

7.3 PREDICTION OF SHEAR STRENGTH FOR SHORT SPAN BEAMS

Section 2.4 of this thesis contains a summary of noteworthy documents providing guidance for the design of deep flexural members. In this section, a detailed analysis of the procedures recommended by the ACI Standard 318-77 and the CIRIA Guide 2 (1977) for estimating the shear capacity of such members is undertaken and compared with results from this experimental programme. These two documents have been selected, since they appear to present the most up-to-date and comprehensive rules for the analysis of deep beams.

7.3.1 ACI 318-77

This document offers a series of rules applicable to members with clear span to effective depth ratio (l_o/d) less than 5 and loaded at the top or compression face when designed for shear. For members subjected to shear and flexure only, the nominal shear strength, V_n, is computed from the nominal shear strength provided by concrete, V_c, and the nominal shear strength provided by shear reinforcement, V_s, so that

$$V_n = V_c + V_s \qquad 7.5$$

The shear strength V_n is limited by the expression

$$V_n < 8\sqrt{f'_c}\ bd \qquad 7.6$$

when l_o/d is less than 2. When l_o/d lies between 2 and 5

$$V_n = 2/3\ (10 + l_o/d)\ \sqrt{f'_c}\ bd \qquad 7.7$$

The ultimate shear strength of the section is given by:

$$V_u \leq \phi\ V_n \qquad 7.8$$

where $\phi = 0.85$

The nominal shear strength provided by the concrete is computed from:

$$V_c = 2\sqrt{f'_c}\ bd \qquad 7.9$$

where f'_c = specified compressive cylinder strength of concrete, psi

b = web thickness, in

d = distance from extreme compression fibre to centroid of longitudinal tension reinforcement.

A more detailed calculation may be carried out using the following equation:

$$V_c = (3.5-2.5(M_u/V_u d))(1.9\sqrt{f'_c} + 2500\ p_w(V_u d/M_u))bd \qquad 7.10$$

where M_u = moment at section

V_u = shear force at section occurring simultaneously with M_u

$p_w = A_s/bd$ where A_s = area of tension reinforcement, in^2

The term $(3.5-2.5(M_u/V_u d))$ should not exceed 2.5 and V_c should not be greater than

$$6\sqrt{f'_c}\ bd \qquad 7.11$$

Shear strength V_s can be computed from:

$$V_s = [(A_v/s)(1 + l_o/d)/12 + (A_{vh}/s_2)(11 - l_o/d)/12]f_y d \qquad 7.12$$

where A_v = area of shear reinforcement perpendicular to flexural tension reinforcement within a distance s

A_{vh} = area of shear reinforcement parallel to flexural reinforcement within a distance s_2

f_y = specified yield strength of reinforcement, psi

For deep beams loaded on the soffit, the explanatory handbook to the ACI code states that if the loads are applied indirectly or at the bottom of the specimen, the design for shear should be the same as for

ordinary members. No advice is given for the case of combined top and bottom loads.

7.3.2 CIRIA Guide 2 (1977)

This document advises that the design for shear of web reinforcement must consider the position of forces either at the top or bottom of the beam.

In the case of deep beams loaded at the bottom, the following equation must be satisfied:

$$V_u < 0.75\ b\ h_a\ \nu_u \qquad 7.13$$

where b = thickness of beam, mm

h_a = effective height, mm

ν_u = maximum value of shear stress taken from CP110 (1972), Tables 6 and 26 for normal and light-weight concretes respectively.

Additionally, loads applied along the whole span to the bottom of the beam must be supported by vertical stirrups at a design stress of $0.87\ f_y$.

The bottom-load shear capacity, V_{cb} is defined as the lesser of $0.75bh_a\nu_u$ and the resulting force that the web reinforcement withstands.

In the case of deep beams loaded at the top the effective clear shear span dimension, x_e must be specified. The value of x_e should be assumed to be either a) the clear shear span for a load which contributes more than 50 percent of the total shear force at the support, or b) 0.25 L for a load uniformly distributed over the whole span.

The following conditions must be satisfied:

$$V_u < 2bh_a^{\,2}\ \nu_c\ k_s/x_e \qquad \text{(a)}$$

and

$$V_u < bh_a\ \nu_u \qquad \text{(b)} \qquad 7.14$$

where ν_c = ultimate concrete shear stress, given by CP110, Tables 5 and 25 for normal and light-weight concretes, respectively.

k_s = 1.0 if $h_a/b < 4$

= 0.6 if $h_a/b > 4$

The top-load shear capacity, V_{ct}, is defined as the smaller figure derived from equations 7.14(a) and 7.14(b).

When combined top and bottom loading action is present, the following condition must be satisfied:

$$V_{at}/V_{ct} + V_{ab}/V_{cb} < 1 \qquad 7.15$$

where V_{at} = applied shear from top loads,

V_{ab} = applied shear from bottom loads

and V_{ct}, V_{cb} are as defined earlier.

Equation 7.15 controls the permissible amount of top and bottom load for a given deep beam. Based on this equation, Fig. 7.3 presents three curves which show graphically the acceptable total load depending on the ratio of the applied top and bottom loads for different percentages of vertical reinforcement, as used in the specimens W1, W2 and W3. It is interesting to note that the three curves predict the same total load when the specimens are loaded entirely on the top level. This occurs since this method does not consider the contribution of web reinforcement to resist shear forces. The top-load shear capacity, V_{ct}, is calculated utilising only those values of the ultimate shear stress (which CP110 gives as a constant for concretes of grade 40 or better), the clear shear span and the effective height.

The straight line on the upper section of the graph represents the hypothetical maximum top and bottom loads that could possibly be applied using this method. This limit is reached when 2.59 percent of the specific vertical reinforcement is provided. Any increase in the percentage of vertical reinforcement beyond this point would not

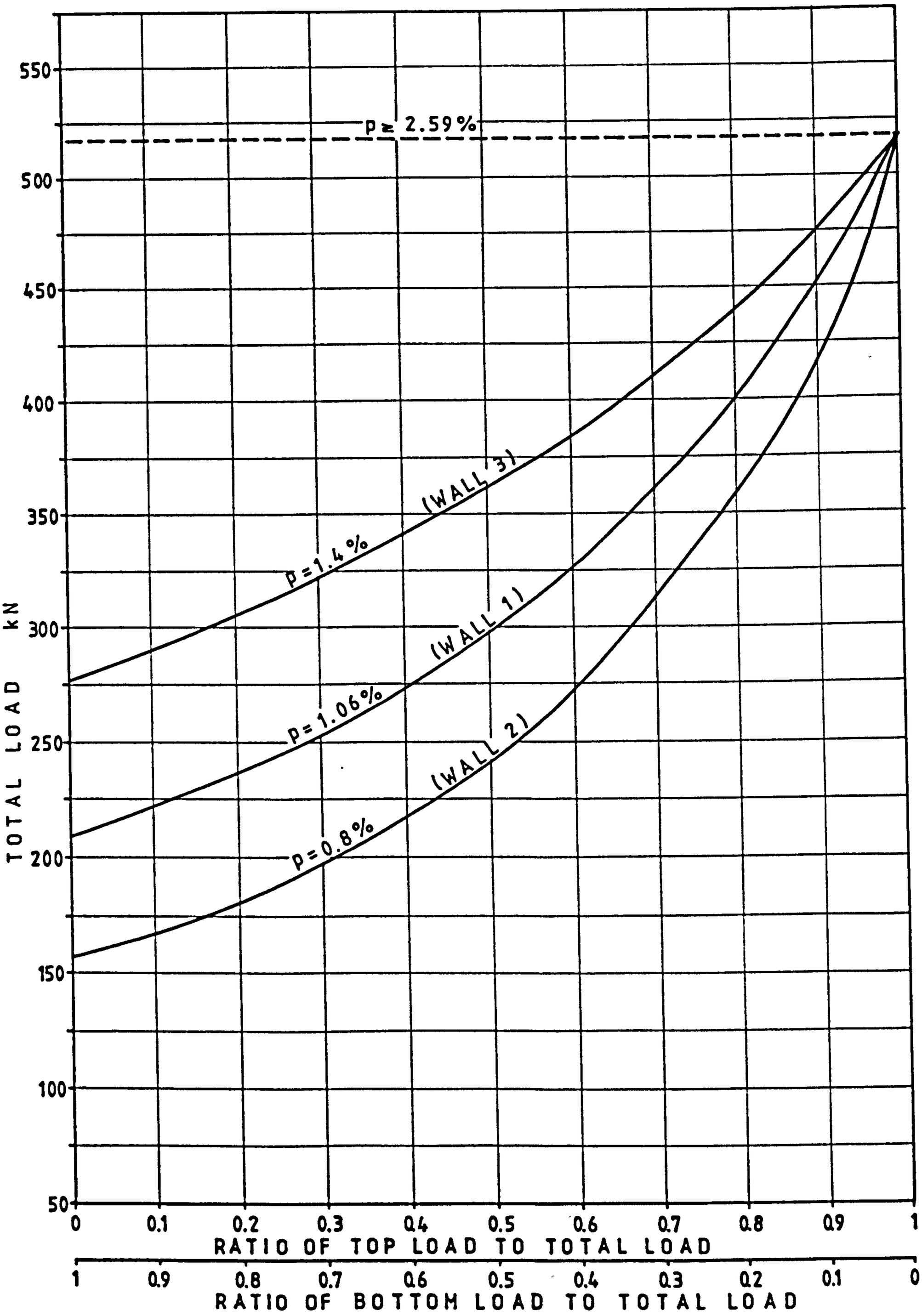

Fig. 7.3 Relationship of bottom and top loads to total load for various percentages of vertical steel as predicted by the simple rules of CIRIA Guide 2.

improve the theoretical capacity of the wall to carry bottom-load, since Eq 7.13 becomes the upper limit. This is the maximum shear force allowed on the section for bottom loads.

In addition to the simple rules explained above for predicting the capacity of an unreinforced web to resist top-load shear forces, the CIRIA Guide gives an alternative procedure which does consider the web reinforcement. This procedure is based on the ultimate shear strength equation postulated by Kong et al (1972). The ultimate shear capacity of a reinforced web in which the clear shear span to effective depth ratio (x_e/h_a) lies between 0.23 and 0.7 can be deduced from:

$$V/bh_a < \lambda_1(1-0.35\ x_e/h_a)\sqrt{f_{cu}} + \lambda_2 \Sigma 100\ A_i y_i \sin^2\theta_i/bh_a^2 \qquad 7.16$$

where λ_1 = 0.44 for normal weight aggregates and

= 0.32 for lightweight aggregates

λ_2 = 1.95 N/mm^2 for deformed bars and

= 0.85 N/mm^2 for plain round bars

A_i, y_i and θ_i are shown in Fig. 7.4

The first and second terms in the equation represent the concrete and steel contributions to the shear strength respectively.

The ultimate shear capacity of the section is limited by the following expression

$$V/bh_a < 1.3\ \lambda_1 \sqrt{f_{cu}} \qquad 7.17$$

and the contribution of the reinforcement to the shear strength must be larger than 0.2V.

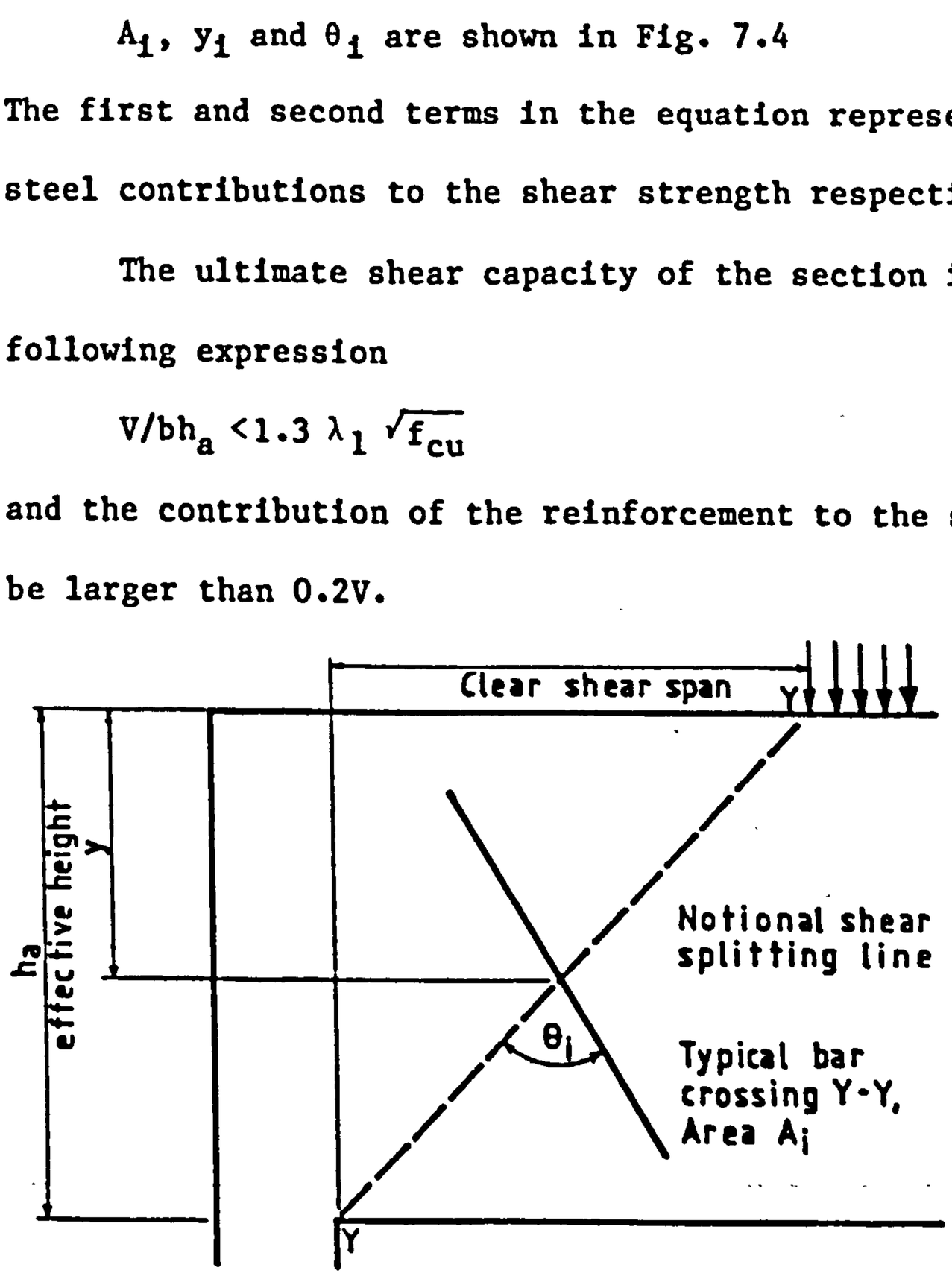

Fig. 7.4 Clear shear span for top loads.

7.4 COMPARISON OF EXPERIMENTAL RESULTS TO ACI AND CIRIA VALUES. TOP LOAD.

7.4.1 ACI Standard 318-77

The ultimate shear strengths for specimens W1-L1, W2-L1 and W3-L1 which were loaded on the top only, have been calculated by using the ACI rules explained earlier and the results of these calculations are presented in Table 7.1. Line 1 of Table 7.1 shows the maximum nominal shear V_n allowed for the section, as calculated by Eq. 7.6. Line 2 gives the contribution of the concrete (V_c) towards the nominal shear strength as calculated using the detailed procedure of Eq. 7.10. Line 3 presents the maximum shear strength allowed for the concrete as derived from Eq. 7.11. This last figure is an upper limit for the value of V_c. In the case of the three walls considered in Table 7.1, the shear strength V_c is governed by the results obtained using Eq 7.10. The contribution to shear strength by the web reinforcement is estimated by Eq. 7.12; these figures are given in line 4. Surprisingly, these values are very high, close to the figure shown in line 1, representing the maximum nominal shear strength. Therefore, the contribution of the steel to the nominal shear strength is limited to the values shown in line 5, given by $V_s = V_n - V_c$. The ultimate shear strength of the section appears in line 7 and the total ultimate load on the top of the wall in line 8. An interesting point in Table 7.1 is the large contribution of the web reinforcement to the shear strength as predicted by Eq. 7.12, only to be limited by Eq. 7.6 to the relatively smaller value shown in line 5. The procedure recommended by the ACI Standard (1977) for calculating the shear strength of deep flexural elements thus appears to be somewhat ambiguous.

Table 7.1 Calculation of shear resistance of specimens W1-L1, W2-L1 and W3-L1 based on ACI standard 318-77

		Equation	W1-L1 kN	W2-L1 kN	W3-L1 kN
1	V_n	7.6	247.9	258.4	272.3
2	V_c	7.10	180.9	187.1	195.2
3	V_c	7.11	185.9	193.8	204.2
4	V_s	7.12	252.1	242.7	265.4
5	V_s	V_n-V_c	67.0	71.3	77.1
6	V_n	7.5	247.9	258.4	272.3
7	V_u	7.8	210.7	219.6	231.5
8		2 V_u	421.4	439.2	463.0

7.4.2 CIRIA Guide 2 (1977)

Table 7.2 discloses the predicted values of the ultimate load capacity for specimens W1-L1, W2-L1 and W3-L1, based on the shear strength for top-loaded deep beams, calculated by the CIRIA procedures explained previously. Line 1 of Table 7.2 gives the values of the ultimate load capacity computed for the three walls by using Eq. 7.14. Lines 2 to 5 present the contribution to the load-carrying capacity of the concrete section and the different reinforcements of the top-loaded walls. This proposed contribution results from the second term of Eq. 7.16 and line 6 of the same table contains the total steel contribution (V_s) to the load carrying capacity. Finally, line 7 indicates the total load capacity based on the ultimate shear values derived using Eq. 7.16.

It can be seen in Table 7.2 that after the concrete section, the main reinforcement contributes most to the shear strength, followed by

Table 7.2 Calculated values of ultimate load carrying capacity of specimens W1-L1, W2-L1 and W3-L1, based on the shear strength as predicted by CIRIA

		W1-L1 kN	W2-L1 kN	W3-L1 kN
1	Load	518.4	518.4	518.4
2	V_c	373.3	389.1	410.0
3	V_{sm}	114.7	114.7	114.7
4	V_{sh}	38.7	38.7	38.7
5	V_{sv}	1.1	0.7	1.3
6	V_s	154.5	154.1	154.8
7	Load	527.8	543.4	564.9

Note V_c = Contribution of concrete to the ultimate load

V_{sm} = Contribution of main reinforcement

V_{sh} = Contribution of horizontal web reinforcement

V_{sv} = Contribution of vertical web reinforcement

the horizontal web reinforcement and lastly the vertical web steel. The contribution to the total shear strength provided by the vertical steel is negligible (about 0.2 percent) when compared to the total shear capacity of the section.

Table 7.3 compares the ultimate load capacity of specimens W1-L1, W2-L1 and W3-L1 as specified by ACI and CIRIA. The load at which the first diagonal crack was noticed in these specimens is also given. It can be observed in Table 7.3 that the ACI propositions are much more conservative than those from CIRIA. This difference is accentuated by the strength reduction factor, ϕ, imposed by the ACI standard upon the

nominal strength in order to calculate the design load. The strength reduction factor accounts for uncertainties in design computation and variations in material strength, workmanship and dimensions. It corresponds to 0.85 for shear strength calculations. The CIRIA figures are closer to the cracking load and for wall W2-L1, the predicted ultimate load is 9 percent higher than the load at which the first crack was detected. Also, in Table 7.3 the failure load for those three specimens appears as more than twice the shear strength calculated by CIRIA rules. In addition, collapse of these specimens was due to bearing failure, suggesting an even greater capacity of the section to resist shear.

In conclusion, the CIRIA (1977) procedure has approximately produced the load at which the first diagonal cracks were observed in these walls, with the actual ultimate shear strength being more than twice the predicted figure. The ACI model was even more conservative.

Table 7.3 Ultimate load predicted by ACI 318-77 and CIRIA Guide 2 and experimental diagonal cracking load

Specimen	ACI		CIRIA	Cracking Load	Failure Load
	Nominal Load (kN)	Design Load (kN)	kN	kN	kN
W1-L1	495.8	421.4	527.8	600	1100
W2-L1	516.8	439.2	543.4	500	1100
W3-L1	544.6	463.0	564.9	600	1300

7.5 COMPARISON OF EXPERIMENTAL RESULTS TO CIRIA VALUES. BOTTOM AND COMBINED LOADS

Of recent documents dealing with recommendations for reinforced concrete design, only CIRIA Guide 2 (1977) has specific regulations for designing deep flexural members when loaded at the soffit or under combined top and bottom loads. Therefore, in the following analysis, this is the only numerical procedure employed.

7.5.1 Bottom load

Table 7.4 presents data concerning the five walls tested under load at the soffit. This data is listed in relation to the ascending percentage of vertical reinforcement in the specimens. Wall W4-L2, without any vertical reinforcement, sustained 130 kN before it cracked horizontally. This crack extended along the whole span, forming a slender beam at the lower level of the wall, whose flexural rigidity continued carrying the load. A small increase in the cracking load can be observed when using 0.8 percent of vetical reinforcement in specimen W2-L2. For the increase in reinforcement from 0.8 to 2.0 percent, the load at which the first horizontal crack was detected remained almost unaffected. That load noted for specimen W3-L2 is inconsistent and was thought to be due to human error in failing to detect the crack at initiation. However, this was checked by examining the load-displacement curve for this specimen and a change in the stiffness was observed at the load step between 167 and 200 kN, suggesting that the detection of cracks at 200 kN was probably correct.

Table 7.4 Effect of vertical reinforcement on cracking load and comparison with CIRIA ultimate load prediction for walls loaded at the bottom

Specimen	Vertical Reinforcement Percentage	CIRIA kN	Cracking Load kN
W4-L2	0	0	130.0
W2-L2	0.80	158.2	167.0
W1-L2	1.06	209.6	167.0
W3-L2	1.40	276.8	200.0
W5-L2	2.00	395.4	160.0

7.5.2 Combined top and bottom loads

The validity of Eq. 7.15 for controlling the values of top and bottom loads applied together on a flexural element is tested in this section.

Figures 7.5 to 7.7 compare the predicted ultimate load to the experimental load at which cracks were first observed in walls W1, W2 and W3. For walls W2 with 0.8 percent of vertical reinforcement (Fig. 7.5) the calculated ultimate load was similar to the experimental cracking load. This implies that for the specimen W2 loaded entirely at the soffit, once cracking occurred, the stress in the reinforcement was close to 0.87 f_y. Figure 7.6 presents the same comparison for specimens W1 with 1.06 percent of vertical reinforcement. Here, for those specimens mainly or totally loaded at the soffit, there is a large difference between the ultimate predicted load and the

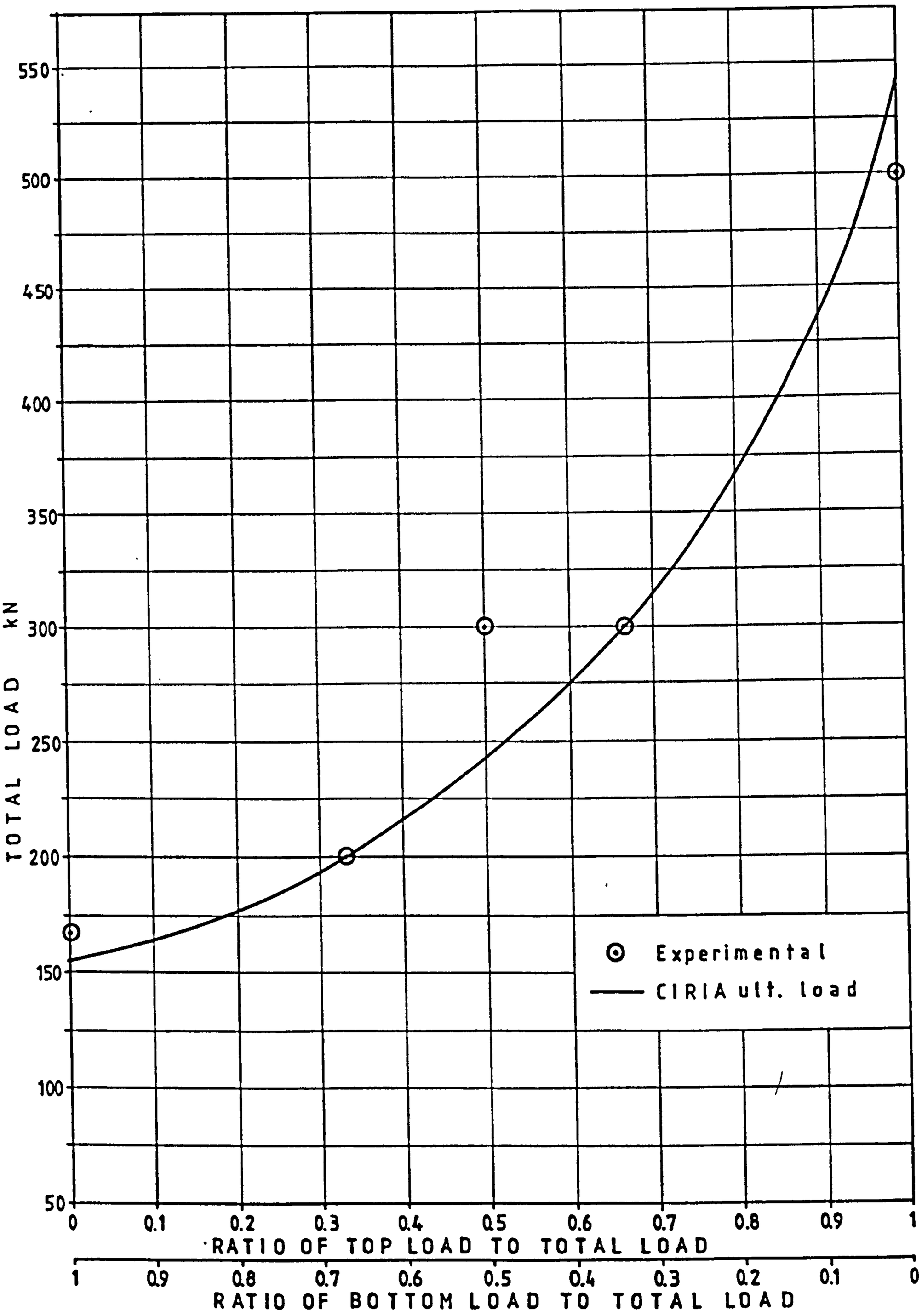

Fig. 7.5 Comparison of CIRIA Guide 2 prediction of ultimate load with experimental cracking load for walls W2 with 0.8 percent vertical reinforcement.

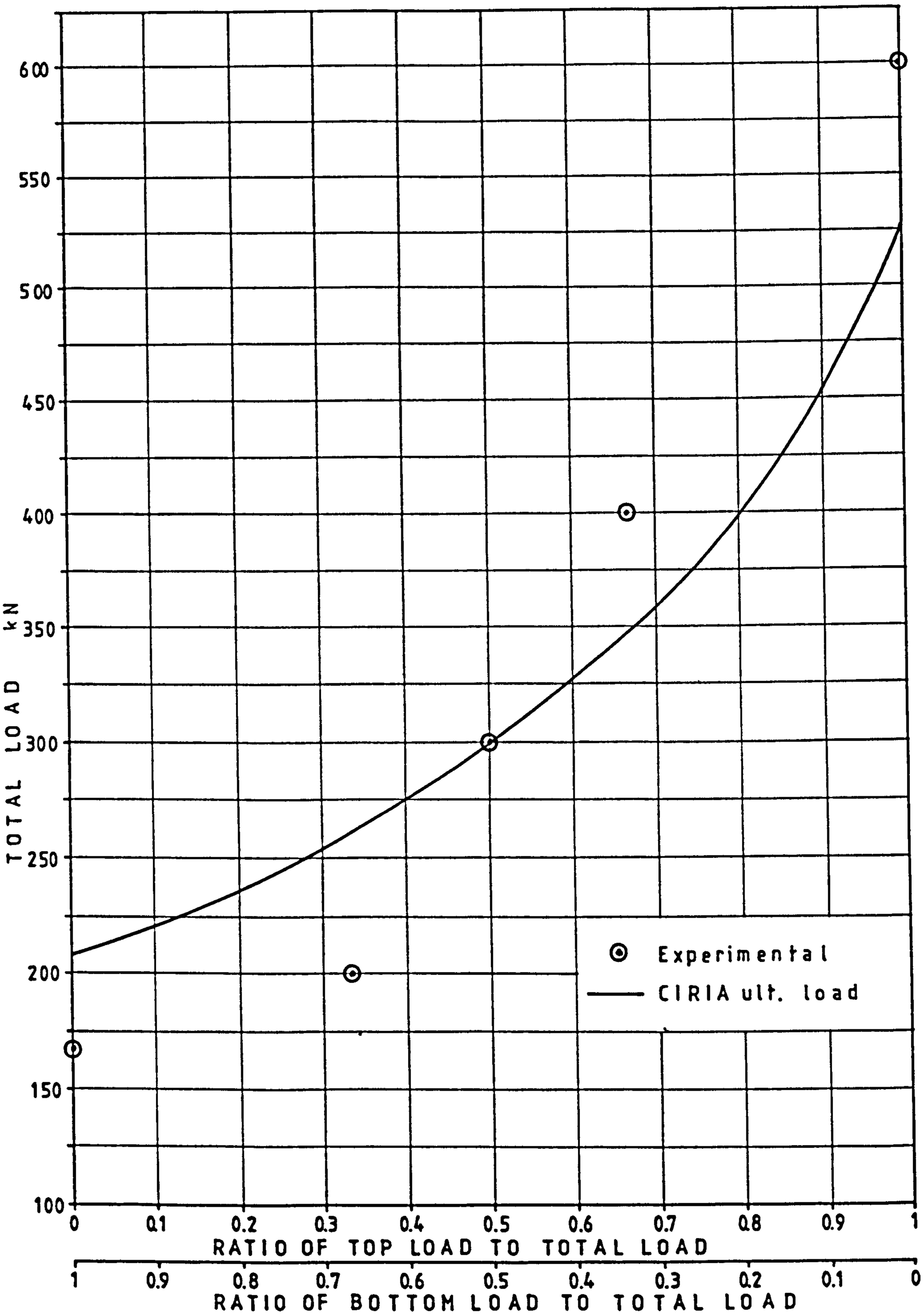

Fig. 7.6 Comparison of CIRIA Guide 2 prediction of ultimate load with experimental cracking load for walls W1 with 1.06 percent vertical reinforcement.

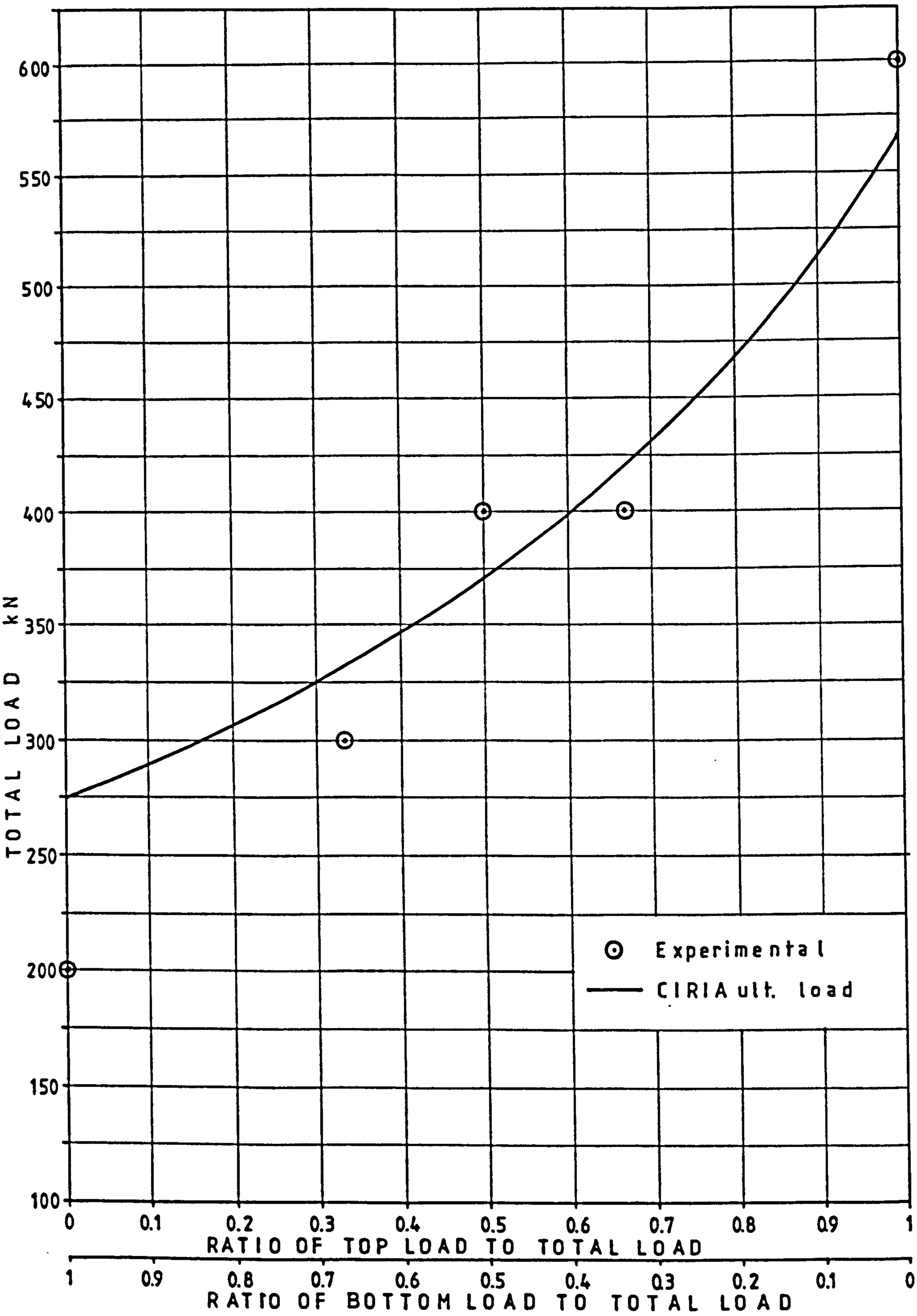

Fig. 7.7 Comparison of CIRIA Guide 2 prediction of ultimate load with experimental cracking load for walls W3 with 1.4 percent vertical reinforcement.

experimental cracking load, indicating a considerable capacity of the specimen to withstand further load beyond cracking. Very similar behaviour is demonstrated by specimen W3 (Fig. 7.7) with 2.0 percent of vertical reinforcement. Here, the difference between the cracking and the estimated ultimate load increases.

Figures 7.5, 7.6 and 7.7 illustrate that for those specimens with more than 0.8 percent vertical reinforcement, the concrete section had cracked before reaching the suspended ultimate load predicted as $0.87\ f_y\ A_{sv}$. Unlike the top loaded specimens, which showed diagonal cracks at loads above the predicted ultimate load, those loaded at the soffit cracked before reaching the design ultimate load, because of the minimal strength of concrete in tension. Higher percentages of reinforcement reduced the crack widths but were insufficient to retard their initiation.

In figures 7.5 to 7.7 it can be observed that the relationship between top and bottom loads provided by Eq. 7.15 is adequate. The only point of concern is the term V_{ab} in this equation, which allows the presence of cracks below the design ultimate load when using percentages of vertical reinforcement above 0.8 percent.

The effect of the type of loading on diagonal tension can be appreciated by examining Table 7.5. In it, the forces causing diagonal tensile cracking are given for the specimens loaded at the top (L1) and under the combined loading type L4, in which 2/3 of the total load is applied on top. For load type L4, the diagonal cracking load is approximately equal to the cracking load under load type L1 multiplied by the ratio of top to total load (0.67). When the load is applied on the soffit, tensile forces are induced, which add to the diagonal tensile stresses arising from the arch action of loads transmitted to the supports. This causes the concrete to reach its maximum tensile

Table 7.5 Comparison of diagonal cracking load (kN) and angle of inclination of cracks between specimens under load types L1 and L4

Load type / Specimen	L1 Angle of inclination of crack	L1 Load kN	L4 Angle of inclination of crack	L4 Load kN
W1	68°	600	62°	400
				268*
W2	65°	500	56°	300
				200*
W3	60°	600	55°	400
				263*

*Load applied on top

strength earlier than under top loads only. The angle of inclination of the diagonal crack is altered by the vertical tensile forces, as shown in Table 7.5, when loads are applied at the soffit.

7.6 CONTROL OF CRACKS

When designing reinforced concrete members, the control of cracks is an important consideration. Cracks are commonly regarded as a source of concern among reinforced concrete designers because of the possibility of corrosive action on the reinforcement. Nevertheless, Beeby (1978) believes that cracks only help to initiate corrosion and that their development does not depend on the crack width, but on the concrete properties. He concluded that the definition of permissible crack widths serves no useful function as a corrosion protection measure.

In hydraulic structures, such as fluid containers, the presence of cracks could severely undermine their function depending on the fluid type. In other cases, cracks are objectionable from the aesthetic point of view; visible cracks impair the confidence of the users of a building although it could be structurally safe.

For serviceability purposes CP110 (1972) limits the crack width to 0.3 mm in general and for members exposed to a severely aggressive environment, it recommends that the crack width should not exceed 0.004 times the nominal cover to the main reinforcement. The Comité Européen du Béton (1970) has similar proposals, in which the crack width is restricted to 0.1 mm for aggressive environments, 0.2 mm for normal external conditions and 0.3 mm for normal internal conditions. A design which does not allow cracking would produce the most stringent serviceability limit. Thus, a definiton of a cracking load is necessary.

Table 7.6 shows the loads at which the crack widths of 0.05, 0.1, 0.2 and 0.3 mm were observed for the specimens tested. For all the walls, there is no doubt that the general crack width limit of 0.3 mm is satisfied below the ultimate load estimated by CIRIA's rules and even the crack width limit of 0.1 mm for aggressive environments demanded by C.E.B. (1970) is fulfilled. For these members, a cover to reinforcement of 12 mm was employed, 3 mm less than the nominal cover recommended in CP110 for mild environmental conditions. It is thought that 3 mm extra cover would not have affected the crack width on the surface of these specimens much. For very severe conditions of exposure CP110 recommends nominal cover up to 60 mm. The test results obtained are not reliable enough to predict the outcome if the cover for severe conditions was used. However, ignoring the fact that the specimens did not have adequate cover for very severe conditions of

Table 7.6 Load at which the crack width limits of 0.05, 0.10, 0.2 and 0.3 mm were observed

Specimen	Ultimate load CIRIA kN	Crack width 0.05	0.1	0.2	0.3	Maximum exp. load kN	
W1-L1	527.8	600	700	-	-	1100	F
W1-L2	209.6	180	210	237	253	375	C
W1-L3	294.1	360	422	485	510	750	C
W1-L4	345.8	440	625	713	765	1000	C
W1-L5	262.1	250	325	400	427	570	C
W2-L1	543.4	575	700	1000	-	1100	F
W2-L2	158.2	167	190	217	227	300	C
W2-L3	240.5	305	318	343	365	600	C
W2-L4	289.6	470	565	635	662	900	C
W2-L5	206.7	200	250	305	325	400	C
W3-L1	564.9	650	800	1100	-	1300	F
W3-L2	276.8	255	315	358	375	500	C
W3-L3	365.2	575	645	685	700	940	F
W3-L4	416.8	860	1000	-	-	1200	F
W3-L5	332.8	450	510	550	570	800	F
W4-L2	-	130	130	130	130	150	C
W5-L2	395.4	275	425	-	-	375	S

Note: F = Failure of support

C = Test suspended due to large crack width and extensive damage to concrete

S = Test suspended

exposure it can be pointed out that most of the members did comply with the limit of 0.05 mm crack width at the estimated ultimate load. The exceptions were those elements loaded mainly on the soffit, i.e., load types L2 and L5 and which had more than 0.8 percent vertical reinforcement.

7.7 DEFINITION OF THE CRACKING LOAD

A basic assumption in the design of reinforced concrete tensile members is that the tensile forces are taken entirely by the reinforcement, ignoring the minimal tensile strength of concrete before cracking. By adopting this assumption, the designer accepts the existence of cracks under working loads in order to have an economical structure.

In the case of walls with a uniformly distributed load at the bottom, the load is carried by the combined performance of the concrete and reinforcement before the first horizontal crack appears. Stress-strain relationships can be considered linear and also the strain in both concrete and steel is the same, corresponding to the elastic theory. All this is possible due to the bond between the reinforcement and concrete, which is taken as being totally effective at early loading stages.

The condition of strain compatibility can be expressed as

$$\varepsilon_c = \varepsilon_s \qquad 7.18$$

where ε_c, ε_s = concrete strain and steel strain respectively.

Equation 7.18 corresponds to

$$f_c/E_{ct} = f_s/E_s \qquad 7.19$$

where f_c = stress in concrete

f_s = stress in steel

E_{ct} = modulus of elasticity of concrete in tension

E_s = modulus of elasticity of steel

Equation 7.19 yields the stress in the concrete and steel as functions of the elastic moduli

$$f_s = \alpha_t f_c \qquad 7.20$$

where $\alpha_t = E_s/E_{ct}$ = modular ratio

From the condition of equilibrium, the suspended load carried by a wall at the soffit before cracking, is given by

$$W = bLf_c + f_s A_{hs} \qquad 7.21$$

where b = thickness of the wall

L = span

The load sustained by the section when the concrete first cracks is defined by

$$W_{cr} = bLf_{ct} + f_s A_{hs} \qquad 7.22$$

where f_{ct} = strength of concrete in tension

In this analysis the strength of concrete in tension is taken to be equal to the cylinder splitting strength.

From Eqs. 7.20 and 7.22

$$W_{cr} = bLf_{ct} + \alpha_t f_{ct} A_{hs} \qquad 7.23$$

or $$W_{cr} = bLf_{ct}(1 + \alpha_t p) \qquad 7.24$$

where $p = A_{hs}/bL$

Equation 7.24 defines the load at which cracking of the section is expected.

Immediately after cracking occurs, all of the tensile force can be considered to be concentrated in the reinforcement at that cracked section, if the crack width is small enough. This situation is represented by the expression

$$W_{cr} = A_{hs} f_s \qquad 7.25$$

From Eqs. 7.24 and 7.25 the stress in the steel at the cracking load is expressed as

$$f_s = f_{ct}(1/p + \alpha_t) \qquad 7.26$$

and the ratio of the stress in the reinforcement to the yielding stress (f_s/f_y) at the cracking load is given by

$$\phi_{cr} = f_{ct}/f_y\ (1/p + \alpha_t) \qquad 7.27$$

Figures 7.8 to 7.11 compare the ratio of stress to yield strength of the vertical reinforcement as calculated by Eq. 7.27 to the experimental ratios obtained from the load at which cracks were first observed for each deep member loaded on the soffit only. Since the properties of the concrete vary within the depth of the walls, two curves are shown, one calculated on the basis of the concrete strength obtained from the control specimens and the second considering the results obtained in Chapter 6. For the latter, a concrete cube strength equal to 62 percent of the strength of the control specimens was assumed; the modulus of elasticity, was derived from Table 1 of CP110. The concrete splitting strength was deduced from the following empirical equation

$$f_{ct} = 0.13(f_{cu})^{0.8} \qquad 7.28$$

given by Brooks and Neville (1977). Table 7.7 presents the assumed properties of the concrete at the level of the cracks for the bottom loaded specimens.

The experimental ratio of stress to yield strength of the reinforcement is shown as a range of values, since the crack would have occurred during a loading step and the exact cracking load was not observed. In general, the values estimated by Eq. 7.27 have been shown to agree well with the experimental results. The results are not precise because of the following uncertainties: first, on the actual strength of the concrete at the level of the crack and second, the exact cracking load as explained earlier. Nevertheless, the validity of Eq. 7.27 is clearly established. Figures 7.8 to 7.11 also highlight

Table 7.7 Assumed concrete strength at the level of the horizontal cracks

	SPECIMEN				
	W1-L2	W2-L2	W3-L2	W5-L2	W5-L2
f_{cu} N/mm^2	24.1	26.2	27.8	25.9	29.3
f_{ct} N/mm^2	1.66	1.77	1.86	1.76	1.94
E_c kN/mm^2	25.8	26.4	27.1	26.4	27.7

how uneconomical the use of large percentages of reinforcement would be if cracking was the serviceability limit.

Table 7.8 compares the outcome of Eq. 7.24 (using the figures of Table 7.7) to the experimental cracking loads for the specimens loaded at the bottom (L2). In general, both sets of values compare reasonably well. These results apply to short term load conditions; long term loads are beyond the scope of this experimental analysis.

Table 7.8 Experimental and calculated cracking loads for walls loaded at the soffit

Specimen	Cracking load	
	Experimental	Eq. 7.24
W1-L2	167	129.3
W2-L2	167	135.1
W3-L2	200	147.8
W4-L2	130	127.9
W5-L2	160	159.9

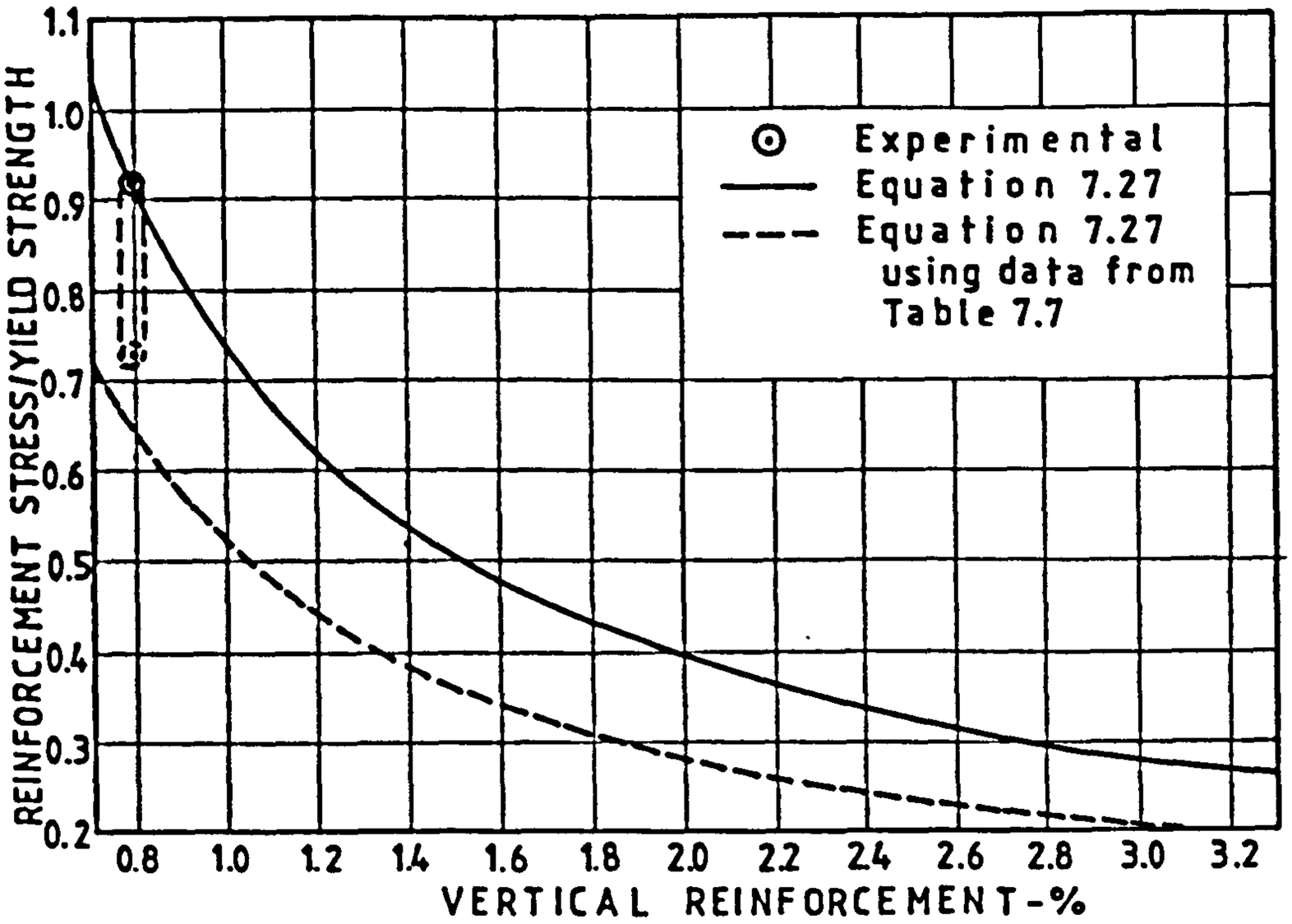

Fig. 7.8 Comparison of the experimental to the calculated ratio (Eq. 7.27) of stress to yield strength of the vertical reinforcement for wall W2-L2.

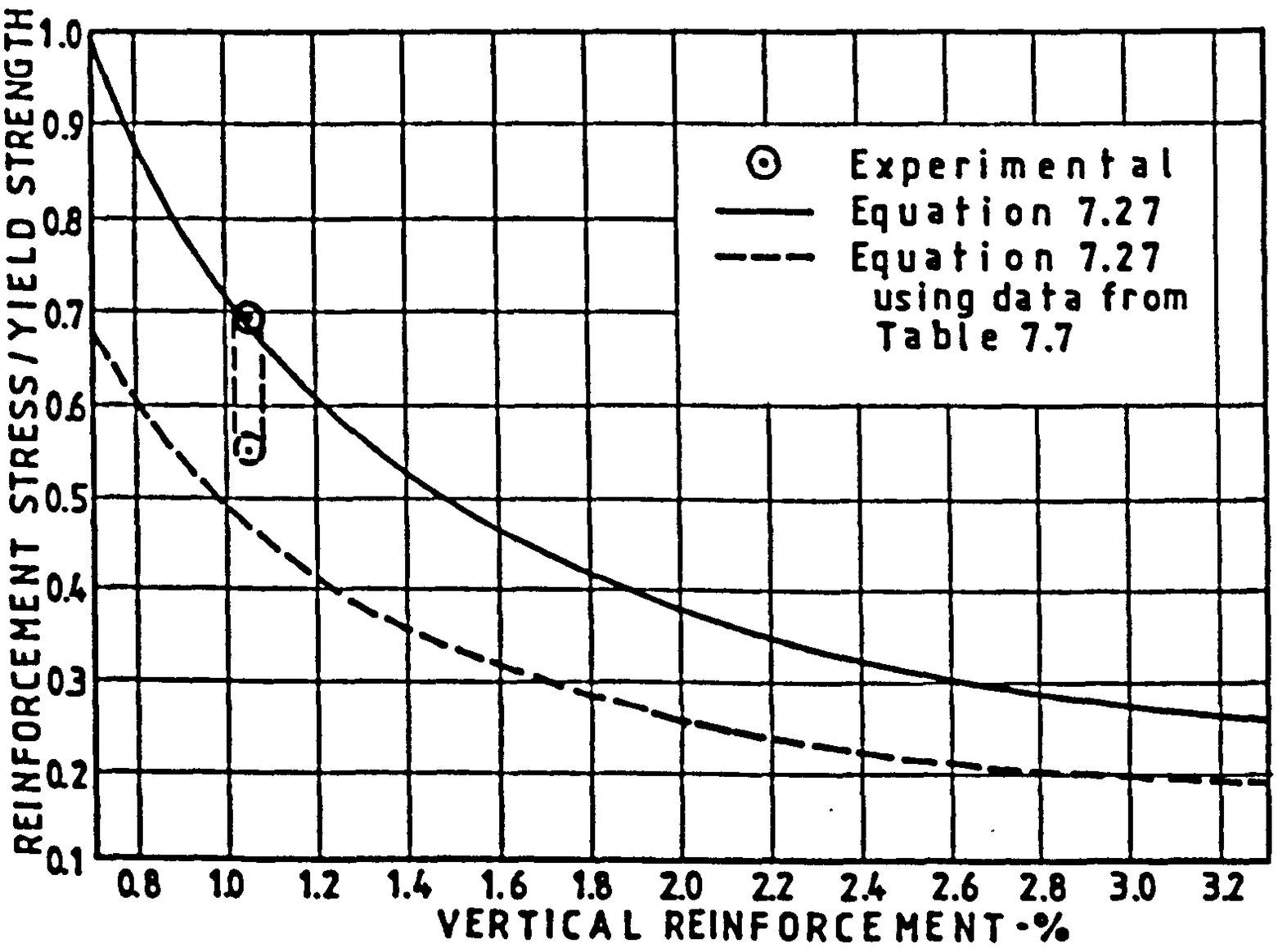

Fig. 7.9 Comparison of the experimental to the calculated ratio (Eq. 7.27) of stress to yield strength of the vertical reinforcement for wall W1-L2.

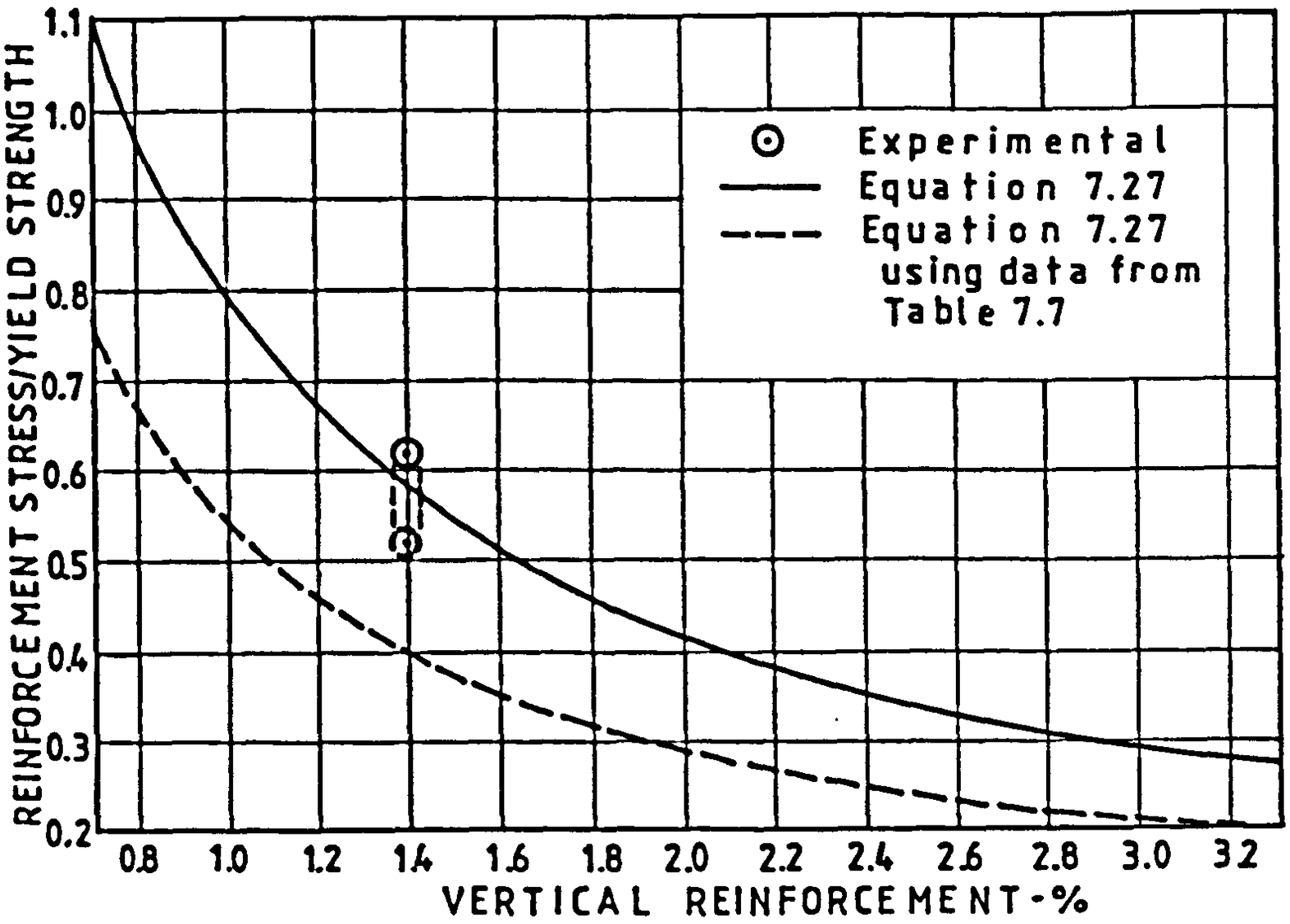

Fig. 7.10 Comparison of the experimental to the calculated ratio (Eq. 7.27) of stress to yield strength of the vertical reinforcement for wall W3-L2.

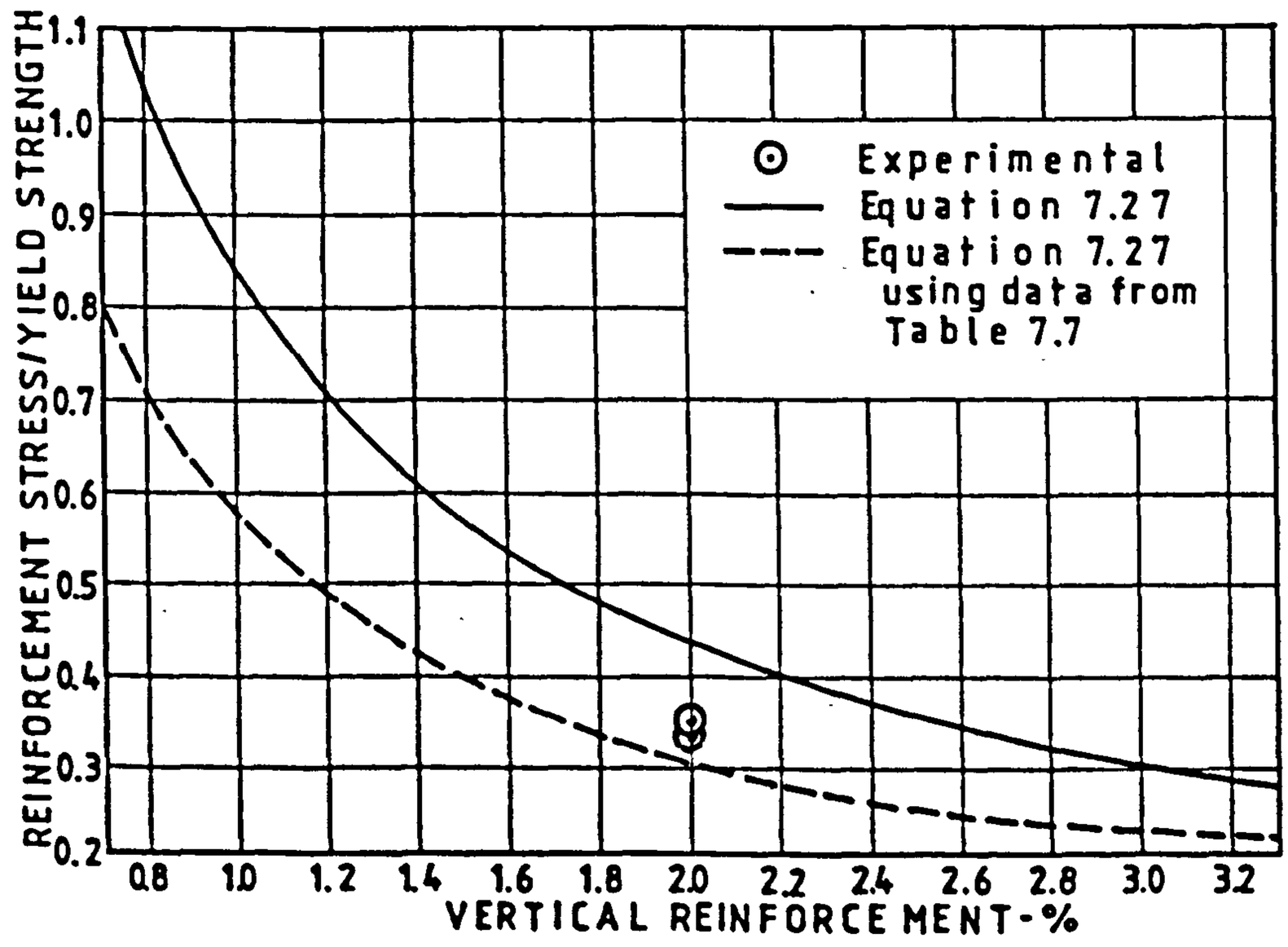

Fig. 7.11 Comparison of the experimental to the calculated ratio (Eq. 7.27) of stress to yield strength of the vertical reinforcement for wall W3-L2.

7.8 CONCLUSIONS

From the analyses performed in this chapter, the following conclusions have been drawn:

a) The CIRIA (1977) procedure for top loaded deep beams has approximately produced the load at which the first diagonal cracks were observed in these walls, with the actual ultimate shear strength being more than twice the predicted figure. The ACI 318-77 model was more conservative.

b) For an increase in vertical reinforcement from 0.8 to 2.0 percent, the load at which the first horizontal crack was detected remained almost unaffected. Those specimens loaded at the soffit cracked before reaching the designed ultimate load; larger percentages of reinforcement reduced the crack widths.

c) When the load is applied on the soffit, tensile forces are induced, which add to the diagonal tensile stresses arising from the arch action of loads transmitted to the supports. This causes the concrete to reach its maximum tensile strength earlier than under top loads only. The angle of inclination of the diagonal crack is reduced by the vertical tensile forces.

d) For these specimens, there is no doubt that the general crack width limit of 0.3 mm is satisfied under the ultimate load estimated by CIRIA's rules and even the crack width limit of 0.1 mm for aggressive environments demanded by C.E.B. (1970) is met.

e) The cracking load for walls loaded at the soffit can be calculated from the elastic properties of the materials using the following equation

$$W_{cr} = bLf_{ct}(1+ \alpha_t\ p)$$

This equation, with adequate safety factors could be used to derive the term V_{ab} for Eq. 7.15 when combined top and bottom loading action is present and where initial cracking is the serviceability limit.

CHAPTER 8

BEARING STRENGTH

8.1 INTRODUCTION

The geometrical characteristics of deep flexural members allow them additional load carrying capacity in terms of shear and bending. This enhanced capacity, if used fully, would impose larger stresses onto the bearing zones, which do not benefit from the geometry of the member. For this reason, whereas in slender beams the bearing capacity is rarely a matter of concern, it can become a serious problem when dealing with elements of large depth/span ratios.

The importance of controlling and improving the bearing strength of deep flexural elements has been demonstrated by this experimental programme. Crushing of the bearing zone was a frequent mode of failure, especially in those specimens with depth/span ratios larger than 1. Since there are no specific guides for predicting the ultimate bearing strength of these structural elements, a brief survey of the literature concerned with the bearing capacity of plain and reinforced concrete has been carried out in order to observe the factors influencing the local bearing strength and ways of improving it.

The bearing strength of plain and reinforced concrete has received some attention from researchers; however, the published work dedicated to the bearing strength of deep beams and wall-beams is sparse. Understanding of the bearing capacity of concrete deep flexural elements seems to be still in its initial stages. Stresses in the bearing zone are complex and elastic analyses are limited in value by the brittle behaviour of concrete. Nevertheless, some authors have persevered in this field as has Guyon (1951), who assumed linear elastic

behaviour for concrete as a basis for the solution of stresses in symmetrically loaded concrete blocks; at loads near failure, this solution disagrees with the actual nonlinear stress-strain curve of concrete. Iyengar (1962) questioned the accuracy of the figures calculated by Guyon's solution. Assumptions of concrete being a perfectly plastic material were used by Chen and Drucker (1969) to formulate a solution for the prediction of bearing strength of concrete. This solution provided an upper bound to the bearing capacity of concrete blocks, which is of very little use for designers, who are interested in a safe and reliable figure. The limitations of this solution were presented by Hyland and Chen (1970).

In this chapter, a brief revision of the general knowledge on concrete bearing capacity is undertaken; also an analysis of data available in the literature on deep beams and from this experimental work is presented.

8.2 BEARING STRENGTH OF PLAIN CONCRETE

The bearing capacity of a concrete block subjected to a localized load is known to be larger than the compressive strength of cubes due to the confining pressure developed around the loaded area. Meyerhof (1953) compared this behaviour to that shown by concrete in triaxial compression tests. This has been confirmed by Shelson (1958) who carried out a test programme on 200 mm concrete cubes, loaded through steel plates corresponding to footing area/loaded area ratios, R, of 64, 32, 16, 8 and 7. Results from this test programme confirmed that the bearing pressure improves as the ratio R increases.

Figure 8.1 shows Shelson's experimental results. It demonstrates that in this case, the bearing pressure apparently approaches an upper limit, 5 times the cylinder compressive strength, for ratios R greater

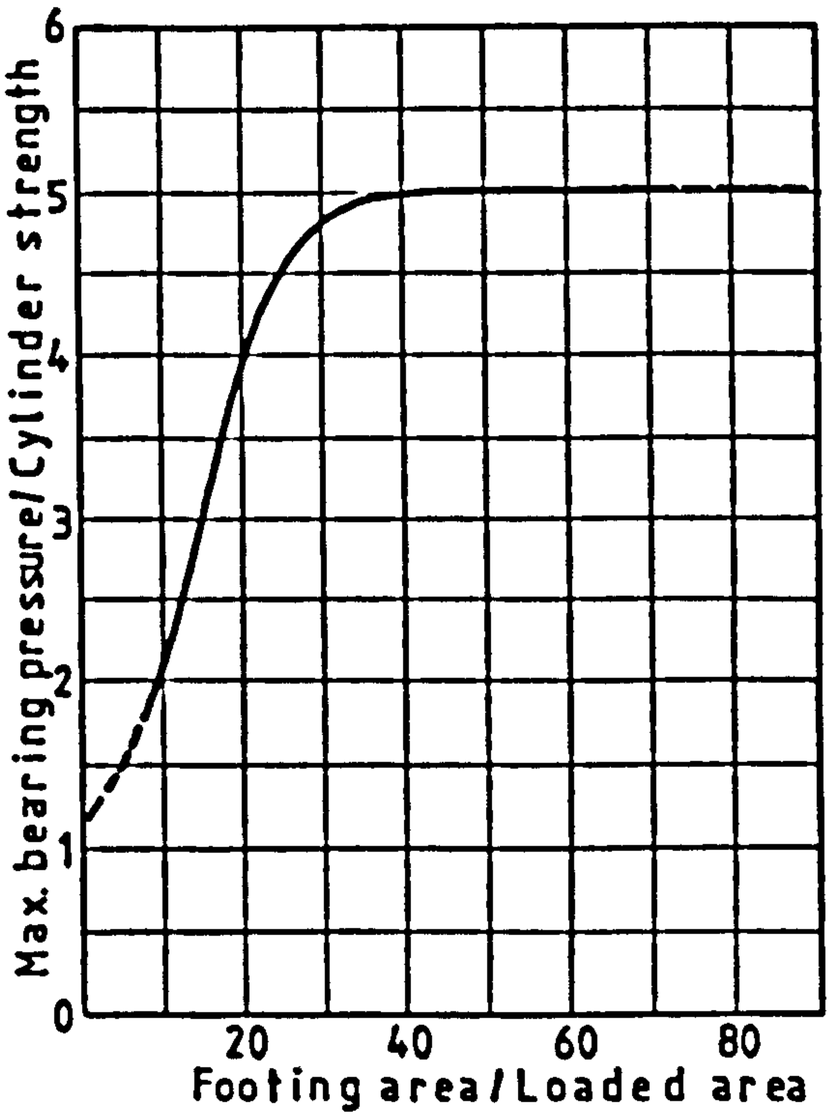

Fig. 8.1 Effect of ratio R on the bearing strength of concrete blocks (Shelson, 1958)

than approximately 30. From the test results it can be observed that the initial section of the curve is almost linear. Shelson observed that failure occurred after the formation of a wedge under the bearing plate. The wedge-shaped segment was forced down, splitting the block.

A similar experimental work was undertaken by Au and Baird (1960). This study dealt with concrete blocks loaded with larger bearing plates and R ratios ranging from 2 to 16. In addition to those aspects studied by Shelson, Au and Baird investigated the effect of maximum aggregate size and height of specimens upon the bearing capacity. Two maximum aggregate sizes were used: 6 and 12 mm. The failure mode observed was similar to that described by Shelson, with the formation of a wedge under the bearing plate; it was an invariable feature in all the tests carried out on cubes. This contradicts Shelson's results, who found that for the smaller R ratios the formation of a distinctly inverted wedge did not occur. Au and Baird explained that this difference in results could be caused by bending due to the uneven bottom surface of the concrete blocks.

Figure 8.2 shows some of Au and Baird's results. It confirms that the bearing strength of concrete under a confined contact area is larger than the unconfined strength. Also demonstrated, is the fact that a larger aggregate size improved the bearing capacity of concrete. The higher bearing capacity exhibited by the more shallow concrete

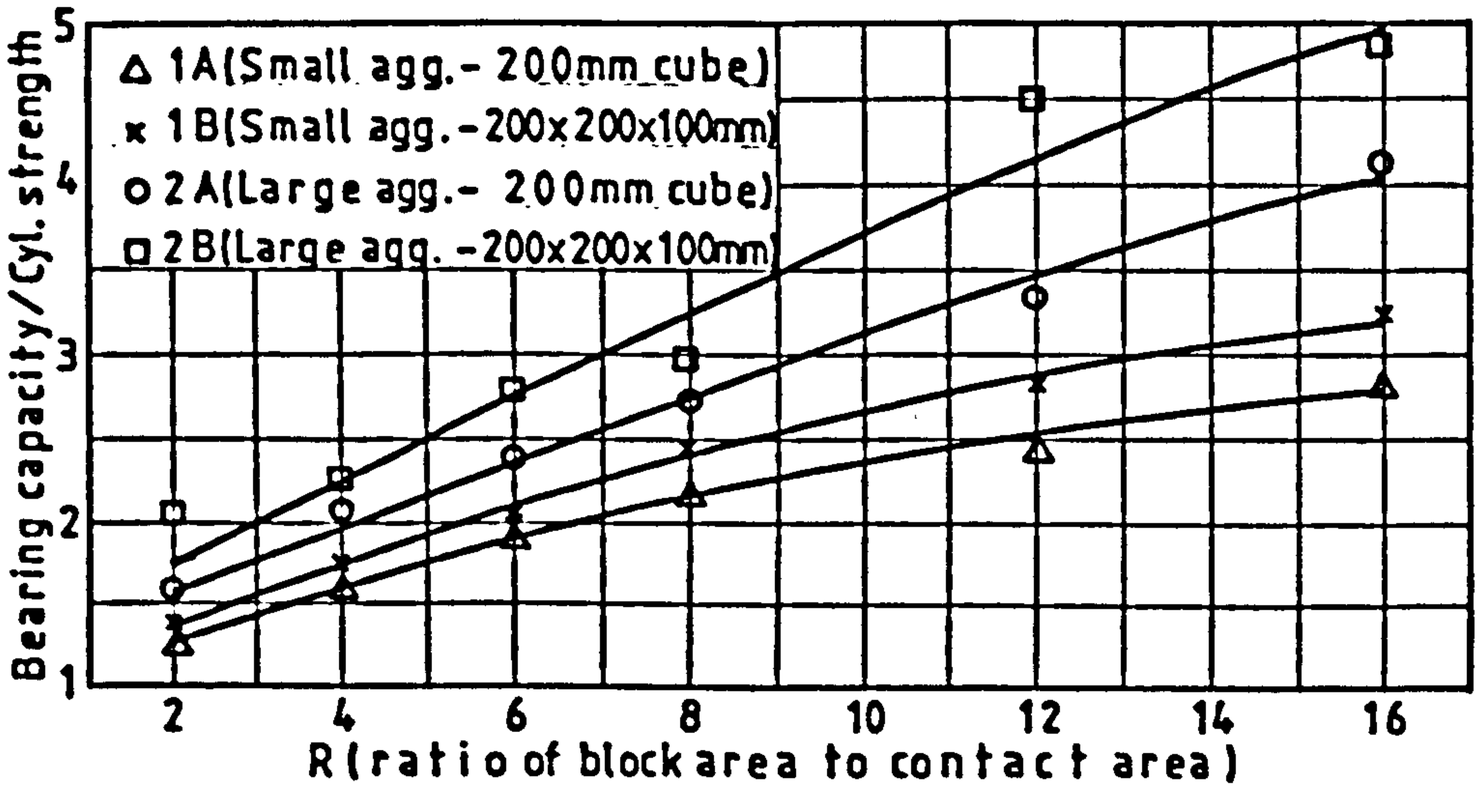

Fig. 8.2 Effect of ratio R̂ and aggregate size on the bearing strength of concrete (Au and Baird, 1960)

blocks was said to arise from the additional restraint provided by friction between the bottom of the block and the support plate.

Muguruma and Okamoto (1965) recognized large differences in the bearing capacity of concrete blocks of different heights under the same concentrated loading condition. The difference was larger for smaller R ratios, higher specimens showing the smaller bearing strength. Specimens with height/breadth ratios from 0.5 to 2.0 were included in the tests. Niyogi (1973) and Hawkins (1970) also reported results in which the bearing strength decreased with increasing height of the specimens, especially at R ratios about 8 or less. Figure 8.3 shows the influence of relative height on the bearing strength of concrete tested under strip bearings as reported by Niyogi (1973).

Hyland and Chen (1970) performed experiments to investigate the effect of base friction. For this, three base conditions were used: a) a steel plate with the intention of providing high base friction, b) a polytetrafluoroethylene film and c) a double punch system, both used

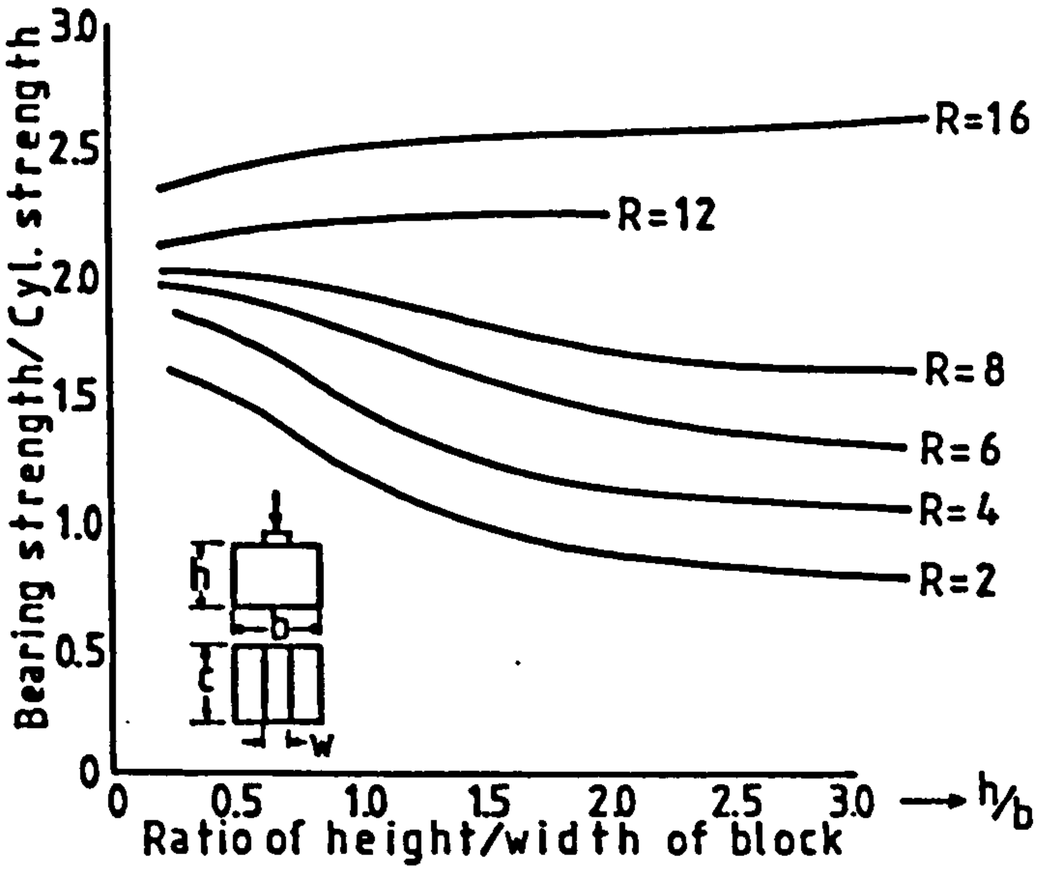

Fig. 8.3 Effect of height of specimen and R ratio on the bearing strength of concrete blocks under strip loading (Niyogi, 1973)

to reduce and eliminate friction respectively. Results from this experimental analysis indicated that friction on the base causes no increase in the bearing capacity. The authors pointed out the difficulty in separating the effect of friction on the base of the concrete blocks from other factors affecting their bearing capacity. The findings of Hyland and Chen contradict the results of other authors previously mentioned.

Hawkins (1968) reported an experimental programme in which some 230 concrete specimens were tested through rigid plates in order to observe the effects of loading geometry, size of specimen and type and strength of concrete on the bearing strength. The majority of the specimens were 150 mm cubes, some of them loaded concentrically and others eccentrically. Figure 8.4 shows the results for two concretes with considerably different strengths, although the aggregate size and type were the same. It can be observed that for a given ratio R, the

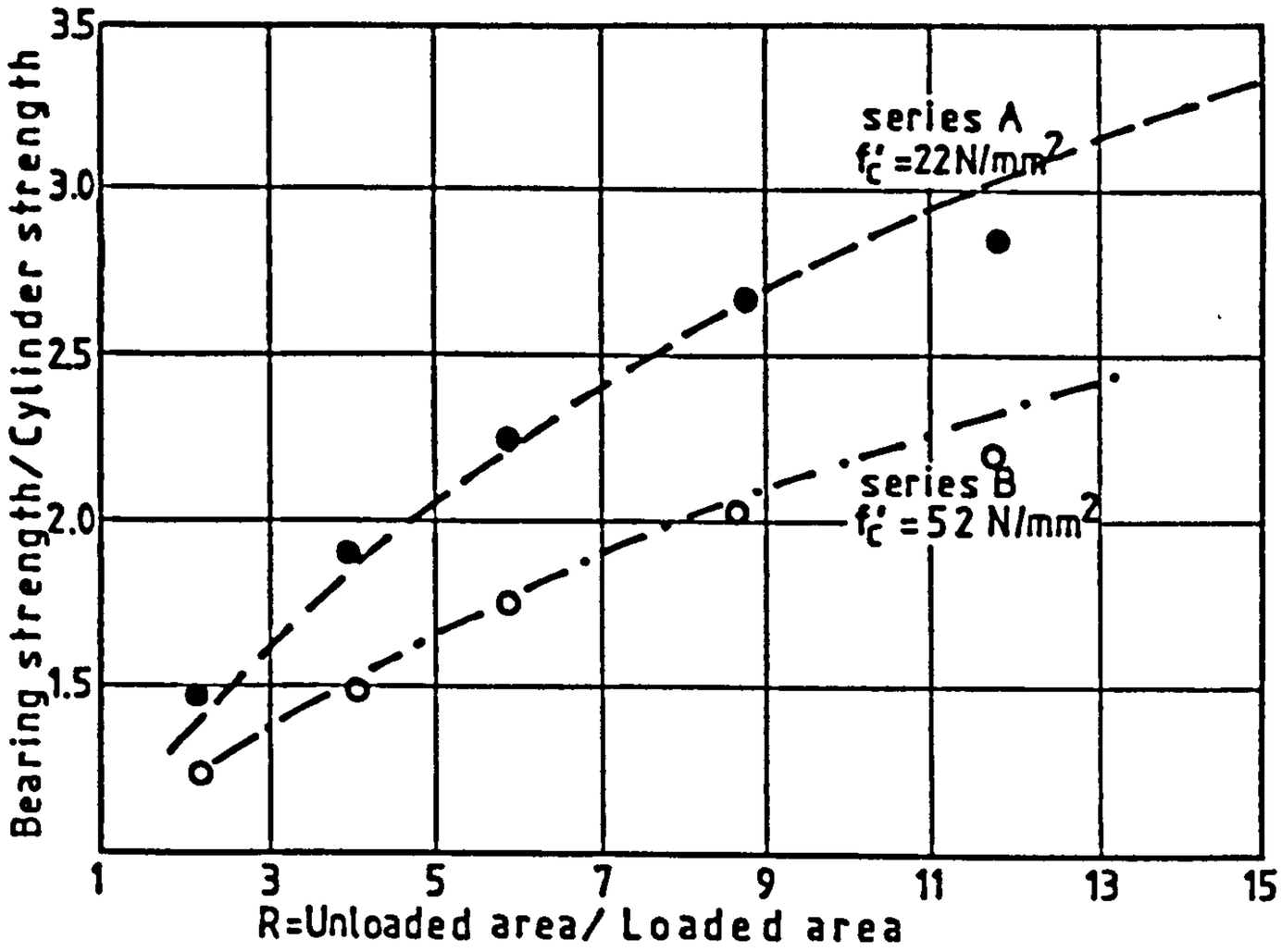

Fig. 8.4 Effect of concrete strength upon bearing capacity (Hawkins, 1968)

higher the strength of the concrete the lower was the resulting ratio of bearing strength to compressive strength, n. Similar conclusions were reached by Niyogi (1974) who found that concrete of richer mixes registered lower n values than leaner mixes.

From the tests on specimens loaded eccentrically, Hawkins (1968) found that bearing strength decreased with the eccentricity of the load and that specimens with smaller loaded areas were affected more than those under larger loaded areas.

The effect of compressible beds onto the bearing strength of concrete blocks loaded concentrically was studied experimentally by Niyogi (1974). Specimens for tests on compressible beds were seated

either on a rubber pad or on sand in a steel box. In general, it was found that specimens tested on yielding beds gave smaller bearing strength ratios, n, compared to specimens on rigid steel beds. The influence of supporting bed on the bearing strength of 200 mm cubes under strip loading is shown in Table 8.1.

Table 8.1 Influence of supporting bed on ratio n for 200 mm cubes under strip loading (Niyogi, 1974)

PLATE SIZE		R	SAND	RUBBER	STEEL
w	b				
25	200	64	7.01	7.14	7.38
33	200	32	4.72	4.61	4.86
50	200	16	2.60	2.47	3.30
100	200	8	1.39	1.49	2.12
200	200	4	0.79	0.83	1.52

Shallow blocks were more affected by the compressible bed than deep blocks. Specimens with a height twice the width were unaffected by the yielding beds. Niyogi explains that the loss in bearing strength due to yielding beds occurred because of a concentration of reaction on the central section of the block at the support surface. This created the effect of the specimen being loaded and supported by two localized loads. Williams (1979) concluded that the type of support does not have any effect on the strength of specimens with a depth to width ratio greater than 1.5.

Kriz and Raths (1963) tested 38 plain concrete specimens with geometry and dimensions as shown in Fig. 8.5. The length of the bearing

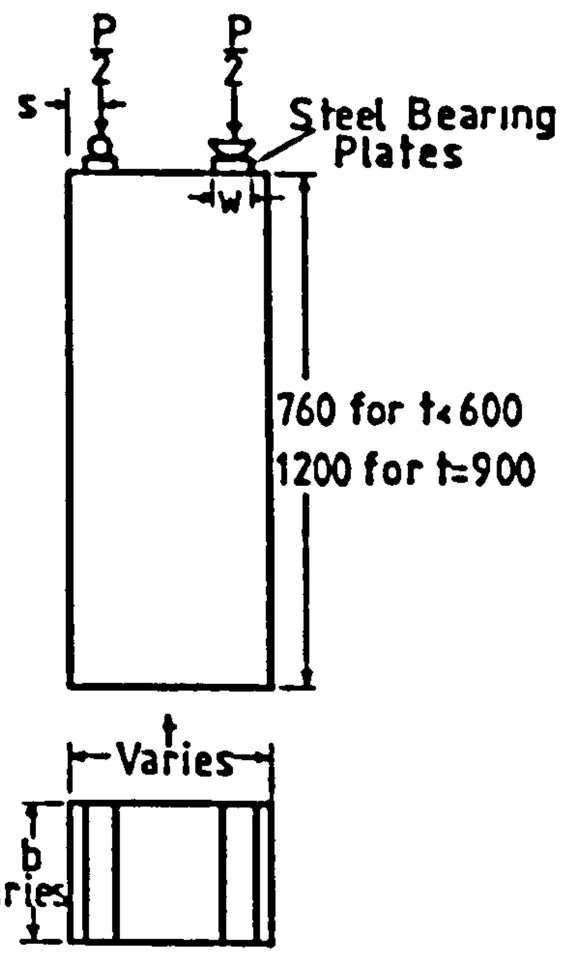

Fig. 8.5 Plain concrete column heads (Kriz and Raths, 1963)

plates was equal to the width, b, for each specimen. It was reported that three modes of failure were observed, depending upon the distance s of the bearing plate from the edge of the specimen (Fig. 8.5). When the distance s was larger than 40 mm, failure was attained by splitting along a vertical plane, forming a wedge under the bearing plate; the second mode of failure was similar to the one explained previously, but the vertical split was intersected by a secondary horizontal fracture of the outer part of the column. The third mode of failure was observed when the distance s was less than 40 mm and consisted of an inclined fracture which intersected the vertical face of the specimen. It was concluded that the bearing strength of the plain concrete specimens tested was not influenced by their dimensions. The following equation was proposed for estimating the bearing strength of plain concrete column heads:

$$f_b = 5.73 \sqrt{f'_c}\ \sqrt[3]{s/w} \qquad 8.1$$

where f_b = bearing strength, N/mm^2

f'_c = cylinder compressive strength, N/mm^2

s = distance from edge of specimen to centre line of bearing plate

w = width of bearing plate

It was demonstrated that experimental bearing strength and the calculated figures from Eq. 8.1 compared well. The average of the

ratio of experimental bearing strength to the estimated values was said to be equal to 1.

Results from the experimental work carried out by Hawkins (1970) have been used to assess the accuracy of the predictions of Eq. 8.1.

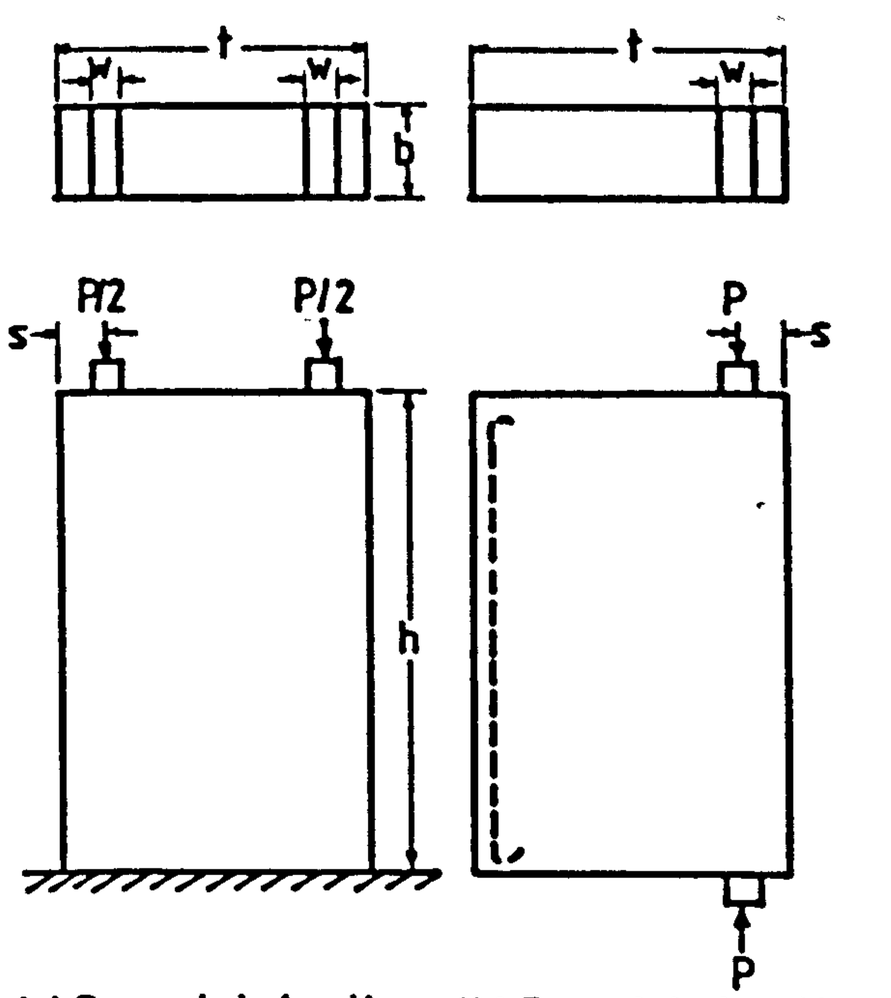

Fig. 8.6 Cross-sectional dimensions for test specimens (Hawkins, 1970)

Figure 8.6 shows the geometrical characteristics and details of the specimens tested by Hawkins and Table 8.2 presents their dimensions. Not all the specimens tested by Hawkins are used in this analysis. Those with reinforcement close to the upper surface and between the loaded points have been omitted to avoid any possibility of using experimental data from specimens which had their bearing strength affected by the proximity of reinforcement.

The ratios in column 11 of Table 8.2 show that Eq. 8.1 predicts reasonably well the ultimate bearing strength of those specimens tested by Hawkins (1970). The average of these ratios is 1.17, showing that in general, the equation underestimates the value by about 17 percent.

The following factors, drawn from this review of work carried out on plain concrete, affect the bearing strength of concrete:

a) Ratio R of footing area to loaded area. This is perhaps the best established factor affecting the bearing strength of concrete; as the ratio R becomes larger, the bearing strength increases,

b) Maximum aggregate size. It has been found that larger aggregate sizes improve the bearing capacity,

Table 8.2 Properties of test specimens and test results from Hawkins (1970)

SPECIMEN No.	SIZE b mm	2T mm	h mm	w mm	s mm	f'_c N/mm^2	P_u kN	f_b test N/mm^2	f_b calc N/mm^2	$\frac{f_b \text{ Test}}{f_b \text{ Calc}}$
D1	152	381	712	19	19	27.9	196	33.9	30.3	1.12
D2	152	381	712	19	38	27.9	254	44.0	38.1	1.15
D3	152	381	712	19	57	27.9	302	52.3	43.6	1.20
D4	152	381	712	19	76	27.9	342	59.2	48.0	1.23
D5	152	381	712	19	95	27.9	369	63.9	51.7	1.23
D6	152	381	712	25.4	19	84.5	441	57.1	47.8	1.19
D7	152	381	712	25.4	38	84.5	628	81.3	60.3	1.35
D8	152	381	712	25.4	57	84.5	672	87.0	69.0	1.26
D9	152	381	712	25.4	76	84.5	730	94.5	75.9	1.24
D10	152	381	712	25.4	95	84.5	752	97.4	81.7	1.19
D20	102	457	1015	25.4	38	48.1	276	53.3	45.5	1.17
D21	102	457	1015	25.4	76	46.8	392	75.7	56.5	1.34
D22	102	457	1015	25.4	127	46.8	490	94.6	67.0	1.41
D23	102	457	1015	25.4	229	35.5	245	47.3	71.0	0.66
D24	102	457	1015	50.8	76	40.9	401	38.7	41.9	0.92
D25	102	457	1015	50.8	38	40.9	401	38.7	33.3	1.16
D26	102	457	762	50.8	38	43.1	401	38.7	34.2	1.13
D27	102	457	635	50.8	38	43.1	401	38.7	34.2	1.13
D28	102	457	508	50.8	38	43.1	445	42.9	34.2	1.25
D29	102	457	381	50.8	38	43.1	468	45.2	34.2	1.32
ECCENTRIC LOADING									AVERAGE =	1.18
C1	102	457	1015	25.4	38	41.6	116	44.8	42.3	1.06
C2	102	457	1015	25.4	76	41.6	147	56.7	53.3	1.07
C3	102	457	1015	25.4	127	43.2	222	85.7	64.4	1.33
C4	102	457	1015	50.8	38	43.2	200	38.6	34.2	1.13
C5	102	457	1015	50.8	76	43.2	231	44.6	43.1	1.03
C6	102	457	1015	50.8	127	43.2	289	55.8	51.1	1.09
									AVERAGE =	1.12

c) Concrete compressive strength. It has been observed that the greater the strength of concrete, the lower the resulting ratio of bearing strength to compressive strength,

d) Eccentricity of the load. Specimens loaded eccentrically showed lower bearing strength,

e) Horizontal component of load. The presence of horizontal forces as components of the load reduces bearing strength,

f) Height/width ratio. Taller specimens gave smaller bearing strengths; this has been associated with friction at the support,

g) Type of bearing bed. The bearing strength was found to be affected by yielding supports. Specimens with height/width ratios greater than 1.5 were unaffected by the type of support.

8.3 BEARING STRENGTH OF REINFORCED CONCRETE

Most of the work published on bearing strength of concrete is based almost entirely on plain concrete specimens and data on the influence of reinforcement is lacking. Here, a summary of the sparse knowledge on the contribution of reinforcement to the bearing strength of concrete is presented.

The experimental work published by Niyogi (1975) provides a general idea of the influence of reinforcement on the bearing capacity of concrete blocks under concentrated load. This experimental programme was carried out on 200 mm concrete cubes reinforced either with spiral steel or reinforcing grid; vertical steel was provided to hold the lateral reinforcement. Eight different types of specimen were used, the variables being the percentage of steel in terms of volume of concrete, the distribution of reinforcement within the depth and breadth of the specimen and type of reinforcement, i.e., spiral or grid reinforcement. In general, it was found that the cracking strength improved with reinforcement, depending on the size of the bearing plate, amount of steel and form of reinforcement. Large spirals with large concrete cores (Fig. 8.7) were the most effective reinforcement against cracking. Reinforcement was less effective against initial cracking when larger bearing plates were used. This is demonstrated in Table 8.3, where the bearing stress ratios at cracking, n_c, are shown for plain and reinforced specimens (Fig. 8.7) which contain 1.0 percent of reinforcement.

Table 8.3 Bearing stress ratio at cracking n_c (Niyogi, 1975)

SPECIMEN	STEEL percent	R 32	16	8
Plain	0	4.67	2.86	1.62
BH	1.0	7.30	3.99	2.45

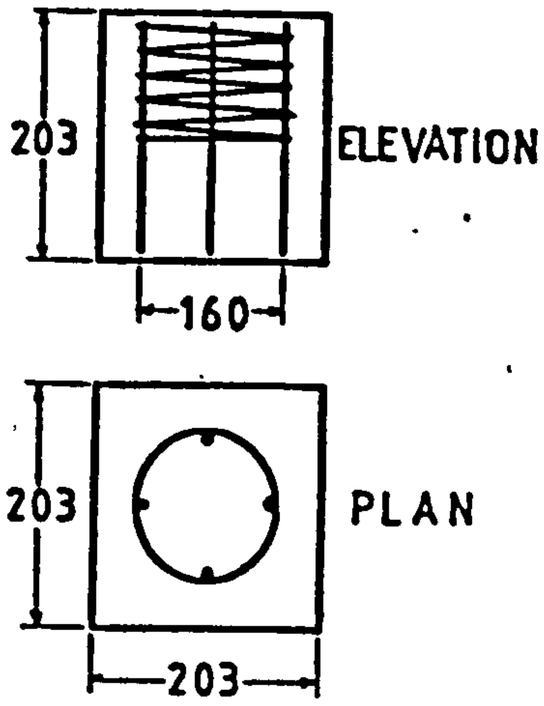

Fig. 8.7 BH type specimens tested by Niyogi, 1975

Among the types of reinforcement tested, single large spirals were the most efficient for ultimate load, giving the highest values of ultimate bearing strength ratio, n, for the same percentage of steel. Also, the reinforcement placed nearer to the loaded surface was more effective than that distributed along the whole depth of the specimen. Table 8.4 presents the ultimate bearing strength ratios (n) for the specimens BH and different R ratios. Note the increasing value of the ultimate bearing strength ratio as the ratio R increases.

Table 8.4 Ultimate bearing strength ratio (Niyogi, 1975)

SPECIMEN	STEEL percent	R 32	16	8
BH	1.0	8.74	5.80	3.55

Muguruma and Okamoto (1965) also found similar results in the test of reinforced concrete cubes. The ultimate bearing capacity increased proportionally to the percentage of reinforcement. Also it

was shown that the use of small diameter circular spiral reinforcement was more effective at increasing the ultimate bearing capacity as well as the first cracking bearing stress. The other type of reinforcement used was rectangular spirals.

Kriz and Raths (1963) tested 185 reinforced concrete column heads, 203 x 305 mm in cross section and 762 mm high. The effect of reinforcement on the bearing capacity of these specimens was analysed and also the reduction of bearing strength by combining horizontal and vertical forces as a means of loading. Figure 8.8 illustrates the types and details of the reinforcement used. The vertical loading was applied as shown in Fig. 8.5 and the method of applying loads with a horizontal component is demonstrated in Fig. 8.9. In the case of large horizontal components of load, an epoxy resin was used to bond the bearing plates to the specimen and prevent slippage.

Two modes of failure were observed in those specimens loaded under vertical loads only. The specimens with the bearing plates close to the edges failed along an inclined plane in a manner similar to that explained previously for unreinforced specimens. When the bearing plates were positioned away from the edges, the specimens failed by crushing of concrete in the bearing zone. It is reported that all the modifications made to the reinforcement had only a small effect on the behaviour of the specimens. The introduction of horizontal forces into the loading reduced the bearing strength of the specimens considerably, compared to those specimens loaded under vertical load only. From the experimental work, Kriz and Raths concluded that the major variables affecting the bearing strength of reinforced concrete columns under strip loading are:

a) concrete compressive strength, b) width of bearing plates, c) distance of bearing plates from column edges, d) amount of lateral

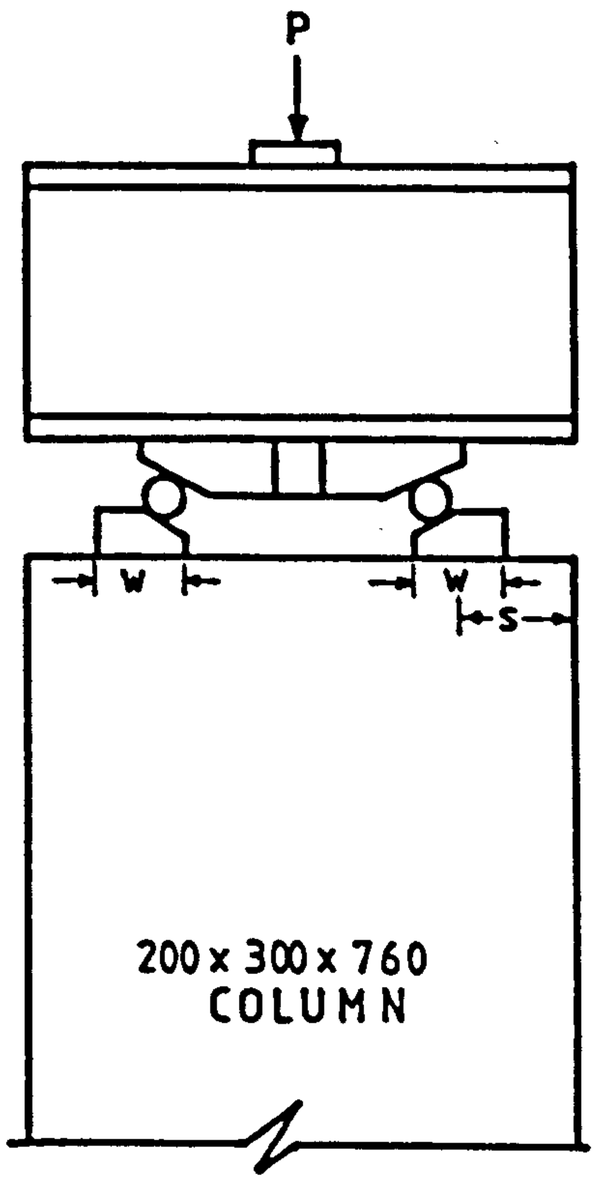

Fig. 8.9 Loading arrangement for combined horizontal and vertical loading (Kriz and Raths, 1963)

reinforcement near the loaded surface and e) the ratio of horizontal to vertical components of the load.

The first three variables were combined in Eq. 8.1 which predicts the bearing strength of plain concrete. The influence of lateral reinforcement was added to Eq. 8.1 and this became:

$$f_b = 5.73 \sqrt{f'_c} \sqrt[3]{s/w} (1 + 0.198 C_1 \sqrt{A_{s1}/b}) \quad / \quad 8.2$$

where A_{s1} = total cross sectional area of the lateral reinforcement, mm^2

b = length of the bearing plate, mm

C_1 = 0 for $s < 40$ mm

C_1 = 2.5 for $s \geq 40$ mm

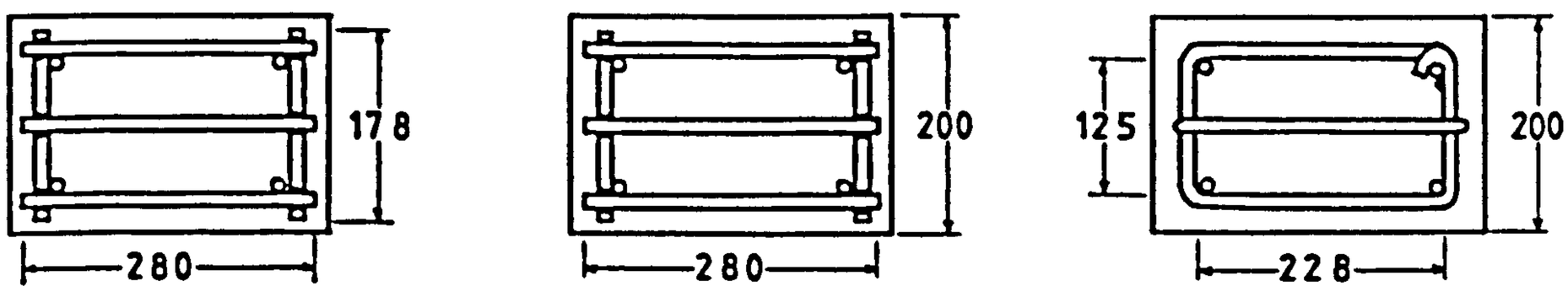

Fig. 8.8 Reinforced concrete column heads tested by Kriz and Raths (1963) a) Group I, welded lateral reinforcement, b) Group V, welded lateral reinforcement in layers, c) Group VI, bent lateral reinforcement, d) Group VII, lateral reinforcement welded to plates, e) Group VIII, lateral reinforcement welded to plates.

On the right hand side of Eq. 8.2 the term in brackets caters for the increase in bearing strength due to lateral reinforcement.

Kriz and Raths compared the prediction of Eq. 8.2 to the experimental results from 54 reinforced concrete column heads tested with vertical load only. They reported that the average ratio of the ultimate bearing strength to the predicted strength of Eq. 8.2 resulted in a value of 1.02 and a standard deviation of 0.17 which demonstrates the validity of Eq. 8.2 for predicting the bearing strength of these particular specimens.

To include the reduction in bearing strength due to the outward horizontal component of the load, the factor $(sw/51613)^{H/V}$ was introduced in Eq. 8.2 producing the final equation below:

$$f_b = 5.73 \sqrt{f'_c} \sqrt[3]{s/w} (1 + 0.198 C_1 \sqrt{A_{s1}/b})(sw/51613)^{H/V} \qquad 8.3$$

where H/V = ratio of horizontal and vertical components of applied load,

and sw should not exceed 5800 mm^2.

Comparison of predictions of Eq. 8.3 to results from 37 specimens tested by Kriz and Raths under loads with ratio H/V = 0.25 gave a factor of 1.20 for the average ratio of experimental bearing strength to calculated bearing strength and a standard deviation of 0.27. For 43 specimens tested by the same authors under H/V = 0.5, they found an average ratio of 1.33 for the experimental results to the calculated values and a standard deviation of 0.47. For 4 specimens tested under H/V = 0.75 the average ratio of test to predicted bearing strength was 1.70. From these results, it is clear that the reduction factor incorporated in Eq. 8.3 to consider the effect of outward horizontal forces becomes more conservative as the ratio H/V increases.

8.4 EXISTING RECOMMENDATIONS FOR BEARING STRENGTH

8.4.1 CP110 (1972)

In the rules for precast concrete construction, this document stipulates that the compressive stresses in the contact area should not exceed 0.4 f_{cu} under ultimate loads. Higher stresses, up to 0.8 f_{cu}, are allowed, if some measures are taken, such as providing binding reinforcement to prevent splitting or spalling. Although this measure is mentioned, a specific procedure for designing such additional reinforcement is absent. Stresses in excess of 0.8 f_{cu} are allowed only in cases justified by testing of prototype units.

In the rules for wall design, this code limits the bearing stresses to 0.6 f_{cu} for concrete grade 25 or more. For other concrete grades, the stresses are limited to 0.5 f_{cu}.

8.4.2 ACI-318-77

This document mandates that the bearing stress in concrete shall be controlled by the following equation

$$f_b < \phi(0.85\ f'_c) \qquad 8.4$$

where ϕ = strength reduction factor

= 0.7 for normally reinforced compression members

= 0.75 for spirally reinforced compression members

f'_c = cylinder compressive strength, psi

For cases in which the supporting surface is wider on all sides than the loaded area, such as footings, the maximum allowable bearing stress could be calculated as

$$f_b < \phi\,(0.85\ f'_c)\ \sqrt{A_2/A_1} \qquad 8.5$$

where A_1 = loaded area

A_2 = maximum area of the portion of the supporting surface that is geometrically similar to and

concentric with the loaded area.

In Eq. 8.5 the factor $\sqrt{A_2/A_1}$ should not exceed 2.

The recommendation for design given by ACI-318-77 includes the widely known effect of the confining pressure developed around the loaded area when the ratio R is larger than 1. No other allowances are made, for example, for the confining effect of reinforcement.

8.4.3 CIRIA Guide 2 (1977)

This document recommends the use of a maximum bearing stress of 0.4 f_{cu} at supports. This limit might be exceeded up to 0.8 f_{cu} at internal supports and up to 0.6 f_{cu} at external supports provided that the bearing zone is confined adequately. Reinforcement stressed at 0.87 f_y can produce this confinement. The area of reinforcement necessary can be calculated from a load approximately equal to 1/6 of the support reaction and distributed over a depth equal to the width of the member. If the stress above that depth is larger than 0.4 f_{cu}, the same percentage of reinforcement should be supplied up to the height at which that limit is not exceeded.

In these rules, the consideration of reinforcement as a means of increasing the bearing strength of concrete represents a considerable improvement in the design of reinforced concrete. Also, the recognition of larger bearing capacity of supports away from the ends of the deep beams is in accordance with the experimental results previously observed. These measures obviously permit a more rational use of materials.

8.5 ANALYSIS OF EXPERIMENTAL RESULTS

Of the 24 specimens tested during this experimental work, 11 failed due to local bearing destruction. Table 8.5 presents the data

concerning the failure load and ultimate bearing stresses. Although it did not show a final bearing failure, specimen W3-L2 is included in this table. Figure 4.12 illustrates that the damage caused to it at the maximum load applied was severe and it was close to failure either by crushing of the supports or by additional deterioration of the mid-span area. The cracks shown by specimen W3-L2 in the area of the supports were consistent with those shown by other specimens prior to a prompt bearing failure. Column 7 of Table 8.5 presents the ratio n of the

Table 8.5 Data concerning specimens which failed due to local bearing destruction

1 SPECIMEN	2 FAILURE LOAD kN	3 SUPPORT AREA mm^2	4 ULTIMATE STRESS N/mm^2	5 f_{cu} N/mm^2	6 f_{cf} N/mm^2	7 $\frac{f_{bu}}{f_{cf}}$
DEEP PANELS						
DB2	900	7200	62.5	53.0	53.0	1.18
DB3	950	7200	66.0	49.3	49.3	1.34
DB4	800	7200	55.6	48.0	48.0	1.16
DB5	940	7200	65.3	49.4	49.4	1.32
DB6	950	7200	66.0	51.6	51.6	1.28
					AVERAGE =	1.26
WALL BEAMS						
W1-L1	1100	10080	54.6	41.7	25.0	2.18
W2-L1	1100	10080	54.6	45.3	27.2	2.01
W3-L1	1300	10080	64.5	50.3	30.2	2.14
					AVERAGE =	2.11
W3-L4	1200	10080	59.5	48.6	29.2	2.04
W3-L3	940	10080	46.6	43.6	26.2	1.78
W3-L5	800	10080	39.7	48.9	29.3	1.35
W3-L2	500	10080	24.8	44.9	26.9	0.92

ultimate stress on the contact area of the support to the/cube strength of concrete. The average of this ratio for the deep panels was 1.26 and for the wall specimens loaded on top, it rose to 2.11. It is obvious that an improvement in the bearing capacity of the wall specimens occurred. This increased bearing strength of specimens W loaded directly on top can be attributed to three main factors: 1) the bearing zone in the walls enjoyed some extra degree of confinement, due

to the presence of nibs cast at that level; 2) the amount of main reinforcement in these elements was larger than in the deep panels, allowing additional distribution of the forces in the bearing area and controlling the development of cracks; 3) the steel bearing blocks of the walls had 8 vertical deformed bars welded (8Y12) to them. These bars were 150 mm long and provided 10 percent of reinforcement in the bearing contact area. This is the maximum percentage of steel allowed by CP110, clause 3.11.5 (where bars overlap) in columns. During construction of the cages, it was felt that the efficiency of the vertical steel could have been greatly improved if there had been room to place horizontal stirrups to prevent outward movement. Also, the procedure adopted for assembling the formwork for casting prevented the desired strengthening of the reinforcement around the bearing zone. This concern was later justified during testing, when the specimens failed by crushing of the bearing area and buckling of the vertical reinforcement was observed.

The variation of the ratio n for specimens DB was not significant. It demonstrates that the effect of depth on the bearing strength of these elements was negligible. In the specimens W, under load on top, the ratio n did not show any substantial variation which could be associated with the different amounts of vertical reinforcement in the webs.

Large variation of the ratio n is shown by the specimens of group W3. From the values of column 7 of Table 8.5, the type of loading, i.e., the ratio of top to bottom load can be seen to largely influence the bearing strength. The ratio n for specimen W3-L1 (under top load only) has a value of 2.14 and this decreases to about 0.92 in specimen W3-L2 (under bottom load only). Figure 8.10 compares the ratio n to the ratio of the top load to total load. The first section of the

curve, joining the ratios n for W3-L2 and W3-L5 is presented in the form of a dashed line due to the uncertainty of the final value of n for specimen W3-L2. The true value may have been slightly higher than indicated.

Although the number of tests from this experimental work is not sufficient to substantiate a complete and general formulation with respect to the effect of type of loading on wall-beams, the results obtained are enough to indicate categorically that the combination of top and hanging load reduces the bearing strength of these elements. This loss in bearing strength is proportional to the amount of hanging load.

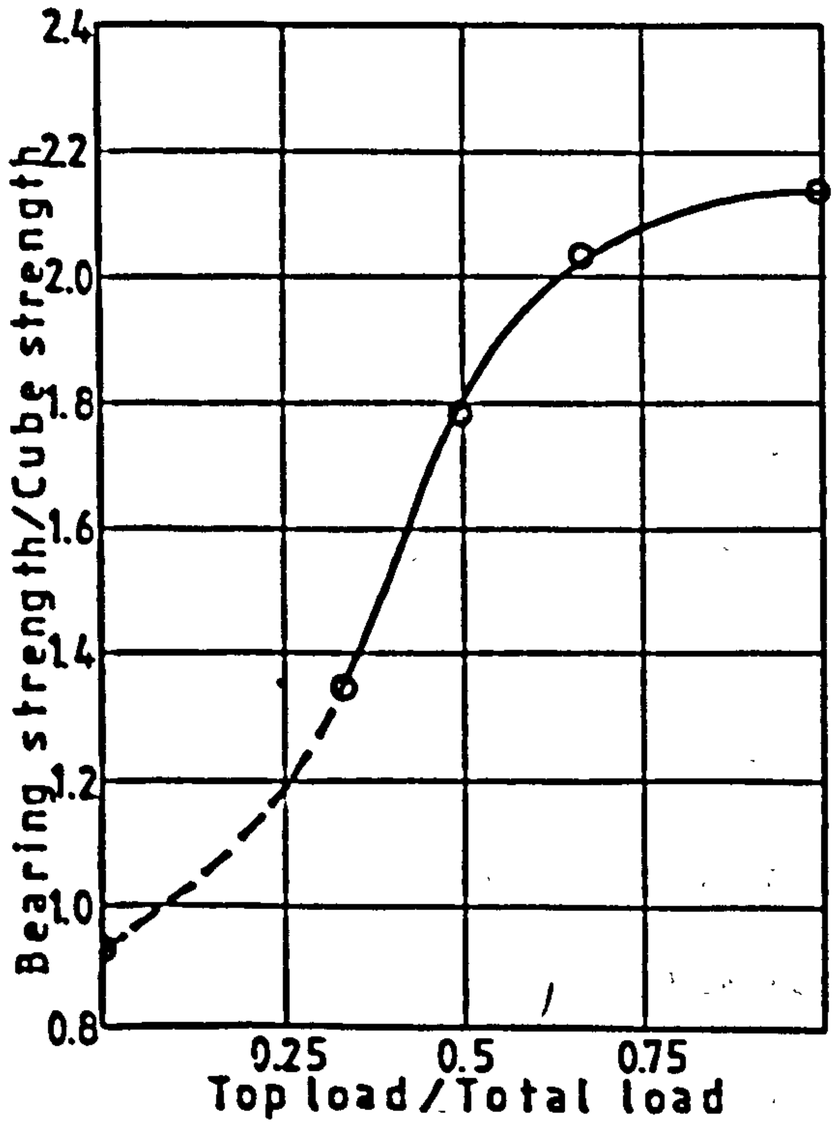

Fig. 8.10 Effect of hanging load on bearing strength of wall-beams

The curve shown in Figure 8.10 can be approximately represented by the following equation:

$$f_{bu}/f_{cu} = 0.92 + (7.0 - 5.83\ K_1)\ K_1^{2.333} \qquad 8.6$$

where f_{bu} = tested ultimate bearing strength

f_{cu} = ultimate cube strength of concrete

$K_1 = P_t/(P_t + P_b)$

where P_t = load applied on the top level

P_b = load applied on the bottom

With loads applied on the soffit, the loss in strength can be attributed to the larger horizontal tensile stresses developed in the region above the bearing area. The arch action resulting in deep beams imposes tensile forces on the face of the bearing area because of the tie created by the main reinforcement, as shown schematically in Figure 8.11. As well as the tensile force generated by the arch mechanism, additonal tensile stresses arise in the bearing area when loads are applied at the soffit of wall beams. In section 7.3 it was observed that the area of wall under direct tension cracked first and that the region underneath the cracks behaves somewhat like a shallow beam with fixed ends. As this shallow beam deflects under the effect of loads, tensile stresses above the bearing area increase because of the negative moment generated at the fixed ends, producing cracks on the face of the supports. This is shown schematically in Fig 8.12.

These cracks reduce the stability and degree of confinement of the "struts" carrying the compressive forces to the supports. Even if the tensile stresses developed in the bearing zone are not high enough to create cracks, the bearing strength is reduced, since the concrete in this region is subjected to a compression-tension biaxial stress system. When the load is directly applied on top of the wall, the tensile force acting on the concrete bearing zone corresponds to that brought about by the reinforcement forming part of the arch-tie mechanism only. Although it has a detrimental effect on the bearing strength of the deep

beam, it is not as damaging as the additional tensile stresses developed from forces acting on the soffit.

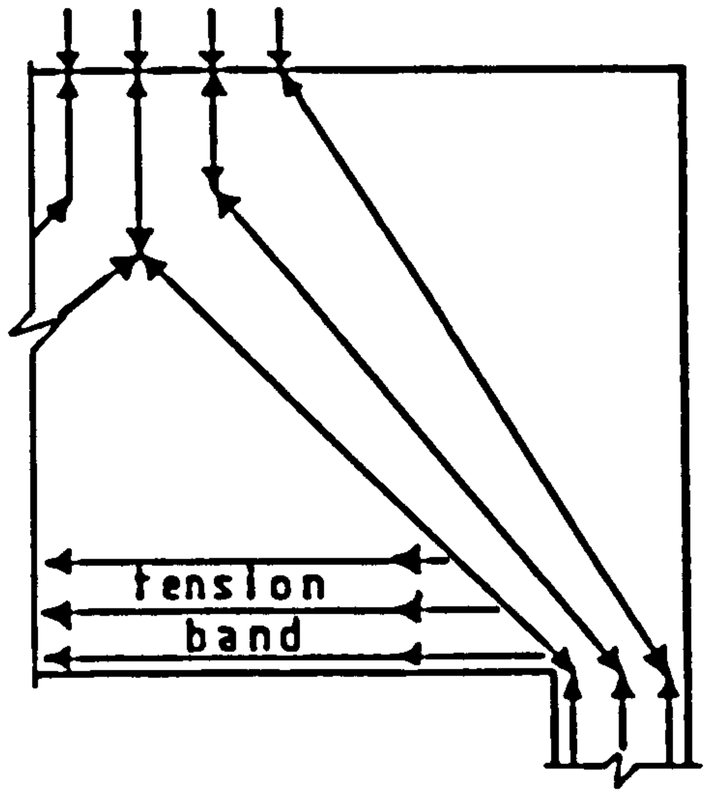

Fig. 8.11 Stress pattern due to the arch mechanism developed in deep beams

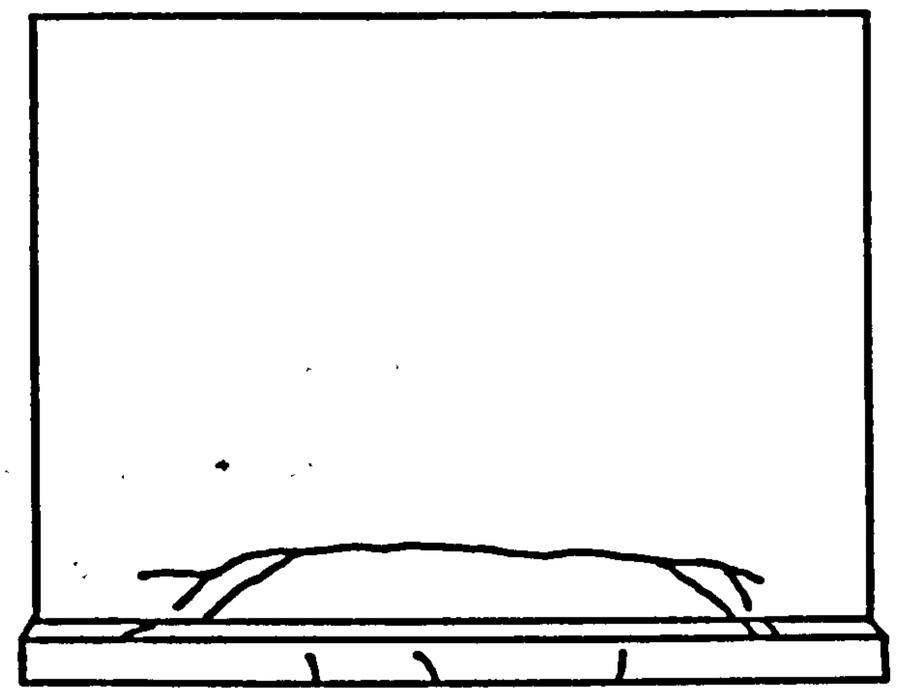

Fig. 8.12 Crack pattern of deep beams loaded at the soffit

Table 8.6 Comparison of experimental failure loads, permissible values from CIRIA (1977) and ACI-318-77, and ultimate strengths from Kriz and Raths (1963).

1	2	3	4	5	6	7	8
SPECIMEN	FAILURE LOAD kN	CIRIA kN	$\frac{2}{3}$	ACI kN	$\frac{2}{5}$	KRIZ AND RATHS kN	$\frac{2}{7}$
DEEP PANELS							
DB2	900	305.3	2.95	360.0	2.50	997.9	0.90
DB3	950	284.0	3.35	337.0	2.82	961.9	0.99
DB4	800	276.5	2.89	328.3	2.44	949.0	0.84
DB5	940	284.5	3.30	338.4	2.78	963.4	0.98
DB6	950	297.2	3.20	354.2	2.68	985.0	0.96
AVERAGE			3.14		2.64		0.93
WALL SPECIMENS							
W1-L1	1100	302.4	3.64	339.9	4.59	1024.1	1.07
W1-L1	1100	329.0	3.34	261.5	4.21	1068.5	1.03
W3-L1	1300	365.3	3.56	290.3	4.48	1129.0	1.15
AVERAGE			3.51		4.43		1.08

Table 8.6 gives the permisible bearing loads as calculated by the CIRIA rules, the ACI-318-77, the model from Kriz and Raths (1963) and the ultimate bearing strength registered during tests. Predicted CIRIA values for the deep panels were calculated on the basis of 0.4 f_{cu} and 0.6 f_{cu} for the wall specimens, since additional confinement was provided by the nibs and the transverse reinforcement. In column 4 it can be observed that the average ultimate load from the tested deep panels is 3.14 times the average permissible strength calculated by the CIRIA rules. For the wall specimens, this ratio increases to an average of 3.51. Column 6 of Table 8.6 shows that the average ratio of experimental ultimate load to permissible ACI load is 2.64 for the DB specimens and 4.43 for the walls. Both the CIRIA and ACI prediction provide a large safety factor against failure and this safety margin is increased for the walls.

Values for ultimate bearing strength from Kriz and Raths are presented in column 7. For the deep panels, the average ratio of the ultimate load to the predicted figure from Eq. 8.2 was 0.93, as shown in column 8 and 1.08 for the W specimens. Obviously, this model overestimates the ultimate bearing strength capacity of the deep panels and underestimates the strength of the walls. The underestimated values for the W specimens are consistent with the earlier discussion in relation to the improved confinement provided to the bearing area by the nibs.

Since the model proposed by Kriz and Raths was developed empirically from tests on column heads, it does not include the loss of bearing strength due to the tensile force transmited to the supports by the main reinforcement in a deep flexural member. This appears to be the main reason for the overestimation of the bearing capacity of the deep panels by Eq. 8.2. Tensile forces acting at the bottom of a

simply supported deep beam are proportional to the bending moment to which it is submitted and hence to the shear span. Based on the data of this experimental programme, a regression analysis has produced the expression $(1-x_s/3430)$ as a reduction factor for Eq. 8.2, which therefore becomes

$$f_b = 5.73\sqrt{f'_c}\ \sqrt[3]{s/w}(1+0.198C_1\ \sqrt{A_{s1}/b})\ (1-x_s/3430) \qquad 8.7$$

where x_s = shear span.

The ratio of the average bearing strength of the deep panels included in Table 8.6 to the calculated figures from Eq. 8.7 is equal to 1.00. This ratio for the wall specimens increased to 1.17.

In practice, Eq. 8.7 can be simplified to

$$f_b = 5\sqrt{f_{cu}}\ \sqrt[3]{s/w}(1+0.2C_1\sqrt{A_{s1}/b})(1-x_s/3400) \qquad 8.8$$

In Eq. 8.8 the concrete cube strength (f_{cu}) is used instead of the cylinder strength (f'_c).

8.6 ANALYSIS OF RESULTS FROM OTHER AUTHORS

Data extracted from the literature available on deep flexural concrete members is compared here with the predictions of Eqs. 8.2 and 8.7. Only those elements which clearly showed local bearing failure were selected for this analysis.

Robins (1971) conducted on extensive analysis of deep beams, with the purpose of studying the effectiveness of different types of web reinforcement. Table 8.7 presents data on some elements which failed by crushing of the concrete at the supports or at the top loaded points. Column 6 of this table gives the ratios m of the experimental values to the estimated values of bearing strength obtained using Eq. 8.2. The average ratio m for specimens which failed at the supports is 0.86 while for those failing at the top loaded points is 1.03. This difference of both ratios corroborates further the negative

Table 8.7 Data from Robins (1971). Comparison with equations 8.2 and 8.7.

1	2	3	4	5	6	7	8
SPECIMEN	FAILURE LOAD kN	f'_c N/mm^2	f_{bu} N/mm^2	Eq.8.2 N/mm^2	m 4/5	Eq. 8.7 N/mm^2	m 4/7
N2-30	498	19.2	42.9	47.1	0.91	43.6	0.98
N8-30	559	23.2	48.1	51.8	0.93	48.0	1.00
N7-30A	505	25.1	43.5	53.9	0.81	49.9	0.87
N7-30C	518	25.1	44.6	53.9	0.83	49.9	0.89
N5-25	416	19.2	35.8	47.1	0.76	43.6	0.82
N8-25	540	23.8	46.5	52.5	0.89	48.6	0.96
AVERAGE					0.86		0.92
FAILURE AT THE TOP							
N3-30	552	22.5	47.5	51.0	1.07	51.0	1.07
N6-30	615	26.1	53.0	55.0	1.11	55.0	1.11
N3-25	450	20.9	38.8	49.2	0.91	49.2	0.91
AVERAGE					1.03		1.03

effect of the tensile forces on the bearing strength of the supports. Column 8 presents the ratios m for results derived using Eq. 8.7. Note that in the case of specimens failing at the supports the ratio m increased to 0.92, while for those failing at the loaded points it remained unchanged, since the top of the member is in compression and the reduction factor is not applied.

Table 8.8 presents results provided by Kong et al (1972) in which the effect of different amounts of inclined web reinforcement was studied. The ratios m for the ultimate bearing stress to the estimated stress from Eq. 8.2 are given in column 6. From these a mean ratio equal to 0.90 was deduced. Column 8 presents the ratios m obtained in conjunction with Eq. 8.7; here the mean value increased to 0.97, demonstrating an improved correlation.

Table 8.8 Data from Kong et al (1972). Comparison with equations 8.2 and 8.7

1	2	3	4	5	6	7	8
SPECIMEN	FAILURE LOAD kN	f'_c N/mm^2	f_{bu} N/mm^2	Eq. 8.2 N/mm^2	m 4/5	Eq. 8.7 N/mm^2	m 4/7
S-30	575.6	22.2	49.6	52.9	0.94	49.0	1.01
S-25	562.9	21.3	48.5	51.9	0.93	48.0	1.01
D-30	557.0	23.1	48.0	54.1	0.89	50.1	0.95
D-25	538.4	23.8	46.4	54.8	0.85	50.7	0.92
AVERAGE					0.90		0.97

A series of reinforced concrete blocks loaded concentrically were tested by Al-Najjim (1981). Details of reinforcement and geometry are shown in Figs. 8.13(a) and 8.13(b). Table 8.9 presents results from 20 of these specimens and compares the ultimate bearing stress sustained under load to the calculated values from Eq. 8.2. All the specimens experienced local bearing failure. Column 7 gives the ratio m of the experimental to the estimated bearing strength values. The average of the ratio m was calculated as 0.97, which proves the accuracy of Eq. 8.2 at predicting the bearing capacity of concentrically loaded reinforced concrete blocks.

Figures 8.13(c) and 8.13(d) illustrate the geometrical details and pattern of reinforcement for the cross-blocks tested by Al-Najjim. In these tests the variable was the amount of vertical reinforcement joining both blocks. Details of the amount of vertical reinforcement and ultimate load are given in Table 8.10. Column 8 provides the ratio of ultimate bearing stress to the concrete cube compressive strength. This ratio increases from 1.69 for specimen F/1 with 2 percent of reinforcement to 2.0 for specimen F/3 with 8 percent. Column 9 discloses the values of bearing strength calculated by Eq. 8.2. The

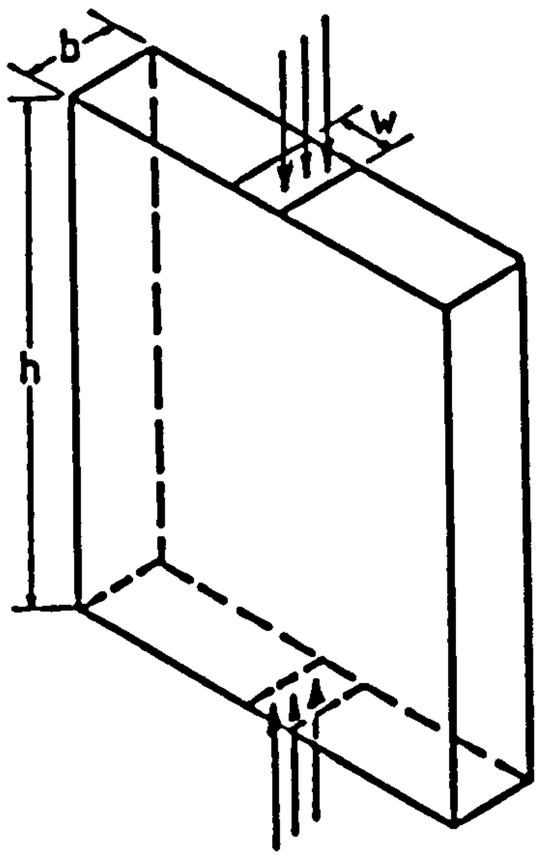

(a)

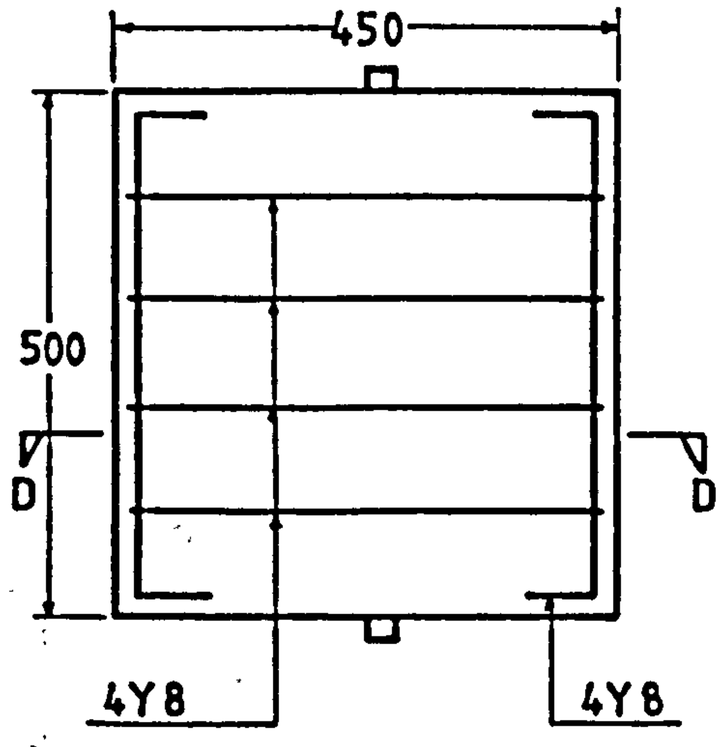

(b)

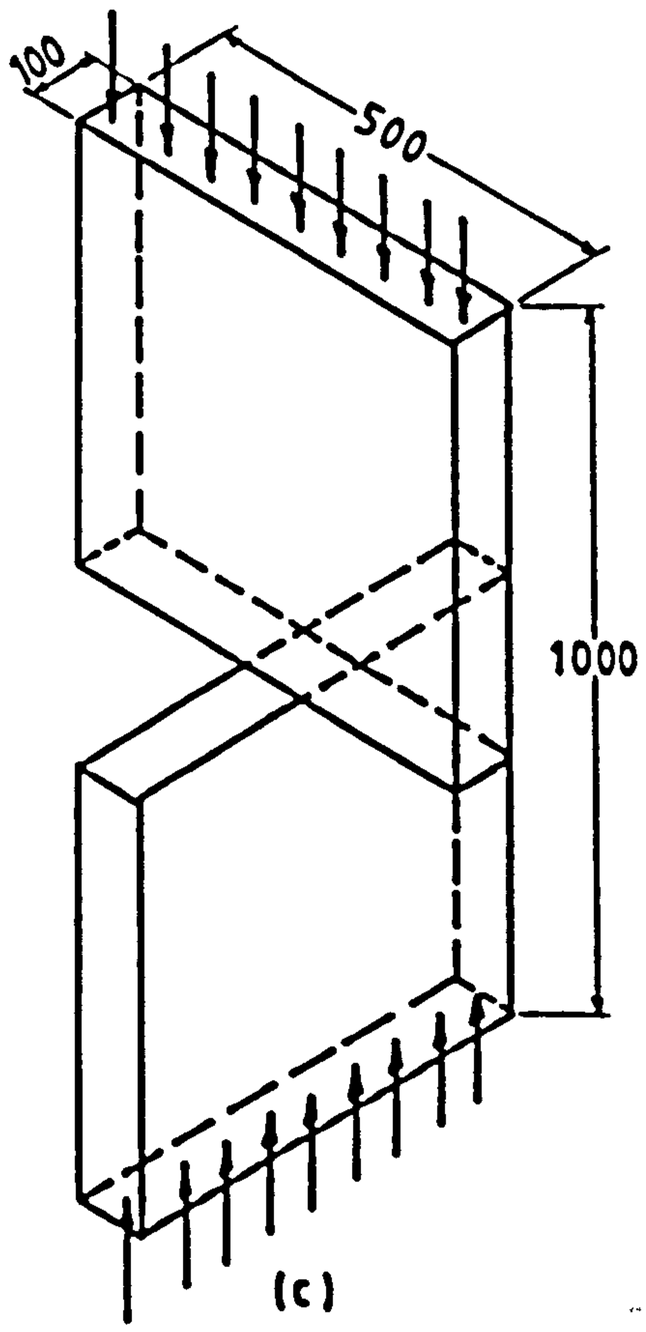

(c)

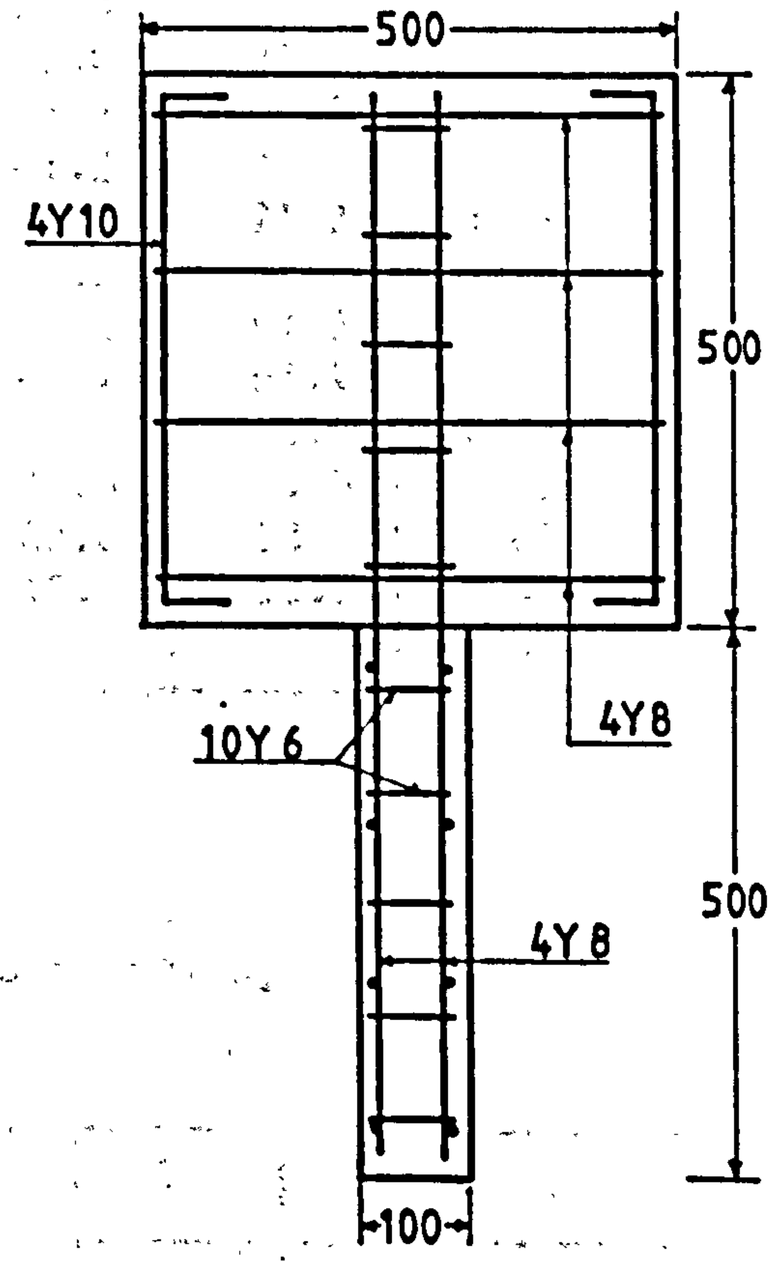

(d)

Fig. 8.13 Geometrical and reinforcement details of specimens tested by Al-Najjim (1981). a) Isometric view of blocks A-E, b) typical reinforcement of blocks A-E, c) isometric view of cross-blocks, and d) typical reinforcement of cross-blocks specimens.

Table 8.9 Data from Al-Najjim (1981). Rectangular blocks loaded concentrically.

1	2	3	4	5	6	7
SPECIMEN	FAILURE LOAD kN	f_{cu} N/mm^2	f'_c N/mm^2	f_{bu} N/mm^2	Eq.8.2 N/mm^2	m 5/6
A/1	120	51.5	41.2	120.0	111.0	1.08
A/2	250	55.0	44.0	125.0	124.9	1.00
A/3	393	57.0	45.6	131.0	128.7	1.02
A/4	569	63.6	50.9	142.3	157.2	0.91
B/1	200	51.5	41.2	100.0	88.9	1.12
B/2	410	55.0	44.0	102.5	98.0	1.05
B/3	555	57.0	45.6	92.5	108.1	0.86
B/4	922	63.6	50.9	115.3	115.9	0.99
C/1	190	51.5	41.2	63.3	83.1	0.76
C/2	600	55.0	44.0	100.0	95.8	1.04
C/3	700	63.6	50.9	77.8	103.9	0.75
C/4	1214	63.6	50.9	101.2	102.5	0.99
D/1	275	51.5	41.2	68.8	74.2	0.93
D/2	650	55.0	44.0	81.3	89.7	0.91
D/3	766	63.6	50.9	63.8	97.3	0.66
D/4	1426	63.6	50.9	89.1	95.1	0.94
E/1	64	31.0	24.8	64.0	58.9	1.09
E/2	141	31.0	24.8	70.5	54.0	1.31
E/3	248	31.0	24.8	62.0	58.9	1.05
E/4	385	31.0	24.8	48.1	53.2	0.90
AVERAGE						0.97

Table 8.10 Data from Al-Najjim (1981). Cross-block specimens.

1	2	3	4	5	6	7	8	9	10
SPEC.	FAILURE LOAD kN	f_{cu} N/mm^2	f'_c N/mm^2	REINF.	REINF. %	f_{bu} N/mm^2	n 7/3	Eq.8.2 N/mm^2	m 7/9
F/1	600	35.6	28.5	4Y8	2.0	60.0	1.69	57.7	1.04
F/2	700	35.6	28.5	4Y12	4.5	70.0	1.97	57.7	1.21
F/3	1000	50.0	40.0	4Y16	8.0	100.0	2.00	68.5	1.46

ratios of the experimental bearing strength to the values calculated by Eq.8.2 are given in column 10. These ratios demonstrate that for a low percentage of vertical reinforcement, Eq. 8.2 predicts fairly accurately the ultimate bearing strength of these blocks. As the percentage of vertical reinforcement increases, the bearing strength becomes larger but Eq. 8.2 does not cater for this, therefore, the ratio m deviates from unity.

8.7 CONCLUSIONS

1. From the experimental results, it is concluded that the variation in depth of the specimens tested did not affect their bearing strength.

2. Top and bottom load combinations have a considerable influence on the bearing strength. Hanging loads reduced the bearing capacity of the specimens. For the elements tested, Eq. 8.6 approximately gives the bearing strength as a function of the top and bottom loads.

3. The equations proposed by Kriz and Raths (1963) are fairly accurate at predicting the ultimate bearing strength of concentrically loaded unreinforced and reinforced concrete specimens under strip load. This accuracy decreased when used for calculating the bearing strength of deep beams.

4. It has been shown that the Kriz and Raths equations together with a reduction factor as follows

$$f_b = 5.73\sqrt{f'_c}\,\sqrt[3]{s/w}(1+0.198C_1\sqrt{A_{s1}/b})(1-x_s/3430)$$

can be used for deriving the bearing strength of deep flexural elements directly loaded on top. This factor takes into account the losses due to the in-plane tensile forces to which the bearing zones are submitted.

5. For practical purposes the equation stated in point 4 can be simplified to

$$f_b = 5.00\sqrt{f_{cu}}\,\sqrt[3]{s/w}(1+0.2C_1\sqrt{A_{s1}/b})(1-x_s/3400)$$

in which the concrete cube strength (f_{cu}) is used.

CHAPTER 9

CONCLUSIONS AND SUGGESTIONS FOR FURTHER RESEARCH

9.1 BEHAVIOUR OF DEEP PANELS WITH DEPTH/SPAN RATIOS LARGER THAN 1

9.1.1 Diagonal cracking load

The CIRIA Guide 2 (1977) limits the shear strength of deep beams to that calculated within an active height equal to the span. Results from this research contradict this limitation. It has been shown that the load at which diagonal cracks occurred became larger as the depth/span ratio increased from 1 to 3. Thereafter, it appears that the diagonal cracking load was unaffected by the height of the panel. For a specimen with depth equal to span, the cracking load was predicted accurately using equation 7.16 recommended by CIRIA Guide 2:

$$V/bH_a < \lambda_1(1-0.35\ x_e/h_a)\ \sqrt{f_{cu}} + \lambda_2\ \Sigma 100A_i y_i\ \sin^2\theta_i/bh_a^2$$

where V = shear strength of the section, N.

The shear strength for specimens with height/span larger than 1 approximately corresponded to that of equation 5.2:

$$V_{cr} = V + (H/L - 1)\ 75000$$

where V_{cr} = shear strength of section, corresponding to the diagonal cracking strength, N,

and V is calculated using Eq. 7.16 and (H/L - 1) should not exceed 2.

9.1.2 Modes of failure

The specimen with depth equal to span failed in shear with a diagonal fracture joining the loaded and supported points. Specimens with depth/span ratios larger than 1 failed by crushing of the bearing blocks. This was the most common mode of failure among these members and was exhibited by panels with depth/span ratios between 1.5 and 3.5.

9.1.3 Horizontal (out-of-plane) displacement

By measuring the horizontal displacements, it was intended to detect deformation or buckling of the panels in a vertical axis and to make sure that the supports and loading mechanisms did not permit a substantial horizontal translation of the specimens under test. This was successfully achieved.

No detectable bending took place in specimens with depth/thickness ratios from 10 to 25. At a depth/thickness ratio of 30 or higher, the phenomenon of buckling can occur although this mode of failure was not attained effectively until a depth/thickness ratio of 40 was reached.

9.1.4 Comparison of experimental stresses with numerical elastic results

In order to establish an agreement between linear Finite Element analysis and the experimental results, the longitudinal and vertical stresses were compared. Before cracking, measured concrete stresses agreed well with the pattern found by linear finite element analysis, but after flexural or diagonal cracking, this similarity disappeared at these cracked sections.

Generally, the longitudinal stresses in the central section (within the height) of the deep panels proved to be small when compared to the maximum tensile and compressive stresses at the bottom and top. For design purposes the upper and lower sections extending to depths of span/3 from the top and bottom of the wall should be carefully considered since significant longitudinal stresses are concentrated at these levels.

The maximum longitudinal compressive and tensile stresses reduce considerably as the depth/span ratio increases up to a value of 1. On

reaching a value of 1.5, the stresses decrease slightly and thereafter the effect of depth is extremely small.

9.2 BEHAVIOUR OF WALL BEAMS UNDER COMBINED TOP AND BOTTOM LOADS

9.2.1 Cracking load for walls loaded on top

The CIRIA Guide 2 (1977) procedure for calculating shear strength of deep beams has approximately predicted the load at which the first diagonal cracks were observed in the walls, with the actual ultimate shear strength being more than twice the predicted figure. Collapse of these specimens was due to bearing failure, suggesting an even greater capacity of the section to resist shear.

9.2.2 Cracking load for walls loaded at the soffit

For an increase in vertical reinforcement from 0.8 to 2.0 percent, the load at which the first horizontal crack was detected remained almost unaffected. Those specimens loaded at the soffit, cracked before reaching the designed ultimate load. Higher percentages of reinforcement were ineffective in retarding crack initiation, although they reduced crack widths. The cracking load (Newtons) for walls loaded at the soffit can be calculated from the elastic properties of the materials using equation 7.24:

$$W_{cr} = bL\ f_{ct}\ (1 + \alpha_t p)$$

This expression applies to short term loading conditions.

Failure of these specimens occurred due to deterioration of the lower section of the wall and excessive crack widths.

9.2.3 Diagonal cracking under combined top and bottom load

When the load is applied at the soffit, tensile forces are induced, which add to the diagonal tensile stresses arising from the

arch action of loads transmitted to the supports. This causes the concrete to reach its maximum tensile strength earlier than under top loads only. The angle of inclination of the diagonal crack is lowered by the vertical tensile forces.

9.2.4 Crack width control

For serviceability purposes, codes of practice and recommendations for design of reinforced concrete structures limit crack widths. In these tests, the specimens satisfied the crack width limits for normal and agressive environments, under the ultimate load estimated by using the CIRIA Guide 2 (1977) rules, while subjected to any combination of top and bottom loads.

9.3 BEARING STRENGTH

This experimental programme has demonstrated the importance of controlling and improving the bearing strength of deep flexural members. Crushing of the bearing zone was a frequent mode of failure. From the experimental results it is concluded that:

a) Bearing strength is unaffected by the variation in depth of the specimens tested.

b) The Kriz and Raths (1963) equations together with a reduction factor (Eq. 8.7)

$$f_b = 5.73 \sqrt{f'_c} \sqrt[3]{s/w} \, (1 + 0.198 C_1 \sqrt{A_{s1}/b})(1 - x_s/3430)$$

can be used for deriving the bearing strength (N/mm^2) of deep flexural elements directly loaded on top. The reduction factor $(1 - x_s/3430)$ takes into account the issues due to the in-plane tensile forces to which the bearing zones are subjected.

c) For practical purposes the equation stated above can be simplified to (Eq. 8.8)

$f_b = 5.00 \sqrt{f_{cu}}\ \sqrt[3]{s/w}\ (1 + 0.2C_1 \sqrt{A_{s1}/b})(1 - x_s/3400)$

in which the concrete cube strength (f_{cu}) is used.

d) Top and bottom load combinations have a considerable influence on the bearing strength. Hanging loads reduced the bearing capacity of the specimens. For the elements tested, Equation 8.6

$f_{bu}/f_{cu} = 0.92 + (7.0-5.83K_1)\ K_1^{2.333}$

approximately gives the bearing strength (N/mm^2) as a function of top and bottom loads.

9.4 QUALITY OF CONCRETE IN VERTICAL STRUCTURES

Compaction of concrete in any structure causes migration of light components, such as air and water, towards the top, creating a weaker concrete in the upper levels. This phenomenon is more critical in structures with large vertical dimensions and cast in their vertical position, for example, walls and columns. Because of the special characteristics of the mixes used for the walls and due to the difficulties experienced during casting, it was felt that verification of the actual concrete strength was necessary. Bearing in mind that these walls were cast upside-down, it was observed that:

a) The maximum strength of concrete occurs at the top of the walls, where the quality of concrete would be equal to that obtained from the control specimens. At the bottom, the actual concrete quality was less than 60 percent of the theoretical quality.

b) In the upper half of the specimen, the rate of change of strength of concrete with depth was greater, while the lower half showed a tendency to a more moderate variation.

c) Concrete strength in the middle vertical strip was on average 91 percent of that strength from the side strips.

9.5 SUGGESTIONS FOR FURTHER RESEARCH

During the development of this research, the necessity for further investigation into the bearing strength of deep flexural elements and means of improving it in order to utilise fully their structural strength in shear and flexure, has been demonstrated. Special attention should be directed towards enhancing the bearing zone confinement by incorporating additional transverse reinforcement. The effects of vertical bars extending from columns or any other type of discrete support needs to be studied further. Also, since almost all the data obtained experimentally has been based on rigid beds, more tests simulating the actual support provided by column heads are recommended.

The load-carrying capacity of deep beams beyond their diagonal and flexural cracking load has been widely recognised. However, the presence of cracks may be detrimental to serviceability, preventing an efficient use of the structural characteristics of these elements. The possibility of retarding cracks by employing prestressing should be considered together with an analysis of the cost implications of its use.

REFERENCES

1. American Concrete Institute (1977) A.C.I. 318-77, Building code requirements for reinforced concrete, Detroit.

2. Al-Najjim, A.G. (1981) Post-cracking behaviour of reinforced concrete beams. PhD Thesis, Polytechnic of Central London.

3. Archer, F.E. and Kitchen, E.M. (1960) Stress distributions in deep beams. Civil Engineering and Public Works Review, Vol. 55, No. 643, February, pp 230-234.

4. Au, T. and Baird, D.L. (1960) Bearing capacity of concrete blocks. Journal of the American Concrete Institute, Vol. 56, No. 9, March, pp 869-879.

5. Beeby, A.W. (1978) Cracking: what are crack width limits for? Concrete, Vol. 12, July, pp 31-33.

6. Bellander, U. (1979) Concrete strength in finished structures-destructive testing methods, relationships and reasonable criteria. R.I.L.E.M., Vol. 1, pp 27-35.

7. Bhargava, J. (1969) Strength of concrete members cast in deep forms. National Swedish Insitute for Building Research, Document No. 5.

8. Bloem, D.L. Concrete strength measurement, cores versus cylinders. Proceedings of the American Society of Testing Materials, Vol. 65, pp 668-696.

9. Bowman, S.A.W. (1980) Discussion on paper published in the Magazine of Concrete Research, Vol. 31, No. 107, June 1979, by J.H. Bungey. Magazine of Concrete Research, Vol. 32, No. 111, June, pp 124-125.

10. Brooks, J.J. and Neville, A.M. (1977) A comparison of creep, elasticity and strength of concrete in tension and in compression. Magazine of Concrete Research, Vol. 29, No. 100, September, pp 131-141.

11. B.S.812 (1975) Method for sampling and testing of mineral aggregates, sands and fillers. British Standards Institute, London.

12. B.S.1881 (1970) Methods of testing concrete. British Standards Institute, London.

13. Bungey, J.H. (1979) Determining concrete strength by using small-diameter cores. Magazine of Concrete Research, Vol. 31, No. 107, June, pp 91-98.

14. Campbell, R.H. and Tobin, R.E. (1967) Core and cylinder strengths of natural and lightweight concrete. Journal of the American Concrete Insitute, Vol. 64, No. 4, April, pp 190-195.

15. Carpenter, J.E. and Hanson, N.W. (1969) Tests of reinforced concrete wall beams with large web openings. Proceedings, American Concrete Institute, Vol. 66, No. 9, September, pp 756-766.

16. Cervenka, V. and Gerstle, K.H. (1971) Inelastic analysis of reinforced concrete panels: theory. Publications I.A.B.S.E., Vol. 31, pp 31-45

17. Cervenka, V. and Gerstle, K.H. (1972) Inelastic analysis of reinforced concrete panels: experimental verification and application. Publications I.A.B.S.E., Vol. 32, pp 25-39.

18. Chen, W.F. and Drucker, D.C. (1969) Bearing capacity of concrete blocks or rock. Proceedings of the American Society of Civil Engineers, Vol. 95, No. EM4, August, pp 955-978

19. Cheng, D.H. and Pei, M.L. (1954) Continuous deep beams. Proceedings of the American Society of Civil Engineers, Structural Division, Vol. 80, No. 450, June, pp 1-17.

20. Chow, L., Conway, H.D. and Winter, G. (1952) Stresses in deep beams. Proceedings of the American Society of Civil Engineers, Structural Division, Vol 78, Separate No. 127, May, pp 1-17.

21. Chow, L., Conway, H.D. and Winter, G. (1953) Stresses in deep beams. Transactions of the American Society of Civil Engineers, Vol. 118, No. 2557, pp 686-708.

22. C.I.R.I.A. (1977) CIRIA Guide 2. The design of deep beams in reinforced concrete. CIRIA Publication, London.

23. Comite Europeen du Beton - F.I.P. (1970) International recommendations for the design and construction of concrete structures, Principles and recommendations. Proceedings of the Sixth F.I.P. Congress, Prague, Czechoslovakia.

24. Concrete Society (1976) Concrete core testing for strength. Report No. 11. London.

25. Conway, H.D., Chow, L. and Morgan, G.W. (1951) Analysis of deep beams. Journal of Applied Mechanics, Vol. 18, No. 2, June, pp 163-172.

26. Coull, A. (1966) Stress analysis of deep beams and walls. The Engineer, Vol. 221, No. 5744, February, pp 310-312.

27. C.P.110 (1972) Code of practice for the use of concrete. British Standards Institute, London.

28. Dally, J.W. and Riley, W.F. (1978) Experimental stress analysis. Second Edition, McGraw-Hill Book Company, New York.

29. De Paiva, H.A.R. and Siess, C.P. (1965) Strength and behaviour of deep beams in shear. Proceedings of the American Society of Civil Engineers, Structural Division, Vol. 91, No. ST5, October, pp 19-41.

30. Department of the Environment (1976) Programme for the analysis and design of reinforced concrete and prestressee concrete slab bridges. HECB/B/13, Strand - Version 2, Program PSALM.

31. Dischinger, F. (1932) Beitrag zur theorie der halbscheibe und des wandartigen balkens. Publications I.A.B.S.E., Vol. 1, pp 69-32.

32. Fereig, S.M. and Smith, K.N. (1977) Indirect loading on beams with short shear spans. Journal of the American Concrete Institute, Vol. 74, No. 5, May, pp 220-222.

33. Ferguson, P.M. (1956) Some implications of recent diagonal tension tests. Journal of the American Concrete Institute, Vol. 53, No.2, August, pp 157-172.

34. Fintel, M, Bernard, P. and Derecho, A. (1968) Staggered transverse wall beams for multi-story concrete buildings - A detailed study. Portland Cement Association, Report XS6813.

35. Geer, E. (1960) Stresses in deep beams. Journal of the American Concrete Institute, Vo. 56, No. 1, January, pp 651-661.

36. Graf, O., Brenner, E. and Bay, H. (1943) Versuche mit einem wandartigen trager aus stahlbeton. Deutscher Ausschuss Für Stahlbeton, Heft 99, Berlin.

37. Guyon, Y. (1951) Contraintes dans les pièces prismatiques soumises á des forces appliquées sur leurs bases, au voisinage de ces bases. Publications I.A.B.S.E., Vol. 11, pp 165-226.

38. Guzman, A.M. and Luisoni, C.J. (1948) Solución variacional del problema de la viga rectangular simplemente apoyada de gran altura. Ciencia y Técnica, Vol. 111, No. 555, September, pp 119-143.

39. Hawkins, N.M. (1968) The bearing strength of concrete loaded through rigid plates. Magazine of Concrete Research, Vol. 20, No. 62, March, pp 31-40.

40. Hawkins, N.M. (1970) The bearing strength of concrete for strip loadings. Magazine of Concrete Research, Vol. 22, No. 71, June, pp 87-98.

41. Hyland, M.W. and Chen, W.F (1970) Bearing capacity of concrete blocks. Journal of the American Concrete Institute, Vol. 67, No. 3, March, pp 228-236.

42. Iyengar, K.T.S.R. (1962) Two-dimensional theories of anchorage zone stresses in post-tensioned prestressed beams. Journal of the American Concrete Institute, Proceedings, Vol. 59, No. 10, October, pp 1443-1466.

43. Kaar, P.H. (1957) Stresses in centrally loaded deep beams. Proceedings of the Society for Experimental Stress Analysis, Vol. 15, No. 1, pp 77-84.

44. Kani, G.N.J. (1966) Basic facts concerning shear failure. Journal of the American Concrete Institute, Proceedings, Vol. 63, No. 6, June, pp 675-692.

45. Kaplan, M.F. (1958) Compressive strength and ultrasonic pulse velocity relationships for concrete in columns. Journal of the American Concrete Institute, Proceedings, Vol. 5, No. 8, February, pp 675-688.

46. Kazimi, S.M.A. and Coull, A. (1964) Application of line solution techniques to the solution of plane-stress problems. International Journal of Mechanical Sciences, Vol. 6, pp 390-396.

47. Kemi, T. and Hiraga, T. (1979) On the distribution of the strength of concrete structures. Proceedings of the Congress on Quality Control of Concrete Structures, Stockholm, Sweden, pp 97-104.

48. Kong, F.K., Robins, P.J. and Cole, D.F. (1970) Web reinforcement effects on deep beams. Journal of the American Concrete Institute, Vol. 67, No. 12, December, pp 1010-1017.

49. Kong, F.K. and Robins, P.J. (1971) Web reinforcement effects on lightweight concrete deep beams. Journal of the American Concrete Institute, Vol. 68, No. 7, July, pp 514-520.

50. Kong, F.K. and Robins, P.J. (1972) Shear strength of reinforced concrete deep beams. Concrete, Vol. 6, No. 3, March, pp 34-36.

51. Kong, F.K., Robins, P.J., Kirby, D.P. and Short, D.R. (1972) Deep beams with inclined web reinforcement. Journal of the American Concrete Institute, Vol. 69, No. 3, March, pp 172-176.

52. Kong, F.K., Robins, P.J., Singh, A. and Sharp, G.R. (1972b) Shear analysis and design of reinforced concrete deep beams. The Structural Engineer, Vol. 50, No. 11, October, pp 405-409.

53. Kong, F.K. and Sharp, G.R. (1973) Shear strength of lightweight reinforced concrete deep beams with web openings. The Structural Engineer, Vol. 51, No. 8, August, pp 267-275.

54. Kong, F.K. and Sharp, G.R. (1977) Structural idealization for deep beams with web openings. Magazine of Concrete Research, Cement and Concrete Association, Vol. 29, No. 99.

55. Kong, F.K., Sharp, G.R., Appleton, S.C., Beaumont, C.J. and Kubik, L.A. (1978) Structural idealization for deep beams with web openings: further evidence. Magazine of Concrete Research, Cement and Concrete Association, Vol. 30, No. 103.

56. Kong, F.K. and Singh, A. (1972) Diagonal cracking and ultimate loads of lightweight concrete deep beams. Journal of the American Concrete Institute, Vol. 69, August, pp 513-521.

57. Kong, F.K. and Singh, A. (1974) Shear strength of lightweight concrete deep beams subjected to repeated loads. American Concrete Institute Special Publication, Shear in reinforced concrete, SP 42-21, Vol. 2, pp 461-476.

58. Kriz, L.B. and Raths, C.H. (1963) Connections in precast concrete structures - bearing strength of column heads. Journal of the Prestressed Concrete Institute, Vol. 8, No. 6, December, pp 45-75.

59. Laupa, A., Siess, C.P. and Newmark, N.M. (1955) Strength in shear of reinforced concrete beams. Bulletin of the Experiment Station, No. 428, University of Illinois.

60. Leonhardt, F. (1965) Reducing the shear reinforcement in reinforced concrete beams and slabs. Magazine of Concrete Research, Vol. 17, No. 53, December, pp 187-198.

61. Leonhardt, F. (1966) Discussion on "strength and behaviour of deep beems in shear" by H. de Paiva and C. Siess. Proceedings of the American Society of Civil Engineers, Vol. 92, ST2, April, pp 427-432.

62. Leonhardt, F. and Walther, R. (1962) Beiträge zur Behandlung der Schubprobleme im Stahlbetonbau. Beton und Stahlbetonbau, Vol. 57, pp 32-44.

63. Leonhardt, F. and Walther, R. (1966) Wandartige Träger. Deutscher Ausschuss für Stahlbeton, Heft 178, Wilhelm Ernst and Sohn, Berlin.

64. Lewis, R.K. (1980) Discussion on "Determining concrete strength by using small diameter cores", by Bungey, J.H. Magazine of Concrete Research, Vol. 32, No. 111, June, pp 123-124.

65. Mather, B. and Tynes, W.O. (1961) Investigation of compressive strength of molded cylinders and drilled cores of concrete. Journal of the American Concrete Insitute, Proceedings, Vol. 57, No. 7, pp 767-778.

66. McHenry, D. (1943) A lattice analogy for the solution of stress problems. Journal of the institution of Civil Engineers, Vol. 21, December, pp 59-82.

67. Meininger, R.C. (1968) Effect of core diameter on measured concrete strength. Journal of Materials, Vol. 3, No. 2, June, pp 320-336.

68. Mendoza, C.J. and Casillas, J. (1965) Variación de la resistencia con la altura en especimenes de concreto colados verticalmente. Revista IMCYC, Vol. 3, No. 13, March, pp 51-70.

69. Meyerhof, G.G. (1953) The bearing capacity of concrete and rock. Magazine of Concrete Research, Vol. 4, No. 12, April, pp 107-116.

70. Morice, P.B. and Base, G.D. (1953) The design and use of a demountable mechanical strain gauge for concrete structures. Magazine of Concrete Research, Vol. 5, No. 13, August, pp 37-42.

71. Muguruma, H. and Okamoto, S. (1965) Study on bearing capacity of concrete. Proceedings of the Eight Japan Congress on Testing Materials. Non-metallic Materials.

72. Murphy, W.E. (1979) The assessment of concrete strength in structures. Proceedings of the Congress on Quality Control of Concrete Structures, RILEM, Stockholm, Sweden, pp 135-142.

73. Nasser, K.W., Acavalos, A. and Daniel, H.R. (1967) Behaviour and design of large openings in reinforced concrete beams. Journal of the American Concrete Institute, Proceedings, Vol. 64, No. 1, January, pp 25-33.

74. Neville, A.M. (1959) Some aspects of the strength of concrete. Civil Engineering and Public Works Review, Vol. 54, No. 639, pp 1153-1156, No. 640, pp 1308-1310, No. 641, pp 1435-1439.

75. Neville, A.M. (1981) Properties of concrete. 3rd Edition, Pitman Publishing Limited, London.

76. Niyogi, S.K. (1973) Bearing strength of concrete - geometric variations. Proceedings of the American Society of Civil Engineers, Structural Division, Vol. 99, No. 7, July, pp 1471-1490.

77. Niyogi, S.K. (1974) Concrete bearing strength - support, mix, size effect. Proceedings of the American Society of Civil Engineers, Structural Division, Vol. 100, No. 8, August, pp 1685-1702.

78. Niyogi, S.K. (1975) Bearing strength of reinforced concrete blocks. Proceedings of the American Society of Civil Engineers, Structural Division, Vol. 101, No. 5, May, pp 1125-1137.

79. Petersons, N. (1964) Strength of concrete in finished structures. Swedish Cement and Concrete Research Institute, Reprint 26, Stockholm.

80. Portland Cement Association (1946) Design of deep girders. Concrete Information No. ST66.

81. Ramakrishnan, V. and Ananthanarayana, Y. (1968) Ultimate strength of deep beams in shear. Journal of the American Concrete Institute, Proceedings, Vol. 65, No. 2, February, pp 87-98.

82. Ramirez, J.L. and Barcena, J.L. (1979) Some data on concrete cores strength evaluation. Proceedings of the Congress on Quality Control of Concrete Structures, RILEM, Stockholm, Sweden, pp 165-173.

83. Robins, P.J. (1971) Reinforced concrete deep beams studied experimentally and by the finite element method. Ph.D. Thesis, University of Nottingham.

84. Rowe, R.E. and Base, G.D. (1966) Model analysis and testing as a design tool. Proceedings of the Institution of Civil Engineers, Vol. 33, February, pp 183-199.

85. Saad, S. and Hendry, A.W. (1961) Stresses in a deep beam with a central concentrated load. Proceedings of the Society for Experimental Stress Analysis, Vol. 38, No. 1, June, pp 192-198.

86. Saad, S. and Hendry, A.W. (1961b) Gravitational stresses in deep beams. The Structural Engineer, Vol. 39, No. 6, June, pp 185-194.

87. Schütt, H. (1956) Uber das Tragvermögen wandartiger Stahlbetontrager. Beton und Stahlbeton, Vol. 51, pp 220-224.

88. Sciammarella, C.A. and Palacio, M.A. (1949) Ensayo fotoelástico de una viga de gran altura. Ciencia y Técnica, Vol. 113, No. 569, November, pp 249-275.

89. Sciammarella, C.A. and Palacio, M.A. (1951) Ensayo fotoelástico de una viga de gran altura. Ciencia y Técnica, Vol. 117, No. 589, July, pp 1-31.

90. Shelson, W. (1958) Bearing capacity of concrete. Journal of the American Concrete Institute, Proceedings, Vo. 54, No. 5, pp 405-414.

91. Smith, K.N. and Vantsiotis, A.S. (1982) Shear strength of deep beams. Journal of the American Concrete Institute, Proceedings, Vol. 79, No. 3, May-June, pp 201-213.

92. Taylor, R. (1960) Some shear tests on reinforced concrete beams without shear reinforcement. Magazine of Concrete Research, Vol. 12, No. 36, November, pp 145-154.

93. Thon, R. (1958) Beitrag zur Berechnung und Bemessung durchlaufender wandartiger Träger. Beton und Stahlbetonbau, Vol. 53, No. 12, December, pp 297-305.

94. Timoshenko, S.P. and Goodier, J.N. (1970) Theory of elasticity. Third Edition, McGraw-Hill Kogakusha, Ltd., Tokyo.

95. Timoshenko, S. and Woinowsky-Krieger, S. (1959) Theory of plates and shells. Second Edition, McGraw-Hill Kogakusha, Ltd., Tokyo.

96. Uhlman, H.L.B. (1952) The theory of girder walls with special reference to reinforced concrete design. The Structural Engineer, Vol. 30, No. 8, August, pp 172-181.

97. Varghese, P.C. and Krishnamoorthy, C.S. (1966) Strength and behaviour of deep reinforced concrete beams. Indian Concrete Journal, Vol. 40, No. 3, March, pp 104-108.

98. Williams, A. (1979) The bearing capacity of concrete loaded over a limited area. Cement and Concrete Association, Technical Report 526.

99. Zsutty, T.C. (1968) Beam shear strength prediction by analysis of existing data. Journal of the American Concrete Institute, Proceedings, Vol. 65, No. 11, November, pp 943-951.

100. Zsutty, T.C. (1971) Shear strength prediction for separate categories of simple beam tests. Journal of the American Concrete Institute, Proceedings, Vol. 68, No. 15, February, pp 138-143.